UiT The Arctic University of Norway

Faculty of Biosciences, Fisheries and Economics

Norwegian College of Fishery Science

Bioactivity profiling and mode of action studies of antibacterial and antibiofilm agents of marine origin

Ataur Rahman

A dissertation for the degree of Philosophiae Doctor

January 2024

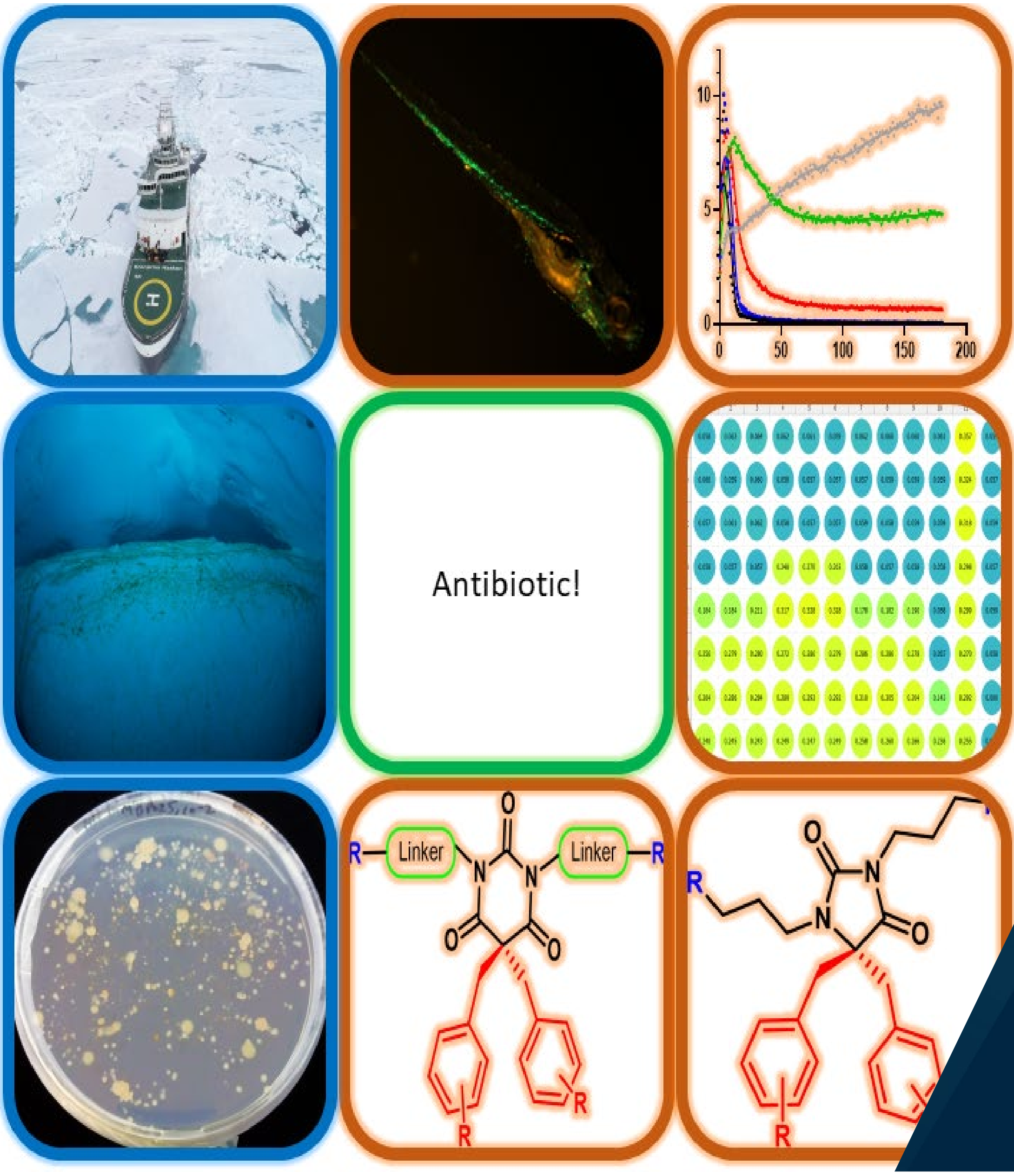

A dissertation for the degree of Philosophiae Doctor

Bioactivity profiling and mode of action studies of antibacterial and antibiofilm agents of marine origin

Ataur Rahman

November 2023

The work for this thesis was carried out from May 2019 to November 2023 at the Marine Bioprospecting research group, Norwegian College of Fishery Science, Faculty of Biosciences, Fisheries and Economics, UiT The Arctic University of Norway. The work was part of the AntifoMar project funded by UiT The Arctic University of Norway.

Table of Contents

Acknowledgments

I stand on the cliff of a monumental personal and professional milestone, completing a journey that has been as challenging as it has been rewarding, fulfilling my doctoral studies. It is a journey I have not walked alone; its chapters are infused with the wisdom, support, and encouragement of numerous individuals to whom I owe immense gratitude. With a deep sense of appreciation, I take this opportunity to acknowledge those whose contributions have been instrumental in pursuing and attaining my PhD.

First and foremost, I extend my heartfelt thanks to my principal supervisor, Prof. Klara Stensvåg, whose expertise and insight have been my guiding light throughout this process. Her patience and unwavering belief in my capabilities have strengthened and inspired me. The intellectual rigour she demanded of me and the generosity with which she shared her profound knowledge have shaped this thesis and my entire approach to scientific inquiry. Her mentorship extends beyond academic guidance; it has been a personal growth experience for which I am profoundly grateful.

I am equally thankful to my co-supervisors, Professor Johanna U Ericson, Professor Morten B. Strøm, Professor Annette Bayer, Associate Professor Hans-Matti Blencke, Associate Professor Gabriel Magno de Freitas Almeida and Dr. Ekaterina Mishchenko, for their wise critiques and valuable suggestions that have greatly enhanced the quality of my research. Their perspectives and association with CANS, Centre for New Antibacterial Strategies, have added a valuable layer of depth to my work.

My sincere appreciation goes to the faculty and staff of the UiT The Arctic University of Norway. Each interaction has added a stone to the edifice of my learning. I would like to acknowledge my colleagues, especially Manuel Karl Langer, Andrea Iselin Elvheim, Christoffer Sivertsen, Hymonti Dey, and Jonathan Hira, for their companionship and for the thought-provoking discussions that have often led to significant breakthroughs in my research. Collaborating with them has been both a pleasure and an enriching experience.

I am grateful to the engineers (Ida Kristine Østnes Hansen, Hege Devold, Frode Jacobsen Øyen) and administrative and technical staff whose support has allowed me to focus on my research without distraction. Their contributions, often behind the scenes, have been invaluable.

This thesis would not have been possible without my family's constant support and patience. To my wife, Wasifa Kabir, I owe a special debt of gratitude. Her understanding, love, and encouragement, even when sacrifices were required, have been a source of personal peace and confidence. Her ability to endure the ups and downs alongside me has been nothing short of extraordinary. To my son, Rihanur Rahman, a bundle of joy and boundless energy, who has brought laughter and light into my toughest days - his hugs have been my haven.

Parents (my and my wife's) and siblings deserve special mention for their unwavering faith and prayers. They instilled in me the value of perseverance and hard work, which have been my companions on this academic voyage.

Finally, I would like to thank UiT The Arctic University of Norway, for the financial assistance and belief in the importance of my research.

Each of you mentioned here, many not named but remembered, have my deepest gratitude. This thesis stands as a testament to your collective support and belief in my potential. Thank you.

Ataur Rahman

Abstract

The emergence of drug-resistant strains and new pathogens intensifies the need for new antimicrobials. Additionally, bacterial biofilms, which contribute to persistent infections, further complicate treatment efforts. The increasing difficulty in discovering and developing new antimicrobials adds to this challenge. However, marine environments, with their vast biodiversity, offer a promising avenue for antibiotic discovery, particularly through natural products synthesized by marine microorganisms. These organisms are a rich source of novel bioactive secondary metabolites with potential therapeutic applications. Additionally, synthetic mimics of antimicrobial peptides represent another promising direction in the quest for new antimicrobials.

Paper I elucidate the structure-activity relationship of cationic amphipathic N,N'-dialkylated-5,5-disubstituted barbiturates as marine eusynstyelamide mimics, investigating their potential as antimicrobial agents. The library of 58 compounds, synthesized through a strategic approach, demonstrated the significance of cationic groups, hydrocarbon linkers, and lipophilic side chains on antimicrobial and haemolytic activities. Notably, guanidyl and amine groups showed broad-spectrum activity, while trimethylated quaternary amines were more selective for Gram-positive bacteria. The compounds, especially 11lG, 13jA, and 13jG, showed potent antimicrobial effects with low haemolytic activity, with the guanidine derivative 11lG significantly disrupting bacterial membranes.

In **paper II**, the investigation into tetrasubstituted, cationic, amphipathic heterocycles as antimicrobial peptide (AMP) mimics identified hydantoin as a favourable scaffold, influencing haemolytic activity and antimicrobial potency. Among the hydantoin derivatives studied, three leads (2dA, 6cG, and 6dG) exhibited promising broad-spectrum activity, with 6dG showing notably low minimum inhibitory concentration values. The mode of action studies revealed a pronounced membranolytic effect on the inner and outer bacterial membranes, emphasizing the importance of structural arrangement in AMP mimics.

In **paper III**, the antibiofilm capabilities and *in vivo* efficacy of these peptidomimetics were explored using a zebrafish model, discovering that 13iA and 2cA presented remarkable biofilm inhibition and eradication potentials, along with moderate activity against resistant clinical isolates. Their lack of toxicity, immunogenicity, and promising *in vivo* antibacterial activity in the zebrafish model up to 16 mg/kg dose showcases their potential as templates for new antibiotics against antimicrobial resistance (AMR).

In **paper IV**, the bioprospecting work focused on Arctic marine bacterial isolates from various habitats near Tromsø and towards the North Pole indicated the presence of biosynthetic gene clusters (BGCs) with antimicrobial activity. Of the 158 isolates, 65 exhibited antibacterial activity, and 37 confirmed the presence of nonribosomal peptide synthetase (NRPS) or polyketide synthase (PKS) BGCs, with genome sequencing and mining unveiling multiple BGCs. Seven of these isolates displayed activity against both Gram-positive and Gram-negative pathogens and contained NRPS or PKS BGCs, advancing them as promising sources of novel antimicrobial agents.

These combined efforts contribute valuable insights into the design and discovery of new antimicrobials, addressing the urgent global challenge of AMR with innovative solutions derived from marine bioprospecting and synthetic peptidomimetic chemistry.

List of papers

This thesis comprises two published articles and two manuscripts, denoted by Roman numerals.

Paper I

Title: A concise SAR-analysis of antimicrobial cationic amphipathic barbiturates for an improved activity-toxicity profile.

Authors: Manuel K. Langer*, **Ataur Rahman***, Hymonti Dey, Trude Anderssen, Francesco Zilioli, Tor Haug, Hans-Matti Blencke, Klara Stensvåg, Morten B. Strøm, Annette Bayer
* The authors contributed equally to this work.
Journal: European Journal of Medicinal Chemistry, available online on 5 August 2022

Paper II

Title: Investigation of tetrasubstituted heterocycles reveals hydantoins as a promising scaffold for development of novel antimicrobials with membranolytic properties.

Authors: Manuel K. Langer, **Ataur Rahman**, Hymonti Dey, Trude Anderssen, Hans-Matti Blencke, Tor Haug, Klara Stensvåg, Morten B. Strøm, Annette Bayer
Journal: European Journal of Medicinal Chemistry, available online on 24 January 2023

Paper III

Title: Peptidomimetic tetrasubstituted barbiturates and hydantoins: Investigation of their antibiofilm, in vivo toxicity and antimicrobial activity.

Authors: Ataur Rahman, Manuel Karl Langer, Bartosz Michno, Gabriela Żyłka, Jonathan Hira, Hege Devold, Ida Kristine Østnes Hansen, Ekaterina Mishchenko, Morten B. Strøm, Annette Bayer, Johanna U Ericson, Tomasz Prajsnar, Klara Stensvåg

Manuscript

Paper IV

Title: Antimicrobial potential of marine bacteria from the Arctic and sub-Arctic regions.

Authors: Ataur Rahman*, Andrea Iselin Elvheim*, Christoffer Ågnes, Ida Kristine Østnes Hansen, Hege Devold, Frode Jacobsen Øyen, Gabriel Magno de Freitas Almeida, Hans-Matti Blencke, Bjarne Landfald, Tor Haug, Klara Stensvåg
* The authors contributed equally to this work.

Manuscript

Authors contribution

	Paper I	Paper II	Paper III	Paper IV
Concept and idea	MKL*, **AR***, TH, HMB, KS, MBS, AB	MKL, **AR**, HMB, TH, KS, MBS, AB	**AR**, MKL, EM, MBS, AB, JUE, TP, KS	**AR***, AIE*, CÅ, HMB, BL, TH, KS
Study design and methods	MKL*, **AR***, HDY, TA, FZ, TH, HMB, KS, MBS, AB	MKL, **AR**, HDY, TA, HMB, TH, KS, MBS, AB	**AR**, MKL, EM, JUE, TP, KS	**AR***, AIE*, CÅ, HMB, BL, TH, KS
Data gathering and interpretation	MKL*, **AR***, HDY, TA, FZ, TH, HMB, KS, MBS, AB	MKL, **AR**, HDY, TA, HMB, TH, KS, MBS, AB	**AR**, MKL, BM, GŻ, JH, HDD, IKØH, EM, JUE, TP, KS	**AR***, AIE*, CÅ, IKØH, HDD, FJØ, HMB, BL, TH, KS
Manuscript preparation	MKL*, **AR***, HDY, TA, FZ, TH, HMB, KS, MBS, AB	MKL, **AR**, HDY, TA, HMB, TH, KS, MBS, AB	**AR**, MKL, BM, GŻ, JH, HDD, IKØH, EM, MBS, AB, JUE, TP, KS	**AR***, AIE*, CÅ, IKØH, HDD, FJØ, GMDFA, HMB, BL, TH, KS

MKL - Manuel K. Langer, AR - Ataur Rahman, HDY - Hymonti Dey, TA - Trude Anderssen, FZ - Francesco Zilioli, TH - Tor Haug, HMB - Hans-Matti Blencke, KS - Klara Stensvåg, MBS - Morten B. Strøm, AB - Annette Bayer, BM - Bartosz Michno, GŻ - Gabriela Żyłka, JH - Jonathan Hira, HDD - Hege Devold, IKØH - Ida Kristine Østnes Hansen, EM - Ekaterina Mishchenko, JUE - Johanna U Ericson, TP - Tomasz Prajsnar, AIE - Andrea Iselin Elvheim, CÅ - Christoffer Ågnes, FJØ - Frode Jacobsen Øyen, GMDFA - Gabriel Magno de Freitas Almeida, BL - Bjarne Landfald.

Abbreviations

AMP(s)	Antimicrobial peptide(s)
AMR	Antimicrobial resistance
BGC(s)	Biosynthetic gene cluster(s)
CANS	Centre for New Antibacterial Strategies
EC_{50}	Effective concentration to produce 50% of the maximum response
FICI	Fractional inhibitory concentration index
hpi	Hour(s) post-infection
IM	Inner membrane
IY	Intrayolk
MBSM(s)	Marine bacterial secondary metabolite(s)
MIC	Minimum inhibitory concentration
MNP(s)	Marine natural product(s)
MoA	Mode of action
NPN	1-N-phenylnaphthylamine
NP(s)	Natural product(s)
NRPS	Nonribosomal peptide synthetase
OM	Outer membrane
OSMAC	One strain many compounds
PCR	Polymerase chain reaction
PKS	Polyketide synthase
RBC	Red blood cell
RNA-seq	RNA sequencing
SAMP(s)	Synthetic antimicrobial peptide(s)
SAR	Structure-activity relationship
SI	Selectivity index
SMAMP(s)	Synthetic mimic of antimicrobial peptide(s)
TLR(s)	Toll-like receptor(s)
WHO	World Health Organization

1 Introduction

The development of new antibiotics is essential to combat the growing threat of infectious diseases and antibiotic resistance. However, traditional drug discovery approaches have faced several challenges and development of new antibiotics is slow. Natural products (NPs) discovery and synthetic biology are promising approaches to antibiotic drug development[1]. This thesis focuses on identifying producers of antimicrobial secondary metabolites and their link to biosynthetic gene clusters (BGCs) from marine bacteria. Additionally, evaluation of the structure-activity relationship (SAR) of synthetic mimics of antimicrobial peptides (SMAMPs) inspired from marine natural products (MNPs).

1.1 The challenges

1.1.1 Infectious diseases

Infectious diseases remain a significant global health challenge[2,3], spreading rapidly due to globalization and interconnectedness, posing a serious public health concern[4]. They contribute significantly to the global burden of diseases, particularly in low-resource settings with inadequate infrastructure and poor healthcare access[2]. The availability of healthcare can prevent disease progression and improve health outcomes. Inadequate investment in public health infrastructure and disease surveillance, particularly in resource-limited countries, hinders effective response and management of infectious diseases[5].

The rise of drug-resistant strains and new pathogens underscores the need for effective infectious disease management[6]. Key challenges include developing diagnostic devices for the real-time detection of multiple disease markers[7] and establishing robust surveillance systems to identify outbreaks and monitor disease spread. The irrational use of antibiotics further complicates disease control, fostering multidrug-resistant pathogens[8]. Global trade and intensive livestock systems create opportunities for the transmission of disease between species, perpetuating the emergence of infectious agents and posing an economic challenge to the global economy[9]. Globalization, overpopulation, and the movement of people and goods across borders exacerbate the spread of the disease, making containment difficult[10-12]. The persistent threat of infectious diseases highlights the need for effective treatment and management[13].

1.1.2 Antimicrobial resistance

Antimicrobial resistance (AMR) is a pressing global health issue[14-16]. AMR is not limited to specific countries or income levels; it is a substantial problem worldwide[17]. The clinical and financial burden imposed by AMR is significant and affects healthcare systems globally[17]. The economic impact of AMR is predicted to cost more than $105 billion annually worldwide, with Africa being the region most affected[18]. AMR is a complex issue that arises when microorganisms evolve and develop resistance to drugs designed to kill them (**Figure 1**)[19,20]. AMR spread can occur through several mechanisms, such as the acquisition of AMR genes through horizontal gene transfer or mutation of existing genes (**Figure 1**).

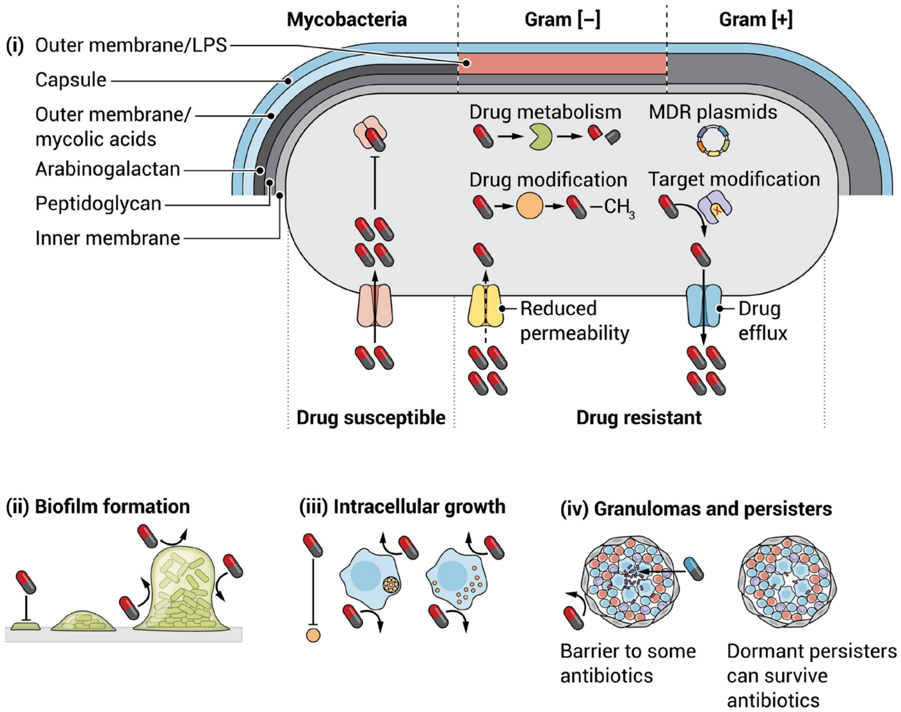

Figure 1. AMR takes many forms*, from (i) the intrinsic physical barrier of the cell envelope; direct interventions by different resistance genes; modification in the physical compartmentalization of (ii) biofilms, (iii) intracellular environments, and (iv) granulomas; to persistent states of low metabolic activity. Permission from American Association for the Advancement of Science (AAAS). Based on Cook et al. (2022)[19].*

Society's failure to protect antibiotics, a precious resource, has contributed to the emergence of antibiotic-resistant bacteria[21]. Various factors, including the misuse and overuse of antibiotics without rational prescription or reason in human medicine, veterinary medicine, and agriculture[22,23], inadequate infection control practices and lack of effective surveillance systems contribute to antibiotic resistance development and spread. This issue of antibiotic resistance is further exacerbated by the lack of national guidelines for antibiotic use and the limited access to laboratory facilities for antimicrobial drug susceptibility tests[24-26]. The World Health Organization (WHO) has identified 12 bacteria or bacterial families that pose the greatest threat to human health and for which new antibiotics are desperately needed[27]. These challenges highlight the urgent need to discover new antibiotics to continually combat multidrug-resistant bacterial strains.

1.1.3 Bacterial biofilm

Bacterial biofilms pose significant problems in various contexts, including healthcare settings and industrial systems. These biofilms, formed by a community of microorganisms embedded within an extracellular matrix, can cause persistent infections and make treatment challenging (**Figure 2**)[28,29]. Biofilms are frequently associated with infections in implanted medical devices. These infections can be challenging to resolve and cause significant morbidity in patients. Additionally, bacteria that grow in biofilms are more resistant to antibiotics and host immune responses, making infections chronic and difficult to manage[30]. The increased prevalence of drug-resistant microorganisms that form biofilms during treatment or after surgery further complicates the challenges in combating biofilm-related infections[31].

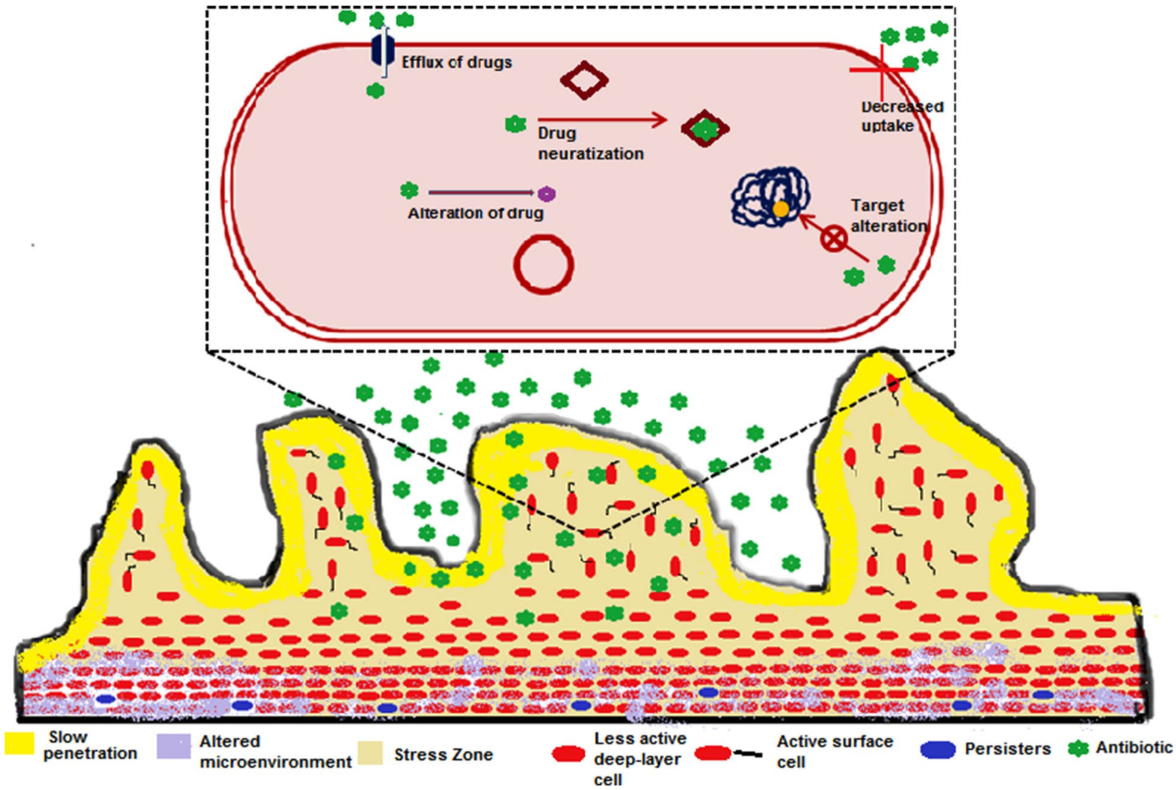

Figure 2. Biofilm and possible mechanisms of antibiotic resistance in biofilm communities; *Sharma et al. (2019)*[32].

In addition, bacterial biofilms exhibit an increased tolerance to antibiotics compared to planktonic bacteria (**Figure 1i**i and **Figure 2**)[32,33]. This increased tolerance is a multifactorial problem arising from the physical and genetic characteristics of biofilms (**Figure 2**). Extracellular polymeric substances in the biofilm matrix create a physical barrier that hinders the diffusion and penetration of antibiotics into the biofilm (**Figure 2**). In addition to the physical barrier, bacterial biofilms also possess inherent genetic resistance mechanisms (**Figure 2**). These mechanisms can include the production of enzymes that can inactivate antibiotics, alterations in the target sites of antibiotics, and up-regulation of efflux pumps that can actively pump antibiotics out from bacterial cells (**Figure 1** and **Figure 2**)[19,32].

1.1.4 Antibacterial discovery void

The first antibiotic, salvarsan, was developed and used in 1910[34]. Antibiotics gained widespread use to treat infections with the discovery of penicillin in 1928[19,34]. The mid-20th century marked the golden age of antibiotic discovery, introducing many new classes, such as cephalosporins, tetracyclines, and aminoglycosides (**Figure 3**)[34]. These antibiotics revolutionized the treatment of infectious diseases against an extensive range of bacteria[19]. The current void in discovery and development is a pressing issue because of increasing antimicrobial resistance. Investing in prospective research to discover new antimicrobial substances has become crucial, as many of the current therapies will no longer be effective in the future, even for common infections, if no new agents are discovered.

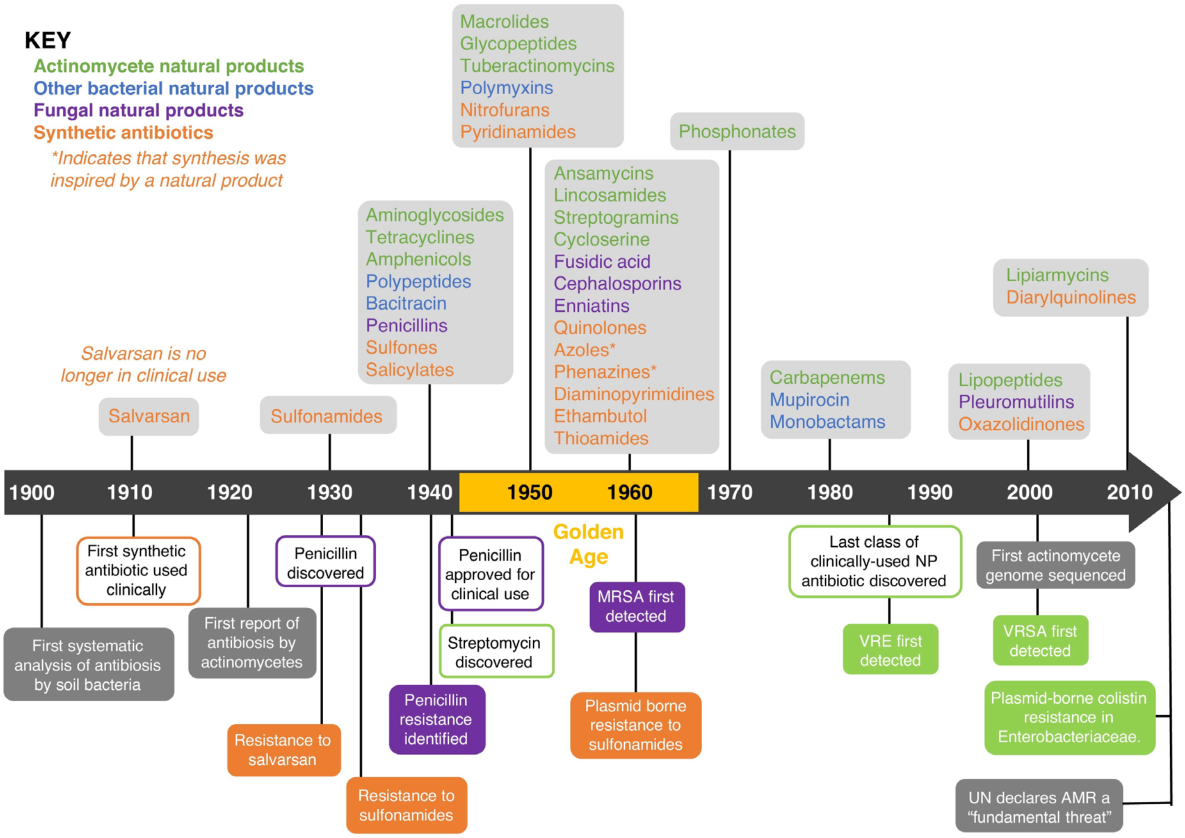

Figure 3. The timeline shows the decade in which new classes of antibiotics entered the clinic. *Antibiotics are colored according to their source: green = actinomycetes, blue = other bacteria, purple = fungi, and orange = synthetic. Permission by Elsevier: Hutchings et al. (2019)*[34].

The lack of discovery of new antimicrobials can be attributed to several factors[35]. First, the over-reliance on existing antibiotics due to their success has led to reduced funding and research efforts for new compounds[35]. Additionally, alternative approaches like combinatorial chemistry have not adequately enriched the drug pipeline. Large pharmaceutical companies, facing regulatory, scientific, and financial challenges, lack motivation for new antimicrobial development[35]. The prolonged research timelines exacerbate this void, leaving the responsibility mainly to small start-ups and academic laboratories[35,36]. The paucity of new antibiotics in the past five decades underscores the need for innovative approaches, as traditional methods produce diminishing returns[37].

1.2 Solutions

This gap in new antibiotics has created a pressing need for alternative approaches to antibiotic discovery. To solve the issue mentioned above, a number of non-traditional/novel/innovative sources (1.2.1, 1.2.2), structures (1.2.2, 1.2.3, 1.2.4), and discovery approaches/workflows (1.2.5) are suggested and discussed in this work.

1.2.1 Marine environment as a source of natural products (NPs)

The marine environment is one potential source to discover new antimicrobial compounds[38-40]. Exploring and exploiting vast and largely underexplored marine environments as a potential source of new antimicrobial compounds is a promising strategy. The unique conditions of the marine environment, especially the Arctic, such as high salinity, high pressure, and low temperatures, provide a habitat for organisms that have evolved unique biochemical and physiological adaptations (**Figure 4**)[41-43]. These adaptations often result in the production of bioactive natural products (NPs) with potent antimicrobial properties.

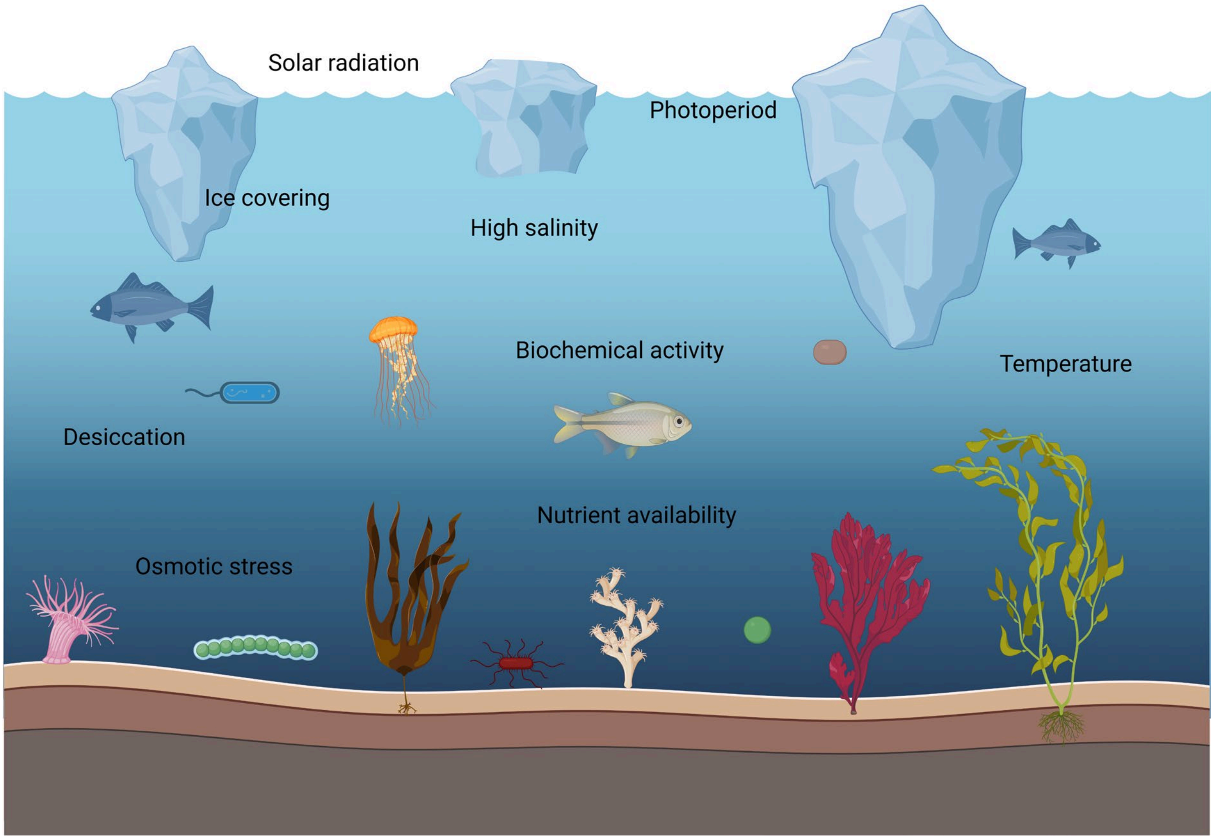

Figure 4. Illustration of stress factors in Arctic marine environments.

Marine bioprospecting, the exploration of marine organisms for bioactive compounds, offers a rich source of novel molecules for drug development, particularly antimicrobials. This approach is enhanced when combined with peptidomimetics (**Figure 5**), where natural peptide structures are mimicked and modified to improve their stability, bioavailability, and specificity. They might be candidates for LEAD compounds for further innovative development if they are found active in bioassays. Thus, the constructive integration in bioprospection leverages the vast chemical diversity of marine natural products and the versatility of peptidomimetics, allowing for the creation of novel compounds with potential therapeutic applications, including combating antimicrobial resistance. Altogether, this integrated strategy enables overcoming the limitations inherent in natural compounds and peptides, paving the way for innovative lead and drug development.

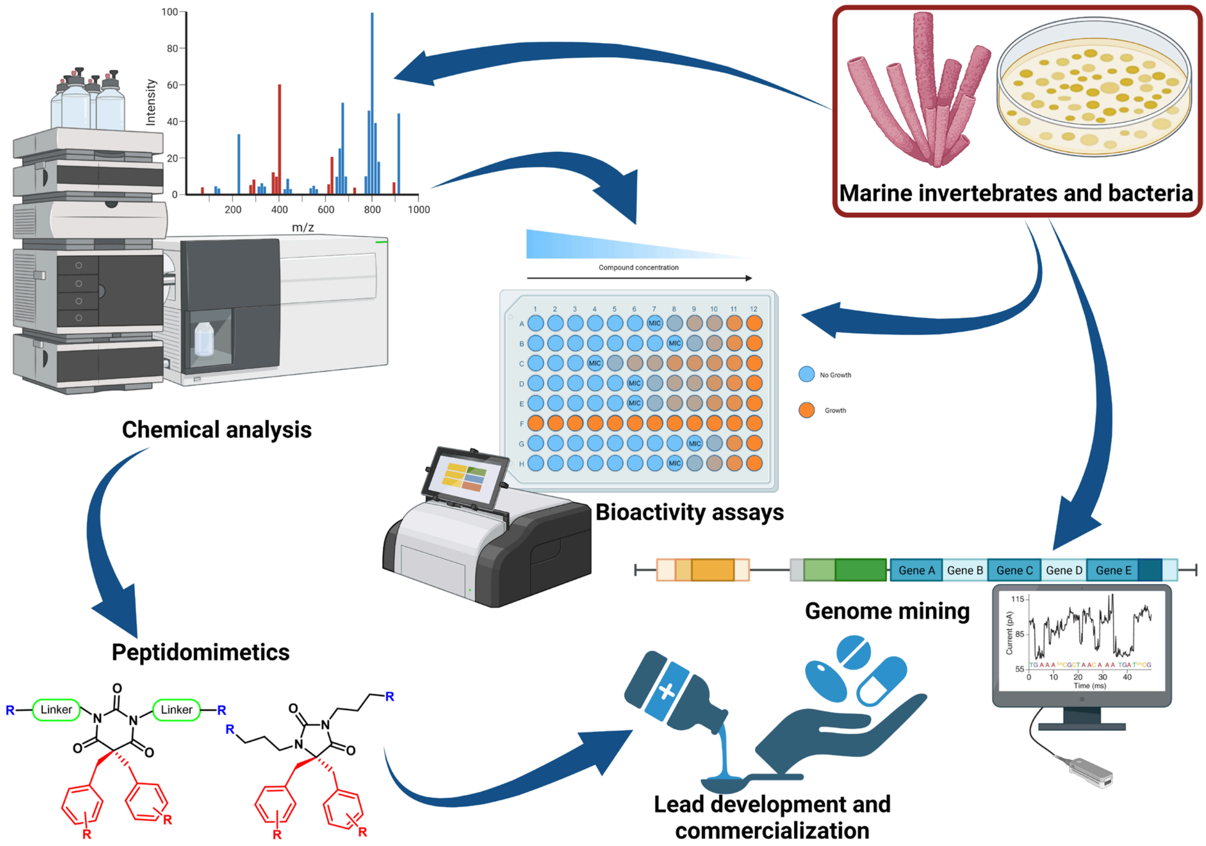

Figure 5. Marine bioprospecting approach, which can be combined with peptidomimetics for drug development.

1.2.2 Marine bacteria as a source of NPs

Most clinically relevant classes of antibiotics derived from NP are of terrestrial origin[34,44,45] (**Figure 6**). However, one potential solution to find new antibiotics lies in the vast biodiversity of marine environments. Marine microorganisms have been found to be a rich source of novel bioactive secondary metabolites with potential for therapeutic applications[38,46].

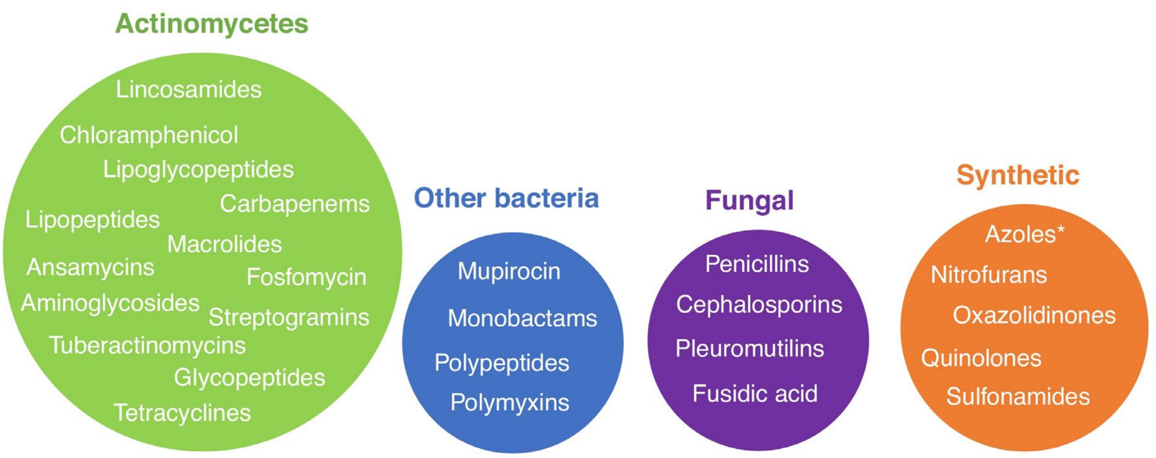

Figure 6. The most relevant class of antibiotics in clinical practice comes from natural products. *Permission by Elsevier: Hutchings et al. (2019)*[34].

The isolation and testing of microorganisms for their ability to produce antibiotically active compounds is a prospective approach [47]. This innovative strategy involves exploring uncharted microbial territories and investigating their potential as sources of new antimicrobial compounds. By venturing beyond the well-known sources of antimicrobials, researchers can discover novel structures and mechanisms of actions. Using high-throughput screening and innovative screening techniques can also aid in the discovery of new antimicrobials. Advances in bioprospection technologies have allowed the collection of samples from deep sea, thermal vents, and polar regions, allowing the discovery of potential secondary metabolites with strong antibiotic activity against drug-resistant pathogens[41]. Furthermore, the application of advanced technologies and techniques, such as metagenomics and genome mining, can accelerate the discovery process by allowing researchers to screen large volumes of marine microorganisms and analyse their genetic potential for producing antimicrobial compounds. BGCs, encompassing polyketide synthase (PKS) and nonribosomal peptide synthetase (NRPS), and their derivatives underpin life-saving drugs for acute and chronic diseases (**Figure 7**)[44,48]. Notable antibiotics include nonribosomal penicillin and polyketide erythromycin A[48]. This prompted investigations into the machinery of these systems, seeking to understand nature's utilization of large proteins for small molecule synthesis[48]. Furthermore, this knowledge aids the genetic engineering of these enzymes to create potentially valuable analogs[48].

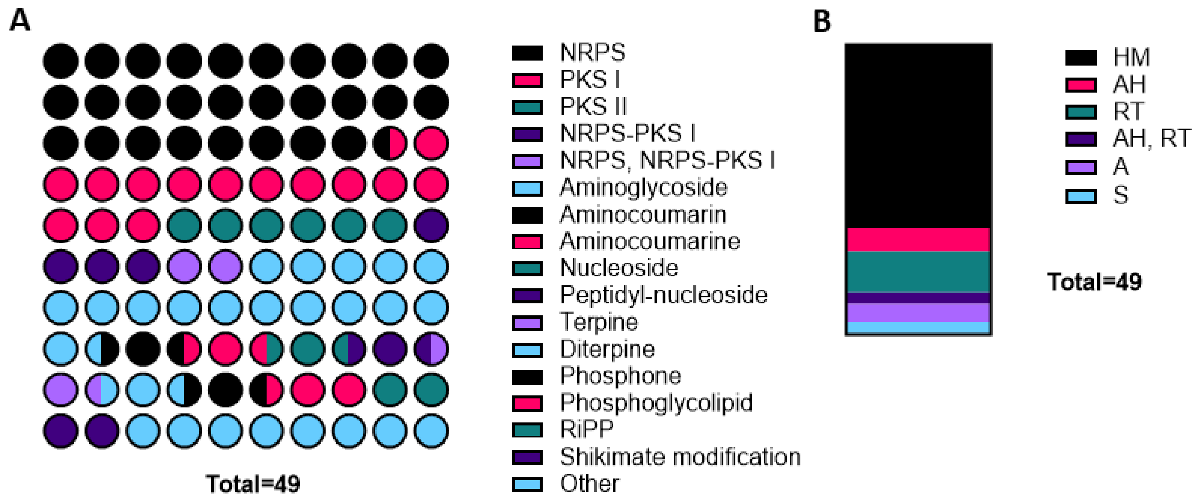

Figure 7. Natural products with antimicrobial activity are produced as secondary metabolites by bacteria or fungi. *Data from Katz et al. (2016)[44]. A. Dot plot showing the distribution of their biosynthetic origin, where NRPS - nonribosomal peptide synthetase, PKS - polyketide synthase, RiPP - ribosomally synthesized and post-translationally modified peptide. B. Major uses as antibacterial, where HM – human medicine, AH - animal health, RT - research tool, and S - scaffold for chemical semi-synthesis.*

The discovery of NPs with antimicrobial activity from marine bacteria dates back to the 1950s, but it was not until the 1970s that antibiotic properties of marine bacterial metabolites were first reported[49]. Since then, numerous studies have been conducted to investigate the antibiotic potential of marine bacteria. These studies have led to the isolation and characterization of novel NPs with diverse chemical structures and potent antimicrobial activity. Various studies have highlighted the potential of marine bacteria as a source of new antibiotics. For example, a study by Schinke et al. isolated a marine bacterium from deep-sea sediments that produced a compound with potent antibacterial activity against methicillin-resistant *Staphylococcus aureus*[50].

Marine bacteria, including Cyanobacteria, Actinobacteria, Roseobacter clade, and Pseudoalteromonas genus, have been found to produce NPs with interesting pharmacological properties[38]. Not limited to these genera, other marine bacteria from various marine sources have been investigated for producing antimicrobial compounds, including sponges, seaweeds, sediments, thermal vents, and symbiotic associations with marine invertebrates[42] (**Table 1**).

Table 1. Antimicrobial activities associated with the main phyla of marine bacteria. *Reprinted by permission of Informa UK Limited, trading as Taylor & Taylor & Francis Group: Stincone et al. (2020)[42], modified.*

Source	***Antimicrobial producing bacteria***	**Target microorganism**
Aquaculture system	*Bacillus velezensis*	As
Cephalopod	*Leisingera* sp.	Vf, Va, Vp
Coral	*Micromonospora, Brachybacterium, Nocardia, Micrococcus, Arthrobacter, Rhodococcus* and *Streptomyces*	Sa, Bs, Ec
Coral	*S. variabilis*	Ec, Vc, Kp, Pa, *Enterobacter* sp., *Streptococcus* sp.
Chordate	*Streptomyces* sp. ZZ338	Sa, Ec, Ca
Gastropod	*Pseudomonas aeruginosa*	*Alteromonas* sp., *Pseudomonas* sp.
Mixture of invertebrate	*Streptomyces* sp.	Pa, Ca, Sa, Ef, Ec, Lm
Mussel	*Bacillus licheniformis*	Vh, Pa
Nudibranch	*Vibrio* and *Pseudoalteromonas*	Ap, Ec, Sa
Seaweed	*B. subtilis* MTCC 10407	Vp
Seaweed	Mixture	Sa, Ec, Ca
Sediment	*Verrucosispora* sp. MS100047	Sa, Mt, Bs, Pa, Ca
Sediment	*Micromonospora harpali*	Bs
Sediment	*Staphylococcus saprophyticus* SBPS 15	Ec, St, Sp, Kp, Vp, Vp, Pm, Spn, Bs, Bc, Sa
Sediment	*Rhodococcus* sp.	Bc, Bs, Ec, Pa, St, Sma, Sf, Sa, Ca
Sediment	*Streptomyces* sp. NIOT-Ch-40	Bs, Ml, Sa, Se, MRSA
Sediment	*Streptomyces, Micromonospora, Nocardiopsis, Saccharomonospora, Actinomadura, Glycomyces,* and *Nocardia*	Kp, Bs, Sa, Ec, *Enterococcus* sp.
Sediment	*Rheinheimera japonica* KMM 9513	Ec, Sa, Se, Bs
Sediment	*Streptomyces* sp. WU20	Sa, Bs, Ec
Sediment	*Streptomyces* sp. H-KF8	Sa, Lm, Se Ec, Pa
Sediment	*Streptomyces* sp., *Kocuria* sp., *Dietzia* sp., and *Nocardiopsis* sp.	Bs, Sa, Pa, Ca
Sediment	*Streptomyces* sp., and *Nocardia* sp.	St, Kp, Pa, Pm, Sa , Ec, *Shigella* sp.
Sediment	*Variovorax* sp.	Sw, Pv, MRSA, VRE
Sediment	*Streptomyces* sp.	Ab, Ec, Ef, Kp, Pa, Pm, Sa,VRE
Sediment	*Aequorivita* sp.	MRSA
Shellfish	*Lactobacillus* sp.	Sa, Vp, Ec, Kc
Sponge	*Streptomyces* sp.	Bs, Bc, Ca, Ec, Sa, Pa,
Sponge	*Acinetobacter, Bacillus, Photobacterium, Shewanella,* and *Vibrio*	Ec, Kp, Pa, Sa, Sh, Ef, Kp, Pa, Sa, MRSA, VRE
Sponge	*Vibrio, Pseudomonas/Marinobacter* and *Bacillus*	Bs, Ec, Vp, Vh, Ca
Sponge	*Vibrio,* etc	Pa, Sa, Bs, Ec, Ca
Sponge	*Rhodococcus sp.*	Sa
Sponge	*B. zhangzhouensis, B. pumilus, Psychrobacter alimentarius,*and *Arthrobacter citreus*	Bc, Se, Ms, Bc, Sen

Source	*Antimicrobial producing bacteria*	Target microorganism
Sponge	Mixture	Sa, Pa, Ec, St
Water	*Bacillus* sp., *Arthrobacter,* and *Brevundimonas*	Ec, Sa, Pa
Water	*Pseudoalteromonas haloplanktis* TAC125	Ec
Water	*Bacillus* sp. and *Pseudomonas* sp.	Ec, Sa
Water/ Sediment	*Pontibacter korlensis* SBK-47	Sm, Sa, Ec, St, Sp, Vp, Vc, Bs, Ml, Ef, Kp
Collection of marine bacteria	*Bacillus pumilus*	Sa, Lm

Ab: *Acinetobacter baumannii*; As: *Aeromonas salmonicida*; Ap: *Arthrobacter psychrolactophilus*; Bc: *Bacillus cereus*; Bs: *Bacillus subtilis*; Ca: *Candida albicans*; Ec: *Escherichia coli*; Ef: *Enterococcus faecalis*; Kp: *Klebsiella pneumoniae*; Lm: *Listeria monocytogenes*; Ml: *Micrococcus luteus*; Ms: *Mycobacterium smegmatis*; Mt: *Mycobacterium tuberculosis*; Pa: *Pseudomonas aeruginosa*; Pm: *Proteus mirabilis*; Pv: Proteus *vulgaris*; Sa: *Staphylococcus aureus*; Se: *Staphylococcus epidermidis*; Sh: *Staphylococcus hominis*; Sw: *Staphylococcus warneri*; Sf: *Shigella flexneri*; Sen: *Salmonella entrica*; Sp: *Salmonella paratyphi*; St: *Salmonella typhi*; Spn: *Streptococcus pneumoniae*; Sm: *Streptococcus mutans*; Sma: *Serratia marcescens*; Va: *Vibrio angluillarum*; Vc: *Vibrio cholerae*; Vf: *Vibrio fischeri*; Vh: *Vibrio harveyi*; Vp: *Vibrio parahaemolyticus*; MRSA: methicillin-resistant *Staphylococcus aureus*; VRE: vancomycin-resistant *Enterococcus*.

1.2.3 Eusynstyelamides, a novel scaffold from marine invertebrates

Not only marine bacteria, but also marine invertebrates and their associated microorganisms are rich sources of bioactive compounds[51,52]. The main phyla of marine invertebrates explored include sponges, cnidarians, molluscs, echinoderms, and ascidians[51,52] (**Figure 8**). However, cold-water bryozoans (moss animals, phylum Ectoprocta) contain many bioactive metabolites and have produced 35 published natural products[53,54].

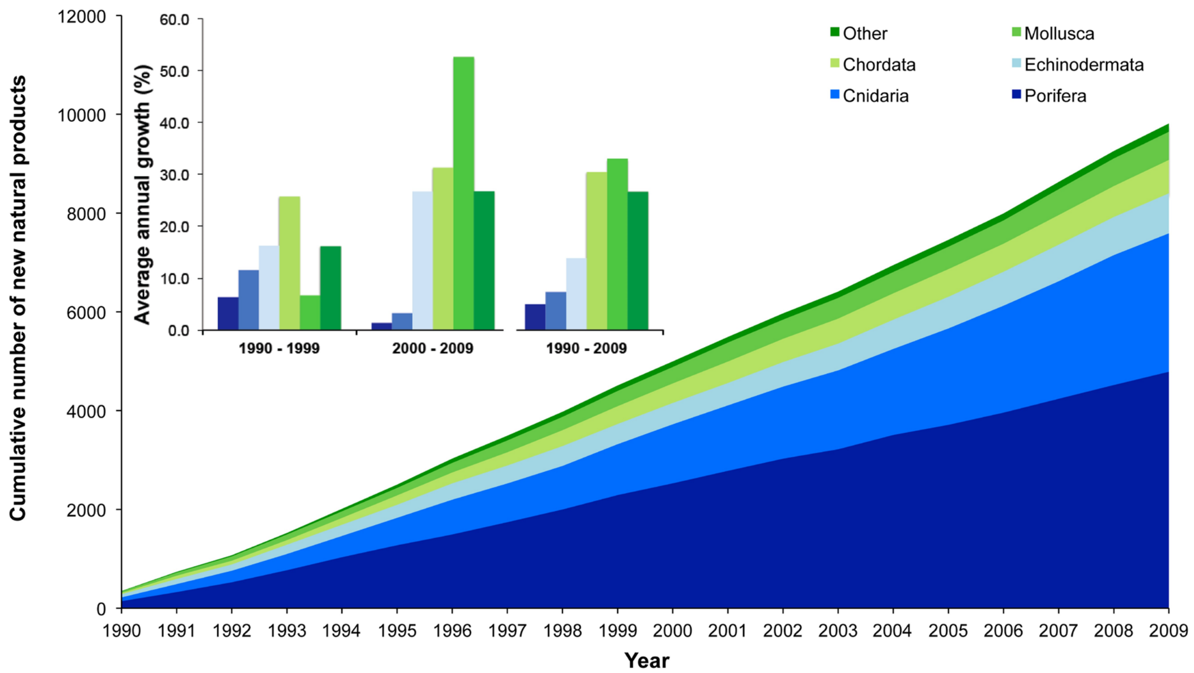

Figure 8. The phyla of marine invertebrates as a source of new natural products. *The cumulative number of new natural products discovered from different marine invertebrate phyla between 1990 and 2009 (Group "Other phyla" include Annelida, Arthropoda, Brachiopoda, Hemichordata, Platyhelmintes, and Bryozoa). Inset: The annual growth of the number of new marine natural products from different marine invertebrates discovered in the 1990s, 2000s and during both decades; Leal et al. (2012)[52].*

In a study investigating the chemistry of the Arctic bryozoan *Tegella cf. spitzbergensis*, researchers isolated and determined the structures of ent-eusynstyelamide B and several new derivatives, including eusynstyelamides D, E and F[55] (**Figure 9**). These compounds exhibited antibacterial activity and were characterized using high-resolution mass spectrometry and NMR techniques[55]. This is the first report on bioactive metabolites of Tegella species[55]. Eusynstyelamide B, a brominated tryptophan metabolite, was previously isolated from the ascidian Eusynstyela latericius[56]. Eusynstyelamides A, B, and C have inhibition of neuronal nitric oxide synthase and modest anticancer and antibacterial activities[56]. Eusynstyelamide A was later found to contain an open central motif instead of the five-membered ring and an additional hydroxy group[56].

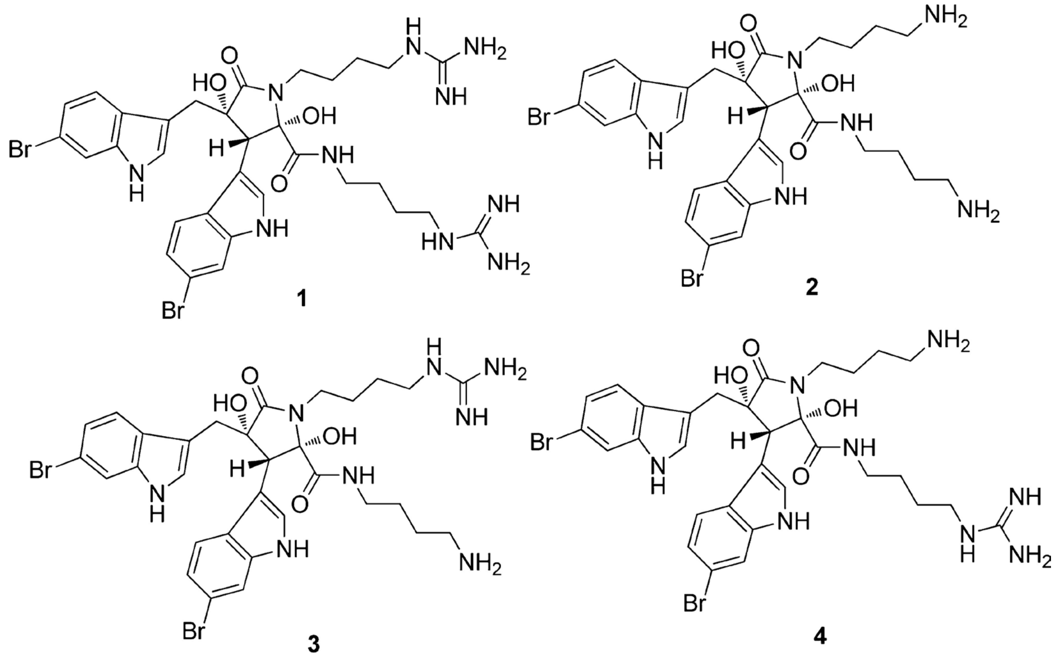

Figure 9. Eusynstyelamides from the Arctic Bryozoan **Tegella cf. spitzbergensis.** *1. ent-eusynstyelamide B, 2. eusynstyelamides D, 3. Eusynstyelamides E, and 4. Eusynstyelamides F. Permission of the American Chemical Society (ACS): Tadesse et al. (2011)[55].*

Overall, these findings highlight the potential of cold-water bryozoans and ascidians as sources of bioactive metabolites. The discovery of new compounds with antibacterial activity from *Tegella spitzbergensis* expands our understanding of the chemical diversity of these organisms. Furthermore, identification of eusynstyelamide B and its isomers in different ascidian species suggests the widespread occurrence of these metabolites in marine environments. More research is needed to explore the therapeutic potential of these compounds and understand their mechanisms of action.

1.2.4 Synthetic mimics of antimicrobial peptides (SMAMPs)

Antimicrobial peptides (AMPs) are naturally occurring molecules that play a crucial role in innate immune defence against microbial pathogens[57,58]. AMPs typically have 12 to 100 amino acid residues and show rapid and effective antimicrobial activity against various pathogens[59,60] (**Figure 10**). However, the development of AMPs as therapeutics has been hindered by challenges such as high production costs, limited stability, and potential toxicity[61]. Researchers have turned to synthetic antimicrobial peptides (SAMPs) and synthetic mimics of antimicrobial peptides (SMAMPs) to overcome these challenges. SAMPs and SMAMPs are artificially designed peptides that mimic the structure and function of natural AMPs. SMAMPs have earned attention as a crucial solution amid the growing threat of antibiotic resistance[58,62]. A decline in antibiotic discoveries in recent decades (**Figure 3**) has led to a shortage of effective antibiotics, necessitating innovative approaches to combat resistant bacterial infections[63]. These SMAMPs can be modified to enhance their activity, stability, and selectivity against specific bacteria[61].

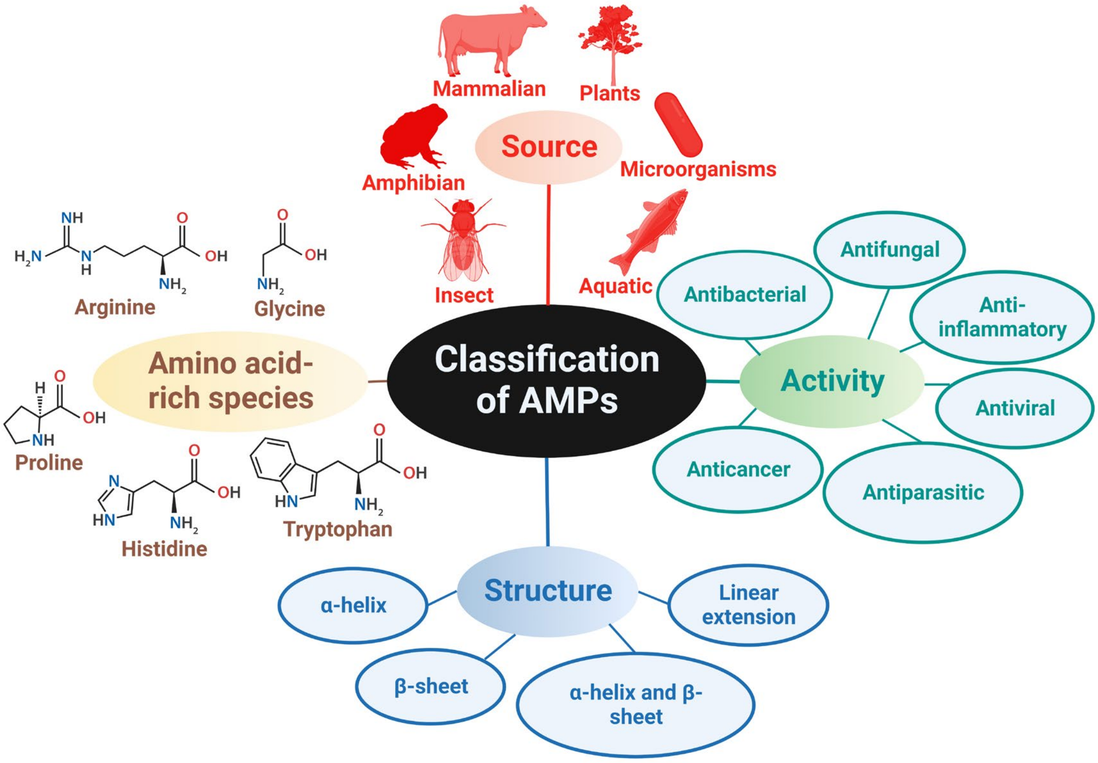

***Figure 10. Classification of antimicrobial peptides (AMPs)**; Huan et al. (2020)[64], modified.*

SMAMPs offer several advantages as a potential solution for new antibiotics. Firstly, SMAMPs have a broad spectrum of activity against various bacterial strains, including drug-resistant ones[58]. Therefore, SMAMPs have the potential to target a wide range of bacteria, making them effective against different types of infections (**Figure 11**) with different modes of action.

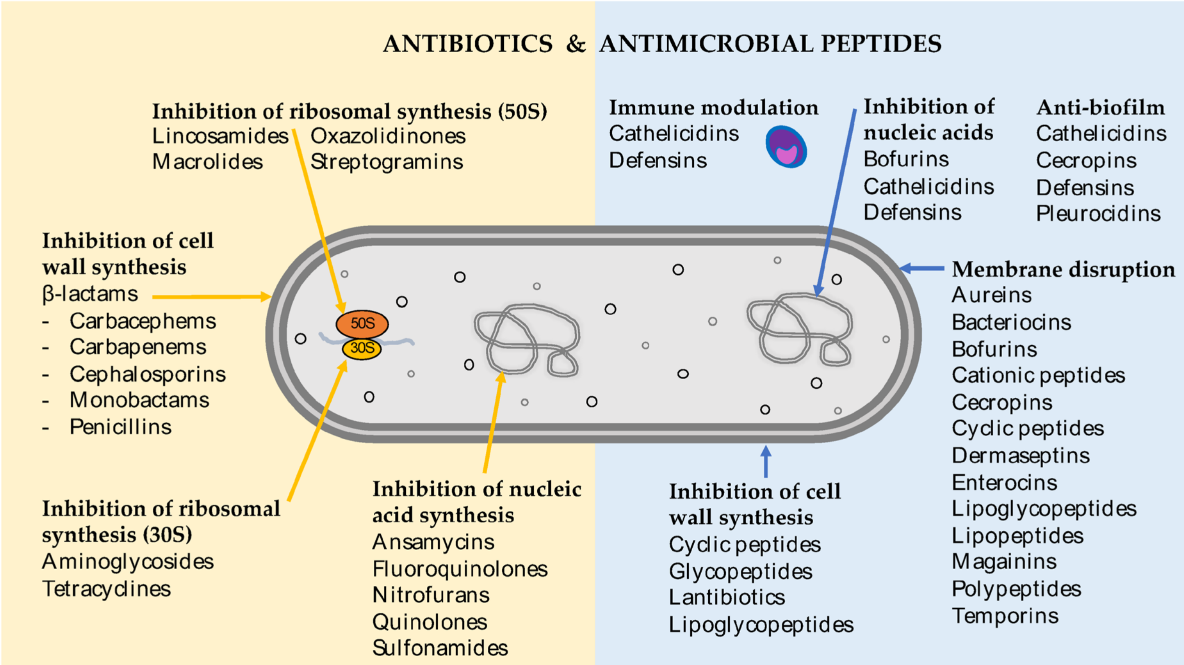

Figure 11. The mechanistic targets of antibiotics and antimicrobial peptides (AMPs)*; Browne et al. (2020)*[58].

Additionally, bacteria have been shown to have a low tendency to develop resistance toward SMAMPs. This is because SMAMPs target multiple bacterial structures and pathways, making it difficult for bacteria to develop resistance[58]. Furthermore, SMAMPs have been found to have a rapid bactericidal effect. Thus, they can kill bacteria quickly, which is crucial in treating severe bacterial infections[58]. Another advantage of SMAMPs is their potential to enhance the activity of other antimicrobial agents. For example, studies have shown that SMAMPs can enhance the activity of traditional antibiotics, making them more effective in combating bacterial infections[58]. Another benefit of SMAMPs is their potential to be customized and optimized[58].

Additionally, SMAMPs offer the advantage of being less prone to being toxic compared to traditional antibiotics[65]. SMAMPs also provide a cost-effective and easily synthesized alternative to naturally occurring antimicrobial compounds. Several commercially available AMPs of natural and synthetic origin (**Table 2**) represent a promising solution for the development of new antibiotics.

Table 2. Commercially available peptide-based antibiotics; *Browne et al. (2020)*[58]*, modified.*

Active Ingredient	**Origin**	**Target Organism**	**Class**	**Mechanism of Action**	**Indication**	**Route of Administration**
Bacitracin	Bacteria (*Bacillus subtilis*)	Gram-positive bacteria	Cyclic peptide	Inhibits cell wall synthesis	Skin infections	Topical Ophthalmic Intramuscular
Dalbavancin	Teicoplanin derivative	Gram-positive bacteria	Lipoglycopeptide	Inhibits cell wall synthesis	Skin infections	Intravenous
Daptomycin	Bacteria (*Streptomyces roseosporus*)	Gram-positive bacteria	Lipopeptide	Membrane lysis	Skin infections	Intravenous
Colistin	Bacteria (*Bacillus polymyxa*)	Gram-negative bacteria	Cyclic peptide	Membrane lysis	Gram-negative infections resistant to multi-drugs	Intravenous
Gramicidin D	Bacteria (*Bacillus brevis*)	Gram-positive bacteria, some Gram-negative bacteria	Mix of three polypeptides	Membrane poration/lysis	Skin and eye infection	Topical Ophthalmic
Oritavancin	Vancomycin derivative	Gram-positive bacteria	Lipoglycopeptide	Membrane lysis and inhibits cell wall synthesis	Skin infections	Intravenous
Polymyxin B	Bacteria (*Bacillus polymyxa*)	Gram-negative bacteria	Polypeptide	Membrane lysis	Urinary tract and bloodstream infections	Ophthalmic Topical Intravenous
Teicoplanin	Bacteria (*Actinoplanes teichomyceticus*)	Gram-positive bacteria	Glycopeptide	Inhibits cell wall synthesis	Serious Gram-positive infections	Intramuscular Intravenous
Telavancin	Vancomycin derivative	Gram-positive bacteria	Lipoglycopeptide	Membrane lysis and inhibits cell wall synthesis	Skin infections	Intravenous
Vancomycin	Bacteria (*Amycolatopsis orientalis*)	Gram-positive bacteria	Glycopeptide	Inhibits cell wall synthesis	Serious Gram-positive infections	Oral Intravenous

1.2.5 AntifoMar

The UiT supported ongoing bioprospection research activity at the University by funding the multidisciplinary strategic project AntifoMar associated to CANS. The project is a collaboration between three faculties at UiT and the Nord University. The primary objective of the AntifoMar project was to develop biofilm-inhibiting and -eradicating compounds for therapeutic and industrial purposes. This is achieved by an intensive four PhD collaboration using marine invertebrates, including genes and associated microbial symbionts, as sources for model compounds. Methods for the isolation, characterization, and bioevaluation of model compounds are established and will be complemented with the synthesis of optimized derivatives and bioinformatics. Marine organisms are a rich source of biofilm-inhibiting compounds. Isolated compounds and improved synthetic derivatives will lead to innovative solutions for biofilm inhibition with relevance in preventing marine biofouling and improving public health.

Milestones of the AntifoMar project (see **Figure** 12 for WPs):
1) Identify biofilm-inhibiting molecules from unexploited marine organisms.
2) Identify the actual producer (host or associated microorganisms).
3) Synthesize and optimize identified antibiofilm molecules and derivatives.
4) Provide innovative lead compounds for therapeutic/industrial applications.
5) Provide interdisciplinary R&D education for four PhDs.

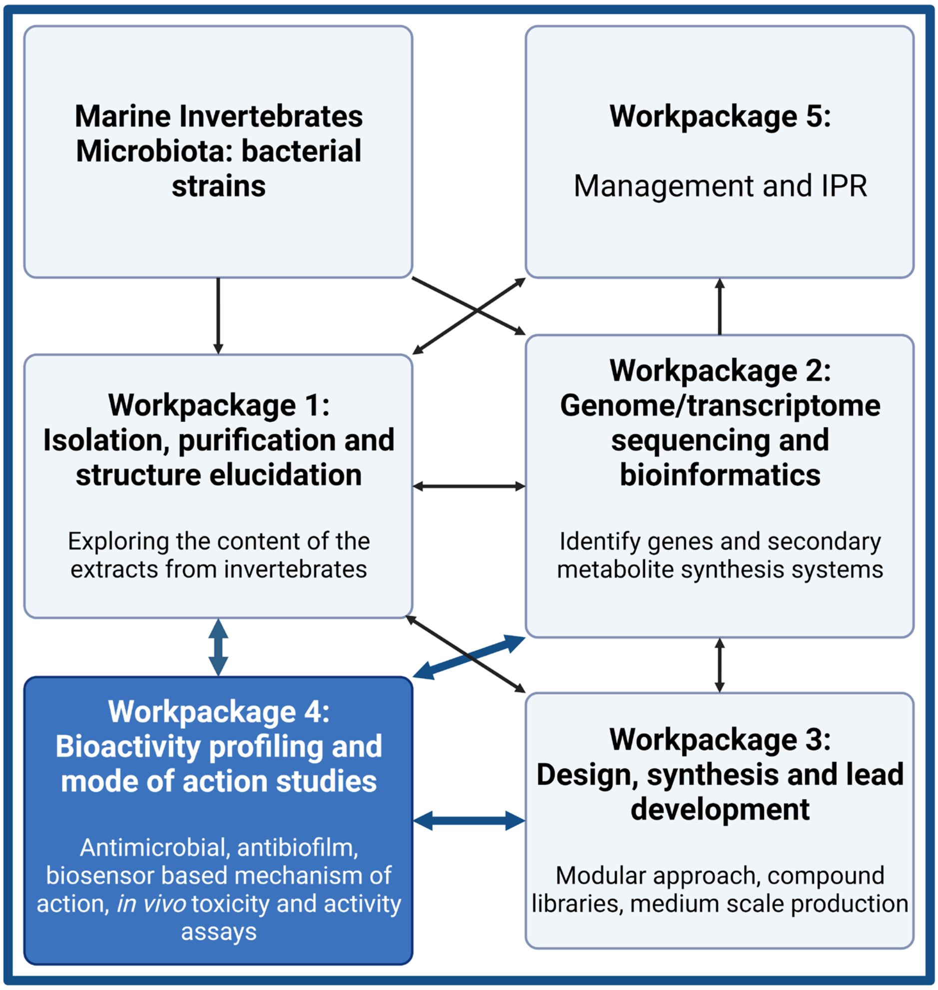

Figure** 12. **Outline of the AntifoMar project's different work packages and indicated information flow.

2 Research objectives

This project was done in the Marine Bioprospecting group at the Norwegian College of Fishery Science within the WP 4 of the project AntifoMar.

The main aim of the research project was to evaluate the development and characterize antimicrobials, biofilm inhibitors, and biofilm-eradicating compounds of marine origin for therapeutic purposes.

The project was divided into two approaches with the following sub-goals to achieve the goal. The sub-goals of the approaches were as follows:

Approach A: Evaluation of synthetic analogues based on natural products

- Identify candidate antimicrobials, biofilm-inhibitors, and -eradicators from a library of designed and chemically synthesized compounds by evaluating the antibacterial and antibiofilm activities.
- Determine the mode of action of the most promising candidates using optimized *in vitro* test systems.
- Evaluate *in vitro* and *in vivo* toxicity and activity of the most promising candidates.

Approach B: Natural products (NPs) from marine bacteria

- Identify and evaluate producers of antimicrobials, biofilm-inhibitors, and -eradicators of natural origin, with a specific focus on marine bacteria.
- Evaluate the selected marine bacteria as a potential source of antimicrobials, biofilm-inhibitors, and -eradicators.

3 Research design

The research design of this project is based on the sub-goals of the two approaches (**Figure 13** and **Figure 14**) that address the main aim. This research design is formed to identify and characterize biofilm-inhibiting and eradicating compounds of marine origin.

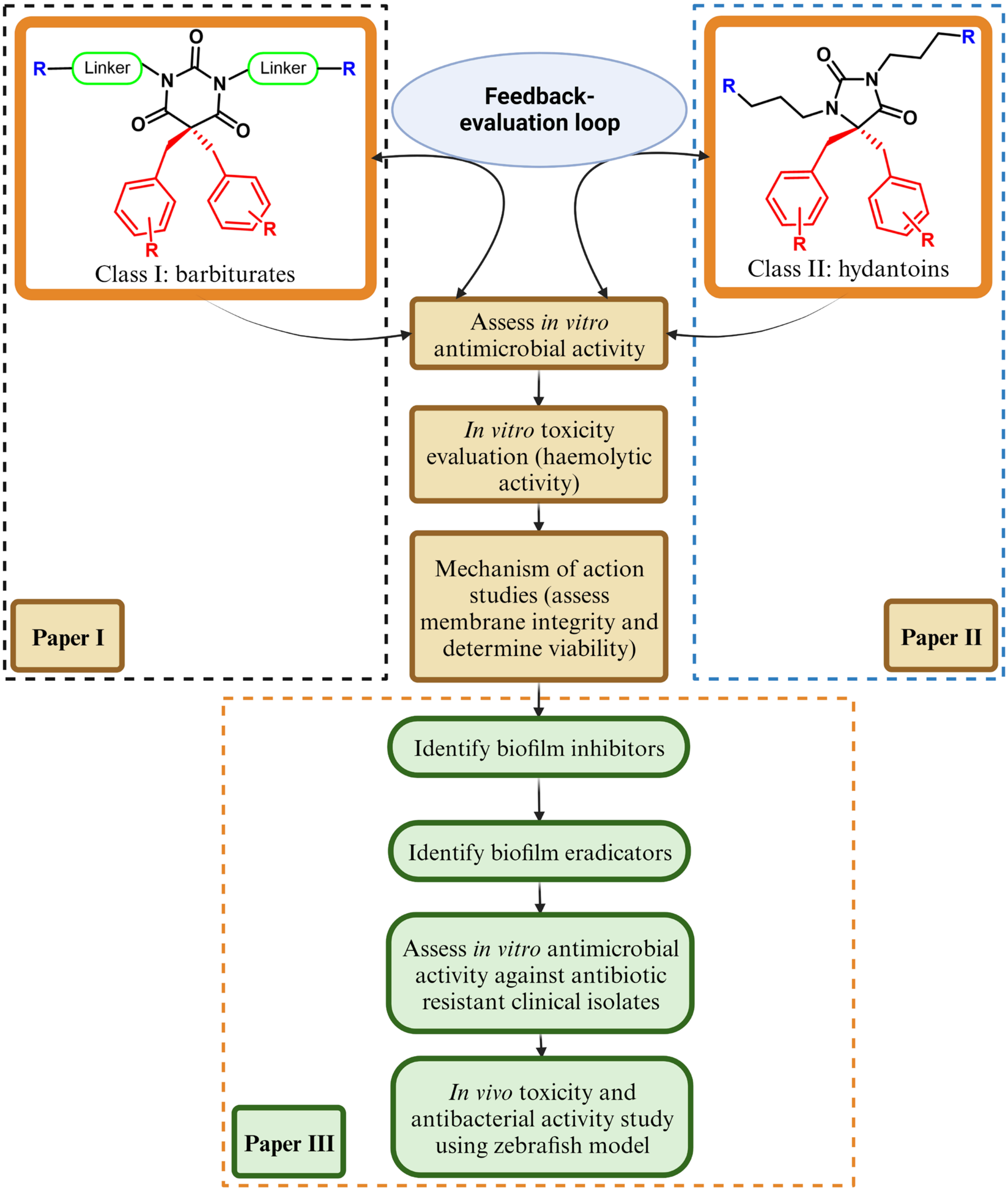

***Figure 13. Approach A**: Characterization of synthetic analogues based on natural products.*

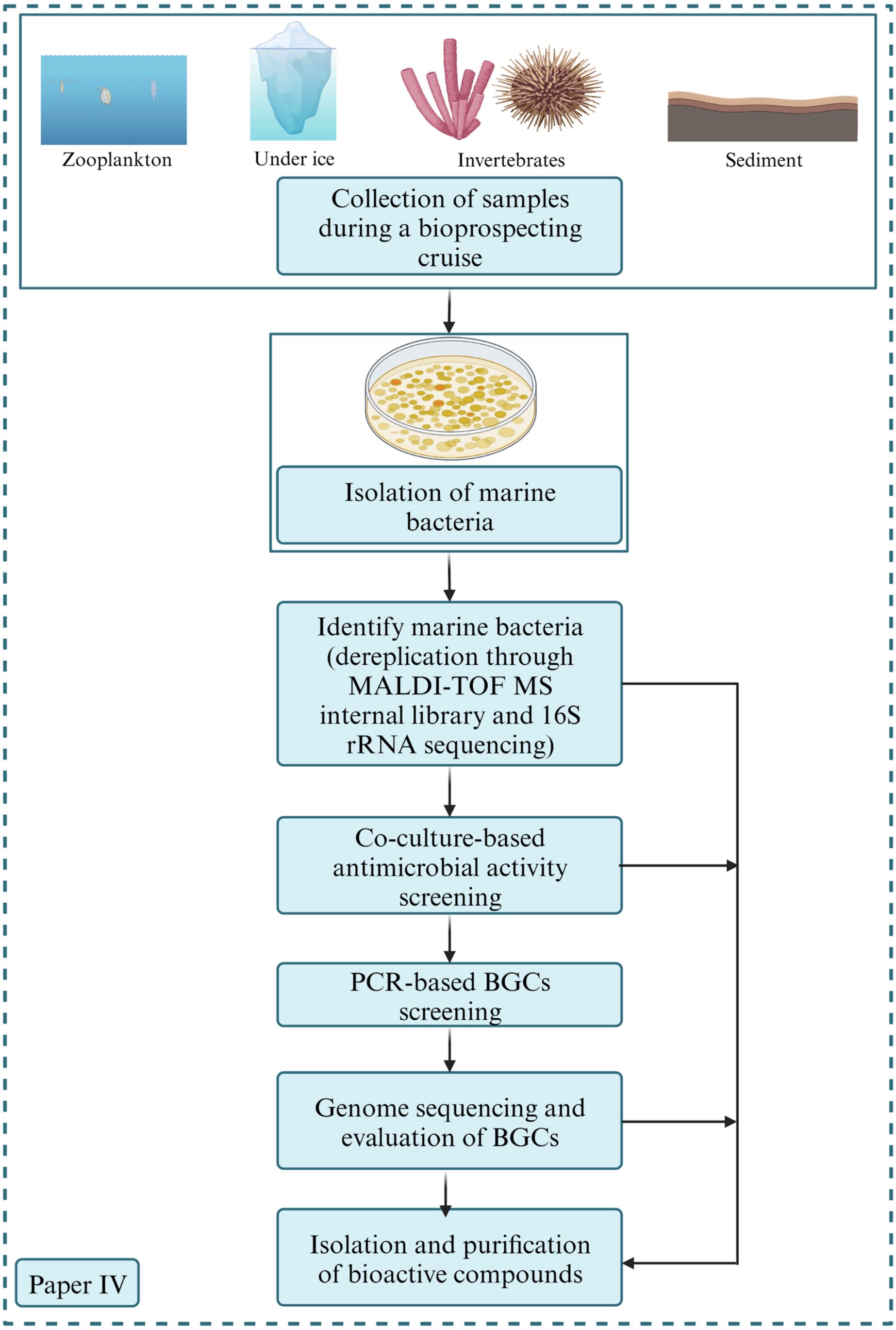

Figure 14. Approach B: *Natural products (NPs) of marine bacteria.*

4 Summary of the main results

4.1 Paper I

Title: A concise SAR-analysis of antimicrobial cationic amphipathic barbiturates for an improved activity-toxicity profile.

Highlights (Figure 15):

– An efficient synthesis of tetrasubstituted barbiturates with diverse cationic and lipophilic side chains is established.
– The careful choice of structural components provides a good balance of antibacterial and haemolytic activity.
– Guanidyl head groups combined with n-butyl linkers give the highest potency.
– The n-Propyl linkers provide the best balance between antibacterial and haemolytic activity.
– Disruption of membrane integrity is the main mode of antibacterial action.

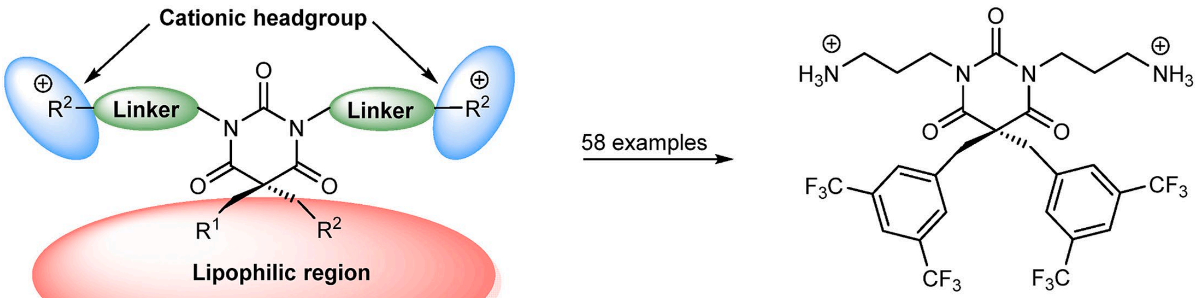

13jA

broad-spectrum potency (MIC: 4 – 8 µg/mL)
low haemolytic activity (EC50: 176 µg/mL)
membranolytic

Figure 15. Graphical abstract of antimicrobial cationic amphipathic barbiturates.

Conclusions:

The qualitative influence of the individual structural components of *N,N*-dialkylated-5,5-disubstituted amphipathic barbiturates on their bioactivity was investigated. Studies on membrane integrity and viability of bacterial cells suggest that compounds exert their bactericidal activity by disrupting the bacterial cell wall of Gram-positive *B. subtilis* in a concentration-dependent manner, as exemplified by barbiturate 11lG. In Gram-negative *E. coli* both the inner and outer membranes were supposedly rapidly disrupted at higher compound concentrations, but a second mechanism of action might also be present. This detailed analysis can help to devise new amphipathic cationic mimics of antimicrobial peptides.

4.2 **Paper II**

Title: Investigation of tetrasubstituted heterocycles reveals hydantoins as a promising scaffold for development of novel antimicrobials with membranolytic properties.

Highlights (Figure 16):

- The hydantoin scaffold was the most promising AMP mimetic of the five heterocycles studied.
- n-Butyl linkers combined with guanidine head groups delivered the highest antimicrobial potency.
- Lead structures 6cG and 6dG delivered high selectivity indices.
- Disruption of the bacterial cytoplasmic membrane was their main mode of action.

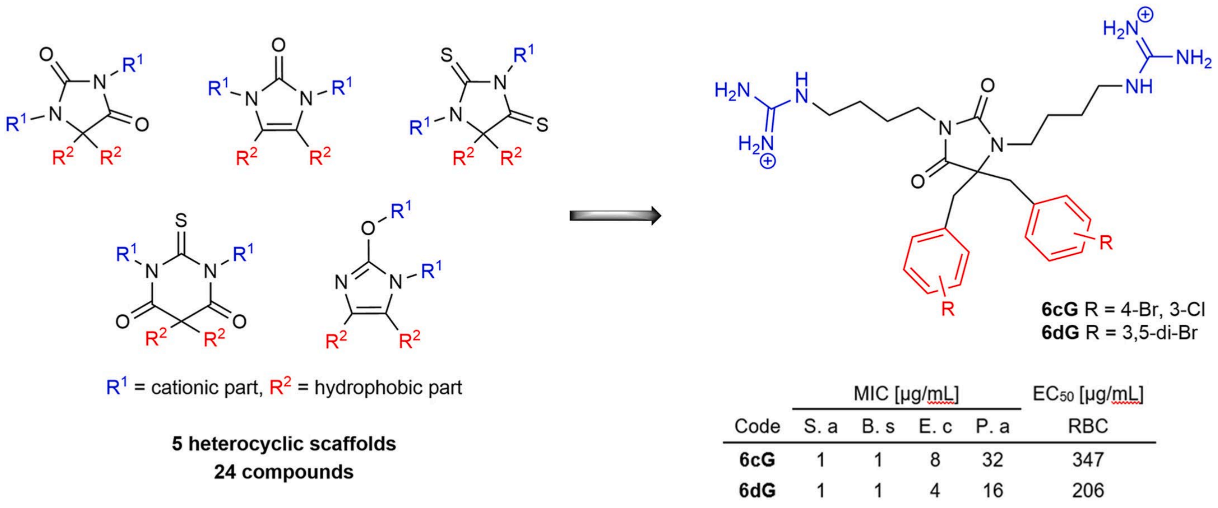

Figure 16. Graphical abstract of hydantoins as a promising scaffold for development of novel antimicrobials.

Conclusions:

We investigated five scaffolds for their suitability for developing novel tetrasubstituted, amphipathic SMAMP antimicrobials, revealing the hydantoin structure as a promising template for antibacterial drug lead development. The results obtained from the viability and membrane integrity assays suggested a rapid membranolytic effect, as demonstrated for hydantoin 6cG in *B. subtilis* and *E. coli*. Interestingly, both the inner and the outer membranes in *E. coli* appeared to be disrupted at a similar speed. We believe that our findings on the qualitative contribution of the scaffold structures can help the development of novel small-molecule analogues of AMPs or SMAMPs.

4.3 Paper III

Title: Peptidomimetic tetrasubstituted barbiturates and hydantoins: Investigation of their antibiofilm, in vivo toxicity and antimicrobial activity.

Highlights (Figure 17):

- Several biofilm inhibitors and -eradicators from barbiturates and hydantoins were identified.
- The lead compounds 13iA of barbiturates and 2cA of hydantoins showed outstanding biofilm inhibition and eradication against *Staphylococcus epidermidis* RP62A.
- With broad spectrum activity of 13iA, it also showed excellent biofilm inhibition and eradication against *Pseudomonas aeruginosa* PAO1.
- Both lead compounds showed promising antimicrobial activity against antimicrobial resistant clinical isolates.
- Compounds 13iA and 2cA did not show toxicity at a dose of 16 mg/kg, similar to the positive control, tetracycline.
- Compound 2cA showed significant antimicrobial activity against *S. aureus,* and compound 13iA was against *S. epidermidis*, better than the positive control, tetracycline.

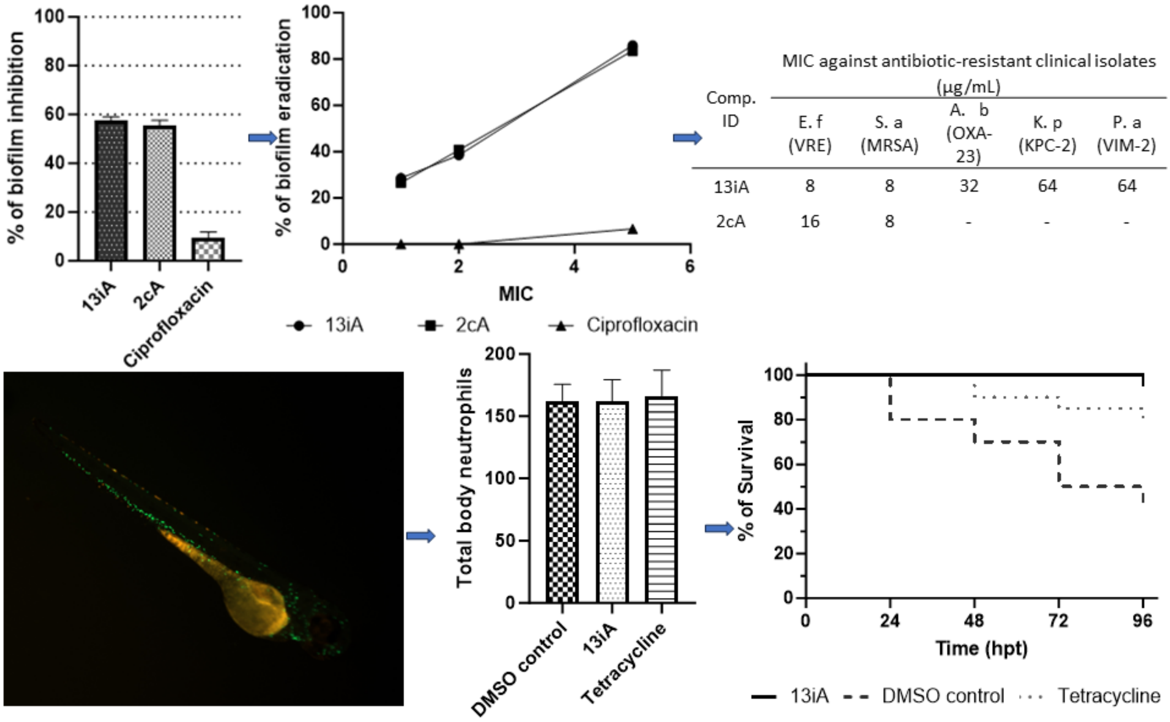

Figure 17. Graphical abstract of in vivo toxicity and activity of barbituric acid and hydantoin derivatives with antibacterial and antibiofilm activity.

Conclusions:

Barbituric acid and hydantoin derivatives showed excellent antibiofilm potential to inhibit biofilm formation and eradicate formed biofilm. They showed dose-dependent inhibition and eradication of biofilms against *S. epidermidis* RP62A, *S. epidermidis* 5179-R1, and *P. aeruginosa* PAO1. The lead compounds showed promising antibacterial activity against both antibiotic-resistant Gram-positive and negative bacteria, almost the same as the activity against reference bacteria. Compounds 13iA and 9 showed excellent in vivo antibacterial activity against *S. epidermidis* RP62A and *S. aureus*.

4.4 Paper IV

Title: Antimicrobial potential of marine bacteria from the Arctic and sub-Arctic regions.

Highlights (Figure 18):

- 158 marine bacteria were isolated in the Arctic regions during a bioprospecting cruise in 2019.
- Moritella, Psychromonas, and Shewanella cover almost half of the identified genera.
- 65 marine bacterial isolates showed antimicrobial activity against at least one strain of the panel of human pathogen-related bacteria.
- 37 isolates indicated the presence of NRPS or PKS gene clusters.
- From genome mining and screening, *Shewanella sp.* MBP011.13.1 and *Pseudomonas sp.* MBP027.4 was the most promising marine bacterial isolates with antibacterial activity and positive for NRPS or PKS and several other BGCs.

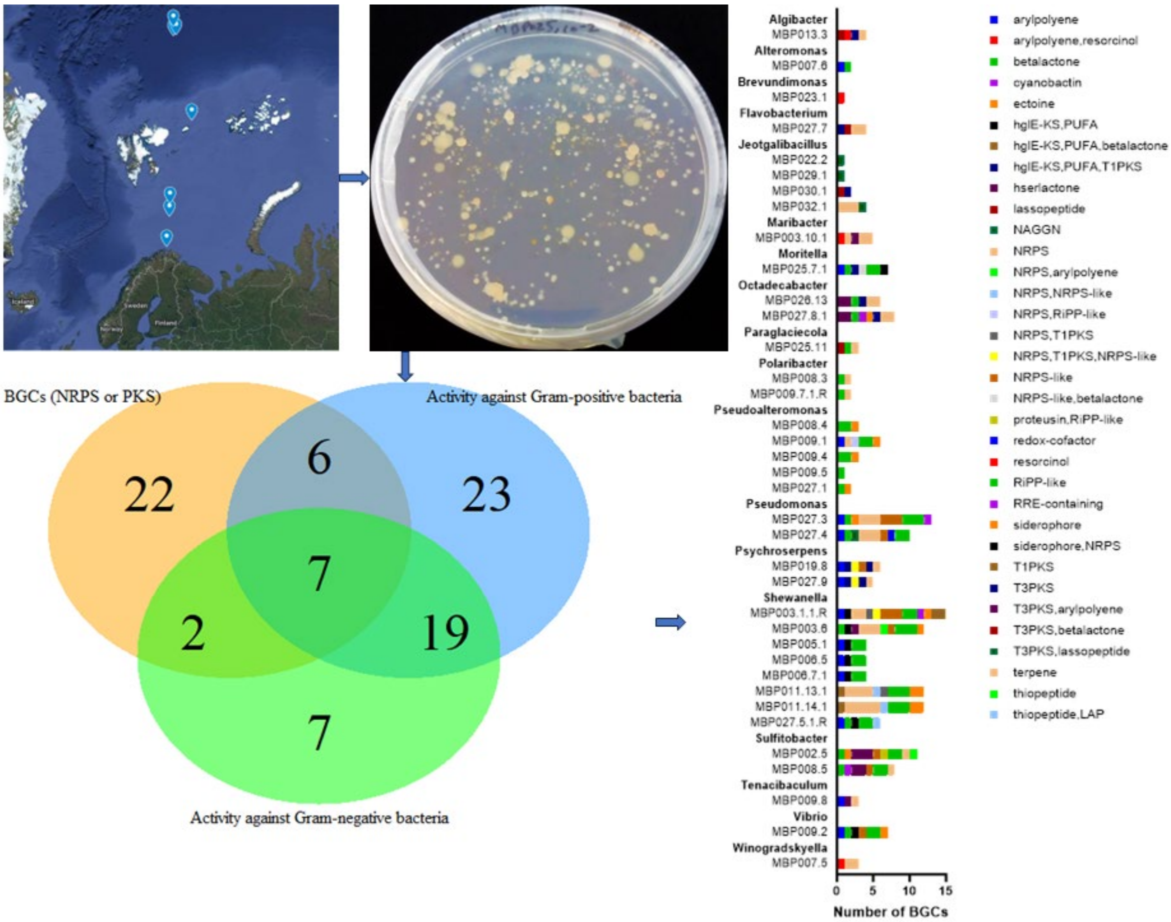

Figure 18. Antimicrobial potential of marine bacteria from the Arctic regions during a bioprospecting cruise in 2019.

Conclusions:

This bioprospecting study of Arctic marine bacterial isolates demonstrates how co-culture and genome mining can be used to identify bioactive marine bacteria as a potential source of antimicrobial compounds. Two marine invertebrates (Porifera), zooplankton, samples from under the ice, and sediments of 452 m deep were the source of the isolates with the most potent antibacterial activity. Genome mining also facilitated the identification of potential BGCs that could encode the antimicrobial compounds.

5 General discussion

Antibiotics have greatly impacted modern medicine, but the rise of antibiotic resistance poses a significant global health concern. The imperative to counteract this threat necessitates the complex and challenging task of discovering and developing novel antibiotics. Multiple factors, such as the complexity of bacterial physiology and a high candidate failure rate, complicate this process[19]. However, promising antibiotic candidates are emerging from diverse sources, underscoring the ongoing efforts in this critical field.

This study was part of the larger multidisciplinary project, AntifoMar. The goal was to identify the producer of antimicrobial compounds of marine origin by collaborating with all other work packages involved in the AntifoMar project. Also, to identify and develop biofilm-inhibiting and eradicating compounds. Additionally, this project evaluated the mode of action, toxicity, and antimicrobial activity both *in vitro* and *in vivo*.

Screening of the SMAMPs library resulted in several promising lead compounds with antimicrobial activity against antibiotic-resistant clinical isolates and antibiofilm properties against Gram-positive and Gram-negative bacteria. Furthermore, *in vivo* toxicity and antibacterial activity were assessed using the zebrafish model. This part of the study resulted in three **papers (I-III)**. Moreover, the screening of marine bacteria as producers of NPs with antimicrobial activities resulted in one p**aper (IV)**.

5.1 Pipeline and challenges associated with the AntifoMar project

The flow of information between different work packages in the AntifoMar project (**Figure 12**) facilitated productive collaboration from various angles, creating constructive interaction between these packages. Since the work packages of the AntifoMar project started simultaneously, they cannot follow a bioprospecting flow as outlined in **Figure 5**. The bioprospecting pipeline involves identifying lead compounds from marine natural sources like invertebrates or bacteria and then employing a peptidomimetic strategy based on the identified scaffolds (**Figure 5** and **Figure 12**). In the AntifoMar project, on the other hand, we had to use the previously identified scaffold, eusynstyelamide, from the Arctic bryozoan, (**Paper I and II**), as the starting point for the peptidomimetics.

For the development of synthetic mimics of antimicrobial peptides (SMAMPs or peptidomimetics), a feedback evaluation loop was essential to optimize their structure and increase their activity. SMAMPs were synthesized in various batches, with each batch undergoing evaluations of antibacterial and haemolytic activities, followed by SAR analysis. This analysis informed the synthesis of subsequent batches. Ultimately, the SMAMPs library consisted of several series of derivatives, encompassing all these batches (**Paper I and II**). Selected derivatives were then subjected to further testing to pinpoint the most promising candidates. This included MOA analysis (as detailed in **Papers I** and **II**), evaluation of antibacterial activity against antibiotic-resistant clinical isolates, and antibiofilm studies (discussed in **Paper III**). This process of SAR and MOA investigation is crucial in the drug discovery pipeline (**Figure 5**), shaping the future stages of development.

The search for animal models to study *in vivo* toxicity and antibacterial activity efficiently, cost-effectively, and without regulatory barriers was challenging in a short period of time. The zebrafish model was opted to assess the toxicity and activity of the shortlisted lead compounds. However, there was a lack of expertise in Norway regarding this infection model. The search extended to Europe to find a suitable group to learn the techniques and conduct the necessary studies. Fortunately, the connection with a group at Jagiellonian University in Poland was experienced in the infection model, where toxicity and activity studies were conducted on compounds using the zebrafish model (**Paper III**), supported by a Research Stay Abroad grant.

Both culture-dependent bioprospecting[66] (as depicted in WP4 and WP2 of **Figure 12**) and culture-independent metagenomics[67] (WP2 of **Figure 12**) have their respective merits and demerits. Classical cultivation techniques are limited in that they can isolate only a small percentage of all microbial species[66,68]. Meanwhile, metagenomic approaches face challenges due to limitations in the availability of microbial DNA[69]. This issue becomes particularly pronounced in low-biomass environments or when dealing with microbiomes of low abundance[69]. Similar problems can occur during the separation of microbial cells from host tissues, especially if the host organisms harbor's low densities of associated microbes or if the separation process yields low quantities[69]. Nevertheless, advancements in cultivation techniques are broadening the scope of cultivable isolates, allowing for more extensive phenotypic screening using cell-based assays[70].

In the marine bioprospecting pipeline (**Figure 5**), numerous biosynthetic gene clusters of marine bacteria remain unexpressed under conventional laboratory conditions, leading to the frequent isolation of already known compounds[71]. Over the last decade, the 'one strain many compounds' (OSMAC) approach has been employed to activate these BGCs[72], primarily encoding enzymes for secondary metabolite biosynthesis[73]. Various culture conditions, such as aeration rate, temperature, and nutrient composition, were modified to successfully activate these BGCs[73]. However, applying the OSMAC approach to psychrophilic bacteria from the Arctic marine environment presented difficulties. Most of these bacteria only thrive at temperatures between 4-10 degrees Celsius and grow in specific media such as marine broth and modified half-strength marine broth (FMAP) medium (**Paper IV**). An alternative strategy involved co-culturing these bacteria with human pathogen relatives, simulating the complex ecological interactions of microbial life[66,71]. This ecology-driven method aimed to activate silent gene clusters to explore the metabolic potential for novel bioactive secondary metabolites[71]. Yet, challenges persisted due to temperature constraints and media compatibility, as Arctic marine bacteria prefer temperatures of 4-10 degrees Celsius (some between 10-20 degrees), and human pathogen relatives exhibit limited growth in marine broth, particularly at lower temperatures. To overcome these obstacles, the co-culture method underwent optimization (**Paper IV**).

5.2 Source of novel antibacterial compounds

Novel antimicrobial compounds can come from various sources, including marine bacteria and synthetic antimicrobial peptides. Marine bacteria, such as those from Streptomyces, are known to produce unique secondary metabolites with antimicrobial properties[74]. Furthermore, synthetic antimicrobial peptides, designed through rational peptide engineering, exhibited promising antimicrobial activity against various pathogens[75,76]. These sources provide attractive opportunities for the discovery of new antimicrobial compounds.

5.2.1 Synthetic mimics of antimicrobial peptides (SMAMPs)

Papers I and **II** describe the SMAMPs library as a source of novel antimicrobials, taking inspiration from the eusynstyelamide NP class[55,56]. After previous demonstration of the efficacy of new tetrasubstituted barbiturates[77], the **paper I** aimed to enhance their therapeutic index by designing a second generation of derivatives, retaining the barbituric acid core and methodically examining the effects of cationic groups, linkers, and lipophilic side chains on antimicrobial and haemolytic activities, as shown in **Figure 19**.

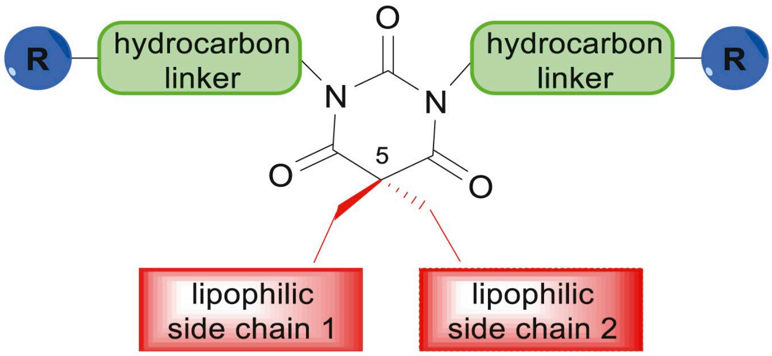

Figure 19. The general structure of the barbituric acid derivatives, mimics of eusynstyelamide.

The derivatives were categorized into five series, each of which alters one moiety while sustaining the rest of the molecular structure. The emphasis of each series was on 1) cationic groups, 2) new lipophilic side chains, 3) a combination of two different lipophilic side chains based on the results of the previous study[77] and series 2 of this **Papers I**, 4) various hydrocarbon linkers, and 5) the most efficient combinations from series 1-4.

Paper II explored how different central scaffolds affect biological activity after investigating the structural components of amphipathic barbiturates in Paper I. The substitution pattern was applied from earlier studies to five heterocycles structurally similar to barbituric acid (**4bA**, **Paper I**), as shown in **Figure 20**. In **Paper II**, imidazolidine-2,4-dione (**2, Paper II**), known as hydantoin, which is acknowledged in medicinal chemistry but seldom in antimicrobials, and 4-imidazolidin-2-one (**3, Paper II)** for its unique geometry and increased lipophilicity, were chosen. Taking into account the relevance of sulfur in drugs, including antimicrobials such as penicillins and cephalosporins, we investigated its impact within an amide (**4, Paper II**) and urea-type bond (**5, Paper II**). Unexpectedly, 2-(hydroxy)-1H-imidazole (**15, Paper II**) emerged as a byproduct during synthesis, prompting its inclusion. Having assessed each structure, **Paper II** focused on hydantoin for a targeted library, forming the basis for the third generation of derivatives.

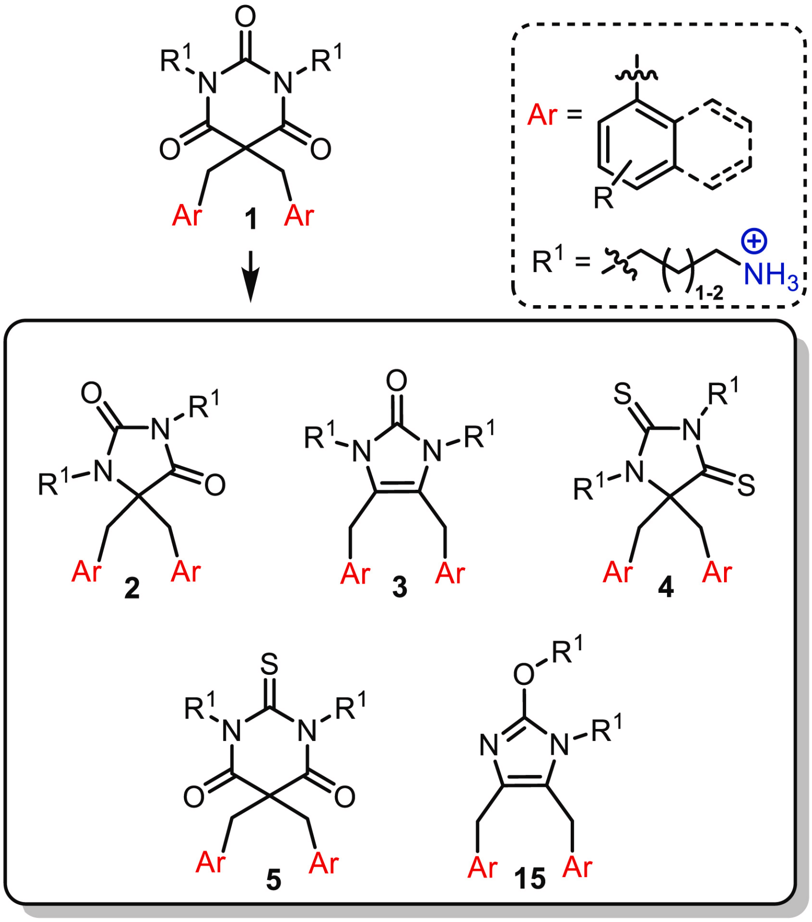

Figure 20. ***Previously utilized barbituric acid 1[77] and core structures 2–5 and 15 were used in this study****. Ar = lipophilic side chain, R1 = n-alkyl linker with a cationic head group. Red: lipophilic part; blue: cationic part.*

5.2.2 Marine bacterial secondary metabolites (MBSMs)

The diversity of marine bacteria and the unique chemical and biological properties of marine bacterial secondary metabolites (MBSMs) make them attractive candidates for the development of new antimicrobials against a wide range of pathogens[74]. In **Paper IV**, 158 marine bacterial isolates were isolated (**Figure 21**) and assessed for their antimicrobial activity against a panel of Gram-positive and -negative human pathogen-related bacteria, including ESKAPE relatives. Additionally, polymerase chain reaction (PCR) screening for NRPS and PKS BGCs and genome mining revealed that at least seven of these marine bacterial isolates should be further investigated for their potential of containing antimicrobial compounds (**Figure 24**).

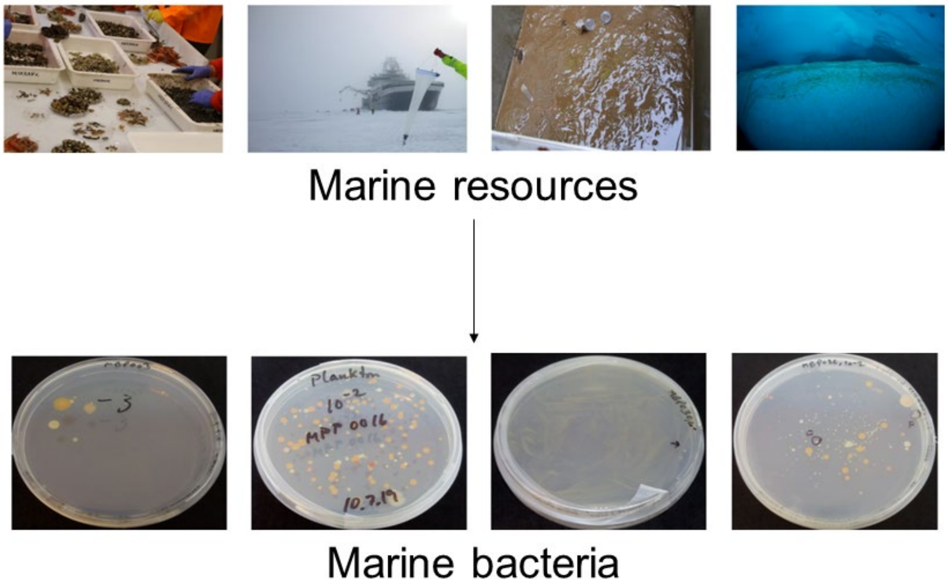

Figure 21. Collection of marine bacteria during a bioprospecting cruise in 2019 in the Arctic region.

5.3 *In vitro* activity assessments

5.3.1 Barbituric acid derivatives – a potential scaffold

Fifty-eight compounds were assessed for antimicrobial potency, indicated by MIC values, and systemic toxicity, reflected in EC_{50} values for haemolysis in the RBC assay. Among the compounds tested, some demonstrated selective activity against Gram-positive strains, while others were effective against both Gram-positive strains and *E. coli*, or against all strains examined. Key trends are highlighted below and in **Figure** *22*. Complete MIC data are available in Tables 1-5 in **Paper I**.

In Series 1, (poly)-methylation of primary amines reduced activity against *P. aeruginosa*, likely due to a decreased effective charge on the cationic groups. Previously used amine and guanidine head groups yielded the most comprehensive broad-spectrum activity.

In Series 2 and 3, the antimicrobial potency and haemolytic activity were predominantly affected by the side chains' lipophilicity; greater lipophilicity increased both potency and haemolysis. Side chains with CLogP values over 4.50 resulted in high haemolytic activity and poor solubility. Combining two distinct lipophilic side chains effectively moderated overall lipophilicity.

In Series 4, linkers such as N-pentyl, n-hexyl, cyclobutyl, and cyclohexyl showed high antimicrobial potency but also high haemolytic activity. The n-propyl linker combined with a guanidine head group was the least haemolytic, followed by an ethyl linker with guanidine.

In Series 5, the n-propyl linker and guanidyl cationic group emerged as the optimal combination for broad-spectrum activity. This configuration enabled the creation of barbiturates with identical or diverse lipophilic groups, yielding promising candidates with reduced haemolytic toxicity.

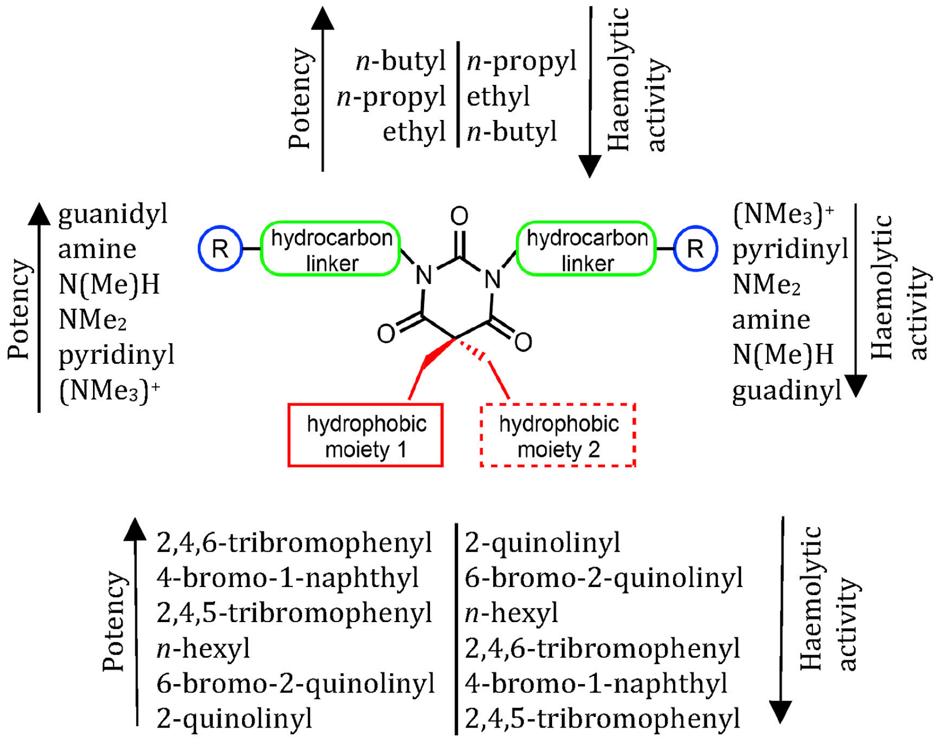

Figure 22. Overview of the general trends observed during the SAR investigation. *The trends for haemolytic activity were assessed for the average between the respective amines and guanidines.*

Paper I examined 17 narrow-spectrum barbiturates against Gram-positive bacteria and 14 broad-spectrum derivatives against Gram-positive and Gram-negative bacteria. Utilizing the luciferase-based biosensor assays, **paper I** confirmed the concentration-dependent membrane disruption for all tested compounds on *B. subtilis* and *E. coli* cytoplasmic membranes. Additionally, a broad-spectrum barbiturate, 11lG (**Paper I**), was assessed using the 1-N-phenylnaphthylamine (NPN) fluorescent probe to examine its impact on *E. coli*'s outer membrane (OM). Low concentrations (0.8x MIC) increased OM permeability without affecting cell viability. However, at higher concentrations (6.4-12.8x MIC), OM disruption occurred at rates comparable to the inner membrane (IM). These findings indicate a concentration-dependent OM and IM disruption mechanism as the primary antibacterial action.

5.3.2 Hydantoin derivatives – another potential scaffold

Twenty-four compounds were tested for antimicrobial efficacy and haemolysis using assays described in **Paper I** and **II** and a comprehensive data set in **Paper II**, Tables 1 and 2. Thioamides and thioureas rendered compounds less haemolytic and less effective against Gram-negative *P. aeruginosa* or led to instability, as with 5A (**Paper II**). Hydantoins were generally less haemolytic than 4-imidazolidin-2-ones (3A, **Paper II**) and 2-(hydroxy)-1H-imidazol (15A, **Paper II**). In the hydantoin series, guanidine derivatives were more potent and haemolytic than amine derivatives with an n-butyl linker but less so with an n-propyl linker, aligning with trends from **Paper I**. All compounds, except 2eA (EC_{50}: 69 µg/mL), had EC_{50} values over 200 µg/mL.

The investigation into tetrasubstituted amphipathic hydantoins confirmed their membranolytic properties using a biosensor assay. Thirteen hydantoins were studied in *B. subtilis,* and six with broad-spectrum activity in *E. coli*, showing concentration-dependent effects on viability and membrane integrity, with a faster action observed in Gram-positive *B. subtilis*. OM permeability in *E. coli* was assessed with NPN fluorescence, where 6cG (4-Br, 3-Cl) at 0.4x MIC increased OM permeability without affecting viability. At 1.6-3.2x MIC, reduced fluorescence suggested possible rapid OM disruption or an intact OM while viability was reduced. These results imply that OM disruption may occur as swiftly as IM disruption, but further research is required to determine whether high concentrations facilitate translocation across the OM without its disruption.

5.3.3 Antibiofilm activity of barbiturate and hydantoin derivatives

The selection of 44 (**Paper III**) out of 82 synthesized compounds from barbiturate (**Papers I**) and hydantoin (**Papers II**) derivatives for biofilm inhibition studies was addressed on a balance of antimicrobial efficacy, low haemolytic activity, and high selectivity index (SI). Evaluating these compounds on biofilm formation by *S. epidermidis* RP62A and *P. aeruginosa* PAO1 at sub-MIC concentrations showed that six compounds were effective against *S. epidermidis* by inhibiting biofilm formation above 50%. Besides, three compounds inhibited the biofilm formation of *P. aeruginosa* by over 50% (Table S1, **Paper III**).

The data indicated that seven out of eleven compounds achieved over 80% eradication of *S. epidermidis* RP62A biofilms, and four out of ten compounds were effective against *P. aeruginosa* PAO1 biofilms at 5x MIC concentrations (Table S1, **Paper III**).

The lead compounds 13iA and 2cA (**Figure 23**) notably demonstrate exceptional biofilm inhibition at sub-MIC concentrations and eradication capabilities at 5x MIC concentrations against *S. epidermidis* RP62A. Compound 13iA also showed excellent biofilm eradication potential (more than 90%) against *P. aeruginosa* PAO1 at 5x MIC concentrations. These findings suggest a potent therapeutic potential of these compounds in resolving established biofilm infections, which is a critical aspect of treating chronic and device-related infections.

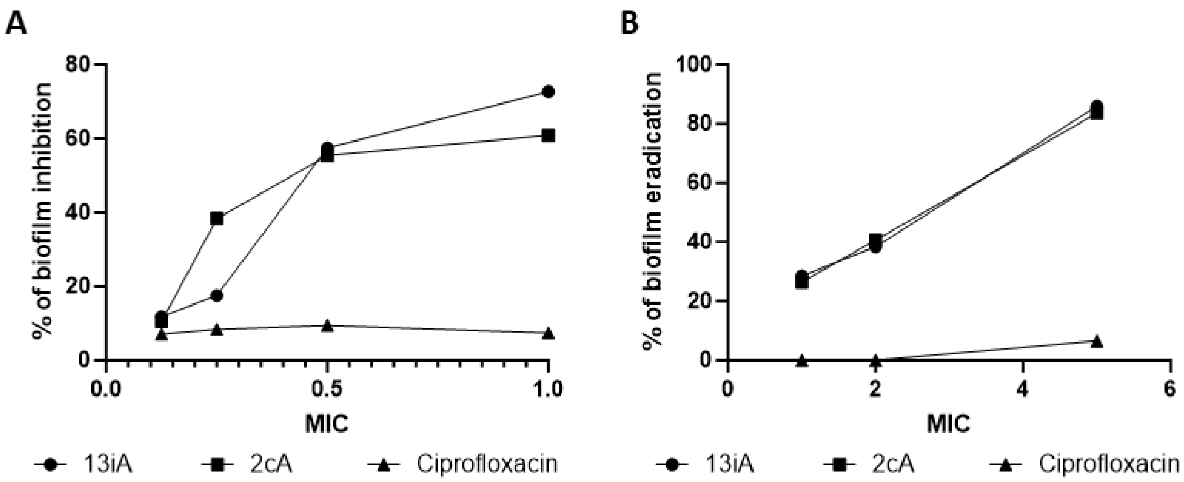

Figure 23. Dose-dependent biofilm inhibition and eradication of compounds 13iA and 2cA against* S. epidermidis *RP62A.

5.3.4 Potential BGCs from marine bacterial isolates

In **Paper IV**, 158 marine bacteria were isolated from various Arctic samples during a 2019 bioprospecting cruise. Co-culture and PCR-based screenings, supplemented by genome sequencing, assessed the potential of BGCs for antimicrobial activity. These bacteria, harvested from benthic invertebrates, sediment from the ocean floor, zooplankton, and biomass from under the sea ice across seven Arctic locations (Figure 9, Figure S1, and Table S1 of **Paper IV**), were evaluated for antimicrobial properties.

Sixty-five isolates inhibited at least one pathogenic strain in a ten human pathogen-related bacteria panel (Tables 1 and Table S3 of **Paper IV**) and five biofilm-forming marine strains (Tables 1 and Table S4 of **Paper IV**). PCR screening using literature-sourced primers (Table S5 of **Paper IV**) identified NRPS or PKS gene clusters in 37 isolates (Table 1 and Table S2 of **Paper IV**). The seven most promising, which contain NRPS or PKS gene clusters and exhibit activity against both Gram-negative and Gram-positive pathogens, belonged to genera *Shewanella* (three isolates), *Pseudomonas* (two), and one each from *Paraglaciecola* and *Pseudoaltermonas* (**Figure 24**).

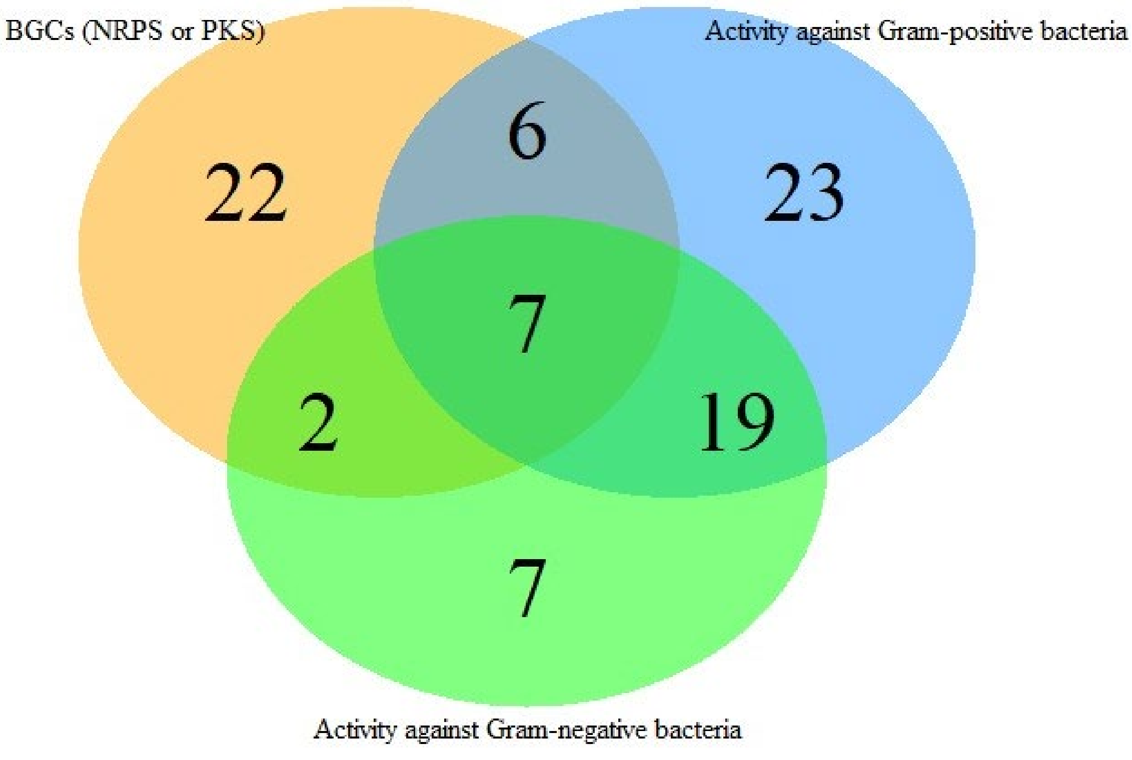

Figure 24. Marine bacterial secondary metabolites (MBSMs) are a potential source of new antimicrobials.

5.4 *In vivo* activity assessments

In **Paper III**, 31 barbiturate and hydantoin derivatives, discussed in **Papers I** and **II**, were selected for zebrafish embryo toxicity studies. Despite the high toxicity observed with the immersion method (Tables S4-S6 of **Paper III**), intrayolk (IY) microinjections of five compounds were non-toxic at 2-8 mg/kg (Table S7 of **Paper III**), aligning with the preclinical dose for this model[78].

Zebrafish-absorbed molecules tend to be more lipophilic than known drugs, and in most cases, their physiochemical properties fall within a narrow range of values compared to the Lipinski rules[79]. Although the physiochemical properties of our compounds do not fall within a narrow range of values compared to the Lipinski rules (Table S8 of **Paper III**), the amphipathic nature of our compounds could hamper gaseous exchange, which could suffocate the fish, thus explaining our observed toxicity in the immersion method. Consequently, IY injections were employed for subsequent in vivo toxicity and antibacterial efficacy studies[78].

Zebrafish possess toll-like receptors (TLRs) with high homology to their counterparts in other vertebrates, including humans[80,81], and bacterial and viral infections upregulate these TLRs[81,82], making zebrafish an excellent infection model. Compounds 13iA and 9 demonstrated significant antibacterial effects against *S. epidermidis* RP62A (Figure 6A and Table S8 of **Paper III**) and 2cA against *S. aureus* (Figure 6B and Table S8 of **Paper III**). Repeated daily dosing proved necessary for infection control, as seen with enhanced survival in *S. aureus*-infected zebrafish treated with compound 9 (**Figure 25**).

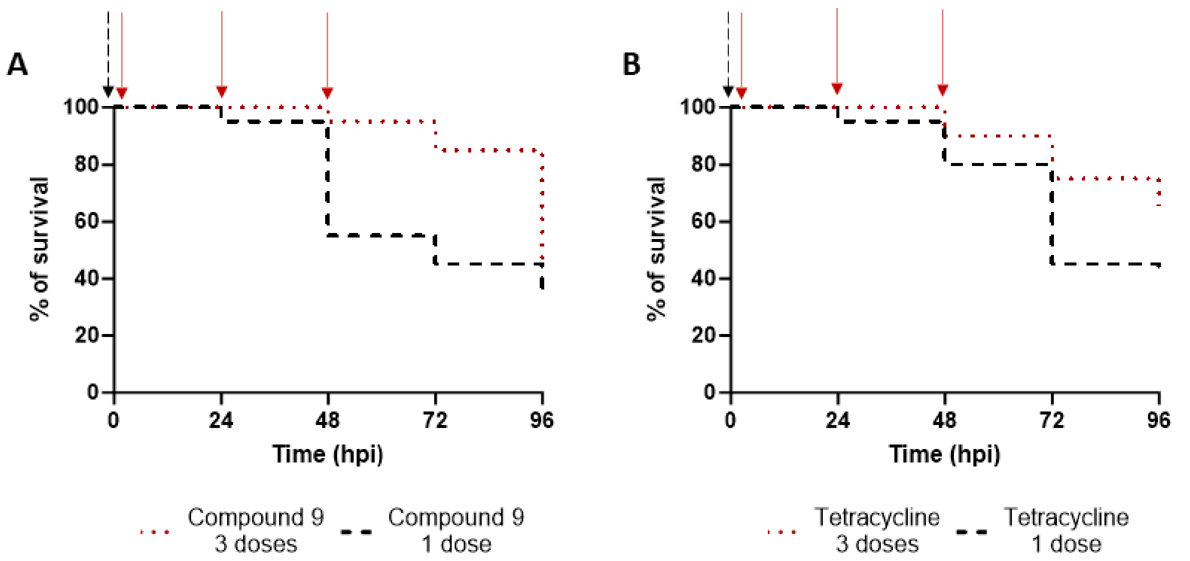

Figure 25. Improved antibacterial activity against* Staphylococcus aureus *when administered in repeated doses daily through IY. A) Compound 9. B) Positive control, tetracycline.

5.5 Potential outcomes of this AntifoMar project

SMAMPs outperform natural AMPs, displaying increased stability, reduced toxicity, and a broader spectrum of antibacterial action. Researchers are focusing on novel peptidomimetics to tackle diverse and resistant bacterial strains, a critical front against antimicrobial resistance[83]. Antimicrobial activity against clinical isolates (**Paper III**) highlights that barbiturate (**Paper I**) and hydantoin (**Paper II**) derivatives have the potential to fight resistant bacteria.

SMAMPs can enhance or complement the efficacy of traditional antibiotics. Pt5-1c, for instance, synergistically improved the efficacy of oxacillin against *S. aureus* USA500 and azithromycin against *K. pneumoniae* 2182, with a fractional inhibitory concentration index (FICI) of 0.5 or less, signifying superior bacterial growth inhibition compared to individual treatments[84]. Additionally, Pt5-1c showed additive effects with vancomycin against *S. aureus* USA500 and with streptomycin against *E. coli* 577, indicated by fractional inhibitory concentration index (FICI) values above 0.5 but at or below 1.0, reflecting a modestly enhanced bacterial growth reduction when used in combination[84].

Paper III highlights the efficacy of barbiturate (**Paper I**) and hydantoin (**Paper II**) derivatives in targeting biofilm-related infections. In **Paper III**, the compounds 13iA and 2cA significantly inhibit biofilm formation by *S. epidermidis* RP62A at sub-MIC concentrations and can eradicate biofilms at concentrations five times the MIC. Furthermore, 13iA demonstrates over 90% eradication of *P. aeruginosa* PAO1 biofilms at 5x MIC concentrations. Other SMAMPs have similar antibiofilm activity; for example, Pt5-1c exhibits potent antibiofilm activity against three tested MDR bacteria (*S. aureus* USA500, *E. coli* 577, and *K. pneumoniae* 2182)[84].

AMPs and SMAMPs are increasingly used to coat biomedical implants, with preclinical and clinical research demonstrating their efficacy in preventing implant-associated infections across various animal models[85].

AMPs and SMAMPs exhibit immunomodulatory effects, such as recruiting and activating immune cells, modulating cytokine production, and promoting wound healing[86,87]. They recruit various immune cells, including neutrophils, macrophages, and dendritic cells, to infection sites and enhance the bactericidal capabilities of immune cells, like stimulating neutrophils to produce reactive oxygen species[86]. They can also regulate cytokine production, increasing pro-inflammatory cytokines for immune response coordination and anti-inflammatory cytokines to resolve inflammation and prevent tissue damage[86]. Additionally, they support wound healing by stimulating angiogenesis and tissue formation[86].

There are other applications of AMPs and SMAMPs, such as Pexiganan for diabetic foot ulcers, LL-37 for leg ulcers and rosacea, and iseganan for ventilator-associated pneumonia exemplify peptidomimetics that have progressed to clinical trials, signifying their potential as therapeutic agents[83].

On the other hand, marine bacteria, including actinobacteria, streptomyces, and bacillus, are prolific producers of bioactive secondary metabolites[58,88]. These MBSMs display a spectrum of biological activities—antimicrobial, antifungal, anti-parasitic, anti-cancer, anti-inflammatory, and immunosuppressive—showcasing their potential in diverse therapeutic applications[58,88].

Exploiting SMAMPs[89] and MNPs[90] as antifouling agents indeed represents a promising avenue toward developing environmentally benign antifouling coatings. Their broad biological activity spectrum, lower environmental impact, and reduced toxicity to non-target marine species enhance their appeal[89,90]. Continued research and development in this field could yield advanced coatings for a range of marine infrastructure, significantly mitigating biofouling while aligning with environmental sustainability goals[89,90].

6 Future perspective

The results obtained in this project should be followed up in further detail, and some of the work is already in progress.

- The assessment of synergistic effects between SMAMPs and antibiotics is a pivotal area of investigation, especially considering increasing antibiotic resistance[84,91]. Exploring these interactions may reveal effective combination therapies that reduce the required doses of antibiotics, limit toxicity, and mitigate the development of resistance[91]. Incorporating these findings into **Paper III** will significantly enhance the paper's contribution to the field, potentially offering new insights into combinatorial treatment strategies.

- Studying the adaptive resistance to SMAMPs and comparing it with that of traditional antibiotics is critical for understanding the long-term efficacy of these compounds. This research will clarify whether SMAMPs retain their effectiveness over time and how quickly bacteria can develop resistance to them compared to conventional antibiotics[92]. Adding these findings to **Paper III** will enrich the discussion on the sustainability of using SMAMPs as a viable alternative or adjunct to existing antimicrobial therapies. Additionally, these findings can be combined with bacteriophage treatment, for example, if there are any resistant bacteria against these SMAMPS or biofilm-related infections, which can be treated with bacteriophage alone or as a combination therapy[93-95].

- In **Papers I** and **II**, the membranolytic mode of action of these SMAMPs has been demonstrated. However, the possibility of a dual mode of action for SMAMPs is an intriguing aspect that merits further investigation. As seen with the N-terminal fragment of Bac7, concentration-dependent behaviour could reveal alternative intracellular targets at sub-membranolytic levels, such as interactions with proteins like DnaK or ribosomes, which could lead to additional or even more specific antimicrobial mechanisms[96-99].

- Certainly, confocal microscopy and flow cytometry offer advanced methodologies to distinguish the effects of SMAMPs on planktonic versus biofilm states of bacteria. Confocal microscopy can provide detailed, three-dimensional images of biofilms, allowing for visualization of the penetration and distribution of SMAMPs within the biofilm matrix[100,101]. Flow cytometry, conversely, can yield quantitative data on the viability and physiological state of individual bacterial cells within a population, whether in biofilms or planktonic form[102,103]. Together, these techniques in **Paper III** can elucidate the distinct responses of bacteria in different states to SMAMP treatment, potentially identifying unique susceptibilities of biofilm-associated bacteria that could be exploited for more effective treatment strategies.

- RNA sequencing (RNA-seq) is a powerful tool to study the overall transcriptional response of bacterial cells to SMAMPs, allowing for a thorough assessment of gene expression changes associated with biofilm inhibition and eradication[104-109]. By comparing the transcriptomic profiles of biofilm-forming bacteria before and after SMAMP treatment, it is likely to identify which genes and pathways are differentially regulated, thus offering an understanding of the molecular mechanisms supporting the mode of action of SMAMPs[104-109]. This evidence can guide the development of targeted strategies to improve the efficacy of SMAMPs and could be a valuable addition to the outcomes of **Paper III**.

- Specific marine bacteria, such as *Shewanella* sp. MBP011.13.1, should be explored to pinpoint antimicrobial compounds and their respective BGCs is an insightful strategy (**Paper IV**). A combination of bioassay-guided fractionation and high-throughput sequencing techniques could be utilized to elucidate these compounds and to identify the gene clusters involved in the biosynthesis of these compounds[110]. This information can then be exploited for heterologous expression, optimization of production conditions, or even synthetic modification to enhance antimicrobial activity[111-113]. Integrating such findings into the broader context of MBSMs research could significantly advance the field.

7 Conclusions

This project aimed to characterize SMAMPs as antimicrobial and antibiofilm agents and identify the producer of antimicrobial compounds from marine bacteria as MBSMs. Four papers were generated from this part of the project in AntifoMar.

Evaluation of synthetic analogues

Firstly, it was identified how N,N-dialkylated-5,5-disubstituted amphipathic barbiturates' structural components affected the bioactivity (**Paper I**). N-propyl linkers balanced antibacterial potency and haemolytic activity well (*in vitro* toxicity), while n-butyl linkers increased the potency. Guanidyl head groups enhanced the antimicrobial potency, and trimethylated amines were suited for narrow-spectrum use. Notably, compounds 13aG, 13jG, and 13jA outperformed the starting compound 1aG in selectivity.

Secondly, five scaffolds were explored for the antibacterial activity of tetrasubstituted, amphipathic SMAMPs and identified the hydantoin structure as a promising basis for antibacterial leads (**Paper II)**. Analysis of derivatives of these hydantoins with various lipophilic side chains, n-alkyl linkers, and cationic groups, and the tetrahalogenated hydantoins demonstrated that 2dA, 6cG, and 6dG were found to be promising leads.

Membrane integrity and bacterial viability studies indicated that compounds like 11lG (**Paper I)** disrupted *B. subtilis* cell walls and affected both *E. coli* membranes, suggesting a primary bactericidal mechanism at high concentrations, with a possible secondary mechanism.

Viability and membrane integrity assays indicated an immediate membranolytic effect on *B. subtilis* and *E. coli*, with 6cG rapidly disrupting both *E. coli* membranes simultaneously (**Paper II**).

Both the barbituric acid and hydantoin derivatives demonstrated strong antibiofilm activity, inhibiting formation and clearing established biofilms in a dose-dependent manner against *S. epidermidis* RP62A, *S. epidermidis* 5179-R1, and *P. aeruginosa* PAO1 (P**aper III)**. They were effective against antibiotic-resistant Gram-positive bacteria, showing similar MIC values to those for susceptible strains, while for resistant Gram-negative bacteria, MICs were up to four times higher.

The *in vivo* toxicity and antibacterial activity were evaluated using a zebrafish model (**Paper III**). Intrayolk injection at 2-8 mg/kg dose in zebrafish was non-toxic and showed promising *in vivo* antibacterial activity. Compounds 13iA and 9 were notably effective against *S. epidermidis* RP62A, and 2cA against *S. aureus in vivo*. For some compounds (9), repeated doses enhanced survival in *S. aureus*-infected zebrafish, indicating a need for consistent treatment for infection control.

Natural products (NPs) from marine bacteria

The study on Arctic marine bacterial isolates (P**aper IV)** identified bioactive marine bacteria for antimicrobial compound discovery using co-culture techniques and genome mining. The most bioactive isolates were obtained from two marine invertebrates (Porifera), zooplankton, under-ice, and sediments (452 m deep).

8 References

1 Boyd, N. K., Teng, C. & Frei, C. R. Brief overview of approaches and challenges in new antibiotic development: a focus on drug repurposing. *Frontiers in cellular and infection microbiology* **11**, 684515 (2021).

2 Hierink, F., Okiro, E. A., Flahault, A. & Ray, N. The winding road to health: A systematic scoping review on the effect of geographical accessibility to health care on infectious diseases in low-and middle-income countries. *Plos one* **16**, e0244921 (2021).

3 Van Der Meer, J. W. The infectious disease challenges of our time. *Frontiers in Public Health* **1**, 7 (2013).

4 Kumar Kulabhusan, P., Hussain, B. & Yüce, M. Current perspectives on aptamers as diagnostic tools and therapeutic agents. *Pharmaceutics* **12**, 646 (2020).

5 Lee, H.-A., Kung, H.-H., Lee, Y.-J., Chao, J. C., Udayasankaran, J. G., Fan, H.-C., Ng, K.-K., Chang, Y.-K., Kijsanayotin, B. & Marcelo, A. B. Global infectious disease surveillance and case tracking system for COVID-19: development study. *JMIR Medical Informatics* **8**, e20567 (2020).

6 Wang, P.-W., Lee, W.-T., Wu, Y.-N. & Shieh, D.-B. Opportunities for Nanomedicine in Clostridioides difficile Infection. *Antibiotics* **10**, 948 (2021).

7 Archibald, M. M., Rizal, B., Connolly, T., Burns, M. J., Naughton, M. J. & Chiles, T. C. A nanocoaxial-based electrochemical sensor for the detection of cholera toxin. *Biosensors and Bioelectronics* **74**, 406-410 (2015).

8 Cui, F., Zhou, Z. & Zhou, H. S. Molecularly imprinted polymers and surface imprinted polymers based electrochemical biosensor for infectious diseases. *Sensors* **20**, 996 (2020).

9 Halasa, T. & Dürr, S. Modeling disease spread and control. **4**, 199 (2017).

10 Wang, Y. & Liu, G. Dynamics Analysis for a Stochastic SIRI Model Incorporating Media Coverage. *Mathematical Problems in Engineering* **2022** (2022).

11 Smith, K. F., Goldberg, M., Rosenthal, S., Carlson, L., Chen, J., Chen, C. & Ramachandran, S. Global rise in human infectious disease outbreaks. *Journal of the Royal Society Interface* **11**, 20140950 (2014).

12 Baker, R. E., Mahmud, A. S., Miller, I. F., Rajeev, M., Rasambainarivo, F., Rice, B. L., Takahashi, S., Tatem, A. J., Wagner, C. E. & Wang, L.-F. Infectious disease in an era of global change. *Nature Reviews Microbiology* **20**, 193-205 (2022).

13 Kim, J., Mohamed, M. A. A., Zagorovsky, K. & Chan, W. C. State of diagnosing infectious pathogens using colloidal nanomaterials. *Biomaterials* **146**, 97-114 (2017).

14 Chioro, A., Coll-Seck, A. M., Høie, B., Moeloek, N., Motsoaledi, A., Rajatanavin, R. & Touraine, M. Antimicrobial resistance: a priority for global health action. *Bull World Health Organ* **93**, 439-439 (2015).

15 Murray, C. J., Ikuta, K. S., Sharara, F., Swetschinski, L., Aguilar, G. R., Gray, A., Han, C., Bisignano, C., Rao, P. & Wool, E. Global burden of bacterial antimicrobial resistance in 2019: a systematic analysis. *The Lancet* **399**, 629-655 (2022).

16 Marathe, N. P., Grevskott, D. H., Salva-Serra, F., Nimje, P. S., Svanevik, C. S., Lunestad, B. T. & Moore, E. R. Seawater from Bergen harbor is a reservoir of conjugative multidrug-resistance plasmids carrying genes for virulence. *International Journal of Hygiene and Environmental Health* **248**, 114108 (2023).

17 Collignon, P., Beggs, J. J., Walsh, T. R., Gandra, S. & Laxminarayan, R. Anthropological and socioeconomic factors contributing to global antimicrobial resistance: a univariate and multivariable analysis. *The Lancet Planetary Health* **2**, e398-e405 (2018).
18 Codjoe, F. S. & Donkor, E. S. Carbapenem resistance: a review. *Medical Sciences* **6**, 1 (2017).
19 Cook, M. A. & Wright, G. D. The past, present, and future of antibiotics. *Science Translational Medicine* **14**, eabo7793 (2022).
20 Nadeem, S. F., Gohar, U. F., Tahir, S. F., Mukhtar, H., Pornpukdeewattana, S., Nukthamna, P., Moula Ali, A. M., Bavisetty, S. C. B. & Massa, S. Antimicrobial resistance: more than 70 years of war between humans and bacteria. *Critical Reviews in Microbiology* **46**, 578-599 (2020).
21 Carlet, J., Collignon, P., Goldmann, D., Goossens, H., Gyssens, I. C., Harbarth, S., Jarlier, V., Levy, S. B., N'Doye, B. & Pittet, D. Society's failure to protect a precious resource: antibiotics. *The Lancet* **378**, 369-371 (2011).
22 Llor, C. & Bjerrum, L. Antimicrobial resistance: risk associated with antibiotic overuse and initiatives to reduce the problem. *Therapeutic advances in drug safety* **5**, 229-241 (2014).
23 Marshall, B. M. & Levy, S. B. Food animals and antimicrobials: impacts on human health. *Clinical microbiology reviews* **24**, 718-733 (2011).
24 Phillips, C. J., Wisdom, A. J., McKinnon, R. A., Woodman, R. J. & Gordon, D. L. Interventions targeting the prescribing and monitoring of vancomycin for hospitalized patients: a systematic review protocol. *Infectious Diseases and Therapy* **6**, 557-563 (2017).
25 Ayukekbong, J. A., Ntemgwa, M. & Atabe, A. N. The threat of antimicrobial resistance in developing countries: causes and control strategies. *Antimicrobial Resistance & Infection Control* **6**, 1-8 (2017).
26 Iskandar, K., Molinier, L., Hallit, S., Sartelli, M., Hardcastle, T. C., Haque, M., Lugova, H., Dhingra, S., Sharma, P. & Islam, S. Surveillance of antimicrobial resistance in low-and middle-income countries: a scattered picture. *Antimicrobial Resistance & Infection Control* **10**, 1-19 (2021).
27 Wu, Y., Wang, B., Lu, H., Zhao, H., Yang, B., Li, L., Lu, Y., Zhang, D., Sun, N. & Huang, H. Identification of novel tricyclic benzo [1, 3] oxazinyloxazolidinones as potent antibacterial agents with excellent pharmacokinetic profiles against drug-resistant pathogens. *Journal of Medicinal Chemistry* **64**, 3234-3248 (2021).
28 Reid, G. Biofilms in infectious disease and on medical devices. *International journal of antimicrobial agents* **11**, 223-226 (1999).
29 Fisher, L. E., Yang, Y., Yuen, M.-F., Zhang, W., Nobbs, A. H. & Su, B. Bactericidal activity of biomimetic diamond nanocone surfaces. *Biointerphases* **11** (2016).
30 Iseppi, R., Di Cerbo, A., Aloisi, P., Manelli, M., Pellesi, V., Provenzano, C., Camellini, S., Messi, P. & Sabia, C. In vitro activity of essential oils against planktonic and biofilm cells of extended-spectrum β-lactamase (ESBL)/carbapenamase-producing gram-negative bacteria involved in human nosocomial infections. *Antibiotics* **9**, 272 (2020).
31 Torres, M. D. T. & de la Fuente-Nunez, C. Reprogramming biological peptides to combat infectious diseases. *Chemical Communications* **55**, 15020-15032 (2019).
32 Sharma, D., Misba, L. & Khan, A. U. Antibiotics versus biofilm: an emerging battleground in microbial communities. *Antimicrobial Resistance & Infection Control* **8**, 1-10 (2019).
33 Hall, C. W. & Mah, T.-F. Molecular mechanisms of biofilm-based antibiotic resistance and tolerance in pathogenic bacteria. *FEMS microbiology reviews* **41**, 276-301 (2017).
34 Hutchings, M. I., Truman, A. W. & Wilkinson, B. Antibiotics: past, present and future. *Current opinion in microbiology* **51**, 72-80 (2019).

35 Wasan, H., Singh, D., Reeta, K. & Gupta, Y. K. Landscape of Push Funding in Antibiotic Research: Current Status and Way Forward. *Biology* **12**, 101 (2023).
36 Regen, S. L. Improving the cellular selectivity of a membrane-disrupting antimicrobial agent by monomer control and by taming. *Molecules* **26**, 374 (2021).
37 Zhu, Y., Cleaver, L., Wang, W., Podoll, J. D., Walls, S., Jolly, A. & Wang, X. Tetracyclic indolines as a novel class of β-lactam-selective resistance-modifying agent for MRSA. *European journal of medicinal chemistry* **125**, 130-142 (2017).
38 Vynne, N. G., Mansson, M. & Gram, L. Gene sequence based clustering assists in dereplication of Pseudoalteromonas luteoviolacea strains with identical inhibitory activity and antibiotic production. *Marine Drugs* **10**, 1729-1740 (2012).
39 Karthikeyan, A., Joseph, A. & Nair, B. G. Promising bioactive compounds from the marine environment and their potential effects on various diseases. *Journal of Genetic Engineering and Biotechnology* **20**, 1-38 (2022).
40 Ameen, F., AlNadhari, S. & Al-Homaidan, A. A. Marine microorganisms as an untapped source of bioactive compounds. *Saudi Journal of Biological Sciences* **28**, 224-231 (2021).
41 Wibowo, J. T., Bayu, A., Aryati, W. D., Fernandes, C., Yanuar, A., Kijjoa, A. & Putra, M. Y. Secondary Metabolites from Marine-Derived Bacteria with Antibiotic and Antibiofilm Activities against Drug-Resistant Pathogens. *Marine Drugs* **21**, 50 (2023).
42 Stincone, P. & Brandelli, A. Marine bacteria as source of antimicrobial compounds. *Critical reviews in biotechnology* **40**, 306-319 (2020).
43 Lo Giudice, A. & Rizzo, C. Bacteria associated with marine benthic invertebrates from polar environments: unexplored frontiers for biodiscovery? *Diversity* **10**, 80 (2018).
44 Katz, L. & Baltz, R. H. Natural product discovery: past, present, and future. *Journal of Industrial Microbiology and Biotechnology* **43**, 155-176 (2016).
45 Newman, D. J. & Cragg, G. M. Natural products as sources of new drugs over the nearly four decades from 01/1981 to 09/2019. *Journal of natural products* **83**, 770-803 (2020).
46 Needham, J., Andersen, R. J. & Kelly, M. T. Biosynthesis of oncorhyncolide, a metabolite of the seawater bacterial isolate MK 157. *Journal of the Chemical Society, Chemical Communications*, 1367-1369 (1992).
47 Oberhofer, M., Wackerlig, J., Zehl, M., Büyük, H., Cao, J. J., Prado-Roller, A., Urban, E. & Zotchev, S. B. Endophytic Akanthomyces sp. LN303 from Edelweiss produces emestrin and two new 2-hydroxy-4 pyridone alkaloids. *ACS omega* **6**, 2184-2191 (2021).
48 Weissman, K. J. The structural biology of biosynthetic megaenzymes. *Nature Chemical Biology* **11**, 660-670 (2015).
49 Wang, W., Park, K.-H., Lee, J., Oh, E., Park, C., Kang, E., Lee, J. & Kang, H. A New Thiopeptide Antibiotic, micrococcin P3, from a marine-derived Strain of the bacterium Bacillus stratosphericus. *Molecules* **25**, 4383 (2020).
50 Schinke, C., Martins, T., Queiroz, S. C., Melo, I. S. & Reyes, F. G. Antibacterial compounds from marine bacteria, 2010–2015. *Journal of natural products* **80**, 1215-1228 (2017).
51 Romano, G., Almeida, M., Varela Coelho, A., Cutignano, A., Gonçalves, L. G., Hansen, E., Khnykin, D., Mass, T., Ramšak, A. & Rocha, M. S. Biomaterials and bioactive natural products from marine invertebrates: From basic research to innovative applications. *Marine Drugs* **20**, 219 (2022).
52 Leal, M. C., Puga, J., Serodio, J., Gomes, N. C. & Calado, R. Trends in the discovery of new marine natural products from invertebrates over the last two decades–where and what are we bioprospecting? *PLoS One* **7**, e30580 (2012).

53 Lebar, M. D., Heimbegner, J. L. & Baker, B. J. Cold-water marine natural products. *Natural Product Reports* **24**, 774-797 (2007).

54 Sharp, J. H., Winson, M. K. & Porter, J. S. Bryozoan metabolites: an ecological perspective. *Natural Product Reports* **24**, 659-673 (2007).

55 Tadesse, M., Tabudravu, J. N., Jaspars, M., Strøm, M. B., Hansen, E., Andersen, J. H., Kristiansen, P. E. & Haug, T. The antibacterial ent-eusynstyelamide B and eusynstyelamides D, E, and F from the Arctic bryozoan Tegella cf. spitzbergensis. *Journal of natural products* **74**, 837-841 (2011).

56 Tapiolas, D. M., Bowden, B. F., Abou-Mansour, E., Willis, R. H., Doyle, J. R., Muirhead, A. N., Liptrot, C., Llewellyn, L. E., Wolff, C. W. & Wright, A. D. Eusynstyelamides A, B, and C, nNOS inhibitors, from the ascidian Eusynstyela latericius. *Journal of natural products* **72**, 1115-1120 (2009).

57 Diamond, G., Beckloff, N., Weinberg, A. & Kisich, K. O. The roles of antimicrobial peptides in innate host defense. *Current pharmaceutical design* **15**, 2377-2392 (2009).

58 Browne, K., Chakraborty, S., Chen, R., Willcox, M. D., Black, D. S., Walsh, W. R. & Kumar, N. A new era of antibiotics: the clinical potential of antimicrobial peptides. *International journal of molecular sciences* **21**, 7047 (2020).

59 Ganz, T. & Lehrer, R. I. Antibiotic peptides from higher eukaryotes: biology and applications. *Molecular medicine today* **5**, 292-297 (1999).

60 Hof, W. v. t., Veerman, E. C., Helmerhorst, E. J. & Amerongen, A. V. N. Antimicrobial peptides: properties and applicability. *Biological Chemistry* **382**, 597 – 619 (2001).

61 Chen, C. H. & Lu, T. K. Development and challenges of antimicrobial peptides for therapeutic applications. *Antibiotics* **9**, 24 (2020).

62 Guo, X., Yan, T., Rao, J., Yue, X., Pei, X., Deng, J., Sun, W., Yang, W., Zhang, B. & Xie, J. Potent Antimicrobial and Antibiofilm Activities of Feleucin-K3 Analogs Modified by α-(4-Pentenyl)-Ala against Multidrug-Resistant Bacteria. *Biomolecules* **11**, 761 (2021).

63 Alves Ferreira, D., Martins, L. M., Fernandes, A. R. & Martins, M. A tale of two ends: repurposing metallic compounds from anti-tumour agents to effective antibacterial activity. *Antibiotics* **9**, 321 (2020).

64 Huan, Y., Kong, Q., Mou, H. & Yi, H. Antimicrobial peptides: classification, design, application and research progress in multiple fields. *Frontiers in microbiology* **11**, 2559 (2020).

65 Laverty, G., Gorman, S. P. & Gilmore, B. F. The potential of antimicrobial peptides as biocides. *International journal of molecular sciences* **12**, 6566-6596 (2011).

66 Marcolefas, E., Leung, T., Okshevsky, M., McKay, G., Hignett, E., Hamel, J., Aguirre, G., Blenner-Hassett, O., Boyle, B. & Lévesque, R. C. Culture-dependent bioprospecting of bacterial isolates from the Canadian high Arctic displaying antibacterial activity. *Frontiers in microbiology* **10**, 1836 (2019).

67 Kodzius, R. & Gojobori, T. Marine metagenomics as a source for bioprospecting. *Marine genomics* **24**, 21-30 (2015).

68 Ward, D. M., Weller, R. & Bateson, M. M. 16S rRNA sequences reveal numerous uncultured microorganisms in a natural community. *Nature* **345**, 63-65 (1990).

69 Elvheim, A. I., Li, C. & Landfald, B. Conservation of Genomic Information in Multiple Displacement Amplified Low-Quantity Metagenomic Material from Marine Invertebrates. *Marine Drugs* **21**, 165 (2023).

70 Vartoukian, S. R., Palmer, R. M. & Wade, W. G. Strategies for culture of 'unculturable' bacteria. *FEMS microbiology letters* **309**, 1-7 (2010).

71 Peng, X.-Y., Wu, J.-T., Shao, C.-L., Li, Z.-Y., Chen, M. & Wang, C.-Y. Co-culture: Stimulate the metabolic potential and explore the molecular diversity of natural products from microorganisms. *Marine Life Science & Technology*, 1-12 (2021).
72 Romano, S., Jackson, S. A., Patry, S. & Dobson, A. D. Extending the "one strain many compounds"(OSMAC) principle to marine microorganisms. *Marine drugs* **16**, 244 (2018).
73 Schwarz, J., Hubmann, G., Rosenthal, K. & Lütz, S. Triaging of culture conditions for enhanced secondary metabolite diversity from different bacteria. *Biomolecules* **11**, 193 (2021).
74 Srinivasan, R., Kannappan, A., Shi, C. & Lin, X. Marine bacterial secondary metabolites: A treasure house for structurally unique and effective antimicrobial compounds. *Marine Drugs* **19**, 530 (2021).
75 Cardoso, P., Glossop, H., Meikle, T. G., Aburto-Medina, A., Conn, C. E., Sarojini, V. & Valery, C. Molecular engineering of antimicrobial peptides: Microbial targets, peptide motifs and translation opportunities. *Biophysical reviews* **13**, 35-69 (2021).
76 Torres, M. D., Pedron, C. N., Higashikuni, Y., Kramer, R. M., Cardoso, M. H., Oshiro, K. G., Franco, O. L., Silva Junior, P. I., Silva, F. D. & Oliveira Junior, V. X. Structure-function-guided exploration of the antimicrobial peptide polybia-CP identifies activity determinants and generates synthetic therapeutic candidates. *Communications biology* **1**, 221 (2018).
77 Paulsen, M. H., Engqvist, M., Ausbacher, D., Anderssen, T., Langer, M. K., Haug, T., Morello, G. R., Liikanen, L. E., Blencke, H.-M. & Isaksson, J. Amphipathic barbiturates as mimics of antimicrobial peptides and the marine natural products eusynstyelamides with activity against multi-resistant clinical isolates. *Journal of Medicinal Chemistry* **64**, 11395-11417 (2021).
78 Guarin, M., Ny, A., De Croze, N., Maes, J., Léonard, M., Annaert, P. & de Witte, P. A. Pharmacokinetics in zebrafish embryos (Zfe) following immersion and intrayolk administration: A fluorescence-based analysis. *Pharmaceuticals* **14**, 576 (2021).
79 Long, K., Kostman, S. J., Fernandez, C., Burnett, J. C. & Huryn, D. M. Do zebrafish obey lipinski rules? *ACS Medicinal Chemistry Letters* **10**, 1002-1006 (2019).
80 Jault, C., Pichon, L. & Chluba, J. Toll-like receptor gene family and TIR-domain adapters in Danio rerio. *Molecular immunology* **40**, 759-771 (2004).
81 Meijer, A. H., Krens, S. G., Rodriguez, I. A. M., He, S., Bitter, W., Snaar-Jagalska, B. E. & Spaink, H. P. Expression analysis of the Toll-like receptor and TIR domain adaptor families of zebrafish. *Molecular immunology* **40**, 773-783 (2004).
82 Phelan, P. E., Mellon, M. T. & Kim, C. H. Functional characterization of full-length TLR3, IRAK-4, and TRAF6 in zebrafish (Danio rerio). *Molecular immunology* **42**, 1057-1071 (2005).
83 Molchanova, N., Hansen, P. R. & Franzyk, H. Advances in development of antimicrobial peptidomimetics as potential drugs. *Molecules* **22**, 1430 (2017).
84 Duan, H., Zhang, X., Li, Z., Yuan, J., Shen, F. & Zhang, S. Synergistic effect and antibiofilm activity of an antimicrobial peptide with traditional antibiotics against multi-drug resistant bacteria. *Microbial Pathogenesis* **158**, 105056 (2021).
85 Drexelius, M. G. & Neundorf, I. Application of antimicrobial peptides on biomedical implants: Three ways to pursue peptide coatings. *International Journal of Molecular Sciences* **22**, 13212 (2021).
86 Anbarasu, A. Antimicrobial peptides as Immunomodulators and Antimycobacterial agents to combat Mycobacterium tuberculosis: a critical review. *Probiotics and Antimicrobial Proteins*, 1-28 (2022).

87 Skovbakke, S. L., Holdfeldt, A., Forsman, H., Bylund, J. & Franzyk, H. The role of formyl peptide receptors for immunomodulatory activities of antimicrobial peptides and peptidomimetics. *Current pharmaceutical design* **24**, 1100-1120 (2018).

88 Al-Shaibani, M. M., Radin Mohamed, R. M. S., Sidik, N. M., Enshasy, H. A. E., Al-Gheethi, A., Noman, E., Al-Mekhlafi, N. A. & Zin, N. M. Biodiversity of secondary metabolites compounds isolated from phylum actinobacteria and its therapeutic applications. *Molecules* **26**, 4504 (2021).

89 Saha, R., Bhattacharya, D. & Mukhopadhyay, M. Advances in modified antimicrobial peptides as marine antifouling material. *Colloids and Surfaces B: Biointerfaces*, 112900 (2022).

90 Liu, L.-L., Wu, C.-H. & Qian, P.-Y. Marine natural products as antifouling molecules–a mini-review (2014–2020). *Biofouling* **36**, 1210-1226 (2020).

91 Wu, X., Li, Z., Li, X., Tian, Y., Fan, Y., Yu, C., Zhou, B., Liu, Y., Xiang, R. & Yang, L. Synergistic effects of antimicrobial peptide DP7 combined with antibiotics against multidrug-resistant bacteria. *Drug design, development and therapy*, 939-946 (2017).

92 Som, A., Vemparala, S., Ivanov, I. & Tew, G. N. Synthetic mimics of antimicrobial peptides. *Peptide Science* **90**, 83-93 (2008).

93 Li, X., He, Y., Wang, Z., Wei, J., Hu, T., Si, J., Tao, G., Zhang, L., Xie, L. & Abdalla, A. E. A combination therapy of Phages and Antibiotics: Two is better than one. *International Journal of Biological Sciences* **17**, 3573 (2021).

94 Osman, A.-H., Kotey, F. C., Odoom, A., Darkwah, S., Yeboah, R. K., Dayie, N. T. & Donkor, E. S. The potential of bacteriophage-antibiotic combination therapy in treating infections with multidrug-resistant bacteria. *Antibiotics* **12**, 1329 (2023).

95 Akturk, E., Melo, L. D., Oliveira, H., Crabbé, A., Coenye, T. & Azeredo, J. Combining phages and antibiotic to enhance antibiofilm efficacy against an in vitro dual species wound biofilm. *Biofilm* **6**, 100147 (2023).

96 Graf, M., Mardirossian, M., Nguyen, F., Seefeldt, A. C., Guichard, G., Scocchi, M., Innis, C. A. & Wilson, D. N. Proline-rich antimicrobial peptides targeting protein synthesis. *Natural product reports* **34**, 702-711 (2017).

97 Podda, E., Benincasa, M., Pacor, S., Micali, F., Mattiuzzo, M., Gennaro, R. & Scocchi, M. Dual mode of action of Bac7, a proline-rich antibacterial peptide. *Biochimica et Biophysica Acta (BBA)-General Subjects* **1760**, 1732-1740 (2006).

98 Scocchi, M., Lüthy, C., Decarli, P., Mignogna, G., Christen, P. & Gennaro, R. The proline-rich antibacterial peptide Bac7 binds to and inhibits in vitro the molecular chaperone DnaK. *International Journal of Peptide Research and Therapeutics* **15**, 147-155 (2009).

99 Mardirossian, M., Grzela, R., Giglione, C., Meinnel, T., Gennaro, R., Mergaert, P. & Scocchi, M. The host antimicrobial peptide Bac71-35 binds to bacterial ribosomal proteins and inhibits protein synthesis. *Chemistry & biology* **21**, 1639-1647 (2014).

100 Reichhardt, C. & Parsek, M. R. Confocal laser scanning microscopy for analysis of Pseudomonas aeruginosa biofilm architecture and matrix localization. *Frontiers in microbiology* **10**, 677 (2019).

101 Schlafer, S. & Meyer, R. L. Confocal microscopy imaging of the biofilm matrix. *Journal of microbiological methods* **138**, 50-59 (2017).

102 Gelle, M., Jacquelin, L. & Choisy, C. in *Annales Pharmaceutiques Francaises.* 243-252.

103 Khomtchouk, K., Weglarz, M., Bekale, L., Koliesnik, I., Bollyky, P. & Santa Maria, P. Quantitative assessment of bacterial growth phase utilizing flow cytometry. *Journal of microbiological methods* **167**, 105760 (2019).

104 Zhao, X., Liu, Z., Liu, Z., Meng, R., Shi, C., Chen, X., Bu, X. & Guo, N. Phenotype and RNA-seq-Based transcriptome profiling of Staphylococcus aureus biofilms in response to tea tree oil. *Microbial Pathogenesis* **123**, 304-313 (2018).

105 Abouelhassan, Y., Zhang, Y., Jin, S. & Huigens III, R. W. Transcript profiling of MRSA biofilms treated with a halogenated phenazine eradicating agent: a platform for defining cellular targets and pathways critical to biofilm survival. *Angewandte Chemie International Edition* **57**, 15523-15528 (2018).

106 Tan, X., Qin, N., Wu, C., Sheng, J., Yang, R., Zheng, B., Ma, Z., Liu, L., Peng, X. & Jia, A. Transcriptome analysis of the biofilm formed by methicillin-susceptible Staphylococcus aureus. *Scientific reports* **5**, 11997 (2015).

107 Qin, N., Tan, X., Jiao, Y., Liu, L., Zhao, W., Yang, S. & Jia, A. RNA-Seq-based transcriptome analysis of methicillin-resistant Staphylococcus aureus biofilm inhibition by ursolic acid and resveratrol. *Scientific reports* **4**, 5467 (2014).

108 Song, Z.-M., Zhang, J.-L., Zhou, K., Yue, L.-M., Zhang, Y., Wang, C.-Y., Wang, K.-L. & Xu, Y. Anthraquinones as potential antibiofilm agents against methicillin-resistant Staphylococcus aureus. *Frontiers in Microbiology* **12**, 709826 (2021).

109 She, P., Luo, Z., Chen, L. & Wu, Y. Efficacy of levofloxacin against biofilms of Pseudomonas aeruginosa isolated from patients with respiratory tract infections in vitro. *Microbiologyopen* **8**, e00720 (2019).

110 Pheiffer, F., Schneider, Y. K.-H., Hansen, E. H., Andersen, J. H., Isaksson, J., Busche, T., Rückert, C., Kalinowski, J., Zyl, L. v. & Trindade, M. Bioassay-Guided Fractionation Leads to the Detection of Cholic Acid Generated by the Rare Thalassomonas sp. *Marine Drugs* **21**, 2 (2022).

111 Baiden, N., Gandini, C., Goddard, P. & Sayanova, O. Heterologous expression of antimicrobial peptides S-thanatin and bovine lactoferricin in the marine diatom Phaeodactylum tricornutum enhances native antimicrobial activity against Gram-negative bacteria. *Algal Research* **69**, 102927 (2023).

112 Zhan, N., Zhang, L., Yang, H., Zheng, Y., Wei, X., Wang, J. & Shan, A. Design and heterologous expression of a novel dimeric LL37 variant in Pichia pastoris. *Microbial Cell Factories* **20**, 1-13 (2021).

113 Hoelscher, M. P., Forner, J., Calderone, S., Krämer, C., Taylor, Z., Loiacono, F. V., Agrawal, S., Karcher, D., Moratti, F. & Kroop, X. Expression strategies for the efficient synthesis of antimicrobial peptides in plastids. *Nature communications* **13**, 5856 (2022).

Paper I

European Journal of Medicinal Chemistry 241 (2022) 114632

Contents lists available at ScienceDirect

European Journal of Medicinal Chemistry

journal homepage: www.elsevier.com/locate/ejmech

A concise SAR-analysis of antimicrobial cationic amphipathic barbiturates for an improved activity-toxicity profile

Manuel K. Langer [a,1], Ataur Rahman [b,1], Hymonti Dey [b], Trude Anderssen [c], Francesco Zilioli [a], Tor Haug [b], Hans-Matti Blencke [b], Klara Stensvåg [b], Morten B. Strøm [c,**], Annette Bayer [a,*]

[a] Department of Chemistry, UiT The Arctic University of Norway, NO-9037, Tromsø, Norway
[b] The Norwegian College of Fishery Science, Faculty of Biosciences, Fisheries and Economics, UiT The Arctic University of Norway, NO-9037, Tromsø, Norway
[c] Department of Pharmacy, Faculty of Health Sciences, UiT The Arctic University of Norway, NO-9037, Tromsø, Norway

ARTICLE INFO

Keywords:
Antibacterial
Barbiturates
Peptidomimetics
SMAMPs
Synthetic mimics of antimicrobial peptides

ABSTRACT

An amphipathic barbiturate mimic of the marine eusynstyelamides is reported as a promising class of antimicrobial agents. We hereby report a detailed analysis of the structure-activity relationship for cationic amphipathic *N,N′*-dialkylated-5,5-disubstituted barbiturates. The influence of various cationic groups, hydrocarbon linkers and lipophilic side chains on the compounds' antimicrobial potency and haemolytic activity was studied. A comprehensive library of 58 compounds was prepared using a concise synthetic strategy. We found cationic amine and guanidyl groups to yield the highest broad-spectrum activity and cationic trimethylated quaternary amine groups to exert narrow-spectrum activity against Gram-positive bacteria. *n*-Propyl hydrocarbon linkers proved to be the best compromise between potency and haemolytic activity. The combination of two different lipophilic side chains allowed for further fine-tuning of the biological properties. Using these insights, we were able to prepare both, the potent narrow-spectrum barbiturate **8a** and the broad-spectrum barbiturates **11lG**, **13jA** and **13jG**, all having low or no haemolytic activity. The guanidine derivative **11lG** demonstrated a strong membrane disrupting effect in luciferase-based assays. We believe that these results may be valuable in further development of antimicrobial lead structures.

1. Introduction

Since the golden age of antibiotics, the developing rate of new agents has decreased notably, while antimicrobial resistance (AMR) has been rising to a global threat [1]. The prominence of this problem is well demonstrated by the World Health Organization (WHO) enacting a global action plan on fighting antimicrobial resistance [2]. While the action plan is focusing on a framework at many different levels, the need for potent antimicrobials stays. As the antibiotics employed for decades start to lose activity against resistant bacteria, several alternative approaches have been investigated. Among these are combination therapy [3,4], bacteriophage therapy [5], photodynamic therapy [6], antibacterial antibodies [7], phytochemicals [5], nanoparticles [8] and antimicrobial peptides [9,10].

From the above stated list, the short, cationic antimicrobial peptides (AMPs) are an intriguing class of compounds. They constitute the first line of host defense in virtually all eukaryotic species including plants, mammals, insects, etc. [11] They generally feature between 20 and 50% hydrophobic residues and have an overall positive charge (+2 to +9) at neutral pH [12–14]. Their amphipathic nature is the basis of their most common mode of action, to permeabilize bacterial membranes. AMPs attach to the negatively charged cytoplastic membrane by electrostatic interactions and subsequently disrupt the apolar bilayer with their hydrophobic part [15]. It is believed that due to these non-specific interactions, bacterial resistance is less likely to be induced [16]. This makes AMPs a promising group of compounds despite their generally lower activity compared to marketed antibiotics [17].

Despite these promising properties, the clinical application of peptide based drugs is often limited by their poor oral uptake and proteolytic instability [18]. Therefore, considerable efforts towards the development of synthetic AMP analogues have been made, cumulating in the development of a variety of different groups of analogues [19–27].

* Corresponding author.
** Corresponding author.
E-mail addresses: Morten.strom@uit.no (M.B. Strøm), Annette.bayer@uit.no (A. Bayer).
[1] Authors contributed equally to this work.

https://doi.org/10.1016/j.ejmech.2022.114632
Received 20 May 2022; Received in revised form 15 July 2022; Accepted 24 July 2022
Available online 5 August 2022

Focusing on small molecules, we have recently reported substituted barbituric acid derivatives [28], inspired by a family of marine natural products, the *eusynstyelamides,* [29,30] as peptidomimetics of AMPs. The lead structure **1aG** (Fig. 1) from our previous study [28] demonstrated good *in vitro* and *in vivo* activity as a proof of principle.

Encouraged by the *in vivo* activity of **1aG** we herein describe an in-depth SAR investigation to improve the potency and selectivity of these peptidomimetics. Several series of amphipathic barbiturates with systematically varying substituents were designed and synthesized. Our aim was to assess the qualitative influence of each structural component aside from the barbituric acid on the antimicrobial and haemolytic activity. Once the impact of each component is identified, improved narrow- and broad-spectrum compounds may be prepared. All new compounds were screened for activity against a panel of antibiotic susceptible strains to determine their minimal inhibitory concentration (MIC) values. Cytotoxicity was assessed by determining the EC_{50} values for the lysis of human red blood cells (RBC). Promising candidates were investigated for their antibacterial mode of action (MoA), using three luciferase-based assays of the viability and integrity of the cytoplasmic inner and outer membrane of bacterial cells.

2. Results and discussion

2.1. Design of the study

To systematically study the influence of structural components of **1aG** [28] (Fig. 1) on the antibacterial and haemolytic activity, we devised several series of compounds based on the general structure shown in Fig. 2. All structures consisted of a central barbituric acid core, which was kept constant. Three structural parts were varied in the design of the compound library: (i) the cationic head groups (blue placeholder in Fig. 2) attached to the nitrogen atoms of the barbiturate core by (ii) a hydrocarbon linker chain (green placeholder) and (iii) the two lipophilic side chains (red placeholders) connected to the barbiturate C-5 carbon.

The influence of the cationic head groups (R; Fig. 2) was investigated by including 1° amines, methylated 2°, 3° and 4° amines and imine derivatives containing guanidino or pyridinium groups in the library design. The cationic groups were chosen based on the prospect of varying the interactions with bacterial membranes and their ability to cross the latter and accumulate in Gram-negative *Escherichia coli* (*E. coli*) [31,32]. Compounds with varying cationic groups are found in compound *series 1*.

The lipophilic side chains (Fig. 2) were hypothesized to influence the compounds' ability to insert into the hydrophobic lipid bilayer of the bacteria. In our library design haloaryls, hetero-aryls, and linear and cyclic hydrocarbons were chosen as lipophilic side chains. The selection was based on results from our previous study [28] and commercial availability. Two different compound series were included in the study; in *series 2* the two lipophilic side chains were identical, while in *series 3* two different lipophilic side chains were combined resulting in

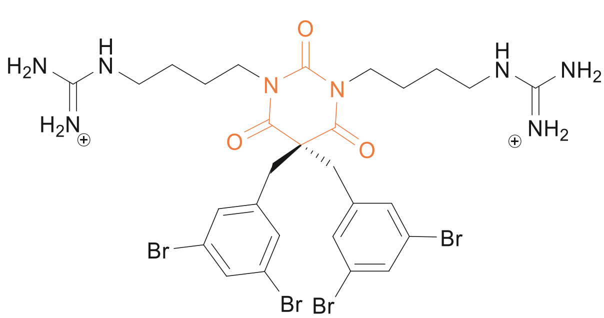

Fig. 1. Lead structure **1aG** from our previous study [28] with the barbituric acid core highlighted in orange.

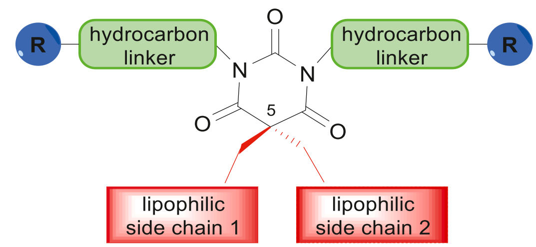

Fig. 2. General structure of the tetrasubstituted barbituric acids used in this study. R = cationic group. The individual parts were evaluated in five series, namely screening of the cationic moieties (*series 1*), lipophilic side chains (*series 2* side chain 1 = side chain 2 and *series 3* side chain 1 ≠ side chain 2), hydrocarbon linker chains (*series 4*) and optimized structures (*series 5*).

derivatives with mixed side chains.

The hydrocarbon linkers (Fig. 2) were chosen on the premises of investigating the influence of the flexibility and distance of the cationic groups relative to the barbiturate core. Linear hydrocarbon chains of 2–6 carbons length gave flexible linkers, while cyclic hydrocarbon linkers (cyclobutyl and cyclohexyl) gave more restricted analogues. Compounds with varying linkers are included in *series 4*.

Based on the results from *series 4* we prepared a range of compounds included in *series 5*, having *n*-propyl linkers.

2.2. Synthesis

Our previously reported synthesis of 5,5-dialkylated barbiturates provided amine and guanidine analogues in six or eight synthetic steps, respectively [28]. In the present study, the demand for a large library of compounds prompted us to develop a shorter synthetic approach. Both amines and guanidines were successfully obtained in three steps from barbituric acid.

The synthetic strategy started with the preparation of symmetrical (**3a-j**) or unsymmetrical (**3k-q**) 5,5-dialkylated barbituric acid (Scheme 1). For the preparation of identically dialkylated compounds, barbituric acid **2** could be di-substituted at the C-5 carbon using organohalides to give **3a-j** in 5–92% yield in the presence of $NaHCO_3$ in PEG-400 (Scheme 1-I). Low yields (5–35%) were obtained for primary alkyl halides and heteroaryls, whereas haloaryls delivered good to excellent yields (70–92%). PEG-400 served as a green solvent alternative and phase transfer catalyst [33]. Commonly applied conditions [34] employing an inorganic base such as K_2CO_3 and benzyltriethylammonium chloride (BTEAC) in $CHCl_3$ performed worse. Weak electrophiles, such as alkyl halides posed an inherent problem. Harsher conditions were needed, which inevitably led to additional *N*-alkylation due to the acidity of the *N*–H protons ($pK_a = 7–9$ [35,36] compared to the pK_a (H–C5) = 3–4 [36,37]).

To obtain unsymmetrically 5,5-dialkylated barbituric acids **3k-q** a different approach was needed, since mono-alkylation enhances the nucleophilicity of the barbiturate C-5 carbon leading to inevitable dialkylation [37]. We investigated several reported methods for selective monoalkylation and *in situ* reductions [37–39], which did not work well in our hands. We therefore decided to use a stepwise approach as shown in Scheme 1-II. Barbituric acid **2** and 3,5-dibromobenzaldehyde were condensed [40] to give compound **4** and subsequent reduction with $NaBH_4$ in EtOH [41] gave the C-5 mono-substituted derivative **5** in 80% yield. We found **5** being an approximate 2:1 mixture of the keto and enol form. This mixture was alkylated a second time using the conditions employed for 5,5-dialkylation of barbituric acid to deliver intermediates **3k-q**. Yields ranged from 5 to 61%, depending on the reactivity of the employed electrophiles.

Starting from intermediates **3**, a wide range of *N,N′*-dialkylated barbituric acid derivatives were prepared, employing a range of methods for *N*-alkylation depending on the availability of reactants

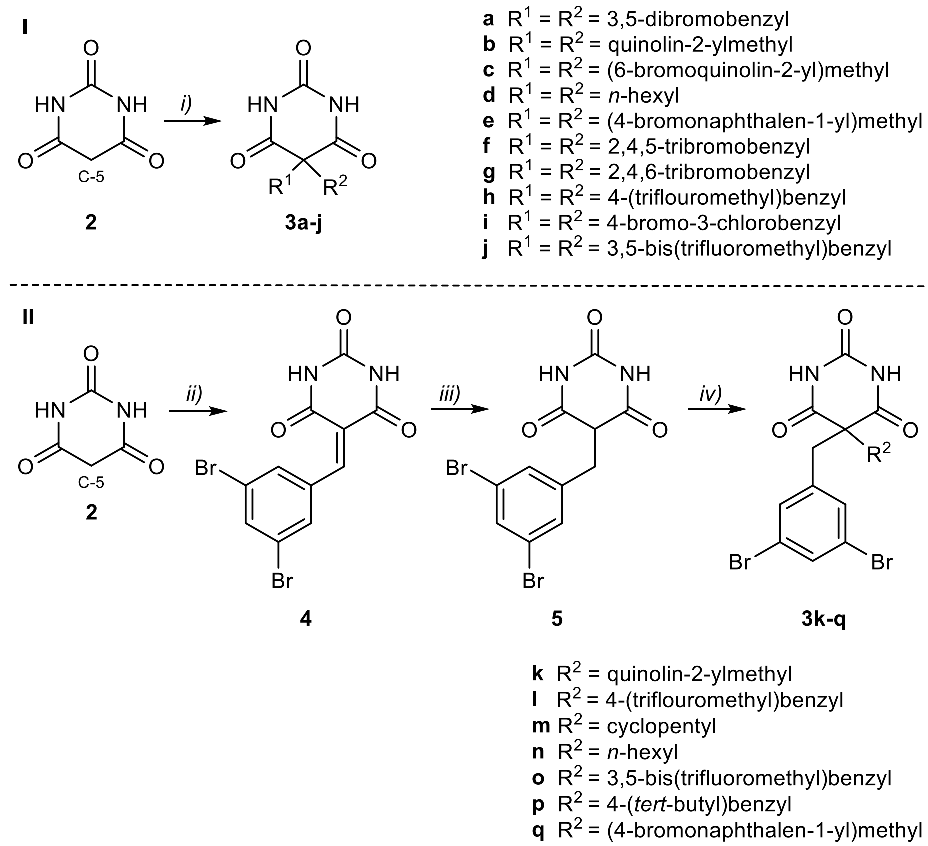

Scheme 1. Synthesis of core structures **3a-q**. **I**: Reaction conditions: i) Alkylating agent, $NaHCO_3$, PEG-400, 45–100 °C, 5–92%. **II**: Reaction conditions: ii) 3,5-dibromobenzaldehyde, H_2O/EtOH (3:1), 105 °C, 58%; iii) $NaBH_4$, EtOH, 70 °C, 80%; iv) Alkyl bromide, $NaHCO_3$, PEG-400, 50–100 °C, 5–61%.

(Scheme 2).

All compounds synthesized are summarized in Tables 1–5. Compounds denoted with capital **A** have an amine as a cationic group and those denoted with capital **G** have cationic guanidino groups, correspondingly. The compounds are grouped into five series (*series 1–5*) based on their structural variations.

Series 1 (Table 1) encompasses compounds with varying cationic groups, while the C-5 substituents (3,5-dibromobenzyl) and hydrocarbon linker (*n*-butyl) were kept unchanged. To obtain the methylated amines and pyridinium containing compounds **6a-9a**, 5,5-bis(3,5-dibromobenzyl)barbituric acid **3a** was *N,N′*-dialkylated with either 1-bromo-4-chlorobutane or 1,4-dibromobutane and Cs_2CO_3 in acetone (Scheme 2-**I**). Subsequent S_N2 substitution of the terminal halo substituent with methylated ammonia or pyridine in acetonitrile at elevated temperature led to compounds **6a-9a** in 33–88% yield. Having a bromide as leaving group proved to be necessary for substitution with methylamine and dimethylamine. Substitutions were only successful with organic solutions of the amines, while hydrohalo salts of the amines could not be used. An optimized method for preparation of the previously reported 1° amine **1aA** and guanidine **1aG** [28] is described in the next paragraph.

Compound *series 2* (Scheme 2-II) contained identically 5,5-disubstituted barbiturates and *series 3* (Scheme 2-II) contained unsymmetrically 5,5-disubstituted barbiturates, while the hydrocarbon linker for both series was a *n*-butyl chain. As cationic groups, both amino (**A**) or guanidino (**G**) groups were explored. Compounds were synthesized from the barbituric acid derivatives **3b-g** or **3k-q** by *N,N′*-dialkylation with *N*-Boc protected 4-aminobutanol or *N,N′*-di-Boc protected 1-(4-hydroxybutyl)guanidine (Scheme 2-**II**). Due to the low p*K*a value of the imidic hydrogens [42] a Mitsunobu protocol using diisopropylazodicarboxylate (DIAD) and PPh_3 could be employed. Removal of the Boc protection mediated by TFA:DCM and subsequent reversed phase (RP) chromatography gave target *series 2* ($R^1 = R^2$) and *series 3* ($R^1 \neq R^2$) as di-TFA salts in 20–89% yield. In some cases the TFA salts were contaminated with reduced DIAD, which could largely be removed by trituration with Et_2O. Interestingly, employment of the more reactive coupling system 1,1′-(azodicarbonyl)dipiperidine ADDP/P(n-Bu$)_3$ and *N,N,N′,N′*-tetramethyldicarboxamide TMAD/P(n-Bu$)_3$ [42] led to lower yields and mono-alkylation.

Series 4 (Table 4) contained compounds with varying linkers, such as aliphatic chains with 2–6 carbons length as well as cyclic hydrocarbons. The C-5 substituents were set to 3,5-dibromobenzyl and the cationic groups were either amino (**A**) or guanidino (**G**) groups. As the relevant linkers were commercially available as *N*-Boc-amino alcohols, we decided to explore the above Mitsunobu protocol in a stepwise synthetic approach (Scheme 2-**III**). The 5,5-bis(3,5-dibromobenzyl)barbituric acid **3a** was *N,N′*-dialkylated with the appropriate Boc-protected amino alcohol using the Mitsunobu conditions followed by TFA:DCM treatment to obtain compounds **12aA-19aA** in 23–73% over 2 steps. Treatment of the amines **12aA-19aA** with *N,N′*-Di-Boc-1*H*-pyrazole-1-carboxamidine and DIPEA or DBU, followed by Boc removal with TFA in DCM delivered the guanidines **12aG-18aG** in 14–92% yield. Employing the well-known and cheaper alternative *N,N′*-bis(*tert*-butoxycarbonyl)-*S*-methylisothiourea [43,44] led to an inseparable mixture of Boc protected amine and Boc protected guanyl compounds.

Based on the bioactivities observed for *series 1–4*, a fifth collection of compounds (*series 5*, Table 5), exploring the effect of an *n*-propyl linker more broadly, was prepared. *Series 5* contained selected identically (*series 2*) or unsymmetrically (*series 3*) 5-substituted barbiturates with both 1-propyl-3-amino (**A**) or 1-propyl-3-guanidino groups (**G**) as *N,N′*-substituents. Starting from compounds **3c, e, h, i, j, l, p**, *N,N′*-alkylation with *N*-Boc *n*-propylbromide, followed by TFA mediated Boc removal and purification by RP chromatography gave identically **13(c,e,h,i,j)A**

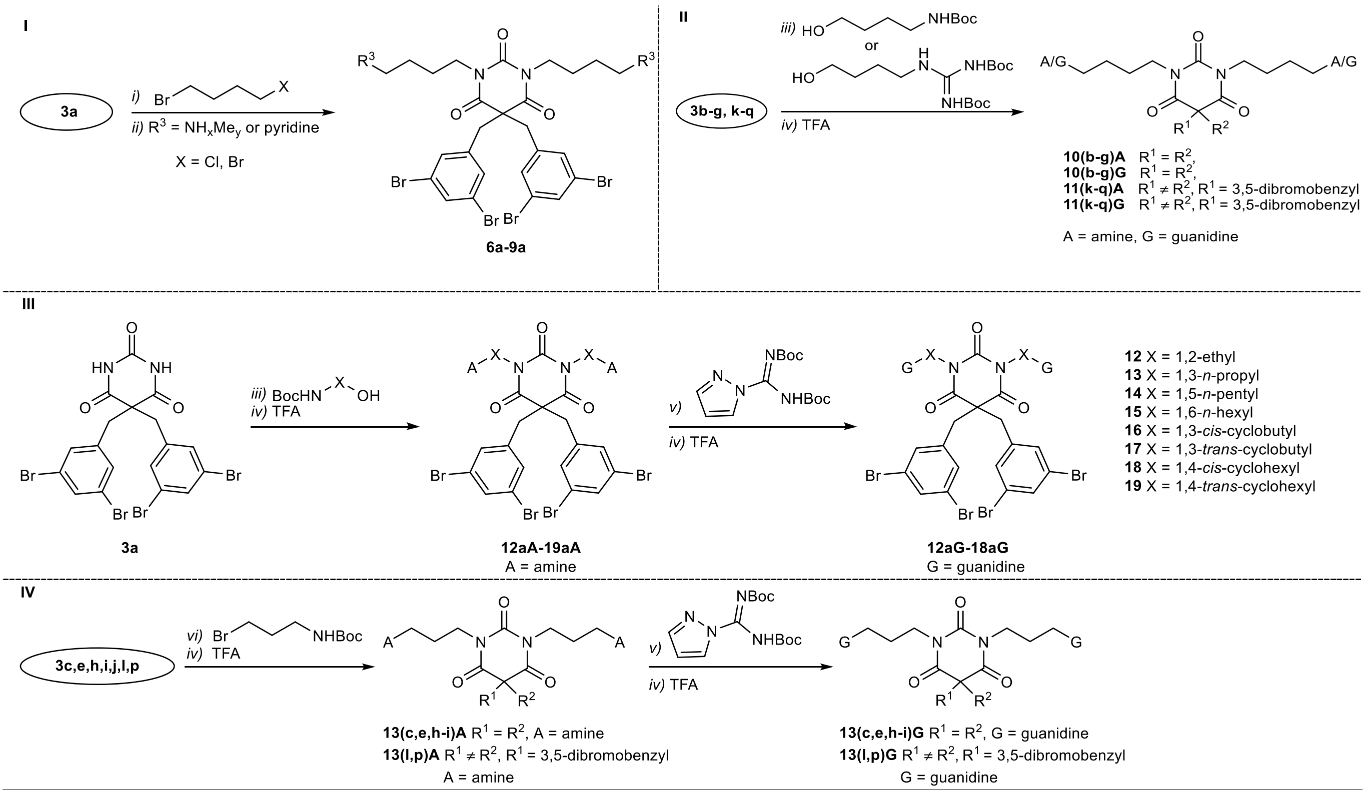

Scheme 2. Synthetic approach to target *series 1–5*, where **A** denotes amine head groups and **G** the guanidine derivatives. All final compounds were obtained as di-TFA salts. **I** R^3 = NH_2Me, $NHMe_2$, NMe_3, pyridinyl; Reaction conditions: i) Cs_2CO_3, acetone, 55 °C, 57-85%; ii) MeCN, 70–90 °C, 33–88%. **II** Reaction conditions: iii) DIAD, PPh_3, anhydrous DCM or THF, 0 °C to r.t., iv) TFA, DCM, r.t., 20–89% o2s. **III** Reaction conditions: iii) DIAD, PPh_3, anhydrous DCM or THF, 0 °C to r.t., iv) TFA, DCM, r.t., 23–73% o2s, v) DIPEA or DBU, THF, 45 °C, 14–92% o2s (after TFA deprotection). **IV** Reaction conditions: vi) base, TBAI, acetone, 50–70 °C, *then* iv) TFA, DCM, r.t., 34–76% o2s (after TFA deprotection); v) DIPEA or DBU, THF, 45 °C, *then* iv) TFA, DCM, r.t., 20–91% o2s (after TFA deprotection).

Table 1
Antimicrobial activity (MIC in μg/mL) against bacterial reference strains and haemolytic activity against human RBC (EC_{50} in μg/mL) for compounds in *series 1*.

Core structure	Comp. ID	R^3	CLogP[a]	Antimicrobial activity				EC_{50}[b]
				S. a	B. s	E. c	P. a	
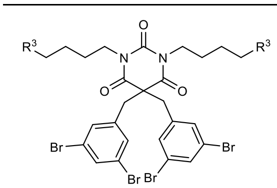	**1aG**[c]	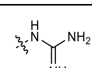	−2.39	2	2	2	8	62
	1aA[d]	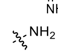	−1.20	4	2	4	8	79
	6a	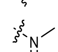	−0.66	8	4	8	16	73
	7a	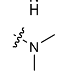	−0.52	8	4	8	64	157
	8a	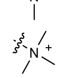	0.42	4	8	128	256	>539
	9a	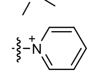	0.72	2	4	8	128	>559
Ciprofloxacin				0.06	<0.03	<0.03	0.25	

Bacterial reference strains: S. a – *Staphylococcus aureus* ATCC 9144, B.s – *Bacillus subtilis* 168, E. c – *Escherichia coli* ATCC 25922, and P. a – *Pseudomonas aeruginosa* ATCC 27853. All compounds were tested as di-TFA salts.
[a] CLogP values were calculated for the respective non protonated cationic group (calculated with ChemBioDraw Ultra v19.0.0.1.28).
[b] Values given as greater than correspond to the highest concentration (500 μM) tested in the RBC assay.
[c] We have reported this compound previously having the following MIC values: S. a: 1 μg/mL, B. s: 2 μg/mL, E. c: 2 μg/mL, P. a: 4 μg/mL [28].
[d] Values were taken from Ref. [28].

or unsymmetrically **13(l,p)A** substituted primary amines in 34–76% yield (Scheme 2-**IV**). The Mitsunobu protocol was evaluated but discarded due to difficulties with purification of some compounds. Treatment of the primary amines with *N,N′*-di-Boc-1*H*-pyrazole-1-carboxamidine and DIPEA, followed by TFA facilitated Boc removal and RP flash chromatography purification yielded the respective guanidines **13(c,e,h,i,j,l,p)G** in 20–91% yield.

2.3. SAR analysis

All compounds were screened for antimicrobial activity against antibiotic susceptible Gram-positive and Gram-negative reference

Table 2
Antimicrobial activity (MIC in µg/mL) against bacterial reference strains and haemolytic activity against human RBC (EC_{50} in µg/mL) for compounds in *series 2*.

Core structure	Comp. ID	$R^1 = R^2$	A/G	CLogP[a]	Antimicrobial activity				EC_{50}[b]
					S. a	B. s	E. c	P. a	
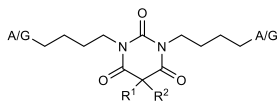	**10bA**	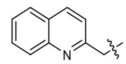	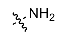	2.53	256	64	>256	>256	>390
	10bG		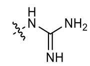	2.53	8	16	128	>256	>432
	10cA	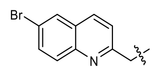	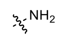	3.39	16	4	256	256	>469
	10cG		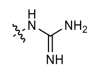	3.39	2	4	16	128	461
	10dA	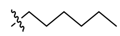	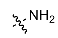	3.87	16	8	32	64	>333
	10dG		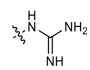	3.87	2	2	4	16	143
	10eA	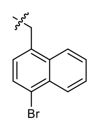	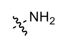	4.68	2	2	4	4	27
	10eG		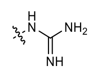	4.68	4	4	4	8	36
	10fA	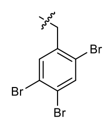	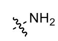	5.03	4	4	8	8	27
	10fG		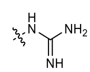	5.03	4	4	4	8	32
	10gA	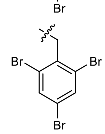	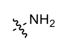	5.03	2	2	4	4	30
	10gG		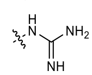	5.03	2	1	4	4	30

Bacterial reference strains: S. a – *Staphylococcus aureus* ATCC 9144, B.s – *Bacillus subtilis* 168, E. c – *Escherichia coli* ATCC 25922, and P. a – *Pseudomonas aeruginosa* ATCC 27853. All compounds were tested as di-TFA salts.

[a] CLogP values were calculated for the respective lipophilic side chains (calculated with ChemBioDraw Ultra v19.0.0.1.28).

[b] Values given as *greater than* correspond to the highest concentration (500 µM) tested in the RBC assay.

strains (Tables 1–5). Haemolytic activity against human red blood cells (RBCs), expressed by the EC_{50} value, was used as a measurement of cytotoxicity. We have earlier reported compounds **1aA** and **1aG** [28], which here are used as reference compounds together with the known antibiotic ciprofloxacin as a positive control. The descriptors for amine derivatives (**A**) and guanidine derivatives (**G**) are omitted for derivatives with other cationic groups.

2.3.1. *Compound series 1: Exploring the cationic head group (R^3)*

First, we set out to investigate the influence of the effective charge of the cationic groups (Table 1, R^3 group and Fig. 2, blue space holders). Upon *N*-methylation the electron density at the nitrogen increases, as does its basicity, but the polarity decreases. Successive introduction of one (**6a**), two (**7a**) or three (**8a**) methyl groups had no noteworthy influence on the activity against the Gram-positive strains (MIC: 4–8 µg/mL), but the activity against the Gram-negative strains dropped considerably for compound **8a** (MIC: 128–256 µg/mL). It is suggested that, among other factors, the electrostatic interaction between these compounds and bacterial membrane plays an important role in the compound's activity [45]. Successive introduction of methyl groups lowers the effective charge of the amine head groups, thus reducing their interaction with the lower charge per area membrane of Gram-negative bacteria compared to Gram-positive strains [46]. Additionally, quaternary ammonium compounds (quats or QACs) are known for their impaired ability to cross the outer membrane of Gram-negative *Pseudomonas aeruginosa* (*P. aeruginosa*) [47]. Recent studies showed generally impaired uptake of compounds containing methylated primary amines in *E. coli* [31]. Despite that presumably lower uptake, secondary (**6a**) and tertiary amines (**7a**) were still active against *E. coli* (MIC: 8 µg/mL). By replacing the quaternary trimethylated ammonium (**8a**) with a pyridinium group (**9a**), the activity against the Gram-positive strains improved (MIC: 2–4 µg/mL) and the activity against *E. coli* was restored (MIC: 8 µg/mL), probably due to increased accumulation [32]. Tertiary (**7a**), EC_{50}: 157 µg/mL) and quaternary amines (**8a** and **9a**; both EC_{50}: >500 µg/mL) displayed lower haemolytic activity compared to the primary (**1aA**, EC_{50}: 79 µg/mL) and secondary (**6a**, EC_{50}: 73 µg/mL) amines.

The quaternary ammonium compound **8a** exhibited narrow-spectrum antimicrobial activity against Gram-positive strains and was non-haemolytic. Compared to the above investigated head groups, the recently reported amine (**1aA**) and guanidine derivatives (**1aG**) appeared to be the most effective against the Gram-negative strains, thus rendering them suitable for broad-spectrum applications. The consecutively developed compounds were therefore synthesized with either amino or guanidino groups.

2.3.2. *Compound series 2: Exploring new lipophilic side chains ($R^1 = R^2$)*

In *series 2*, the influence of heterocyclic, aliphatic and highly brominated lipophilic side chains (Table 2, R^1/R^2 groups and Fig. 2, red space holders) on the biological activity was examined. Both side chains employed were identical.

The antimicrobial activity for the amine barbiturates **10(b-g)A** ranged from MIC: 2–256 µg/mL and for the guanidine barbiturates **10(b-g)G** from MIC: 1–16 µg/mL against the Gram-positive strains *Staphylococcus aureus* (*S. aureus*) and *Bacillus subtilis* (*B. subtilis*). Against the Gram-negative strains *E. coli* and *P. aeruginosa* both, the amine and guanidine derivatives, showed MIC values of 4 – >256 µg/mL. We included quinoline and 6-bromoquinoline as heterocyclic alternatives. The amine derivative **10bA** (R^1/R^2 = quinolin-2-ylmethyl) was neither antibacterial (MIC: ≥64 µg/mL) nor haemolytic, whereas the guanidine derivative **10bG** exhibited some activity against the Gram-positive strains (MIC: 8–16 µg/mL).

Table 3
Antimicrobial activity (MIC in μg/mL) against bacterial reference strains and haemolytic activity against human RBC (EC_{50} in μg/mL) for compounds in *series 3*.

Core structure	Comp. ID	R^2	A/G	CLogP[a]	Antimicrobial activity				EC_{50}[b]
					S. a	B. s	E. c	P. a	
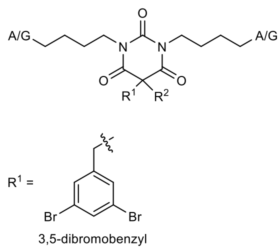	**11kA**	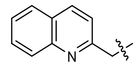	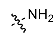	3.45	32	8	128	256	>444
	11kG		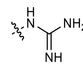	3.45	2	4	32	32	450
	11lA	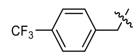	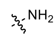	3.95	16	8	32	64	342
	11lG		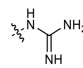	3.95	2	4	2	16	161
	11mA	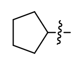	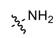	3.58	16	8	64	64	>407
	11nA	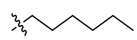	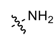	4.12	4	4	16	16	144
	11nG		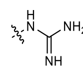	4.12	2	4	4	8	58
	11oA	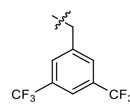	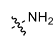	4.39	8	2	8	8	93
	11oG		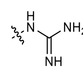	4.39	2	2	2	4	36
	11pA	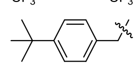	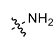	4.42	4	4	8	8	82
	11pG		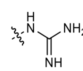	4.42	2	2	2	4	39
	11qA	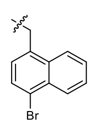	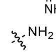	4.52	4	4	4	8	47
	11qG		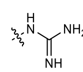	4.52	1	4	4	8	58

Bacterial reference strains: S. a – *Staphylococcus aureus* ATCC 9144, B.s – *Bacillus subtilis* 168, E. c – *Escherichia coli* ATCC 25922, and P. a – *Pseudomonas aeruginosa* ATCC 27853. Guanidyl barbiturate **11mG** could not be obtained. All compounds were tested as di-TFA salts.

[a] CLogP values were calculated for the respective lipophilic side chains and are presented as the average for the two substituents. (calculated with ChemBioDraw Ultra v19.0.0.1.28).

[b] Values given as *greater than* correspond to the highest concentration (500 μM) tested in the RBC assay.

Upon inserting a bromine in the 6-position for **10cA** (R^1/R^2 = (6-bromoquinolin-2-yl)methyl) the CLogP rose considerably, and the amine derivative became active against the Gram-positive bacteria (MIC: 4–16 μg/mL). The respective guanidine **10cG** was found to be active against both the Gram-positive strains and *E. coli* (MIC: 2–16 μg/mL), while being nonhaemolytic. The bromine substituent seemed to be essential for good antimicrobial activity against Gram-positive strains and *E. coli*.

In the next step we replaced the aromatic side chains by alkyl chains as found in antimicrobial quats [48,49]. We decided to incorporate two hexyl chains, which mimic the single long alkyl chain commonly found in quats [50]. The amine derivative **10dA** (R^1/R^2 = *n*-hexyl) showed weak activity against all bacterial strains (MIC: 8–64 μg/mL), whereas the guanidine derivative **10dG** showed high antibacterial activity with MIC values of 2–4 μg/mL against all strains except for *P. aeruginosa*. Haemolysis was still moderate, with EC_{50}: 143 μg/mL. Interestingly, the shorter hexyl chains perform just as good as the longer alkyl chains in quats [48], suggesting that the overall hydrophobic bulk is more important than the actual chain length.

Compounds **10e** (R^1/R^2 = (4-bromonaphthalen-1-yl)methyl) were prepared based on the previously reported (4-fluoronaphthalen-1-yl) methyl barbituric acid [28]. Introduction of electron withdrawing fluorine into molecules is known to hamper *in vivo* oxidation of aromatic side chains during Phase I metabolism [51,52]. Replacing the fluorine for a bromine increases the hydrophobic bulk, while having similar electronic effects [53]. Surprisingly, the amine derivative **10eA** was equally potent as the guanidine **10eG** with MIC values of 2–8 μg/mL against all reference strains. However, both, **10eA** and **10eG**, were also highly haemolytic (EC_{50}: 27–36 μg/mL).

Previously, we have found bromo substituents on the phenyl ring having a positive effect on the biological activity, with 3,5-dibromophenyl providing the highest activity [26]. We therefore prepared derivatives **10fA** and **10fG** (R^1/R^2 = 2,4,5-tribromobenzyl) and **10gA** and **10gG** (R^1/R^2 = 2,4,6-tribromobenzyl) being at the far end of the hydrophobicity scale. They all displayed potent antibacterial activity, with MIC values ≤8 μg/mL against all strains. However, haemolytic activity also increased for all these compounds (EC_{50}: 27–32 μg/mL). The positioning of the bromines on the phenyl ring had a minor influence on antibacterial activity, with **10gA** and **10gG** being most potent.

In summary, halogenated heterocycles are promising side chains for narrow-spectrum application. The hydrophobicity of the C-5 substituents had the greatest influence, while the structure being secondary. When exceeding CLogP ≈4.50, the structures mostly became too haemolytic to be of interest for further studies.

2.3.3. Compound series 3: Exploring mixed lipophilic groups ($R^1 \neq R^2$)

A series of compounds containing two different side chains were prepared to tune lipophilicity and side chain structure with respect to antimicrobial activity and haemolytic activity. We intended to pair the potent 3,5-dibromobenzyl side chain (R^1) with side chains (R^2) of different varying lipophilicity (Table 3; R^2 group; Fig. 2, red space holders).

First, we chose to incorporate previously documented non potent side chains (see *series 2* and previously reported [26,28]) in compounds **11k** (R^2 = quinolin-2-ylmethyl and **11l** (R^2 = 4-(trifluoromethyl) benzyl). The amine derivatives **11kA** and **11lA** displayed weak activity, mainly against *B. subtilis* (MIC: 8 μg/mL) but can be considered non-haemolytic. The guanidine derivatives **11kG** and **11lG** were still

Table 4
Antimicrobial activity (MIC in μg/mL) against bacterial reference strains and haemolytic activity against human RBC (EC_{50} in μg/mL) for compounds in *series 4*.

Core structure	Comp. ID	X	A/G	CLogP[a]	Antimicrobial activity				EC_{50}
					S. a	B. s	E. c	P. a	
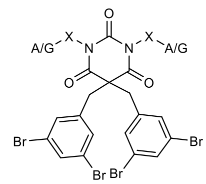	**12aA**	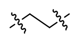	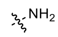	1.75	4	4	4	8	39
	12aG		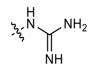	1.75	2	2	4	16	164
	13aA	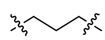	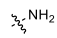	2.28	4	4	8	8	99
	13aG		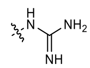	2.28	2	2	4	8	187
	14aA	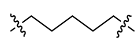	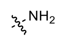	3.34	4	4	8	8	24
	14aG		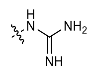	3.34	4	4	4	8	29[b]
	15aA	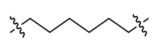	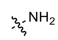	3.87	4	4	4	16	30
	15aG		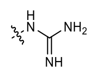	3.87	4	4	4	32	57[b]
	16aA	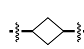	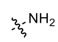	2.24	8	4	4	8	50
	16aG		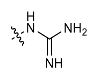	2.24	2	2	4	8	75
	17aA	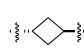	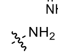	2.24	4	4	4	8	93
	17aG		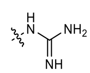	2.24	2	4	4	8	62
	18aA	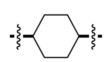	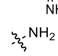	3.35	4	4	4	8	15
	18aG		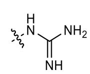	3.35	2	1	4	4	30
	19aA	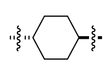	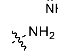	3.35	2	2	2	4	16

Bacterial reference strains: S. a – *Staphylococcus aureus* ATCC 9144, B.s – *Bacillus subtilis* 168, E. c – *Escherichia coli* ATCC 25922, and P. a – *Pseudomonas aeruginosa* ATCC 27853. All compounds were tested as di-TFA salts. Compound **19aG** was not obtained in satisfying purity.
[a] CLogP values were calculated for the respective hydrocarbon linkers (calculated with ChemBioDraw Ultra v19.0.0.1.28).
[b] Precipitation in the RBC assay observed.

almost non-haemolytic (EC_{50}: down to 161 μg/mL) and displayed potent activity against the Gram-positive strains (MIC: 2–4 μg/mL).

The derivative **11lG** showed additionally good activity against the Gram-negative *E. coli* (MIC: 4 μg/mL). The superior performance of **11lG** over **11kG** may be attributed to the higher average CLogP value of the lipophilic side chain of **11lG**. The polar nitrogen atom in the quinolinyl side chain (**11lG**) might also reduce the compounds' activity.

Next, we tested two hydrocarbon analogues **11m** (R^2 = cyclopentyl) and **11n** (R^2 = *n*-hexyl), with comparable average hydrophobicity to **11k** and **11l,** respectively. Compound **11mA** was potent against both Gram-positive strains and non-haemolytic. The amine derivative **11nA** was mainly acting against the Gram-positive strains (MIC: 4 μg/mL) but showed 3-fold higher haemolytic activity compared to **11lA**. The guanyl derivative **11nG** exhibited potent antibacterial activity, with MIC-values of 2–8 μg/mL against all strains tested. Even though its average CLogP was only marginally higher than **11lG**, its haemolytic activity was pronouncedly higher (EC_{50}: 58 μg/mL). The compounds **11m** and **11n** indicated that a combination of an aromatic and a hydrocarbon lipophilic side chain leads to higher haemolytic activity, compared to two aromatic side chains.

To study the influence of the structure of the lipophilic side chains we prepared structurally different, but of similar lipophilicity, compounds **11o** (R^2 = 3,5-bis(trifluoromethyl)benzyl), **11p** (R^2 = 4-(*tert*-butyl) benzyl), and **11q** (R^2 = (4-bromonaphthalen-1-yl)methyl). All their amine derivatives displayed low MIC values of 2–8 μg/mL against all reference strains and **11oA** was least haemolytic (EC_{50}: 93 μg/mL). Upon guanylation, a further improvement in antimicrobial activity was achieved, but haemolytic activity was also increased. Thus, **11oG** and **11pG** became twice as potent and haemolytic (EC_{50}: 36–39 μg/mL), rendering them unfavorable for systemic *in vivo* treatment. The bromonaphthyl containing **11qG** became more potent against *S. aureus* (MIC: 1 μg/mL), yet haemolytic activity (EC_{50}: 58 μg/mL) was still unfavorably high. No clear trend for the antimicrobial activity could be deduced, based on the structure of the lipophilic side chains.

Taken all together, **11kG** displayed promising narrow-spectrum activity against Gram-positive strains and absence of haemolytic activity. Compounds **11oG** and **11pG** are highly potent derivatives but displayed high haemolytic activity.

2.3.4. Compound series 4: Exploring the hydrocarbon linker chain (X)

We incorporated various linear and cyclic hydrocarbon linkers (Tables 4 and X group; Fig. 2, green space holder) between the central scaffold and the cationic residue. 3,5-Dibromobenzyl was kept fixed as the lipophilic side chain and the previously reported compounds **1aA** and **1aG** (both X = *n*-butyl) served as reference substances for comparison. Shortening or elongating the alkyl chains to 2, 3, 5 or 6 methylene groups (**12aA-15aA**) led to no significant change in antibacterial activity (MIC: 4–16 μg/mL against all strains). The haemolytic activity increased slightly compared to **1aA** (X = *n*-butyl), except for **13aA** (X = *n*-propyl), which became slightly less haemolytic. So far, guanidine derivatives tended to have a higher haemolytic activity (*vide supra)* compared to amine derivatives. In contrast, **13aG** (X = *n*-propyl) and

Table 5
Antimicrobial activity (MIC in μg/mL) against bacterial reference strains and haemolytic activity against human RBC (EC_{50} in μg/mL) for compounds in *series 5*.

Core structure	Comp ID	R^1	R^2	A/G	CLogP[a]	Antimicrobial activity				EC_{50}[b]
						S. a	B. s	E. c	P. a	
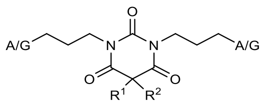	**13cA**	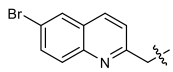	$R^2 = R^1$	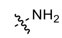	3.39	32	8	64	256	>455
	13cG			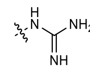	3.39	8	4	64	>128	>497
	13hA	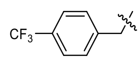	$R^2 = R^1$	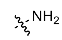	3.87	64	16	64	128	>393
	13hG			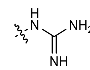	3.87	8	4	128	256	>435
	13iA	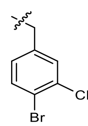	$R^2 = R^1$	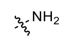	4.08	8	4	8	16	323
	13iG			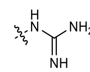	4.08	2	2	8	32	348
	13eA	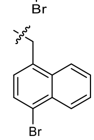	$R^2 = R^1$	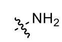	4.68	2	2	4	4	23
	13eG			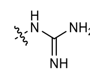	4.68	2	2	4	8	61
	13jA	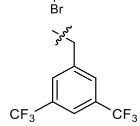	$R^2 = R^1$	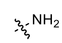	5.03	8	4	8	8	176
	13jG			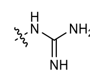	5.03	4	2	8	16	445
	13lA	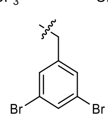	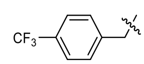	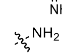	3.95	32	8	16	32	>438
	13lG			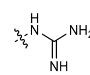	3.95	4	4	16	64	>480
	13pA	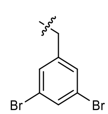	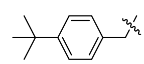	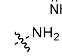	4.42	4	2	8	8	47
	13pG			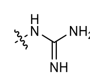	4.42	1	1	2	16	169

Bacterial reference strains: S. a – *Staphylococcus aureus* ATCC 9144, B.s – *Bacillus subtilis* 168, E. c – *Escherichia coli* ATCC 25922, and P. a – *Pseudomonas aeruginosa* ATCC 27853. All compounds were tested as di-TFA salts.

[a] CLogP values were calculated for the respective lipophilic side chains. For non-identical side chains, the value stated is the average of both individual side chains. Values were calculated for substituted benzyl groups (calculated with ChemBioDraw Ultra v19.0.0.1.28).

[b] Values given as *greater than* correspond to the highest concentration (500 μM) tested in the RBC assay.

12aG (X = ethyl) were observed to exhibit 2-fold and 4-fold decreased haemolytic activity, respectively, compared to their amine counterparts. The activity against the Gram-positive strains was slightly improved, whereas the potencies against the Gram-negative *P. aeruginosa* were retained or a little diminished. The derivatives **14aA** and **14aG** (X = *n*-pentyl) displayed virtually the same MIC and EC_{50} values, whereas **15aG** (X = *n*-hexyl) was less potent against *P. aeruginosa* (MIC: 32 μg/mL) compared to **15aA** (X = *n*-hexyl) (MIC: 16 μg/mL). Both guanylated compounds were less potent than the previously investigated derivative **1aG** (X = *n*-butyl) and their haemolytic levels were comparably high (EC_{50}: 29–57 μg/mL). Compounds **14aG** (X = *n*-pentyl) and **15aG** (X = *n*-hexyl) led also to precipitation in the RBC assay upon sample preparation, possibly due to their higher overall hydrophobicity, demonstrating an unfavorable solubility profile.

To investigate if the conformational freedom of the linker influenced the compounds potency, 1,3-cyclobutyl and 1,4-cyclohexyl were used as surrogates for the *n*-propyl and *n*-butyl chains, taking advantage of their restricted spatial arrangement. Compounds **16aA** (X = *cis*-1,3-cyclobutyl) and **17aA** (X = *trans*-1,3-cyclobutyl) displayed the same MIC values (4–8 μg/mL) as **13aA** (X = *n*-propyl) against all strains, but **16aA** (*cis*) was almost twice as haemolytic as **13aA** (X = *n*-propyl) and **17aA** (*trans*). Their guanylated counterparts **16aG** (*cis*) and **17aG** (*trans*), were more potent against the Gram-positive strains, but no change in MIC was observed against the Gram-negative strains. Both derivatives exhibited considerably higher haemolytic activity compared to **13aG** (X = *n*-propyl).

While being equally haemolytic (EC_{50}: 15 μg/mL) and 5-times more haemolytic than **1aA** (X = *n*-butyl), **19aA** (X = *trans*-1,4-cyclohexyl) was twice as potent as **18aA** (X = *cis*-1,4-cyclohexyl). The guanidine derivative **18aG** (*cis*) was highly potent (MIC: 1–4 μg/mL) against all bacterial strains, but its haemolytic activity was also too high to be of therapeutical value for systemic application. Of note, the guanylated derivative (**18aG**) was nevertheless less haemolytic than the amine derivative (**18aA**).

In summary, compounds with rigid cyclic linkers showed similar or slightly higher potency compared to their linear analogues, but they tended to be more haemolytic. Furthermore, compounds with pentyl and hexyl linkers showed furthermore decreased water solubility. The amine derivatives having ethyl, *n*-propyl or *n*-butyl linkers displayed similar antibacterial bioactivity profiles, whereas the equivalent guanidine derivatives displayed descending antimicrobial activity as follows: *n*-butyl > *n*-propyl > ethyl. The best balance between high antimicrobial activity and low haemolytic activity was presented by compounds having *n*-propyl hydrocarbon linker chains.

2.3.5. Compound series 5: Investigating compounds with a n-propyl hydrocarbon linker

In *series 5* (Table 5), we studied the effect of the *n*-propyl linker more closely due to the promising balance between high antimicrobial activity and low haemolytic activity seen in *series 4*. We selected the lipophilic side chains (R^1/R^2) based on our previous findings. We reasoned that compounds **13c**, **13h** and **13l** would mainly act against

Gram-positive strains, whereas compounds **13e**, **13i**, **13j** and **13p** should provide a higher broad-spectrum activity. Amines **13cA** (R^1/R^2 = (6-bromoquinolin-2-yl)methyl) and **13hA** (R^1/R^2 = 4-(trifluoromethyl) benzyl) displayed generally low antibacterial activity against all strains (MIC: 8–256 μg/mL). However, the guanyl equivalents **13cG** and **13hG** exhibited fair activity and selectivity for Gram-positive strains (MIC: 4–8 μg/mL) and weak activity towards Gram-negative strain (MIC: ≥64 μg/mL). None of the four compounds was haemolytic.

Compound **13iA** (R^1/R^2 = 4-bromo-3-chlorobenzyl) displayed good activity against all strains (MIC: 4–8 μg/mL) except for the Gram-negative *P. aeruginosa* (MIC: 16 μg/mL). The guanyl derivative **13iG** displayed further improved activity against the Gram-positive strains (MIC: 2 μg/mL), but the activity against *P. aeruginosa* was lost. Noteworthy, the amine **13iA** and guanidine **13iG** derivatives were non-haemolytic (EC_{50}: >300 μg/mL), despite the relatively high CLogP values of their lipophilic side chains.

Derivatives **13eA** and **13eG** contained the bulky bromo-naphthyl (R^1/R^2 = (4-bromonaphthalen-1-yl)methyl) group. The amine derivative **13eA** was highly potent (MIC: 2–4 μg/mL) against all strains, but too haemolytic to be of practical use (EC_{50}: 23 μg/mL). Upon guanylation, **13eG** still had good activity against all strains (MIC: 2–8 μg/mL) and an almost three-fold decrease in haemolytic activity (EC_{50}: 61 μg/mL) was observed. The relatively high haemolytic activity was still unfavorable, but the positive effect of exchanging *n*-butyl linkers (**10eG**) for *n*-propyl linkers (**13eG**) was well demonstrated.

The amine derivative **13jA**, featuring 3,5-bis(trifluoromethyl)benzyl side chains, was potent against all strains (MIC: 4–8 μg/mL) and displayed low haemolytic activity (EC_{50}: 176 μg/mL). The guanyl analogue **13jG** was twice as potent against the Gram-positive strains, while the activity against *P. aeruginosa* was reduced (MIC: 16 μg/mL). Pleasingly, the guanylation rendered the compound non-haemolytic.

The unsymmetrically C-5 substituted amine **13lA** (R^1 = 3,5-dibromobenzyl, R^2 = 4-(trifluoromethyl)benzyl) displayed acceptable activity only against *B. subtilis* (MIC: 8 μg/mL). The guanyl derivative **13lG** exhibited good activity against both Gram-positive strains (MIC: 4 μg/mL), but its intermediate activity against Gram-negative *E. coli* (MIC: 16 μg/mL) limits its narrow-spectrum application against Gram-positive bacteria.

The unsymmetrically substituted amine **13pA** (R^1 = 3,5-dibromobenzyl, R^2 = 4-(*tert*-butyl)benzyl) was potent against all strains tested (MIC: 2–8 μg/mL) but was quite haemolytic (EC_{50}: 47 μg/mL). The guanyl derivative **13pG** became more potent against all strains but *P. aeruginosa* (MIC: 16 μg/mL), accompanied by an almost 4-fold decrease in haemolytic activity (EC_{50}: 169 μg/mL), rendering it a very promising candidate for further studies.

Using *n*-propyl linkers clearly had a positive effect and led to development of the potent derivatives **13iA**, **13jA**, **13jG**, **13lG** and **13pG** with broad-spectrum activity. All five derivatives displayed low haemolytic activity, making them promising candidates for further evaluation.

2.3.6. Trends in haemolytic activity

When examining the haemolytic activity of our compounds we saw a pronounced difference between compounds having *n*-propyl and *n*-butyl linkers. The core findings are presented in the following paragraph and a more detailed section on how the structures were compared can be found in chapter 1 of the Supporting Information.

For our comparison, we selected 24 compounds and assorted them into four scaffold groups (Fig. S1) based on the combination of linkers and cationic head groups. Compounds with (i) *n*-propyl linkers and amine groups were placed in group 3CA, (ii) *n*-propyl linkers and guanidyl groups in group 3CG, (iii) *n*-butyl linkers and amine groups in group 4CA and (iv) *n*-butyl linkers and guanidyl groups in group 4CG. Each scaffold group contained compounds with the following side chain combinations: **a** (3,5-dibromobenzyl), **e** ((4-bromonaphthalen-1-yl) methyl), **i** (4-bromo-3-chlorobenzyl), **j** (3,5-bis(trifluoromethyl)benzyl), **l** (R^2 = 4-(trifluoromethyl)benzyl) and **p** (4-(*tert*-butyl)benzyl). To represent the trends, we have looked at the difference in EC_{50} values between 3CG – 3CA and 4CG – 4CA (Fig. S2) as well as 3CA – 4CA and 4CG – 3CG (Fig. S3).

First, we compared guanidyl- and amine-containing compounds with the same linkers and lipophilic side chains. For compounds with *n*-butyl linkers (4CG – 4CA), all guanidyl containing compounds were more haemolytic than their amine counterparts except for when the (4-bromonaphthalen-1-yl)methyl (**e**) was present. Comparing *n*-propyl containing derivatives (3CG – 3CA), we observed the reversed trend. The guanidyl derivatives were equally to pronouncedly less haemolytic than their amine counterparts. The difference in EC_{50} values ranged from 0 μg/mL for side chain combination **l** to 269 μg/mL for side chain combination **j**.

Next, we compared the *n*-butyl with *n*-propyl linkers in the presence of amine groups (3CA – 4CA). For side chain combinations **a**, **e**, **j** and **p** the compounds were of comparable haemolytic activity regardless of the linker length. Only for side chain combinations **i** and **l** the derivatives with *n*-propyl linkers (3CA) were less haemolytic by 151 and 158 μg/mL, respectively, compared to their *n*-butyl counterparts (4CA). The difference between *n*-butyl and *n*-propyl linkers was most eminent in the presence of guanidyl groups (4CG – 3CG). All compounds having *n*-propyl linkers (3CG) were less haemolytic than compounds with *n*-butyl linkers (4CG). The difference ranged from 25 μg/mL for side chain combination **e** to an impressive 347 μg/mL for side chain combination **j**.

This comparison clearly shows that *n*-propyl linkers not only led to derivatives with good broad-spectrum activity, but also low haemolytic activity. Despite the often noteworthy difference in EC_{50} values for the two linkers, no obvious SAR could be delineated.

2.3.7. Summary of SAR analysis

The general trends of our SAR analysis are summarized in Fig. 3. When assessing the potency of the lipophilic side chains and the hydrocarbon linkers, amine and guanidine derivatives were not distinguished, as they generally follow the same trends.

We found that the antimicrobial activity decreased along the line of *n*-butyl > *n*-propyl > ethyl and haemolytic activity increased as follows: *n*-propyl < ethyl < *n*-butyl. The cyclic hydrocarbons, *n*-pentyl and *n*-*hexyl* displayed varying MIC values, but where all too haemolytic to be of any practical use and were therefore excluded from the list. Guanyl compounds with *n*-butyl linkers were more haemolytic than their amine counterparts. As mentioned before, for ethyl and *n*-propyl linkers this

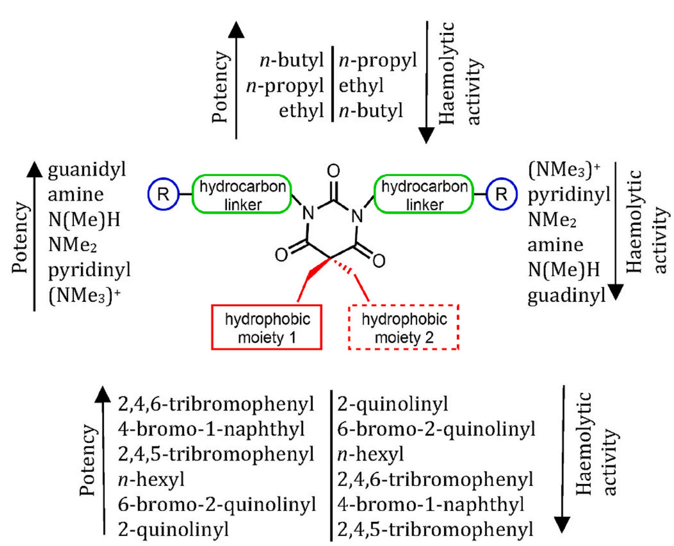

Fig. 3. Overview over the general trends observed during the SAR investigation. The trends for haemolytic activity were assessed for the average between the respective amines and guanidines.

trend was reversed. Based on this, *n*-propyl seemed to be the best compromise to achieve high antimicrobial activity and moderate haemolytic activity.

In line with our previous findings, the compounds potency and haemolytic activity increased with higher CLogP values of the lipophilic side chains for both, amines and guanidines. Bromines proved to be a good modulator of the hydrophobicity of aryl groups. The structure of the side chains seemed thereby to be secondary. The most potent compounds proved to be too haemolytic for future therapeutic considerations. By combining two lipophilic side chains of different structure and hydrophobicity (**11kG** and **11lG**), antimicrobial potency and haemolytic activity of the compounds could be fine-tuned.

To achieve good broad-spectrum activity, amine or guanidine groups proved to be necessary. Methylated primary amines showed reduced activity against Gram-negative *P. aeruginosa* alongside reduced haemolytic activity. The least haemolytic cationic groups were the quaternary ammonium compounds in **8a** and **9a**. Due to its lack of haemolytic activity and high activity against Gram-positive bacterial strains, **8a** could proof valuable for narrow-spectrum applications against Gram-positive bacteria.

2.4. Selectivity index

A common measurement for the efficiency of antimicrobial agents is the selectivity index (SI) given by the ratio EC_{50}/MIC values (for all SI values see Table S1). Our efforts led to promising candidates for narrow- as well as broad-spectrum applications. We have grouped them into three groups (Table 6) based on their activity and SI against Gram-positive strains (entries 1–4), Gram-positive strains and *E. coli* (entries 5–7) and all strains tested (entries 8–11), respectively. Compounds were considered active if the MIC values were ≤16 μg/mL.

The first group, **8a**, **11kG**, **13cG** and **13hG** (Table 6, entries 1–4), comprised compounds that had a SI ≥ 54 for the Gram-positive strains, while showing no activity against Gram-negative strains and human red blood cells. These properties make them ideal candidates for narrow-spectrum application against Gram-positive bacteria.

Compounds in the second group had SI ≥ 40 (Table 6, entries 5–7) against the Gram-positive strains and the Gram-negative *E. coli* and a medium SI (<20) against Gram-negative *P. aeruginosa*. Of the three compounds **9**, **11lG** and **13pG**, only pyridinyl derivative **9** (entry 5) did not show measurable haemolytic activity. But despite having moderate EC_{50} values (161 and 169 μg/mL), guanyl derivatives **11lG** and **13pG** had a high SI.

The third group comprises molecules with a SI ≥ 20 (Table 6, entries 8–11) against all four strains. Compounds **13aG** and **13jA** (entries 8–9) displayed a good overall SI and had also good activity against the Gram-negative *P. aeruginosa* (MIC: 8 μg/mL). Compounds **13jG** and **13iA** (entries 10–11) were mildly potent against *P. aeruginosa* (MIC: 16 μg/mL), but due to their low haemolytic activity they still display promising SI values. Their absence of cytotoxicity makes them promising candidates, despite their mild activity against Gram-negative *P. aeruginosa*, keeping in mind that most naturally occurring AMPs display low activity against this Gram-negative strain as well [17]. Additionally, group 3 compounds generally matched or outperformed our reference compounds **1aA** and **1aG** (entries 12–13).

Table 6
Selectivity index (SI) of the most promising wide and narrow-spectrum antimicrobials. EC_{50} values are given in [μg/mL].

Entry	Comp. ID	SI (EC_{50}/MIC)[a]				EC_{50}[b]
		S. a	B. s	E. c	P. a	
1	**8a**	>135	>67	–	–	>539
2	**11kG**	225	113	–	–	450
3	**13cG**	>62	>124	–	–	>497
4	**13hG**	>54	>109	–	–	>435
5	**9a**	>280	>140	>70	–	>559
6	**11lG**	81	40	81	10	161
7	**13pG**	169	169	85	11	169
8	**13aG**	93	93	47	23	187
9	**13jA**	23	46	23	23	176
10	**13jG**	111	222	56	28	445
11	**13iA**	40	81	40	20	323
12	**1aA**	20	40	20	10	79
13	**1aG**	31	31	31	8	62

Bacterial reference strains: S. a – *Staphylococcus aureus* ATCC 9144, B.s – *Bacillus subtilis* 168, E. c – *Escherichia coli* ATCC 25922, and P. a – *Pseudomonas aeruginosa* ATCC 27853.

[a] No SI was calculated if the MIC was >16 μg/mL.

[b] Values given as *greater than* correspond to the highest concentration (500 μM) tested in the RBC assay.

2.5. Effect of the counterion on solubility and activity

The counterion of acidic and basic drugs is known to greatly influence their overall physicochemical properties such as solubility, membrane permeability and stability [54,55]. From the long list of physiological anions for basic active pharmaceutical ingredients (APIs), hydrochloride salts are predominant [55] and known to improve water solubility [56].

We found that the water solubility of the TFA salts decreased noticeably when the CLogP values of the lipophilic side chains rose beyond 4. To study if we could counteract this trend, we converted selected compounds to HCl salts. Additionally, we wanted to investigate if the counterion affected the biological activity. Table 7 summarizes the re-evaluated MIC and EC_{50} values of selected compounds as hydrochloride salts. Water solubility was assessed qualitatively by setting the threshold at 1 mg/mL. Entries 1–3 show that previously not soluble (−) TFA salts became soluble (+). Compound **13iG** (entry 4) and several others (data not shown) remained poorly soluble in water, especially if several bromine substituents were present in the lipophilic side chain.

Hydrochloride salts of the amine derivatives **13iA** and **13jA** exhibited no change in their MIC values and showed only slightly differing EC_{50} values (entries 1–2). No clear trend could be observed whether hydrochloride salts tended to be more or less haemolytic than TFA salts. Surprisingly, the HCl salts of guanyl derivatives **13iG** and **13jG** displayed improved MIC values against *S. aureus* (Entries 3–4), while the activity against *E. coli* remained unchanged. Compound **13jG** was the only HCl salt being considerably more haemolytic than its TFA counterpart (Entry 3), for yet undetermined reasons. The deceivingly higher haemolytic activity of derivatives **13iA** and **13iG** as HCl salts (Entry 2 and 4) can be attributed to the lower molecular weight of the HCl salts.

2.6. Mode of action studies

Luciferase-based biosensor assays (viability and membrane integrity)

Table 7
MIC and EC_{50} values in μg/mL of selected di-TFA (first value) and di-hydrochloride (HCl, second value) salts. Improved values are highlighted in green.

Entry	Code	MIC [μg/mL][a]		EC_{50} [μg/mL]	Solubility[b]
		S. a	E. c		
1	**13jA**	8/8	8/8	176/224	−/+
2	**13iA**	8/8	8/8	323/271[c]	−/+
3	**13jG**	4/2	8/8	445/118	−/+
4	**13iG**	2/0.5	8/8	348/291[d]	−/−

[a] Bacterial reference strains: S. a – *Staphylococcus aureus* ATCC 9144 and E. c – *Escherichia coli* ATCC 25922.

[b] If solubility in pure water is equal or greater than 1 mg/mL it is denoted with (+), if lower (−).

[c] EC_{50} = 368/375 μM (TFA/HCl).

[d] EC_{50} = 362/362 μM (TFA/HCl).

were performed to explore the mode of action of promising compounds on *B. subtilis* 168 and *E. coli* K12 [57]. The biosensor-based viability assay measures bacterial viability as light production through recombinantly expressed bacterial luciferase originating from the *Photorhabdus luminescens lux* operon. The addition of external substrates does not affect the production of light by the bacterial *lux* operon. The bacterium itself provides the pool of reduced flavin mononucleotide (FMNH2) and long-chain aliphatic aldehydes, which are the substrates responsible for light production. Bacterial luciferase is an excellent real-time sensor for bacterial viability, as NADH, NADPH, and ATP are necessary to constantly top up the substrates' pool.

The biosensor-based membrane integrity assay depends on the luciferase (*lucGR* gene) originating from the luminous click beetle *Pyrophorus plagiophthalamus*. In contrast to bacterial luciferase, the light reaction of *lucGR* is stringently reliant on the substrate D-luciferin, which is added externally. D-luciferin is inadequately crossing intact biological membranes at neutral pH. After the addition of antimicrobial substances, the uptake is explored to determine if the membrane becomes permeable to the substrate D-luciferin. An increase in light production occurs when D-luciferin enters (increased influx) through a compromised membrane. Light production peaks rapidly if membrane integrity is compromised and, thereafter, usually decreases while the ATP from dying cells is consumed.

Based on structural modifications, MIC values, haemolytic activity, and selectivity index, 17 compounds were selected for mode of action studies against *B. subtilis* 168 (see Supporting Information, Table S2) as they were mainly potent against Gram-positive bacteria. Furthermore, based on their broad-spectrum activity, 14 additional compounds were tested against both, the Gram-positive *B. subtilis* 168 and the Gram-negative *E. coli* K12 biosensor strain (see the Supporting Information, Tables S2 and S3). In general, most of the compounds tested affected viability and showed strong membrane disrupting activity against both bacterial strains. However, some of the compounds showed a more pronounced effect on viability and a faster membranolytic effect against *B. subtilis* compared to *E. coli*. For most compounds, both viability and membrane integrity were affected when the concentration of the compounds was higher than the MIC value. Additionally, increasing concentrations affected viability and membranolytic activity in increasing rates, indicating a concentration-dependent killing effect. We could not determine any relationship between structure/activity and the mode of action profiles.

We selected the broad-spectrum barbiturate **11lG** to exemplify the results of the viability and membrane integrity assay in detail (Fig. 4 and Fig. 5). Barbiturate **11lG** clearly affected the viability of *B. subtilis* (Fig. 4A, left). The membrane integrity assay was performed on the *B. subtilis* biosensor strain to confirm that the rapid decrease in bacterial viability was caused by membrane damage. Derivative **11lG** showed a membrane-related mode of action as light emission decreased rapidly in a dose-dependent manner (Fig. 4B, left), similar to chlorhexidine (CHX) (Fig. 4B, right). The reference control CHX is a bactericidal agent recognized for its cell wall and membrane disruptive properties [58], with MIC values of 1.5 μg/mL against both, *B. subtilis* 168 and *E. coli* K12. The disruptive membrane effect of barbiturate **11lG** on *B. subtilis* was shown at a concentration as low as 6.4 μg/mL, which is approximately 1.6 times higher than its MIC (4 μg/mL) (Fig. 4B, left). The lowest concentration (3.2 μg/mL), which is slightly lower than its MIC value, showed a limited membrane disruption effect and the peak emission did not decline during the assay period. The bacterial concentration for these experiments was approximately 100 times higher than the concentration used in the MIC assay, which could explain why slightly higher concentrations of barbiturate **11lG** were needed to affect the viability and membrane integrity.

When it comes to the effects of barbiturate **11lG** on the viability and membrane integrity in the Gram-negative *E. coli*, the picture is somewhat different from that of the Gram-positive *B. subtilis*. The broad-spectrum derivative **11lG** affected the viability of the *E. coli* strain and showed a concentration-dependent killing effect like CHX (Fig. 5A). Although **11lG** affected the viability, a much less prominent inner

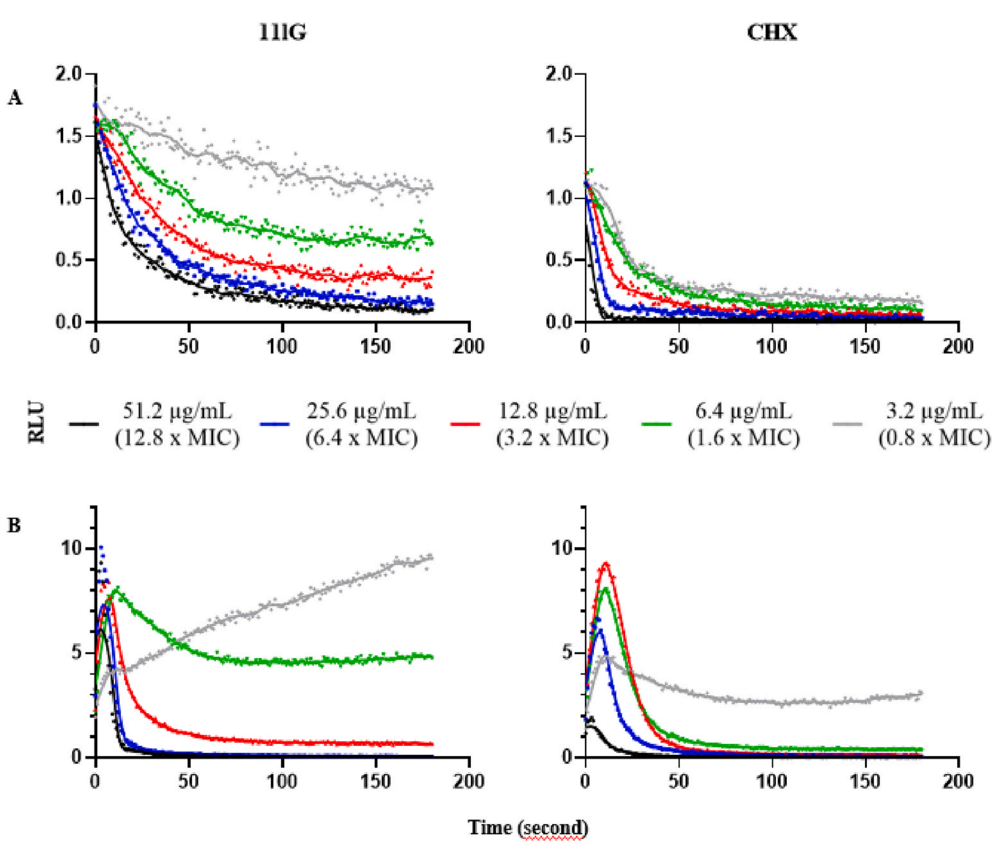

Fig. 4. The effects of **11lG** (broad-spectrum) and CHX (positive control) on the kinetics of (**A**) viability and (**B**) membrane integrity in *B. subtilis* 168. Normalized light emission (normalized with a negative, untreated water control) is plotted as relative light units (RLU) over time (seconds). Light emission was measured each second for 180 s after adding the bacterial cell suspension (with 1 mM D-luciferin for the membrane integrity assay) to the analytes in separate wells. The multiples of the MIC values given in parentheses refers only to compound **11lG**. The figure shows a representative data set from at least three independent experiments.

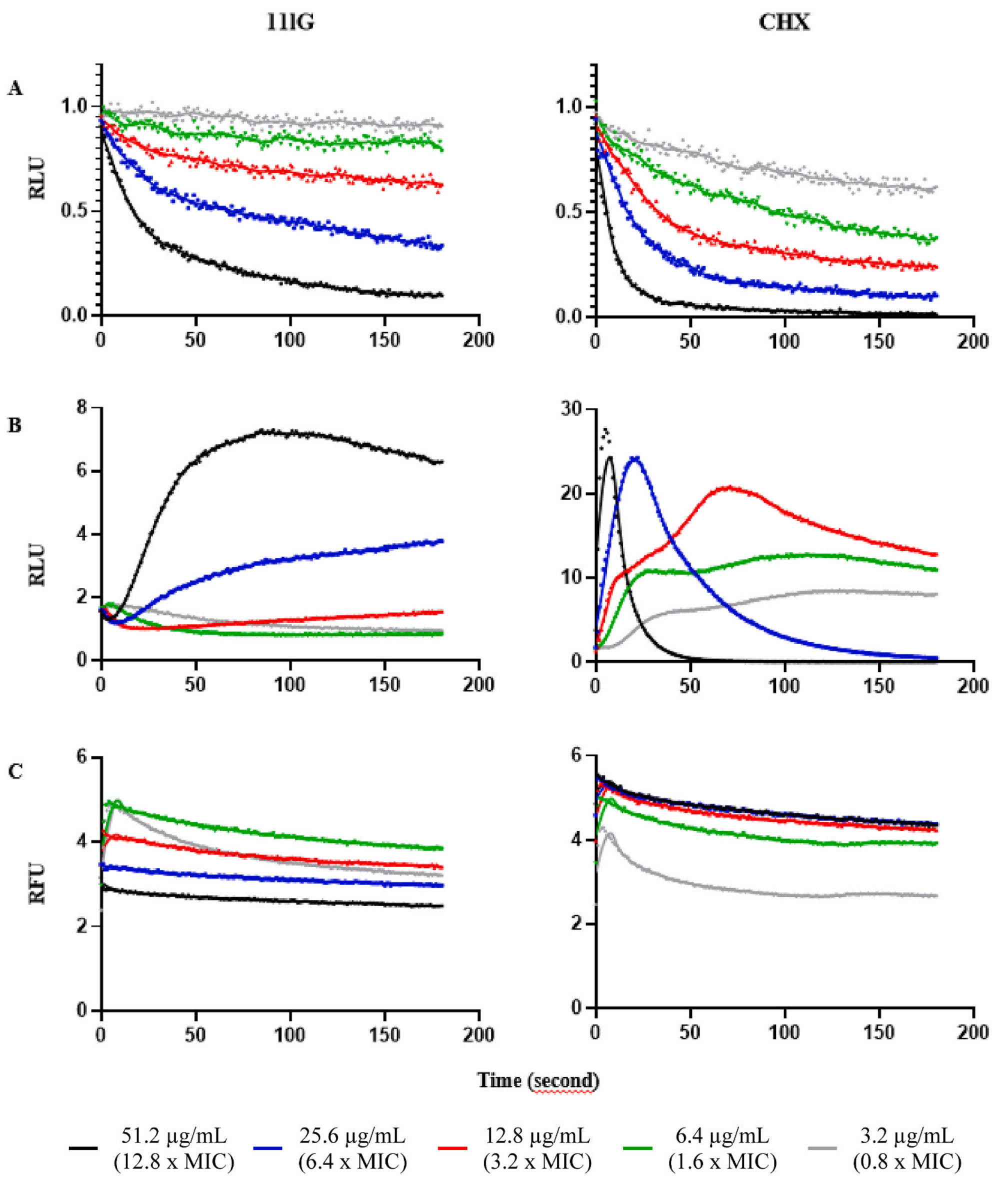

Fig. 5. The effects of **11lG** (broad-spectrum) and a CHX (positive control) on the kinetics of (A) viability and (B) inner membrane integrity (C) outer membrane integrity in *E. coli* K12. Normalized light emission (normalized with a negative, untreated water control) is plotted as relative light units (RLU) over time (seconds) for A and B. For C, normalized fluorescence (normalized with a negative, untreated water control) is plotted as relative fluorescence units (RFU) over time (seconds). Light emission/fluorescence was measured each second for 180 s after adding the bacterial cell suspension (with 1 mM D-luciferin for the inner membrane integrity assay and 20 μM 1-N-phenylnapthylamine for outer membrane integrity assay) to the analytes in separate wells. The multiples of the MIC values given in parentheses refers only to compound **11lG**. The figure shows a representative data set from at least three independent experiments.

membrane disruptive effect was observed as only the two highest concentrations (6.4 – 12.8x MIC) gave a rise in light emission (and did not decline during the test period) (Fig. 5B**,** left). The delayed and reduced action of **11lG** on the membrane integrity might be due to the outer membrane of *E. coli*, which probably acts as an additional barrier.

To confirm the assumption about the outer membrane barrier in *E. coli*, we used the 1-*N*-phenylnapthylamine (NPN) fluorescent probe to determine whether compound **11lG** can affect the outer membrane to become more permeable. The small molecule NPN (219 Da) is weakly fluorescent in an aqueous solution, but when bound to phospholipids, it gives strong fluorescence [59]. The hydrophobic NPN cannot efficiently cross the outer membrane of intact *E. coli* cells, yielding low fluorescence, but if the outer membranes is compromised, NPN can reach the periplasmic space and bind phospholipids of the inner and outer membranes, thus producing increased fluorescence. In this assay, low concentrations (3.2 μg/mL) of barbiturate **11lG** led to higher fluorescence levels (Fig. 5C, left), but did not initially give any increase in luminescence in the inner membrane integrity assay (Fig. 5B, left). This phenomenon suggests that most of the cells are intact and viable without having significantly compromised integrity of the inner membrane but have increased permeability of the outer membrane. Upon increasing the concentration of barbiturate **11lG**, the fluorescence levels were lower (Fig. 5C, left) indicating either an intact outer membrane or rapid membrane disintegration before the start of the measurement. At the same time the viability of the bacterial cells was clearly reduced (Fig. 5A, left) and the inner membrane integrity was impaired (Fig. 5B, left).

When the 10 μL sample of the NPN assay was spotted on an agar plate after the test period, the viability of the bacterial cells was clearly reduced for concentrations of 25.6–51.2 μg/mL (6.4 – 12.8x MIC) (see Fig. S4), confirming the bactericidal effect of barbiturate **11lG**. Those results strongly suggest that barbiturate **11lG** disrupts both the outer and the inner membrane at the same rate when the concentration is high enough. However, it cannot be excluded that higher concentrations of **11lG** induce a different mode of action, resulting in the compound crossing the outer membrane without disrupting it.

Our results indicate that the primary mode of action for most of the compounds, including the broad-spectrum barbiturate **11lG**, against both the Gram-positive *B. subtilis* and the Gram-negative *E. coli*, is the disruption of the membrane integrity in a concentration-depended manner. However, it is known that certain cationic AMPs exhibit a concentration-dependent dual mode of action [60]. For example, the

N-terminal 1–35 fragment of Bac7 (a proline-arginine-rich AMP) is known to affect the inner membrane at high concentrations and bind to and affect intracellular chaperone protein DnaK and 70S ribosomes at lower concentrations [61–63]. Therefore, there might also be other targets than the bacterial cytoplasmic membrane, and more work is required to conclude if there is any dual mode of action present or not.

3. Conclusion

In the present study, we have investigated the qualitative influence of the individual structural components of *N,N*-dialkylated-5,5-disubstituted amphipathic barbiturates on their bioactivity. We found that *n*-propyl linkers provide the best balance between antibacterial potency and haemolytic activity and *n*-butyl linkers provide the highest potency. Guanidyl head-groups led to the highest antimicrobial potency, whereas trimethylated amines proved to be attractive for narrow-spectrum application. By choosing the individual components carefully, we were able to prepare several compounds having SI values ≥20 and being active towards two (**8a**, **11kG**, **13cG**, **13hG**), three (**9a**, **11lG**, **13pG**) or all four (**13aG**, **13iA**, **13jA**, **13jG**) strains of our test panel. The best compounds (**13aG**, **13jG** and **13jA**) had an improved selectivity index compared to the initial starting point (**1aG**).

Studies on the integrity of the membranes and the viability of bacterial cells suggest that our compounds exert their bactericidal activity by disrupting the bacterial cell wall of Gram-positive *B. subtilis* in a concentration-dependent manner as exemplified by barbiturate **11lG**. In Gram-negative *E. coli* both, the inner and outer membrane, were supposedly rapidly disrupted at higher compound concentration, but a second mechanism of action might be present in addition.

We believe that our detailed analysis can help to devise new amphipathic cationic mimics of antimicrobial peptides.

4. Experimental section

For a detailed description of all chemical and biological experimental procedures, chemical analysis, and supporting results, see the Supporting Information. Additional raw data is available through the DataverseNO repository, link: https://doi.org/10.18710/GNTWOG.

Author contributions

M.K.L, A.B. and M.B.S. designed the compound library; M.K.L and F. Z. performed the compound synthesis and analysis; A.R., H.D., H.-M.B., T.H. and K.S. determined the biological assays; A.R., H.D., T.A. performed the biological assays and M.K.L, A.R., H.D., H.-M.B., T.H., K.S., A.B. and M.B.S. analysed and interpreted the data. The manuscript was written through contributions of all authors. All authors have given approval to the final version of the manuscript.

Declaration of competing interest

The authors declare that they have no known competing financial interests or personal relationships that could have appeared to influence the work reported in this paper.

Data availability

Additional raw data is available through the DataverseNO repository, link: https://doi.org/10.18710/GNTWOG.

Acknowledgements

MKL, AR and HD thank for a PhD fellowship provided by UiT as part of the AntifoMar and LeadScAMR grants.

Appendix A. Supplementary data

Supplementary data to this article can be found online at https://doi.org/10.1016/j.ejmech.2022.114632.

References

[1] M.I. Hutchings, A.W. Truman, B. Wilkinson, Antibiotics: past, present and future, Curr. Opin. Microbiol. 51 (2019) 72–80.
[2] Global Action Plan on Antimicrobial Resistance, World Health Organization, Geneva, 2015.
[3] P.D. Tamma, S.E. Cosgrove, L.L. Maragakis, Combination therapy for treatment of infections with gram-negative bacteria, Clin. Microbiol. Rev. 25 (2012) 450–470.
[4] M. Laws, A. Shaaban, K.M. Rahman, Antibiotic resistance breakers: current approaches and future directions, FEMS Microbiol. Rev. 43 (2019) 490–516.
[5] S.M. Mandal, A. Roy, A.K. Ghosh, T.K. Hazra, A. Basak, O.L. Franco, Challenges and future prospects of antibiotic therapy: from peptides to phages utilization, Front. Pharmacol. 5 (2014) 1–12.
[6] M.R. Hamblin, T. Hasan, Photodynamic therapy: a new antimicrobial approach to infectious disease? Photochem. Photobiol. Sci. 3 (2004) 436–450.
[7] A. DiGiandomenico, B.R. Sellman, Antibacterial monoclonal antibodies: the next generation? Curr. Opin. Microbiol. 27 (2015) 78–85.
[8] N. Beyth, Y. Houri-Haddad, A. Domb, W. Khan, R. Hazan, Alternative antimicrobial approach: nano-antimicrobial materials, Evid. base Compl. Alternative Med. 2015 (2015), 246012.
[9] M.S. Mulani, E.E. Kamble, S.N. Kumkar, M.S. Tawre, K.R. Pardesi, Emerging strategies to combat ESKAPE pathogens in the era of antimicrobial resistance: a review, Front. Microbiol. 10 (2019) 1–24.
[10] R.E. Hancock, A. Patrzykat, Clinical development of cationic antimicrobial peptides: from natural to novel antibiotics, Curr. Drug Targets: Infect. Disord. 2 (2002) 79–83.
[11] M. Mahlapuu, J. Håkansson, L. Ringstad, C. Björn, Antimicrobial peptides: an emerging category of therapeutic agents, Front. Cell. Infect. Microbiol. 6 (2016) 1–12.
[12] R.E.W. Hancock, H.-G. Sahl, Antimicrobial and host-defense peptides as new anti-infective therapeutic strategies, Nat. Biotechnol. 24 (2006) 1551–1557.
[13] M. Pasupuleti, A. Schmidtchen, M. Malmsten, Antimicrobial peptides: key components of the innate immune system, Crit. Rev. Biotechnol. 32 (2012) 143–171.
[14] M.R. Yeaman, N.Y. Yount, Mechanisms of antimicrobial peptide action and resistance, Pharmacol. Rev. 55 (2003) 27–55.
[15] R.E.W. Hancock, Peptide antibiotics, Lancet 349 (1997) 418–422.
[16] K.L. Brown, R.E.W. Hancock, Cationic host defense (antimicrobial) peptides, Curr. Opin. Immunol. 18 (2006) 24–30.
[17] A. Ebbensgaard, H. Mordhorst, M.T. Overgaard, C.G. Nielsen, F.M. Aarestrup, E. B. Hansen, Comparative evaluation of the antimicrobial activity of different antimicrobial peptides against a range of pathogenic bacteria, PLoS One 10 (2015), e0144611.
[18] K. Fosgerau, T. Hoffmann, Peptide therapeutics: current status and future directions, Drug Discov. Today 20 (2015) 122–128.
[19] Y. Yang, Z. Cai, Z. Huang, X. Tang, X. Zhang, Antimicrobial cationic polymers: from structural design to functional control, Polym. J. 50 (2018) 33–44.
[20] A. Strassburg, F. Kracke, J. Wenners, A. Jemeljanova, J. Kuepper, H. Petersen, J. C. Tiller, Nontoxic, hydrophilic cationic polymers—identified as class of antimicrobial polymers, Macromol. Biosci. 15 (2015) 1710–1723.
[21] D. Liu, W.F. DeGrado, De novo design, synthesis, and characterization of antimicrobial β-peptides, J. Am. Chem. Soc. 123 (2001) 7553–7559.
[22] P. Sang, Y. Shi, P. Teng, A. Cao, H. Xu, Q. Li, J. Cai, Antimicrobial AApeptides, Curr. Top. Med. Chem. 17 (2017) 1266–1279.
[23] T. Hansen, T. Alst, M. Havelkova, M.B. Strøm, Antimicrobial activity of small β-peptidomimetics based on the pharmacophore model of short cationic antimicrobial peptides, J. Med. Chem. 53 (2010) 595–606.
[24] P. Teng, A. Nimmagadda, M. Su, Y. Hong, N. Shen, C. Li, L.-Y. Tsai, J. Cao, Q. Li, J. Cai, Novel bis-cyclic guanidines as potent membrane-active antibacterial agents with therapeutic potential, Chem. Commun. 53 (2017) 11948–11951.
[25] M.H. Paulsen, E.A. Karlsen, D. Ausbacher, T. Anderssen, A. Bayer, P. Ochtrop, C. Hedberg, T. Haug, J.U. Ericson Sollid, M.B. Strøm, An amphipathic cyclic tetrapeptide scaffold containing halogenated $\beta^{2,2}$-amino acids with activity against multiresistant bacteria, J. Pept. Sci. 24 (2018) e3117.
[26] M.H. Paulsen, D. Ausbacher, A. Bayer, M. Engqvist, T. Hansen, T. Haug, T. Anderssen, J.H. Andersen, J.U.E. Sollid, M.B. Strøm, Antimicrobial activity of amphipathic α,α-disubstituted β-amino amide derivatives against ESBL – CARBA producing multi-resistant bacteria; effect of halogenation, lipophilicity and cationic character, Eur. J. Med. Chem. 183 (2019), 111671.
[27] M. Wang, X. Feng, R. Gao, P. Sang, X. Pan, L. Wei, C. Lu, C. Wu, J. Cai, Modular design of membrane-active antibiotics: from macromolecular antimicrobials to small scorpionlike peptidomimetics, J. Med. Chem. 64 (2021) 9894–9905.
[28] M.H. Paulsen, M. Engqvist, D. Ausbacher, T. Anderssen, M.K. Langer, T. Haug, G. R. Morello, L.E. Liikanen, H.-M. Blencke, J. Isaksson, E. Juskewitz, A. Bayer, M. B. Strøm, Amphipathic barbiturates as mimics of antimicrobial peptides and the marine natural products eusynstyelamides with activity against multi-resistant clinical isolates, J. Med. Chem. 64 (2021) 11395–11417.
[29] D.M. Tapiolas, B.F. Bowden, E. Abou-Mansour, R.H. Willis, J.R. Doyle, A. N. Muirhead, C. Liptrot, L.E. Llewellyn, C.W. Wolff, A.D. Wright, C.A. Motti,

B. Eusynstyelamides A, C. nNOS inhibitors, From the ascidian Eusynstyela latericius, J. Nat. Prod. 72 (2009) 1115–1120.
[30] M. Tadesse, J.N. Tabudravu, M. Jaspars, M.B. Strom, E. Hansen, J.H. Andersen, P. E. Kristiansen, T. Haug, The antibacterial ent-eusynstyelamide B and eusynstyelamides D, E, and F from the Arctic bryozoan Tegella cf. spitzbergensis, J. Nat. Prod. 74 (2011) 837–841.
[31] M.F. Richter, B.S. Drown, A.P. Riley, A. Garcia, T. Shirai, R.L. Svec, P. J. Hergenrother, Predictive compound accumulation rules yield a broad-spectrum antibiotic, Nature 545 (2017) 299–304.
[32] S.J. Perlmutter, E.J. Geddes, B.S. Drown, S.E. Motika, M.R. Lee, P.J. Hergenrother, Compound uptake into *E. coli* can Be facilitated by N-alkyl guanidiniums and pyridiniums, ACS Infect. Dis. 7 (2021) 162–173.
[33] S. Zhang, Z. Shi, W. Cao, T. Gao, H. Deng, Synthesis of a series of perfluoroalkyl containing spiro cyclic barbituric acid derivatives, J. Chem. Res. 2009 (2009) 381–383.
[34] S. Kotha, A.C. Deb, R.V. Kumar, Spiro-annulation of barbituric acid derivatives and its analogs by ring-closing metathesis reaction, Bioorg. Med. Chem. Lett. 15 (2005) 1039–1043.
[35] K.T. Mahmudov, M.N. Kopylovich, A.M. Maharramov, M.M. Kurbanova, A. V. Gurbanov, A.J.L. Pombeiro, Barbituric acids as a useful tool for the construction of coordination and supramolecular compounds, Coord. Chem. Rev. 265 (2014) 1–37.
[36] J.T. Bojarski, J.L. Mokrosz, H.J. Bartoń, M.H. Paluchowska, Recent progress in barbituric acid chemistry, in: A.R. Katritzky (Ed.), Adv. Heterocycl. Chem., Academic Press, 1985, pp. 229–297.
[37] J.V. Tate, W.N. Tinnerman II, V. Jurevics, H. Jeskey, E.R. Biehl, Preparation of 5-substituted benzylbarburituric acids and investigation of the effect of the benzyl and substituted benzyl groups on the acidity of barbituric acid, J. Heterocycl. Chem. 23 (1986) 9–11.
[38] D.B. Ramachary, M. Kishor, Y.V. Reddy, Development of pharmaceutical drugs, drug intermediates and ingredients by using direct organo-click reactions, Eur. J. Org. Chem. 2008 (2008) 975–993.
[39] S.J. Kalita, D.C. Deka, 2-Phenyl-2,3-dihydrobenzo[d]thiazole: a mild, efficient, and highly active in situ generated chemoselective reducing agent for the one-pot synthesis of 5-monoalkylbarbiturates in water, Synlett 29 (2018) 477–482.
[40] J.D. Figueroa-Villar, E.R. Cruz, N. Lucia dos Santos, Synthesis of oxadeazaflavines from barbituric acid and aromatic aldehydes, Synth. Commun. 22 (1992) 1159–1164.
[41] A.A. Vieira, B.G. Marinho, L.G. de Souza, P.D. Fernandes, J.D. Figueroa-Villar, Design, synthesis and in vivo evaluation of sodium 2-benzyl-chloromalonates as new central nervous system depressants, MedChemComm 6 (2015) 1427–1437.
[42] S. Fletcher, The Mitsunobu reaction in the 21st century, Org. Chem. Front. 2 (2015) 739–752.
[43] A.R. Katritzky, B.V. Rogovoy, Recent developments in guanylating agents, Archive for Organic Chem. 2005 (2005) 49–87.
[44] T. Gers, D. Kunce, P. Markowski, J. Izdebski, Reagents for efficient conversion of amines to protected guanidines, Synthesis 2004 (2004) 37–42.
[45] K. Midura-Nowaczek, A. Markowska, Antimicrobial peptides and their analogs: searching for new potential therapeutics, Perspect. Med. Chem. 6 (2014) 73–80.
[46] J.S. Dickson, M. Koohmaraie, Cell surface charge characteristics and their relationship to bacterial attachment to meat surfaces, Appl. Environ. Microbiol. 55 (1989) 832–836.
[47] G.M. Bruinsma, M. Rustema-Abbing, H.C. van der Mei, C. Lakkis, H.J. Busscher, Resistance to a polyquaternium-1 lens care solution and isoelectric points of *Pseudomonas aeruginosa* strains, J. Antimicrob. Chemother. 57 (2006) 764–766.
[48] A. Skrzypczak, B. Brycki, I. Mirska, J. Pernak, Synthesis and antimicrobial activities of new quats, Eur. J. Med. Chem. 32 (1997) 661–668.
[49] F. Devínsky, I. Lacko, F. Bittererová, D. Mlynarčík, Quaternary ammonium-salts. 18. Preparation and relationship between structure, IR spectral characteristics, and antimicrobial activity of some new bis-quaternary isosters of 1,5-pentanediammonium dibromides, Chem. Pap. 6 (1987) 803–814.
[50] P. Gilbert, L.E. Moore, Cationic antiseptics: diversity of action under a common epithet, J. Appl. Microbiol. 99 (2005) 703–715.
[51] T. Hansen, M.K. Moe, T. Anderssen, M.B. Strøm, Metabolism of small antimicrobial β2,2-amino acid derivatives by murine liver microsomes, Eur. J. Drug Metab. Pharmacokinet. 37 (2012) 191–201.
[52] E.P. Gillis, K.J. Eastman, M.D. Hill, D.J. Donnelly, N.A. Meanwell, Applications of fluorine in medicinal chemistry, J. Med. Chem. 58 (2015) 8315–8359.
[53] D.H. McDaniel, H.C. Brown, An extended table of hammett substituents constants based on the ionization of substituted benzoic acids, J. Org. Chem. 23 (1958) 420–427.
[54] D. Gupta, D. Bhatia, V. Dave, V. Sutariya, S. Varghese Gupta, Salts of therapeutic agents: chemical, physicochemical, and biological considerations, Molecules 23 (2018) 1719.
[55] A.T.M. Serajuddin, Salt formation to improve drug solubility, Adv. Drug Deliv. Rev. 59 (2007) 603–616.
[56] P.L. Gould, Salt selection for basic drugs, Int. J. Pharm. 33 (1986) 201–217.
[57] M. Virta, K.E.O. Åkerman, P. Saviranta, C. Oker-Blom, M.T. Karp, Real-time measurement of cell permeabilization with low-molecular-weight membranolytic agents, J. Antimicrob. Chemother. 36 (1995) 303–315.
[58] T. Kuyyakanond, L.B. Quesnel, The mechanism of action of chlorhexidine, FEMS Microbiol. Lett. 100 (1992) 211–215.
[59] B. Loh, C. Grant, R.E. Hancock, Use of the fluorescent probe 1-N-phenylnaphthylamine to study the interactions of aminoglycoside antibiotics with the outer membrane of *Pseudomonas aeruginosa*, Antimicrob. Agents Chemother. 26 (1984) 546–551.
[60] M. Graf, M. Mardirossian, F. Nguyen, A.C. Seefeldt, G. Guichard, M. Scocchi, C. A. Innis, D.N. Wilson, Proline-rich antimicrobial peptides targeting protein synthesis, Nat. Prod. Rep. 34 (2017) 702–711.
[61] E. Podda, M. Benincasa, S. Pacor, F. Micali, M. Mattiuzzo, R. Gennaro, M. Scocchi, Dual mode of action of Bac7, a proline-rich antibacterial peptide, Biochim. Biophys. Acta 1760 (2006) 1732–1740.
[62] M.L. Scocchi, P. Decarli, G. Mignogna, P. Christen, R. Gennaro, The proline-rich antibacterial peptide Bac7 binds to and inhibits in vitro the molecular chaperone DnaK, Int. J. Pept. Res. Therapeut. 15 (2009) 147–155.
[63] M. Mardirossian, R. Grzela, C. Giglione, T. Meinnel, R. Gennaro, P. Mergaert, M. Scocchi, The host antimicrobial peptide Bac71-35 binds to bacterial ribosomal proteins and inhibits protein synthesis, Chem. Biol. 21 (2014) 1639–1647.

Supporting Information
for
A concise SAR-analysis of antimicrobial cationic amphipathic barbiturates for an improved activity-toxicity profile

Manuel K. Langer[a#], Ataur Rahman[b#], Hymonti Dey[b], Trude Anderssen[c], Francesco Zilioli[a], Tor Haug[b], Hans-Matti Blencke[b], Klara Stensvåg[b], Morten B. Strøm[c]*, Annette Bayer[a]*
[a] *Department of Chemistry, UiT – The Arctic University of Norway, NO-9037 Tromsø, NORWAY.*
[b] *The Norwegian College of Fishery Science, Faculty of Biosciences, Fisheries and Economics, UiT – The Arctic University of Norway, NO-9037 Tromsø, NORWAY.*
[c] *Department of Pharmacy, Faculty of Health Sciences, UiT – The Arctic University of Norway, NO-9037 Tromsø, NORWAY.*
*# Authors contributed equally; * Corresponding authors.*

Table of Contents

1 Trends in haemolytic activity

We have grouped selected compounds into four scaffold groups for this comparison (**Figure S1**). Each group consisted of compounds with six different hydrophobic side chain combinations **a**, **e**, **i**, **j**, **l** and **p** for a given scaffold: *n*-propyl linkers and amine head groups **3CA** (**13A**, **13eA**, **13iA**, **13jA**, **13lA**, **13pA**) *n*-propyl linkers and guanidine head groups **3CG** (**13G**, **13eG**, **13iG**, **13jG**, **13lG**, **13pG**), *n*-butyl linkers and amine head groups **4CA** (**1aA**, **10eA**, **11lA**, **11pA**) and *n*-butyl linkers and guanidine head groups **4CG** (**1aG**, **10eG**, **11lG**, **11pG**). Compounds having two 6-bromo-2-quinolyl (**10cA, 10cG, 13cA** and **13cG**) or two 4-trifluoromethylbenzyl (**13hA** and **13hG**) side chains were excluded due to their lack of haemolytic activity. EC_{50} values for compounds containing *n*-butyl linkers and hydrophobic moieties 4-bromo-3-chlorobenzyl (**i**) and 3,5-bis(trifluoromethyl)benzyl (**j**) were obtained in our previous study.[1]

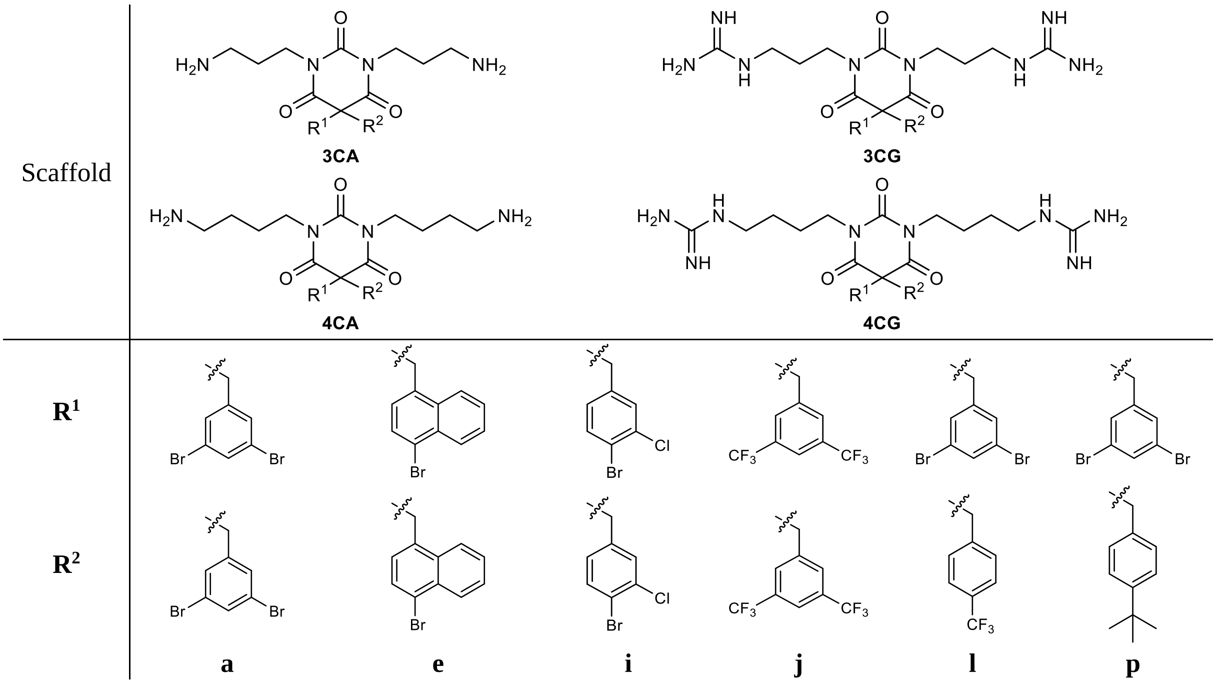

Figure S1. Overview of the scaffolds **3CA** (**13A**, **13eA**, **13iA**, **13jA**, **13lA**, **13pA**), **3CG** (**13G**, **13eG**, **13iG**, **13jG**, **13lG**, **13pG**), **4CA** (**1aA**, **10eA**, **11lA**, **11pA**) and **4CG** (**1aG**, **10eG**, **11lG**, **11pG**) and the linker combinations **a**, **e**, **i**, **j**, **l** and **p**.

1.1 Comparison of amines vs. guanidines by linker length

Figure S2 shows the comparison of haemolytic activity for amine and guanidine derivatives by linker length. For each compound series with a specific linker length (*n*-propyl **3C** or *n*-butyl **4C**) and hydrophobic side chain combination **a**, **e**, **i**, **j**, **l** and **p** we subtracted the EC_{50} values, given in µg/mL, for the amine derivative (**A**) from the guanidyl derivative (**G**). For a negative value, the guanidine derivative was more and for a positive value less heamolytic than its amine counterpart.

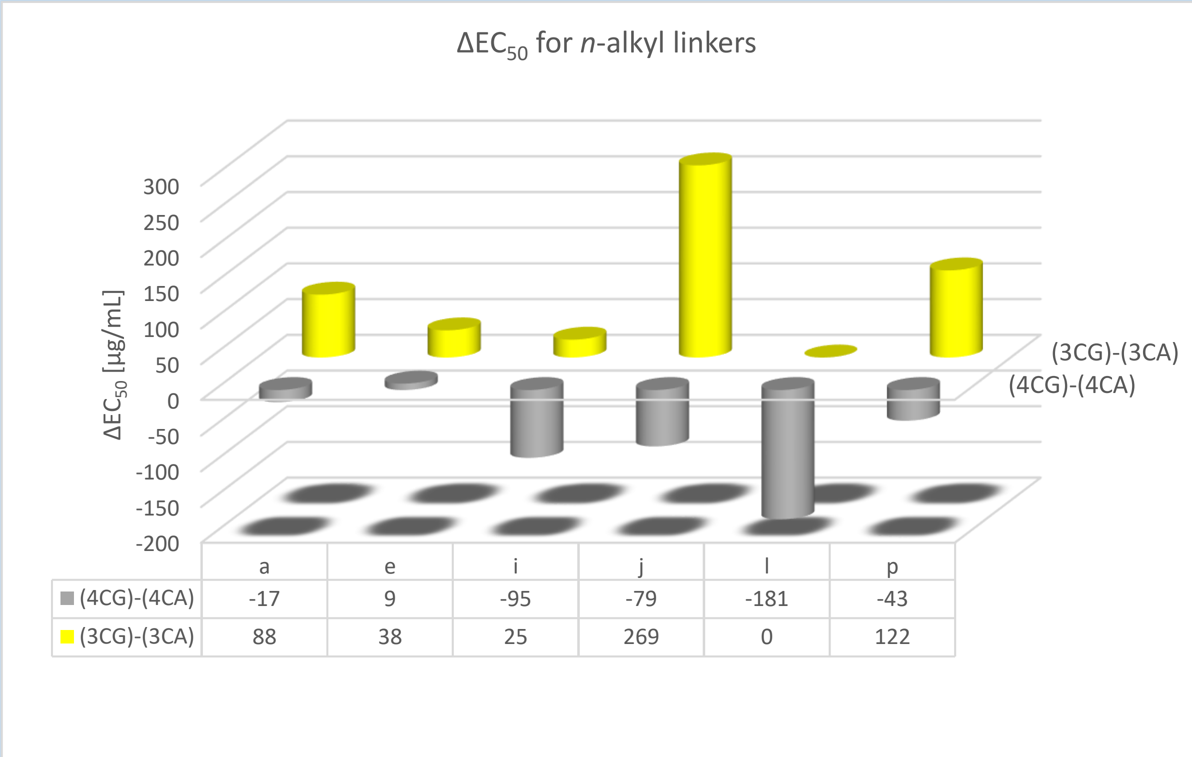

Figure S2. Comparison of the difference in haemolytic activity (EC_{50} values in µg/mL) between the amine and guanidine derivatives for two linker series. For a given hydrophobic side chain combination (**a**, **e**, **i**, **j**, **l** and **p)** and hydrophobic linker (*n*-propyl **3C** or *n*-butyl **4C**), the EC_{50} value of the amine derivative (**A**) was subtracted from the EC_{50} value of the guanidyl derivatives (**G**), stated as (**3CG**)-(**3CA**) and (**4CG**)-(**4CA**). For negative values the guanidine derivative was more haemolytic than the amine. For positive values the guanidine derivative was less haemolytic than the amine. X-axis: hydrophobic moieties **a**, **e**, **i**, **j**, **l** and **p**; Y-axis: ΔEC_{50} values in (µg/mL); Z-axis: linker series. Grey: Comparison of derivatives with a *n*-butyl linker. Yellow: Comparison of derivatives with a *n*-propyl.

1.2 Comparison of *n*-propyl vs. *n*-butyl linkers by cationic group

Using the same grouping (**Figure S1**) we looked at the difference of the haemolytic activity between amine derivatives (**A**) having either a *n*-butyl (**4CA**) or *n*-propyl linker (**3CA**). The same comparison was composed for the guanidine derivatives (**3CG** and **4CG**) (both **Figure S3**). For each compound series with a specific cationic group (**A** or **G**) and hydrophobic side chain combination **a**, **e**, **i**, **j**, **l** and **p**, we subtracted the EC_{50} values, given in µg/mL, for the *n*-butyl linker derivative (**4C**) from the *n*-propyl linker derivative (**3C**). For positive values the *n*-propyl derivatives were less and for negative values more haemolytic than their *n*-butyl containing counterparts.

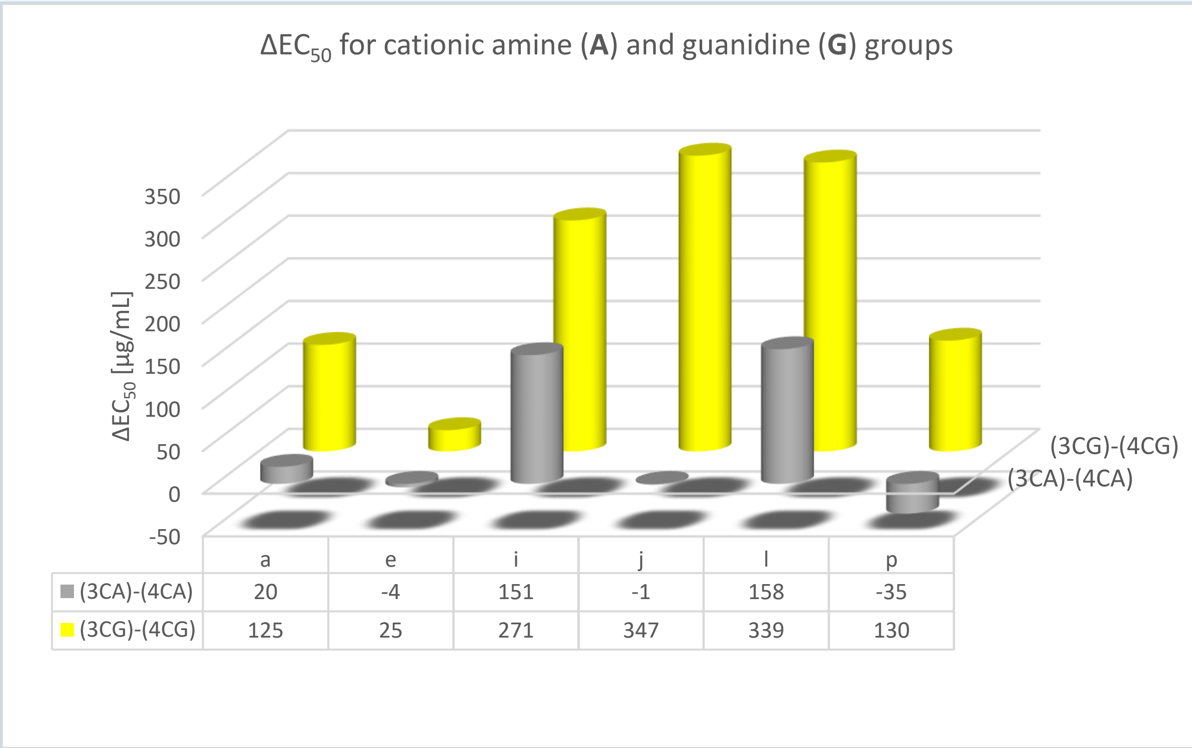

Figure S3. Comparison of the difference in haemolytic activity (EC_{50} values in µg/mL) between the *n*-propyl and *n*-butyl derivatives for the amine and guanidine series. For a given hydrophobic side chain (**a**, **e**, **i**, **j**, **l** and **p)** and cationic group (amine **A** or guanidine **G**), the EC_{50} value of the *n*-butyl (**4C**) was subtracted from the EC_{50} value of the *n*-propyl (**3C**) derivative, stated as (**3CG**)-(**4CG**) and (**3CA**)-(**4CA**). For a positive value the *n*-propyl (**3C**) containing derivatives were less and for a negative value they were more haemolytic than the *n*-butyl derivatives. X-axis: hydrophobic moieties **a**, **e**, **i**, **j**, **l** and **p**; Y-axis: ΔEC_{50} values in (µg/mL); Z-axis: cationic group series. Grey: Comparison of derivatives with an amine group (**A**). Yellow: Comparison of derivatives with a guanidine group (**G**).

2 Experimental procedures

2.1 General methods

Unless otherwise noted, purchased chemicals were used as received without further purification. Solvents were dried according to standard procedures over molecular sieves of appropriate size. Normal phase flash chromatography was carried out on silica gel 60 (230−400 mesh) or on an interchim® PuriFlash XS420 flash system with the sample preloaded on a Samplet® cartridge belonging to a Biotage SP-1 system. Purification by reversed phase (RP) C18 column chromatography (H_2O with 0.1 % TFA/MeCN with 0.1 % TFA) was performed on an interchim® PuriFlash XS420 flash system with the sample preloaded on a Samplet® cartridge. Thin layer chromatography was carried out using Merck TLC Silica gel 60 F254 and visualized by short-wavelength ultraviolet light or by treatment with an appropriate stain.

NMR spectra were obtained on a 400 MHz Bruker Advance III HD spectrometer equipped with a 5 mm SmartProbe BB/1H (BB = 19F, 31P-15N) at 20 °C. The chemical shifts are reported in ppm relative to the solvent residual peak ($CDCl_3$: δH 7.26 and δC 77.16; Methanol-d4: δH 3.31 and δC 49.00; deuterium oxide: δH 4.79; DMSO-d6 δH 2.51 and δC 39.52). ^{13}C NMR spectra were obtained with ^{1}H decoupling. Data are represented as follows: chemical shift, multiplicity (s = singlet, d = doublet, t = triplet, q = quartet, p = pentet, h = heptet, dt = doublet of triplet, tt = triplet of triplet, m = multiplet), coupling constant (*J* in Hz) and integration. The raw data was analyzed with MestReNova (Version 14.0.0-23239).

High-resolution mass spectra (HRMS) were recorded from methanol solutions on an LTQ Orbitrap XL (Thermo Scientific) either in negative or in positive electrospray ionization (ESI) mode. The data was analyzed with Thermo Scientific Xcalibur software.

The purity of all tested compounds was determined to be ≥95%. The analyses were carried out on a Waters ACQUITY UPC^2 system equipped with a Torus™ DEA 130Å, 1.7 µm, 2.1 mm x 50 mm column or a Torus™ 2-PIC 130Å, 1.7 µm, 2.1 mm x 50 mm column. Compounds were detected on a Waters ACQUITY PDA detector spanning wavelengths from 190 to 650 nm, coupled to a Waters ACQUITY QDA detector for low resolution mass (LRMS) detection. The derivatives were eluted with a mobile phase consisting of supercritical CO_2 and MeOH containing 0.1 % NH_3 and a linear gradient of 2 – 40 % MeOH over 2 or 4 min followed by isocratic 0.5 min of 40% MeOH. The flow rate was 1.5 mL/min.

2.2 Synthesis of starting materials

1-bromo-4-(bromomethyl)naphthalene[2], 2-(bromomethyl)quinoline[2, 3], 6-bromo-2-(bromomethyl)quinoline[3], *tert*-butyl (2-bromoethyl)carbamate, *tert*-butyl (3-bromopropyl)carbamate [4], *tert*-butyl (2-hydroxyethyl)carbamate[5], *tert*-butyl (4-hydroxybutyl)carbamate[6], *N,N*'-di(tert-butoxycarbonyl)-guanidinylbutanol[7] were prepared as described in literature. *tert*-butyl (5-hydroxypentyl)carbamate and *tert*-butyl (6-hydroxyhexyl)carbamate were purchased from commercial sources. Compounds **1eA** and **1eG** were synthesized as described in literature.[1]

Note: All final compounds were obtained as di-TFA salts. TFA is typically observed at δ 162.1 (q, *J* = 35.7 Hz) *and* δ 117.7 (q, *J* = 290.3 Hz) *in* ^{13}*C-NMR and is not reported for each compound individually*.

2.3 General procedures

<u>*General procedure A*</u>*:* Synthesis of identically *5,5*-disubstituted barbituric acids **3a-j**

Barbituric acid **2** was taken up in PEG-400 and sodium bicarbonate was added. The reaction mixture was stirred for 5 min before the respective benzyl bromide or alkyl halide was added in one portion. The suspension was stirred at elevated temperature until full conversion was achieved (TLC) and was then allowed to cool to ambient temperature. Upon addition of 10% $NaHCO_{3(aq)}$ solution a white solid precipitated, which was filtered off and washed with 10% $NaHCO_{3(aq)}$ solution, water, and heptane. The obtained solid was collected, mixed with water, and the suspension was heated to reflux for 15 min. After the suspension had cooled to ambient temperature, the solid was collected by filtration and lyophilized for 24 h. MeOH was added, and the resulting suspension was sonicated for 5 min. The suspension was filtered, and the residue was collected and dried to yield the 5,5-disubstituted barbituric acids.

If no precipitate was obtained upon addition of 10% $NaHCO_{3(aq)}$ solution, the aqueous layer was extracted with a suitable solvent three times. The combined organics were dried over Na_2SO_4, filtered and the solvent was removed. The crude was purified by column chromatography on silica gel with EtOAc in heptane as eluent.

General procedure B: *N*-alkylation with alkyl halides and subsequent Boc deprotection

The *5,5*-disubstituted barbituric acid **3c**, **e**, **h**, **i**, **j**, **l** or **p** was mixed with acetone and an inorganic base. The reaction mixture was stirred at ambient temperature for 10 min before *tert*-butyl-(3-bromopropyl)carbamate and TBAI were added. The suspension was heated until TLC indicated full conversion. The mixture was allowed to cool to ambient temperature and EtOAc and 10% $NaHCO_3$ (aq) solution were added. The layers were separated, and the organic layer was washed twice with 10 % $NaHCO_3$ (aq) solution. The organic layer was dried over $MgSO_4$, filtered and the solvent was removed under reduced pressure. The crude was purified on an automated flash system equipped with a silica column and EtOAc in heptane as eluent, to deliver the *N*-Boc-protected amines.
To the *N*-Boc-protected amine in DCM, was added TFA and the mixture was stirred at ambient temperature until HRMS indicated full conversion. The solvent was removed, and the crude product was purified on an automated flash system equipped with a C18 column and MeCN/H_2O containing 0.1% TFA as solvents. The product containing fractions were collected, the solvent was removed, and the product lyophilized for 48 h. The amines were obtained as di-TFA salts.

General procedure C: Guanidine formation

The di-TFA salts of the amines were mixed with THF and DIPEA and stirred at ambient temperature for 10 min. *N*,*N′*-Di-Boc-1*H*-pyrazole-1-carboxamidine was added and the solution was stirred at elevated temperatures until TLC indicated full conversion. The mixture was allowed to cool to ambient temperature and sat. $NH_4Cl_{(aq)}$ solution and EtOAc were added. The layers were separated, and the aqueous layer was extracted twice with EtOAc. The combined organics were dried over Na_2SO_4, filtered and the solvent was removed. The crude products were purified on an automated flash system equipped with a silica column and EtOAc/heptane as eluent to yield the *N*,*N'*-di-Boc-protected guanidines.
The *N*,*N'*-di-Boc-protected guanidines were stirred with TFA in DCM at ambient temperature until HRMS indicated full conversion. In some cases, multiple additions of TFA were needed. The solvent was removed, and the crude product was purified on an automated flash system equipped with a C18 column and MeCN/H_2O containing 0.1% TFA as eluent. The product-containing fractions were collected, the solvent was removed, and the product was lyophilized for 48 h. The guanidines were obtained as di-TFA salts.

General Procedure D: *N*-alkylation *via* the Mitsunobu reaction

The respective 5,5-disubstituted barbituric acid **3b-g** and **3k-q**, the alcohol of choice and PPh_3 were mixed with anhydrous DCM in a heat dried vial under argon atmosphere. The mixture was cooled to 0 °C and upon dropwise addition of DIAD a clear yellow solution was obtained. The mixture was left stirring in the melting ice-water bath until TLC indicated full conversion. Then 10% $NaHCO_{3(aq)}$ solution and EtOAc were added, and the layers were separated. The aqueous layer was extracted twice with EtOAc and the combined organics were dried over Na_2SO_4, filtered and the solvent was removed under reduced pressure. The crude product was purified by column chromatography on silica gel with EtOAc/heptane as eluent to yield the *N,N*-alkylated barbituric acids.
To the di-*N*-Boc amines or di-*N,N'*-di-Boc protected guanidines, dissolved in DCM, was added TFA and the mixture was stirred at ambient temperature until HRMS indicated full conversion. Sometimes multiple TFA additions were needed. The solvent was removed, and the crude product was purified on an automated flash system equipped with a C18 column and MeCN/H_2O containing 0.1% TFA as eluent. The product containing fractions were collected, the solvent was removed, and the product was lyophilized for 24 h. The obtained solids were triturated three times with Et_2O or heptane. The solids were dissolved in MeOH, and water was added. The mixture was lyophilized for 48 h to yield the desired amines or guanidines as di-TFA salts.

General Procedure E: Introduction of alkylated amines

1,3-bis(4-chlorobutyl)-5,5-bis(3,5-dibromobenzyl)pyrimidine-2,4,6(1*H*,3*H*,5*H*)-trione **S1** was mixed with MeCN and methylamine, dimethylamine or trimethylamine were added. The mixture was heated until HRMS indicated full conversion. It was allowed to cool to ambient temperature and the solvent was removed. The crude product was purified by automated RP chromatography with MeCN/H_2O containing 0.1% TFA as solvent. The product containing fractions were collected, the solvent was removed, and the product was lyophilized for 48 h. The amines were obtained as di-TFA salts.

General Procedure F: Synthesis of 5,5-disubstituted barbituric acids **3k-q** with mixed substituents

5-monoalkylated barbituric acid **5** was taken up in PEG-400, $NaHCO_3$ was added, and the suspension was stirred at ambient temperature. After 10 min the alkylating agent was added, and the mixture was stirred at elevated temperature until HRMS indicated full conversion. The mixture was allowed to cool to ambient temperature and Et_2O and 10% $NaHCO_{3(aq)}$ solution were added. The layers were separated, and the aqueous layer was extracted once with Et_2O and EtOAc each. The combined organics were dried over Na_2SO_4, filtered and the solvent was removed under reduced pressure. The crude products were purified by column chromatography on silica with EtOAc/heptane as eluent to yield the desired barbituric acids **3k-q**.

General Procedure G: Preparation of di-hydrochloric (HCl) salts

The previously obtained di-TFA salts of the amines and guanidines were taken up in MeOH and HCl in MeOH (1.25 M, 10.0 eq) was added. The solution was stirred for 5 min, before removal of the solvent under a nitrogen stream. The resulting residue was lyophilized for 24 h. The procedure was repeated twice more to yield the respective di-HCl salts. The absence of fluorine was confirmed by ^{19}F NMR (not included).

2.4 Synthesis of barbiturates with identical lipophilic side chains 3a-j

All compounds were synthesized according to General Procedure A

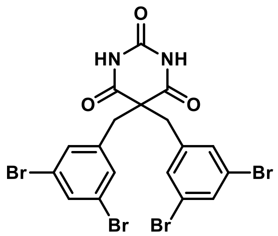

5,5-bis(3,5-dibromobenzyl)pyrimidine-2,4,6(1H,3H,5H)-trione **3a**. Barbituric acid (500 mg, 3.90 mmol, 1.0 eq), PEG-400 (15 mL), $NaHCO_3$ (656 mg, 7.81 mmol, 2.0 eq), 1,3-dibromo-5-(bromomethyl)benzene (2.05 g, 6.25 mmol, 1.6 eq). The mixture was stirred at 45 °C for 20 h. The title compound **3a** (1.62 g, 3.12 mmol, 83%) was obtained as a white solid. **^{1}H NMR** (400 MHz, DMSO-*d6*) δ 11.60 (s, 2H), 7.76 (t, *J* = 1.8 Hz, 2H), 7.22 (d, *J* = 1.8 Hz, 4H), 3.26 (s, 4H). **^{13}C NMR** (101 MHz, DMSO-*d6*) δ 171.3 (2C), 148.9, 139.6 (2C), 132.6 (2C), 131.5 (4C), 122.4 (4C), 58.1, 41.7 (2C). **HRMS** (ESI): calcd for $C_{18}H_{11}Br_4N_2O_3^-$ [M-H]$^-$ 618.7509, found 618.7514.

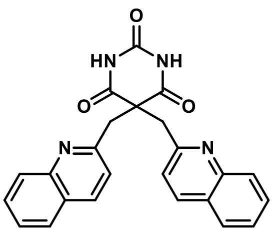

5,5-bis(quinolin-2-ylmethyl)pyrimidine-2,4,6(1H,3H,5H)-trione **3b**. Barbituric acid (600 mg, 4.68 mmol, 1.0 eq), PEG-400 (30 mL), $NaHCO_3$ (786 mg, 9.36 mmol, 2.0 eq), 2-(bromomethyl)quinoline (1.71 g, 7.94 mmol, 1.70 eq). The mixture was stirred at 45 °C for 16 h and then at 60 °C for 24 h. The title compound **3b** (981 mg, 2.39 mmol, 56%) was obtained as a white solid. **^{1}H NMR** (400 MHz, DMSO-*d6*) δ 10.86 (s, 2H), 8.27 (d, *J* = 8.5 Hz, 2H), 7.93 (dd, *J* = 8.1, 1.3 Hz, 2H), 7.77 (dd, *J* = 8.5, 1.4 Hz, 2H), 7.72 (ddd, *J* = 8.3, 6.6, 1.4 Hz, 2H), 7.56 (ddd, *J* = 8.1, 6.6, 1.5 Hz, 2H), 7.40 (d, *J* = 8.5 Hz, 2H), 3.71 (s, 4H). **^{13}C NMR** (101 MHz, DMSO-*d6*) δ 173.7 (2C), 156.8 (2C), 151.3, 146.4 (2C), 136.4 (2C), 129.6 (2C), 128.0 (2C), 127.8 (2C), 126.5 (2C), 126.3 (2C), 121.5 (2C), 52.2, 45.7 (2C). **HRMS** (ESI): calcd for $C_{24}H_{17}N_4O_3^-$ [M-H]$^-$ 409.1306, found 409.1304.

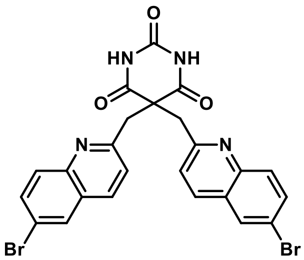

5,5-bis((6-bromoquinolin-2-yl)methyl)pyrimidine-2,4,6(1H,3H,5H)-trione **3c**.

Barbituric acid (90 mg, 0.70 mmol, 1.0 eq), PEG-400 (10 mL), $NaHCO_3$ (112 mg, 1.34 mmol, 1.90 eq), 6-bromo-2-(bromomethyl)quinoline (402 mg, 1.34 mmol, 1.90 eq). The mixture was stirred at 60 °C for 20 h and then at 60 °C for 24 h. The title compound **3c** (109 mg, 0.19 mmol, 27%) was obtained as an off-white solid. **^{1}H NMR** (400 MHz, DMSO-*d6*) δ 11.17 (s, 2H), 8.29 (d, *J* = 8.5 Hz, 2H), 8.26 (d, *J* = 2.2 Hz, 2H), 7.90 (dd, *J* = 8.9, 2.3 Hz, 2H), 7.66 (d, *J* = 8.9 Hz, 2H), 7.48 (d, *J* = 8.6 Hz, 2H), 3.75 (s, 4H). **^{13}C NMR** (101 MHz, DMSO-*d6*) δ 173.5 (2C), 157.6 (2C), 151.2, 145.0 (2C), 135.3 (2C), 132.8 (2C), 130.1 (2C), 129.9 (2C), 127.8 (2C), 122.5 (2C), 119.1 (2C), 52.01, 45.6 (2C). **HRMS** (ESI): calcd for $C_{24}H_{15}Br_2N_4O_3^-$ [M-H]$^-$ 564.9516, found 564.9517.

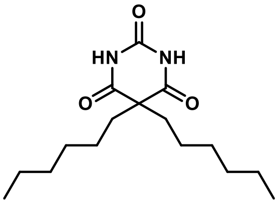

5,5-dihexylpyrimidine-2,4,6(1H,3H,5H)-trione **3d**.

Barbituric acid (445 mg, 3.47 mmol, 1.0 eq), PEG-400 (6 mL), $NaHCO_3$ (730 mg, 8.69 mmol, 2.50 eq), 1-iodohexane (1.33 g, 0.92 mL, 6.25 mmol, 1.80 eq). The mixture was stirred at 100 °C for 48 h and then allowed to cool to ambient temperature and 10% $NaHCO_{3(aq)}$ was added. The aqueous layer was extracted with THF (2x) and MTBE (1x), the combined organics dried over Na_2SO_4, filtered and the solvent was removed under reduced pressure. The crude product was purified by column chromatography on silica with 25% EtOAc in heptane. The title compound **3d** (42 mg, 0.18 mmol, 5%) was obtained as a yellow solid. **^{1}H NMR** (400 MHz, DMSO-*d6*) δ 11.51 (s, 2H), 1.81 – 1.73 (m, 4H), 1.29 – 1.13 (m, 12H), 1.12 – 0.99 (m, 4H), 0.87 – 0.77 (m, 6H). **^{13}C NMR** (101 MHz, DMSO-*d6*) δ 173.2 (2C), 149.8, 55.0, 38.3 (2C), 30.7 (2C), 28.5 (2C), 24.3 (2C), 21.8 (2C), 13.8 (2C). **HRMS** (ESI): calcd for $C_{16}H_{27}N_2O_3^-$ [M-H]$^-$ 295.2027, found 295.2024.

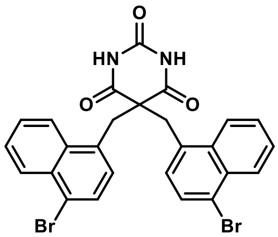

5,5-bis((4-bromonaphthalen-1-yl)methyl)pyrimidine-2,4,6(1H,3H,5H)-trione **3e**.

Barbituric acid (650 mg, 5.07 mmol, 1.0 eq), PEG-400 (15 mL), $NaHCO_3$ (853 mg, 10.15 mmol, 2.0 eq), 1-bromo-4-(bromomethyl)naphthalene (1.71 g, 8.65 mmol, 1.71 eq). The mixture was stirred at 45 °C for 24 h. The title compound **3e** (2.25 g, 3.98 mmol, 92%) was obtained as a white solid. **^{1}H NMR** (400 MHz, DMSO-*d6*) δ 10.44 (s, 2H), 7.57 – 7.46 (m, 2H), 7.38 – 7.30 (m, 2H), 7.00 (d, *J* = 7.8 Hz, 2H), 6.87 (dq, *J* = 12.8, 6.6 Hz, 4H), 6.30 (d, *J* = 7.8 Hz, 2H), 3.16 (s, 4H). **^{13}C NMR** (101 MHz, DMSO-*d6*) δ 172.2 (2C), 149.1, 133.1 (2C), 132.5 (2C), 131.2 (2C), 129.5 (2C), 127.8 (2C), 127.5 (2C), 127.1 (2C), 126.9 (2C), 125.1 (2C), 121.6 (2C), 69.8, 57.5 (2C). **HRMS** (ESI): calcd for $C_{26}H_{17}Br_2N_2O_3^-$ [M-H]$^-$ 562.9611, found 562.9612.

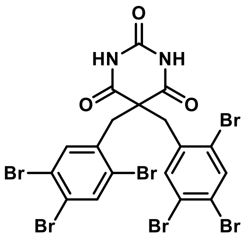

5,5-bis(2,4,5-tribromobenzyl)pyrimidine-2,4,6(1H,3H,5H)-trione **3f**.

Barbituric acid (350 mg, 2.73 mmol, 1.0 eq), PEG-400 (13 mL), $NaHCO_3$ (377 mg, 4.49 mmol, 1.65 eq), 1,2,4-tribromo-5-(bromomethyl)benzene (1.51 g, 3.71 mmol, 1.36 eq). The mixture was stirred at 45 °C for 4.5 d. Instead of sonicating the solids were boiled in MeOH for 30 min, cooled to ambient temperature and filtered. The title compound **3f** (1.07 g, 1.37 mmol, 74%) was obtained as a white solid. **^{1}H NMR** (400 MHz, DMSO-*d6*) δ 11.81 (s, 1H), 8.07 (s, 1H), 7.35 (s, 1H), 3.45 (s, 2H). **^{13}C NMR** (101 MHz, DMSO-*d6*) δ 170.7 (2C), 149.1, 136.7 (2C), 136.4 (2C), 134.5 (2C), 124.7 (2C), 123.7 (2C), 123.1 (2C), 70.2, 55.3 (2C). **HRMS** (ESI): calcd for $C_{18}H_9Br_6N_2O_3^-$ [M-H]$^-$ 774.5719, found 774.5727.

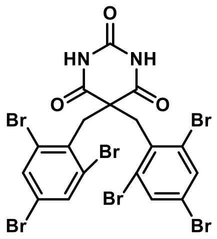

5,5-bis(2,4,6-tribromobenzyl)pyrimidine-2,4,6(1H,3H,5H)-trione **3g**.
Barbituric acid (300 mg, 2.34 mmol, 1.0 eq), PEG-400 (20 mL), $NaHCO_3$ (374 mg, 4.45 mmol, 1.90 eq), 1,3,5-tribromo-2-(bromomethyl)benzene (1.51 g, 3.71 mmol, 1.59 eq). The mixture was stirred at 45 °C for 66 h. Instead of sonicating, the solids were boiled in MeOH for 30 min, cooled to ambient temperature and filtered. The title compound **3g** (1.13 g, 1.37 mmol, 78%) was obtained as a white solid. **^{1}H NMR** (400 MHz, DMSO-*d6*) δ 11.47 (s, 2H), 7.90 (s, 4H), 3.83 (s, 4H). **^{13}C NMR** (101 MHz, DMSO-*d6*) δ 170.7 (2C), 149.7, 135.7 (2C), 134.4 (4C), 127.3 (4C), 121.4 (2C), 54.6, 43.0 (2C). **HRMS** (ESI): calcd for $C_{18}H_9Br_6N_2O_3^-$ [M-H]$^-$ 774.5719, found 774.5718.

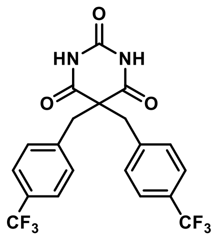

5,5-bis(4-(trifluoromethyl)benzyl)pyrimidine-2,4,6(1H,3H,5H)-trione **3h**.
Barbituric acid (1.25 g, 9.76 mmol, 1.0 eq), PEG-400 (50 mL), $NaHCO_3$ (1.64 g, 19.52 mmol, 2.0 eq), 1-(bromomethyl)-4-(trifluoromethyl)benzene (4.20 g, 17.59 mmol, 1.8 eq). The mixture was stirred at 45 °C for 45 h. The title compound **3h** (1.62 g, 3.12 mmol, 84%) was obtained as a white solid. **^{1}H NMR** (400 MHz, DMSO-*d6*) δ 11.40 (s, 2H), 7.68 (d, *J* = 8.0 Hz, 4H), 7.27 (d, *J* = 8.0 Hz, 4H), 3.40 (s, 4H). **^{13}C NMR** (101 MHz, DMSO-*d6*) δ 171.4 (2C), 148.8, 139.8 (2C), 130.3 (4C), 128.1 (q, *J* = 31.7 Hz, 2C), 125.5 – 125-3 (m, 4C), 124.15 (q, *J* = 272.1 Hz, 2C), 58.4, 43.0 (2C). **HRMS** (ESI): calcd for $C_{20}H_{13}F_6N_2O_3^-$ [M-H]$^-$ 443.0836, found 443.0831.

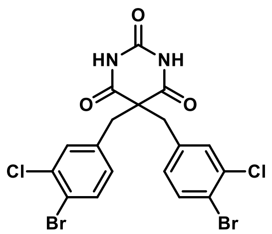

5,5-bis(4-bromo-3-chlorobenzyl)pyrimidine-2,4,6(1H,3H,5H)-trione **3i**.
Barbituric acid (324 mg, 2.53 mmol, 1.0 eq), PEG-400 (30 mL), $NaHCO_3$ (489 mg, 5.82 mmol, 2.3 eq), 1-bromo-4-(bromomethyl)-2-chlorobenzene (1.37 g, 4.81 mmol, 1.9 eq). The mixture was stirred at 45 °C for 15 h and then at 65 °C for 22 h. The crude compound was purified by column chromatography on silica with 15% EtOAc/hepante containing 2.5% MeOH as eluent. The title compound **3i** (752 mg, 1.41 mmol, 56%) was obtained as a white solid. **^{1}H NMR** (400 MHz, DMSO-*d6*) δ 11.51 (s, 2H), 7.71 (d, *J* = 8.2 Hz, 2H), 7.24 (d, *J* = 2.1 Hz, 2H), 6.93 (dd, *J* = 8.3, 2.1 Hz, 2H), 3.26 (s, 4H). **^{13}C NMR** (101 MHz, DMSO-*d6*) δ 171.4 (2C), 148.8, 136.7 (2C), 134.0 (2C), 133.0 (2C), 131.3 (2C), 129.8 (2C), 120.6 (2C), 58.2, 41.9 (2C). **HRMS** (ESI): calcd for $C_{18}H_{11}Br_2Cl_2N_2O_3^-$ [M-H]$^-$ 530.8519, found 530.8520.

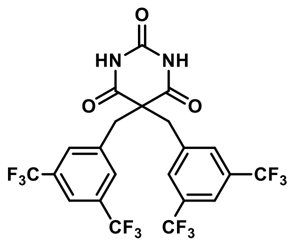

5,5-bis(3,5-bis(trifluoromethyl)benzyl)pyrimidine-2,4,6(1H,3H,5H)-trione **3j**.
Barbituric acid (650 mg, 5.07 mmol, 1.0 eq), PEG-400 (35 mL), $NaHCO_3$ (853 mg, 10.15 mmol, 2.0 eq), 1-(bromomethyl)-3,5-bis(trifluoromethyl)benzene (2.73 g, 1.63 mL, 8.88 mmol, 1.75 eq). The mixture was stirred at 45 °C for 22 h. The title compound **3j** (2.33 g, 4.01 mmol, 79%) was obtained as a white solid. **^{1}H NMR** (400 MHz, DMSO-*d6*) δ 11.64 (s, 2H), 8.04 (s, 2H), 7.71 (d, *J* = 1.7 Hz, 4H), 3.53 (s, 4H). **^{13}C NMR** (101 MHz, DMSO-*d6*) δ 171.2 (2C), 148.6, 138.3 (2C), 130.7 – 130.5 (m, 4C), 130.2 (q, *J* = 32.9 Hz, 4C), 123.2 (q, *J* = 274 Hz), 121.5 – 121.3 (m, 2C), 57.9, 41.3 (2C). **HRMS** (ESI): calcd for $C_{22}H_{11}F_{12}N_2O_3^-$ [M-H]$^-$ 579.0584, found 579.0566.

2.5 Synthesis of barbiturates with mixed hydrophobic residues **3k-q**

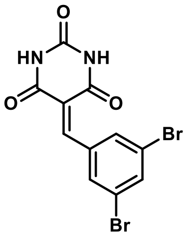

5-(3,5-dibromobenzylidene)pyrimidine-2,4,6(1H,3H,5H)-trione **4**.
Barbituric acid (485 mg, 3.79 mmol, 1.0 eq) was taken up in water (15 mL) and heated to 105 °C until the compound dissolved. 3,5-dibromobenzaldehyde (1.00 g, 3.79 mmol, 1.0 eq) was dissolved in EtOH (5 mL) and added to the aqueous solution. A fine white precipitate formed which dissolved again after 1 min. After a few minutes a yellow precipitate formed. The mixture was stirred for a total of 25 min. After cooling to ambient temperature, it was filtered and the residue was washed with water and EtOAc. The solids were collected and dried to yield pure **4** (817 mg, 2.19 mmol, 58%) as a yellow solid. ^{1}**H NMR** (400 MHz, DMSO-*d6*) δ 11.46 (s, 1H), 11.30 (s, 1H), 8.17 (s, 1H), 8.12 (d, *J* = 1.8 Hz, 2H), 7.94 (t, *J* = 2.0 Hz, 1H). ^{13}**C NMR** (101 MHz, DMSO-*d6*) δ 162.7, 161.3, 150.4, 150.2, 137.1, 135.3, 133.0 (2C), 121.9, 121.7 (2C). **HRMS** (ESI): calcd for $C_{11}H_5Br_2N_2O_3^-$ [M-H]$^-$ 370.8672, found 370.8672.

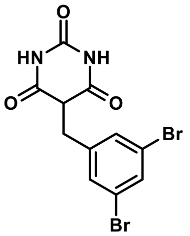

5-(3,5-dibromobenzyl)pyrimidine-2,4,6(1H,3H,5H)-trione **5**.
Compound **4** (1.00 g, 2.67 mmol, 1.0 eq) was taken up in EtOH (22 mL) and $NaBH_4$ (202 mg, 5.35 mmol, 2.0 eq) was added in one portion. After stirring at 70 °C for 5 min the yellow solid turned white. The mixture was allowed to cool to ambient temperature and the mixture was acidified to pH = 1 with 1 N HCl. The solid was collected by filtration to yield **5** (805 mg, 2.14 mmol, 80%) as a white solid. A 2:1 mixture of the Keto and Enol-form was obtained. The mixture was used without further purification.

Keto-**9**: ^{1}**H NMR** (400 MHz, DMSO-*d6*) δ 11.25 (s, 2H), 7.67 (s, 1H), 7.36 (d, *J* = 1.8 Hz, 2H), 4.08 (t, *J* = 5.3 Hz, 1H), 3.22 (d, *J* = 5.3 Hz, 1H). ^{13}**C NMR** (101 MHz, DMSO-*d6*) δ 169.6, 150.7, 143.3, 131.6, 131.0 (2C), 122.2 (2C), 49.2, 31.5.

Enol-**9:** ^{1}**H NMR** (400 MHz, DMSO-*d6*) δ 10.72 (s, 2H), 7.60 (t, *J* = 1.8 Hz, 1H), 7.36 (d, *J* = 1.8 Hz, 2H), 3.55 (s, 1H). ^{13}**C NMR** (101 MHz, DMSO-*d6*) δ 150.4, 146.7, 131.1, 130.4 (2C), 122.6 (2C), 88.2, 27.1. **HRMS** (ESI): calcd for $C_{11}H_7Br_2N_2O_3^-$ [M-H]$^-$ 372.8829, found. 372.8828.

The following compounds were synthesized according to *General Procedure F*:

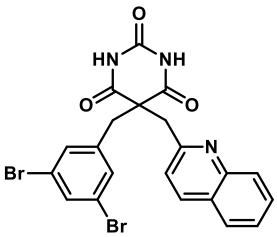

5-(3,5-dibromobenzyl)-5-(quinolin-2-ylmethyl)pyrimidine-2,4,6(1H,3H,5H)-trione **3k**.
Compound **5** (200 mg, 532 µmol, 1.0 eq), 2-(bromomethyl)quinoline (118 mg, 532 µmol, 1.0 eq), $NaHCO_3$ (67 mg, 798 µmol, 1.50 eq) and PEG-400 (3 mL) were stirred at 60 °C for 41 h. The crude was purified with 20-35% EtOAc in heptane to yield **3k** (110 mg, 213 µmol, 40%) as a white solid. ^{1}**H NMR** (400 MHz, Methanol-*d4*) δ 8.15 (d, *J* = 8.1 Hz, 1H), 7.81 (dd, *J* = 7.6, 1.2 Hz, 1H), 7.70 – 7.64 (m, 2H), 7.61 (ddd, *J* = 8.4, 6.7, 1.5 Hz, 1H), 7.48 (ddd, *J* = 8.1, 5.4, 1.4 Hz, 1H), 7.36 (d, *J* = 8.7 Hz, 1H), 7.33 (d, *J* = 1.7 Hz, 2H), 3.92 (s, 2H), 3.28 (s, 2H). ^{13}**C NMR** (101 MHz, Methanol-*d4*) δ 175.1, 158.2, 152.2, 148.0, 140.1, 137.8, 134.4, 132.8, 130.6, 129.1, 128.8, 128.2, 127.4, 123.9, 121.7, 56.4, 45.3, 45.0. **HRMS** (ESI): calcd for $C_{21}H_{14}Br_2N_3O_3^-$ [M-H]$^-$ 513.9407, found.: 513.9406.

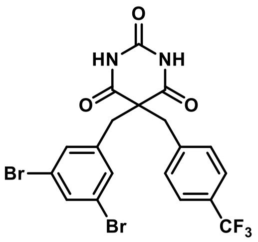

5-(3,5-dibromobenzyl)-5-(4-(trifluoromethyl)benzyl)pyrimidine-2,4,6(1H,3H,5H)-trione **3l**.
Compound **5** (200 mg, 532 µmol, 1.0 eq), 1-(bromomethyl)-4-(trifluoromethyl)benzene (82 µL, 532 µmol, 1.0 eq), $NaHCO_3$ (67 mg, 798 µmol, 1.50 eq) and PEG-400 (3 mL) were stirred at 50 °C for 18h. The crude was purified with 15% EtOAc in heptane to yield **3l** (83 mg, 155 µmol, 29%) as a white solid. ^{1}**H NMR** (400 MHz, Methanol-*d4*) δ 16.82 (t, *J* = 1.8 Hz, 1H), 6.76 (d, *J* = 8.1 Hz, 2H), 6.52 (d, *J* = 8.1 Hz, 2H), 6.49 (d, *J* = 1.7 Hz, 2H), 2.63 (s, 2H), 2.56 (s, 2H). ^{13}**C NMR** (101 MHz, Methanol-*d4*) δ 163.6, 140.6, 131.3 (2C), 124.9, 123.3, 122.0, 121.5 (q, *J* = 32.4 Hz), 117.0 (t, *J* = 3.9 Hz), 116.1 (q, J = 273.0 Hz), 114.5, 51.2, 35.4, 34.4. **HRMS** (ESI): calcd for $C_{22}H_{14}Br_3N_2O_3^-$ [M-H]$^-$ 590.8560, found.: 590.8565.

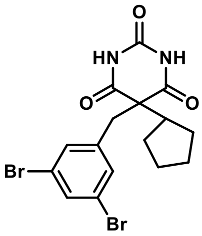

5-cyclopentyl-5-(3,5-dibromobenzyl)pyrimidine-2,4,6(1H,3H,5H)-trione **3m**. Compound **5** (158 mg, 420 µmol, 1.0 eq), bromocyclopentane (43 µL, 399 µmol, 0.95 eq), $NaHCO_3$ (34 mg, 399 µmol, 0.95 eq), TBAI (23 mg, 63 µmol, 0.15 eq) and PEG-400 (2 mL) were stirred at 100 °C for 48 h and then at 140 °C for 72 h. The crude was purified with 15% EtOAc in heptane to yield impure **3m** (9 mg, 20 µmol, 5%) as a yellow solid. **NMR** *no suitable data was obtained*. **HRMS** (ESI): calcd for $C_{16}H_{15}Br_2N_2O_3^-$ $[M-H]^-$ 440.9455, found: 440.9464.

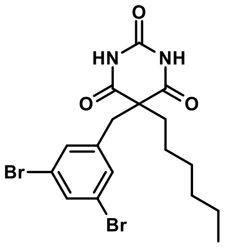

5-(3,5-dibromobenzyl)-5-hexylpyrimidine-2,4,6(1H,3H,5H)-trione **3n**. Compound **5** (200 mg, 532 µmol, 1.0 eq), 1-iodohexane (75 µL, 506 µmol, 0.95 eq), $NaHCO_3$ (45 mg, 532 µmol, 1.00 eq) and PEG-400 (2 mL) were stirred at 100 °C for 5 d. The crude was purified with 0-45% EtOAc in heptane to yield **3n** (129 mg, 280 µmol, 53%) as a colorless foam. **^{1}H NMR** (400 MHz, Methanol-*d4*) δ 7.61 (t, *J* = 1.8 Hz, 1H), 7.24 (d, *J* = 1.8 Hz, 2H), 3.16 (s, 2H), 2.09 – 2.00 (m, 2H), 1.38 – 1.16 (m, 8H), 0.94 – 0.84 (m, 3H). **^{13}C NMR** (101 MHz, Methanol-*d4*) δ 174.0, 150.7, 141.1, 134.2, 132.6, 123.9, 59.0, 44.2, 40.1, 32.4, 30.2, 25.9, 23.5, 14.3. **HRMS** (ESI): calcd for $C_{17}H_{19}Br_2N_2O_3^-$ $[M-H]^-$ 456.9768, found.: 456.9767.

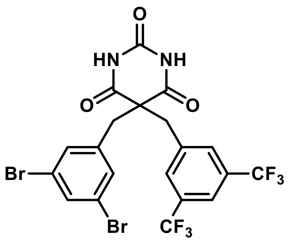

5-(3,5-bis(trifluoromethyl)benzyl)-5-(3,5-dibromobenzyl)pyrimidine-2,4,6(1H,3H,5H)-trione **3o**. Compound **5** (294 mg, 782 µmol, 1.0 eq), 1-(bromomethyl)-3,5-bis(trifluoromethyl)benzene (143 µL, 798 µmol, 1.00 eq), $NaHCO_3$ (99 mg, 1.17 mmol, 1.50 eq), and PEG-400 (20 mL) were stirred at 50 °C for 7 d. 10% $NaHCO_{3(aq)}$ solution was added, the aqueous layer was extracted with DCM (3x) and the combined organic layers dried over $MgSO_4$. The crude was purified with 30% EtOAc in heptane to yield **3o** (471 mg, 327 µmol, 42%) as a white solid. **^{1}H NMR** (400 MHz, DMSO-*d6*) δ 11.63 (s, 2H), 8.05 (s, 1H), 7.77 (d, *J* = 1.8 Hz, 1H), 7.70 (s, 2H), 7.23 (d, *J* = 1.8 Hz, 2H), 3.50 (s, 2H), 3.30 (s, 2H). **^{13}C NMR** (101 MHz, DMSO-*d6*) δ 171.3 (2C), 148.7, 139.5, 138.4, 132.6, 131.6 (2C), 130.6 – 130.4 (m, 2C), 130.2 (q, *J* = 32.8 Hz, 2C), 123.2 (q, *J* = 273.9 Hz, 2C), 122.4 (2C), 121.6 – 121.4 (m, 1C) 58.1, 41.6, 41.5. **HRMS** (ESI): calcd for $C_{20}H_{11}Br_2F_6N_2O_3^-$ $[M-H]^-$ 598.9046, found: 598.9040.

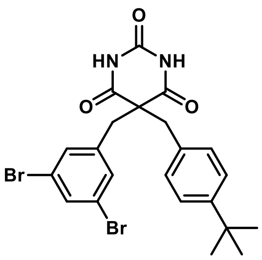

5-(4-(tert-butyl)benzyl)-5-(3,5-dibromobenzyl)pyrimidine-2,4,6(1H,3H,5H)-trione **3p**. Compound **5** (200 mg, 532 µmol, 1.0 eq), 1-(bromomethyl)-4-(tert-butyl)benzene (147 µL, 798 µmol, 1.50 eq), $NaHCO_3$ (67 mg, 798 µmol, 1.50 eq), and PEG-400 (6 mL) were stirred at 100 °C for 21 h. The crude was purified with 10-15% EtOAc in heptane to yield **3p** (169 mg, 324 µmol, 61%) as a white solid. **^{1}H NMR** (400 MHz, DMSO-*d6*) δ 11.40 (s, 2H), 7.75 (t, *J* = 1.8 Hz, 1H), 7.33 – 7.25 (m, 2H), 7.22 (d, *J* = 1.8 Hz, 2H), 7.00 – 6.93 (m, 2H), 3.28 (s, 2H), 3.21 (s, 2H), 1.22 (s, 9H). **^{13}C NMR** (101 MHz, DMSO-*d6*) δ 171.6, 149.7, 148.8, 134.0, 132.5, 131.7, 131.4, 129.0, 125.2, 122.4, 58.5, 43.3, 42.0, 34.2, 31.0. **HRMS** (ESI): calcd for $C_{22}H_{21}Br_2N_2O_3^-$ $[M-H]^-$ 518.9924, found: 518.9924.

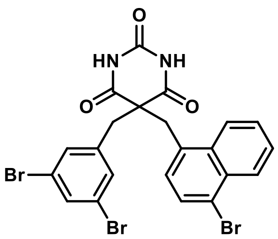

5-((4-bromonaphthalen-1-yl)methyl)-5-(3,5-dibromobenzyl)pyrimidine-2,4,6(1H,3H,5H)-trione **3q**. Compound **5** (75 mg, 200 µmol, 1.0 eq), 1-bromo-4-(bromomethyl)naphthalene (60 mg, 200 µmol, 1.0 eq), $NaHCO_3$ (25 mg, 300 µmol, 1.50 eq) and PEG-400 (1 mL) were stirred at 50 °C for 14h. The crude was purified with 20% EtOAc in heptane to yield **3q** (66 mg, 111 µmol, 56%) as a white solid. **^{1}H NMR** (400 MHz, DMSO-*d6*) δ 1.40 (s, 2H), 8.22 (d, *J* = 7.8 Hz, 1H), 8.16 (dd, *J* = 8.4, 1.4 Hz, 1H), 7.84 (d, *J* = 7.8 Hz, 1H), 7.75 (t, *J* = 1.8 Hz, 1H), 7.70 (ddd, *J* = 8.3, 6.8, 1.2 Hz, 1H), 7.64 (ddd, *J* = 8.3, 6.8, 1.5 Hz, 1H), 7.27 (d, *J* = 1.8 Hz, 2H), 7.13

(d, J = 7.8 Hz, 1H), 3.81 (s, 2H), 3.45 (s, 2H). **^{13}C NMR** (101 MHz, DMSO-*d6*) δ 171.6, 148.7, 140.0, 132.9, 132.5, 132.0, 131.6, 131.2, 129.4, 128.0, 127.8, 127.1, 126.9, 125.0, 122.3, 121.8, 57.9, 41.5. **HRMS** (ESI): calcd for $C_{22}H_{14}Br_3N_2O_3^-$ [M-H]$^-$ 590.8560, found.: 590.8565.

2.6 Synthesis of *series 1*

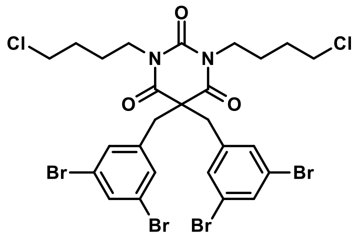

1,3-bis(4-chlorobutyl)-5,5-bis(3,5-dibromobenzyl)pyrimidine-2,4,6(1H,3H,5H)-trione **S1**.
5,5-bis(3,5-dibromobenzyl)pyrimidine-2,4,6(1*H*,3*H*,5*H*)-trione **3a** (250 mg, 400 µmol, 1.0 eq) and Cs_2CO_3 (326 mg, 1.00 mmol, 2.50 eq) were stirred in acetone (5 mL) at ambient temperature for 10 min. 1-bromo-4-chlorobutane (208 µL, 1.80 mmol, 4.50 eq) was added and the mixture was heated to 55 °C for 72 h. EtOAc and 10% $NaHCO_{3(aq)}$ solution were added, the layers were separated and the organic layer was washed with 10% $NaHCO_{3(aq)}$ solution twice. The organic layer was dried over Na_2SO_4, filtered and the solvent was removed. The crude product was purified on an automated flash system equipped with a silica column and gradient 0-30 % EtOAc/heptane. **S1** (273 mg, 339 µmol, 85%) was obtained as a colorless oil. **^{1}H NMR** (400 MHz, Chloroform-*d*) δ 7.53 (dq, J = 3.2, 1.8 Hz, 2H), 7.13 (q, J = 2.2 Hz, 4H), 3.65 (td, J = 7.1, 2.5 Hz, 4H), 3.51 (td, J = 6.4, 2.8 Hz, 4H), 3.36 – 3.25 (m, 4H), 1.62 – 1.53 (m, 4H), 1.53 – 1.43 (m, 4H). **^{13}C NMR** (101 MHz, Chloroform-*d*) δ 169.9 (2C), 149.1, 138.4 (2C), 133.8 (2C), 131.3 (4C), 123.3 (4C), 59.9, 44.2 (2C), 41.4 (2C), 29.8 (2C), 25.4 (2C). **HRMS** (ESI): *not found*.

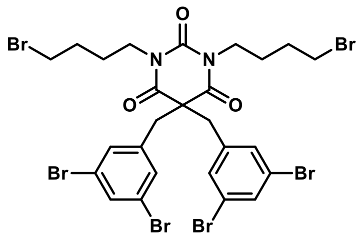

1,3-bis(4-bromobutyl)-5,5-bis(3,5-dibromobenzyl)pyrimidine-2,4,6(1H,3H,5H)-trione **S2**.
5,5-bis(3,5-dibromobenzyl)pyrimidine-2,4,6(1*H*,3*H*,5*H*)-trione **3a** (112 mg, 180 µmol, 1.0 eq) and Cs_2CO_3 (146 mg, 1.00 mmol, 2.50 eq) were stirred in acetone (5 mL) at ambient temperature for 10 min. 1,4-dibromobutane (156 µL, 1.08 mmol, 6.0 eq) was added and the mixture was heated to 55 °C for 72 h. EtOAc and 10% $NaHCO_{3(aq)}$ solution were added, the layers were separated and the organic layer was washed with 10% $NaHCO_{3(aq)}$ solution twice. The organic layer was dried over Na_2SO_4, filtered and the solvent was removed. The crude product was purified on an automated flash system equipped with a silica column and gradient 10-55 % EtOAc/heptane. **S2** (91 mg, 102 µmol, 57%) was obtained as a colorless oil. **^{1}H NMR** (400 MHz, Chloroform-*d*) δ 7.54 (t, J = 1.7 Hz, 2H), 7.14 (d, J = 1.7 Hz, 4H), 3.69 – 3.62 (m, 4H), 3.38 (t, J = 6.7 Hz, 4H), 3.33 (s, 4H), 1.67 (p, J = 6.8 Hz, 4H), 1.49 (p, J = 7.5 Hz, 4H). **^{13}C NMR** (101 MHz, Chloroform-*d*) δ 169.9 (2C), 149.1, 138.4 (2C), 133.8 (2C), 131.3 (4C), 123.3 (4C), 59.9, 44.2 (2C), 41.3 (2C), 29.9 (2C), 26.6 (2C). **HRMS** (ESI): calcd for $C_{26}H_{26}Br_6N_2O_3Na^+$ [M+Na]$^+$ 910.6936, found: 910.6938.

The following compounds were synthesized according to General Procedure E

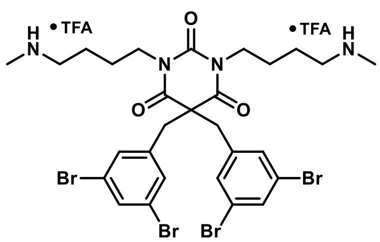

5,5-bis(3,5-dibromobenzyl)-1,3-bis(4-(methylamino)butyl)pyrimidine-2,4,6(1H,3H,5H)-trione **6a**.
S2 (40 mg, 45 µmol, 1.0 eq), methylamine (2M in THF, 179 µL, 358 µmol, 8.0 eq) and MeCN (1 mL) were stirred at 70 °C for 40 h. The crude was purified by automated RP column chromatography with gradient 15-53% MeCN/H_2O + 0.1% TFA to yield the di-TFA salt of **6a** (15 mg, 15 µmol, 33%) as a slightly yellow solid. **^{1}H NMR** (400 MHz, Methanol-*d4*) δ 7.65 (t, J = 1.6 Hz, 2H), 7.22 (d, J = 1.8 Hz, 4H), 3.68 (t, J = 7.6 Hz, 4H), 3.42 (s, 4H), 3.11 – 2.96 (m, 4H), 2.69 (s, 6H), 1.58 (p, J = 7.7 Hz, 4H), 1.41 (p, J = 7.8 Hz, 4H). **^{13}C NMR** (101 MHz, Methanol-*d4*) δ 171.2 (2C), 150.5, 140.5 (2C), 134.5 (2C), 132.7 (4C), 124.1 (4C), 61.2, 49.7 (2C), 44.8 (2C), 42.2 (2C), 33.5 (2C), 26.3 (2C), 24.3 (2C). **HRMS** (ESI): calcd for $C_{28}H_{35}Br_4N_4O_3^+$ [M+H]$^+$ 790.9437, found 790.9436. **SFC**: 98.0%.

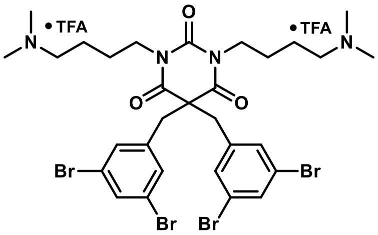

5,5-bis(3,5-dibromobenzyl)-1,3-bis(4-(dimethylamino)butyl)pyrimidine-2,4,6(1H,3H,5H)-trione **7a**.

S2 (40 mg, 45 µmol, 1.0 eq), dimethylamine (2M in THF, 179 µL, 358 µmol, 8.0 eq) and MeCN (1 mL) were stirred at 70 °C for 24 h. The crude was purified by automated RP column chromatography with gradient 15-53% MeCN/H_2O + 0.1% TFA to yield the di-TFA salt of **7a** (35 mg, 33 µmol, 75%) as a slightly yellow solid. **^{1}H NMR** (400 MHz, Methanol-*d4*) δ 7.66 (t, *J* = 1.6 Hz, 2H), 7.22 (d, *J* = 1.8 Hz, 4H), 3.69 (t, *J* = 7.7 Hz, 4H), 3.42 (s, 4H), 3.20 – 3.09 (m, 4H), 2.88 (d, *J* = 1.6 Hz, 12H), 1.70 – 1.55 (m, 4H), 1.40 (p, *J* = 7.7 Hz, 4H). **^{13}C NMR** (101 MHz, Methanol-*d4*) δ 171.2 (2C), 150.5, 140.5 (2C), 134.5 (2C), 132.6 (4C), 124.1 (4C), 61.2, 58.4 (2C), 44.8 (2C), 43.4 (4C), 42.1 (2C), 26.2 (2C), 22.8 (2C). **HRMS** (ESI): calcd for $C_{30}H_{39}Br_4N_4O_3^+$ $[M+H]^+$ 818.9750, found 818.9744. **SFC**: 96.4%.

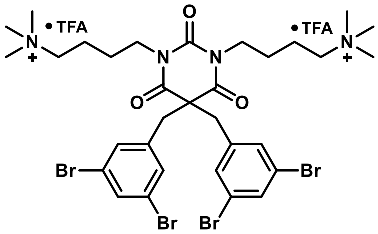

4,4'-(5,5-bis(3,5-dibromobenzyl)-2,4,6-trioxodihydropyrimidine-1,3(2H,4H)-diyl)bis(N,N,N-trimethylbutan-1-aminium) **8a**.

S1 (45 mg, 56 µmol, 1.0 eq), trimethylamine (1M in THF, 783 µL, 783 µmol, 14.0 eq), NaI (15 mg, 100 µmol, 1.8 eq) and MeCN (1 mL) were stirred at 70 °C for 96 h. The crude was purified by automated RP column chromatography with gradient 15-55% MeCN/H_2O + 0.1% TFA to yield the di-TFA salt of **8a** (53 mg, 49 µmol, 88%) as a slightly yellow solid. **^{1}H NMR** (400 MHz, Methanol-*d4*) δ 7.66 (t, *J* = 1.8 Hz, 2H), 7.22 (d, *J* = 1.8 Hz, 4H), 3.78 – 3.66 (m, 4H), 3.43 (s, 4H), 3.41 – 3.34 (m, 4H), 3.13 (s, 18H), 1.82 – 1.68 (m, 4H), 1.39 (tt, *J* = 10.6, 6.4 Hz, 4H). **^{13}C NMR** (101 MHz, Methanol-*d4*) δ 171.2 (2C), 150.4, 139.8 (2C), 134.5 (2C), 132.6 (4C), 124.2 (4C), 67.1 (t, *J* = 3.0 Hz, 2C), 61.1, 53.6 (t, *J* = 4.0 Hz 6C), 44.8 (2C), 42.2 (2C), 26.0 (2C), 21.3 (2C). **HRMS** (ESI): calcd for $C_{32}H_{44}Br_4N_4O_3^{2+}$ $[M]^{2+}$ 424.0068, found 424.0068. **SFC**: 97.7%.

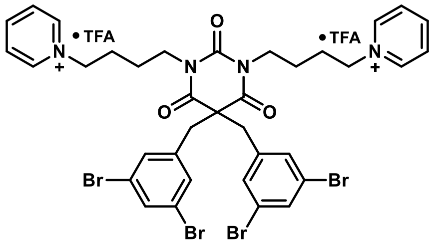

1,1'-((5,5-bis(3,5-dibromobenzyl)-2,4,6-trioxodihydropyrimidine-1,3(2H,4H)-diyl)bis(butane-4,1-diyl))bis(pyridin-1-ium) **9a**.

S1 (28 mg, 35 µmol, 1.0 eq), pyridine (500 µL), NaI (2.6 mg, 17 µmol, 0.5 eq) and MeCN (0.5 mL) were stirred at 90 °C for 64 h. The crude was purified by automated RP column chromatography with gradient 10-70% MeCN/H_2O + 0.1% TFA to yield the di-TFA salt of **9a** (21 mg, 19 µmol, 54%) as a slightly yellow solid. **^{1}H NMR** (400 MHz, Methanol-*d4*) δ 9.10 – 8.99 (m, 4H), 8.64 (tt, *J* = 7.8, 1.3 Hz, 2H), 8.23 – 8.12 (m, 4H), 7.62 (t, *J* = 1.8 Hz, 2H), 7.20 (d, *J* = 1.8 Hz, 4H), 4.75 – 4.65 (m, 4H), 3.80 – 3.68 (m, 4H), 3.44 (s, 4H), 1.95 (p, *J* = 7.5 Hz, 4H), 1.45 (tt, *J* = 9.7, 6.6 Hz, 4H). **^{13}C NMR** (101 MHz, Methanol-*d4*) δ 171.3 (2C), 150.5, 147.2 (2C), 146.0 (4C), 140.5 (2C), 134.5 (2C), 132.6 (4C), 129.7 (4C), 124.1 (4C), 62.1 (2C), 61.2, 44.8 (2C), 42.0 (2C), 29.4 (2C), 25.6 (2C). **HRMS** (ESI): calcd for $C_{36}H_{36}Br_4N_4O_3^{2+}$ $[M]^{2+}$ 443.9755, found. 443.9757 **SFC**: >99.5%.

2.7 Synthesis of *series 2*

The compounds were prepared according to General Procedure D.

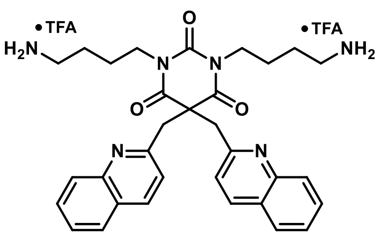

1,3-bis(4-aminobutyl)-5,5-bis(quinolin-2-ylmethyl)pyrimidine-2,4,6(1H,3H,5H)-trione **10bA**.

Barbiturate **3b** (145 mg, 350 µmol, 1.0 eq), *tert*-butyl (4-hydroxybutyl)carbamate (166 mg, 875 µmol, 2.5 eq), PPh_3 (273 mg, 1.05 mmol, 3.0 eq) and DIAD (206 µL, 1.05 mmol, 3.0 eq) were stirred in DCM (2.0 mL) for 25 h. The crude was purified with 0-70% EtOAc in heptane to yield boc-**10bA** (84 mg, 112 µmol, 32%) as a slightly yellow solid.

TFA (130 µL, 1.70 mmol, 15.5 eq) and DCM (1.5 mL) were added, and the mixture was stirred at ambient temperature for 18 h. The crude was purified by automated RP column chromatography with a gradient of 0-70% MeCN/H_2O + 0.1% TFA to yield the di-TFA salt of **10bA** (61 mg, 78 µmol, 22% o2s) as a white solid, m.p. 85-95 °C. **^{1}H NMR** (400 MHz, Methanol-*d4*) δ 8.31 (d, *J* = 8.5 Hz, 2H), 7.93 (d, *J* = 8.2 Hz, 2H), 7.76 (d, *J* = 3.5 Hz, 4H), 7.59 (dt, *J* = 8.1, 4.0 Hz, 2H), 7.45 (d, *J* = 8.6 Hz, 2H), 3.98 (s, 4H), 3.82 (t, *J* = 6.9 Hz, 4H), 2.60 (t, *J* = 7.4 Hz, 4H), 1.51 – 1.30 (m, 8H). **^{13}C NMR** (101 MHz, Methanol-*d4*) δ 174.1 (2C), 158.2 (2C), 153.4, 148.2 (2C), 138.2 (2C), 131.0 (2C), 129.2 (2C), 129.1 (2C), 128.5 (2C), 127.7 (2C), 122.6 (2C), 54.8, 42.0 (2C), 39.9 (2C), 25.9 (2C), 25.7 (2C). *One carbon signal was not observed.* **HRMS** (ESI): calcd for $C_{32}H_{37}N_6O_3^+$ $[M+H]^+$ 553.2922, found 553, 2920. **SFC**: >99.5%.

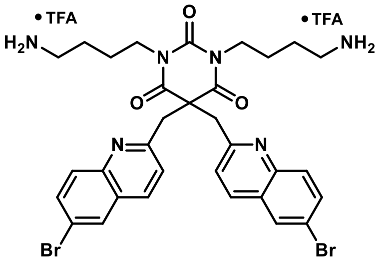

1,3-bis(4-aminobutyl)-5,5-bis((6-bromoquinolin-2-yl)methyl)pyrimidine-2,4,6(1H,3H,5H)-trione **10cA**.

Barbiturate **3c** (39 mg, 69 µmol, 1.0 eq), *tert*-butyl (4-hydroxybutyl)carbamate (32 mg, 172 µmol, 2.5 eq), PPh_3 (54 mg, 206 µmol, 3.0 eq) and DIAD (43 µL, 206 µmol, 3.0 eq) were stirred in DCM (1.0 mL) for 20 h. The crude was purified with 20-62% EtOAc in heptane to yield boc-**10cA** (40 mg, 44 µmol, 64%) as a white solid.
TFA (79 µL, 1.03 mmol, 15.0 eq) and DCM (0.7 mL) were added, and the mixture was stirred at ambient temperature for 17 h. The crude was purified by automated RP column chromatography with a gradient of 10-60% MeCN/H_2O + 0.1% TFA to yield the di-TFA salt of **10cA** (40 mg, 43 µmol, 62% o2s) as a white solid. **^{1}H NMR** (400 MHz, Methanol-*d4*) δ 8.22 – 8.15 (m, 2H), 8.10 (d, *J* = 2.2 Hz, 2H), 7.81 (dd, *J* = 8.9, 2.2 Hz, 2H), 7.61 (d, *J* = 9.0 Hz, 2H), 7.41 (d, *J* = 8.5 Hz, 2H), 3.93 (s, 4H), 3.79 (t, *J* = 6.8 Hz, 4H), 2.66 (t, *J* = 7.2 Hz, 4H), 1.49 – 1.34 (m, 8H). **^{13}C NMR** (101 MHz, Methanol-*d4*) δ 173.8 (2C), 158.9 (2C), 153.3, 146.7 (2C), 137.2 (2C), 134.3 (2C), 131.3 (2C), 131.0 (2C), 129.6 (2C), 123.6 (2C), 121.2 (2C), 54.5, 48.2 (2C), 42.0 (2C), 39.9 (2C), 25.9 (2C), 25.7 (2C). **HRMS** (ESI): calcd for $C_{32}H_{35}Br_2N_6O_3^+$ $[M+H]^+$ 709.1132, found 709.1129. **SFC**: 99.2%.

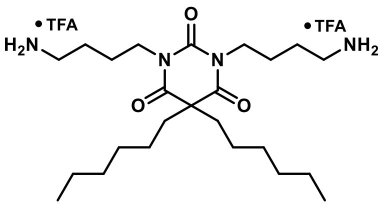

1,3-bis(4-aminobutyl)-5,5-dihexylpyrimidine-2,4,6(1H,3H,5H)-trione **10dA**.

Barbiturate **3d** (37 mg, 125 µmol, 1.0 eq), *tert*-butyl (4-hydroxybutyl)carbamate (59 mg, 312 µmol, 2.5 eq), PPh_3 (98 mg, 375 µmol, 3.0 eq) and DIAD (78 µL, 374 µmol, 3.0 eq) were stirred in DCM (1.0 mL) for 20 h. The crude was purified with 10-40% EtOAc in heptane to yield boc-**10dA** (66 mg, 103 µmol, 83%) as a white solid.
TFA (96 µL, 1.25 mmol, 10.0 eq) and DCM (1.0 mL) were added, and the mixture was stirred at ambient temperature for 22 h. The crude was purified by automated RP column chromatography with a gradient of 10-60% MeCN/H_2O + 0.1% TFA to yield the di-TFA salt of **10dA** (58 mg, 87 µmol, 70% o2s) as a white powder. **^{1}H NMR** (400 MHz, Methanol-*d4*) δ 4.00 – 3.86 (m, 4H), 3.06 – 2.93 (m, 4H), 1.99 – 1.89 (m, 4H), 1.70 (h, *J* = 3.8 Hz, 8H), 1.32 – 1.18 (m, 12H), 1.09 (dt, *J* = 9.5, 4.6 Hz, 4H), 0.87 (t, *J* = 6.8 Hz, 6H). **^{13}C NMR** (101 MHz, Methanol-*d4*) δ 173.2 (2C), 151.9, 57.8, 42.2 (2C), 41.0 (2C), 40.2 (2C), 32.3 (2C), 30.2 (2C), 26.0 (2C), 25.9 (4C), 23.5 (2C), 14.3 (2C). **HRMS** (ESI): calcd for $C_{24}H_{47}N_4O_3^+$ $[M+H]^+$ 439.3643, found 439.3642. **SFC**: 96.5%.

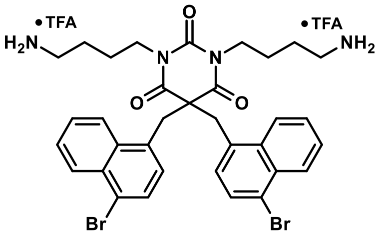

1,3-bis(4-aminobutyl)-5,5-bis((4-bromonaphthalen-1-yl)methyl)pyrimidine-2,4,6(1H,3H,5H)-trione **10eA**.

Barbiturate **3e** (201 mg, 350 µmol, 1.0 eq), *tert*-butyl (4-hydroxybutyl)carbamate (166 mg, 880 µmol, 2.5 eq), PPh_3 (277 mg, 1.06 mmol, 3.0 eq) and DIAD (205 µL, 1.04 mmol, 3.0 eq) were stirred in DCM (2.0 mL) for 24 h. The crude was purified with 0-70% EtOAc in heptane to yield boc-**10eA** (315 mg, 346 µmol, 99%) as a white solid.
TFA (0.42 mL, 5.48 mmol, 15.8 eq) and DCM (2.0 mL) were added, and the mixture was stirred at ambient temperature for 18 h. The crude was purified by automated RP column chromatography with a

gradient of 0-70% MeCN/H_2O + 0.1% TFA to yield the di-TFA salt of **10eA** (153 mg, 163 µmol, 47% o2s) as a white solid, m.p. 105-110°C. **^{1}H NMR** (400 MHz, Methanol-*d4*) δ 8.35 – 8.27 (m, 2H), 8.25 – 8.18 (m, 2H), 7.75 – 7.57 (m, 6H), 7.13 (d, *J* = 7.8 Hz, 2H), 4.10 (s, 4H), 3.35 (t, 4H), 2.60 (t, *J* = 7.7 Hz, 4H), 1.06 (p, 4H), 0.78 (p, *J* = 15.0, 7.6 Hz, 4H). **^{13}C NMR** (101 MHz, Methanol-*d4*) δ 172.0 (2C), 150.7, 134.4 (2C), 133.5 (2C), 133.4 (2C), 130.5 (2C), 129.3 (2C), 128.7 (2C), 128.5 (2C), 128.1 (2C), 126.6 (2C), 123.8 (2C), 60.4, 41.7 (2C), 41.5 (2C), 40.0 (2C), 25.2 (2C), 25.1 (2C). **HRMS** (ESI): calcd for $C_{34}H_{37}Br_2N_4O_3^+$ [M+H]$^+$ 707.1227, found 707.1230. **SFC**: 95.3%.

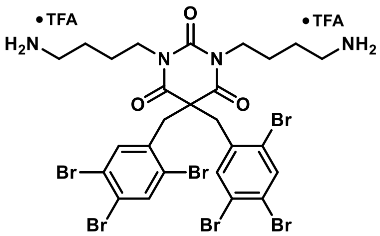

1,3-bis(4-aminobutyl)-5,5-bis(2,4,5-tribromobenzyl)pyrimidine-2,4,6(1H,3H,5H)-trione **10fA**.
Barbiturate **10f** (80 mg, 102 µmol, 1.0 eq), *tert*-butyl (4-hydroxybutyl)carbamate (58 mg, 307 µmol, 3.0 eq), PPh_3 (81 mg, 307 µmol, 3.0 eq) and DIAD (64 µL, 307 µmol, 3.0 eq) were stirred in DCM (0.5 mL) for 12 h. The crude was purified with 0-40% EtOAc in heptane to yield boc-**10fA** (97 mg, 86 µmol, 84%) as a slightly yellow oil.
TFA (66 µL, 0.86 mmol, 10.0 eq) and DCM (1.0 mL) were added, and the mixture was stirred at ambient temperature for 18 h. The crude was purified by automated RP column chromatography with a gradient of 20-45% MeCN/H_2O + 0.1% TFA to yield the di-TFA salt of **10fA** (57 mg, 50 µmol, 49% o2s) as a white powder. **^{1}H NMR** (400 MHz, Methanol-*d4*) δ 7.95 (s, 2H), 7.34 (s, 2H), 3.81 (t, *J* = 7.0 Hz, 4H), 3.64 (s, 4H), 2.92 (t, *J* = 7.4 Hz, 4H), 1.61 – 1.44 (m, 8H). **^{13}C NMR** (101 MHz, Methanol-*d4*) δ 170.6 (2C), 150.9, 138.6 (2C), 137.6 (2C), 136.0 (2C), 125.7 (2C), 125.5 (2C), 124.6 (2C), 58.1, 43.5 (2C), 42.7 (2C), 40.2 (2C), 26.0 (2C), 25.8 (2C). **HRMS** (ESI): calcd for $C_{26}H_{29}Br_6N_4O_3^+$ [M+H]$^+$ 918.7334, found: 918.7343. **SFC**: 98.8%.

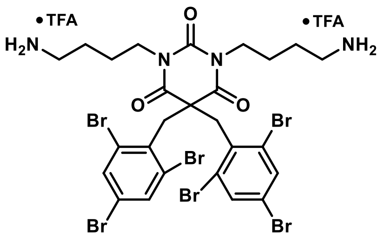

1,3-bis(4-aminobutyl)-5,5-bis(2,4,6-tribromobenzyl)pyrimidine-2,4,6(1H,3H,5H)-trione **10gA**.
Barbiturate **3g** (70 mg, 90 µmol, 1.0 eq), *tert*-butyl (4-hydroxybutyl)carbamate (42 mg, 224 µmol, 2.5 eq), PPh_3 (70 mg, 269 µmol, 3.0 eq) and DIAD (56 µL, 269 µmol, 3.0 eq) were stirred in anhydrous DMPU:dimethylcarbonate (1:1, 4.0 mL) for 24 h. The crude was purified with 10-40% EtOAc in heptane to yield impure boc-**10gA** (101 mg, 90 µmol, 100%) as a colorless viscous oil.
TFA (69 µL, 0.90 mmol, 10.0 eq) and DCM (1.0 mL) were added, and the mixture was stirred at ambient temperature for 18 h. The crude was purified by automated RP column chromatography with a gradient of 15-50% MeCN/H_2O + 0.1% TFA to yield the di-TFA salt of **10gA** (26 mg, 23 µmol, 25% o2s) as a white powder. **^{1}H NMR** (400 MHz, Methanol-*d4*) δ 7.81 (s, 2H), 4.03 (s, 2H), 3.77 (t, *J* = 7.3 Hz, 2H), 2.94 – 2.83 (m, 2H), 1.55 (p, *J* = 7.7 Hz, 2H), 1.43 – 1.32 (m, 2H). **^{13}C NMR** (101 MHz, Methanol-*d4*) δ 170.6 (2C), 151.7, 137.0 (2C), 136.1 (4C), 128.6 (4C), 123.0 (2C), 57.3, 45.7 (2C), 42.6 (2C), 40.2 (2C), 25.9 (2C), 25.6 (2C). *TFA signals were observed but are not reported.* **HRMS** (ESI): calcd for $C_{26}H_{29}Br_6N_4O_3^+$ [M+H]$^+$ 918.7334, found: 918.7332. **SFC**: 96.5%.

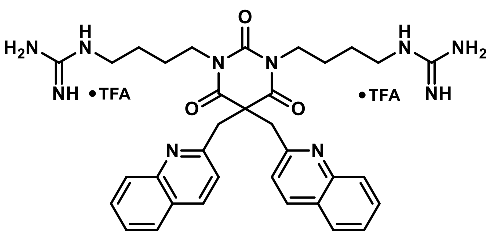

1,1'-((2,4,6-trioxo-5,5-bis(quinolin-2-ylmethyl)dihydropyrimidine-1,3(2H,4H)-diyl)bis(butane-4,1-diyl))diguanidine **10bG**.
Barbiturate **3b** (49 mg, 120 µmol, 1.0 eq), *N,N*'-di(*tert*-butoxycarbonyl)-guanidinylbutanol (80 mg, 240 µmol, 2.5 eq), PPh_3 (273 mg, 1.05 mmol, 3.0 eq) and DIAD (75 µL, 360 µmol, 3.0 eq) were stirred in DCM (1.0 mL) for 16 h. The crude was purified with 10-70% EtOAc in heptane to yield boc-**10bG** (85 mg, 82 µmol, 68%) as a slightly yellow highly viscous oil.
TFA (138 µL, 1.80 mmol, 15.0 eq) and DCM (1.0 mL) were added, and the mixture was stirred at ambient temperature for 17 h. The crude was purified by automated RP column chromatography with a gradient of 0-70% MeCN/H_2O + 0.1% TFA to yield the di-TFA salt of **10bG** (39 mg, 45 µmol, 38% o2s) as a slightly brown solid. **^{1}H NMR** (400 MHz, Methanol-*d4*) δ 8.22 (d, *J* = 8.5 Hz, 2H), 7.93 – 7.82

(m, 2H), 7.75 – 7.66 (m, 4H), 7.55 (dq, *J* = 8.1, 4.5, 4.0 Hz, 2H), 7.37 (d, *J* = 8.5 Hz, 2H), 3.94 (s, 4H), 3.81 (t, *J* = 7.0 Hz, 4H), 2.82 (t, *J* = 7.4 Hz, 4H), 1.40 (p, *J* = 7.1 Hz, 4H), 1.22 – 1.11 (m, 4H). **^{13}C NMR** (101 MHz, Methanol-*d4*) δ 172.9 (2C), 156.9 (2C), 156.7 (2C), 152.1, 146.8 (2C), 136.7 (2C), 129.6 (2C), 127.7 (4C), 127.1 (2C), 126.3 (2C), 121.1 (2C), 53.5, 47.0 (2C), 40.9 (2C), 40.4 (2C), 25.5 (2C), 24.8 (2C). **HRMS** (ESI): calcd for $C_{34}H_{41}N_{10}O_3^+$ [M+H]$^+$ 637.3358, found 637.3353. **SFC**: 99.3%.

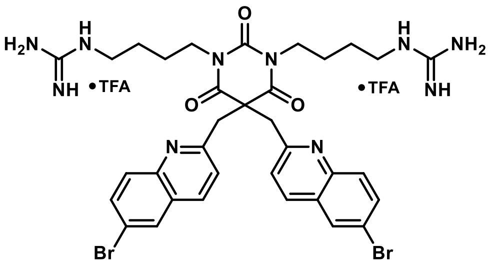

1,1'-((5,5-bis((6-bromoquinolin-2-yl)methyl)-2,4,6-triox-odihydropyrimidine-1,3(2H,4H)-diyl)bis(butane-4,1-diyl))diguanidine **10cG**.
Barbiturate **3c** (35 mg, 62 µmol, 1.0 eq), *N,N*'-di(*tert*-butoxycarbonyl)-guanidinylbutanol (51 mg, 154 µmol, 2.5 eq), PPh_3 (48 mg, 185 µmol, 3.0 eq) and DIAD (39 µL, 185 µmol, 3.0 eq) were stirred in DCM (1.0 mL) for 20 h. The crude was purified with 30-70% EtOAc in heptane to yield boc-**10cG** (72 mg, 60 µmol, 98%) as a yellow highly viscous oil.
TFA (71 µL, 0.92 mmol, 15.0 eq) and DCM (1.0 mL) were added, and the mixture was stirred at ambient temperature for 22 h. The crude was purified by automated RP column chromatography with a gradient of 10-60% MeCN/H_2O + 0.1% TFA to yield the di-TFA salt of **10cG** (41 mg, 40 µmol, 65% o2s) as a white powder. **^{1}H NMR** (400 MHz, Methanol-*d4*) δ 8.17 (d, *J* = 8.5 Hz, 2H), 8.09 (d, *J* = 2.2 Hz, 2H), 7.80 (dd, *J* = 9.0, 2.2 Hz, 2H), 7.60 (d, *J* = 9.0 Hz, 2H), 7.41 (d, *J* = 8.5 Hz, 2H), 3.92 (s, 4H), 3.82 (t, *J* = 7.0 Hz, 4H), 2.85 (t, *J* = 7.4 Hz, 4H), 1.41 (p, *J* = 7.1 Hz, 4H), 1.19 (qd, *J* = 7.1, 5.9, 3.9 Hz, 4H). **^{13}C NMR** (101 MHz, Methanol-*d4*) δ 174.0 (2C), 158.9 (2C), 158.3 (2C), 153.4, 146.7 (2C), 137.3 (2C), 134.3 (2C), 131.3 (2C), 131.0 (2C), 129.6 (2C), 123.5 (2C), 121.2 (2C), 54.5, 48.3 (2C), 42.3 (2C), 41.8 (2C), 26.8 (2C), 26.2 (2C). **HRMS** (ESI): calcd for $C_{34}H_{39}Br_2N_{10}O_3^+$ [M+H]$^+$ 793.1568, found 793.1575. **SFC**: >99.5%.

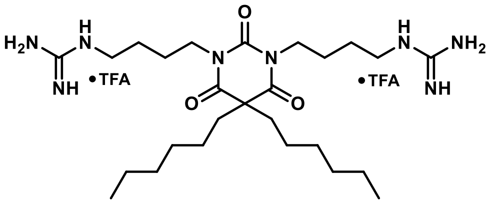

1,1'-((5,5-dihexyl-2,4,6-trioxodihydropyrimidine-1,3(2H,4H)-diyl)bis(butane-4,1-diyl))diguanidine **10dG**.
Barbiturate **3d** (22 mg, 74 µmol, 1.0 eq), *N,N*'-di(*tert*-butoxycarbonyl)-guanidinylbutanol (62 mg, 186 µmol, 2.5 eq), PPh_3 (58 mg, 223 µmol, 3.0 eq) and DIAD (48 µL, 223 µmol, 3.0 eq) were stirred in DCM (1.0 mL) for 20 h. The crude was purified with 10-40% EtOAc in heptane to yield boc-**10dG** (66 mg, 72 µmol, 96%) as a yellow oil.
TFA (85 µL, 1.11 mmol, 15.0 eq) and DCM (1.0 mL) were added, and the mixture was stirred at ambient temperature for 22 h. The crude was purified by automated RP column chromatography with a gradient of 10-60% MeCN/H_2O + 0.1% TFA to yield the di-TFA salt of **10dG** (48 mg, 64 µmol, 86% o2s) as a white powder. **^{1}H NMR** (400 MHz, Methanol-*d4*) δ 3.94 (t, *J* = 6.9 Hz, 4H), 3.23 (t, *J* = 6.8 Hz, 4H), 2.00 – 1.91 (m, 4H), 1.74 – 1.57 (m, 8H), 1.33 – 1.17 (m, 12H), 1.08 (dd, *J* = 10.4, 6.4 Hz, 4H), 0.87 (t, *J* = 6.9 Hz, 6H). **^{13}C NMR** (101 MHz, Methanol-*d4*) δ 173.3 (2C), 158.9 (2C), 152.0, 57.8, 42.4 (2C), 42.0 (2C), 41.1 (2C), 32.4 (2C), 30.1 (2C), 27.2 (2C), 26.2 (2C), 26.0 (2C), 23.5 (2C), 14.3 (2C). **HRMS** (ESI): calcd for $C_{26}H_{51}N_8O_3^+$ [M+H]$^+$ 523.4079, found 523.4078. **SFC**: >99.5%.

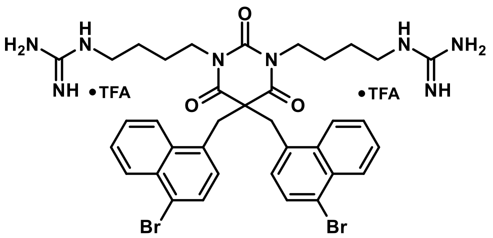

1,1'-((5,5-bis((4-bromonaphthalen-1-yl)methyl)-2,4,6-tri-oxodihydropyrimidine-1,3(2H,4H)-diyl)bis(butane-4,1-diyl))diguanidine **10eG**.
Barbiturate **3e** (71 mg, 125 µmol, 1.0 eq), *N,N*'-di(*tert*-butoxycarbonyl)-guanidinylbutanol (83 mg, 250 µmol, 2.0 eq), PPh_3 (98 mg, 375 µmol, 3.0 eq) and DIAD (79 µL, 275 µmol, 3.0 eq) were stirred in DCM (1.5 mL) for 16 h. The crude was purified with 10-60% EtOAc in heptane to yield boc-**10eG** (124 mg, 104 µmol, 83%) as a colorless oil.
TFA (287 µL, 3.76 mmol, 30.0 eq) and DCM (1.5 mL) were added, and the mixture was stirred at ambient temperature for 36 h. The crude was purified by automated RP column chromatography with a gradient of 0-70% MeCN/H_2O + 0.1% TFA to yield the di-TFA salt of **10eG** (85 mg, 83 µmol, 67%

o2s) as a white solid. **^{1}H NMR** (400 MHz, Methanol-*d4*) δ 8.38 – 8.29 (m, 2H), 8.22 (dt, *J* = 7.8, 2.7 Hz, 2H), 7.68 (d, *J* = 7.8 Hz, 2H), 7.66 – 7.61 (m, 4H), 7.15 (d, *J* = 7.8 Hz, 2H), 4.13 (s, 4H), 3.36 (t, *J* = 7.2 Hz, 4H), 2.87 (t, *J* = 7.1 Hz, 4H), 0.97 (ddd, *J* = 14.3, 7.5, 4.0 Hz, 4H), 0.84 (tt, *J* = 8.4, 6.2 Hz, 4H). **^{13}C NMR** (101 MHz, Methanol-*d4*) δ 172.0 (2C), 158.5(2C), 150.9, 134.4 (2C), 133.5 (2C), 133.4 (2C), 130.4 (2C), 129.4 (2C), 128.7 (2C), 128.5 (2C), 128.1 (2C), 126.2 (2C), 123.8 (2C), 60.4, 42.1 (2C), 41.8 (2C), 41.6 (2C), 26.5 (2C), 25.4 (2C). **HRMS** (ESI): calcd for $C_{36}H_{41}Br_2N_8O_3^+$ [M+H]$^+$ 791.1663, found 791,1665. **SFC**: >99.5%.

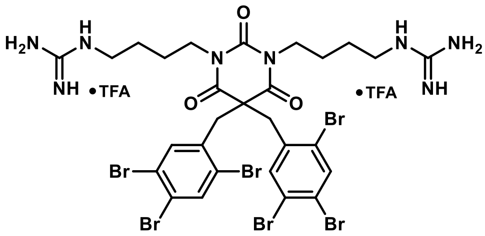

1,1'-((2,4,6-trioxo-5,5-bis(2,4,5-tribromobenzyl)dihydropyrimidine-1,3(2H,4H)-diyl)bis(butane-4,1-diyl))diguanidine **10fG.**

3f (80 mg, 102 µmol, 1.0 eq), *N,N*'-di(*tert*-butoxycarbonyl)-guanidinylbutanol (58 mg, 307 µmol, 3.0 eq), PPh_3 (81 mg, 307 µmol, 3.0 eq) and DIAD (64 µL, 307 µmol, 3.0 eq) were stirred in DCM (0.5 mL) for 12 h. The crude was purified with 0-40% EtOAc in heptane to yield boc-**10fG** (98 mg, 70 µmol, 68%) as a slightly yellow oil.
TFA (80 µL, 1.04 mmol, 15.0 eq) and DCM (1.0 mL) were added, and the mixture was stirred at ambient temperature for 18 h. The crude was purified by automated RP column chromatography with a gradient of 20-45% MeCN/H_2O + 0.1% TFA to yield the di-TFA salt of **10fG** (43 mg, 35 µmol, 34% o2s) as a white powder. **^{1}H NMR** (400 MHz, Methanol-*d4*) δ 7.95 (s, 2H), 7.31 (s, 2H), 3.81 (t, *J* = 6.9 Hz, 4H), 3.64 (s, 4H), 3.16 (t, *J* = 6.6 Hz, 4H), 1.57 – 1.41 (m, 8H). **^{13}C NMR** (101 MHz, Methanol-*d4*) δ 170.7 (2C), 158.6 (2C), 150.9, 138.6 (2C), 137.6 (2C), 135.8 (2C), 125.7 (2C), 125.5 (2C), 124.7 (2C), 58.0, 43.5 (2C), 43.0 (2C), 42.0 (2C), 27.0 (2C), 26.2 (2C). **HRMS** (ESI): calcd for $C_{28}H_{33}Br_6N_8O_3^+$ [M+H]$^+$ 1002.7770, found: 1002.7768. **SFC**: 98.5%.

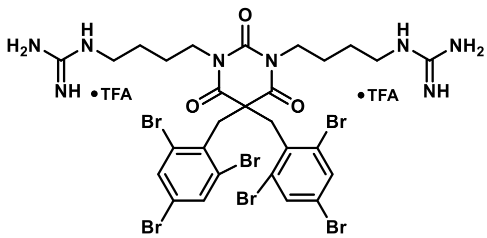

1,1'-((2,4,6-trioxo-5,5-bis(2,4,6-tribromobenzyl)dihydropyrimidine-1,3(2H,4H)-diyl)bis(butane-4,1-diyl))diguanidine **10gG**.

Barbiturate **3g** (70 mg, 90 µmol, 1.0 eq), *N,N*'-di(*tert*-butoxycarbonyl)-guanidinylbutanol (74 mg, 224 µmol, 2.5 eq), PPh_3 (70 mg, 269 µmol, 3.0 eq) and DIAD (56 µL, 269 µmol, 3.0 eq) were stirred in anhydrous DMPU:dimethylcarbonate (1:1, 4.0 mL) for 24 h. The crude was purified with 10-40% EtOAc in heptane to yield boc-**10gG** (79 mg, 56 µmol, 63%) as a colorless oil.
TFA (206 µL, 2.68 mmol, 30.0 eq) and DCM (1.0 mL) were added, and the mixture was stirred at ambient temperature for 43 h. The crude was purified by automated RP column chromatography with a gradient of 20-55% MeCN/H_2O + 0.1% TFA to yield the di-TFA salt of **10gG** (37 mg, 30 µmol, 33% o2s) as a white powder. **^{1}H NMR** (400 MHz, Methanol-*d4*) δ 7.80 (s, 4H), 4.02 (s, 4H), 3.77 (t, *J* = 7.1 Hz, 4H), 3.13 (t, *J* = 7.0 Hz, 4H), 1.52 – 1.31 (m, 8H). **^{13}C NMR** (101 MHz, Methanol-*d4*) δ 170.6 (2C), 158.7 (2C), 151.7, 137.0 (2C), 136.1 (4C), 128.5 (4C), 123.0 (2C), 57.3, 45.8 (2C), 42.9 (2C), 42.0 (2C), 27.2 (2C), 25.8 (2C). **HRMS** (ESI): calcd for $C_{28}H_{34}Br_6N_8O_3$ for [M+2H]$^{2+}$ 501.8922, found: 501.8917. **SFC**: 98.1%.

2.8 Synthesis of *series 3*

The following products were synthesized according to General Procedure D:

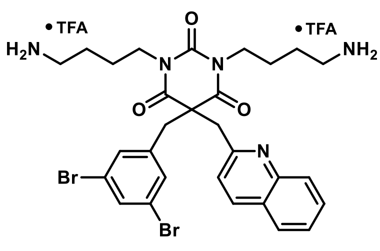

1,3-bis(4-aminobutyl)-5-(3,5-dibromobenzyl)-5-(quinolin-2-ylmethyl)pyrimidine-2,4,6(1H,3H,5H)-trione **11kA**.

Barbiturate **3k** (55 mg, 107 µmol, 1.0 eq), *tert*-butyl (4-hydroxybutyl)carbamate (50 mg, 266 µmol, 2.5 eq), PPh_3 (84 mg, 319 µmol, 3.0 eq) and DIAD (67 µL, 319 µmol, 3.0 eq) were stirred in DCM (0.5 mL) for 16 h. The crude was purified with 10-50% EtOAc in heptane to yield impure boc-**11kA** (145 mg, 169 µmol, 159%) as a colorless oil.

TFA (81 µL, 1.06 mmol, 10.00 eq) and DCM (0.7 mL) were added, and the mixture was stirred at ambient temperature for 21 h. The crude was purified by automated RP column chromatography with a gradient of 15-53% MeCN/H_2O + 0.1% TFA to yield the di-TFA salt of **11kA** (70 mg, 81 µmol, 76% o2s) as a white solid. **^{1}H NMR** (400 MHz, Methanol-*d4*) δ 8.21 (d, *J* = 8.5 Hz, 1H), 7.86 (dd, *J* = 8.1, 1.5 Hz, 1H), 7.72 (t, *J* = 1.7 Hz, 1H), 7.65 (ddd, *J* = 8.4, 6.9, 1.5 Hz, 1H), 7.51 (ddd, *J* = 8.2, 6.9, 1.2 Hz, 1H), 7.48 – 7.44 (m, 1H), 7.41 (d, *J* = 8.5 Hz, 1H), 7.25 (d, *J* = 1.8 Hz, 2H), 4.03 (s, 2H), 3.87 – 3.69 (m, 4H), 3.36 (s, 2H), 2.87 – 2.71 (m, 4H), 1.67 – 1.38 (m, 8H). **^{13}C NMR** (101 MHz, Methanol-*d4*) δ 173.2 (2C), 158.6, 152.4, 147.8, 140.1, 138.11, 134.6, 132.7 (2C), 130.9, 129.2, 128.6, 128.4, 127.5, 124.0 (2C), 122.0, 56.8, 46.4, 45.9, 42.2 (2C), 40.1 (2C), 26.3 (2C), 25.9 (2C). **HRMS** (ESI): calcd for $C_{29}H_{34}Br_2N_5O_3^+$ [M+H]$^+$ 658.1023, found 658.1027. **SFC**: >99.5%.

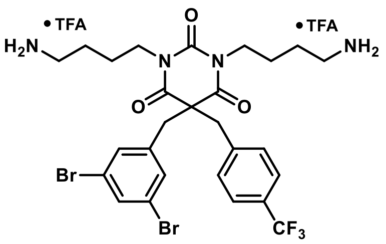

1,3-bis(4-aminobutyl)-5-(3,5-dibromobenzyl)-5-(4-(trifluoromethyl)benzyl)pyrimidine-2,4,6(1H,3H,5H)-trione **11lA**.
Barbiturate **3l** (36 mg, 67 µmol, 1.0 eq), *tert*-butyl (4-hydroxybutyl)carbamate (32 mg, 169 µmol, 2.5 eq), PPh_3 (53 mg, 202 µmol, 3.0 eq) and DIAD (42 µL, 202 µmol, 3.0 eq) were stirred in DCM (0.5 mL) for 16 h. The crude was purified with 10-40% EtOAc in heptane to yield boc-**11lA** (55 mg, 63 µmol, 93%) as a colorless oil. TFA (41 µL, 539 µmol, 8.00 eq) and DCM (0.7 mL) were added, and the mixture was stirred at ambient temperature for 17 h. The crude was purified by automated RP column chromatography with a gradient of 15-60% MeCN/H_2O + 0.1% TFA to yield the di-TFA salt of **11lA** (41 mg, 47 µmol, 69% o2s) as a white powder. **^{1}H NMR** (400 MHz, Methanol-*d4*) δ 7.66 (t, *J* = 1.8 Hz, 1H), 7.57 (d, *J* = 8.1 Hz, 2H), 7.27 (d, *J* = 8.1 Hz, 2H), 7.24 (d, *J* = 1.8 Hz, 2H), 3.70 (ddd, *J* = 13.0, 9.3, 5.7 Hz, 2H), 3.59 (ddd, *J* = 13.0, 9.0, 5.9 Hz, 2H), 3.53 (s, 2H), 3.46 (s, 2H), 2.97 – 2.86 (m, 4H), 1.56 – 1.45 (m, 4H), 1.45 – 1.24 (m, 4H). **^{13}C NMR** (101 MHz, Methanol-*d4*) δ 171.3 (2C), 150.6, 140.8 – 140.7 (m, 2C), 140.7, 134.5, 132.8 (2C), 131.4 (2C), 131.08 (q, *J* = 32.4 Hz). 126.7 (q, *J*, = 3.5 Hz, 2C), 124.1 (2C), 61.1, 45.6, 45.1, 42.1 (2C), 40.2 (2C), 26.0 (2C), 25.7 (2C). *CF_3 carbon was not observed, due to too low intensity*. **HRMS** (ESI): calcd for $C_{27}H_{32}Br_4F_3N_4O_3^+$ [M+H]$^+$ 675.0788, found 675.0793. **SFC**: 95.3%.

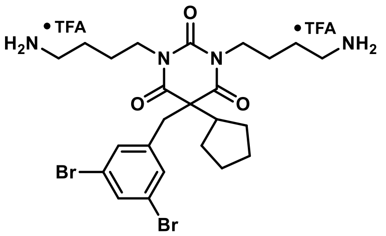

1,3-bis(4-aminobutyl)-5-cyclopentyl-5-(3,5-dibromobenzyl)pyrimidine-2,4,6(1H,3H,5H)-trione **11mA**.
Barbiturate **3m** (45 mg, 101 µmol, 1.0 eq), *tert*-butyl (4-hydroxybutyl)carbamate (48 mg, 253 µmol, 2.5 eq), PPh_3 (81 mg, 304 µmol, 3.0 eq) and DIAD (64 µL, 304 µmol, 3.0 eq) were stirred in DCM (1.0 mL) for 16 h. The crude was purified with 10-50% EtOAc in heptane to yield boc-**11mA** (63 mg, 80 µmol, 79%) as a yellow oil. TFA (116 µL, 1.52 mmol, 15.00 eq) and DCM (1.0 mL) were added, and the mixture was stirred at ambient temperature for 17 h. The crude was purified by automated RP column chromatography with a gradient of 15-60% MeCN/H_2O + 0.1% TFA to yield the di-TFA salt of **11mA** (21 mg, 26 µmol, 25% o2s) as a white powder. **^{1}H NMR** (400 MHz, Methanol-*d4*) δ 7.61 (t, *J* = 1.8 Hz, 1H), 7.23 (d, *J* = 1.8 Hz, 2H), 3.83 (t, *J* = 7.3 Hz, 4H), 3.37 (s, 2H), 3.03 – 2.90 (m, 4H), 2.60 (h, *J* = 8.1 Hz, 1H), 1.78 (d, *J* = 8.9 Hz, 2H), 1.69 – 1.45 (m, 14H). **^{13}C NMR** (101 MHz, Methanol-*d4*) δ 171.6 (2C), 151.4, 141.9, 134.0, 133.1 (2C), 123.8 (2C), 61.3, 51.8, 42.2 (2C), 42.0, 40.3 (2C), 28.4, 26.2 (2C), 25.9, 25.5 (2C). **HRMS** (ESI): calcd for $C_{24}H_{35}Br_2N_4O_3^+$ [M+H]$^+$ 585.1070, found 585.1068. **SFC**: >99.5%.

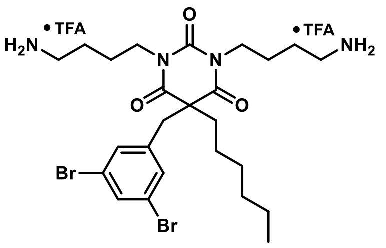

1,3-bis(4-aminobutyl)-5-(3,5-dibromobenzyl)-5-hexylpyrimidine-2,4,6(1H,3H,5H)-trione **11nA**.
Barbiturate **3n** (52 mg, 113 µmol, 1.0 eq), *tert*-butyl (4-hydroxybutyl)carbamate (54 mg, 283 µmol, 2.5 eq), PPh_3 (89 mg, 339 µmol, 3.0 eq) and DIAD (71 µL, 339 µmol, 3.0 eq) were stirred in DCM (1.0 mL) for 20 h. The crude was purified with 10-50% EtOAc in heptane to yield boc-**11nA** (86 mg, 107 µmol, 95%) as a colorless oil.

TFA (87 µL, 1.13 mmol, 10.0 eq) and DCM (1.0 mL) were added, and the mixture was stirred at ambient temperature for 22 h. The crude was purified by automated RP column chromatography with a gradient of 15-60% $MeCN/H_2O$ + 0.1% TFA to yield the di-TFA salt of **11nA** (68 mg, 82 µmol, 73% o2s) as a white powder. **^{1}H NMR** (400 MHz, Methanol-*d4*) δ 7.64 (t, *J* = 1.8 Hz, 1H), 7.17 (d, *J* = 1.8 Hz, 2H), 3.80 (tdd, *J* = 13.0, 8.8, 7.3 Hz, 4H), 3.23 (s, 2H), 2.97 (td, *J* = 7.2, 3.0 Hz, 4H), 2.17 – 2.08 (m, 2H), 1.70 – 1.54 (m, 6H), 1.47 (qt, *J* = 10.6, 3.3 Hz, 2H), 1.34 – 1.20 (m, 6H), 1.11 (tt, *J* = 11.7, 6.6 Hz, 2H), 0.93 – 0.84 (m, 3H). **^{13}C NMR** (101 MHz, Methanol-*d4*) δ 172.1 (2C), 151.1, 140.9, 134.3, 132.6 (2C), 124.0 (2C), 59.4, 45.7, 42.3 (2C), 40.7, 40.3 (2C), 32.3, 30.1, 26.2 (2C), 25.9, 25.8 (2C), 23.5, 14.23. **HRMS** (ESI): calcd for $C_{25}H_{39}Br_2N_4O_3^+$ $[M+H]^+$ 601.1383, found 601.1384. **SFC**: 95.2%.

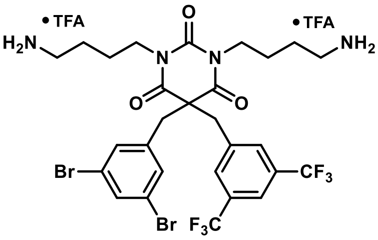

1,3-bis(4-aminobutyl)-5-(3,5-bis(trifluoromethyl)benzyl)-5-(3,5-dibromobenzyl)pyrimidine-2,4,6(1H,3H,5H)-trione **11oA**.

Barbiturate **3o** (90 mg, 150 µmol, 1.0 eq), *tert*-butyl (4-hydroxybutyl)carbamate (85 mg, 449 µmol, 3.0 eq), PPh_3 (118 mg, 449 µmol, 3.0 eq) and DIAD (94 µL, 449 µmol, 3.0 eq) were stirred in anhydrous THF (1.0 mL) for 12 h. The crude was purified with 0-40% EtOAc in heptane to yield boc-**11oA** (110 mg, 117 µmol, 78%) as a pale-yellow oil.

TFA (90 µL, 1.17 mmol, 10.0 eq) and DCM (1.0 mL) were added, and the mixture was stirred at ambient temperature for 18 h. The crude was purified by automated RP column chromatography with a gradient of 20-45% $MeCN/H_2O$ + 0.1% TFA to yield the di-TFA salt of **11oA** (82 mg, 84 µmol, 56% o2s) as a white foam. **^{1}H NMR** (400 MHz, Methanol-*d4*) δ 7.90 (s, 1H), 7.68 – 7.64 (m, 3H), 7.24 (d, *J* = 1.7 Hz, 2H), 3.71 – 3.53 (m, 4H), 3.65 (s, 2H), 3.47 (s, 2H), 2.90 (dd, *J* = 9.1, 6.6 Hz, 4H), 1.59 – 1.48 (m, 4H), 1.46 – 1.26 (m, 4H). **^{13}C NMR** (101 MHz, Methanol-*d4*) δ 171.1 (2C), 150.3, 140.3, 139.6, 134.7, 133.0 (q, *J* = 33.3 Hz, 2C) 132.7 (2C), 131.4 (q, *J* = 2.7 Hz, 2C), 124.6 (q, *J* = 272.2 Hz, 2C), 124.2 (2C), 122.9 – 122.7 (m, 1C), 61.2, 45.3, 44.4, 42.2 (2C), 40.1 (2C), 26.1 (2C), 25.7 (2C). **HRMS** (ESI): calcd for $C_{28}H_{31}Br_2F_6N_4O_3^+$ $[M+H]^+$ 743.0662, found 743.0670. **SFC**: 97.4%.

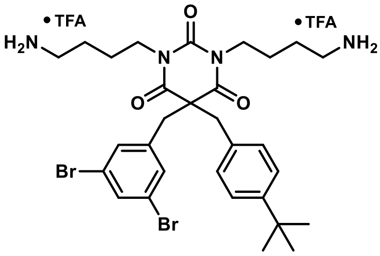

1,3-bis(4-aminobutyl)-5-(4-(tert-butyl)benzyl)-5-(3,5-dibromobenzyl)pyrimidine-2,4,6(1H,3H,5H)-trione **11pA**.

Barbiturate **3p** (56 mg, 107 µmol, 1.0 eq), *tert*-butyl (4-hydroxybutyl)carbamate (51 mg, 268 µmol, 2.5 eq), PPh_3 (85 mg, 322 µmol, 3.0 eq) and DIAD (67 µL, 322 µmol, 3.0 eq) were stirred in DCM (1.0 mL) for 6 h. The crude was purified with 0-45% EtOAc in heptane to yield impure boc-**11pA** (101 mg, 117 µmol, 109%) as a yellow solid.

TFA (82 µL, 1.07 mmol, 10.00 eq) and DCM (1.0 mL) were added, and the mixture was stirred at ambient temperature for 17 h. The crude was purified by automated RP column chromatography with a gradient of 10-65% $MeCN/H_2O$ + 0.1% TFA to yield the di-TFA salt of **11pA** (85 mg, 95 µmol, 89% o2s) as a white powder. **^{1}H NMR** (400 MHz, Methanol-*d4*) δ 7.63 (t, *J* = 1.8 Hz, 1H), 7.30 – 7.25 (m, 2H), 7.24 (d, *J* = 1.7 Hz, 2H), 7.00 – 6.93 (m, 2H), 3.68 (ddd, *J* = 13.0, 8.8, 6.0 Hz, 2H), 3.56 (ddd, *J* = 13.0, 8.7, 6.2 Hz, 2H), 3.44 (s, 2H), 3.38 (s, 2H), 2.91 (td, *J* = 7.2, 1.9 Hz, 4H), 1.57 – 1.44 (m, 4H), 1.44 – 1.30 (m, 4H), 1.25 (s, 9H). **^{13}C NMR** (101 MHz, Methanol-*d4*) δ 171.7 (2C), 152.2, 150.70, 141.21, 134.2, 132.8 (2C), 130.2 (2C), 126.6 (2C), 124.0 (2C), 61.6, 46.5, 44.2, 41.9 (2C), 40.17 (2C), 35.3, 31.7 (3C), 26.0 (2C), 25.7 (2C). **HRMS** (ESI): calcd for $C_{30}H_{41}Br_2N_4O_3^+$ $[M+H]^+$ 663.1540, found 663.1545. **SFC**: 98.8%.

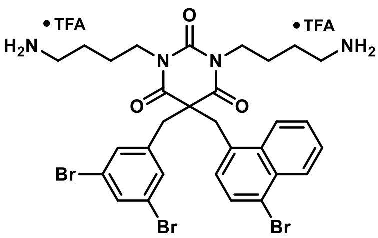

1,3-bis(4-aminobutyl)-5-((4-bromonaphthalen-1-yl)methyl)-5-(3,5-dibromobenzyl)pyrimidine-2,4,6(1H,3H,5H)-trione **11qA**.

Barbiturate **3q** (55 mg, 92 µmol, 1.0 eq), *tert*-butyl (4-hydroxybutyl)carbamate (44 mg, 231 µmol, 2.5 eq), PPh_3 (73 mg, 277 µmol, 3.0 eq) and DIAD (58 µL, 277 µmol, 3.0 eq) were stirred in DCM (0.5 mL) for 16 h. The crude was purified with 10-65% EtOAc in heptane to yield boc-**11qA** (85 mg, 91 µmol, 98%) as a colorless oil.

TFA (57 µL, 740 µmol, 8.00 eq) and DCM (0.7 mL) were added, and the mixture was stirred at ambient temperature for 17 h. The crude was purified by automated RP column chromatography with a gradient of 15-60% MeCN/H_2O + 0.1% TFA to yield the di-TFA salt of **11qA** (62 mg, 66 µmol, 71% o2s) as a white powder. **^{1}H NMR** (400 MHz, Methanol-*d4*) δ 8.30 – 8.22 (m, 1H), 8.17 (dt, *J* = 7.9, 2.6 Hz, 1H), 7.72 (d, *J* = 7.7 Hz, 1H), 7.68 – 7.60 (m, 3H), 7.28 (d, *J* = 1.8 Hz, 2H), 7.15 (d, *J* = 7.8 Hz, 1H), 3.96 (s, 2H), 3.62 (s, 2H), 3.50 (ddd, *J* = 13.1, 8.9, 6.0 Hz, 2H), 3.39 (ddd, *J* = 13.1, 8.9, 5.9 Hz, 2H), 2.88 – 2.73 (m, 4H), 1.31 (h, *J* = 7.4 Hz, 4H), 1.21 – 0.99 (m, 4H). **^{13}C NMR** (101 MHz, Methanol-*d4*) δ 171.5 (2C), 150.5, 141.2, 134.3, 134.2, 133.4, 133.1 (2C), 132.8, 130.6, 128.8, 128.7, 128.3, 126.2, 124.0, 123.9 (2C), 61.1, 44.0, 42.4, 42.0 (2C), 40.2 (2C), 25.7 (2C), 25.6 (2C). **HRMS** (ESI): calcd for $C_{30}H_{34}Br_3N_4O_3^+$ [M+H]$^+$ 735.0176, found 735.0181. **SFC**: 96.1%.

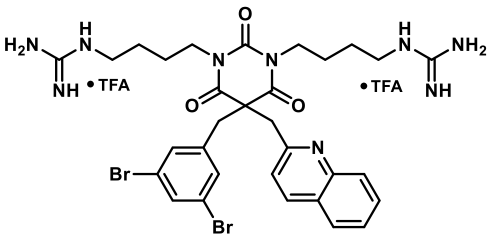

1,1'-((5-(3,5-dibromobenzyl)-2,4,6-trioxo-5-(quinolin-2-ylmethyl)dihydropyrimidine-1,3(2H,4H)-diyl)bis(butane-4,1-diyl))diguanidine **11kG**.

Barbiturate **3k** (42 mg, 81 µmol, 1.0 eq), *N,N*'-di(*tert*-butoxycarbonyl)-guanidinylbutanol (67 mg, 203 µmol, 2.5 eq), PPh_3 (64 mg, 244 µmol, 3.0 eq) and DIAD (51 µL, 245 µmol, 3.0 eq) were stirred in DCM (1.0 mL) for 20 h. The crude was purified with 10-45% EtOAc in heptane to yield impure boc-**11kG** (149 mg, 130 µmol, 160%) as a white solid.

TFA (187 µL, 2.44 mmol, 30.00 eq) and DCM (0.7 mL) were added, and the mixture was stirred at ambient temperature for 48 h. The crude was purified by automated RP column chromatography with a gradient of 15-53% MeCN/H_2O + 0.1% TFA to yield the di-TFA salt of **11kG** (32 mg, 33 µmol, 41% o2s) as a white powder. **^{1}H NMR** (400 MHz, Methanol-*d4*) δ 8.20 (d, *J* = 8.5 Hz, 1H), 7.89 – 7.82 (m, 1H), 7.70 (t, *J* = 1.8 Hz, 1H), 7.64 (ddd, *J* = 8.4, 7.0, 1.4 Hz, 1H), 7.50 (ddd, *J* = 8.1, 7.0, 1.2 Hz, 1H), 7.47 (d, *J* = 8.4 Hz, 1H), 7.41 (d, *J* = 8.5 Hz, 1H), 7.24 (d, *J* = 1.7 Hz, 2H), 4.02 (s, 2H), 3.88 – 3.68 (m, 4H), 3.35 (d, *J* = 2.0 Hz, 2H), 3.11 – 2.91 (m, 5H), 1.67 – 1.33 (m, 8H). **^{13}C NMR** (101 MHz, Methanol-*d4*) δ 173.2 (2C), 158.6 (2C), 158.4, 152.4, 147.8, 140.1, 138.1, 134.5, 132.6 (2C), 130.9, 129.2, 128.6, 128.3, 127.5, 124.0 (2C), 122.0, 56.8, 46.4, 45.9, 42.5 (2C), 42.0 (2C), 27.0 (2C), 26.4 (2C). **HRMS** (ESI): calcd for $C_{27}H_{43}Br_2N_8O_3^+$ [M+H]$^+$ 742.1459, found 742.1456. **SFC**: >99.5%.

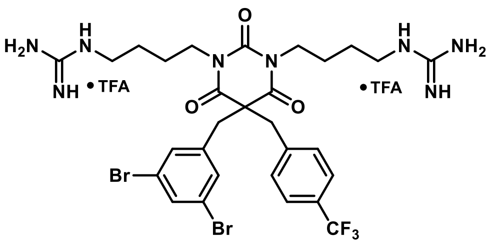

(4-(5-(3,5-dibromobenzyl)-3-(4-guanidinobutyl)-2,4,6-tri-oxo-5-(4-(trifluoromethyl)benzyl)tetrahydropyrimidin-1(2H)-yl)butyl)-l2-azanecarboximidamide **11lG**.

Barbiturate **3l** (43 mg, 81 µmol, 1.0 eq), *N,N*'-di(*tert*-butoxycarbonyl)-guanidinylbutanol (67 mg, 201 µmol, 2.5 eq), PPh_3 (63 mg, 242 µmol, 3.0 eq) and DIAD (51 µL, 242 µmol, 3.0 eq) were stirred in DCM (1.0 mL) for 20 h. The crude was purified with 10-35% EtOAc in heptane to yield boc-**11lG** (82 mg, 71 µmol, 88%) as a white solid.

TFA (185 µL, 2.42 mmol, 30.00 eq) and DCM (0.7 mL) were added, and the mixture was stirred at ambient temperature for 48 h. The crude was purified by automated RP column chromatography with a gradient of 15-60% MeCN/H_2O + 0.1% TFA to yield the di-TFA salt of **11lG** (55 mg, 56 µmol, 69% o2s) as a white powder. **^{1}H NMR** (400 MHz, Methanol-*d4*) δ 7.64 (t, *J* = 1.8 Hz, 1H), 7.59 – 7.53 (m, 2H), 7.26 (d, *J* = 8.7 Hz, 2H), 7.23 (d, *J* = 1.8 Hz, 2H), 3.75 – 3.64 (m, 2H), 3.64 – 3.55 (m, 2H), 3.52 (s, 2H), 3.45 (s, 2H), 3.16 (t, *J* = 6.6 Hz, 4H), 1.48 – 1.28 (m, 8H). **^{13}C NMR** (101 MHz, Methanol-*d4*) δ 171.4 (2C), 158.7 (2C), 150.6, 140.7 (2C), 134.4, 132.9 (2C), 131.4 (2C), 131.1 (q, *J* = 32.4 Hz), 126.6 (q, *J* = 3.8 Hz, 2C), 125.4 (q, *J* = 272.7 Hz), 124.1 (2C), 61.1, 45.7, 45.0, 42.4 (2), 41.9 (2C), 26.9 (2C), 26.1 (2C). **HRMS** (ESI): calcd for $C_{29}H_{36}Br_2F_3N_8O_3^+$ [M+H]$^+$ 759.1224, found 759.1221. **SFC**: 98.5%.

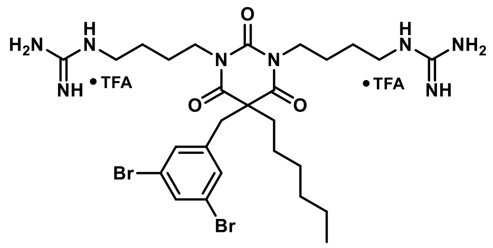

1,1'-((5-(3,5-dibromobenzyl)-5-hexyl-2,4,6-trioxodihydro-pyrimidine-1,3(2H,4H)-diyl)bis(butane-4,1-diyl))diguanidine **11nG**.
Barbiturate **3n** (32 mg, 70 µmol, 1.0 eq), *N,N*'-di(*tert*-butoxycarbonyl)-guanidinylbutanol (58 mg, 174 µmol, 2.5 eq), PPh_3 (55 mg, 209 µmol, 3.0 eq) and DIAD (44 µL, 209 µmol, 3.0 eq) were stirred in DCM (1.0 mL) for 20 h. The crude was purified with 10-42% EtOAc in heptane to yield impure boc-**11nG** (81 mg, 75 µmol, 107%) as a white solid.
TFA (80 µL, 1.04 mmol, 15.00 eq) and DCM (1.0 mL) were added, and the mixture was stirred at ambient temperature for 22 h. The crude was purified by automated RP column chromatography with a gradient of 10-55% MeCN/H_2O + 0.1% TFA to yield the di-TFA salt of **11nG** (54 mg, 59 µmol, 85% o2s) as a white powder. **^{1}H NMR** (400 MHz, Methanol-*d4*) δ 7.63 (t, *J* = 1.8 Hz, 1H), 7.17 (d, *J* = 1.7 Hz, 2H), 3.88 – 3.73 (m, 4H), 3.28 – 3.17 (m, 6H), 2.17 – 2.08 (m, 2H), 1.66 – 1.39 (m, 8H), 1.34 – 1.19 (m, 7H), 1.11 (dd, *J* = 10.6, 5.9 Hz, 2H), 0.93 – 0.85 (m, 3H). **^{13}C NMR** (101 MHz, Methanol-*d4*) δ 172.2 (2C), 158.7, 151.2, 140.9, 134.3, 132.5 (2C), 124.1 (2C), 59.4, 45.6, 42.5 (2C), 42.0 (2C), 40.9, 32.3, 30.1, 27.1 (2C), 26.4 (2C), 26.0, 23.5, 14.3. **HRMS** (ESI): calcd for $C_{27}H_{43}Br_2N_8O_3^+$ [M+H]$^+$ 685.1819, found 685.1821. **SFC**: 99.1%.

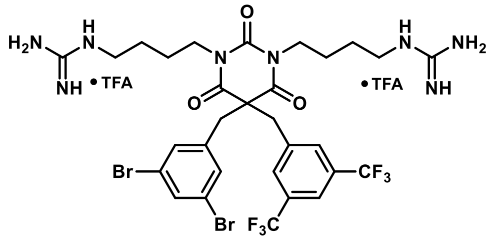

1,1'-((5-(3,5-bis(trifluoromethyl)benzyl)-5-(3,5-dibromo-benzyl)-2,4,6-trioxodihydropyrimidine-1,3(2H,4H)-diyl)bis(butane-4,1-diyl))diguanidine **11oG**.
Barbiturate **3o** (90 mg, 150 µmol, 1.0 eq), *N,N*'-di(*tert*-butoxycarbonyl)-guanidinylbutanol (149 mg, 449 µmol, 3.0 eq), PPh_3 (118 mg, 449 µmol, 3.0 eq) and DIAD (94 µL, 449 µmol, 3.0 eq) were stirred in anhydrous THF (1.0 mL) for 12 h. The crude was purified with 0-40% EtOAc in heptane to yield boc-**11oG** (64 mg, 52 µmol, 35%) as a pale-yellow oil.
TFA (60 µL, 781 µmol, 15.0 eq) and DCM (1.0 mL) were added, and the mixture was stirred at ambient temperature for 18 h. The crude was purified by automated RP column chromatography with a gradient of 20-45% MeCN/H_2O + 0.1% TFA to yield the di-TFA salt of **11oG** (31 mg, 29 µmol, 20% o2s) as a white foam. **^{1}H NMR** (400 MHz, Methanol-*d4*) δ 7.90 (d, *J* = 1.8 Hz, 1H), 7.65 (t, *J* = 1.8 Hz, 1H), 7.64 (d, *J* = 1.5 Hz, 2H), 7.23 (d, *J* = 1.7 Hz, 2H), 3.65 (s, 2H), 3.71 – 3.53 (m, 4H), 3.47 (s, 2H), 3.15 (t, *J* = 6.8 Hz, 4H), 1.50 – 1.26 (m, 8H). **^{13}C NMR** (101 MHz, Methanol-*d4*) δ 171.1 (2C), 158.7 (2C), 150.3, 140.3, 139.6, 134.7, 133.0 (q, *J* = 33.4 Hz, 2C), 132.7 (2C), 131.3 (q, *J* = 2.5 Hz, 2C), 124.5 (q, *J* = 272.1 Hz, 2C), 124.2 (2C), 122.8 – 122.6 (m, 1C), 61.2, 45.2, 44.6, 42.5 (2C), 41.9 (2C), 26.9 (2C), 26.2 (2C). **HRMS** (ESI): calcd for $C_{30}H_{35}Br_2F_6N_8O_3^+$ M+H]$^+$ 827.1098, found: 827.1106. **SFC**: 98.0%.

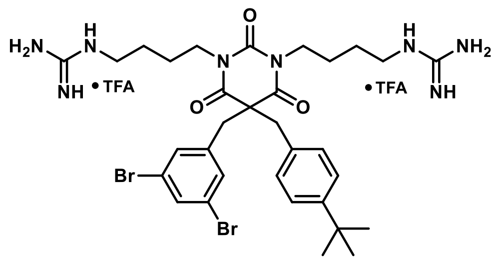

(4-(5-(4-(tert-butyl)benzyl)-5-(3,5-dibromobenzyl)-3-(4-guanidinobutyl)-2,4,6-trioxotetrahydropyrimidin-1(2H)-yl)butyl)-l2-azanecarboximidamide **11pG**.
Barbiturate **3p** (58 mg, 111 µmol, 1.0 eq), *N,N*'-di(*tert*-butoxycarbonyl)-guanidinylbutanol (92 mg, 278 µmol, 2.5 eq), PPh_3 (88 mg, 333 µmol, 3.0 eq) and DIAD (70 µL, 333 µmol, 3.0 eq) were stirred in DCM (1.0 mL) for 48 h. The crude was purified with 0-40% EtOAc in heptane to yield boc-**11pG** (110 mg, 96 µmol, 86%) as a yellow oil.
TFA (128 µL, 166 µmol, 15.0 eq) and DCM (1.0 mL) were added, and the mixture was stirred at ambient temperature for 17 h. The crude was purified by automated RP column chromatography with a gradient of 10-65% MeCN/H_2O + 0.1% TFA to yield the di-TFA salt of **11pG** (82 mg, 84 µmol, 76% o2s) as a white powder. **^{1}H NMR** (400 MHz, Methanol-*d4*) δ 7.61 (t, *J* = 1.8 Hz, 1H), 7.29 – 7.24 (m, 2H), 7.24 (d, *J* = 1.8 Hz, 2H), 7.01 – 6.90 (m, 2H), 3.73 – 3.62 (m, 1H), 3.56 (ddd, *J* = 12.9, 8.0, 5.2 Hz, 2H), 3.43 (s, 2H), 3.37 (s, 2H), 3.16 (t, *J* = 6.6 Hz, 4H), 1.48 – 1.31 (m, 8H), 1.24 (s, 9H). **^{13}C NMR** (101 MHz, Methanol-*d4*) δ 171.8 (2C), 158.7 (2C), 152.2, 150.8, 141.2, 134.2, 132.8, 132.7 (2C), 130.2 (2C), 126.6

(2C), 124.0 (2C), 61.6, 46.6, 44.3, 42.3 (2C), 42.0 (2C), 35.3, 31.7 (3C), 26.9 (2C), 26.1 (2C). **HRMS** (ESI): calcd for $C_{32}H_{45}Br_2N_8O_3^+$ [M+H]$^+$ 747.1976, found: 747.1981. **SFC**: 95.4%.

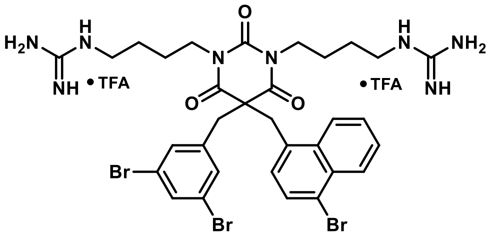

1,1'-((5-((4-bromonaphthalen-1-yl)methyl)-5-(3,5-dibromobenzyl)-2,4,6-trioxodihydropyrimidine-1,3(2H,4H)-diyl)bis(butane-4,1-diyl))diguanidine **11qG**.
Barbiturate **3q** (103 mg, 173 µmol, 1.0 eq), *N,N*'-di(*tert*-butoxycarbonyl)-guanidinylbutanol (143 mg, 434 µmol, 2.5 eq), PPh_3 (136 mg, 519 µmol, 3.0 eq) and DIAD (109 µL, 519 µmol, 3.0 eq) were stirred in DCM (1.0 mL) for 20 h. The crude was purified with 10-38% EtOAc in heptane to yield impure boc-**11qG** (216 mg, 177 µmol, 102%) as a white solid.
TFA (398 µL, 5.20 mmol, 30.00 eq) and DCM (0.7 mL) were added, and the mixture was stirred at ambient temperature for 48 h. The crude was purified by automated RP column chromatography with a gradient of 10-65% MeCN/H_2O + 0.1% TFA to yield the di-TFA salt of **11qG** (133 mg, 128 µmol, 74% o2s) as a white powder. **^{1}H NMR** (400 MHz, Methanol-*d4*) δ 8.28 – 8.20 (m, 1H), 8.20 – 8.13 (m, 1H), 7.71 (d, *J* = 7.7 Hz, 1H), 7.68 – 7.62 (m, 2H), 7.61 (t, *J* = 1.8 Hz, 1H), 7.28 (d, *J* = 1.7 Hz, 2H), 7.15 (d, *J* = 7.8 Hz, 1H), 3.95 (s, 2H), 3.62 (s, 2H), 3.50 (ddd, *J* = 12.9, 8.6, 6.0 Hz, 2H), 3.38 (ddd, *J* = 13.3, 8.4, 5.8 Hz, 2H), 3.04 (t, *J* = 7.0 Hz, 4H), 1.35 – 1.00 (m, 8H). **^{13}C NMR** (101 MHz, Methanol-*d4*) δ 171.6 (2C), 158.6 (2C), 150.6, 141.2, 134.2, 133.4, 133.0 (2C), 132.8, 130.5, 129.7, 128.8, 128.7, 128.3, 126.2, 124.1, 124.0 (2C), 61.1, 44.0, 42.5, 42.3 (2C), 42.0 (2C), 26.7 (2C), 25.9 (2C). **HRMS** (ESI): calcd for $C_{32}H_{38}Br_3N_8O_3^+$ [M+H]$^+$ 819.0612, found 819.0610. **SFC**: 96.3%.

2.9 Synthesis of *series 4*

2.9.1 Amine derivatives

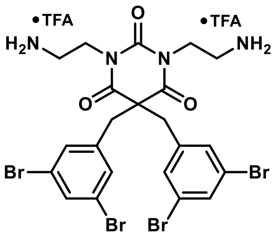

1,3-bis(2-aminoethyl)-5,5-bis(3,5-dibromobenzyl)pyrimidine-2,4,6(1H,3H,5H)-trione **12aA**.
The compound was synthesized according to General Procedure D. Barbiturate **3a** (80 mg, 128 µmol, 1.0 eq), *tert*-butyl (2-hydroxyethyl)carbamate (52 mg, 321 µmol, 2.5 eq), PPh_3 (101 mg, 385 µmol, 3.0 eq) and DIAD (81 µL, 385 µmol, 3.0 eq) were stirred in DCM (1.0 mL) for 20 h. The crude was purified with 10-50% EtOAc in heptane to yield boc-**12aA** (97 mg, 107 µmol, 83%) as a colorless oil. TFA (98 µL, 1.28 mmol, 10.0 eq) and DCM (1.0 mL) were added, and the mixture was stirred at ambient temperature for 22 h. The crude was purified by automated RP column chromatography with a gradient of 10-60% MeCN/H_2O + 0.1% TFA to yield the di-TFA salt of **12aA** (83 mg, 89 µmol, 69% o2s) as a white powder. **^{1}H NMR** (400 MHz, Methanol-*d4*) δ 7.64 (t, *J* = 1.8 Hz, 2H), 7.29 (d, *J* = 1.8 Hz, 4H), 4.00 (t, *J* = 6.6 Hz, 4H), 3.39 (s, 4H), 3.02 (t, *J* = 6.6 Hz, 4H). **^{13}C NMR** (101 MHz, Methanol-*d4*) δ 171.3 (2C), 151.1, 140.3 (2C), 134.6 (2C), 133.0 (4C), 124.0 (4C), 60.7, 44.0 (2C), 40.4 (2C), 38.6 (2C). **HRMS** (ESI): calcd for $C_{22}H_{23}Br_4N_4O_3^+$ [M+H]$^+$ 706.8498, found 706.8502. **SFC**: 96.7%.

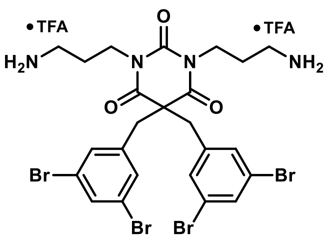

1,3-bis(3-aminopropyl)-5,5-bis(3,5-dibromobenzyl)pyrimidine-2,4,6(1H,3H,5H)-trione **13aA**.
The compound was synthesized according to General Procedure B. Barbiturate **3a** (468 mg, 0.75 mmol, 1.0 eq), *tert*-butyl (3-bromopropyl)carbamate (366 mg, 1.53 mmol, 2.05 eq), K_2CO_3 (311 mg, 2.25 mmol, 3.0 eq), TBAI (28 mg, 75 µmol, 0.1 eq) and acetone (7 mL) were stirred at 50 °C for 20 h. Boc-**13aA** (600 mg, 0.64 mmol, 85%) was obtained as a yellow solid. TFA (0.75 mL, 9.78 mmol, 15.0 eq) and DCM (2.5 mL) were added, and the mixture was stirred at ambient temperature for 17 h. The crude was purified by automated RP column chromatography with a gradient of 0-70% MeCN/H_2O + 0.1% TFA to yield the di-TFA salt of **13aA** (495 mg, 0.42 mmol, 56% o2s) as a white powder, m.p. 208-212 °C. **^{1}H NMR** (400 MHz, Methanol-*d4*) δ 7.67 (s, 2H), 7.25 (d, *J* = 1.8 Hz, 4H), 3.78 (t, 4H), 3.45 (s, 4H), 2.85 (t, *J* = 7.1 Hz, 4H), 1.77 (p, *J* = 7.1 Hz, 4H). **^{13}C NMR** (101 MHz, Methanol-*d4*) δ 171.3 (2C), 150.8, 140.4 (2C),

134.7 (2C), 132.6 (4C), 124.2 (4C), 61.4, 44.8 (2C), 40.2 (2C), 38.2 (2C), 27.3 (2C). **HRMS** (ESI): calcd for $C_{24}H_{27}Br_4N_4O_3^+$ $[M+H]^+$ 734.8811, found 734.8806. **SFC**: >99.5%.

The following compounds were synthesized according to General Procedure D.

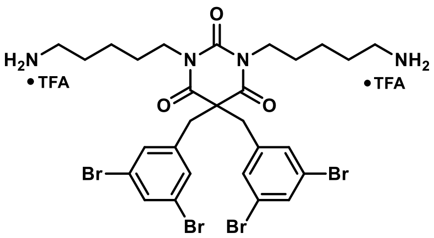

1,3-bis(5-aminopentyl)-5,5-bis(3,5-dibromobenzyl)pyrimidine-2,4,6(1H,3H,5H)-trione **14aA**.
Barbiturate **3a** (82 mg, 131 µmol, 1.0 eq), *tert*-butyl (5-hydroxypentyl)carbamate (67 mg, 329 µmol, 2.5 eq), PPh_3 (103 mg, 394 µmol, 3.0 eq) and DIAD (83 µL, 394 µmol, 3.0 eq) were stirred in DCM (1.0 mL) for 20 h. The crude was purified with 10-50% EtOAc in heptane to yield boc-**14aA** (104 mg, 105 µmol, 80%) as a slightly yellow solid. TFA (101 µL, 1.31 mmol, 10.0 eq) and DCM (1.0 mL) were added, and the mixture was stirred at ambient temperature for 22 h. The crude was purified by automated RP column chromatography with a gradient of 10-60% $MeCN/H_2O$ + 0.1% TFA to yield the di-TFA salt of **14aA** (92 mg, 69 µmol, 69% o2s) as a white powder. **^{1}H NMR** (400 MHz, Methanol-*d4*) δ 7.63 (t, *J* = 1.8 Hz, 2H), 7.20 (d, *J* = 1.7 Hz, 4H), 3.71 – 3.58 (m, 4H), 3.40 (s, 4H), 2.97 – 2.86 (m, 4H), 1.75 – 1.63 (m, 4H), 1.42 – 1.31 (m, 4H), 1.31 – 1.21 (m, 4H). **^{13}C NMR** (101 MHz, Methanol-*d4*) δ 171.1 (2C), 150.3, 140.5 (2C), 134.4 (2C), 132.6 (4C), 124.1 (4C), 61.1, 44.8 (2C), 42.6 (2C), 40.5 (2C), 28.6 (2C), 28.2 (2C), 24.6 (2C).**HRMS** (ESI): calcd for $C_{28}H_{35}Br_4N_4O_3^+$ $[M+H]^+$ 790.9437, found 790.9443. **SFC**: >99.5%.

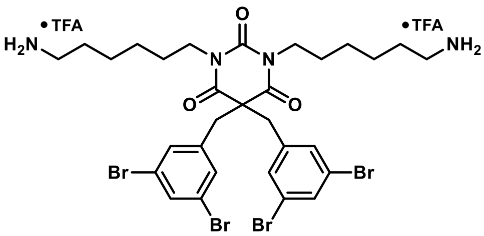

1,3-bis(6-aminohexyl)-5,5-bis(3,5-dibromobenzyl)pyrimidine-2,4,6(1H,3H,5H)-trione **15aA**.
Barbiturate **3a** (80 mg, 128 µmol, 1.0 eq), *tert*-butyl (6-hydroxyhexyl)carbamate (70 mg, 321 µmol, 2.5 eq), PPh_3 (101 mg, 385 µmol, 3.0 eq) and DIAD (81 µL, 385 µmol, 3.0 eq) were stirred in DCM (1.0 mL) for 20 h. The crude was purified with 10-40% EtOAc in heptane to yield boc-**15aA** (105 mg, 103 µmol, 80%) as a colorless oil.
TFA (98 µL, 1.28 mmol, 10.0 eq) and DCM (1.0 mL) were added, and the mixture was stirred at ambient temperature for 22 h. The crude was purified by automated RP column chromatography with a gradient of 10-60% $MeCN/H_2O$ + 0.1% TFA to yield the di-TFA salt of **15aA** (98 mg, 93 µmol, 73% o2s) as a white powder. **^{1}H NMR** (400 MHz, Methanol-*d4*) δ 7.63 (t, *J* = 1.7 Hz, 2H), 7.20 (d, *J* = 1.8 Hz, 4H), 3.72 – 3.56 (m, 4H), 3.39 (s, 4H), 2.97 – 2.86 (m, 4H), 1.71 – 1.57 (m, 4H), 1.38 (dp, *J* = 22.6, 8.1, 7.7 Hz, 8H), 1.25 – 1.13 (m, 4H). **^{13}C NMR** (101 MHz, Methanol-*d4*) δ 171.1 (2C), 150.4, 140.5 (2C), 134.4 (2C), 132.6 (4C), 124.1 (4C), 61.0, 44.9 (2C), 42.8 (2C), 40.6 (2C), 28.9 (2C), 28.5 (2C), 27.2 (2C), 27.0 (2C). **HRMS** (ESI): calcd for $C_{30}H_{39}Br_4N_4O_3^+$ $[M+H]^+$ 818.9750, found 818.9756. **SFC**: 98.5%.

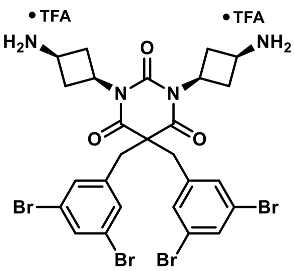

1,3-bis((1s,3S)-3-aminocyclobutyl)-5,5-bis(3,5-dibromobenzyl)pyrimidine-2,4,6(1H,3H,5H)-trione **16aA**.
Barbiturate **3a** (300 mg, 481 µmol, 1.0 eq), *tert*-butyl trans-(3-hydroxycyclobutyl)carbamate (225 mg, 1.20 mmol, 2.5 eq), PPh_3 (378 mg, 1.44 mmol, 3.0 eq) and DIAD (302 µL, 1.44 mmol, 3.0 eq) were stirred in anhydrous DCM (1.5 mL) at ambient temperature for 24 h. The crude was purified with 0-40% EtOAc in heptane to yield boc-**16aA** (404 mg, 420 µmol, 87%) as a colorless oil. Boc-**16aA** (404 mg, 420 µmol, 1.0 eq), TFA (161 µL, 2.10 mmol, 5.0 eq) and DCM (3.0 mL) were combined, and the mixture was stirred at ambient temperature until HRMS indicated full conversion. The crude was purified by automated RP column chromatography with a gradient of 15-45% $MeCN/H_2O$ + 0.1% TFA to yield the di-TFA salt of **16aA** (306 mg, 309 µmol, 64% o2s) as a white solid. **^{1}H NMR** (400 MHz, Methanol-*d4*) δ 7.64 (t, *J* = 1.8 Hz, 2H), 7.25 (d, *J* = 1.8 Hz, 4H), 4.89 (p, *J* = 8.8 Hz, 2H), 3.56 (p, *J* = 7.8 Hz, 2H), 3.43 (s, 4H), 2.82 (tdd, *J* = 10.5, 9.4, 5.7, 1.8 Hz, 4H), 2.70 – 2.60 (m, 4H). *Partial overlap of a methylene signals with residual water.* **^{13}C NMR** (101 MHz, Methanol-*d4*) δ 171.5 (2C), 150.4, 140.4 (2C), 134.6

(2C), 132.7 (4C), 124.2 (4C), 61.6, 44.7 (2C), 43.5 (2C), 40.7 (2C), 33.8 (4C). **HRMS** (ESI): calcd for $C_{26}H_{27}Br_4N_4O_3^+$ $[M+H]^+$ 758.8811, found: 758.8810. **SFC**: >99.5%

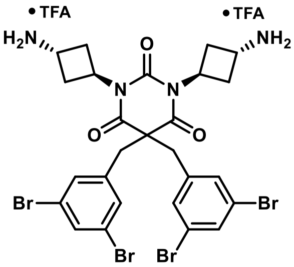

1,3-bis((1r,3R)-3-aminocyclobutyl)-5,5-bis(3,5-dibromobenzyl)pyrimidine-2,4,6(1H,3H,5H)-trione **17aA**.

Barbiturate **3a** (300 mg, 481 µmol, 1.0 eq), *tert*-butyl trans-(3-hydroxycyclobutyl)carbamate (225 mg, 1.20 mmol, 2.5 eq), PPh_3 (378 mg, 1.44 mmol, 3.0 eq) and DIAD (302 µL, 1.44 mmol, 3.0 eq) were stirred in anhydrous THF (2.5 mL) at ambient temperature for 24 h. The crude was purified with 0-40% EtOAc in heptane to yield boc-**17aA** (262 mg, 272 µmol, 67%) as a colorless oil.

Boc-**17aA** (262 mg, 272 µmol, 1.0 eq), TFA (125 µL, 1.63 mmol, 6.0 eq) and DCM (2.0 mL) were combined, and the mixture was stirred at ambient temperature for 38 h. The crude was purified by automated RP column chromatography with a gradient of 15-45% $MeCN/H_2O$ + 0.1% TFA to yield the di-TFA salt of **17aA** (125 mg, 126 µmol, 26% o2s) as a white solid. **^{1}H NMR** (400 MHz, Methanol-*d4*) δ 7.66 (t, *J* = 1.8 Hz, 2H), 7.24 (d, *J* = 1.8 Hz, 4H), 5.41 (ttd, *J* = 10.1, 7.2, 1.0 Hz, 2H), 4.07 (tdd, *J* = 9.1, 4.4, 3.4 Hz, 2H), 3.44 (s, 4H), 2.90 – 2.74 (m, 4H), 2.54 – 2.41 (m, 4H). **^{13}C NMR** (101 MHz, Methanol-*d4*) δ 171.3 (2C), 150.0, 140.5 (2C), 134.5 (2C), 132.6 (4C), 124.2 (4C), 61.5 (2C), 45.3 (2C), 44.8 (2C), 43.5 (2C), 32.7 (4C). **HRMS** (ESI): calcd for $C_{26}H_{27}Br_4N_4O_3^+$ $[M+H]^+$ 758.8811, found: 758.8813. **SFC**: >99.5%

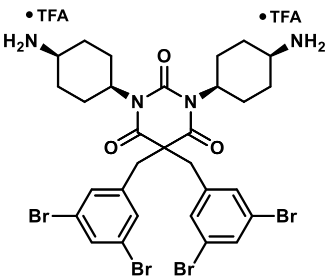

1,3-bis((1s,4S)-4-aminocyclohexyl)-5,5-bis(3,5-dibromobenzyl)pyrimidine-2,4,6(1H,3H,5H)-trione **18aA**.

Barbiturate **3a** (200 mg, 321 µmol, 1.0 eq), *tert*-butyl (*trans*-4-hydroxycyclohexyl)carbamate (173 mg, 801 µmol, 2.5 eq), PPh_3 (252 mg, 962 µmol, 3.0 eq) and DIAD (201 µL, 962 µmol, 3.0 eq) were stirred in DCM (1.0 mL) for 18 h. The crude was purified with 0-40% EtOAc in heptane to yield boc-**18aA** (179 mg, 176 µmol, 55%) as a colorless oil.

Boc-**18aA** (160 mg, 157 µmol, 1.0 eq), TFA (98 µL, 1.28 mmol, 10.0 eq) and DCM (1.0 mL) were combined, and the mixture was stirred at ambient temperature for 22 h. The crude was purified by automated RP column chromatography with a gradient of 15-50% $MeCN/H_2O$ + 0.1% TFA to yield the di-TFA salt of **18aA** (138 mg, 132 µmol, 46% o2s) as a white powder. **^{1}H NMR** (400 MHz, Methanol-*d4*) δ 7.66 (t, *J* = 1.8 Hz, 2H), 7.24 (d, *J* = 1.8 Hz, 4H), 4.61 – 4.41 (m, 2H), 3.54 – 3.47 (m, 2H), 3.43 (s, 4H), 2.54 – 2.21 (m, 4H), 2.06 – 1.94 (m, 4H), 1.94 – 1.78 (m, 4H), 1.29 – 1.17 (m, 4H). **^{13}C NMR** (101 MHz, Methanol-*d4*) δ 171.6 (2C), 149.9, 140.5 (2C), 134.5 (2C), 132.7 (4C), 124.3 (4C), 61.3, 55.2 (2C), 46.8 (2C), 45.0 (2C), 29.2 (4C), 24.1 (4C). **HRMS** (ESI): calcd for $C_{30}H_{35}Br_4N_4O_3^+$ $[M+H]^+$ 814.9437, found 814.9444. **SFC**: >99.5%

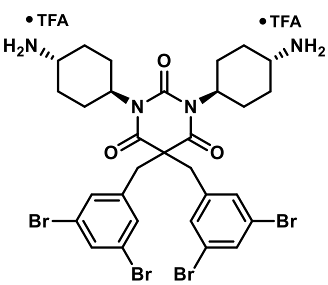

1,3-bis((1r,4R)-4-aminocyclohexyl)-5,5-bis(3,5-dibromobenzyl)pyrimidine-2,4,6(1H,3H,5H)-trione **19aA**.

Barbiturate **3a** (300 mg, 481 µmol, 1.0 eq), *tert*-butyl (cis-4-hydroxycyclohexyl)carbamate (259 mg, 1.20 mmol, 2.5 eq), PPh_3 (378 mg, 1.44 mmol, 3.0 eq) and DIAD (302 µL, 1.44 mmol, 3.0 eq) were stirred in anhydrous THF (2.5 mL) at 45 °C for 72 h. The crude was purified with 0-40% EtOAc in heptane to yield boc-**19aA** (169 mg, 166 µmol, 35%) as a colorless oil.

Boc-**19aA** (169 mg, 166 µmol, 1.0 eq), TFA (127 µL, 1.66 mmol, 10.0 eq) and DCM (2.0 mL) were combined, and the mixture was stirred at ambient temperature until HRMS indicated full conversion. The crude was purified by automated RP column chromatography with a gradient of 15-45% $MeCN/H_2O$ + 0.1% TFA to yield the di-TFA salt of **19aA** (116 mg, 111 µmol, 23% o2s) as a white solid. **^{1}H NMR** (400 MHz, Dimethylsulfoxide-*d6*) δ 7.94 (s, 6H), 7.80 (t, *J* = 1.7 Hz, 2H), 7.13 (d, *J* = 1.8 Hz, 4H), 4.36 – 4.17 (m, 2H), 3.08 – 2.92 (m, 2H), 2.21 – 2.04 (m, 4H), 2.03 – 1.91 (m, 4H), 1.47 – 1.29 (m, 4H), 1.28 – 1.13 (m, 4H). **^{13}C NMR** (101 MHz, Dimethylsulfoxide-*d6*) δ 169.7 (2C), 148.4, 139.0 (2C), 132.8 (2C), 131.3 (4C), 122.8 (4C), 59.5, 53.6 (2C), 48.0 (2C), 43.2 (2C), 29.6

(4C), 26.2 (4C). **HRMS** (ESI): calcd for $C_{30}H_{35}Br_4N_4O_3^+$ $[M+H]^+$ 814.9437, found: 814.9441. **SFC**: 91.0%

2.9.2 Guanidine derivatives

The compounds were synthesized according to General Procedure C.

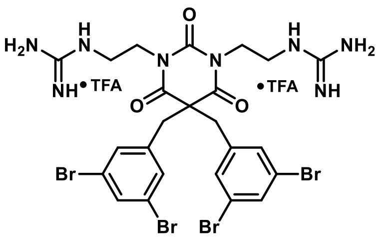

1,1'-((5,5-bis(3,5-dibromobenzyl)-2,4,6-trioxodihydropyrimidine-1,3(2H,4H)-diyl)bis(ethane-2,1-diyl))diguanidine **12aG**.
Barbiturate **12aA** (18 mg, 19 µmol, 1.0 eq), *N,N′*-di-Boc-1*H*-pyrazole-1-carboxamidine (18 mg, 58 µmol, 3.0 eq), DIPEA (10 µL, 57 µmol, 3.00 eq) and THF (1 mL) were stirred at 45 °C for 3.0 h. The crude was purified with 10-45% EtOAc in heptane to yield impure boc-**12aG** (30 mg, 25 µmol, 131%) as a colorless oil.
TFA (22 µL, 287 µmol, 15.0 eq) and DCM (1 mL) were added, and the mixture was stirred at ambient temperature for 40 h. The crude was purified by automated RP column chromatography with a gradient of 25-65% MeCN/H_2O + 0.1% TFA to yield the di-TFA salt of **12aG** (18 mg, 18 µmol, 92% o2s) as a white solid. **^{1}H NMR** (400 MHz, Methanol-*d4*) δ 7.67 (t, *J* = 1.6 Hz, 2H), 7.29 (d, *J* = 1.8 Hz, 4H), 3.88 (t, *J* = 6.5 Hz, 4H), 3.43 (s, 4H), 3.25 (t, *J* = 6.6 Hz, 4H). **^{13}C NMR** (101 MHz, Methanol-*d4*) δ 171.4 (2C), 158.9 (2C), 151.1 (2C), 140.3 (2C), 134.7 (2C), 132.9 (4C), 124.1 (4C), 61.1, 44.4 (2C), 41.6 (2C), 40.5 (2C). **HRMS** (ESI): calcd for $C_{24}H_{28}Br_4N_8O_3^{2+}$ $[M+2H]^{2+}$ 395.9503, found 395.9511. **SFC**: 98.2%.

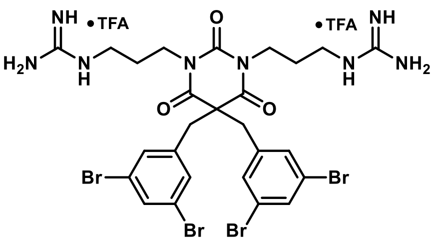

1,1'-((5,5-bis(3,5-dibromobenzyl)-2,4,6-trioxodihydropyrimidine-1,3(2H,4H)-diyl)bis(propane-3,1-diyl))diguanidine **13aG**.
Barbiturate **13aA** (70 mg, 73 µmol, 1.0 eq), *N,N′*-di-Boc-1*H*-pyrazole-1-carboxamidine (56 mg, 181 µmol, 2.50 eq), DIPEA (51 µL, 290 µmol, 4.00 eq) and THF (1 mL) were stirred at 45 °C for 2.5 h. The crude was purified with 20% EtOAc in heptane to yield boc-**13aG** (54 mg, 44 µmol, 61%) as a white foam.
TFA (83 µL, 1.09 mmol, 15.0 eq) and DCM (1 mL) were added, and the mixture was stirred at ambient temperature for 40 h. The crude was purified by automated RP column chromatography with a gradient of 10-60% MeCN/H_2O + 0.1% TFA to yield the di-TFA salt of **13aG** (43 mg, 41 µmol, 57% o2s) as a white powder. **^{1}H NMR** (400 MHz, Methanol-*d4*) δ 7.65 (t, *J* = 1.8 Hz, 2H), 7.23 (d, *J* = 1.8 Hz, 4H), 3.77 – 3.67 (m, 4H), 3.44 (s, 4H), 3.08 (t, *J* = 7.0 Hz, 4H), 1.62 (dq, *J* = 9.2, 7.1 Hz, 4H). **^{13}C NMR** (101 MHz, Methanol-*d4*) δ 171.3 (2C), 158.7 (2C), 150.5, 140.5 (2C), 134.58 (2C), 132.6 (4C), 124.2 (4C), 61.4, 44.8 (2C), 40.4 (2C), 39.6 (2C), 28.9 (2C). **HRMS** (ESI): calcd for $C_{26}H_{31}Br_4N_8O_3^+$ $[M+H]^+$ 818.9247, found 818.9250. **SFC**: >99.5%.

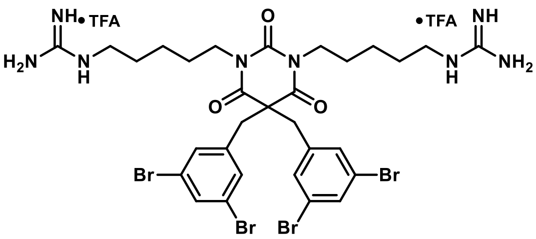

1,1'-((5,5-bis(3,5-dibromobenzyl)-2,4,6-trioxodihydropyrimidine-1,3(2H,4H)-diyl)bis(pentane-5,1-diyl))diguanidine **14aG**.
Barbiturate **14aA** (13 mg, 13 µmol, 1.0 eq), *N,N′*-di-Boc-1*H*-pyrazole-1-carboxamidine (12 mg, 38 µmol, 3.0 eq), DIPEA (7 µL, 38 µmol, 3.00 eq) and THF (1 mL) were stirred at 45 °C for 3.0 h. The crude was purified with 10-45% EtOAc in heptane to yield boc-**14aG** (15 mg, 12 µmol, 92%) as a yellow oil.
TFA (15 µL, 191 µmol, 15.0 eq) and DCM (1 mL) were added, and the mixture was stirred at ambient temperature for 20 h. The crude was purified by automated RP column chromatography with a gradient of 25-65% MeCN/H_2O + 0.1% TFA to yield the di-TFA salt of **14aG** (12 mg, 11 µmol, 85% o2s) as a white solid. **^{1}H NMR** (400 MHz, Methanol-*d4*) δ 7.64 (t, *J* = 1.6 Hz, 2H), 7.21 (d, *J* = 1.7 Hz, 4H), 3.63 (t, *J* = 7.6 Hz, 4H), 3.41 (s, 4H), 3.16 (t, *J* = 7.2 Hz, 4H), 1.62 (p, *J* = 7.3 Hz, 4H), 1.42 – 1.30 (m, 4H), 1.25 (p, *J* = 7.6 Hz, 4H). **^{13}C NMR** (101 MHz, Methanol-*d4*) δ 171.2 (2C), 158.7 (2C), 150.4, 140.6

(2C), 134.4 (2C), 132.6 (4C), 124.1 (4C), 61.1, 44.9 (2C), 42.8 (2C), 42.3 (2C), 29.5 (2C), 28.8 (2C), 24.8 (2C). **HRMS** (ESI): calcd for $C_{30}H_{40}Br_4N_8O_3^{2+}$ [M+2H]$^{2+}$ 437.9973, found 437.9978. **SFC**: 98.4%.

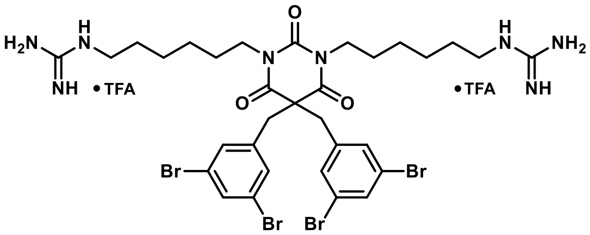

1,1'-((5,5-bis(3,5-dibromobenzyl)-2,4,6-trioxodihydropyrimidine-1,3(2H,4H)-diyl)bis(hexane-6,1-diyl))diguanidine **15aG**.

Barbiturate **15aA** (38 mg, 36 µmol, 1.0 eq), *N,N′*-di-Boc-1*H*-pyrazole-1-carboxamidine (34 mg, 109 µmol, 3.0 eq), DBU (22 µL, 148 µmol, 4.00 eq) and THF (1 mL) were stirred at 45 °C for 3.5 h. The organic layer was washed with 10% citric acid$_{(aq)}$ solution instead of 10% $NaHCO_{3(aq)}$ solution. Partial cleavage of the Boc groups was observed. Boc-**15aG** was used without further purification.

4M HCl in Dioxane (452 µL, 1.81 mmol, 50.0 eq) was added and the mixture was stirred at ambient temperature for 24 h. The crude was purified by RP chromatography with a gradient of 10-70% MeCN/H_2O + 0.1% TFA to yield the di-TFA salt of **15aG** (30 mg, 26 µmol, 73% o2s) as a white solid. **^{1}H NMR** (400 MHz, Methanol-*d4*) δ 7.63 (t, *J* = 1.8 Hz, 2H), 7.20 (d, *J* = 1.7 Hz, 4H), 3.68 – 3.57 (m, 4H), 3.40 (s, 4H), 3.17 (t, *J* = 7.1 Hz, 4H), 1.57 (p, *J* = 7.3 Hz, 4H), 1.47 – 1.27 (m, 8H), 1.20 (p, *J* = 7.7 Hz, 4H). **^{13}C NMR** (101 MHz, Methanol-*d4*) δ 171.2 (2C), 158.6 (2C), 150.5, 140.6 (2C), 134.4 (2C), 132.6 (4C), 124.1 (4C), 61.1, 44.9 (2C), 42.9 (2C), 42.4 (2C), 29.8 (2C), 29.0 (2C), 27.3 (2C), 27.3 (2C). **HRMS** (ESI): calcd for $C_{32}H_{44}Br_4N_8O_3^{2+}$ [M+2H]$^{2+}$ 452.0129, found 452.0137. **SFC**: 98.1%.

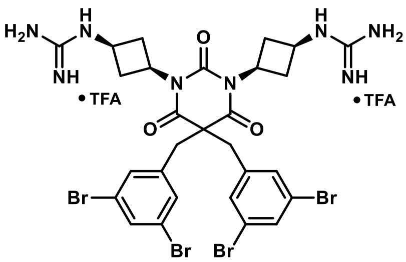

1,1'-((1S,1'S,3s,3's)-(5,5-bis(3,5-dibromobenzyl)-2,4,6-trioxodihydropyrimidine-1,3(2H,4H)-diyl)bis(cyclobutane-3,1-diyl))diguanidine **16aG.**

Barbiturate **16aA** (200 mg, 202 µmol, 1.0 eq), *N,N′*-di-Boc-1*H*-pyrazole-1-carboxamidine (157 mg, 505 µmol, 2.5 eq), DIPEA (140 µL, 808 µmol, 4.0 eq) and THF (4.0 mL) were stirred at 45 °C for 3 h. The crude was purified with 10-45% EtOAc in heptane to yield boc-**16aG** (134 mg, 108 µmol, 53%) as a colorless oil.

TFA (124 µL, 1.61 mmol, 15.0 eq) and DCM (0.5 mL) were added, and the mixture was stirred at ambient temperature until HRMS indicated full conversion. The crude was purified by automated RP column chromatography with a gradient of 18-45% MeCN/H_2O + 0.1% TFA to yield the di-TFA salt of **16aG** (52 mg, 48 µmol, 24% o2s) as a white solid. **^{1}H NMR** (400 MHz, Methanol-*d4*) δ 7.65 (t, *J* = 1.8 Hz, 2H), 7.23 (d, *J* = 1.8 Hz, 4H), 4.67 (tt, *J* = 9.3, 8.1 Hz, 2H), 3.80 – 3.69 (m, 2H), 2.79 – 2.67 (m, 4H), 2.63 – 2.51 (m, 4H). **^{13}C NMR** (101 MHz, Methanol-*d4*) δ 171.6 (2C), 157.7 (2C), 150.3, 140.4 (2C), 134.5 (2C), 132.6 (4C), 124.2 (4C), 61.5, 44.8 (2C), 43.8 (2C), 41.4 (2C), 36.3 (4C). **HRMS** (ESI): calcd for $C_{28}H_{31}Br_4N_8O_3^+$ [M+H]$^+$ 842.9247, found 842.9238. **SFC**: 98.6%.

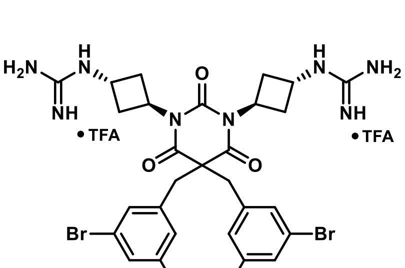

1,1'-((1R,1'R,3r,3'r)-(5,5-bis(3,5-dibromobenzyl)-2,4,6-trioxodihydropyrimidine-1,3(2H,4H)-diyl)bis(cyclobutane-3,1-diyl))diguanidine **17aG**.

Barbiturate **17aA** (87 mg, 88 µmol, 1.0 eq), *N,N′*-di-Boc-1*H*-pyrazole-1-carboxamidine (68 mg, 220 µmol, 2.5 eq), DIPEA (61 µL, 351 µmol, 4.0 eq) and THF (4.0 mL) were stirred at 45 °C for 3 h. The crude was purified with 10-45% EtOAc in heptane to yield impure boc-**17aG** (116 mg, 93 µmol, 106%) as a colorless oil.

TFA (107 µL, 1.39 mmol, 15.0 eq) and DCM (0.5 mL) were added, and the mixture was stirred at ambient temperature until HRMS indicated full conversion. The crude was purified by automated RP column chromatography with a gradient of 15-45% MeCN/H_2O + 0.1% TFA to yield the di-TFA salt of **17aG** (31 mg, 29 µmol, 32% o2s) as a white solid. **^{1}H NMR** (400 MHz, Methanol-*d4*) δ 7.64 (t, *J* = 1.7 Hz, 2H), 7.23 (d, *J* = 1.7 Hz, 4H), 5.32 – 5.20 (m, 2H), 4.26 – 4.17 (m, 2H), 3.42 (s, 4H), 2.97 – 2.85 (m, 4H), 2.36 – 2.25 (m, 4H). **^{13}C NMR** (101 MHz, Methanol-*d4*) δ 171.4 (2C), 158.3 (2C), 150.0, 140.5 (2C), 134.5 (2C), 132.6 (4C), 124.2 (4C), 61.5, 46.5 (2C), 44.8 (2C), 43.9

(2C), 35.2 (4C). **HRMS** (ESI): calcd for $C_{28}H_{31}Br_4N_8O_3^+$ $[M+H]^+$ 842.9247, found 842.9254. **SFC**: 92.1%.

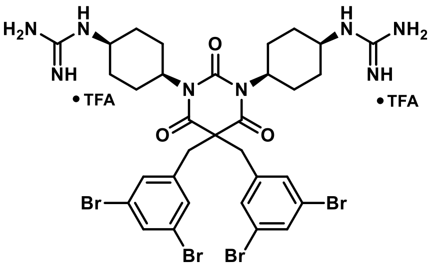

1,1'-((1S,1'S,4s,4's)-(5,5-bis(3,5-dibromobenzyl)-2,4,6-trioxodihydropyrimidine-1,3(2H,4H)-diyl)bis(cyclohexane-4,1-diyl))diguanidine **18gG**.

Barbiturate **18aA** (125 mg, 120 µmol, 1.0 eq), *N*,*N'*-di-Boc-1*H*-pyrazole-1-carboxamidine (93 mg, 299 µmol, 2.5 eq), DIPEA (83 µL, 478 µmol, 4.0 eq) and THF (0.5 mL) were stirred at 45 °C for 17 h. The crude was purified with 45% EtOAc in heptane to yield boc-**18gG** (106 mg, 81 µmol, 68%) as a colorless oil.

TFA (94 µL, 1.22 mmol, 15.0 eq) and DCM (0.5 mL) were added, and the mixture was stirred at ambient temperature until HRMS indicated full conversion. The crude was purified by automated RP column chromatography with a gradient of 15-45% MeCN/H_2O + 0.1% TFA to yield the di-TFA salt of **18gG** (19 mg, 17 µmol, 14% o2s) as a white solid. **^{1}H NMR** (400 MHz, Methanol-*d4*) δ 7.64 (t, *J* = 1.8 Hz, 2H), 7.22 (d, *J* = 1.7 Hz, 4H), 4.60 – 4.32 (m, 2H), 3.80 – 3.70 (m, 2H), 3.40 (s, 4H), 2.55 – 2.18 (m, 4H), 1.93 (d, *J* = 14.0 Hz, 4H), 1.78 – 1.62 (m, 4H), 1.25 – 1.11 (m, 4H). **^{13}C NMR** (101 MHz, Methanol-*d4*) δ 171.6 (2C), 158.0 (2C), 150.0, 140.6 (2C), 134.4 (2C), 132.7 (4C), 124.3 (4C), 61.2, 55.6 (2C), 46.6 (2C), 45.0 (2C), 30.6 (4C), 24.5 (4C). **HRMS** (ESI): calcd for $C_{32}H_{39}Br_4N_8O_3^+$ $[M+H]^+$ 898.9873, found 898.9880. **SFC**: 97.2%.

2.10 Synthesis of *series 5*

2.10.1 Amine derivatives

All compounds were synthesized according to General procedure B:

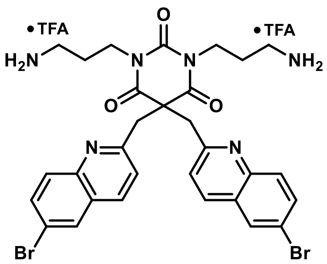

1,3-bis(3-aminopropyl)-5,5-bis((6-bromoquinolin-2-yl)methyl)pyrimidine-2,4,6(1H,3H,5H)-trione **13cA**.

Barbiturate **3c** (54 mg, 95 µmol, 1.0 eq), *tert*-butyl (3-bromopropyl)carbamate (57 mg, 0.24 mmol, 2.50 eq), Cs_2CO_3 (77 mg, 0.24 mmol, 2.50 eq), TBAI (7 mg, 19 µmol, 0.2 eq) and acetone (1.5 mL) were stirred at 60 °C for 40 h. The crude was purified with 10-70% EtOAc in heptane to yield boc-**13cA** (29 mg, 33 µmol, 35%) as a colorless oil.

TFA (73 µL, 0.95 mmol, 10.0 eq) and DCM (0.7 mL) were added, and the mixture was stirred at ambient temperature for 22 h. The crude was purified by automated RP column chromatography with a gradient of 10-60% MeCN/H_2O + 0.1% TFA to yield the di-TFA salt of **13cA** (29 mg, 32 µmol, 34% o2s) as a white powder. **^{1}H NMR** (400 MHz, Methanol-*d4*) δ 8.25 – 8.18 (m, 2H), 8.13 (d, *J* = 2.2 Hz, 2H), 7.83 (dd, *J* = 8.9, 2.2 Hz, 2H), 7.61 (d, *J* = 9.0 Hz, 2H), 7.44 (d, *J* = 8.5 Hz, 2H), 3.97 (s, 4H), 3.89 (t, *J* = 6.9 Hz, 4H), 2.62 (t, *J* = 7.0 Hz, 4H), 1.82 (p, *J* = 7.0 Hz, 4H). **^{13}C NMR** (101 MHz, Methanol-*d4*) δ 174.3 (2C), 158.9 (2C), 153.2, 146.7 (2C), 137.5 (2C), 134.7 (2C), 131.4 (2C), 130.7 (2C), 129.6 (2C), 123.5 (2C), 121.3 (2C), 54.5, 48.2 (2C), 39.9 (2C), 38.1 (2C), 27.0 (2C). **HRMS** (ESI): calcd for $C_{30}H_{31}Br_2N_6O_3^+$ $[M+H]^+$ 681.0819, found 681.0823. **SFC**: >99.5%.

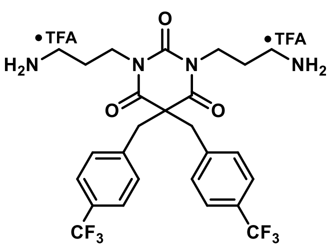

1,3-bis(3-aminopropyl)-5,5-bis(4-(trifluoromethyl)benzyl)pyrimidine-2,4,6(1H,3H,5H)-trione **13hA**.

Barbiturate **3h** (332 mg, 0.75 mmol, 1.0 eq), *tert*-butyl (3-bromopropyl)carbamate (368 mg, 1.55 mmol, 2.07 eq), K_2CO_3 (315 mg, 2.28 mmol, 3.0 eq), TBAI (28 mg, 75 µmol, 0.1 eq) and acetone (8 mL) were stirred at 50 °C for 21 h. Boc-**13hA** (469 mg, 0.62 mmol, 83%) was obtained as a yellow solid and used without further purification.

TFA (0.72 mL, 9.38 mmol, 15.1 eq) and DCM (2.5 mL) were added, and the mixture was stirred at ambient temperature for 17 h. The crude was purified by automated RP column chromatography with a gradient of 0-70% MeCN/H_2O + 0.1% TFA to yield the di-TFA salt of **13hA**

(448 mg, 0.57 mmol, 76% o2s) as a white powder, m.p. 180-184 °C. **^{1}H NMR** (400 MHz, Methanol-*d4*) δ 7.60 (d, *J* = 8.1 Hz, 4H), 7.30 (d, *J* = 8.0 Hz, 4H), 3.70 (t, 4H), 3.58 (s, 4H), 2.72 (t, *J* = 7.3 Hz, 4H), 1.69 (p, *J* = 7.3 Hz, 4H). **^{13}C NMR** (101 MHz, Methanol-*d4*) δ 171.5 (2C), 150.9, 140.6 (2C), 131.4 (4C), 131.2 (q, *J* = 32.4 Hz, 2C), 126.7 (q, *J* = 3.7 Hz, 4C), 125.4 (q, *J* = 271.0 Hz, 2C), 61.3, 45.7 (2C), 40.0 (2C), 38.0 (2C), 26.7 (2C). **HRMS** (ESI): calcd for $C_{26}H_{29}F_6N_4O_3^+$ [M+H]$^+$ 559.2138, found 559.2145. **SFC**: 95.6%.

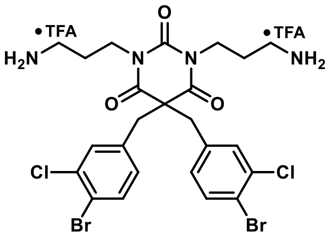

1,3-bis(3-aminopropyl)-5,5-bis(4-bromo-3-chlorobenzyl)pyrimidine-2,4,6(1H,3H,5H)-trione **13iA**.

Barbiturate **3i** (401 mg, 0.75 mmol, 1.0 eq), *tert*-butyl (3-bromopropyl)carbamate (366 mg, 1.54 mmol, 2.05 eq), K_2CO_3 (314 mg, 2.27 mmol, 3.0 eq), TBAI (28 mg, 75 µmol, 0.1 eq) and acetone (7 mL) were stirred at 50 °C for 21 h. Boc-**13iA** (564 mg, 0.68 mmol, 91%) was obtained as a beige highly viscous oil and used without further purification.
TFA (0.78 mL, 10.2 mmol, 15.0 eq) and DCM (2.5 mL) were added, and the mixture was stirred at ambient temperature for 18 h. The crude was purified by automated RP column chromatography with a gradient of 0-70% MeCN/H_2O + 0.1% TFA to yield the di-TFA salt of **13iA** (365 mg, 0.42 mmol, 55% o2s) as a white powder, m.p. 213-216 °C. **^{1}H NMR** (400 MHz, Methanol-*d4*) δ 7.61 (d, *J* = 8.2 Hz, 2H), 7.24 (d, *J* = 2.1 Hz, 2H), 6.94 (dd, *J* = 8.3, 2.1 Hz, 2H), 3.74 (t, 4H), 3.44 (s, 4H), 2.80 (t, *J* = 7.2 Hz, 4H), 1.74 (p, *J* = 7.2 Hz, 4H). **^{13}C NMR** (101 MHz, Methanol-*d4*) δ 171.5 (2C), 150.9, 137.6 (2C), 135.6 (2C), 135.4 (2C), 132.5 (2C), 130.7 (2C), 122.8 (2C), 61.2, 44.8 (2C), 40.1 (2C), 38.1 (2C), 27.0 (2C). **HRMS** (ESI): calcd for $C_{24}H_{27}Br_2Cl_2N_4O_3^+$ [M+H]$^+$ 646.9821, found 646.9832. **SFC**: 95.2%.

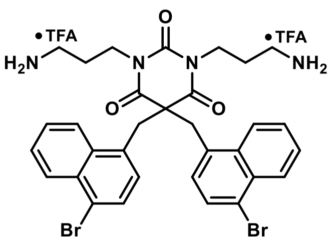

1,3-bis(3-aminopropyl)-5,5-bis((4-bromonaphthalen-1-yl)methyl)pyrimidine-2,4,6(1H,3H,5H)-trione **13eA**.

Barbiturate **3e** (428 mg, 0.75 mmol, 1.0 eq), *tert*-butyl (3-bromopropyl)carbamate (369 mg, 1.55 mmol, 2.07 eq), K_2CO_3 (313 mg, 2.26 mmol, 3.0 eq), TBAI (28 mg, 75 µmol, 0.1 eq) and acetone (7 mL) were stirred at 50 °C for 21 h. The crude was purified with 15-60% EtOAc in heptane to yield boc-**13eA** (379 mg, 0.43 mmol, 57%) as a white solid. TFA (0.49 mL, 6.40 mmol, 15.0 eq) and DCM (2.0 mL) were added, and the mixture was stirred at ambient temperature for 18 h. The crude was purified by automated RP column chromatography with a gradient of 0-70% MeCN/H_2O + 0.1% TFA to yield the di-TFA salt of **13eA** (355 mg, 0.39 mmol, 52% o2s) as a white powder. m.p.: 204-207 °C. **^{1}H NMR** (400 MHz, Methanol-*d4*) δ 8.40 – 8.11 (m, 4H), 7.73 (dd, *J* = 7.8, 2.3 Hz, 2H), 7.70 – 7.59 (m, 4H), 7.26 – 7.03 (m, 2H), 4.15 (s, 4H), 3.41 (t, *J* = 7.0 Hz, 4H), 2.44 (t, *J* = 6.5, 5.4 Hz, 4H), 1.38 (p, *J* = 7.1 Hz, 4H). **^{13}C NMR** (101 MHz, Methanol-*d4*) δ 172.2 (2C), 151.2, 134.4 (2C), 133.4 (2C), 133.3 (2C), 130.5 (2C), 129.1 (2C), 128.8 (2C), 128.7 (2C), 128.4 (2C), 126.3 (2C), 124.0 (2C), 60.2, 41.7 (2C), 39.9 (2C), 37.8 (2C), 26.6 (2C). **HRMS** (ESI): calcd for $C_{32}H_{33}Br_2N_4O_3^+$ [M+H]$^+$ 679.0914, found 679.0903. **SFC**: 96.5%.

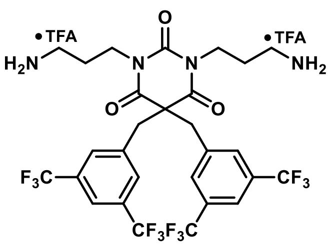

1,3-bis(3-aminopropyl)-5,5-bis(3,5-bis(trifluoromethyl)benzyl)pyrimidine-2,4,6(1H,3H,5H)-trione **13jA**.

Barbiturate **3j** (261 mg, 0.45 mmol, 1.0 eq), *tert*-butyl (3-bromopropyl)carbamate (214 mg, 0.90 mmol, 2.00 eq), Cs_2CO_3 (323 mg, 0.99 mmol, 2.2 eq), TBAI (17 mg, 45 µmol, 0.1 eq) and acetone (2.5 mL) were stirred at 70 °C for 3.5 d. The crude was purified with 0-70% EtOAc in heptane to yield boc-**13jA** (265 mg, 0.30 mmol, 66%) as a white solid. TFA (0.28 mL, 3.60 mmol, 8.0 eq) and DCM (2.0 mL) were added, and the mixture was stirred at ambient temperature for 12 h. The crude was purified by automated RP column chromatography with a gradient of 0-70% MeCN/H_2O + 0.1% TFA to yield the di-TFA salt of **13jA** (251 mg, 0.27 mmol, 61% o2s) as a white powder. **^{1}H NMR** (400 MHz, Methanol-*d4*) δ 7.93 (s, 2H), 7.73 – 7.68 (m, 4H), 3.76 – 3.68 (m, 8H), 2.80 (t, *J* = 7.1 Hz, 4H), 1.67 (dq, *J* = 9.0, 7.2 Hz, 4H). **^{13}C NMR** (101 MHz, Methanol-*d4*) δ 171.1 (2C), 150.6, 139.3 (2C), 133.1 (q, *J* = 33.4 Hz, 4C), 131.6 –

131.4 (m, 4C), 124.6 (q, *J* = 272 Hz, 4C), 123.1 – 122.8 (m, 2C), 61.0, 44.6 (2C), 40.3 (2C), 38.0 (2C), 26.9 (2C). **HRMS** (ESI): calcd for $C_{28}H_{27}F_{12}N_4O_3^+$ [M+H]$^+$ 695.1886, found 695.1884. **SFC**: 95.2%.

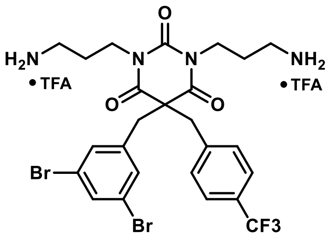

1,3-bis(3-aminopropyl)-5-(3,5-dibromobenzyl)-5-(4-(trifluoromethyl)benzyl)pyrimidine-2,4,6(1H,3H,5H)-trione **13lA**.
Barbiturate **3l** (479 mg, 0.90 mmol, 1.0 eq), *tert*-butyl (3-bromopropyl)carbamate (470 mg, 1.97 mmol, 2.2 eq), K_2CO_3 (372 mg, 2.69 mmol, 3.0 eq), TBAI (33 mg, 90 µmol, 0.1 eq) and acetone (15 mL) were stirred at 50 °C for 18 h. The crude was purified by column chromatography on silica gel with EtOAc in heptane to yield boc-**13lA** (340 mg, 0.40 mmol, 45%) as a pale-yellow oil.
TFA (0.30 mL, 3.88 mmol, 10.0 eq) and DCM (3.0 mL) were added, and the mixture was stirred at ambient temperature for 17 h. The crude was purified by automated RP column chromatography with a gradient of 15-50% MeCN/H_2O + 0.1% TFA to yield the di-TFA salt of **13lA** (334 mg, 0.39 mmol, 44% o2s) as a white powder. **^{1}H NMR** (400 MHz, Methanol-*d4*) δ 7.67 (t, *J* = 1.8 Hz, 1H), 7.60 (d, *J* = 8.0 Hz, 2H), 7.29 (d, *J* = 8.0 Hz, 2H), 7.26 (d, *J* = 1.8 Hz, 2H), 3.81 – 3.67 (m, 4H), 3.56 (s, 2H), 3.48 (s, 2H), 2.89 – 2.71 (m, 4H), 1.82 – 1.62 (m, 4H).δ **^{13}C NMR** (101 MHz, Methanol-*d4*) δ 171.4 (2C), 150.9, 140.7 – 140.6 (m, 1C), 140.5, 134.6, 132.6 (2C), 131.5, 131.2 (q, *J* = 32.5 Hz, 1C) 126.8 (q, *J* = 3.9 Hz, 2C), 125.4 (q, *J* = 271.9 Hz, 1C), 124.2 (2C), 61.4, 45.4, 45.0, 40.1 (2C), 38.1 (2C), 27.0 (2C). **HRMS** (ESI): calcd for $C_{25}H_{28}Br_2F_3N_4O_3^+$ [M+H]$^+$ 647.0475, found 647.0473. **SFC**: 97.3%.

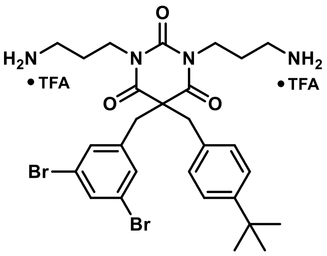

1,3-bis(3-aminopropyl)-5-(4-(tert-butyl)benzyl)-5-(3,5-dibromobenzyl)pyrimidine-2,4,6(1H,3H,5H)-trione **13pA**.
Barbiturate **3p** (100 mg, 192 µmol, 1.0 eq), *tert*-butyl (3-hydroxypropyl)carbamate (84 mg, 479 µmol, 2.5 eq), PPh_3 (151 mg, 575 µmol, 3.0 eq) and DIAD (120 µL, 574 µmol, 3.0 eq) were stirred in anhydrous DCM (0.5 mL) for 16 h. The crude was purified with 0-40% EtOAc in heptane to yield impure boc-**13pA** (161 mg, 192 µmol, 101%) as a colorless oil.
TFA (129 µL, 1.67 mmol, 10.0 eq) and DCM (1.0 mL) were added, and the mixture was stirred at ambient temperature for 18 h. The crude was purified by automated RP column chromatography with a gradient of 15-50% MeCN/H_2O + 0.1% TFA to yield the di-TFA salt of **13pA** (118 mg, 137 µmol, 71% o2s) as a white powder. **^{1}H NMR** (400 MHz, Methanol-*d4*) δ 7.64 (t, *J* = 1.7 Hz, 1H), 7.31 (d, *J* = 8.3 Hz, 2H), 7.26 (d, *J* = 1.7 Hz, 2H), 6.99 (d, *J* = 8.3 Hz, 2H), 3.79 – 3.64 (m, 4H), 3.46 (s, 2H), 3.41 (s, 2H), 2.76 (oct, *J* = 7.1 4H), 1.83 – 1.62 (m, 4H). **^{13}C NMR** (101 MHz, Methanol-*d4*) δ 171.9 (2C), 152.5, 151.1, 141.1, 134.4, 132.7, 132.6 (2C), 130.2 (2C), 126.7 (2C), 124.1 (2C), 61.9, 46.5, 44.2, 40.0 (2C), 38.2 (2C), 35.4, 31.7 (3C), 27.0 (2C). **HRMS** (ESI): calcd for $C_{28}H_{37}Br_2N_4O_3^+$ [M+H]$^+$ 635.1227, found: 635.1232. **SFC**: 97.0%.

2.10.2 Guanidine derivatives

All compounds were synthesized according to General Procedure C:

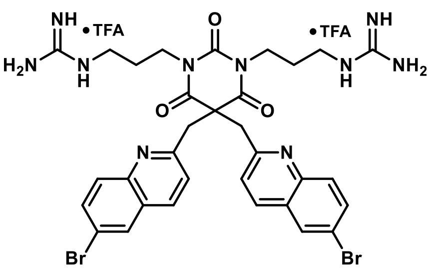

1,1'-((5,5-bis((6-bromoquinolin-2-yl)methyl)-2,4,6-trioxodihydropyrimidine-1,3(2H,4H)-diyl)bis(propane-3,1-diyl))diguanidine **13cG**.
Barbiturate **13aA** (11 mg, 12.1 µmol, 1.0 eq), *N,N'*-di-Boc-1*H*-pyrazole-1-carboxamidine (9.4 mg, 30.2 µmol, 2.50 eq), DIPEA (5.3 µL, 30.2 µmol, 2.50 eq) and THF (0.5 mL) were stirred at 45 °C for 2.5 h. The crude was purified with 20-60% EtOAc in heptane to yield boc-**13cG** (13 mg, 11.1 µmol, 92%) as a white foam.
TFA (28 µL, 181 µmol, 30.0 eq) and DCM (0.5 mL) were added, and the mixture was stirred at ambient temperature for 24 h. The crude was purified by automated RP column chromatography with a gradient of 20-60% MeCN/H_2O + 0.1% TFA to yield the di-TFA salt of **13cG** (11 mg, 11 µmol, 91% o2s) as a

white powder. **^{1}H NMR** (400 MHz, Methanol-*d4*) δ 8.20 (d, *J* = 8.5 Hz, 2H), 8.11 (d, *J* = 2.2 Hz, 2H), 7.81 (dd, *J* = 8.9, 2.2 Hz, 2H), 7.58 (d, *J* = 9.0 Hz, 2H), 7.44 (d, *J* = 8.6 Hz, 2H), 3.97 (s, 4H), 3.86 (t, *J* = 6.8 Hz, 4H), 2.80 (t, *J* = 6.9 Hz, 4H), 1.64 (p, *J* = 6.9 Hz, 4H). **^{13}C NMR** (101 MHz, Methanol-*d4*) δ 174.2 (2C), 159.0 (2C), 158.4, 153.4 (2C), 146.7 (2C), 137.4 (2C), 134.5 (2C), 131.4 (2C), 130.8 (2C), 129.6 (2C), 123.5 (2C), 121.3 (2C), 54.5, 48.3 (2C), 40.2 (2C), 39.7 (2C), 28.5 (2C). **HRMS** (ESI): calcd for $C_{32}H_{35}Br_2N_{10}O_3^+$ [M+H]$^+$ 765.1255, found 765.1259. **SFC**: 97.4%

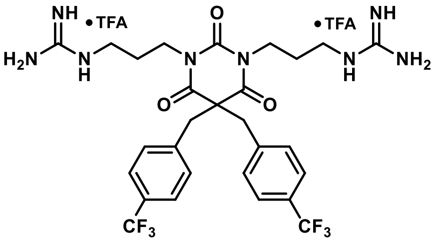

1,1'-((2,4,6-trioxo-5,5-bis(4-(trifluoromethyl)benzyl)dihydropyrimidine-1,3(2H,4H)-diyl)bis(propane-3,1-diyl))diguanidine **13hG**.

Barbiturate **13hA** (70 mg, 89 µmol, 1.0 eq), *N*,*N′*-di-Boc-1*H*-pyrazole-1-carboxamidine (69 mg, 223 µmol, 2.50 eq), DIPEA (62 µL, 356 µmol, 4.00 eq) and THF (1 mL) were stirred at 45 °C for 2.5 h. The crude was purified with 15% EtOAc in heptane to yield boc-**13hG** (73 mg, 70 µmol, 79%) as a white foam.
TFA (102 µL, 1.33 mmol, 15.0 eq) and DCM (1 mL) were added, and the mixture was stirred at ambient temperature for 40 h. The crude was purified by automated RP column chromatography with a gradient of 10-60% MeCN/H_2O + 0.1% TFA to yield the di-TFA salt of **13hG** (61 mg, 70 µmol, 79% o2s) as a white powder. **^{1}H NMR** (400 MHz, Methanol-*d4*) δ 7.57 (d, *J* = 8.0 Hz, 4H), 7.29 (d, *J* = 8.0 Hz, 4H), 3.72 – 3.63 (m, 4H), 3.58 (s, 4H), 2.93 (t, *J* = 6.8 Hz, 4H), 1.53 (dq, *J* = 8.8, 7.0 Hz, 4H). **^{13}C NMR** (101 MHz, Methanol-*d4*) δ 171.5 (2C), 158.7 (2C), 150.8, 140.8 (2C), 131.5 (4C), 131.2 (q, *J* = 32.5 Hz, 2C), 126.7 (q, *J* = 3.7 Hz, 4C), 125.4 (d, *J* = 271 Hz, 4C), 61.2, 45.8 (2C), 40.3 (2C), 39.6 (2C), 28.2 (2C). **HRMS** (ESI): calcd for $C_{28}H_{33}F_6N_8O_3^+$ [M+H]$^+$ 643.2574, found 643.2579. **SFC**: 98.6%.

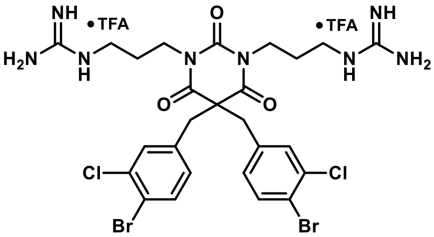

1,1'-((5,5-bis(4-bromo-3-chlorobenzyl)-2,4,6-trioxodihydropyrimidine-1,3(2H,4H)-diyl)bis(propane-3,1-diyl))diguanidine **13iG**.

Barbiturate **13iA** (70 mg, 80 µmol, 1.0 eq), *N*,*N′*-di-Boc-1*H*-pyrazole-1-carboxamidine (62 mg, 200 µmol, 2.50 eq), DIPEA (56 µL, 319 µmol, 4.00 eq) and THF (1 mL) were stirred at 45 °C for 2.5 h. The crude was purified with 20% EtOAc in heptane to yield boc-**13iG** (81 mg, 71 µmol, 90%) as a clear solid.
TFA (92 µL, 1.20 mmol, 15.0 eq) and DCM (1 mL) were added, and the mixture was stirred at ambient temperature for 40 h. The crude was purified by automated RP column chromatography with a gradient of 10-60% MeCN/H_2O + 0.1% TFA to yield the di-TFA salt of **13iG** (61 mg, 64 µmol, 80% o2s) as a white powder. **^{1}H NMR** (400 MHz, Methanol-*d4*) δ 7.57 (d, *J* = 8.3 Hz, 2H), 7.22 (d, *J* = 2.1 Hz, 2H), 6.91 (dd, *J* = 8.3, 2.1 Hz, 2H), 3.75 – 3.67 (m, 4H), 3.42 (s, 4H), 3.00 (t, *J* = 6.9 Hz, 4H), 1.64 – 1.52 (m, 4H). **^{13}C NMR** (101 MHz, Methanol-*d4*) δ 171.4 (2C), 158.7 (2C), 150.7, 137.6 (2C), 135.6 (2C), 135.3 (2C), 132.5 (2C), 130.6 (2C), 122.7 (2C), 61.1, 44.9 (2C), 40.3 (2C), 39.6 (2C), 28.5 (2C). **HRMS** (ESI): calcd for $C_{26}H_{31}Br_2Cl_2N_8O_3^+$ [M+H]$^+$ 731.0257, found 731.0263. **SFC**: >99.5%.

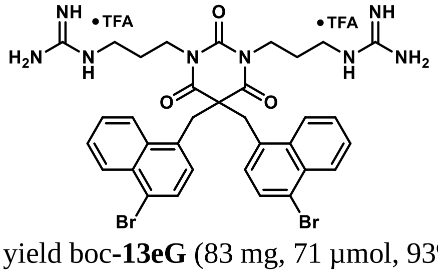

1,1'-((5,5-bis((4-bromonaphthalen-1-yl)methyl)-2,4,6-trioxodihydropyrimidine-1,3(2H,4H)-diyl)bis(propane-3,1-diyl))diguanidine **13eG**.

Barbiturate **13eA** (70 mg, 77 µmol, 1.0 eq), *N*,*N′*-di-Boc-1*H*-pyrazole-1-carboxamidine (60 mg, 193 µmol, 2.50 eq), DIPEA (54 µL, 308 µmol, 4.00 eq) and THF (1 mL) were stirred at 45 °C for 2.5 h. The crude was purified with 15% EtOAc in heptane to yield boc-**13eG** (83 mg, 71 µmol, 93%) as a white foam.
TFA (89 µL, 1.16 mmol, 15.0 eq) and DCM (1 mL) were added, and the mixture was stirred at ambient temperature for 40 h. The crude was purified by automated RP column chromatography with a gradient of 10-60% MeCN/H_2O + 0.1% TFA to yield the di-TFA salt of **13eG** (67 mg, 68 µmol, 88% o2s) as a white powder. **^{1}H NMR** (400 MHz, Methanol-*d4*) δ 8.39 – 8.30 (m, 2H), 8.29 – 8.19 (m, 2H), 7.70 (d, *J* = 7.8 Hz, 2H), 7.65 (td, *J* = 7.0, 6.6, 3.6 Hz, 4H), 7.16 (d, *J* = 7.8 Hz, 2H), 4.17 (s, 4H), 3.45 – 3.35 (m, 4H), 2.57 (t, *J* = 6.9 Hz, 4H), 1.09 (p, *J* = 7.0 Hz, 4H). **^{13}C NMR** (101 MHz, Methanol-*d4*) δ 172.2

(2C), 158.4 (2C), 150.9, 134.4 (2C), 133.4 (2C), 130.4 (2C), 129.3 (2C), 128.8 (2C), 128.6 (2C), 128.2 (2C), 126.5 (2C), 123.9 (2C), 60.6, 41.5 (2C), 40.1 (2C), 39.2 (2C), 27.8 (2C). **HRMS** (ESI): calcd for $C_{34}H_{37}Br_2N_8O_3^+$ [M+H]$^+$ 763.1350, found 763.1356. **SFC**: >99.5%.

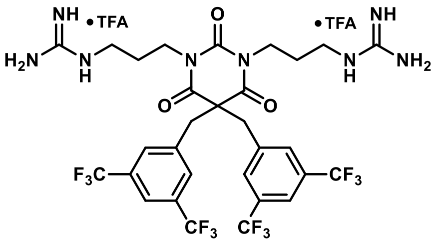

1,1'-((5,5-bis(3,5-bis(trifluoromethyl)benzyl)-2,4,6-trioxodihydropyrimidine-1,3(2H,4H)-diyl)bis(propane-3,1-diyl))diguanidine **13jG**.

Barbiturate **13jA** (50 mg, 54 µmol, 1.0 eq), *N,N'*-di-Boc-1*H*-pyrazole-1-carboxamidine (42 mg, 136 µmol, 2.50 eq), DIPEA (38 µL, 217 µmol, 4.00 eq) and THF (1 mL) were stirred at 45 °C for 2.5 h. The crude was purified with 15% EtOAc in heptane to yield boc-**13jG** (49 mg, 42 µmol, 77%) as a white foam.
TFA (62 µL, 0.81 mmol, 15.0 eq) and DCM (1 mL) were added, and the mixture was stirred at ambient temperature for 40 h. The crude was purified by automated RP column chromatography with a gradient of 10-60% MeCN/H_2O + 0.1% TFA to yield the di-TFA salt of **13jG** (42 mg, 42 µmol, 77% o2s) as a white powder. **^{1}H NMR** (400 MHz, Methanol-*d4*) δ 7.93 (s, 2H), 7.69 (d, *J* = 1.6 Hz, 4H), 3.72 (s, 4H), 3.69 – 3.60 (m, 4H), 3.03 (t, *J* = 6.9 Hz, 4H), 1.49 (dq, *J* = 9.4, 7.0 Hz, 4H).**^{13}C NMR** (101 MHz, Methanol-*d4*) δ 171.1 (2C), 158.7 (2C), 150.2, 139.4 (2C), 133.10 (q, *J* = 33.4 Hz, 4C), 131.5 – 131.3 (m, 4C), 124.5 (q, *J* = 272 Hz, 4C) 123.1 – 122.8 (m, 2C), 61.2, 44.8 (2C), 40.5 (2C), 39.5 (2C), 28.5 (2C). **HRMS** (ESI): calcd for $C_{30}H_{31}F_{12}N_8O_3^+$ [M+H]$^+$ 779.2322, found 779.2324. **SFC**: >99.5%.

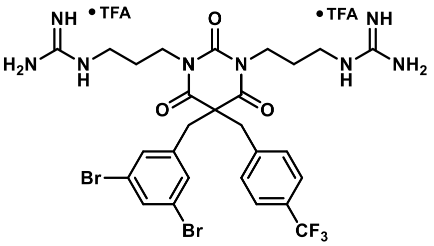

1,1'-((5-(3,5-dibromobenzyl)-2,4,6-trioxo-5-(4-(trifluoromethyl)benzyl)dihydropyrimidine-1,3(2H,4H)-diyl)bis(propane-3,1-diyl))diguanidine **13lG**.

Barbiturate **13lA** (150 mg, 171 µmol, 1.0 eq), *N,N'*-di-Boc-1*H*-pyrazole-1-carboxamidine (90 mg, 291 µmol, 1.7 eq), DIPEA (119 µL, 685 µmol, 4.0 eq) and THF (0.5 mL) were stirred at 45 °C for 2.5 h. The crude was purified with 10-45% EtOAc in heptane to yield boc-**13lG** (121 mg, 107 µmol, 62%) as a white foam.
TFA (246 µL, 3.20 mmol, 30.0 eq) and DCM (1.5 mL) were added, and the mixture was stirred at ambient temperature for 36 h. The crude was purified by automated RP column chromatography with a gradient of 15-45% MeCN/H_2O + 0.1% TFA to yield the di-TFA salt of **13lG** (11 mg, 11 µmol, 20% o2s) as a white powder. **^{1}H NMR** (400 MHz, Methanol-*d4*) δ 7.64 (t, *J* = 1.8 Hz, 1H), 7.57 (d, *J* = 8.0 Hz, 2H), 7.27 (d, *J* = 8.0 Hz, 2H), 7.24 (d, *J* = 1.7 Hz, 2H), 3.74 (ddd, *J* = 13.3, 8.6, 6.2 Hz, 2H), 3.65 (ddd, *J* = 13.2, 8.6, 6.0 Hz, 2H), 3.54 (s, 2H), 3.47 (s, 2H), 1.58 (dddd, *J* = 22.8, 13.3, 6.9, 2.0 Hz, 4H). **^{13}C NMR** (101 MHz, Methanol-*d4*) δ 171.4 (2C), 158.7 (2C), 150.7, 140.6 (2C), 134.5, 132.7 (2C), 131.4, 131.2 (q, *J* = 32.6 Hz, 1C), 126.7 (q, *J* = 3.8 Hz, 2C), 125.4 (q, *J* = 271.1 Hz, 1C) 124.2 (2C), 61.3, 45.7, 44.9, 40.3 (2C), 39.6 (2C), 28.6 (2C). **HRMS** (ESI): calcd for $C_{27}H_{32}Br_2F_3N_8O_3^+$ [M+H]$^+$ 731.0911, found: 731.0919 **SFC**: 97.8%.

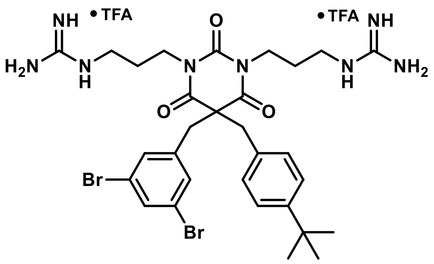

1,1'-((5-(4-(tert-butyl)benzyl)-5-(3,5-dibromobenzyl)-2,4,6-trioxodihydropyrimidine-1,3(2H,4H)-diyl)bis(propane-3,1-diyl))diguanidine **13pG**.

Barbiturate **13pA** (60 mg, 69 µmol, 1.0 eq), *N,N'*-di-Boc-1*H*-pyrazole-1-carboxamidine (54 mg, 174 µmol, 2.5 eq), DIPEA (30 µL, 174 µmol, 2.5 eq) and THF (1.5 mL) were stirred at 50 °C for 2.5 h. The crude was purified with 10-50% EtOAc in heptane to yield impure boc-**13pG** (86 mg, 77 µmol, 111%) as a white solid.
TFA (80 µL, 1.04 mmol, 15.0 eq) and DCM (1.5 mL) were added, and the mixture was stirred at ambient temperature for 24 h. The crude was purified by automated RP column chromatography with a gradient of 10-45% MeCN/H_2O + 0.1% TFA to yield the di-TFA salt of **13pG** (39 mg, 41 µmol, 59% o2s) as a white powder. **^{1}H NMR** (400 MHz, Methanol-*d4*) δ 7.62 (t, *J* = 1.8 Hz, 1H), 7.30 – 7.26 (m, 2H), 7.25 (d, *J* = 1.8 Hz, 2H), 7.00 – 6.94 (m, 2H), 3.72 (ddd, *J* = 13.2, 8.1, 6.7 Hz, 2H), 3.63 (ddd, *J* = 13.5, 8.0,

6.2 Hz, 2H), 3.45 (s, 2H), 3.39 (s, 2H), 2.98 (td, *J* = 6.9, 5.1 Hz, 4H), 1.65 – 1.49 (m, 4H), 1.25 (s, 9H). **^{13}C NMR** (101 MHz, Methanol-*d4*) δ 171.9 (2C), 158.7 (2C), 152.4, 150.9, 141.2, 134.3, 132.7, 130.2 (2C), 126.7 (2C), 124.1 (2C), 61.8, 46.7, 44.1, 40.2 (2C), 39.6 (2C), 35.3, 31.6 (3C), 28.5 (2C). **HRMS** (ESI): calcd for $C_{30}H_{41}Br_2N_8O_3^+$ [M+H]$^+$ 719.1663, found: 719.1664. **SFC**: 98.6%

3 ^{1}H and ^{13}C NMR spectra of final compounds

NMR raw data of all intermediates can be found here: https://doi.org/10.18710/GNTWOG.

3.1 ^{1}H and ^{13}C NMR spectra of compounds in *series 1*

5,5-bis(3,5-dibromobenzyl)-1,3-bis(4-(methylamino)butyl)pyrimidine-2,4,6(1*H*,3*H*,5*H*)-trione di-TFA salt (**6a**)

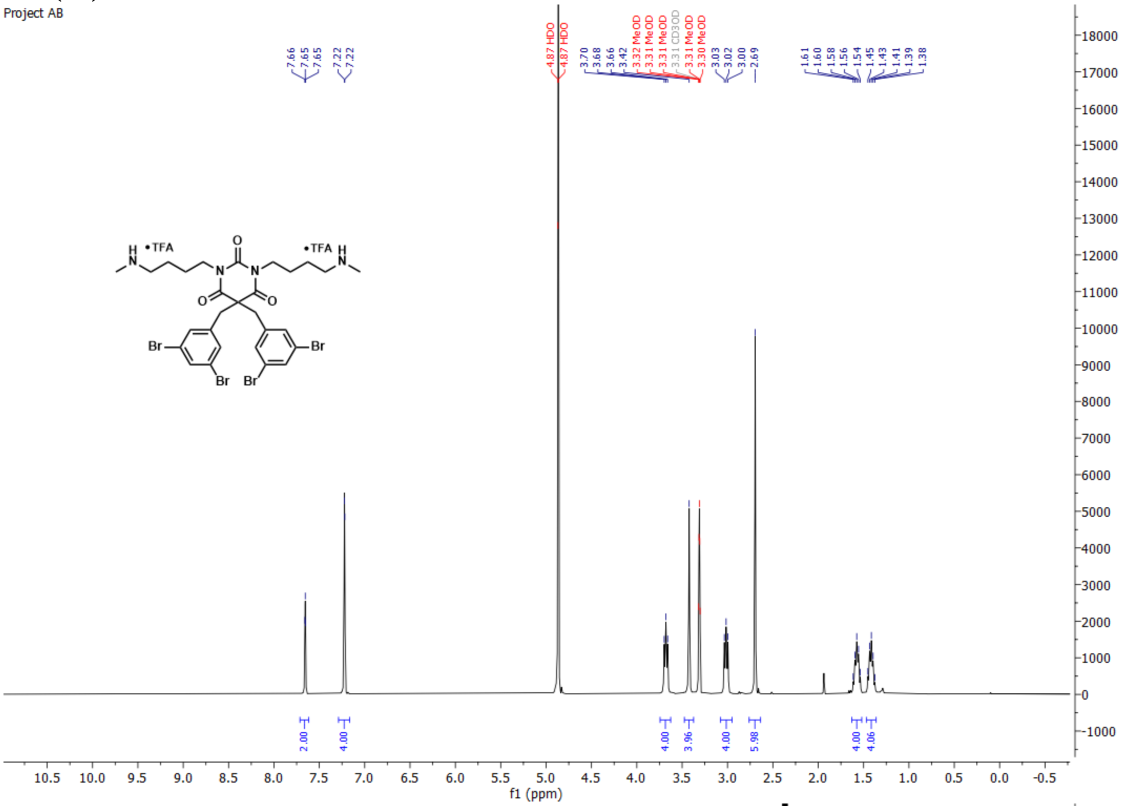

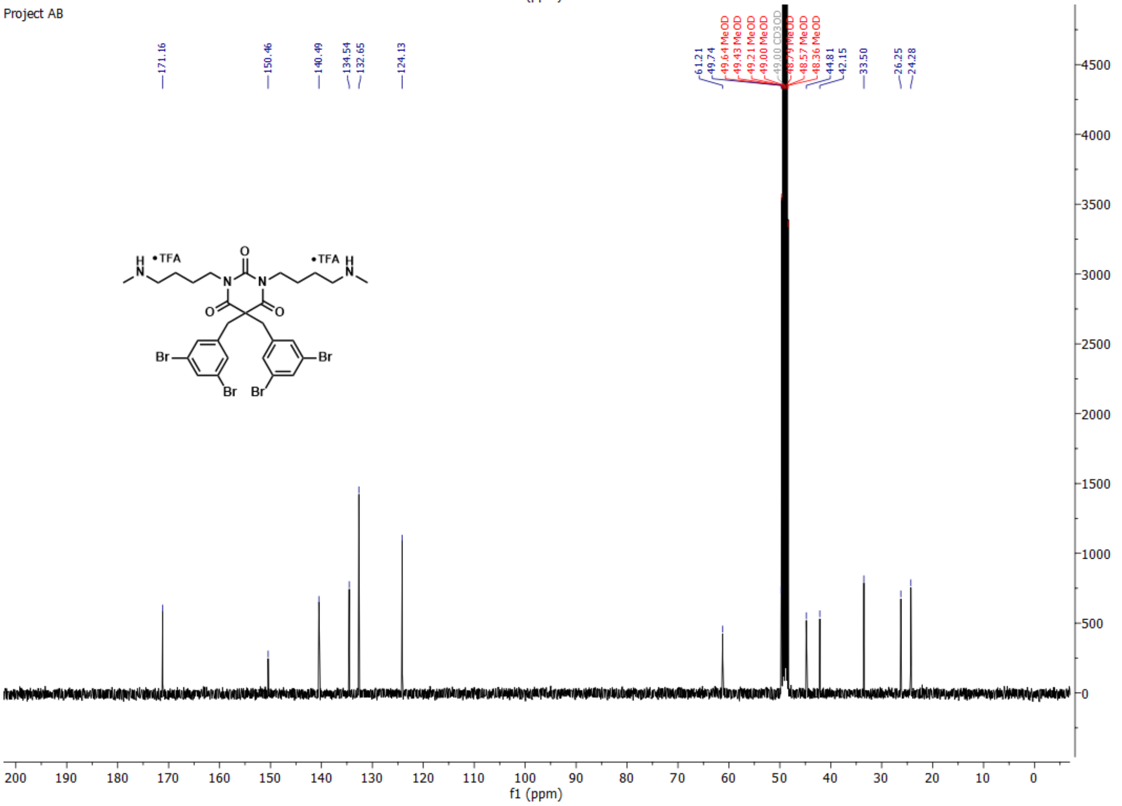

5,5-bis(3,5-dibromobenzyl)-1,3-bis(4-(dimethylamino)butyl)pyrimidine-2,4,6(1*H*,3*H*,5*H*)-trione di-TFA salt (**7a**)

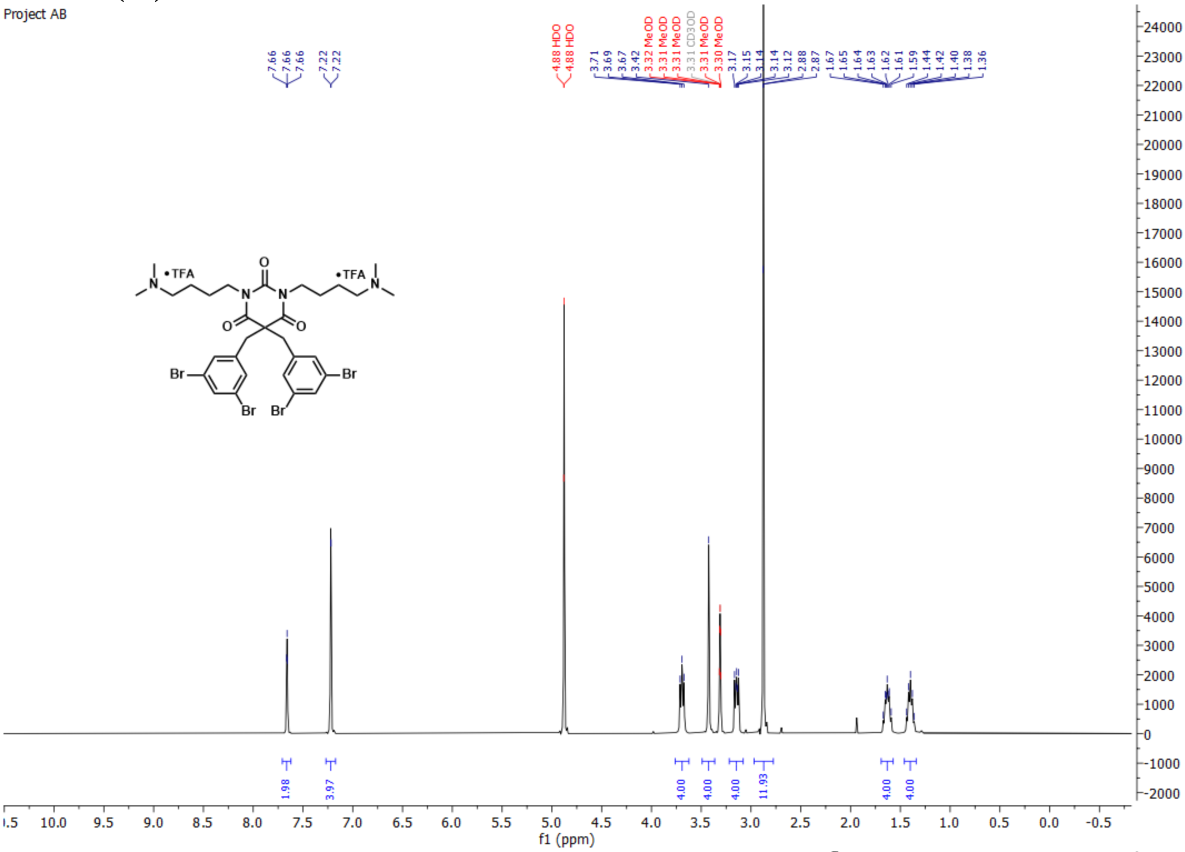

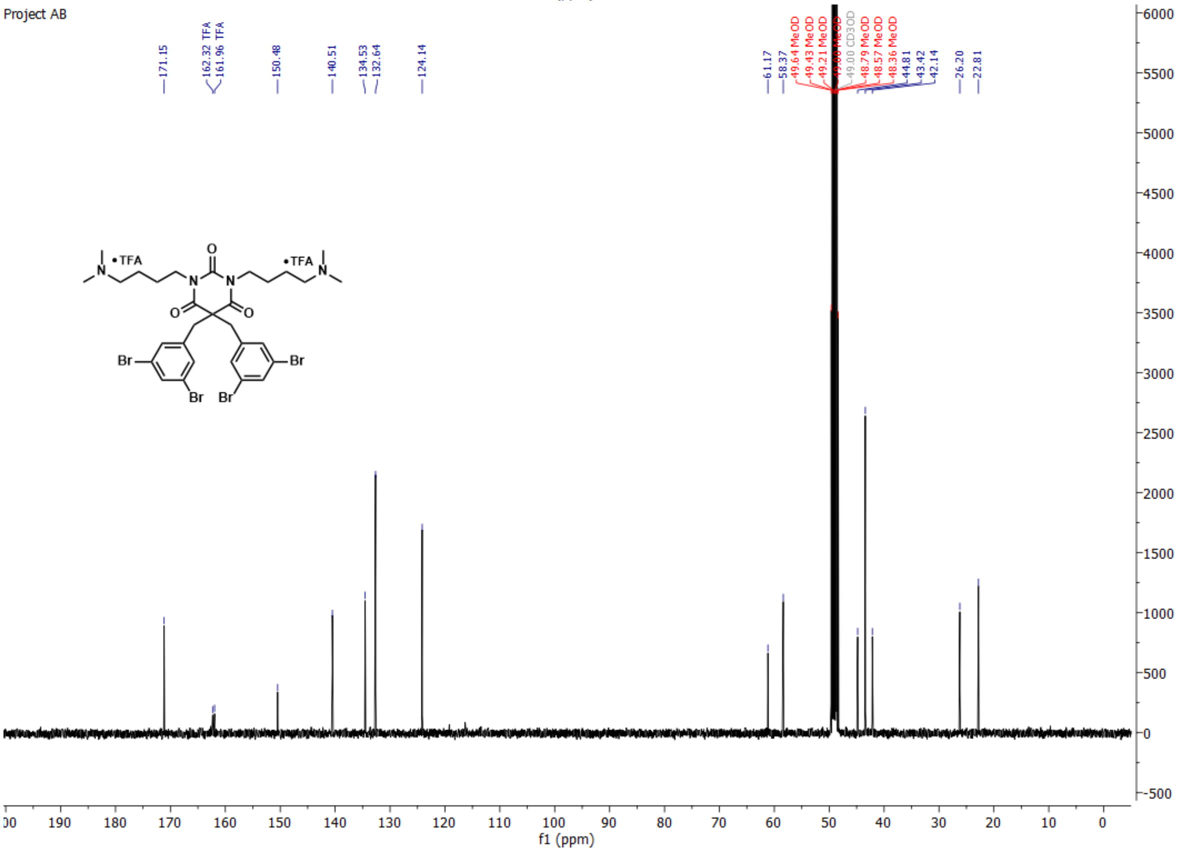

4,4'-(5,5-bis(3,5-dibromobenzyl)-2,4,6-trioxodihydropyrimidine-1,3(2*H*,4*H*)-diyl)bis(*N*,*N*,*N*-trimethyl-butan-1-aminium) di-TFA salt (**8a**)

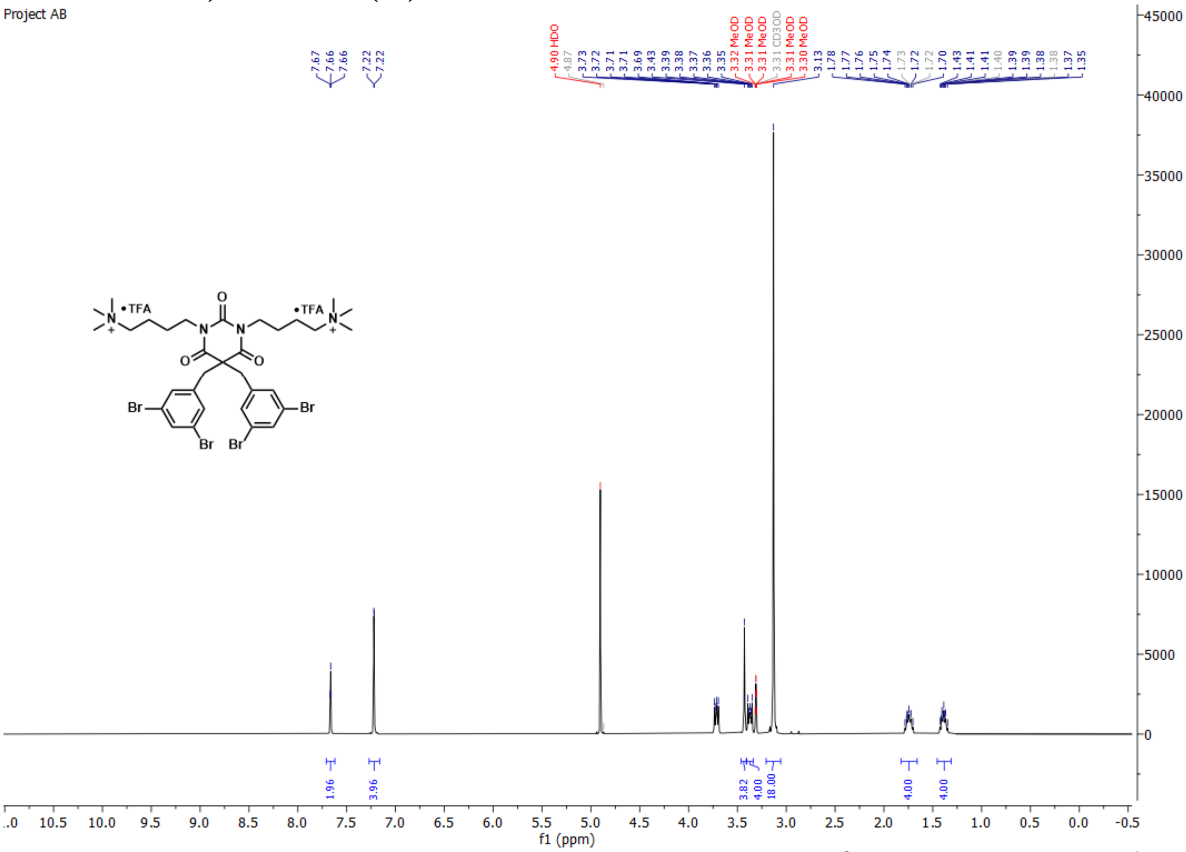

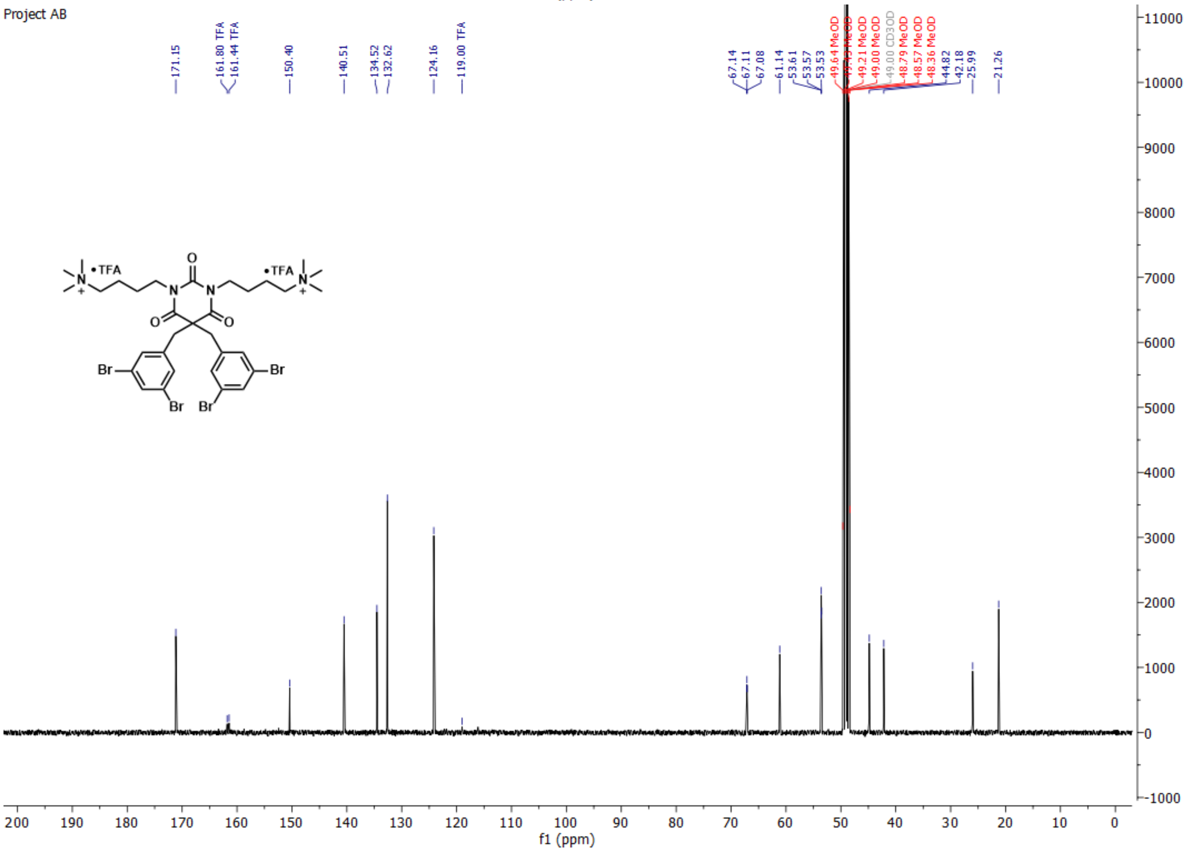

1,1'-((5,5-bis(3,5-dibromobenzyl)-2,4,6-trioxodihydropyrimidine-1,3(2*H*,4*H*)-diyl)bis(butane-4,1-diyl))bis(pyridin-1-ium) di-TFA salt (**9a**)

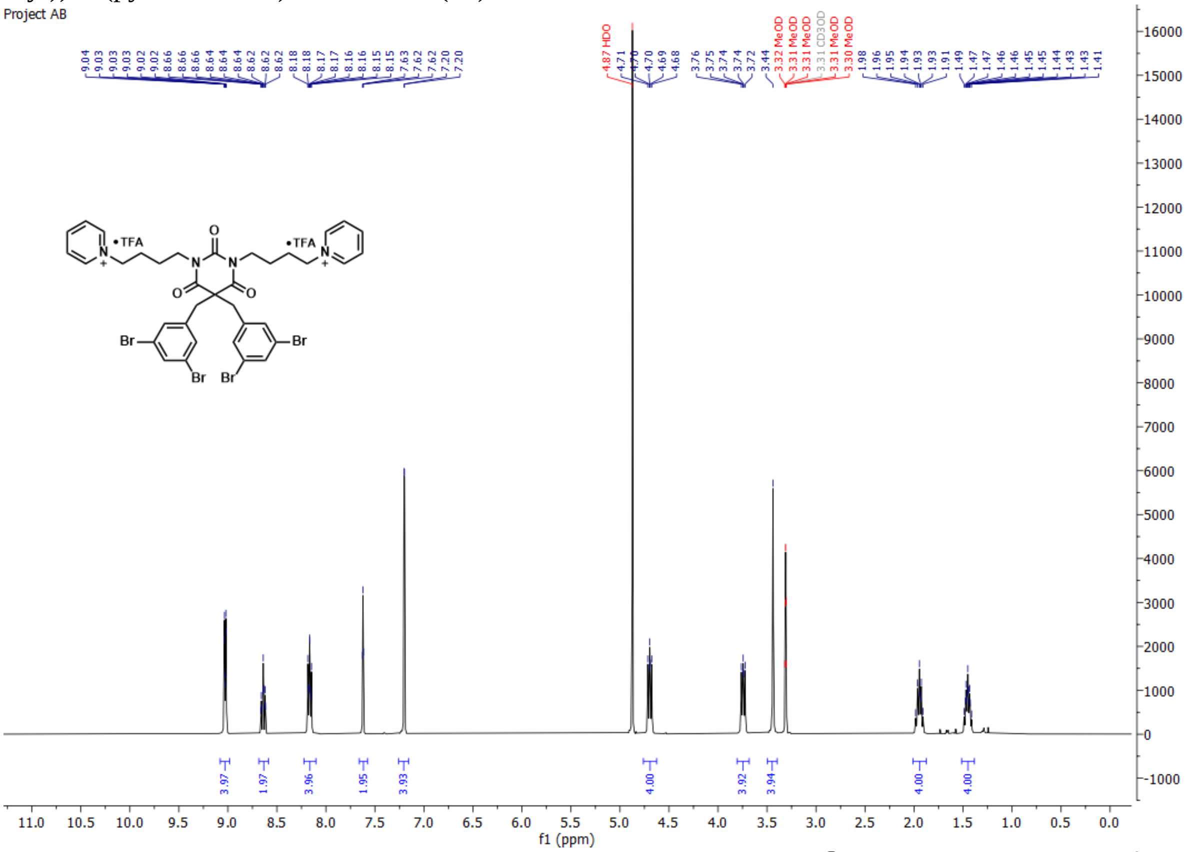

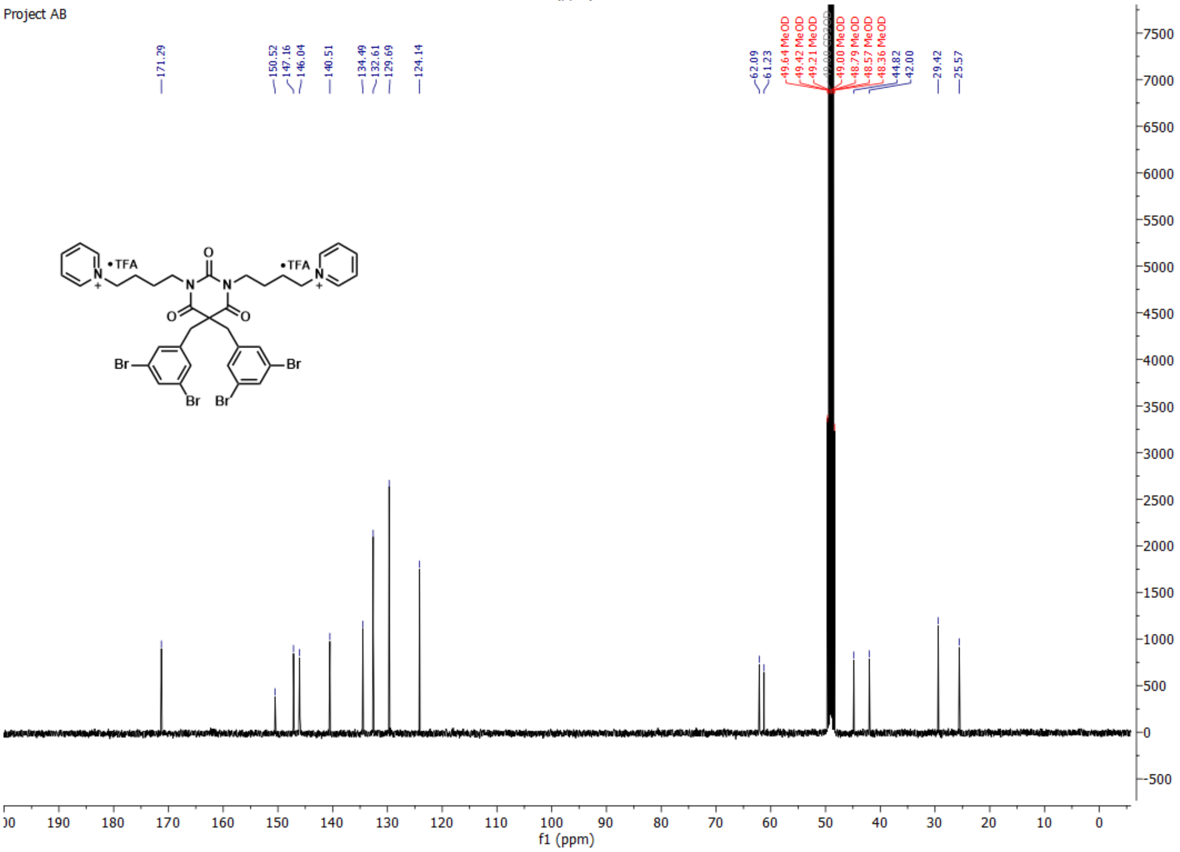

3.2 ^{1}H and ^{13}C NMR spectra of compounds in *series 2*

1,3-bis(4-aminobutyl)-5,5-bis(quinolin-2-ylmethyl)pyrimidine-2,4,6(1*H*,3*H*,5*H*)-trione di-TFA salt **(10bA)**

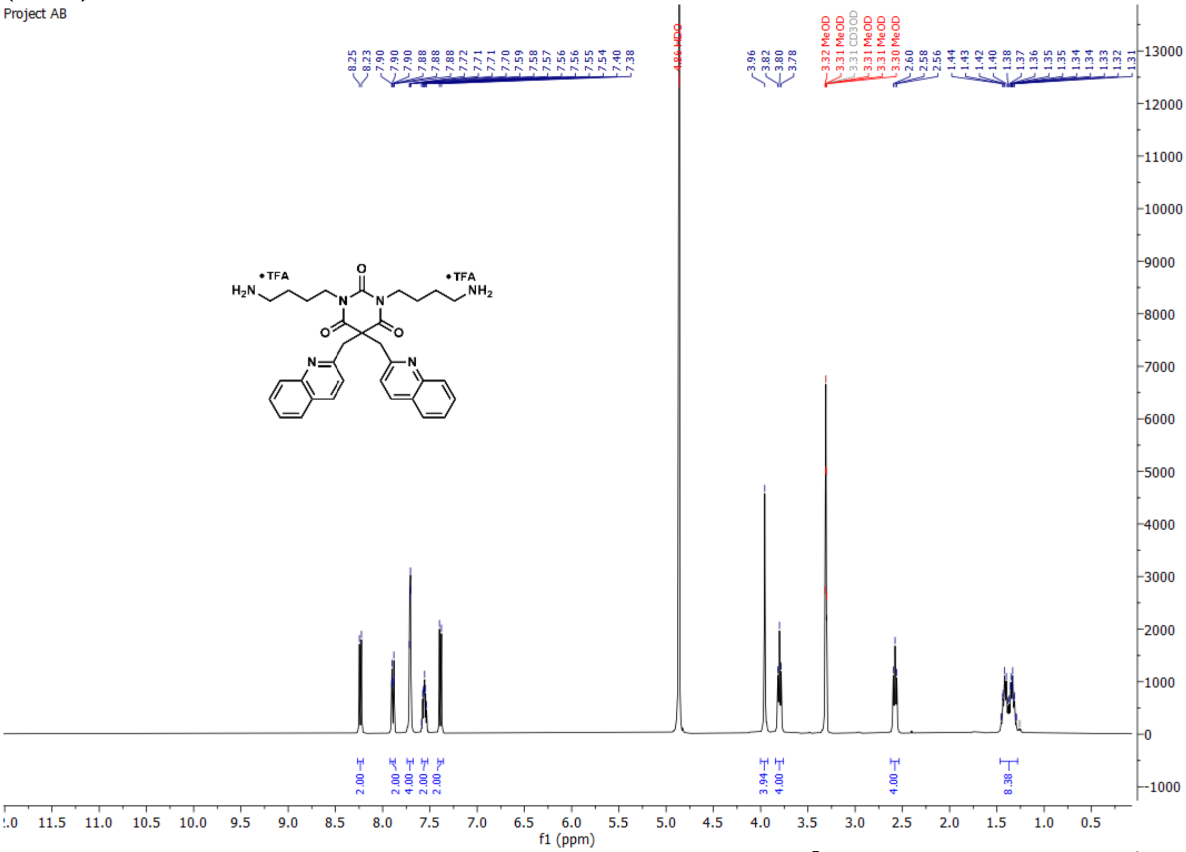

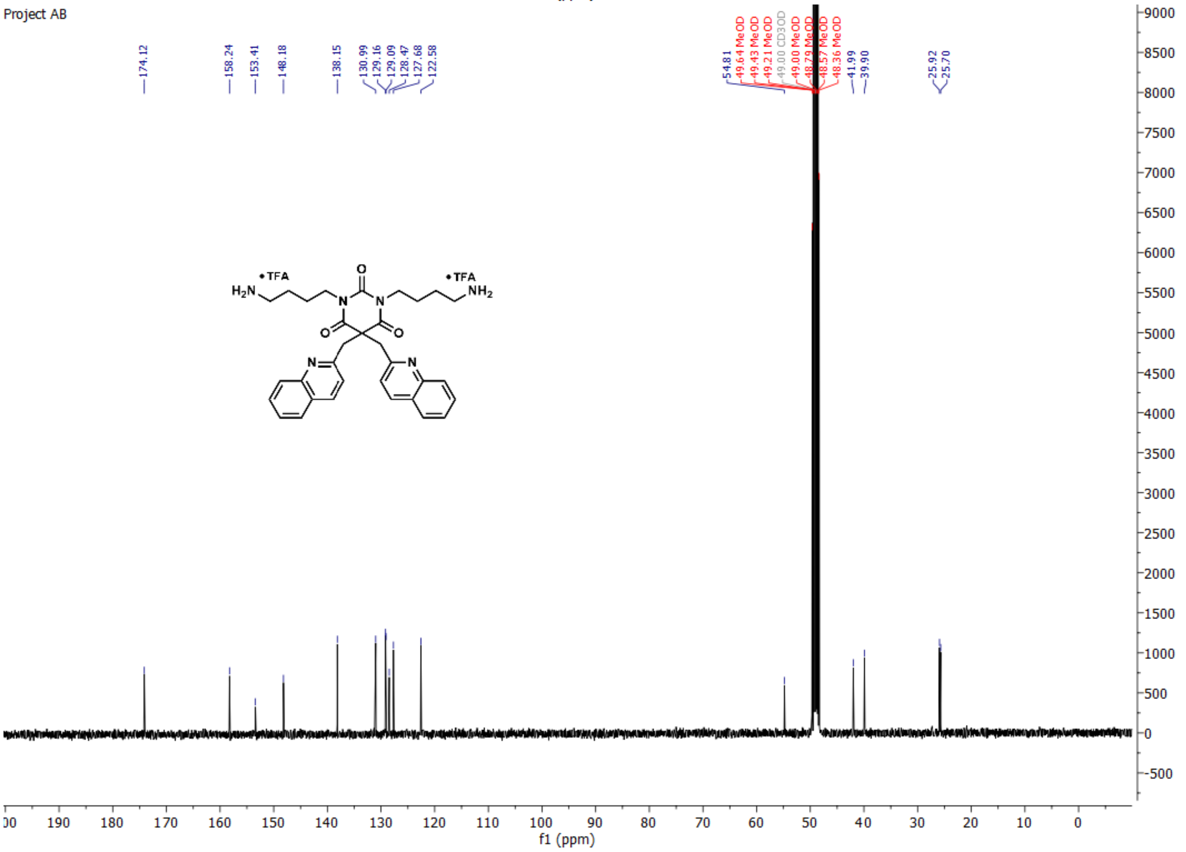

1,3-bis(4-aminobutyl)-5,5-bis((6-bromoquinolin-2-yl)methyl)pyrimidine-2,4,6(1*H*,3*H*,5*H*)-trione di-TFA salt (**10cA**)

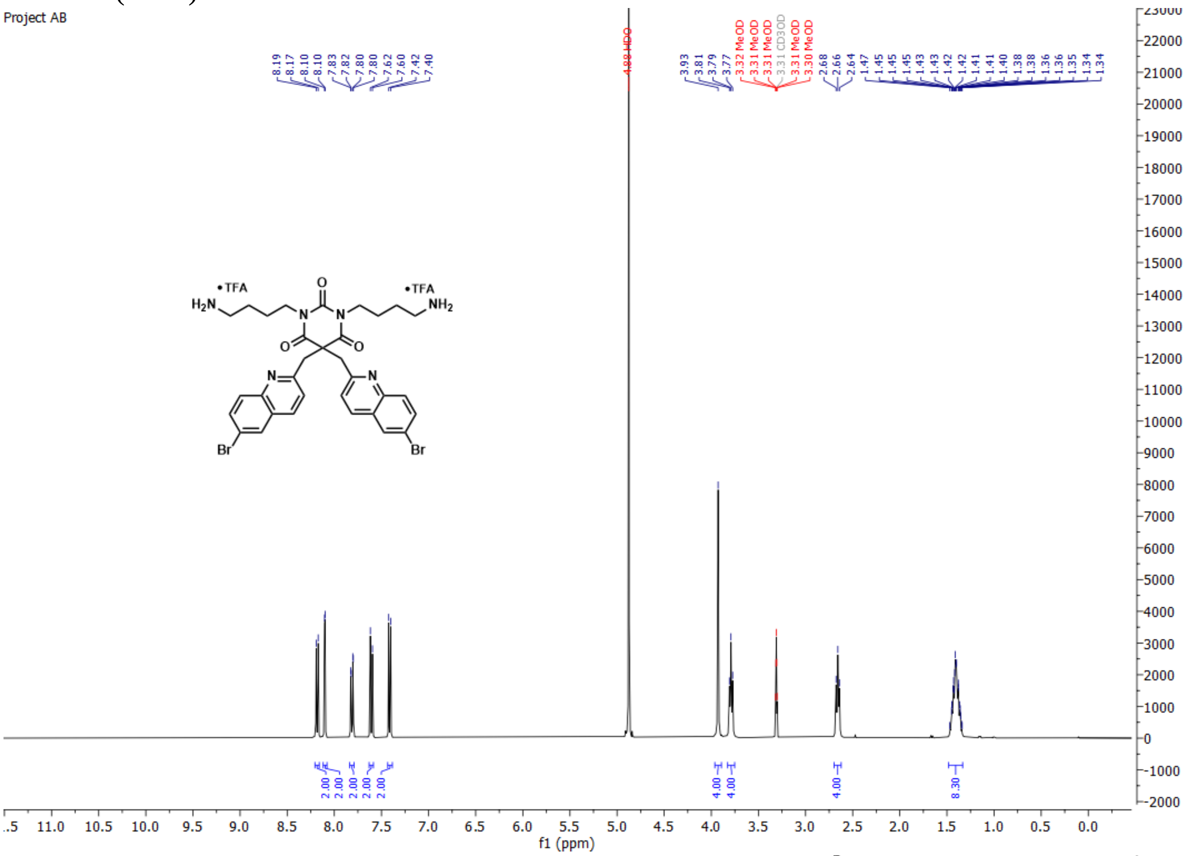

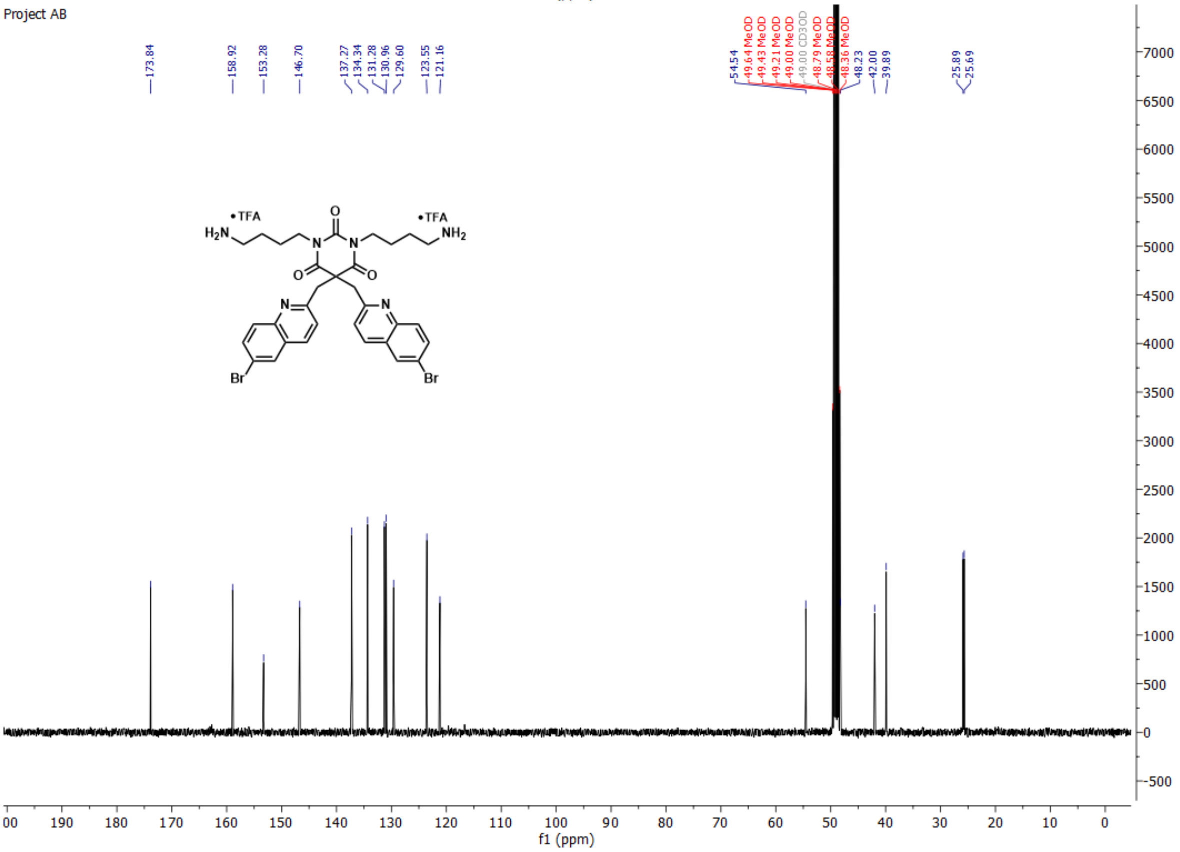

1,3-bis(4-aminobutyl)-5,5-dihexylpyrimidine-2,4,6(1*H*,3*H*,5*H*)-trione di-TFA salt (**10dA**)

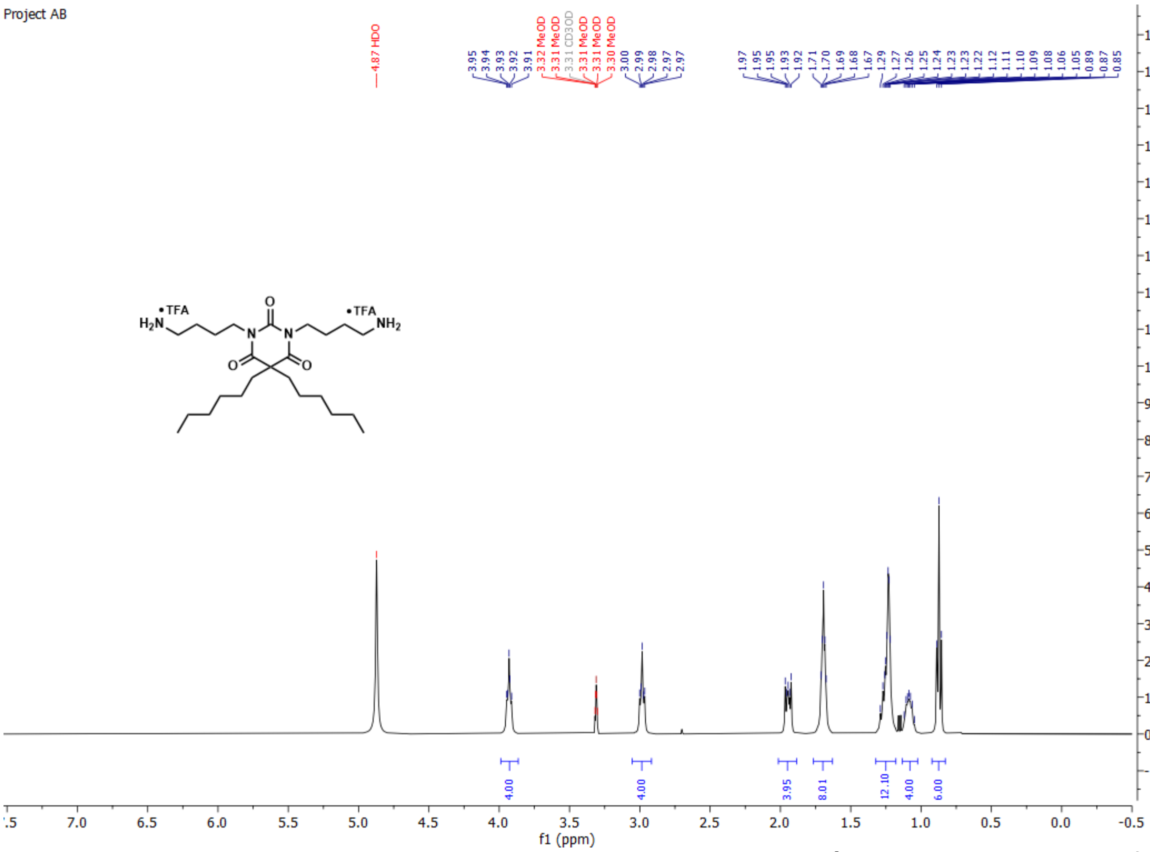

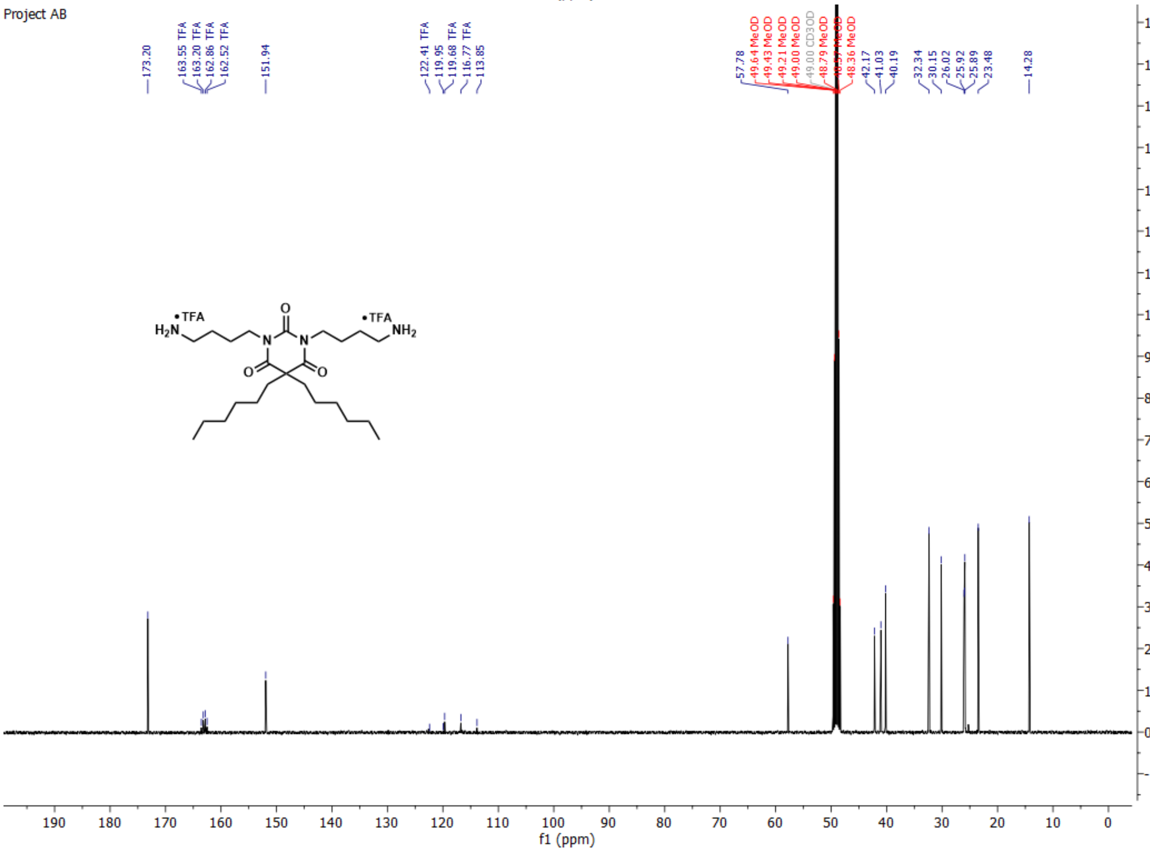

1,3-bis(4-aminobutyl)-5,5-bis((4-bromonaphthalen-1-yl)methyl)pyrimidine-2,4,6(1*H*,3*H*,5*H*)-trione di-TFA salt (**10eA**)

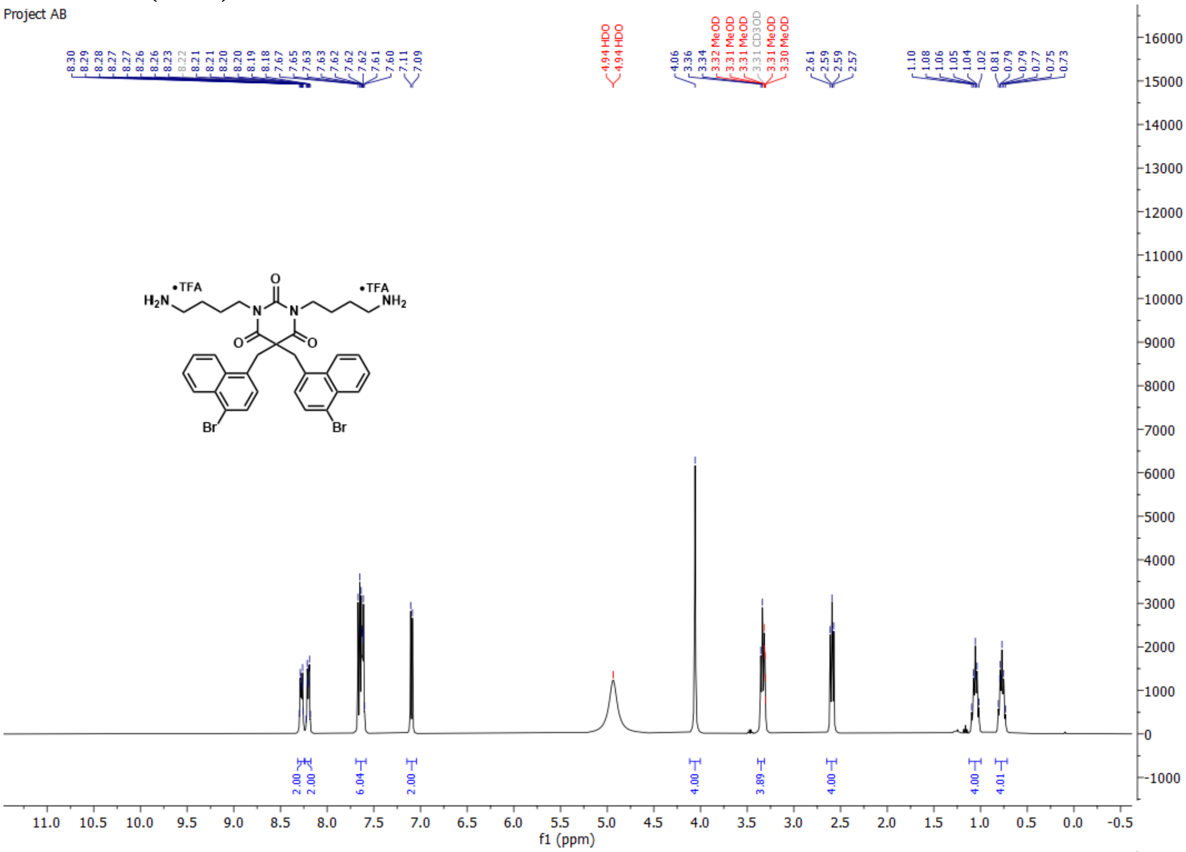

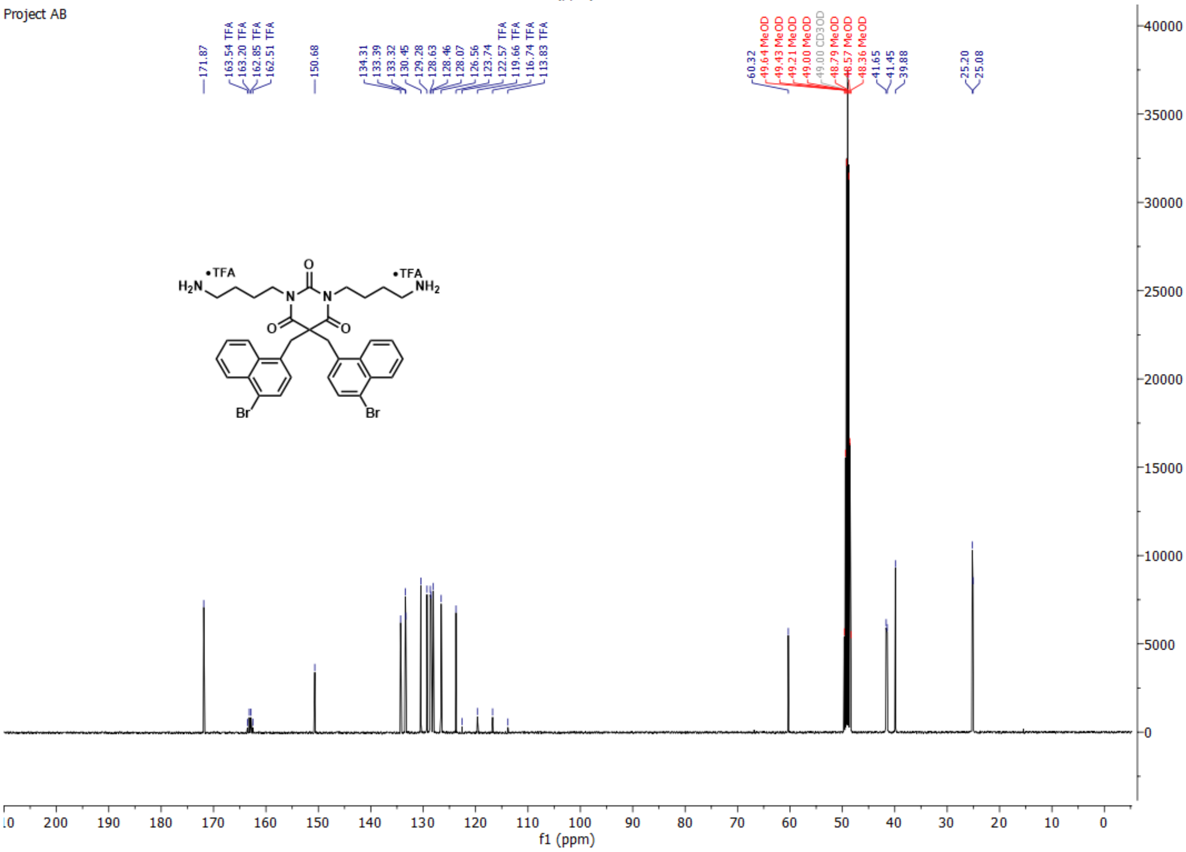

1,3-bis(4-aminobutyl)-5,5-bis(2,4,5-tribromobenzyl)pyrimidine-2,4,6(1*H*,3*H*,5*H*)-trione di-TFA salt (**10fA**)

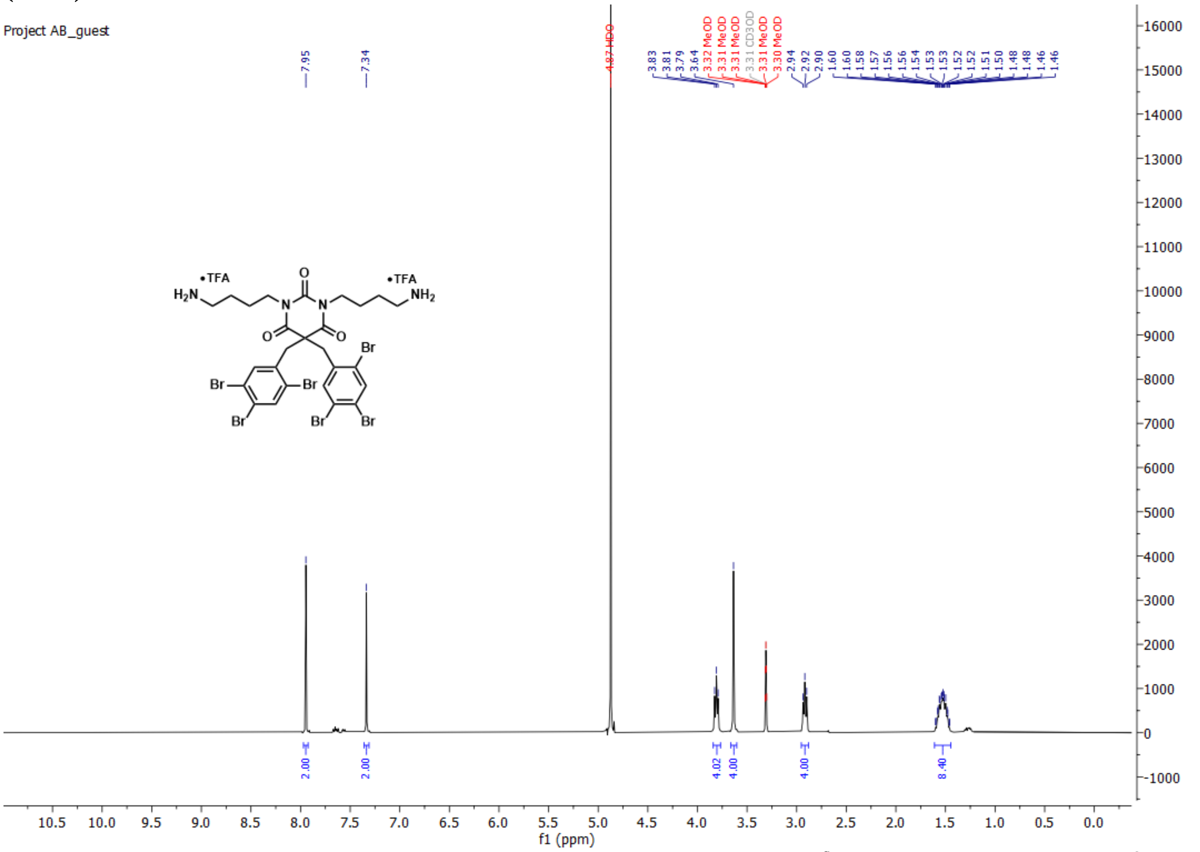

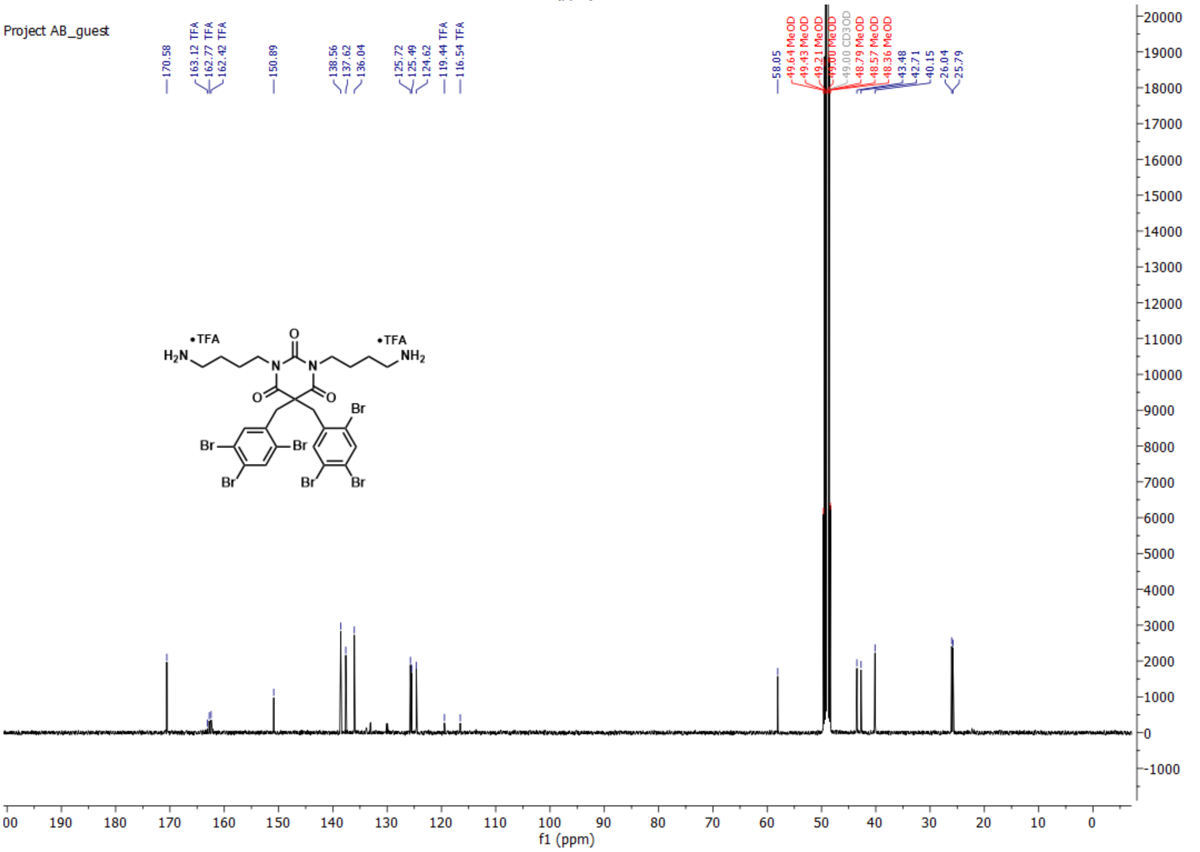

1,3-bis(4-aminobutyl)-5,5-bis(2,4,6-tribromobenzyl)pyrimidine-2,4,6(1*H*,3*H*,5*H*)-trione di-TFA salt (**10gA**)

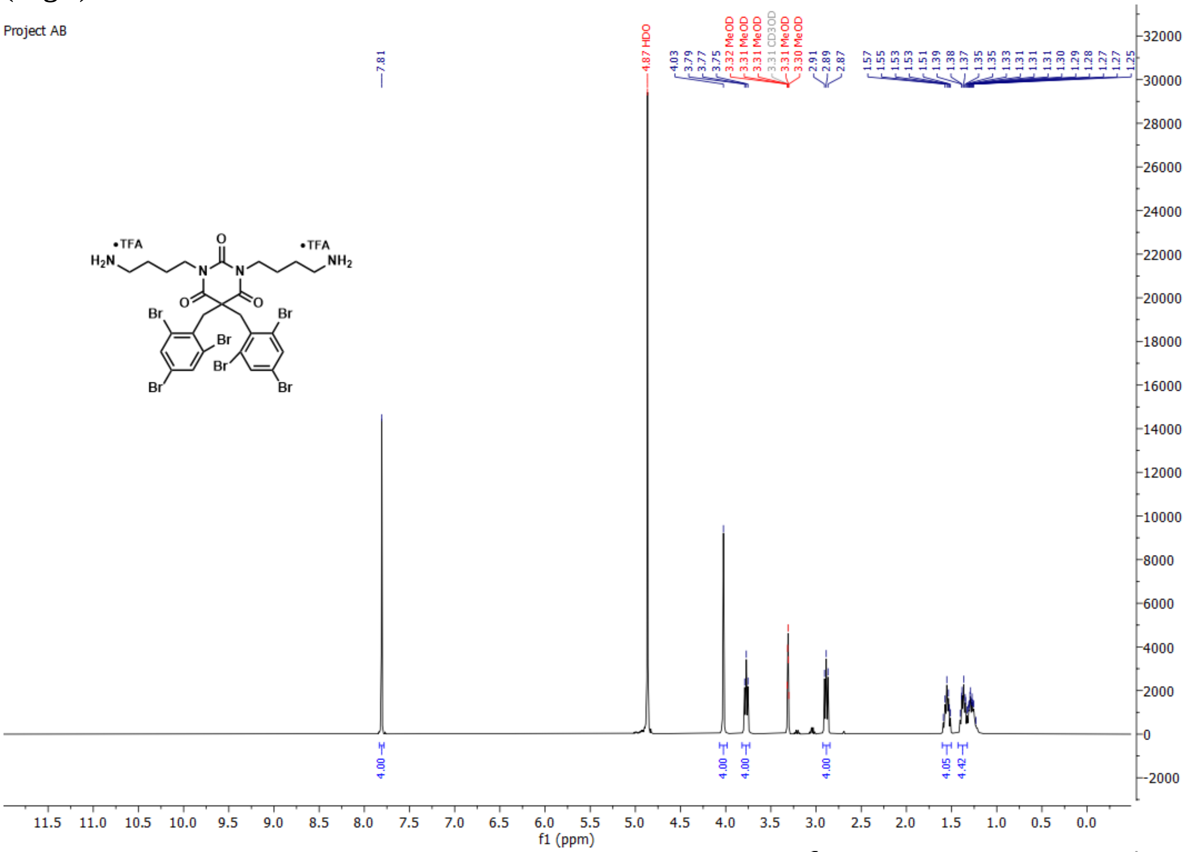

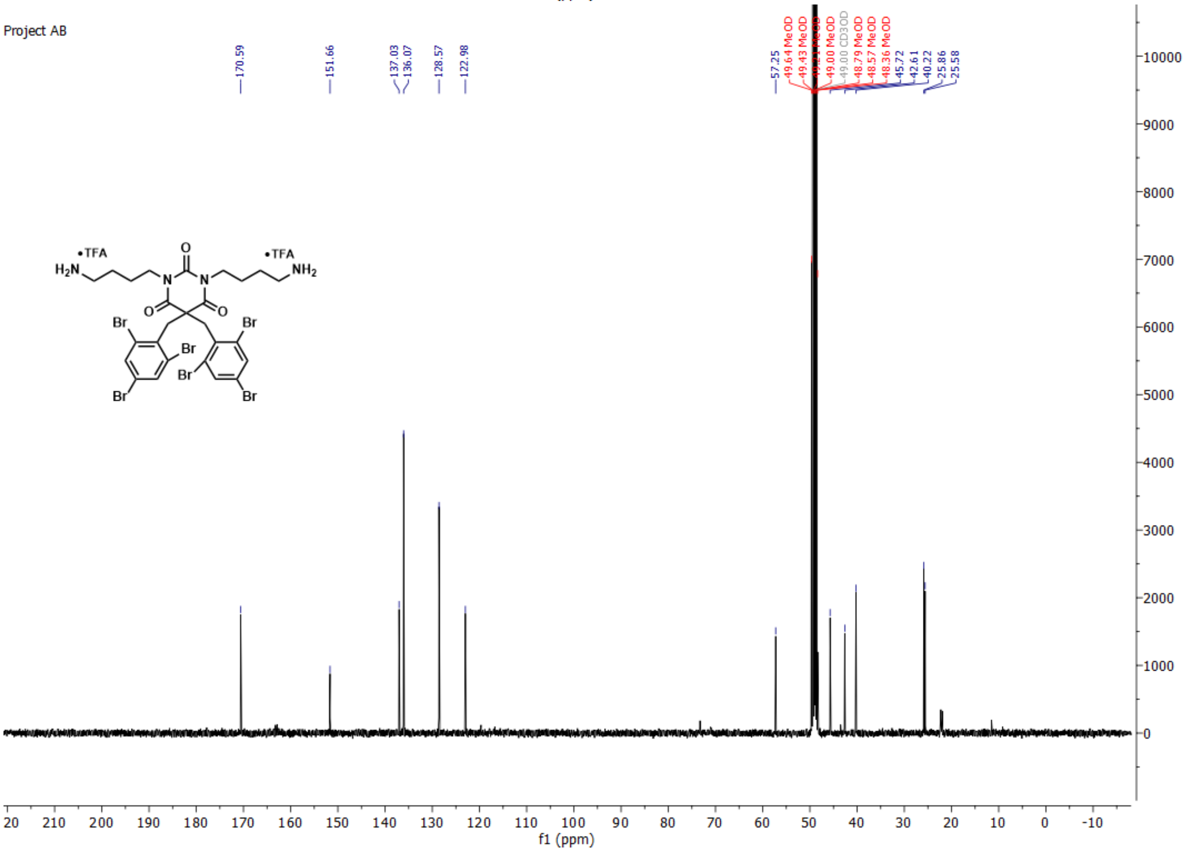

1,1'-((2,4,6-trioxo-5,5-bis(quinolin-2-ylmethyl)dihydropyrimidine-1,3(2*H*,4*H*)-diyl)bis(butane-4,1-diyl))diguanidine di-TFA salt (**10bG**)

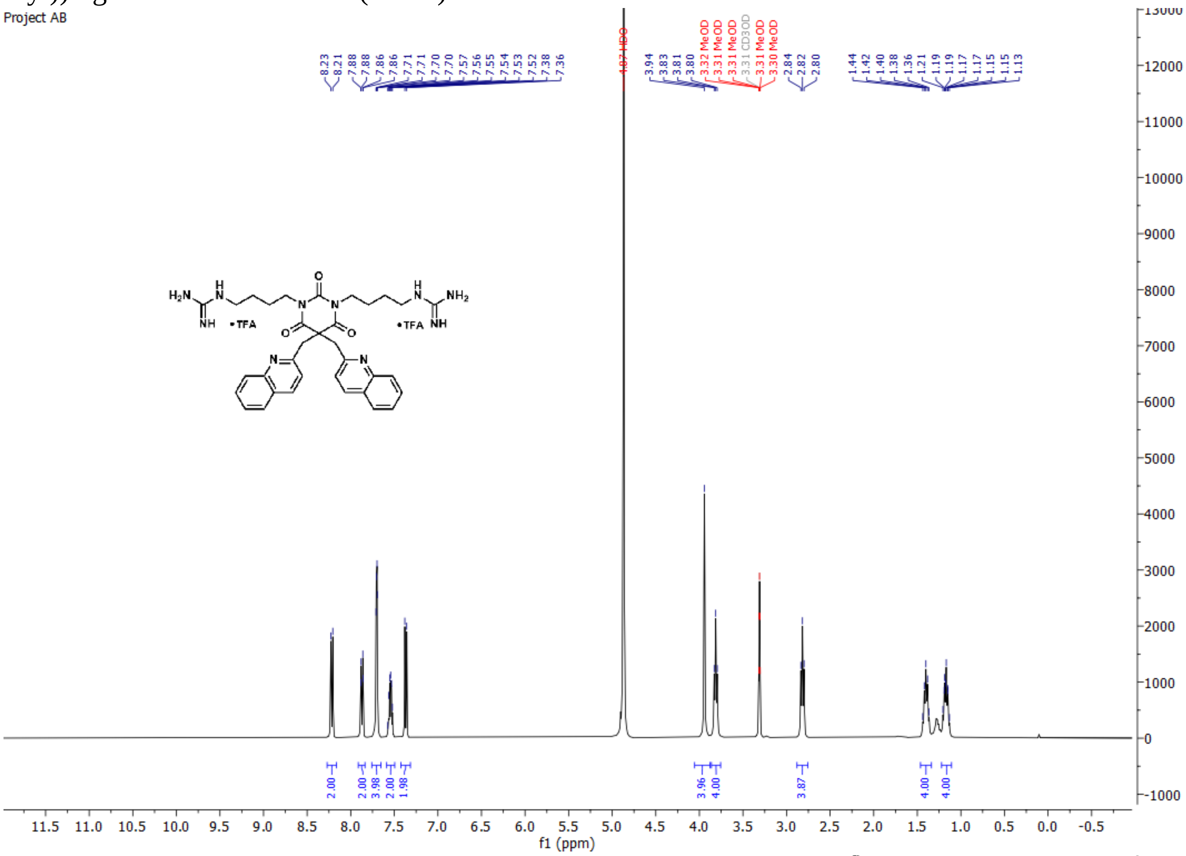

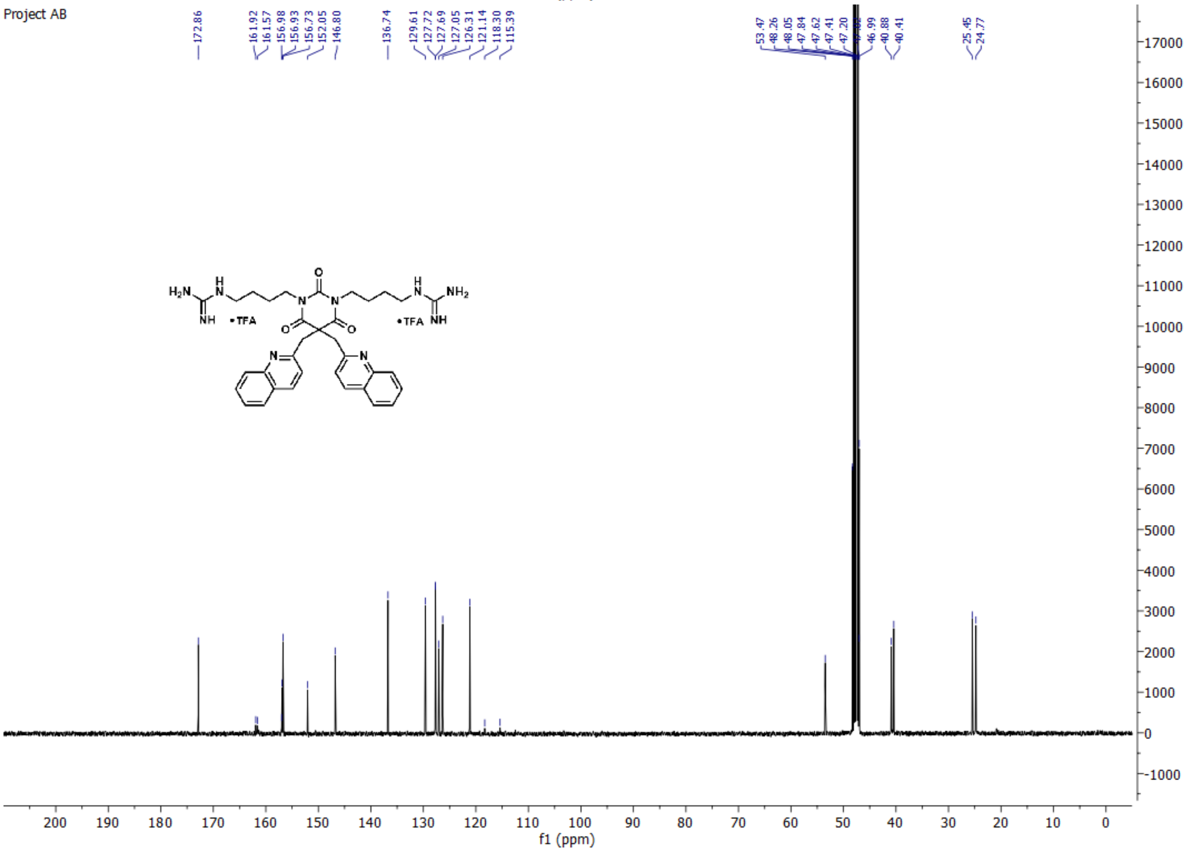

1,1'-((5,5-bis((6-bromoquinolin-2-yl)methyl)-2,4,6-trioxodihydropyrimidine-1,3(2*H*,4*H*)-diyl)bis(butane-4,1-diyl))diguanidine di-TFA salt (**10cG**)

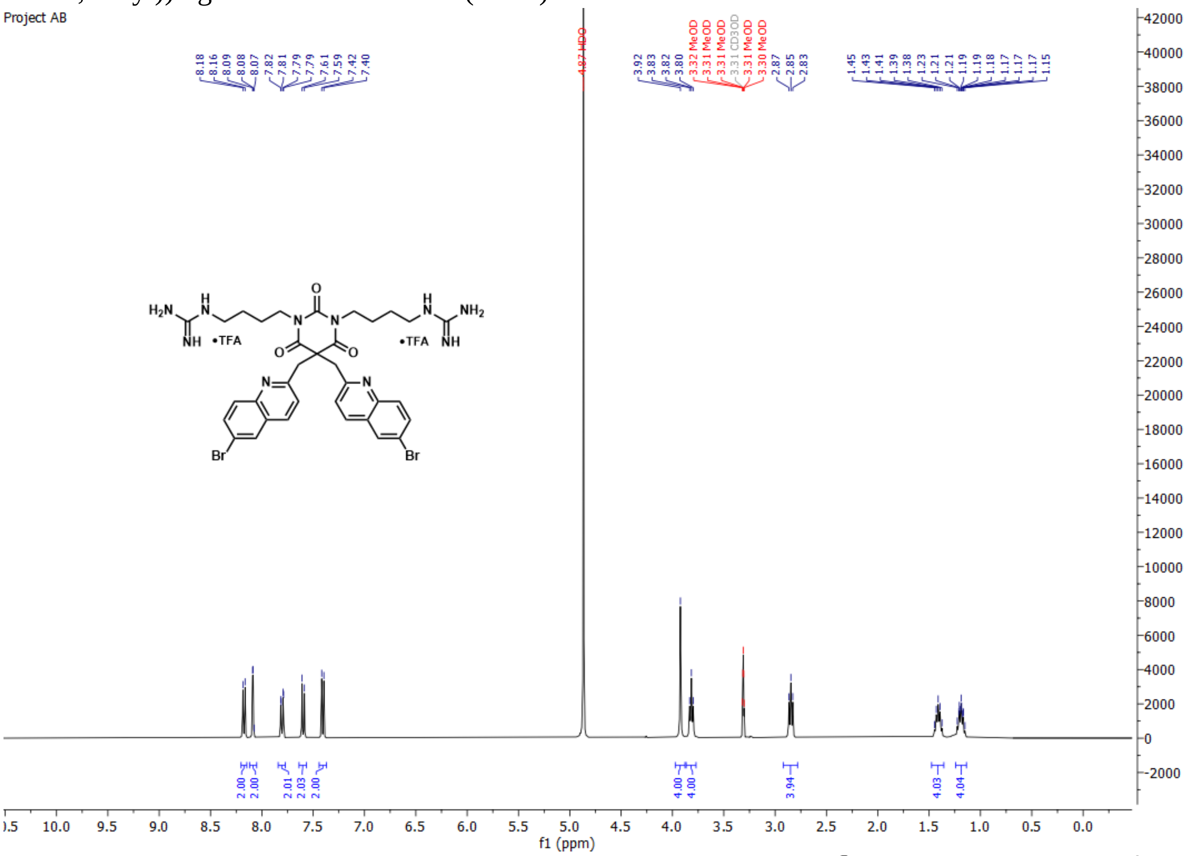

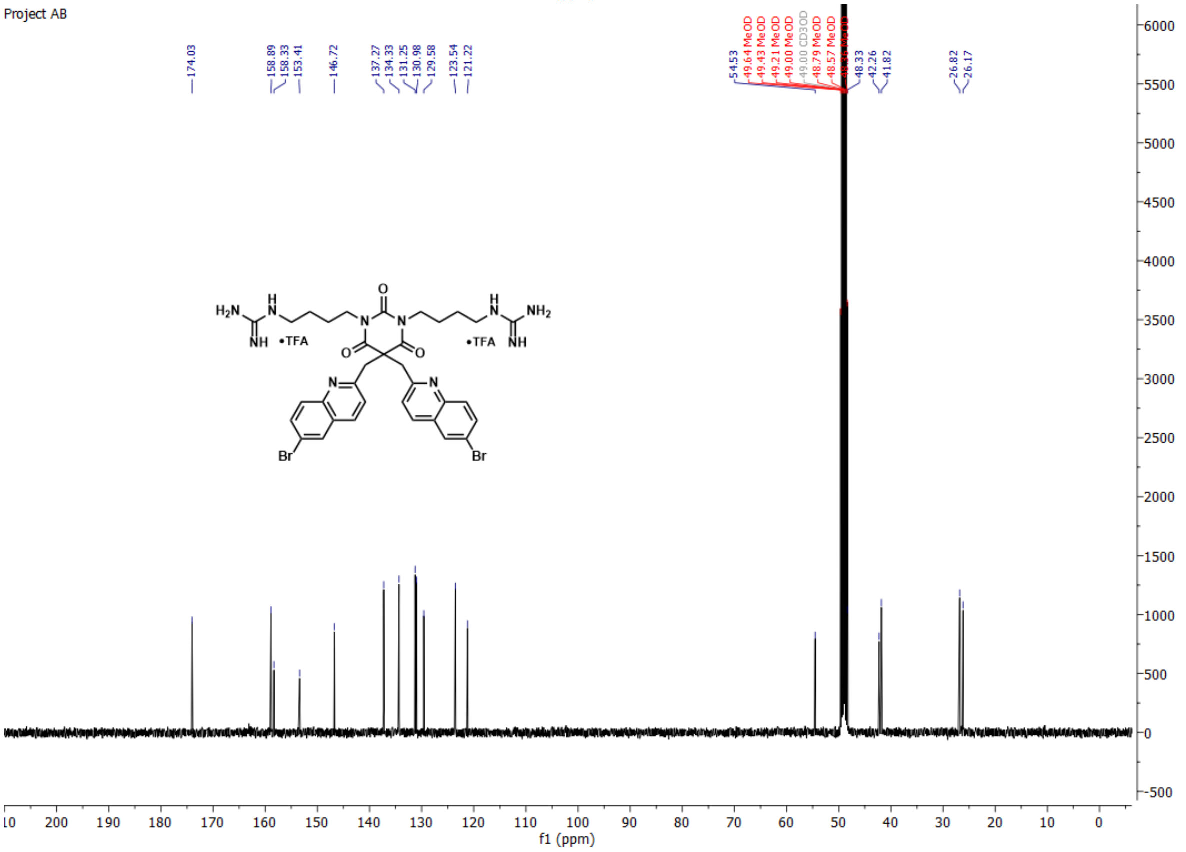

1,1'-((5,5-dihexyl-2,4,6-trioxodihydropyrimidine-1,3(2*H*,4*H*)-diyl)bis(butane-4,1-diyl))diguanidine di-TFA salt (**10dG**)

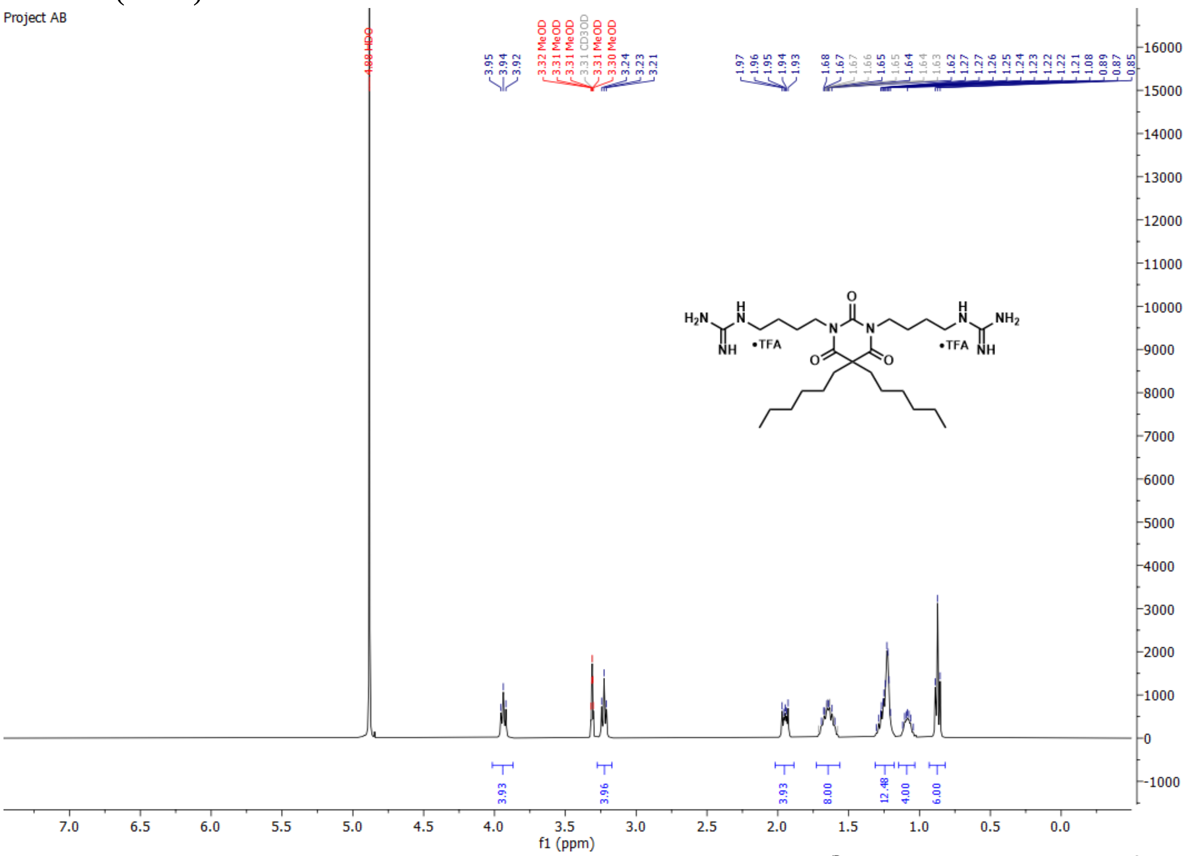

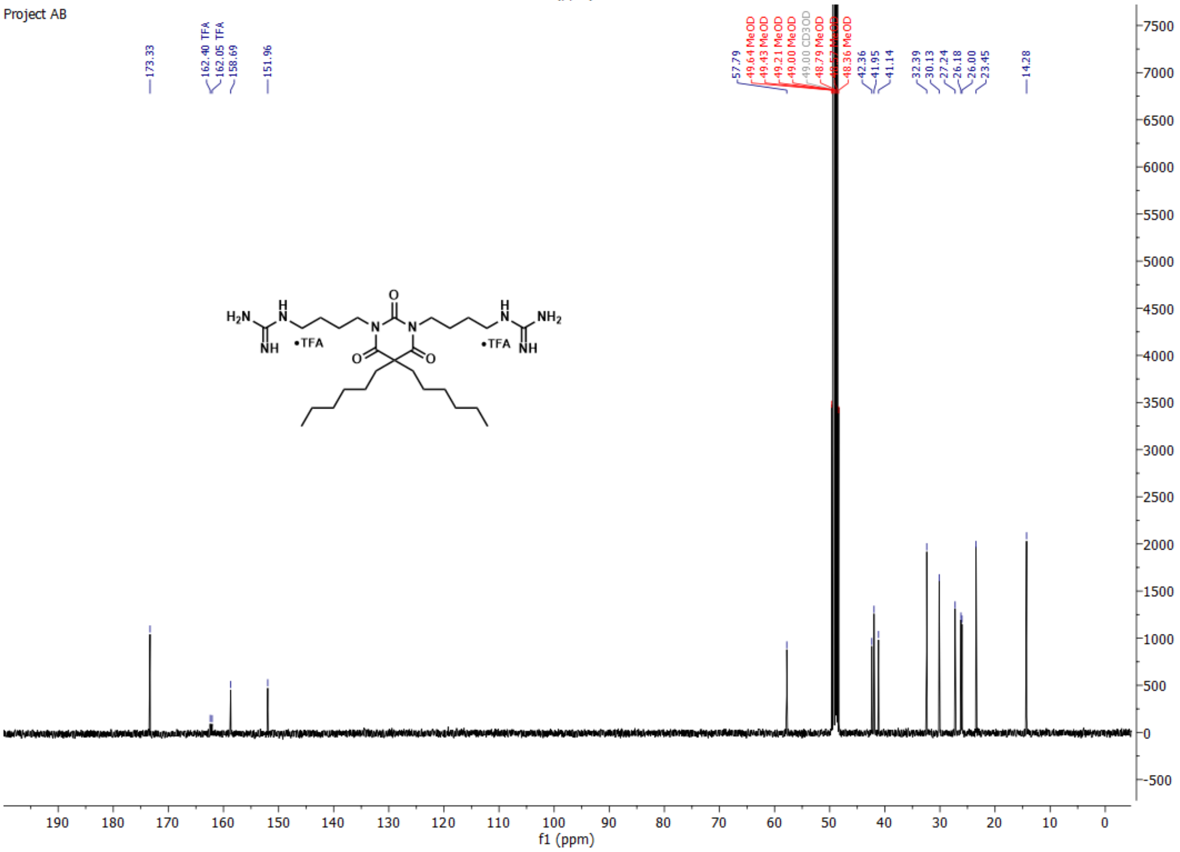

1,1'-((5,5-bis((4-bromonaphthalen-1-yl)methyl)-2,4,6-trioxodihydropyrimidine-1,3(2*H*,4*H*)-diyl)bis(butane-4,1-diyl))diguanidine di-TFA salt (**10eG**)

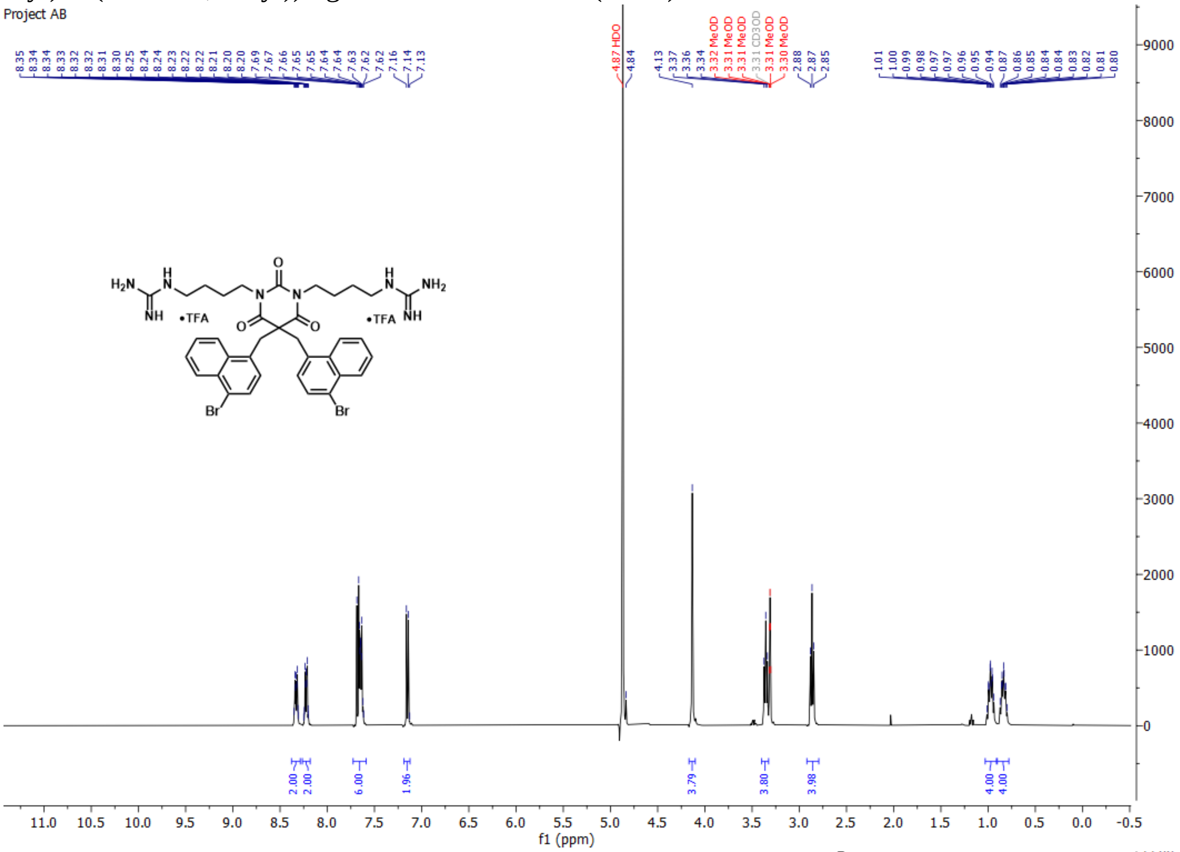

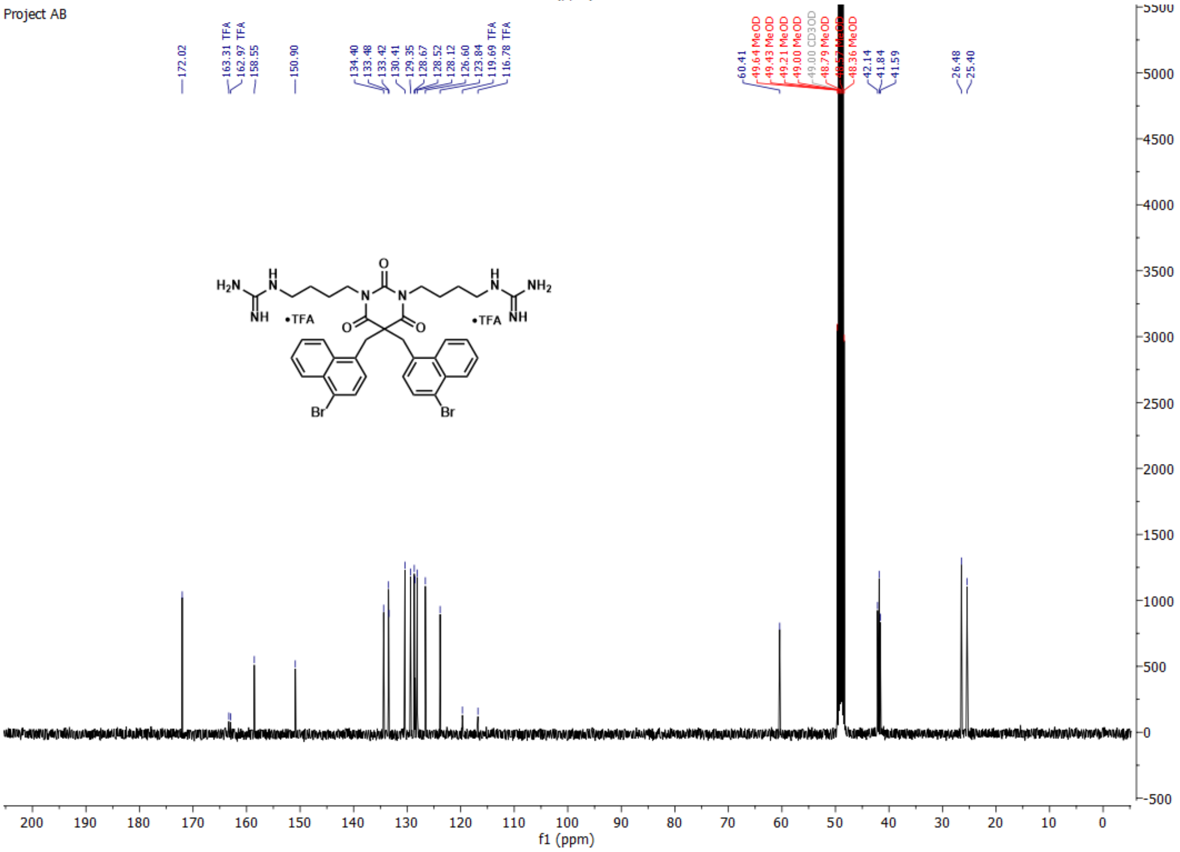

1,1'-((2,4,6-trioxo-5,5-bis(2,4,5-tribromobenzyl)dihydropyrimidine-1,3(2*H*,4*H*)-diyl)bis(butane-4,1-diyl))diguanidine di-TFA salt (**10fG**)

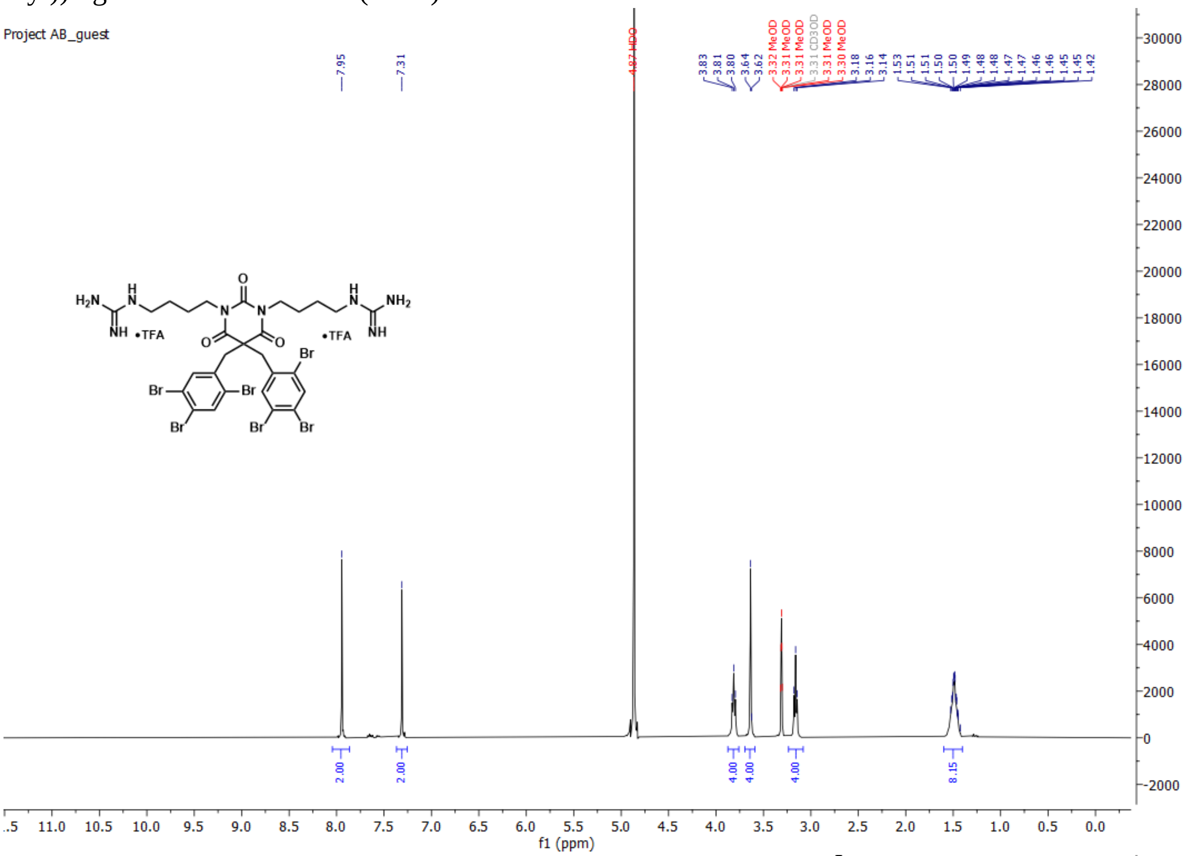

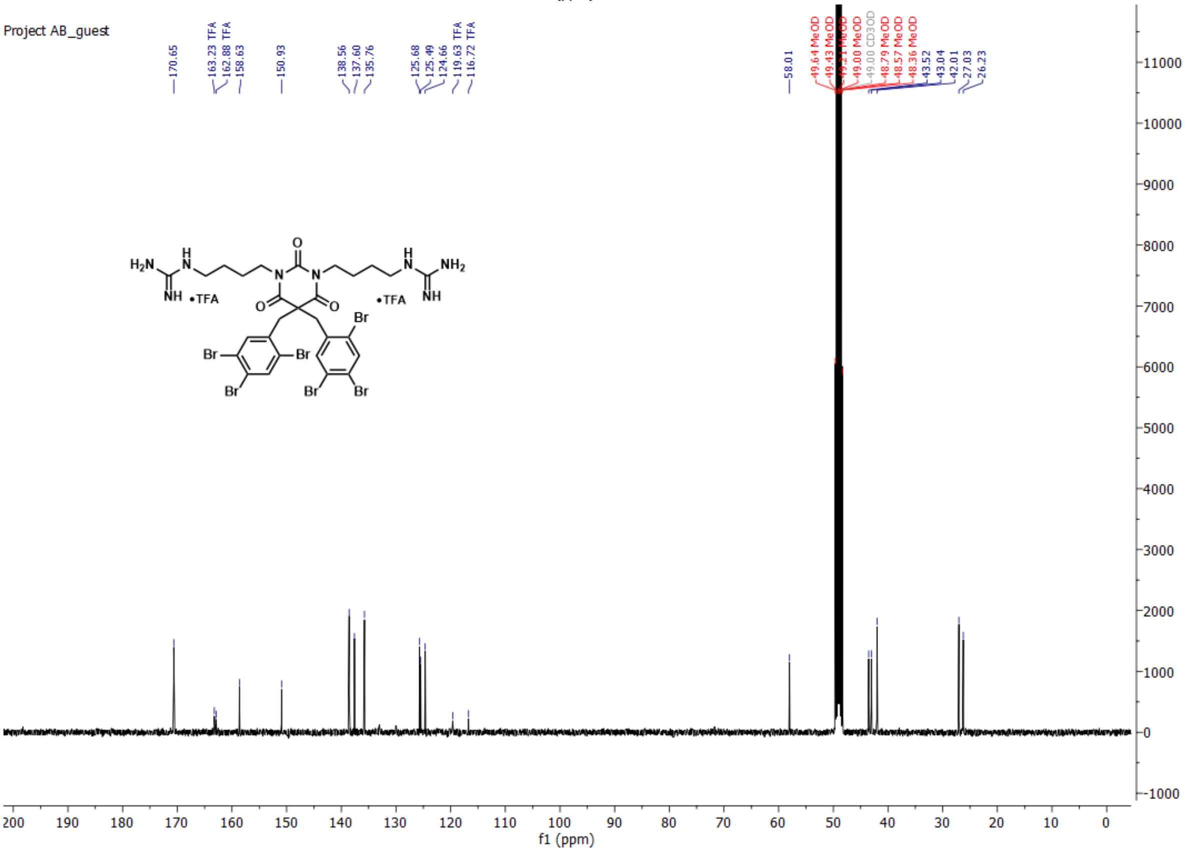

1,1'-((2,4,6-trioxo-5,5-bis(2,4,6-tribromobenzyl)dihydropyrimidine-1,3(2*H*,4*H*)-diyl)bis(butane-4,1-diyl))diguanidine di-TFA salt (**10gG**)

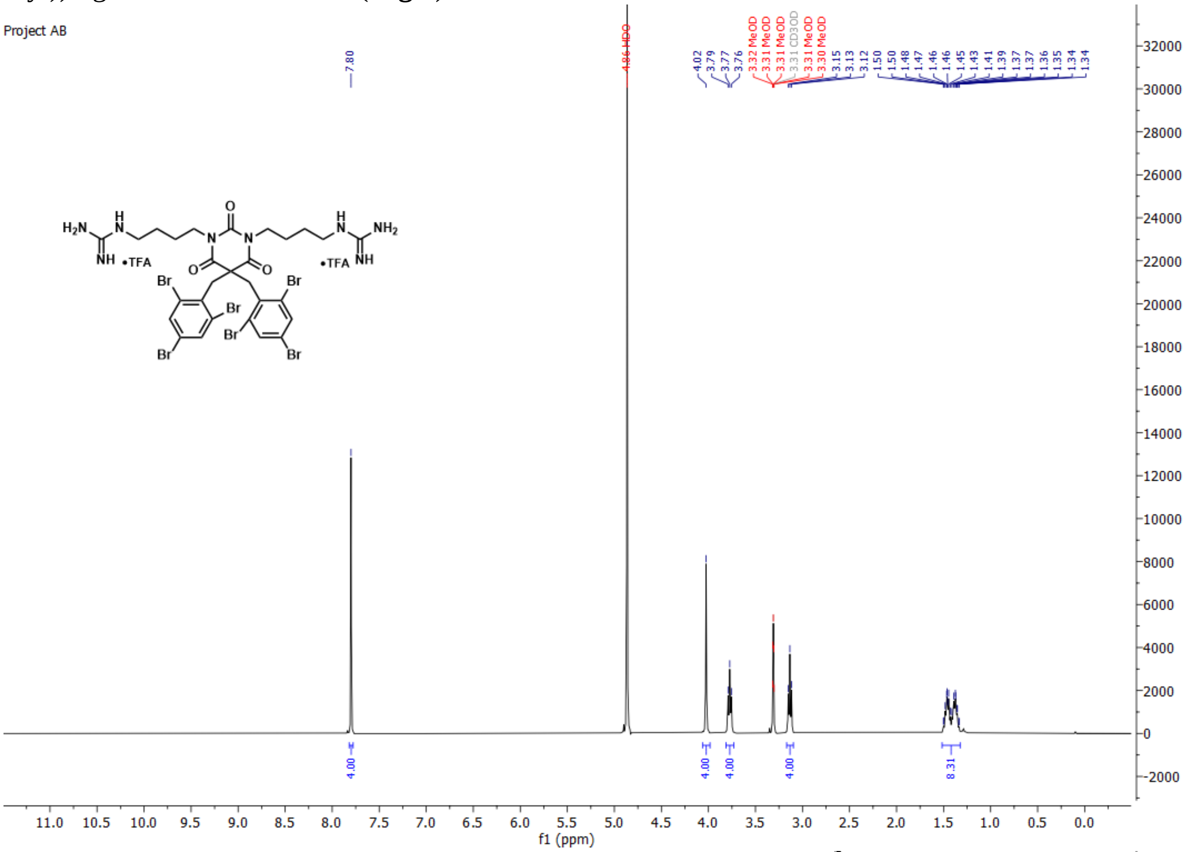

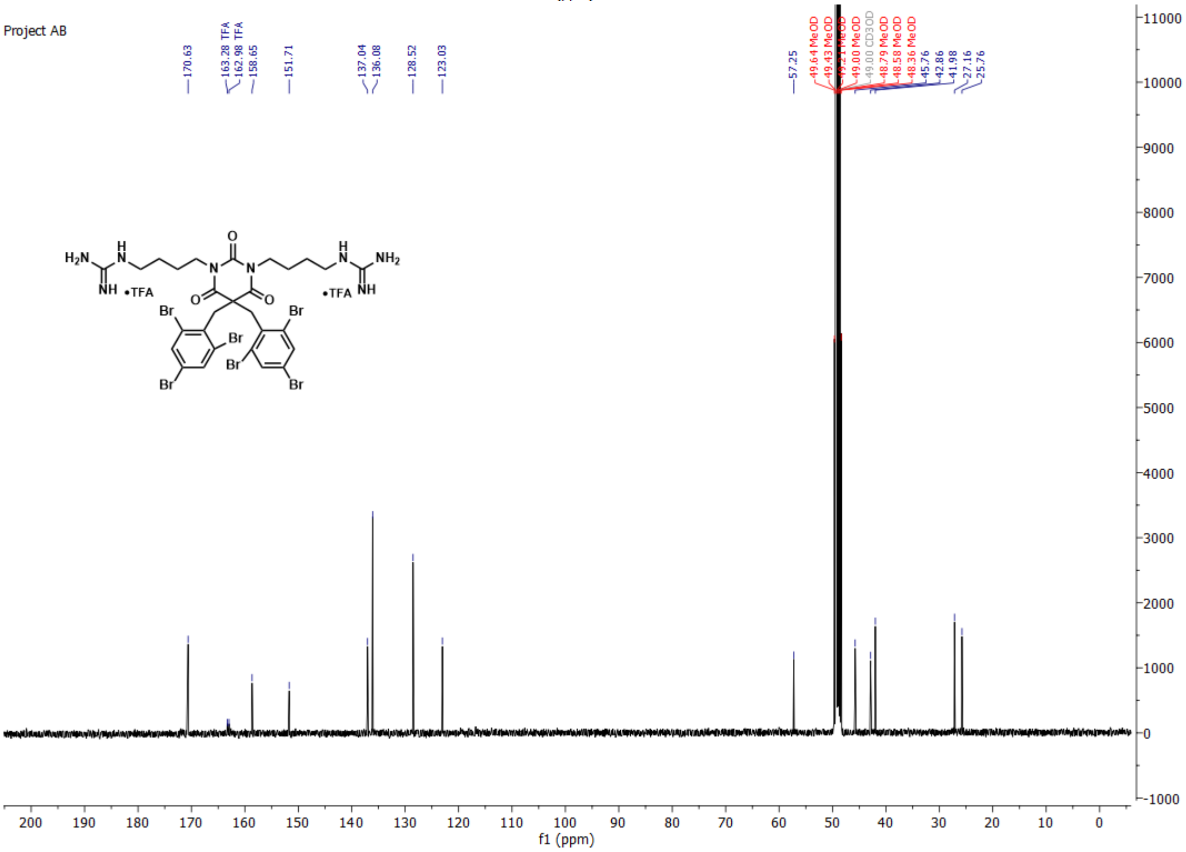

3.3 ^{1}H and ^{13}C NMR spectra of compounds in *series 3*

1,3-bis(4-aminobutyl)-5-(3,5-dibromobenzyl)-5-(quinolin-2-ylmethyl)pyrimidine-2,4,6(1*H*,3*H*,5*H*)-trione di-TFA salt (**11kA**)

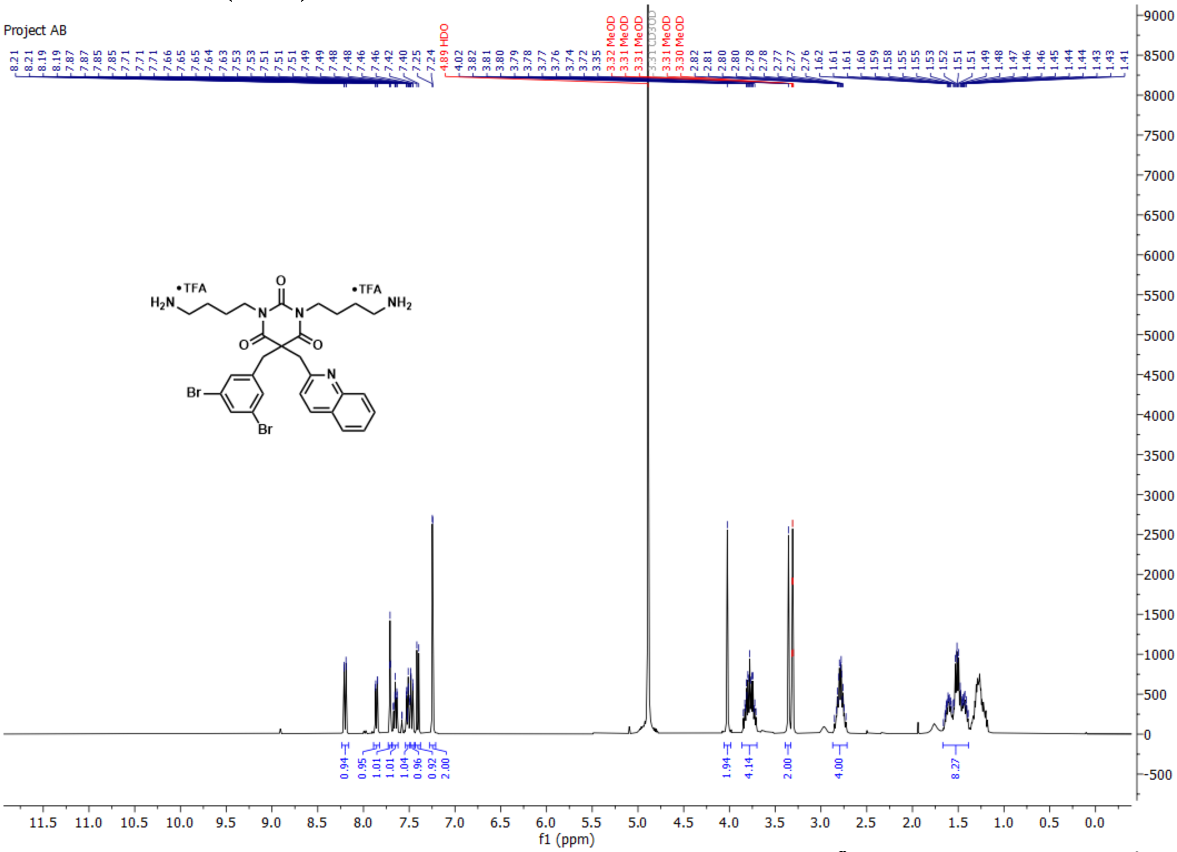

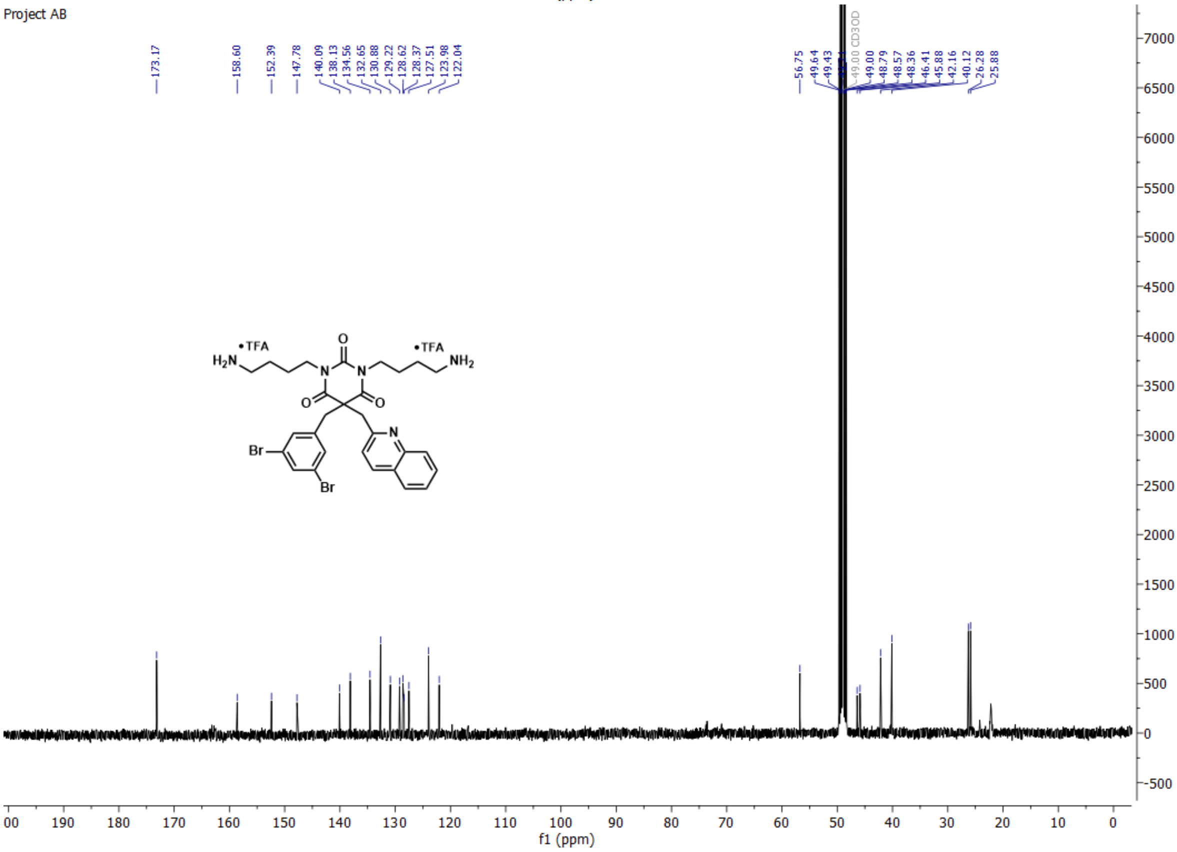

1,3-bis(4-aminobutyl)-5-(3,5-dibromobenzyl)-5-(4-(trifluoromethyl)benzyl)pyrimidine-2,4,6(1*H*,3*H*,5*H*)-trione di-TFA salt (**11lA**)

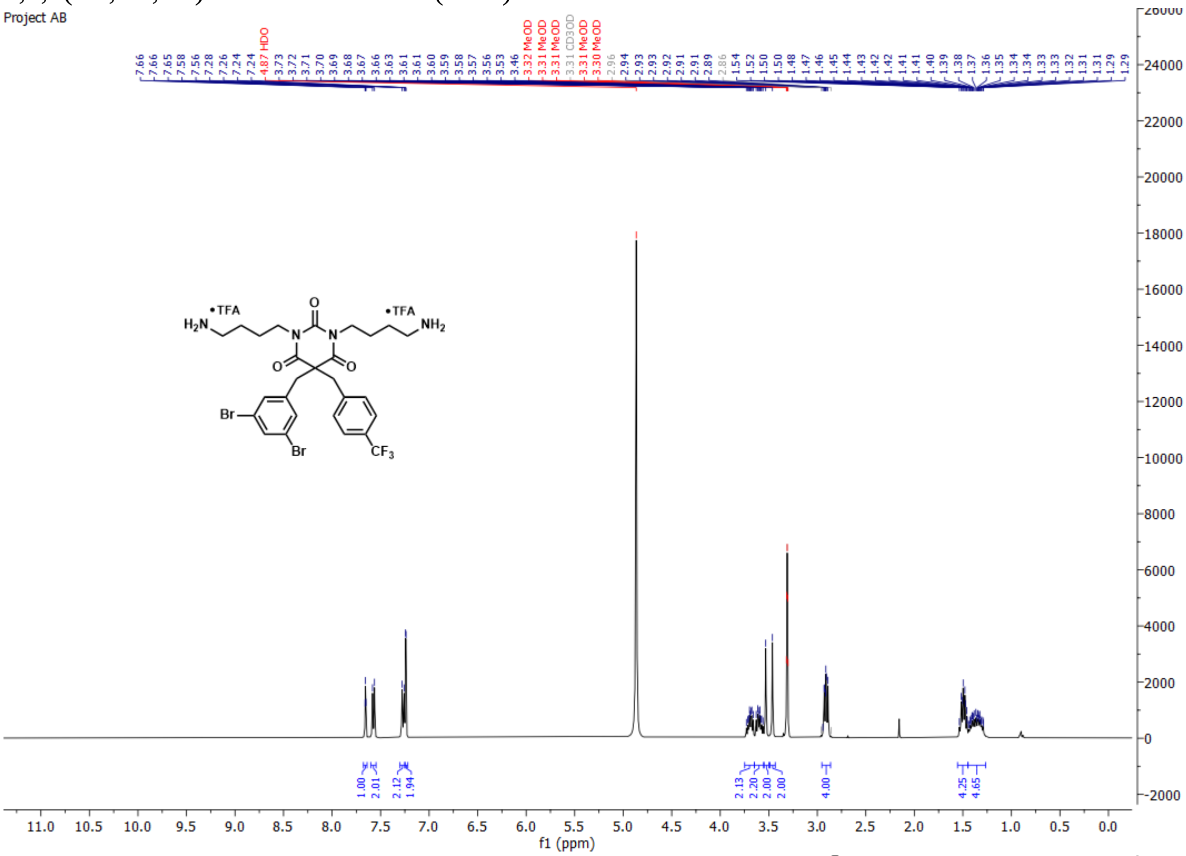

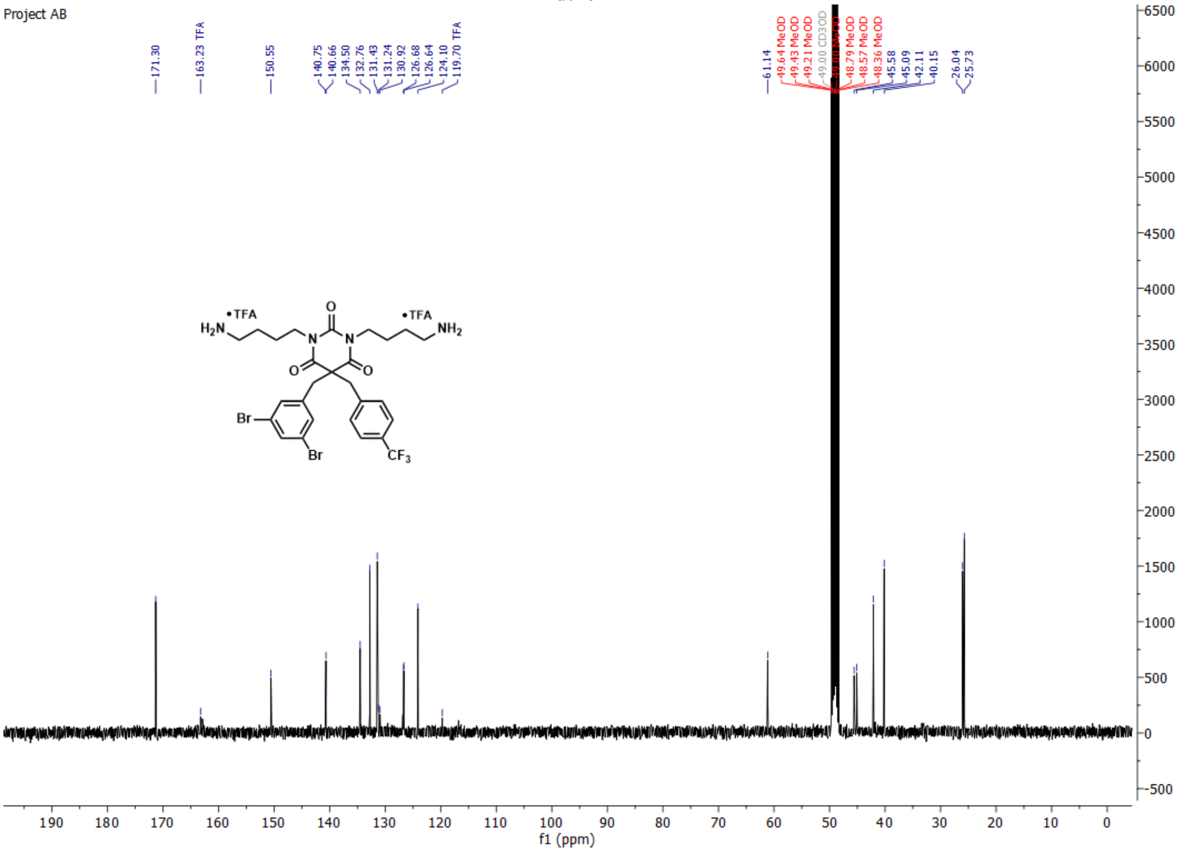

1,3-bis(4-aminobutyl)-5-cyclopentyl-5-(3,5-dibromobenzyl)pyrimidine-2,4,6(1*H*,3*H*,5*H*)-trione di-TFA salt (**11mA**)

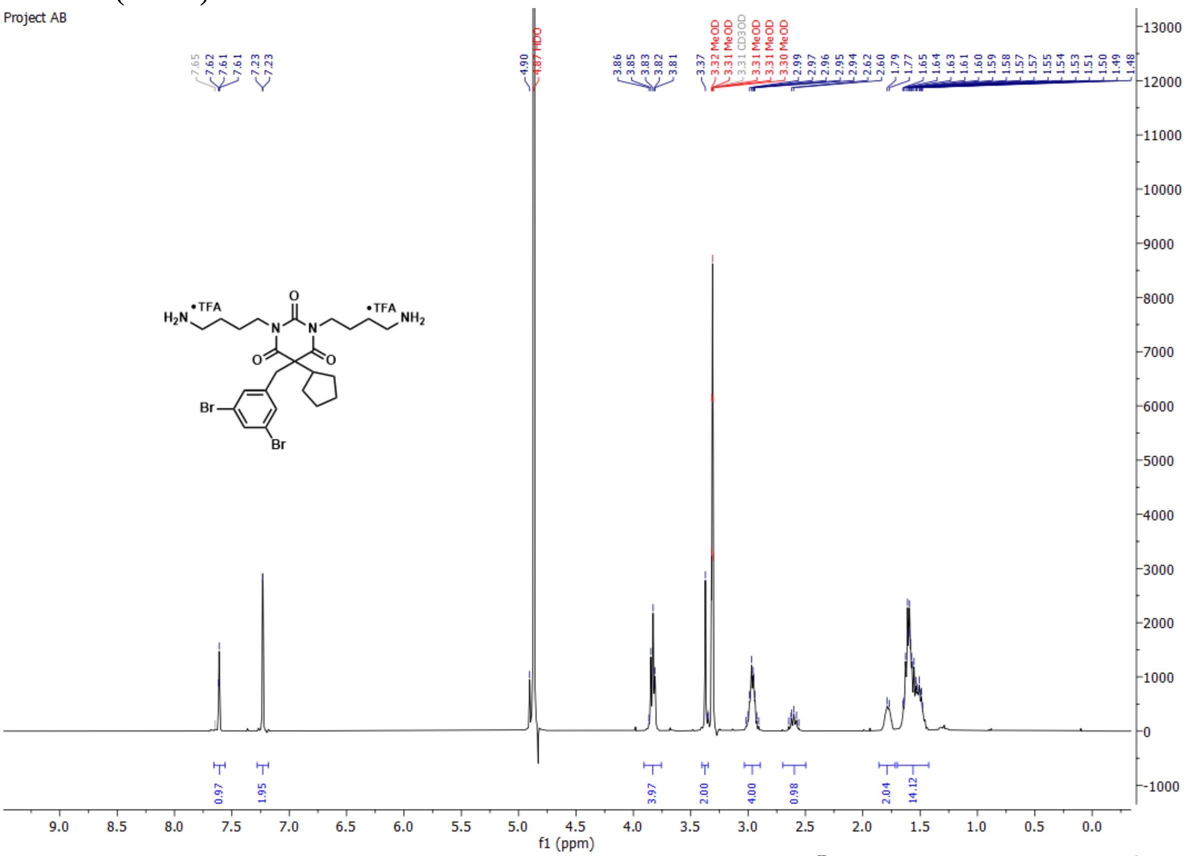

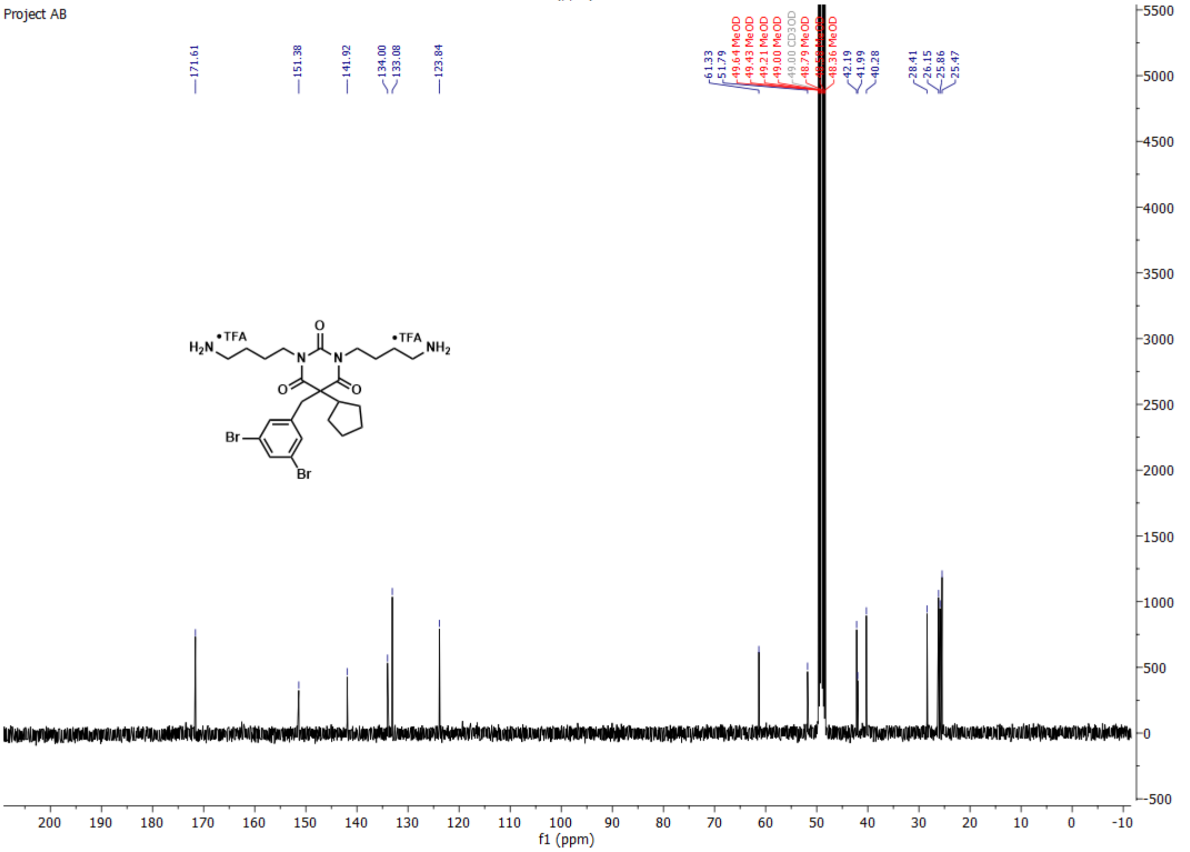

1,3-bis(4-aminobutyl)-5-(3,5-dibromobenzyl)-5-hexylpyrimidine-2,4,6(1*H*,3*H*,5*H*)-trione di-TFA salt **(11nA)**

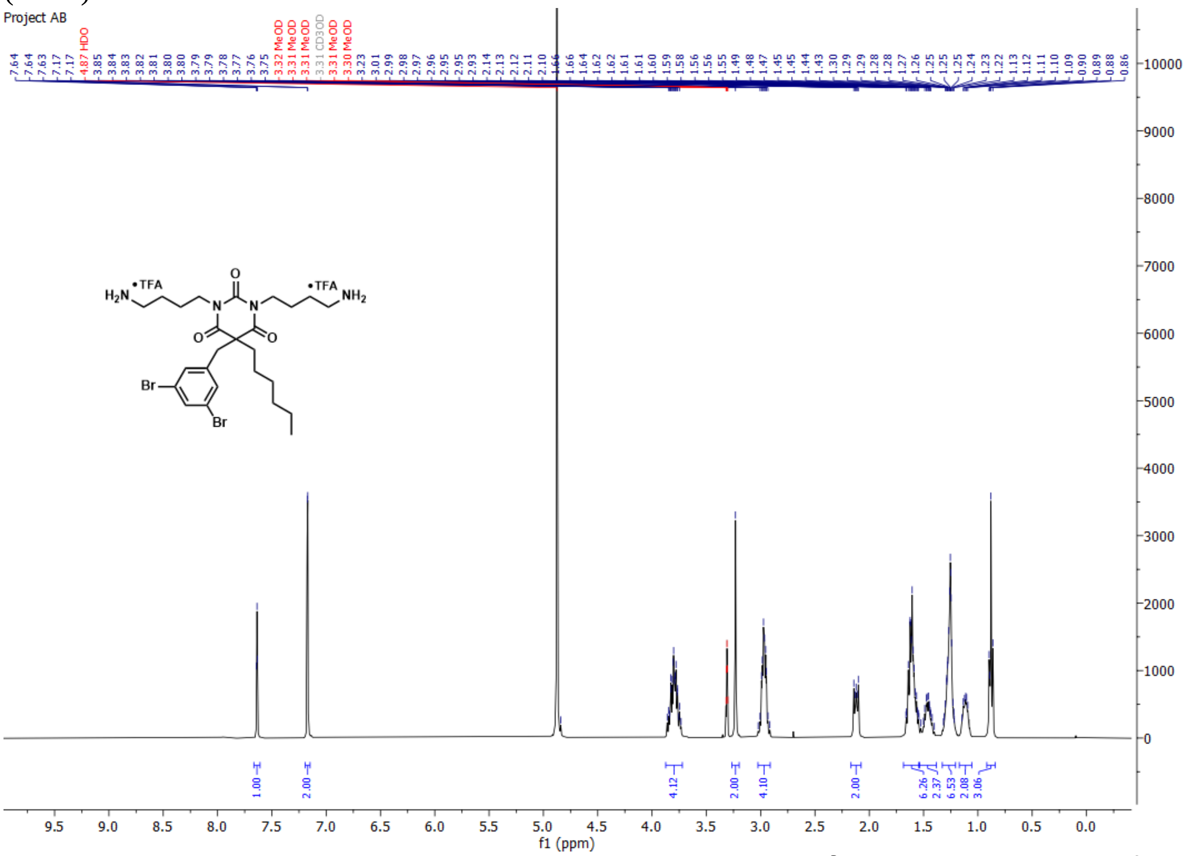

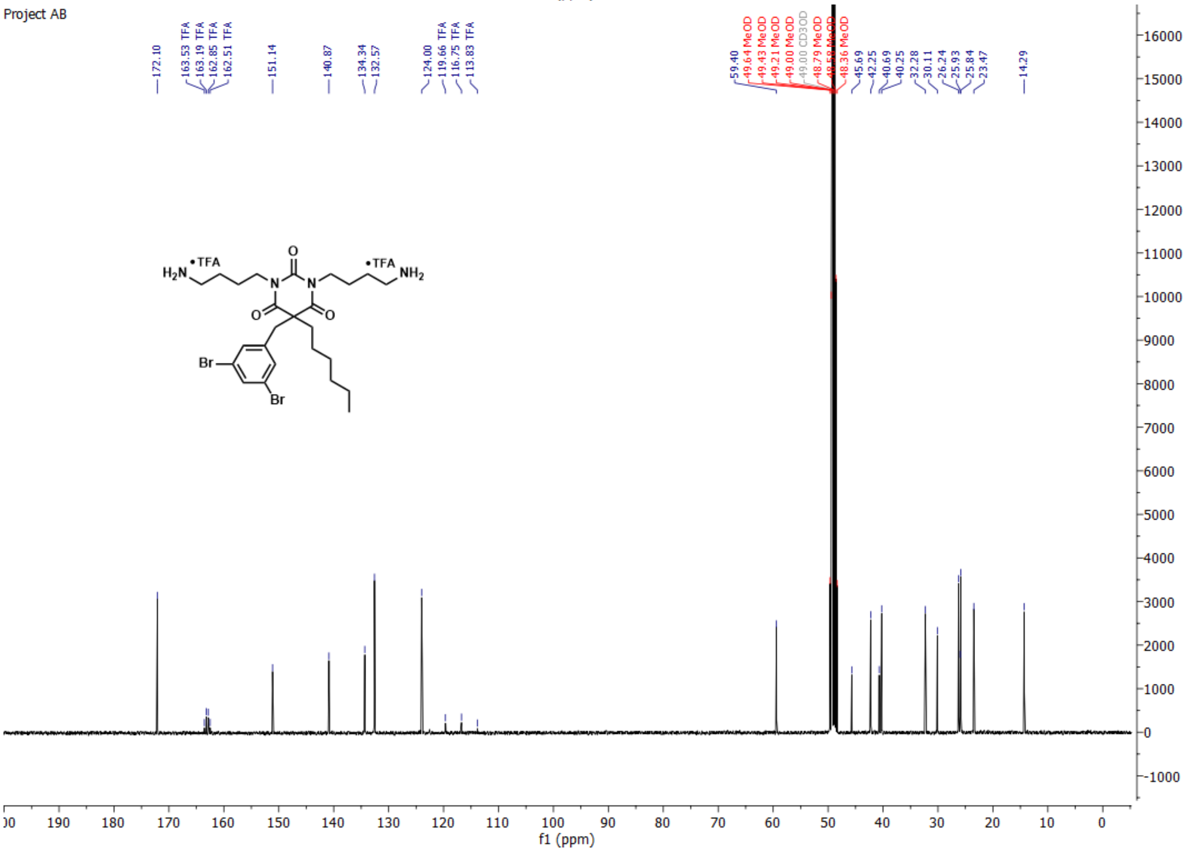

1,3-bis(4-aminobutyl)-5-(3,5-bis(trifluoromethyl)benzyl)-5-(3,5-dibromobenzyl)pyrimidine-2,4,6(1*H*,3*H*,5*H*)-trione di-TFA salt (**11oA**)

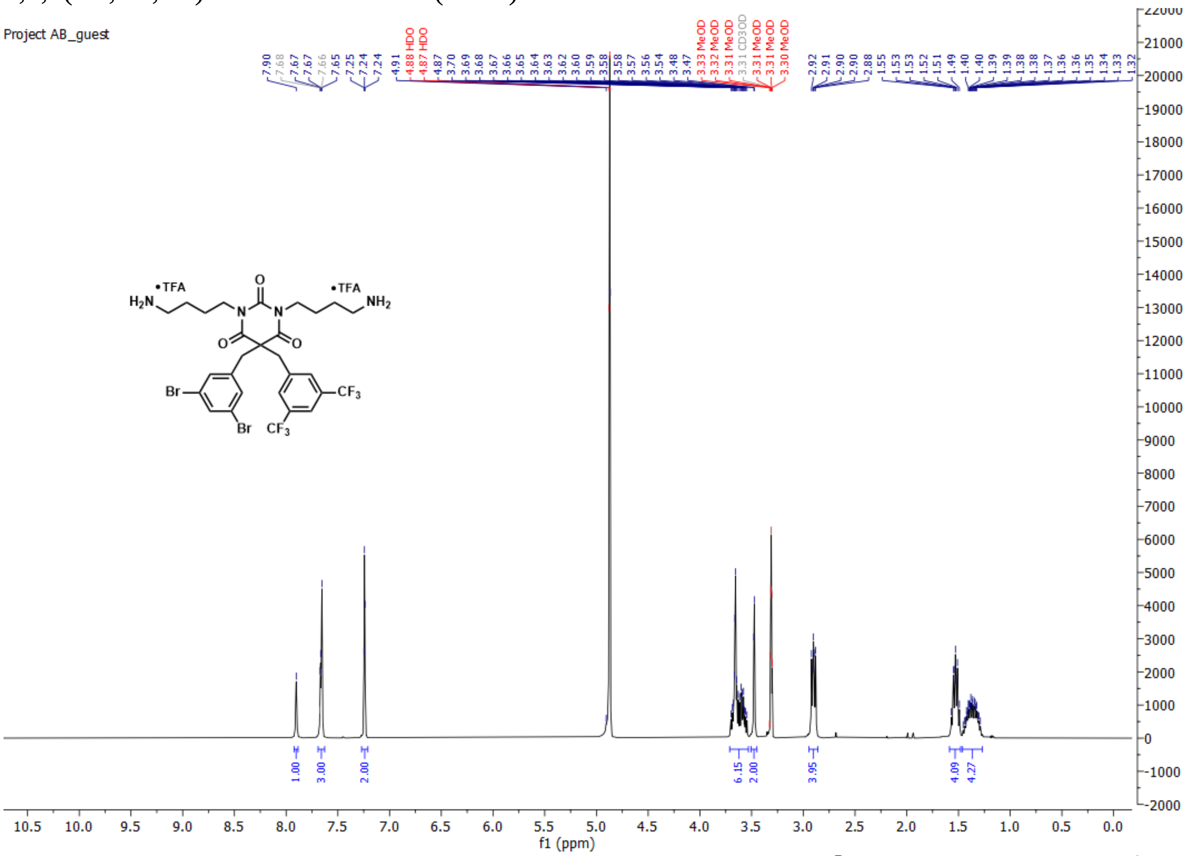

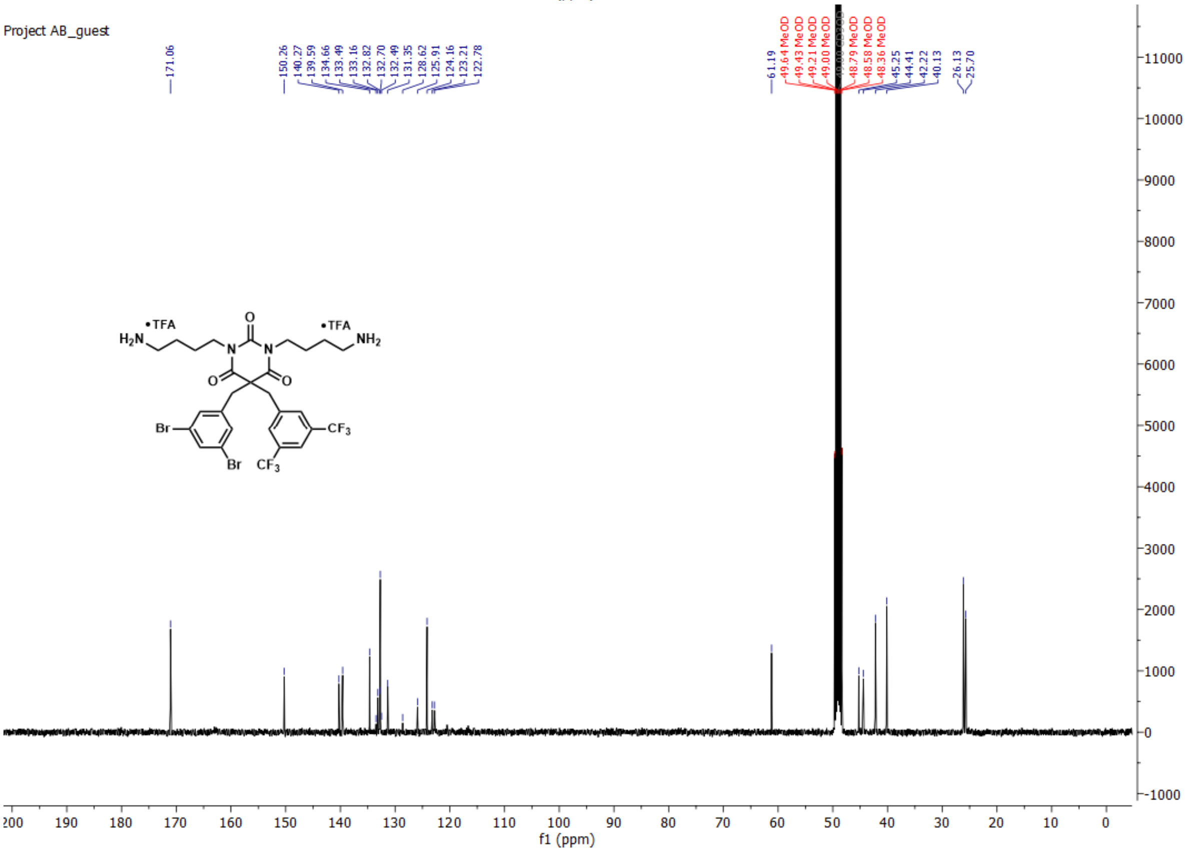

1,3-bis(4-aminobutyl)-5-(4-(*tert*-butyl)benzyl)-5-(3,5-dibromobenzyl)pyrimidine-2,4,6(1*H*,3*H*,5*H*)-trione di-TFA salt (**11pA**)

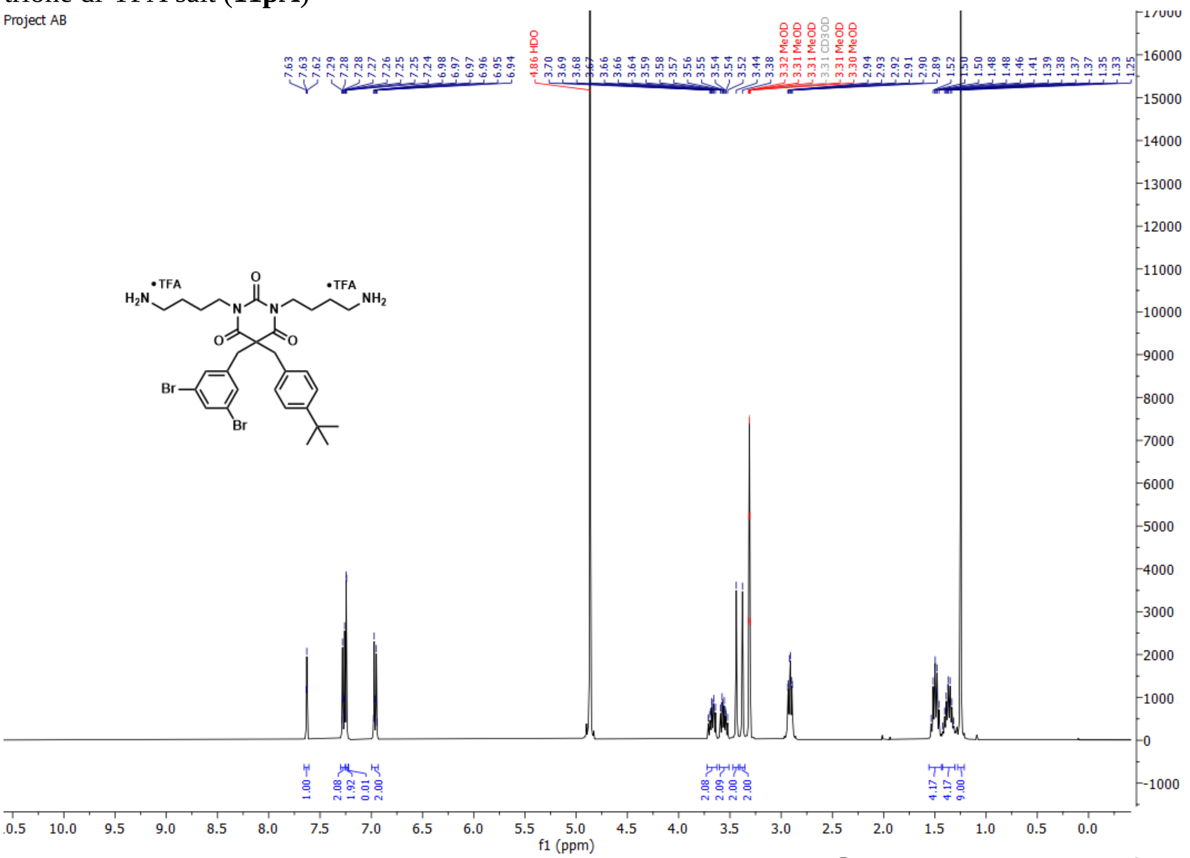

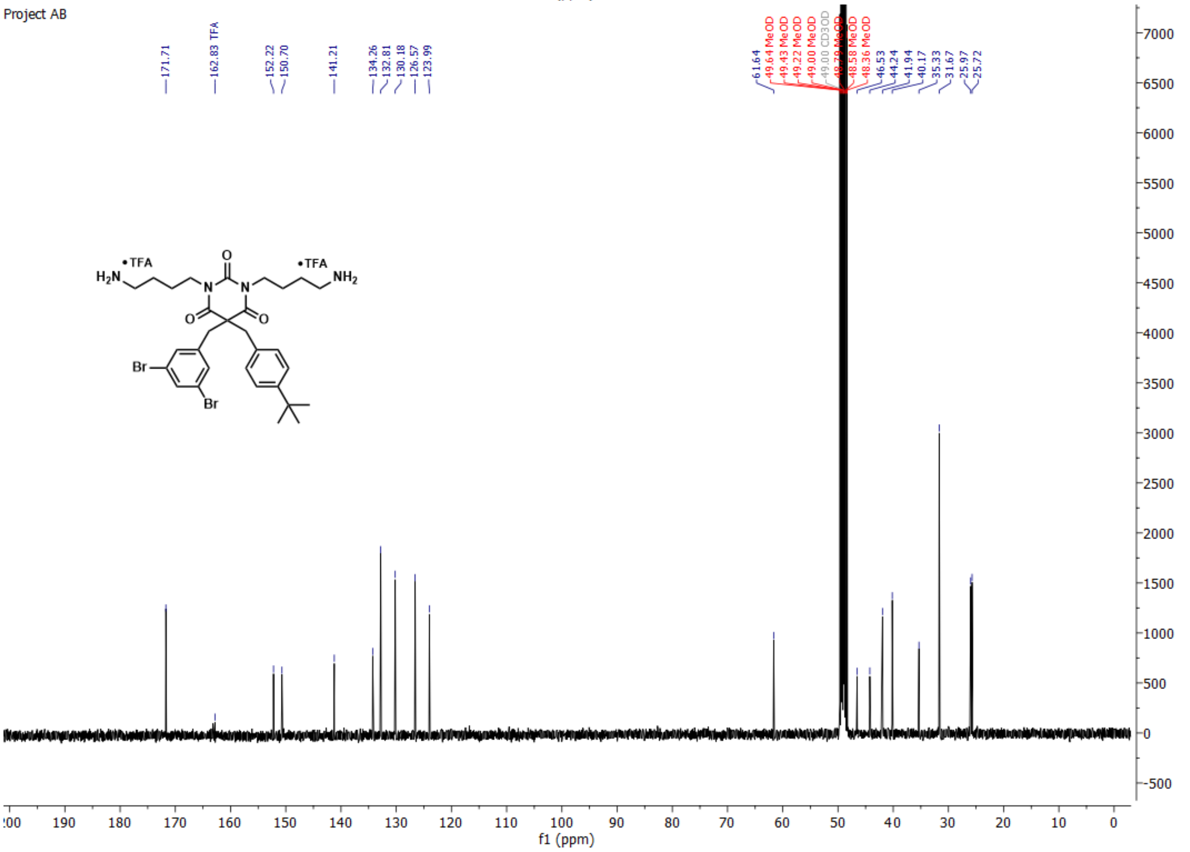

1,3-bis(4-aminobutyl)-5-((4-bromonaphthalen-1-yl)methyl)-5-(3,5-dibromobenzyl)pyrimidine-2,4,6(1*H*,3*H*,5*H*)-trione di-TFA salt (**11qA**)

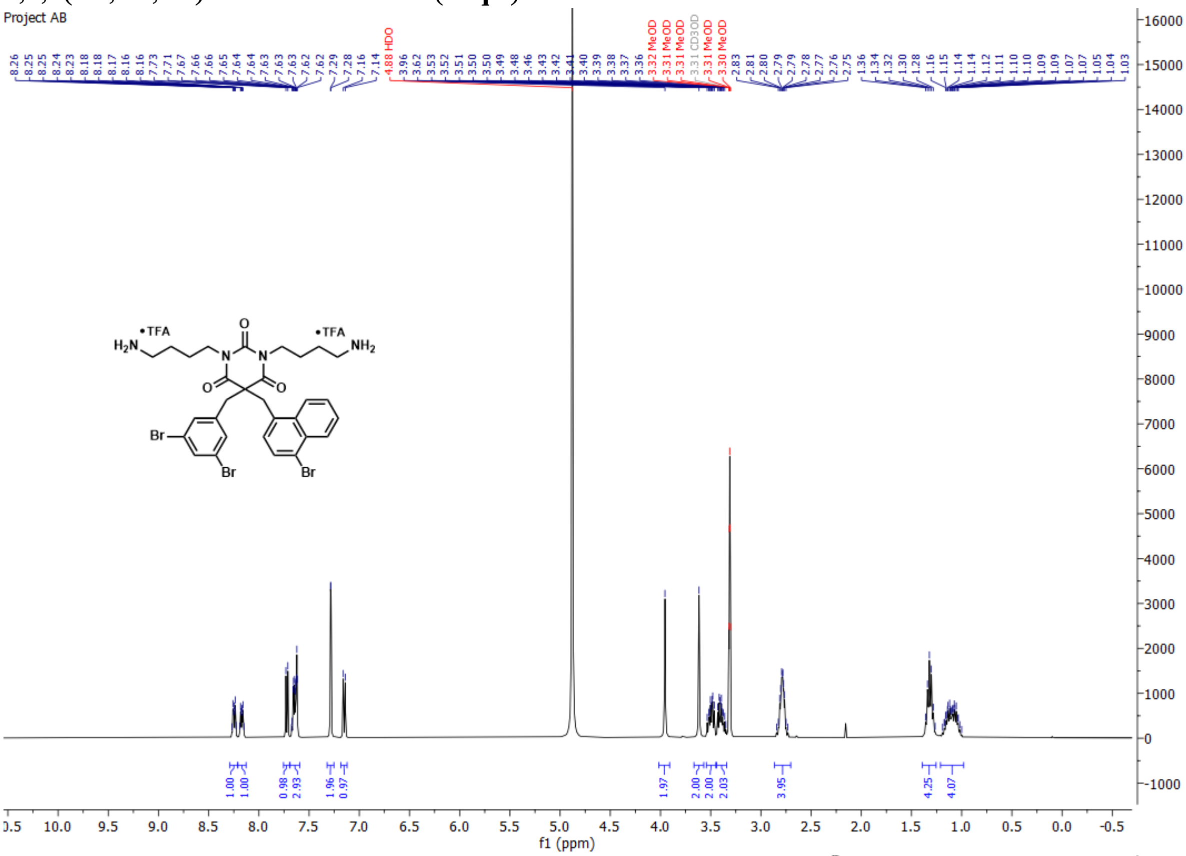

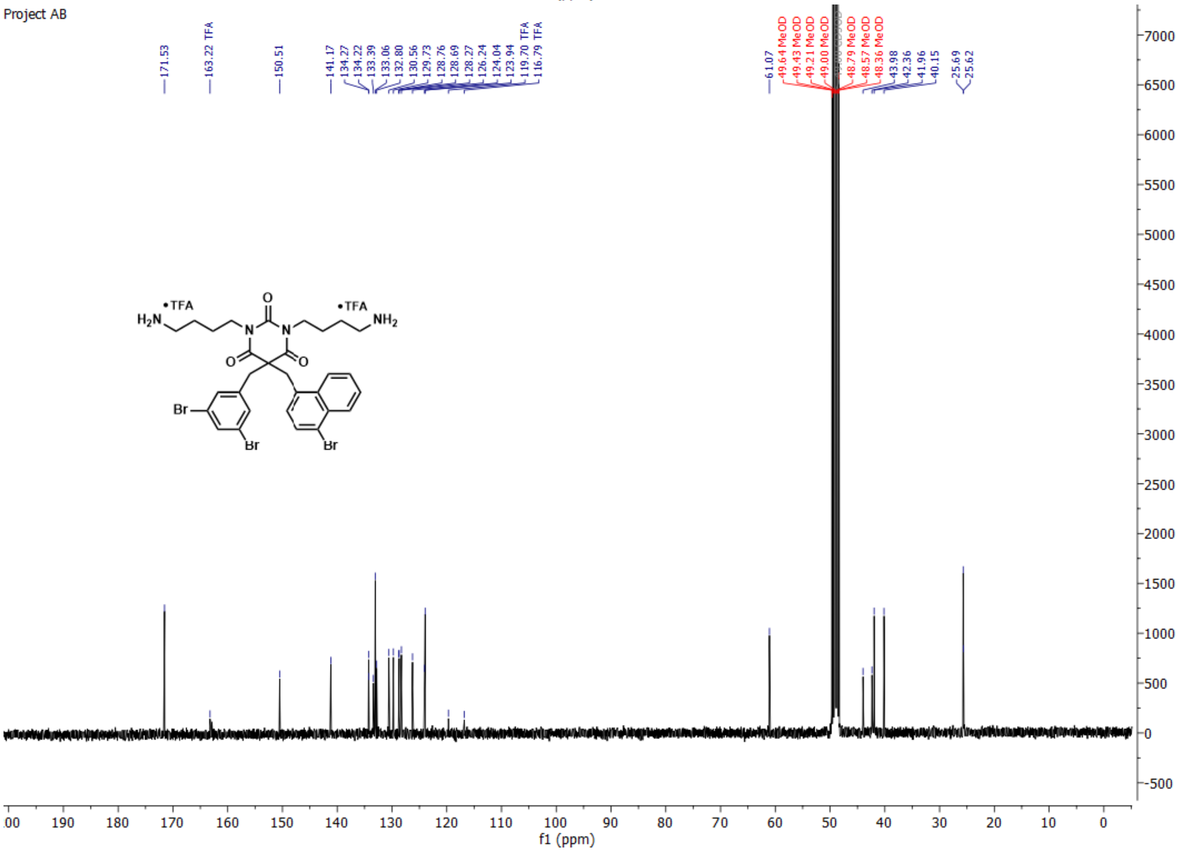

1,1'-((5-(3,5-dibromobenzyl)-2,4,6-trioxo-5-(quinolin-2-ylmethyl)dihydropyrimidine-1,3(2*H*,4*H*)-diyl)bis(butane-4,1-diyl))diguanidine di-TFA salt (**11kG**)

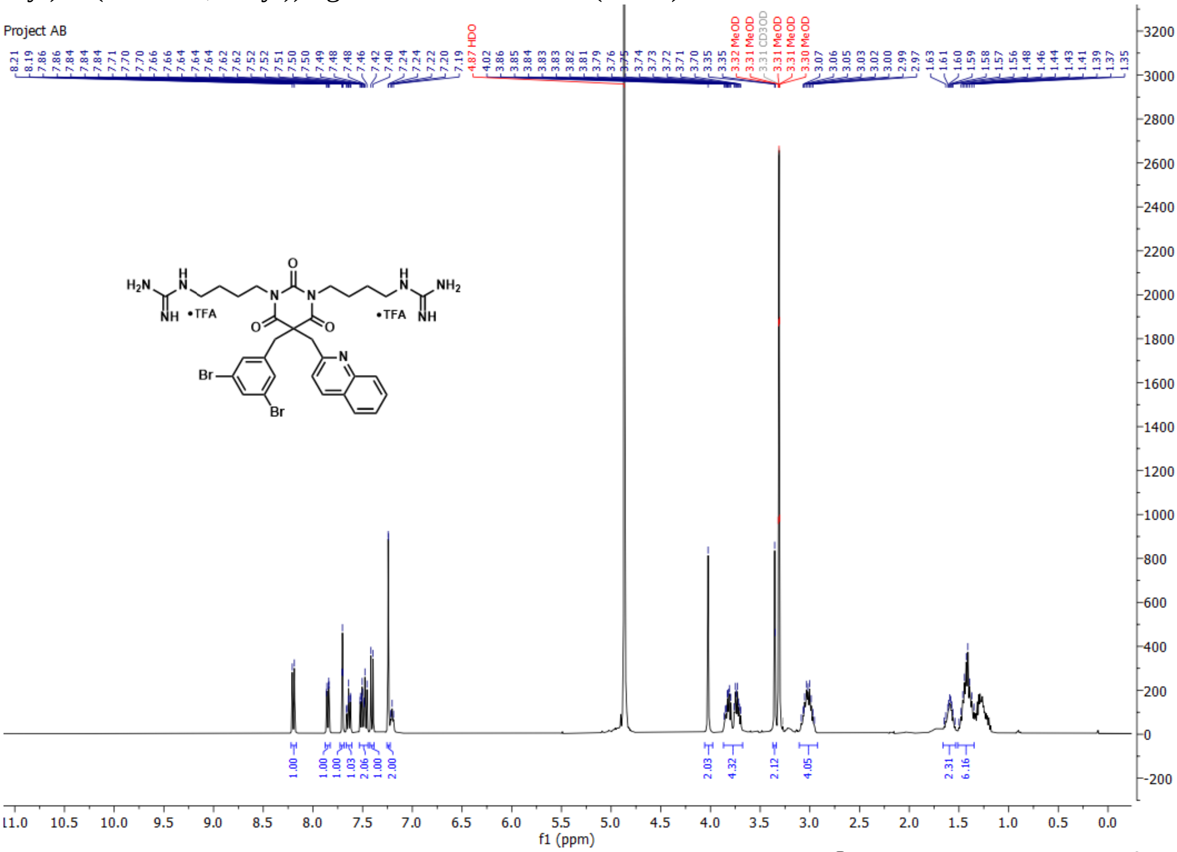

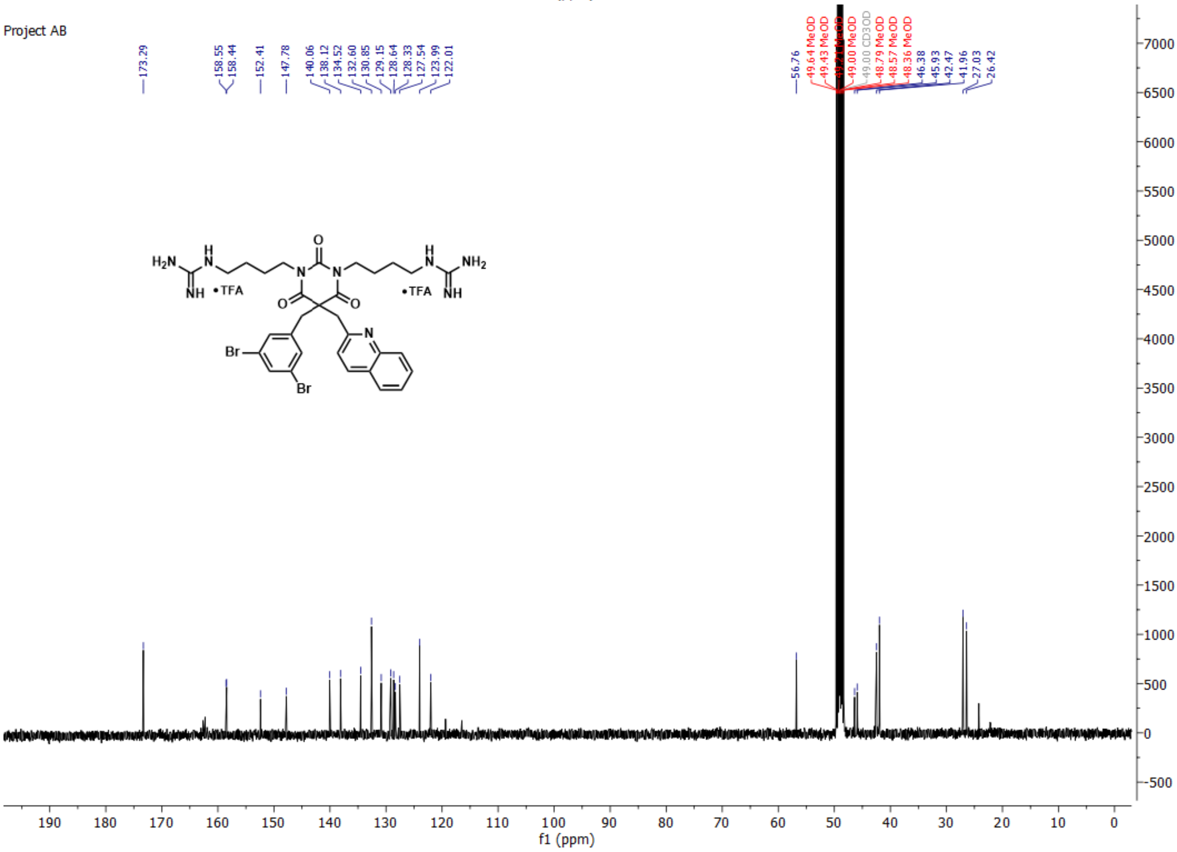

(4-(5-(3,5-dibromobenzyl)-3-(4-guanidinobutyl)-2,4,6-trioxo-5-(4-(trifluoromethyl)benzyl)tetrahydro-pyrimidin-1(2*H*)-yl)butyl)-l2-azanecarboximidamide di-TFA salt (**11lG**)

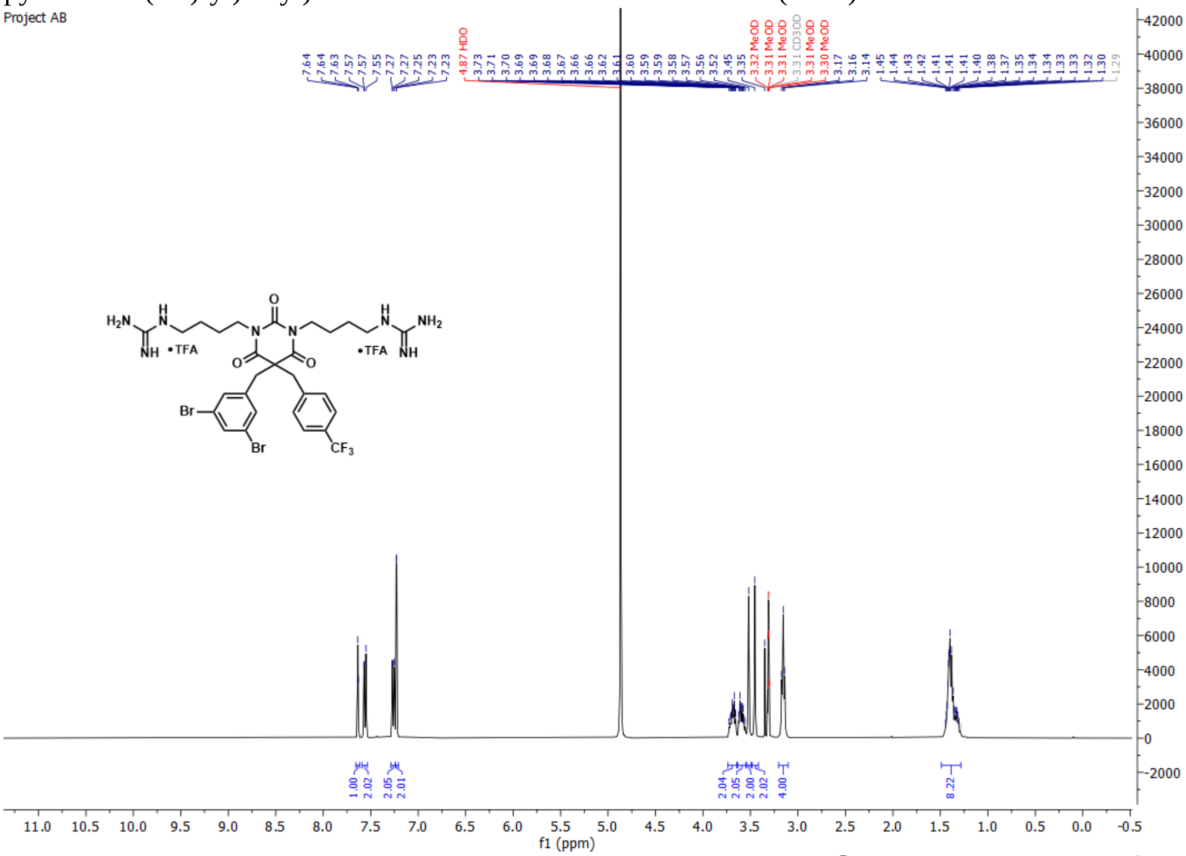

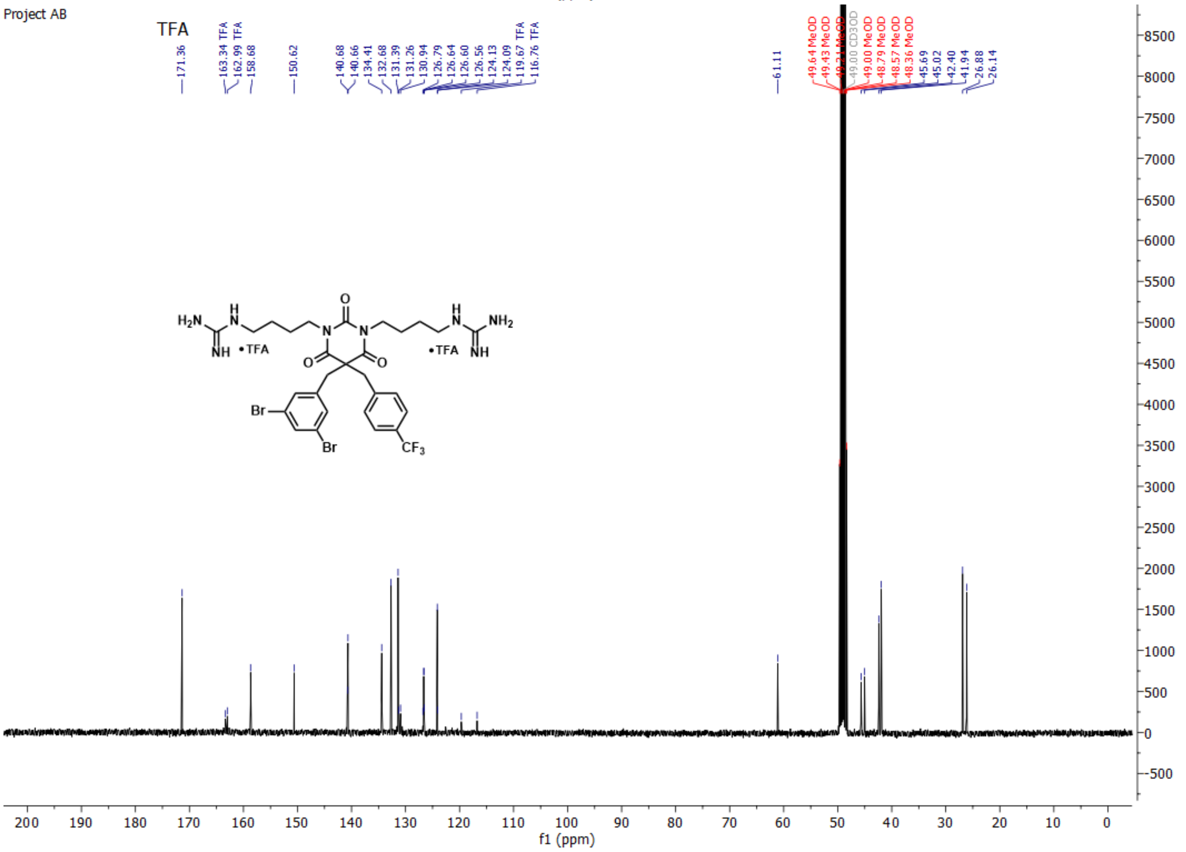

1,1'-((5-(3,5-dibromobenzyl)-5-hexyl-2,4,6-trioxodihydropyrimidine-1,3(2*H*,4*H*)-diyl)bis(butane-4,1-diyl))diguanidine di-TFA salt (**11nG)**

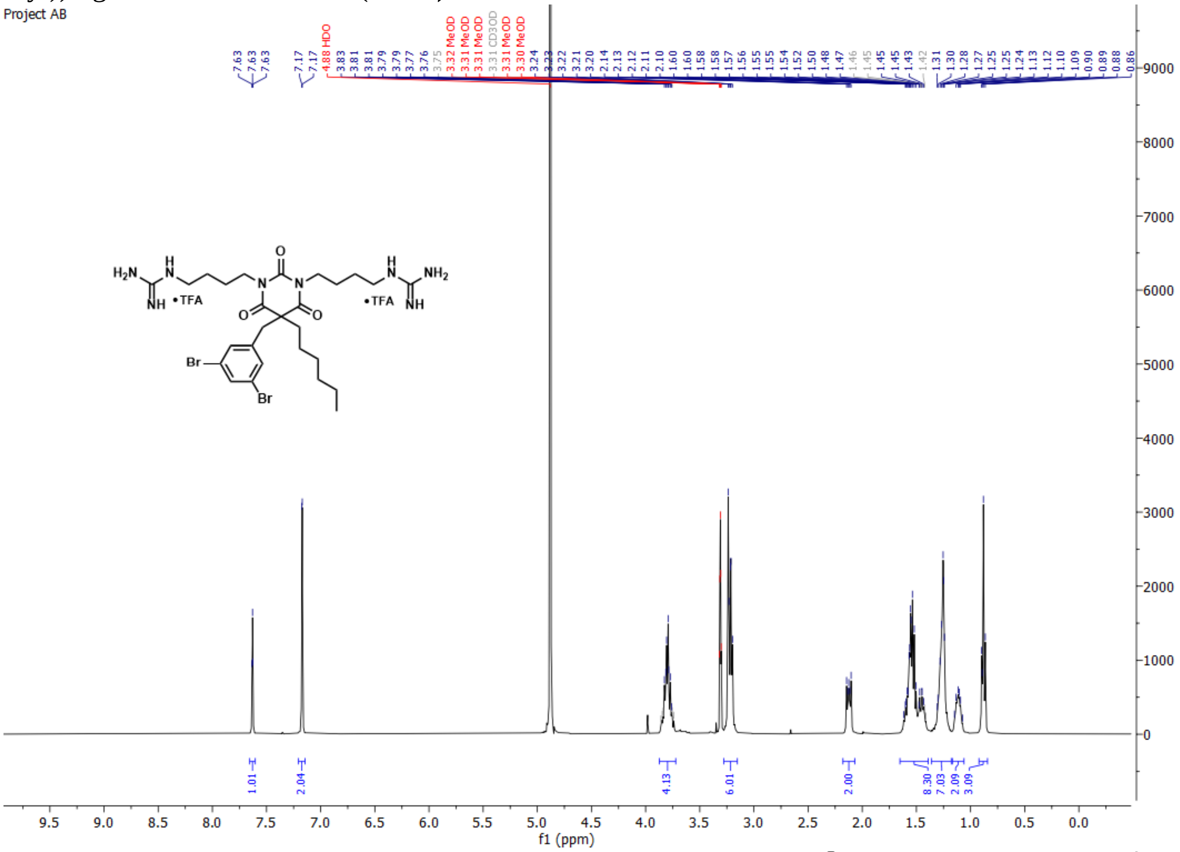

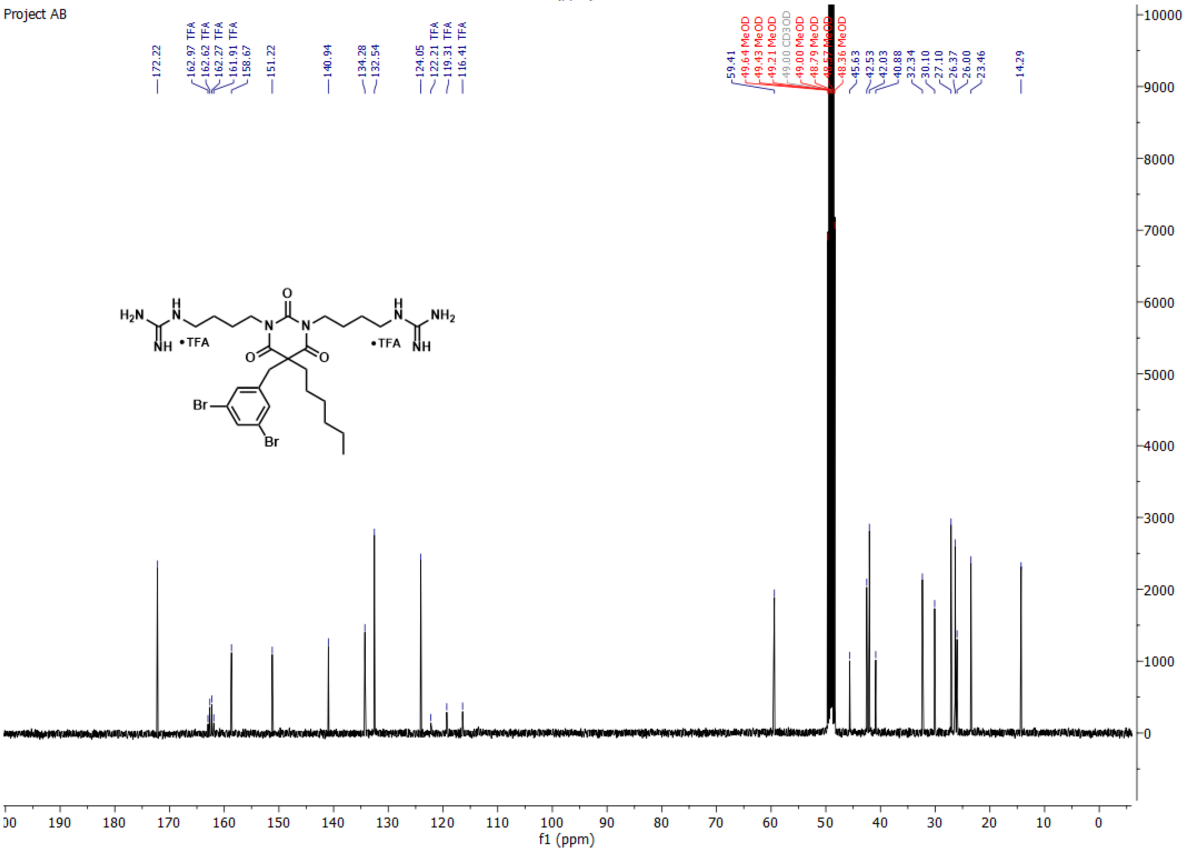

1,1'-((5-(3,5-bis(trifluoromethyl)benzyl)-5-(3,5-dibromobenzyl)-2,4,6-trioxodihydropyrimidine-1,3(2*H*,4*H*)-diyl)bis(butane-4,1-diyl))diguanidine di-TFA salt (**11oG**)

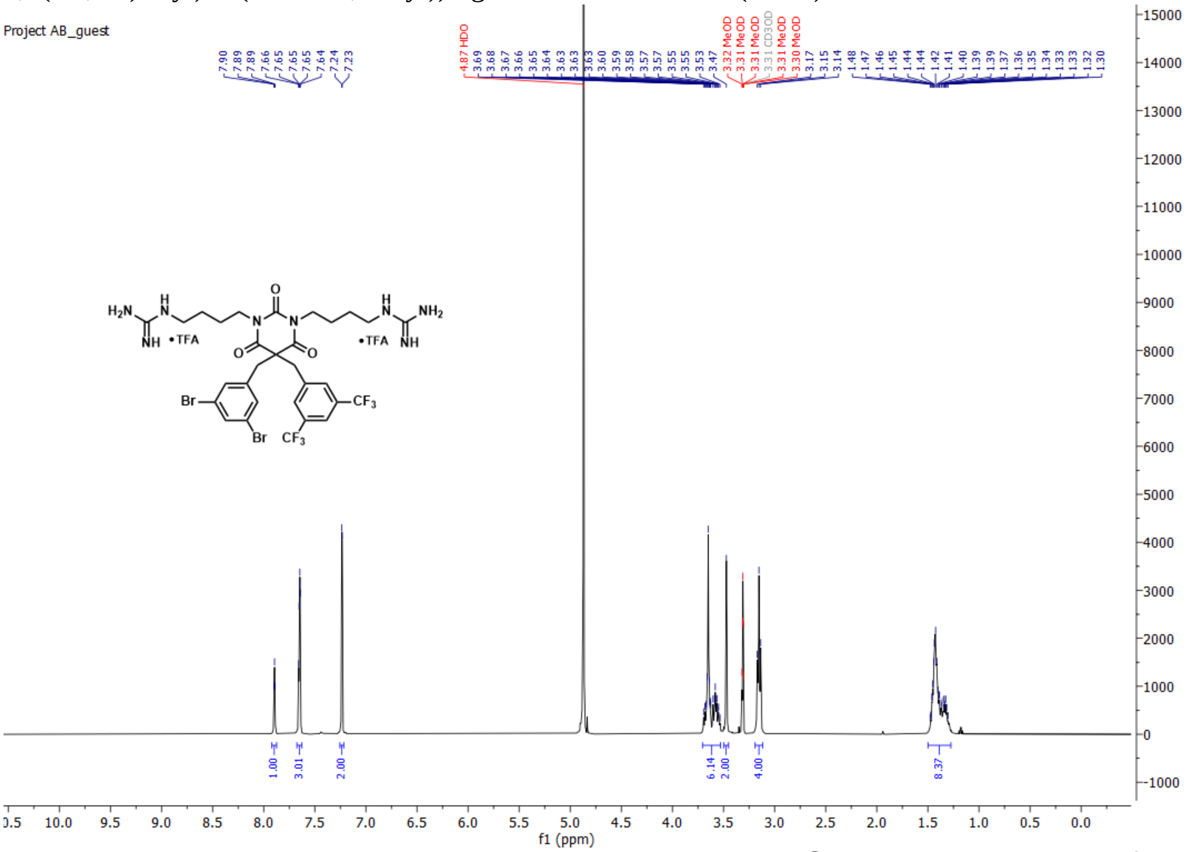

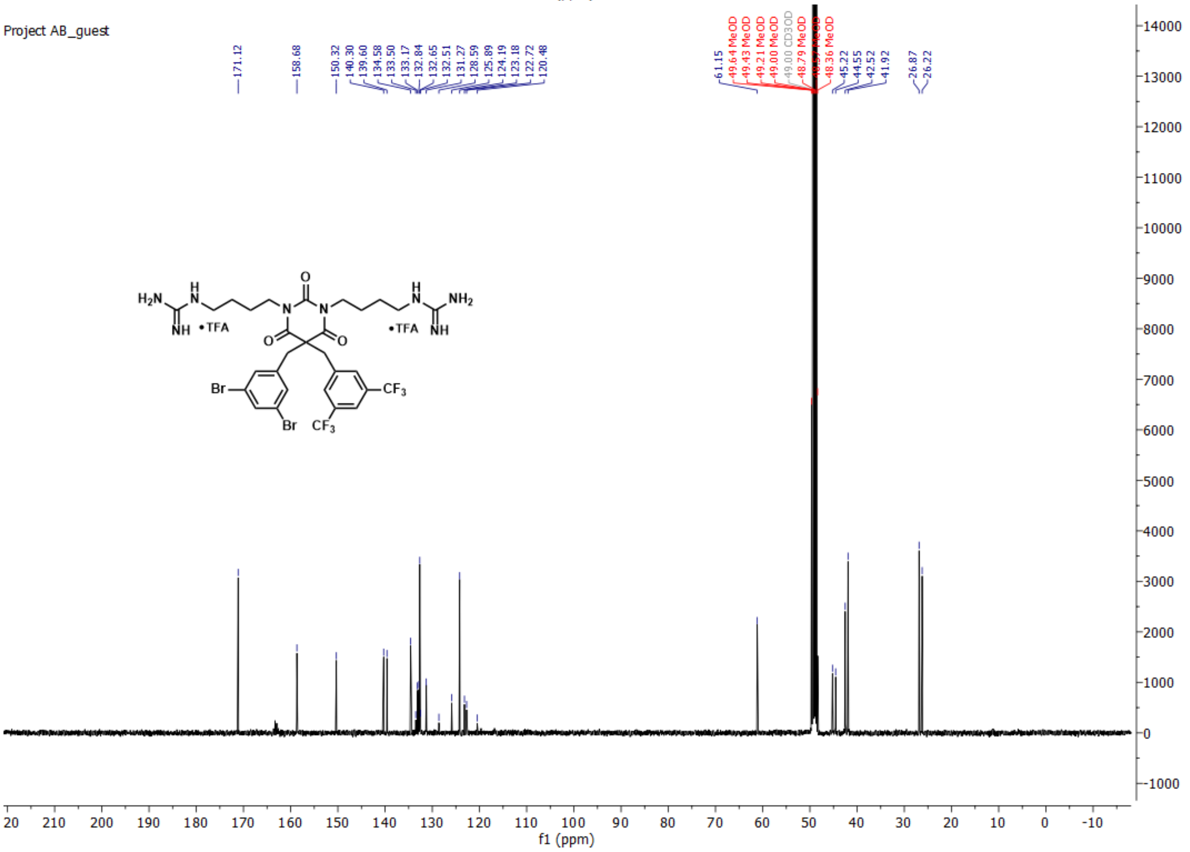

1,1'-((5-(4-(*tert*-butyl)benzyl)-5-(3,5-dibromobenzyl)-2,4,6-trioxodihydropyrimidine-1,3(2*H*,4*H*)-diyl)bis(butane-4,1-diyl))diguanidine di-TFA salt (**11pG**)

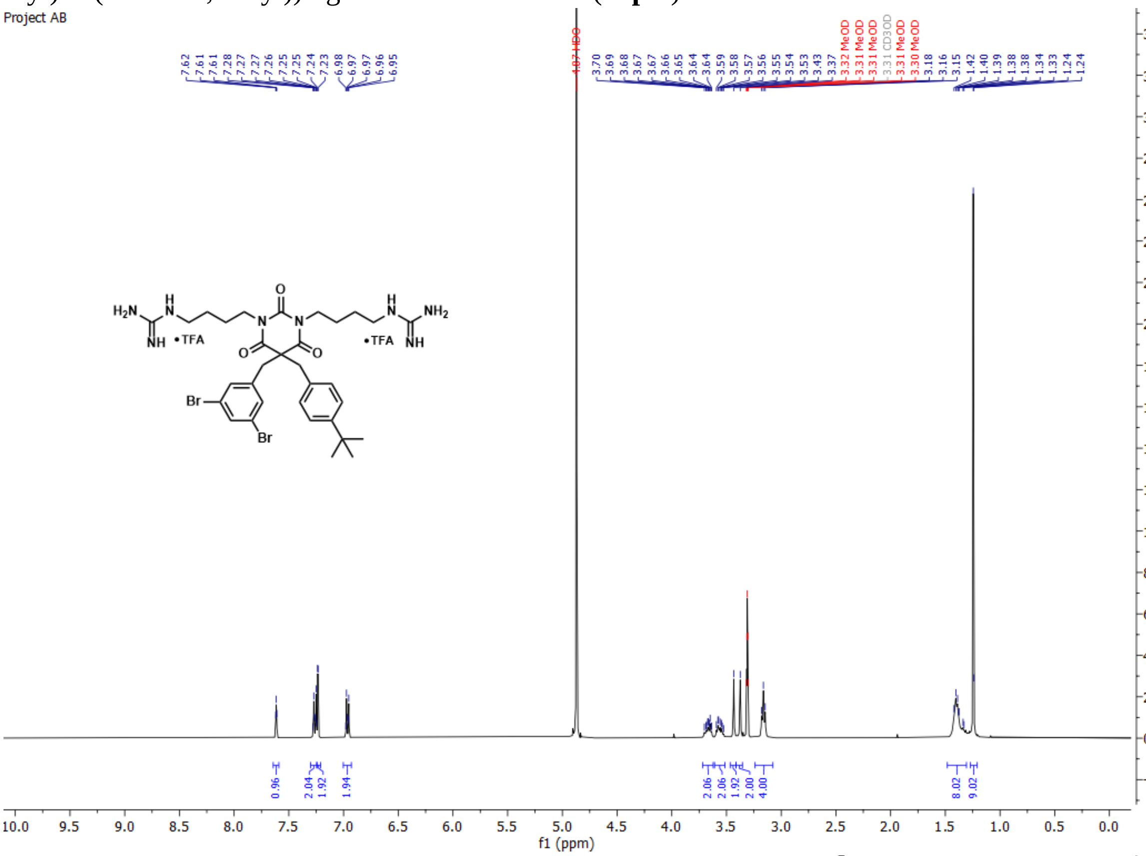

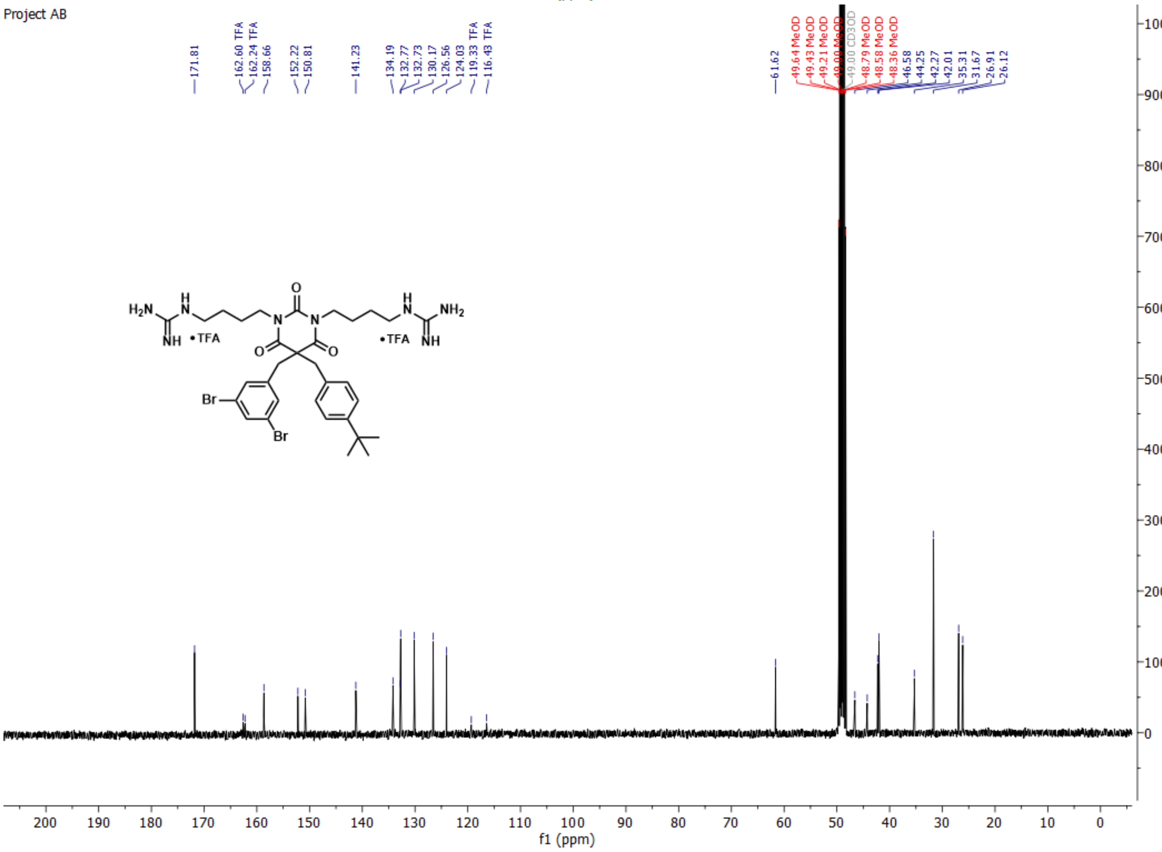

1,1'-((5-((4-bromonaphthalen-1-yl)methyl)-5-(3,5-dibromobenzyl)-2,4,6-trioxodihydropyrimidine-1,3(2*H*,4*H*)-diyl)bis(butane-4,1-diyl))diguanidine di-TFA salt (**11qG**)

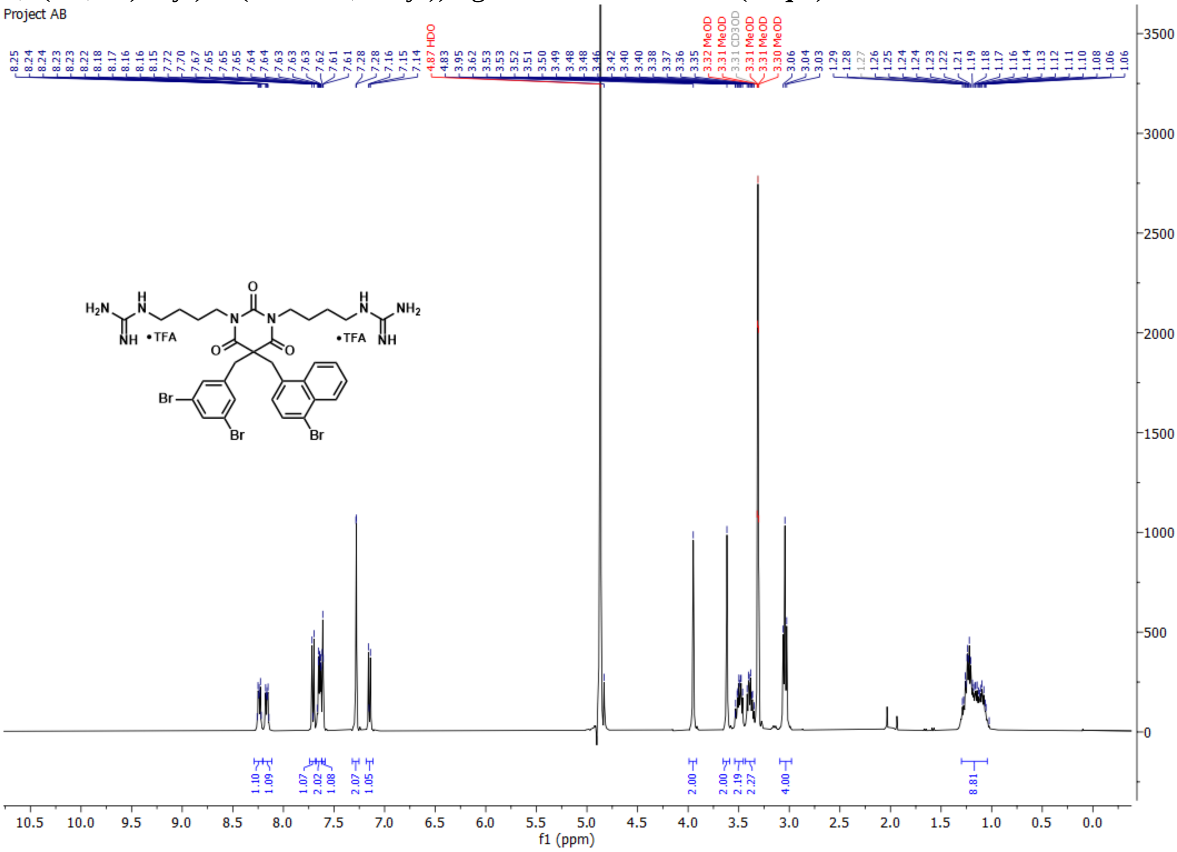

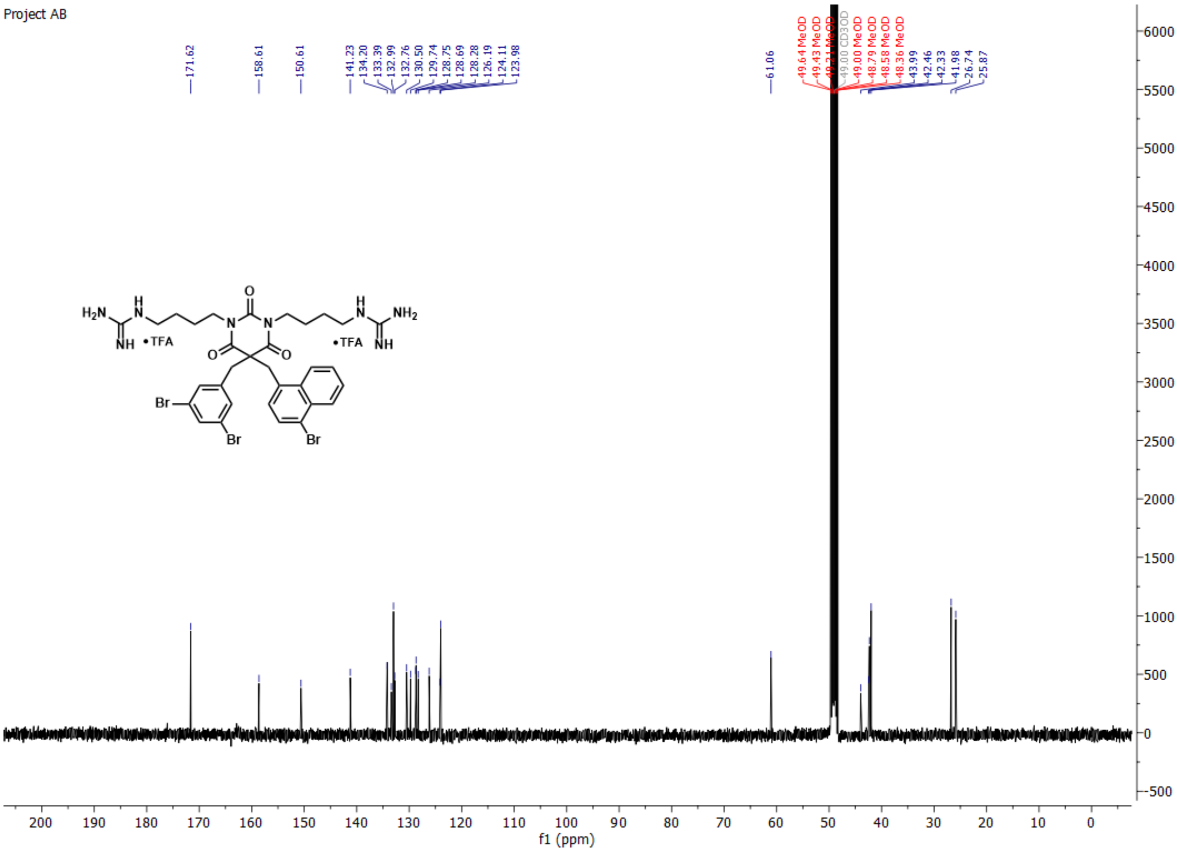

3.4 ^{1}H and ^{13}C NMR spectra of compounds in *series 4*

1,3-bis(2-aminoethyl)-5,5-bis(3,5-dibromobenzyl)pyrimidine-2,4,6(1*H*,3*H*,5*H*)-trione di-TFA salt (**12aA**)

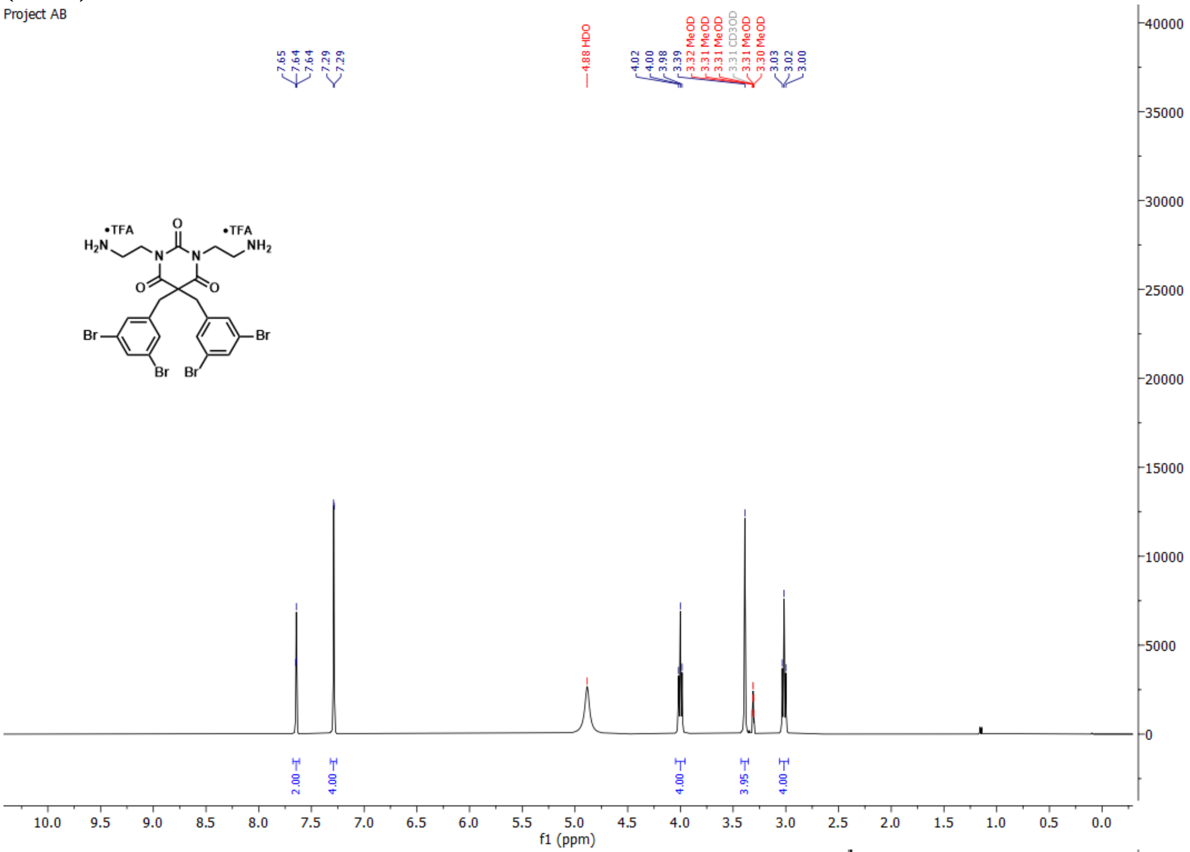

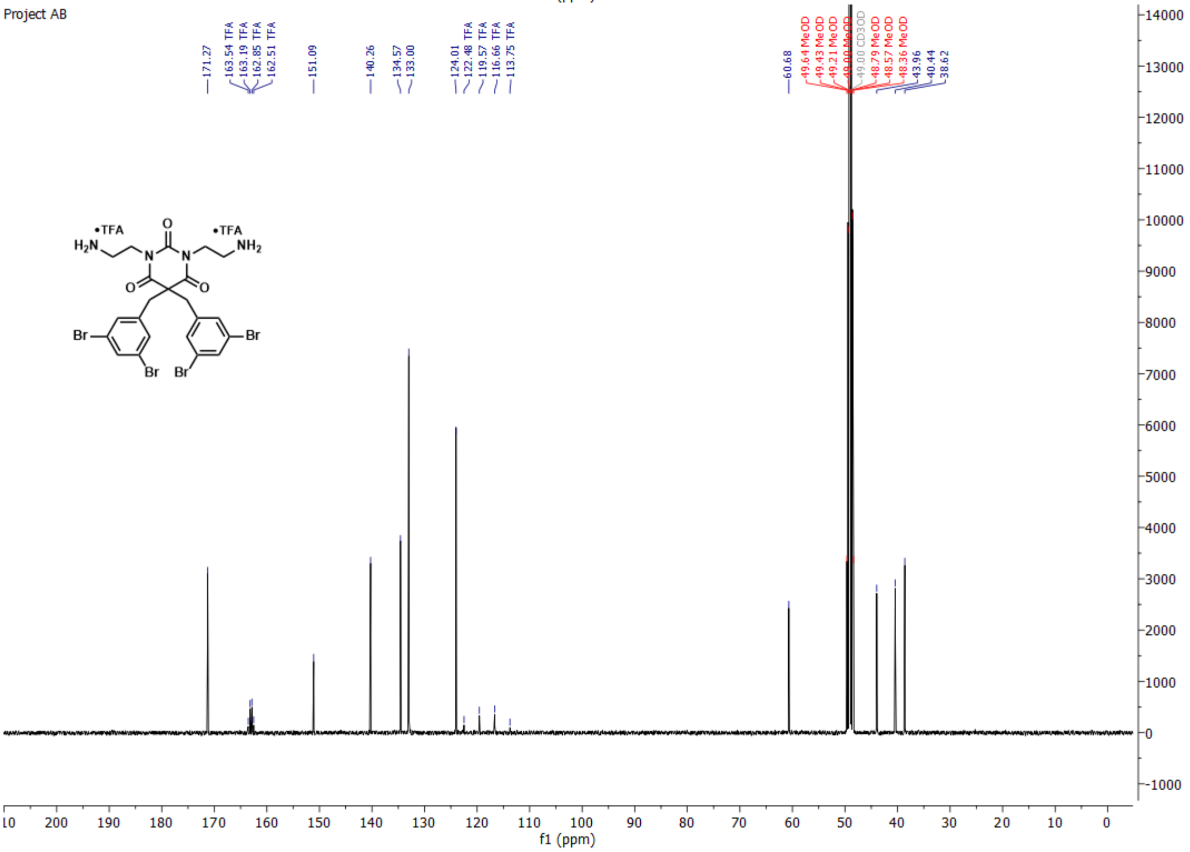

1,3-bis(3-aminopropyl)-5,5-bis(3,5-dibromobenzyl)pyrimidine-2,4,6(1*H*,3*H*,5*H*)-trione di-TFA salt (**13aA**)

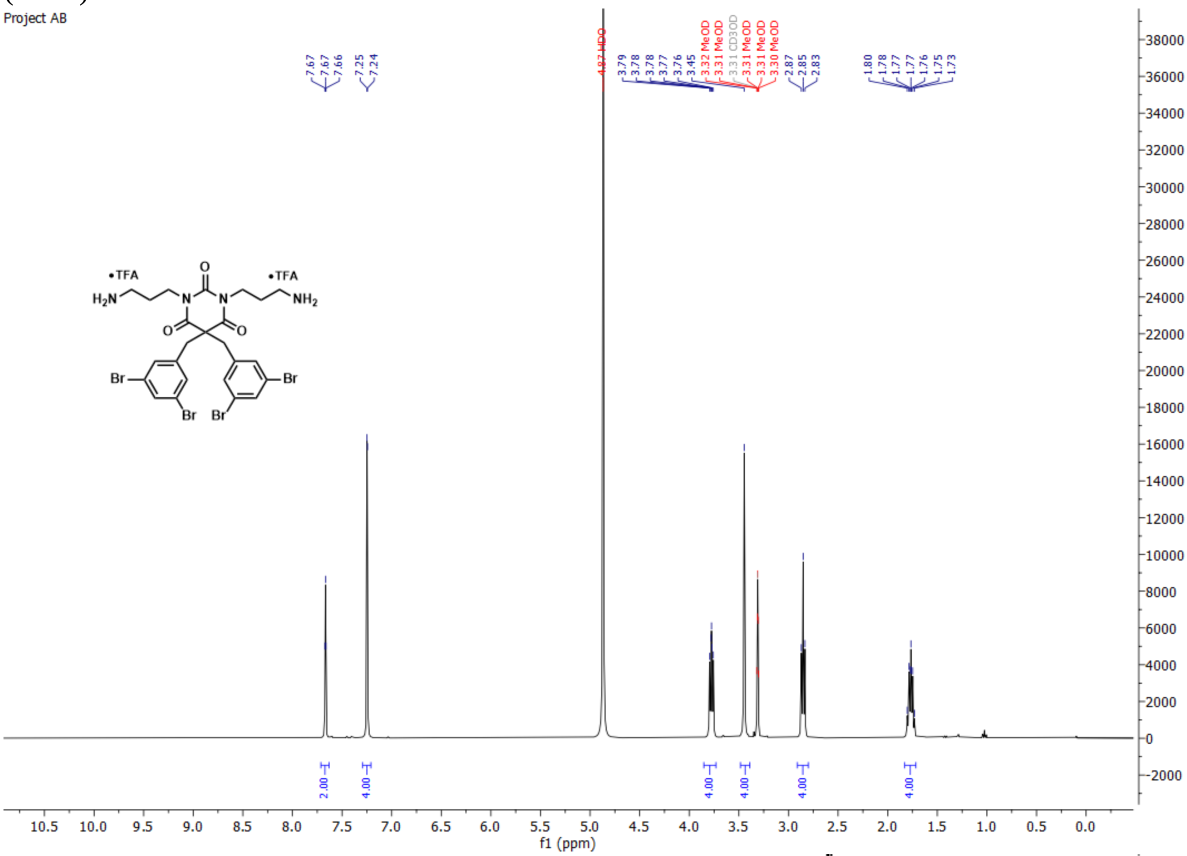

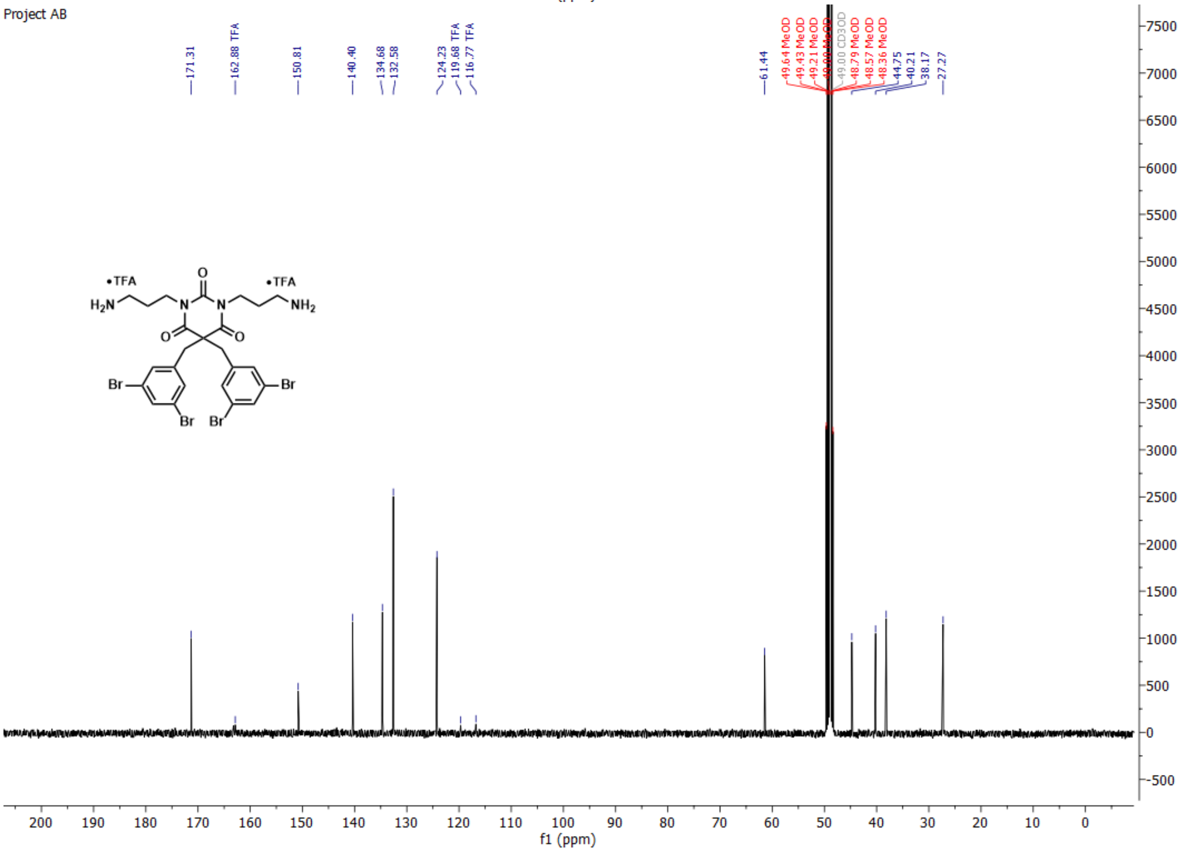

1,3-bis(5-aminopentyl)-5,5-bis(3,5-dibromobenzyl)pyrimidine-2,4,6(1*H*,3*H*,5*H*)-trione di-TFA salt (**14aA**)

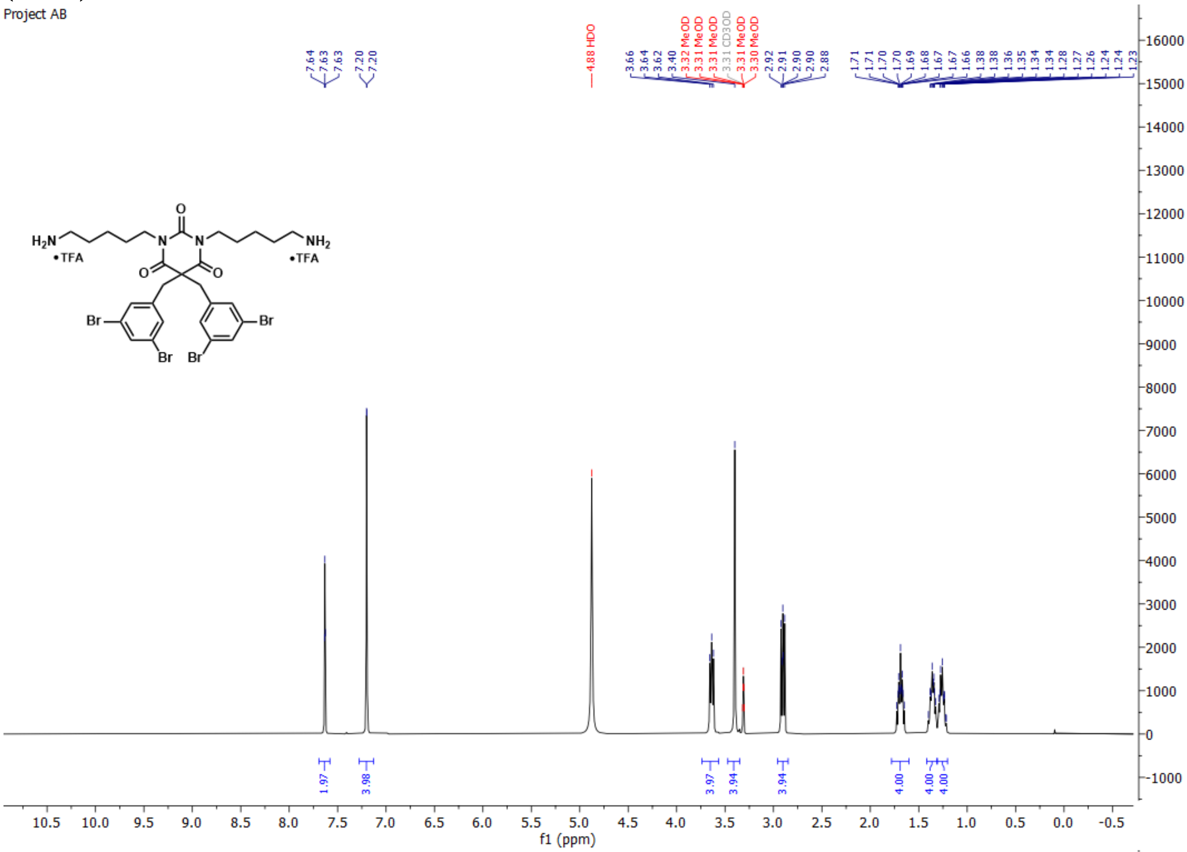

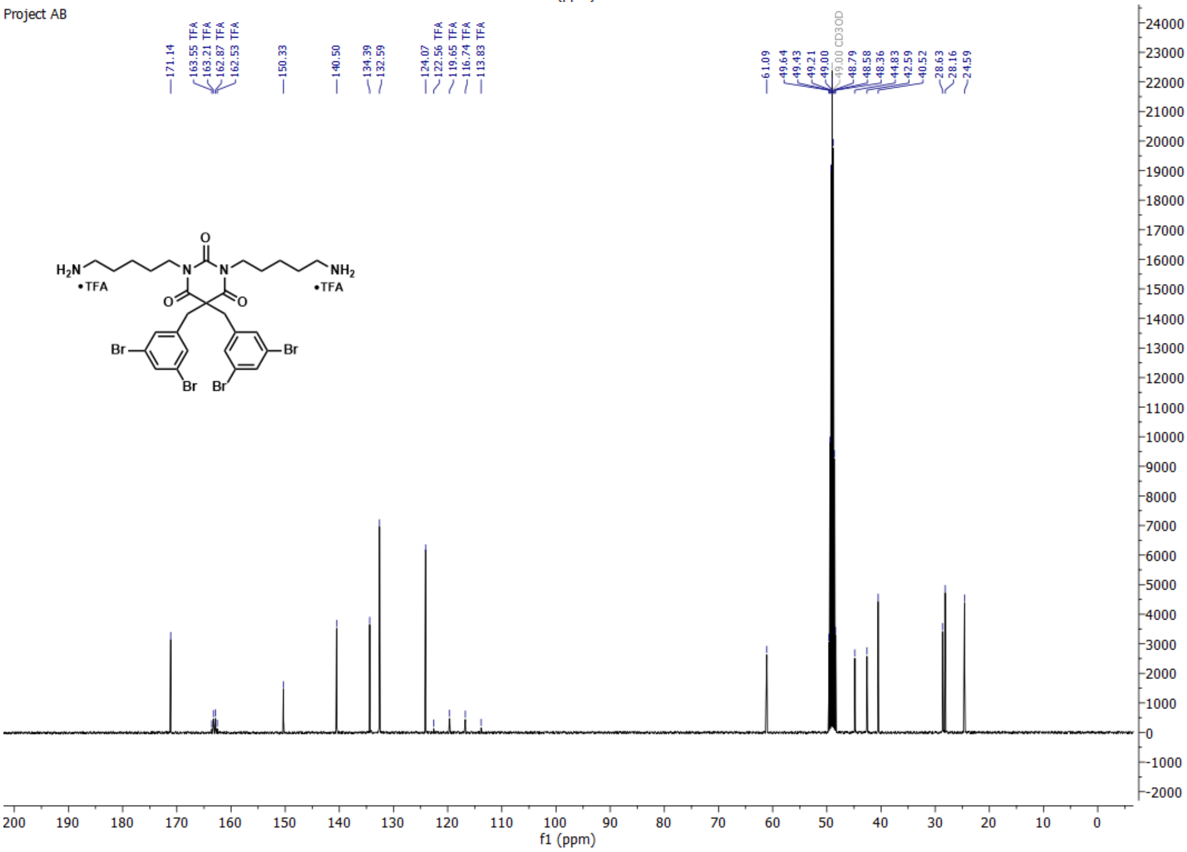

1,3-bis(6-aminohexyl)-5,5-bis(3,5-dibromobenzyl)pyrimidine-2,4,6(1*H*,3*H*,5*H*)-trione di-TFA salt (**15aA**)

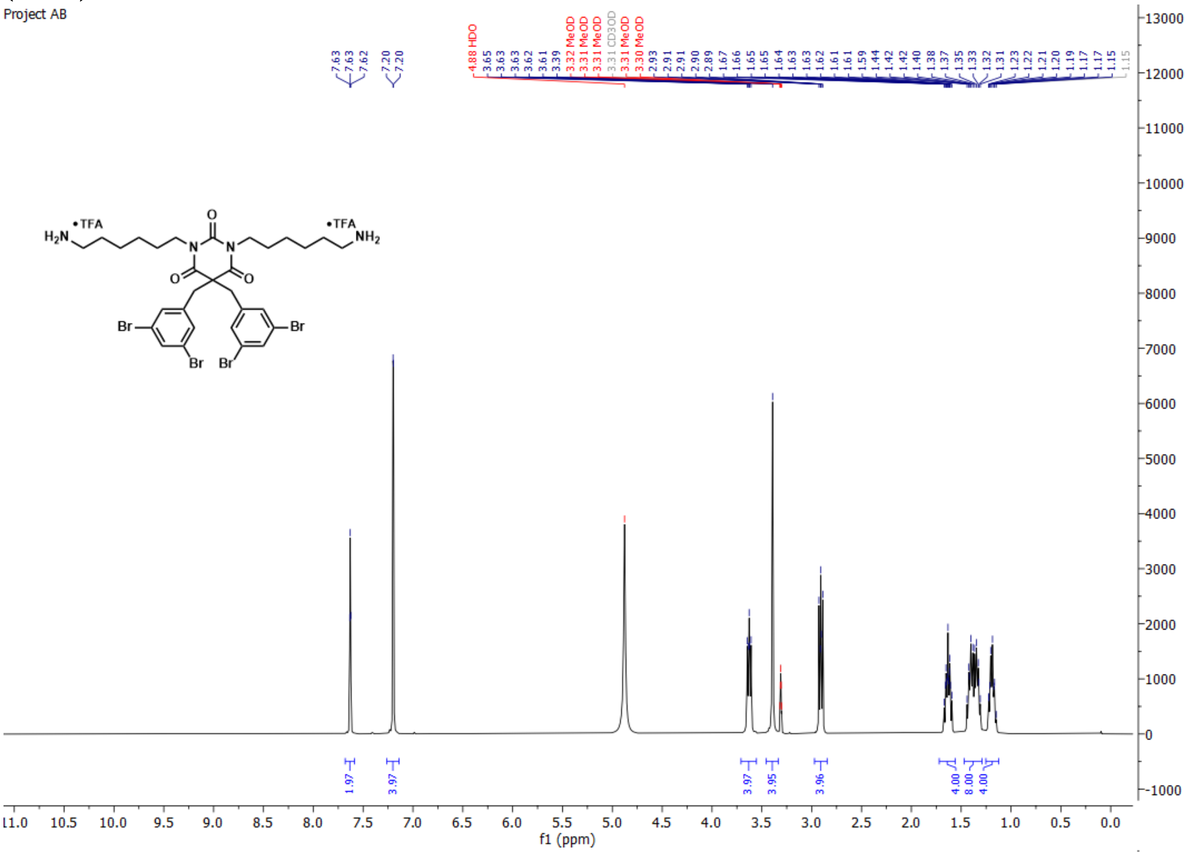

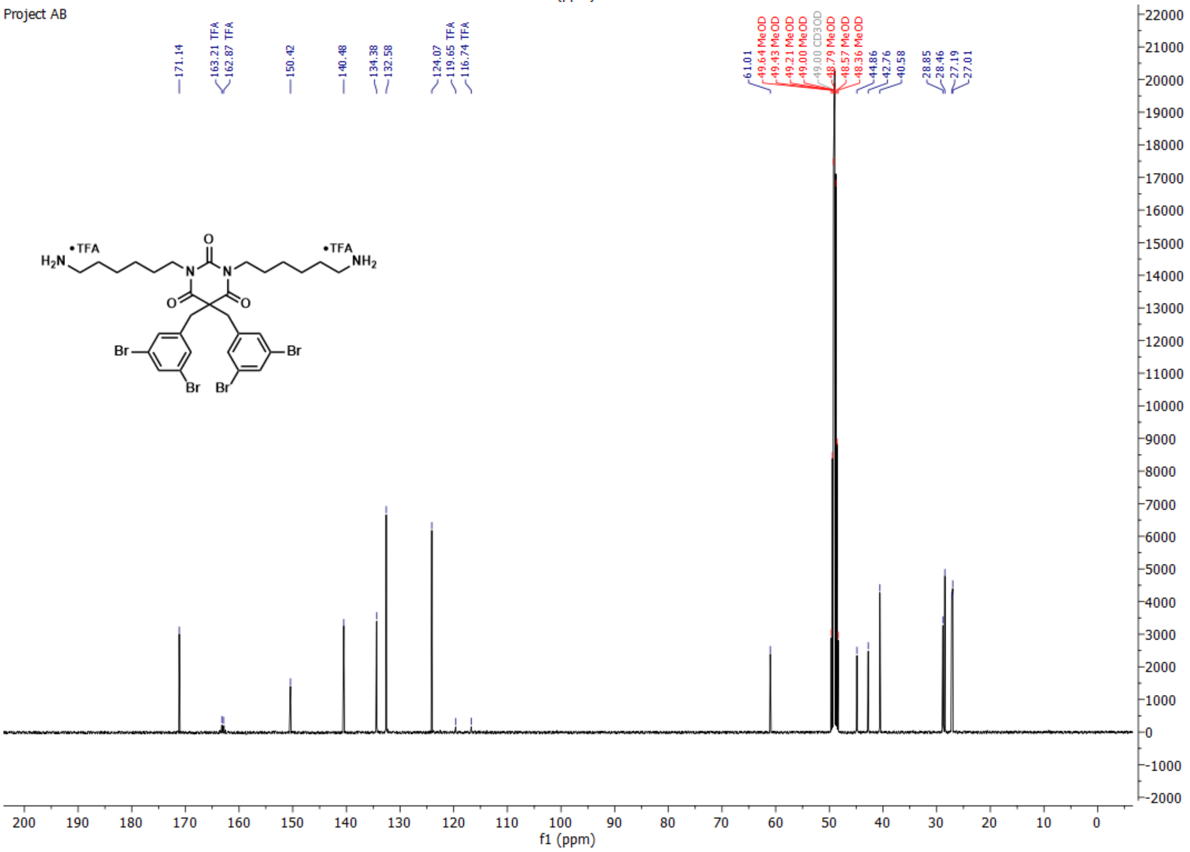

1,3-bis((1*s*,3*S*)-3-aminocyclobutyl)-5,5-bis(3,5-dibromobenzyl)pyrimidine-2,4,6(1*H*,3*H*,5*H*)-trione di-TFA salt (**16aA**)

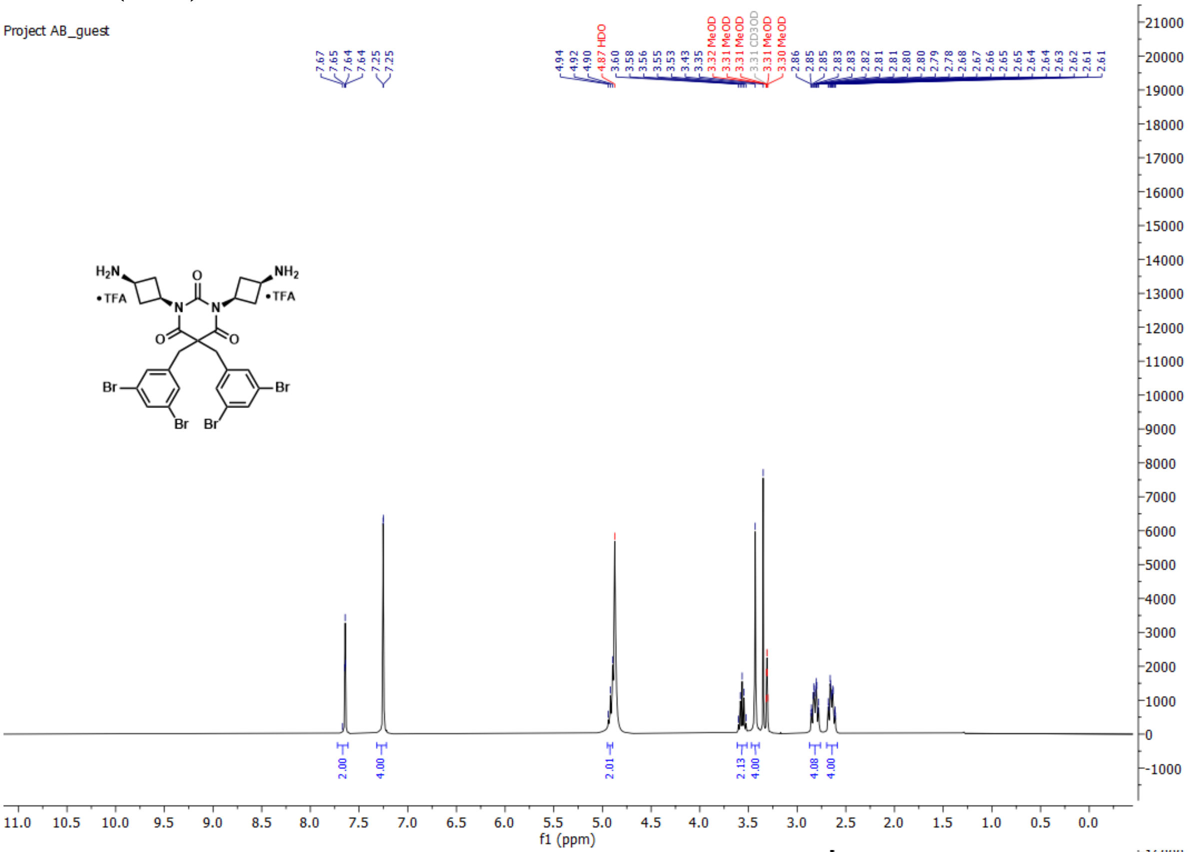

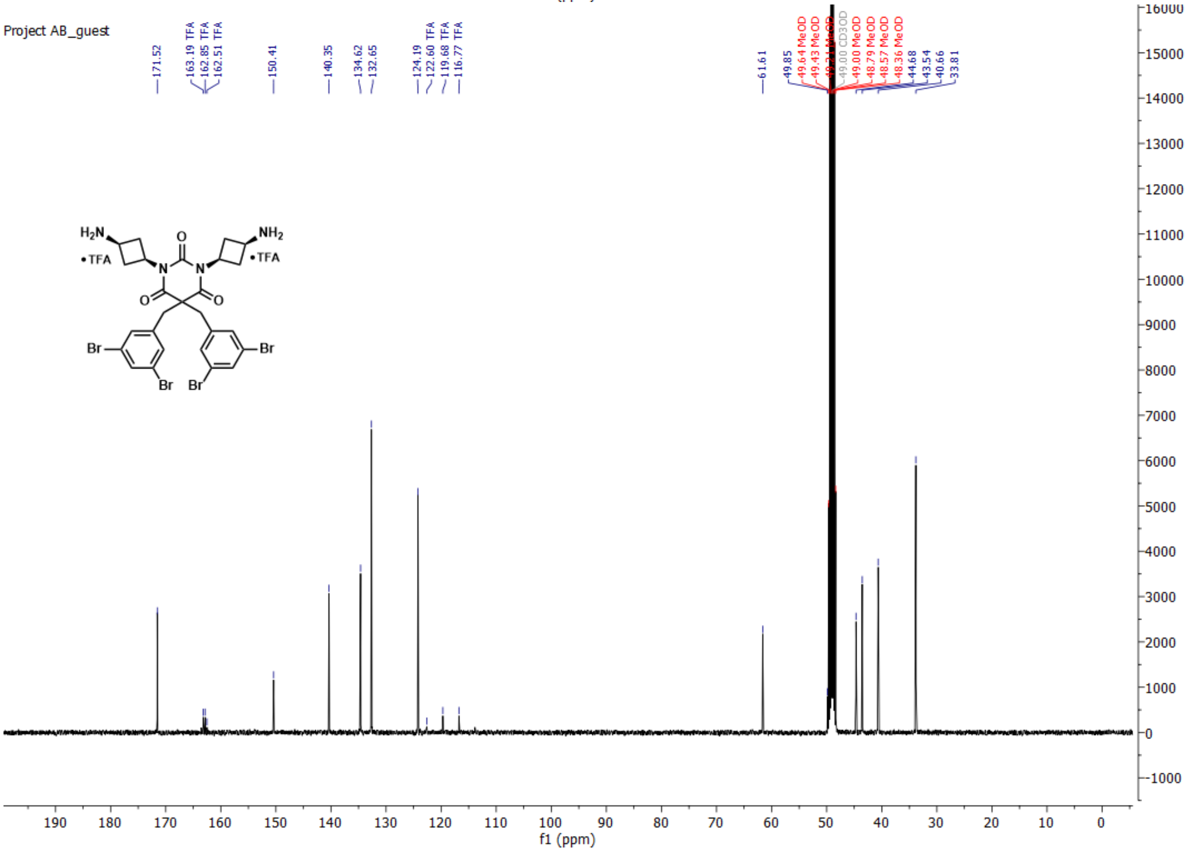

1,3-bis((1*r*,3*R*)-3-aminocyclobutyl)-5,5-bis(3,5-dibromobenzyl)pyrimidine-2,4,6(1*H*,3*H*,5*H*)-trione di-TFA salt (**17aA**)

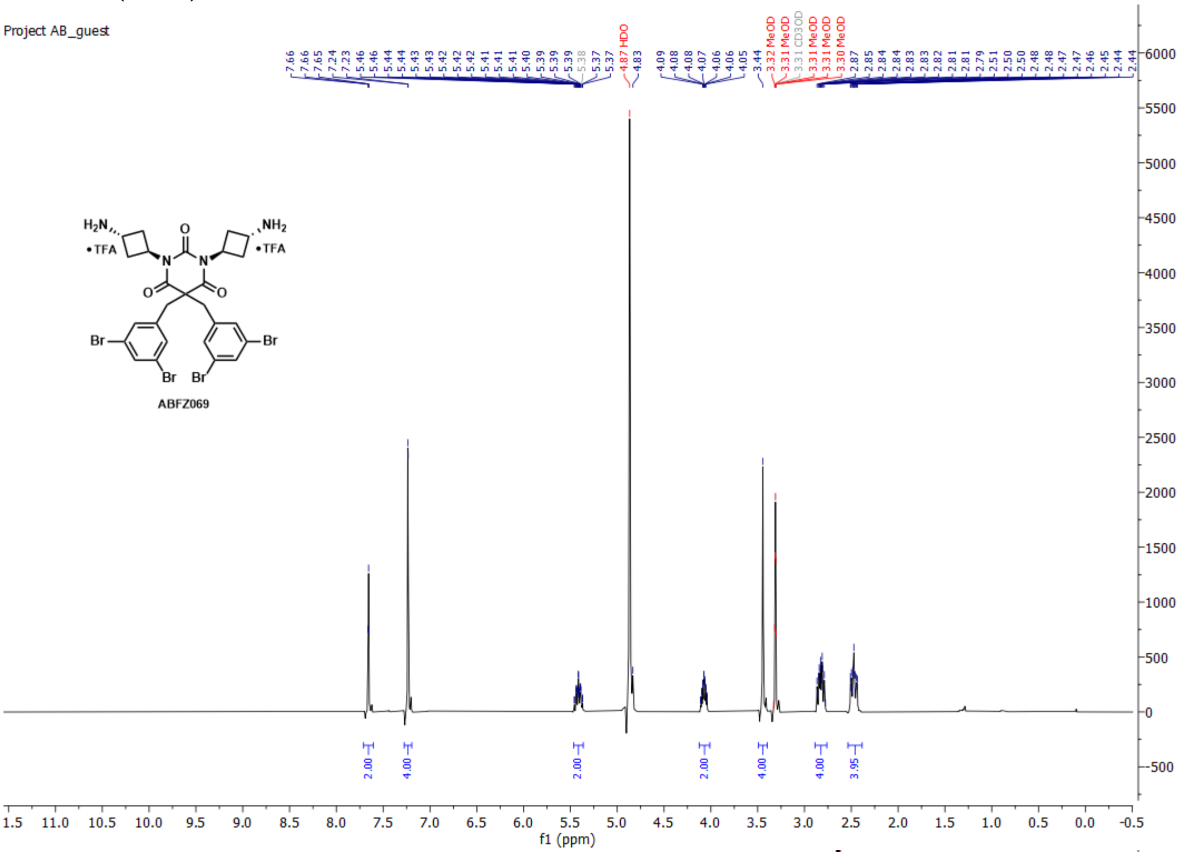

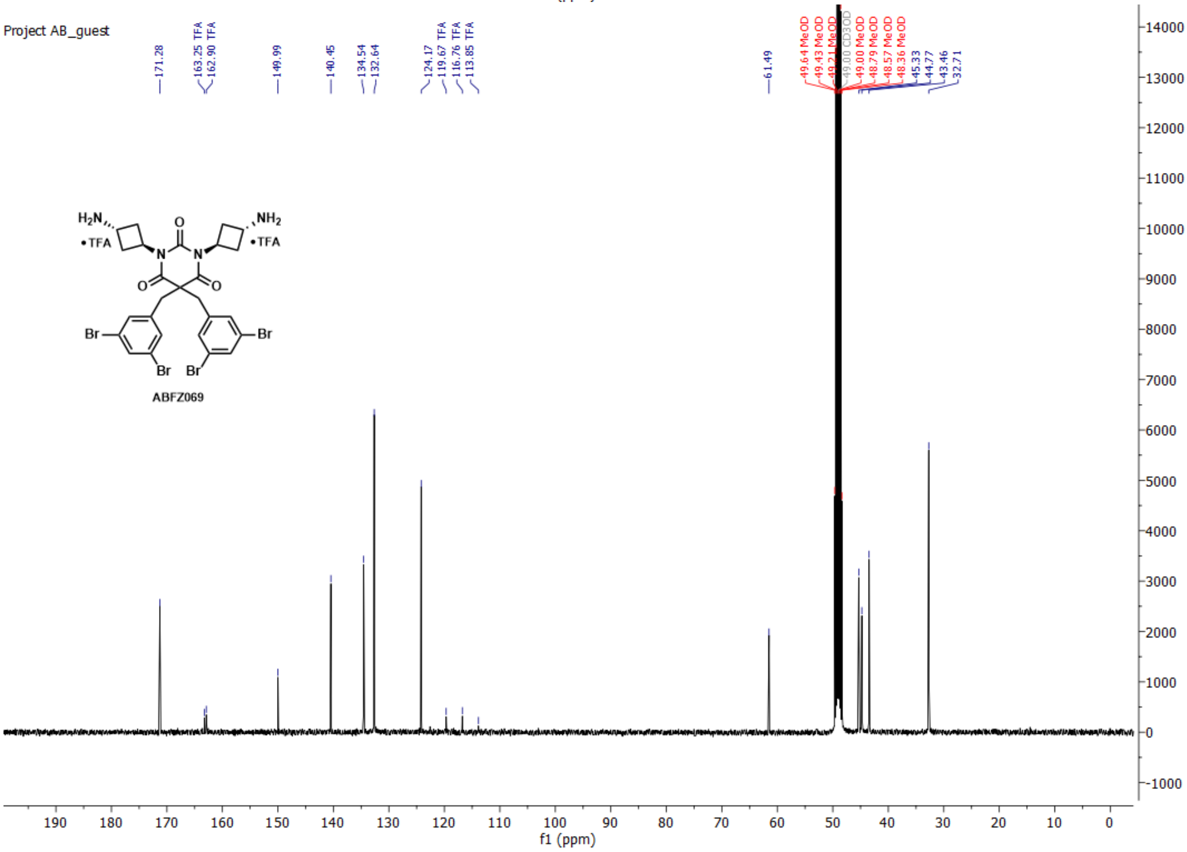

1,3-bis((1*s*,4*S*)-4-aminocyclohexyl)-5,5-bis(3,5-dibromobenzyl)pyrimidine-2,4,6(1*H*,3*H*,5*H*)-trione di-TFA salt (**18aA**)

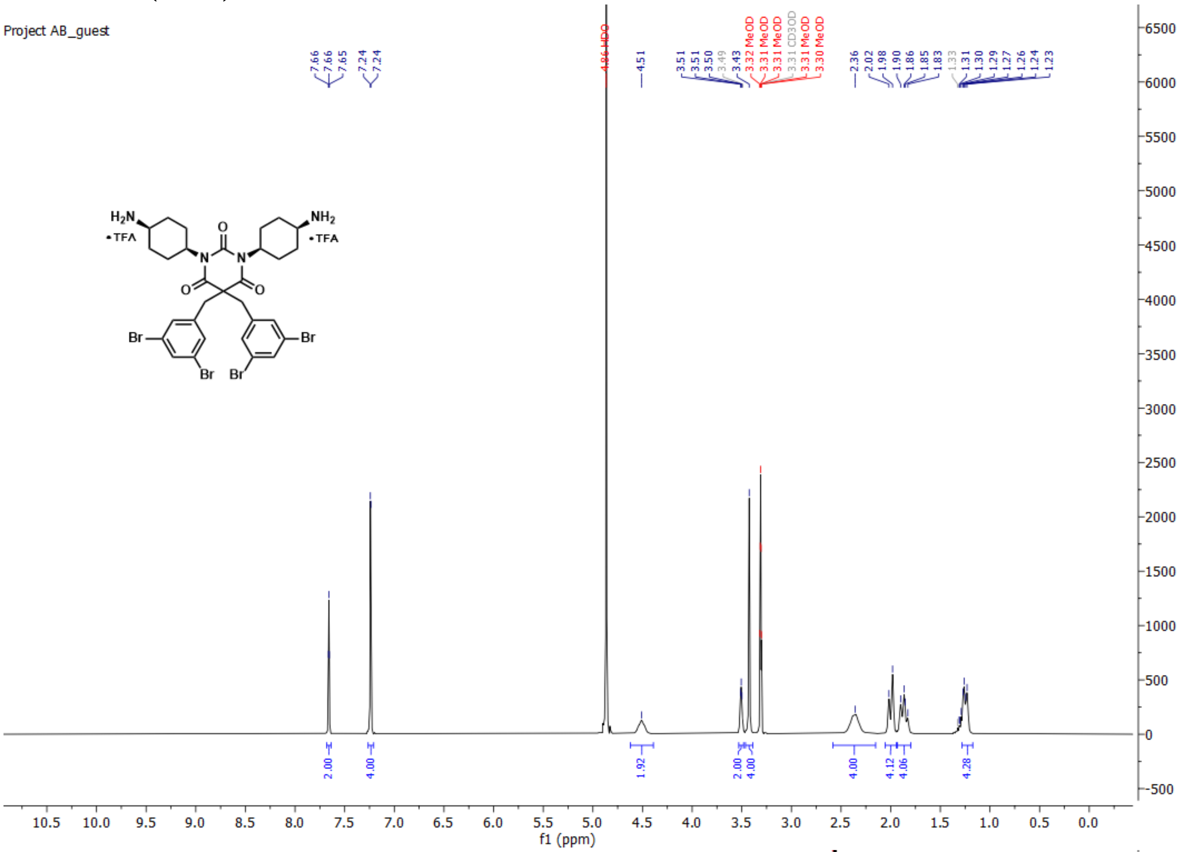

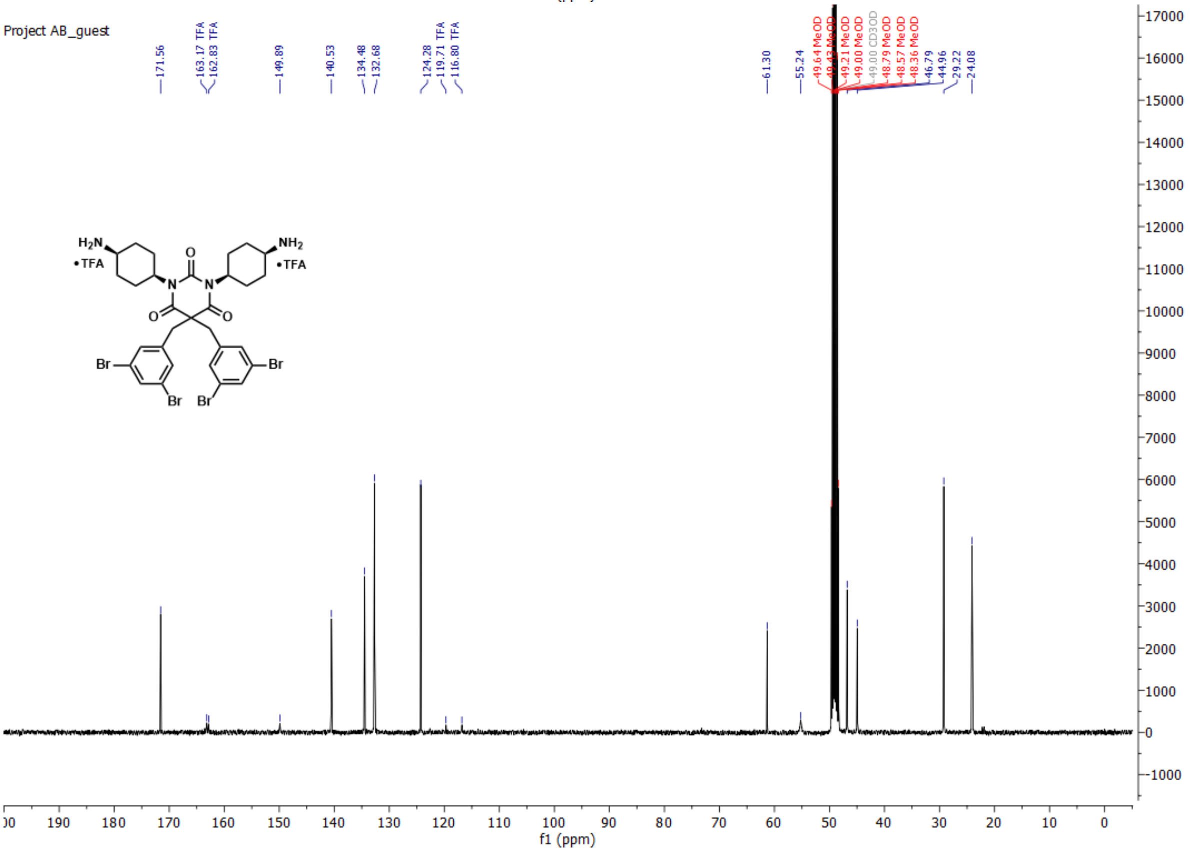

1,3-bis((1*r*,4*R*)-4-aminocyclohexyl)-5,5-bis(3,5-dibromobenzyl)pyrimidine-2,4,6(1*H*,3*H*,5*H*)-trione di-TFA salt (**19aA**)

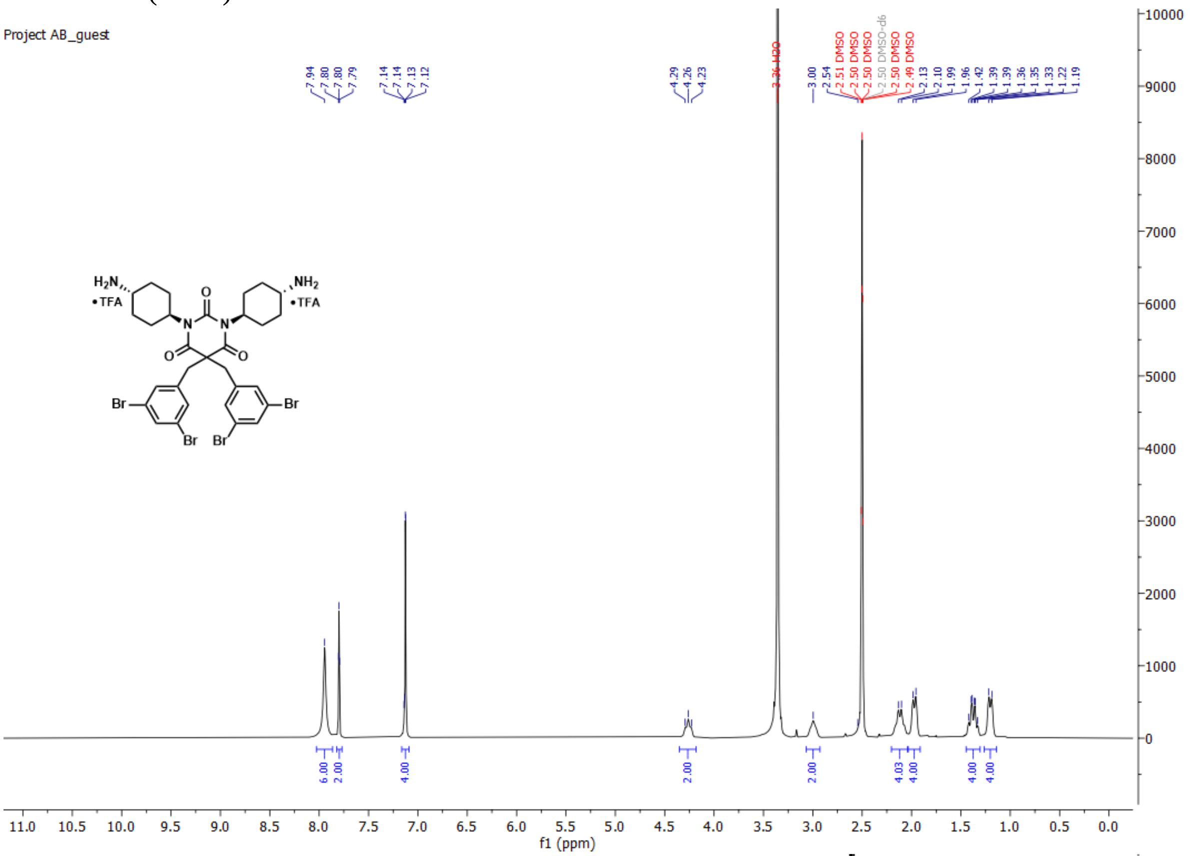

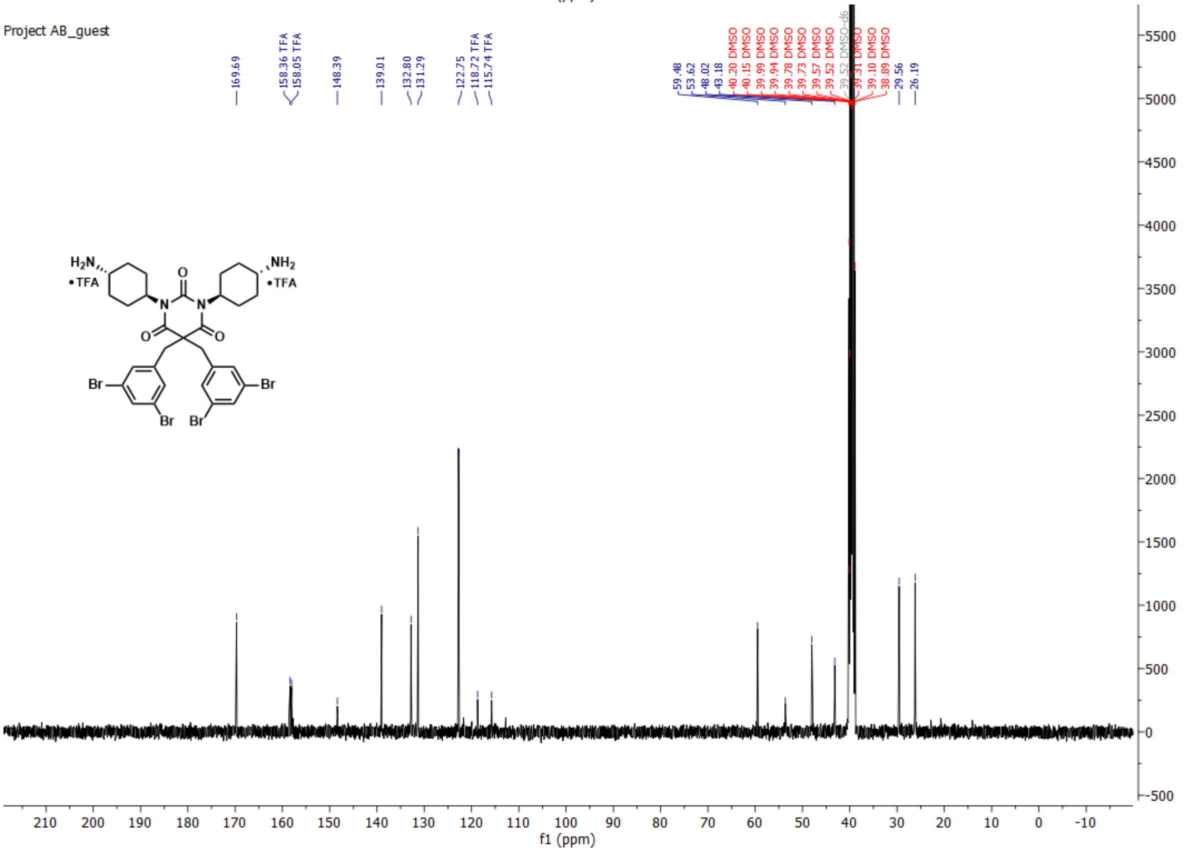

1,1'-((5,5-bis(3,5-dibromobenzyl)-2,4,6-trioxodihydropyrimidine-1,3(2*H*,4*H*)-diyl)bis(ethane-2,1-diyl))diguanidine di-TFA salt (**12aG**)

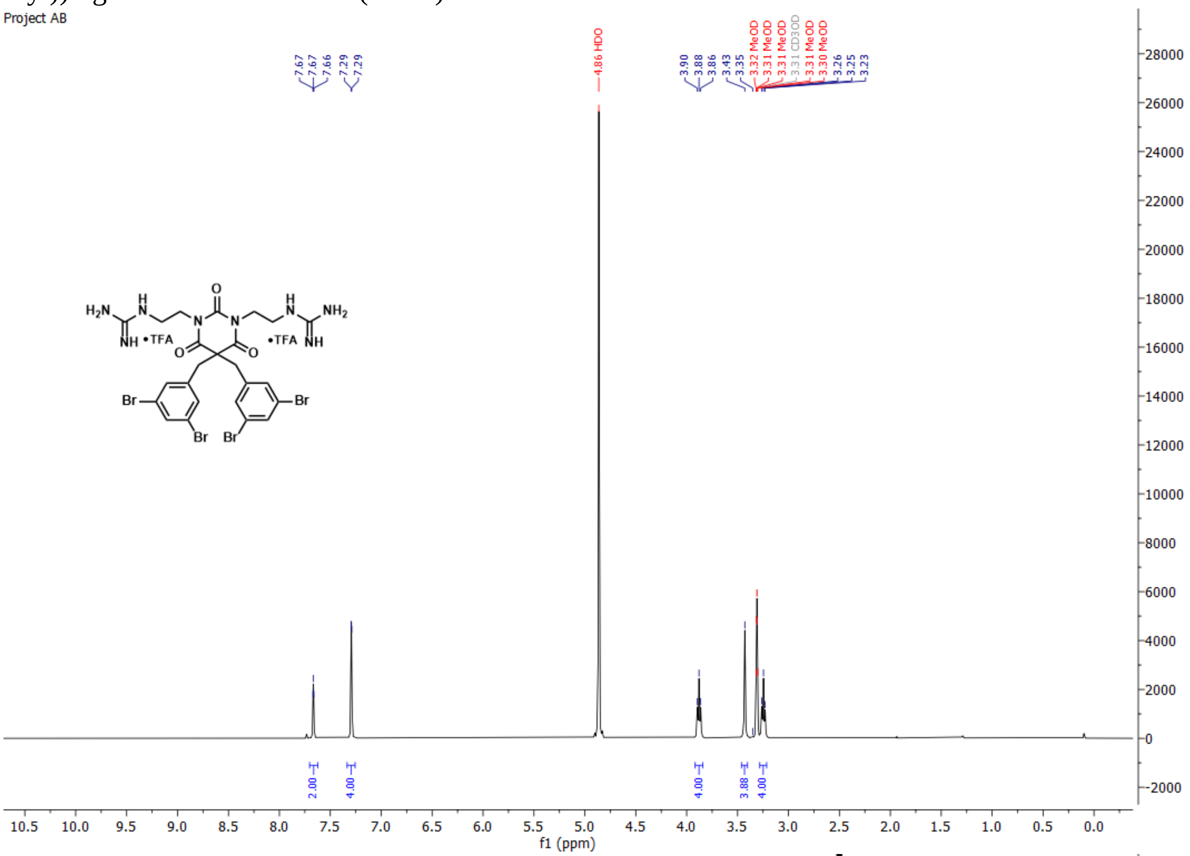

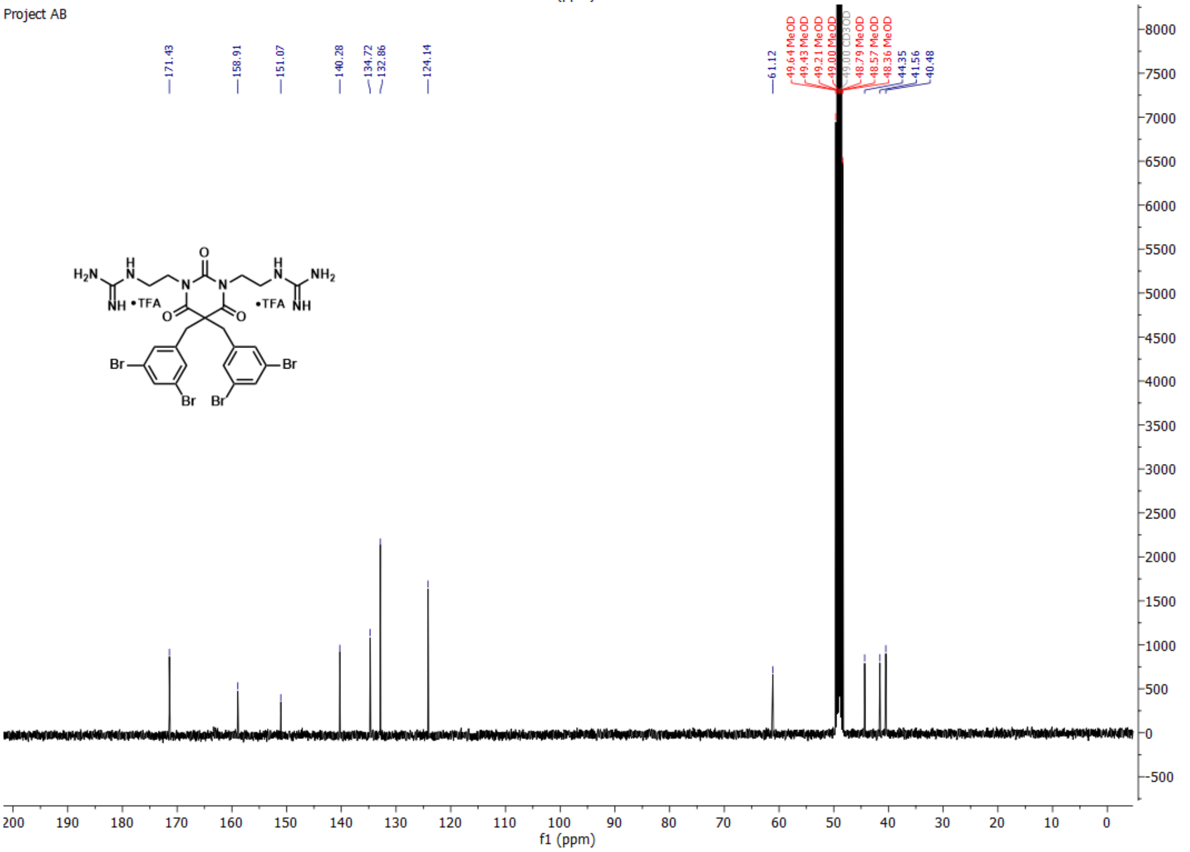

1,1'-((5,5-bis(3,5-dibromobenzyl)-2,4,6-trioxodihydropyrimidine-1,3(2*H*,4*H*)-diyl)bis(propane-3,1-diyl))diguanidine di-TFA salt (**13aG**)

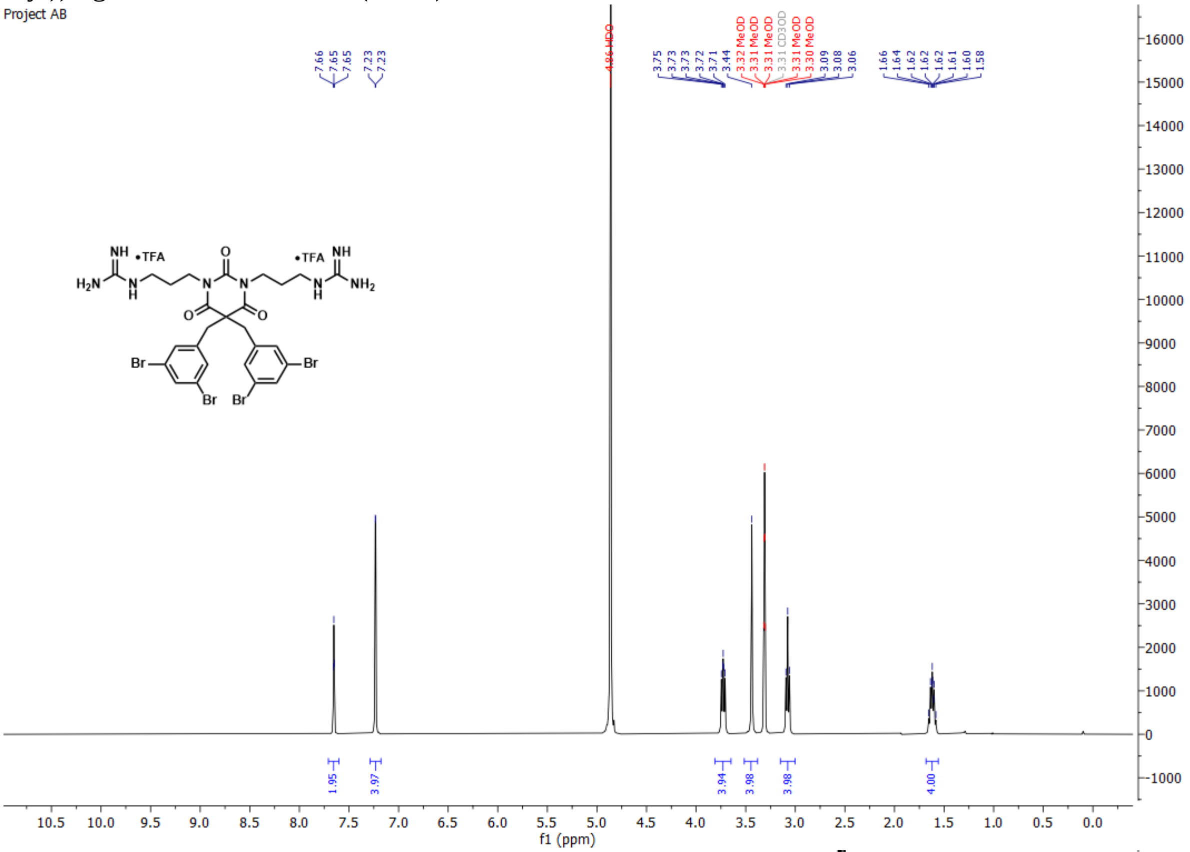

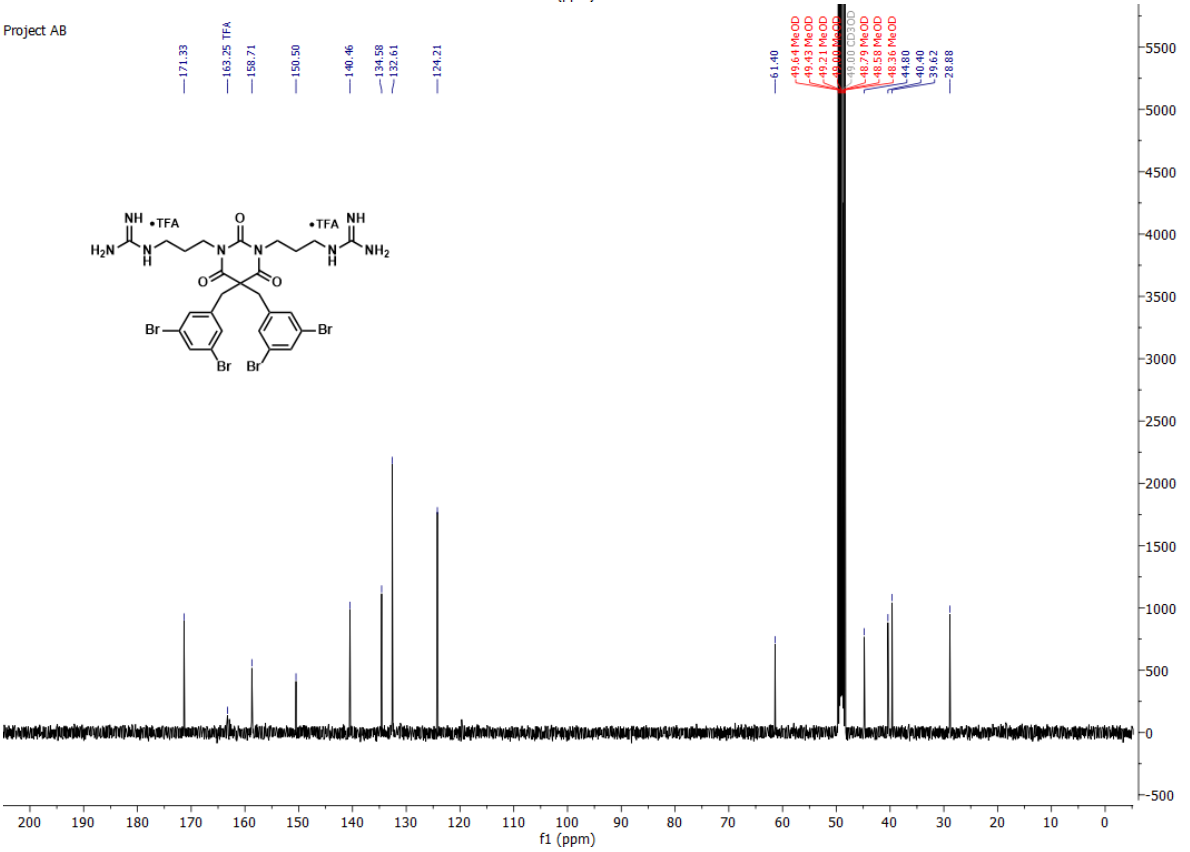

1,1'-((5,5-bis(3,5-dibromobenzyl)-2,4,6-trioxodihydropyrimidine-1,3(2*H*,4*H*)-diyl)bis(pentane-5,1-diyl))diguanidine di-TFA salt (**14aG**)

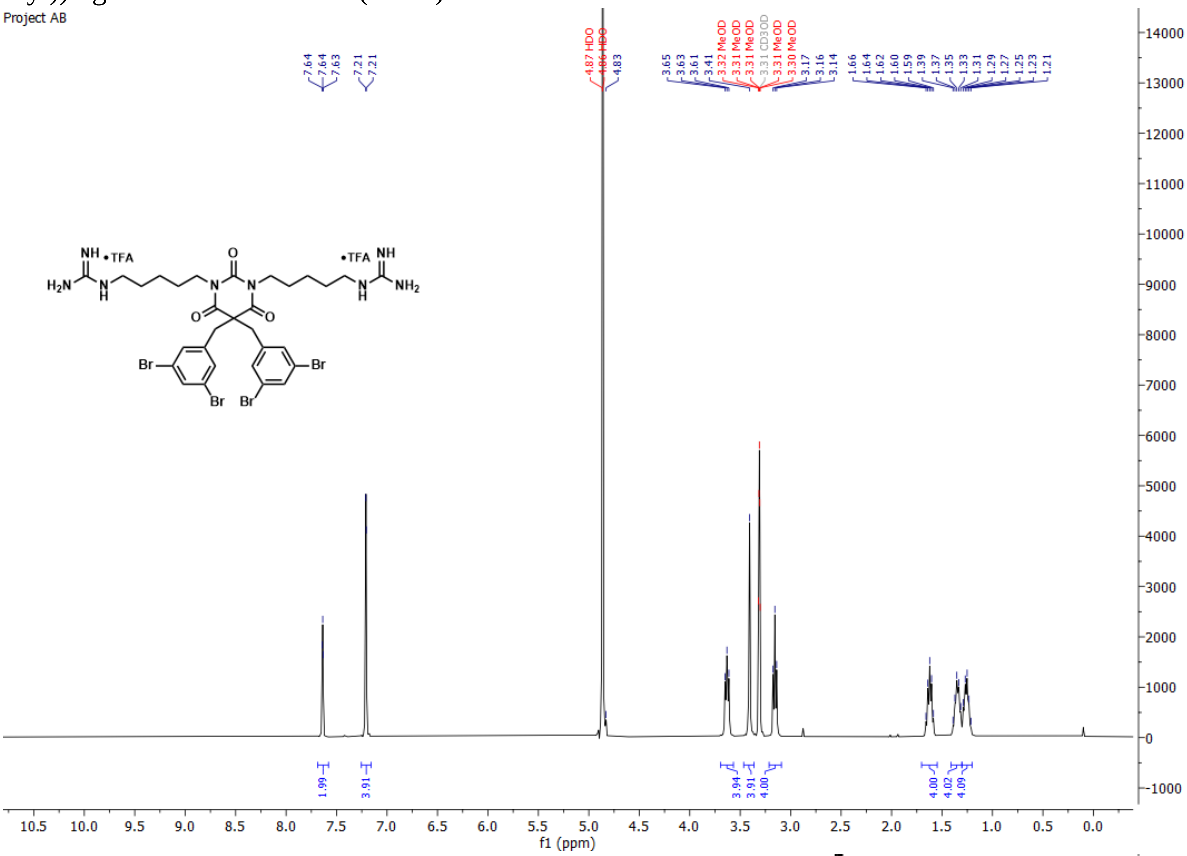

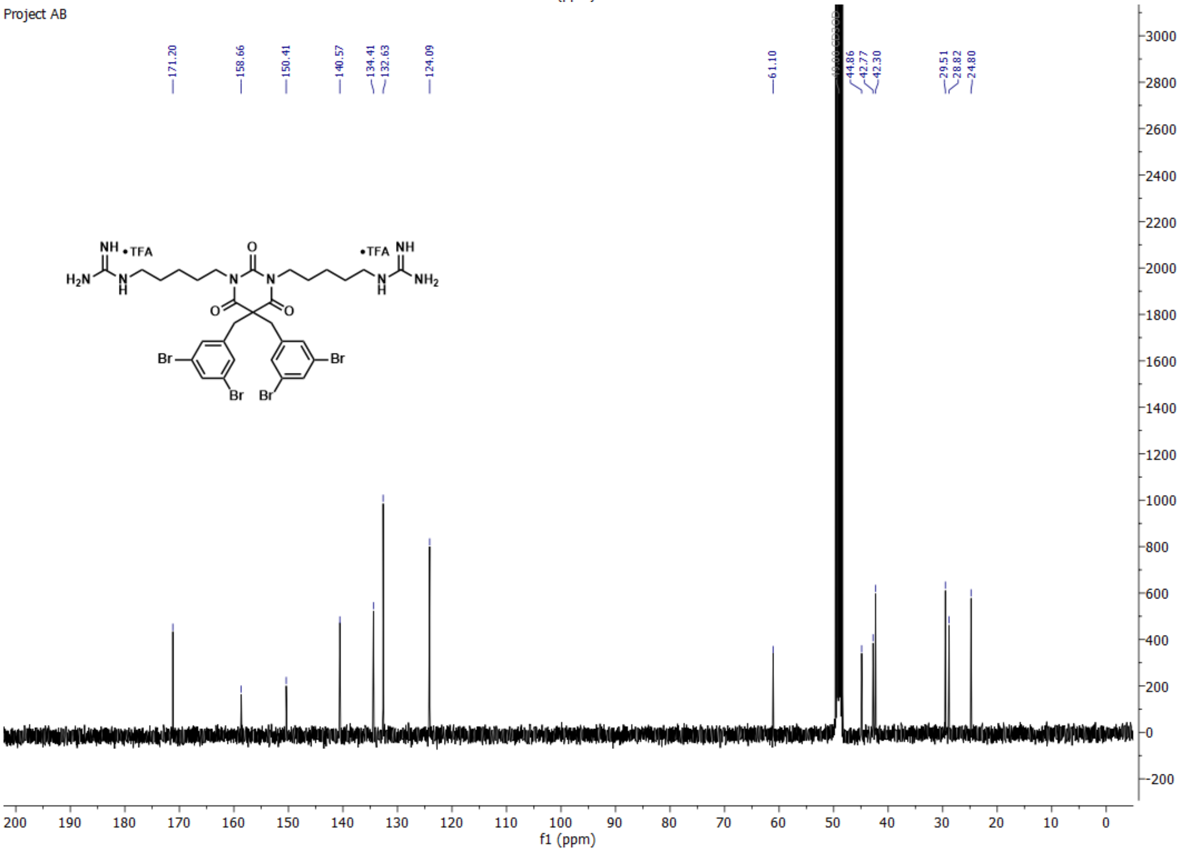

1,1'-((5,5-bis(3,5-dibromobenzyl)-2,4,6-trioxodihydropyrimidine-1,3(2*H*,4*H*)-diyl)bis(hexane-6,1-diyl))diguanidine di-TFA salt (**15aG**)

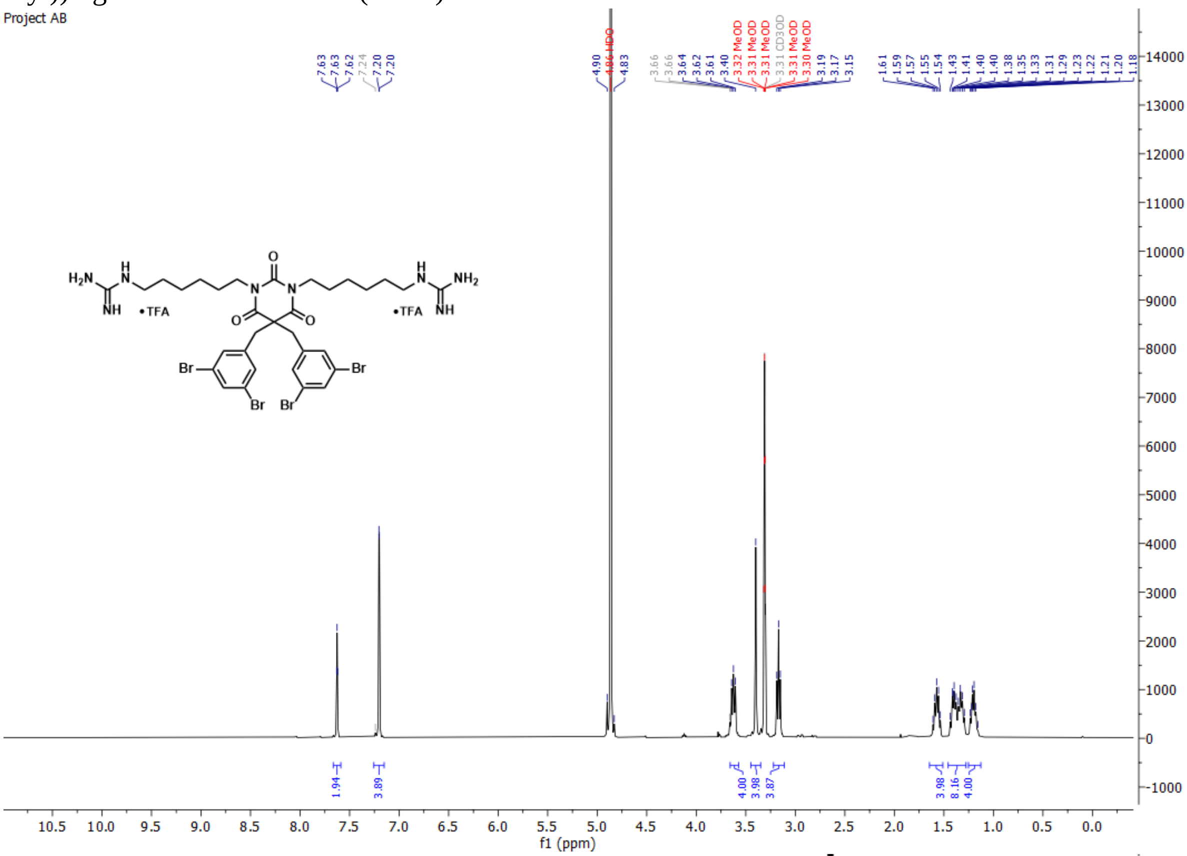

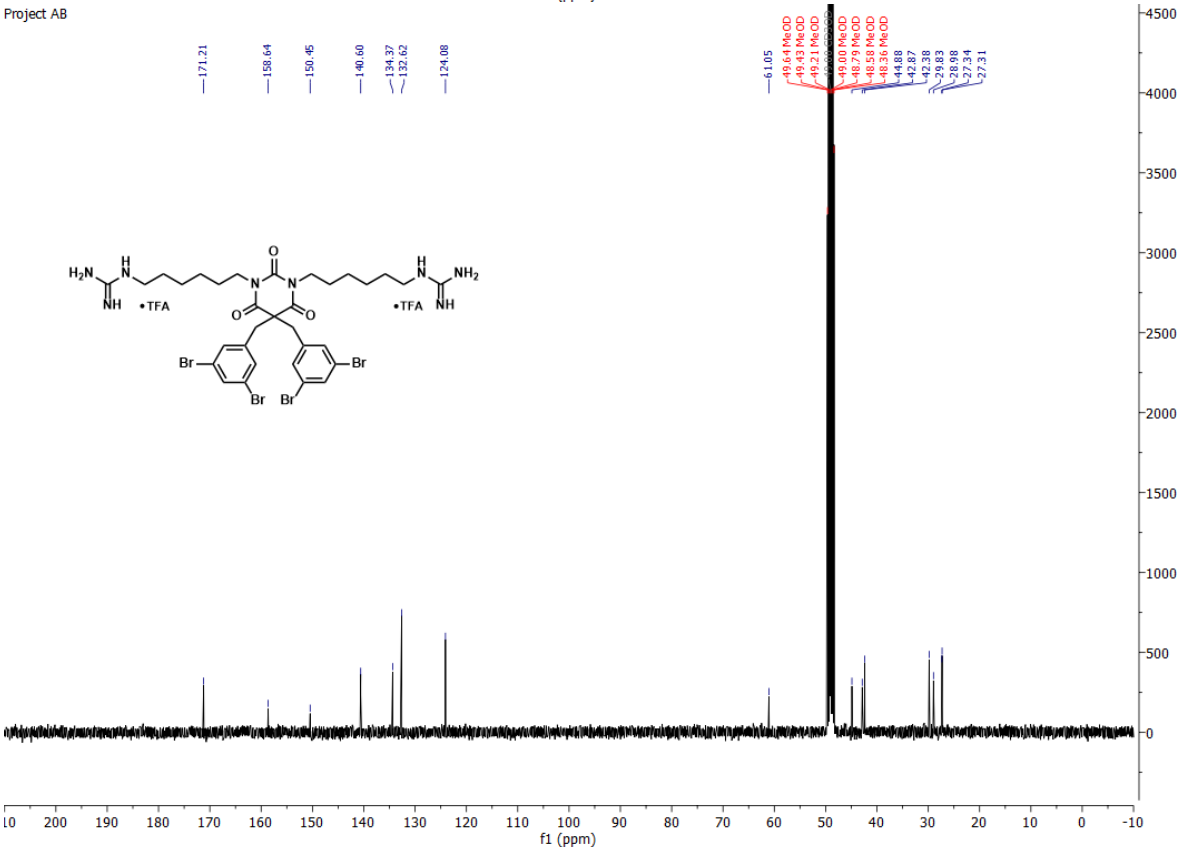

1,1'-((1*S*,1'*S*,3*s*,3'*s*)-(5,5-bis(3,5-dibromobenzyl)-2,4,6-trioxodihydropyrimidine-1,3(2*H*,4*H*)-diyl)bis(cyclobutane-3,1-diyl))diguanidine di-TFA salt (**16aG**)

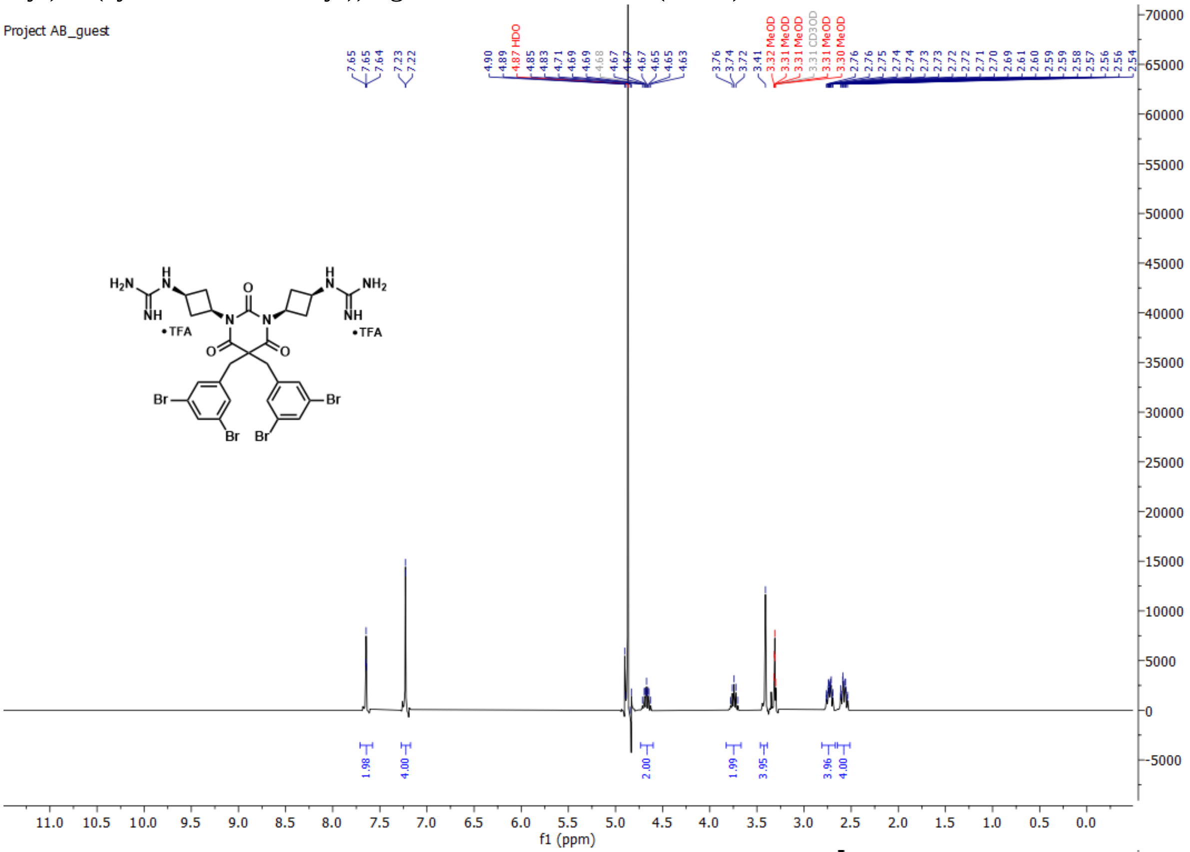

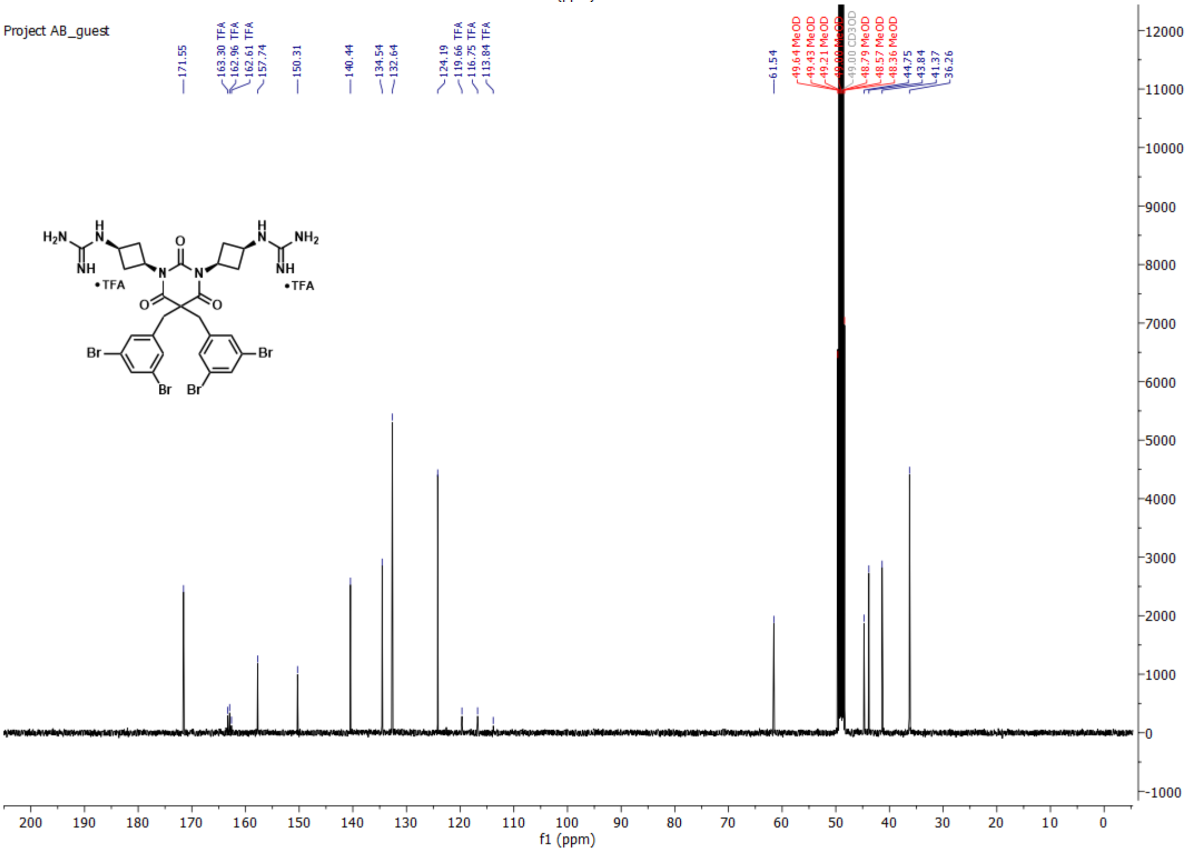

1,1'-((1*R*,1'*R*,3*r*,3'*r*)-(5,5-bis(3,5-dibromobenzyl)-2,4,6-trioxodihydropyrimidine-1,3(2*H*,4*H*)-diyl)bis(cyclobutane-3,1-diyl))diguanidine di-TFA salt (**17aG**)

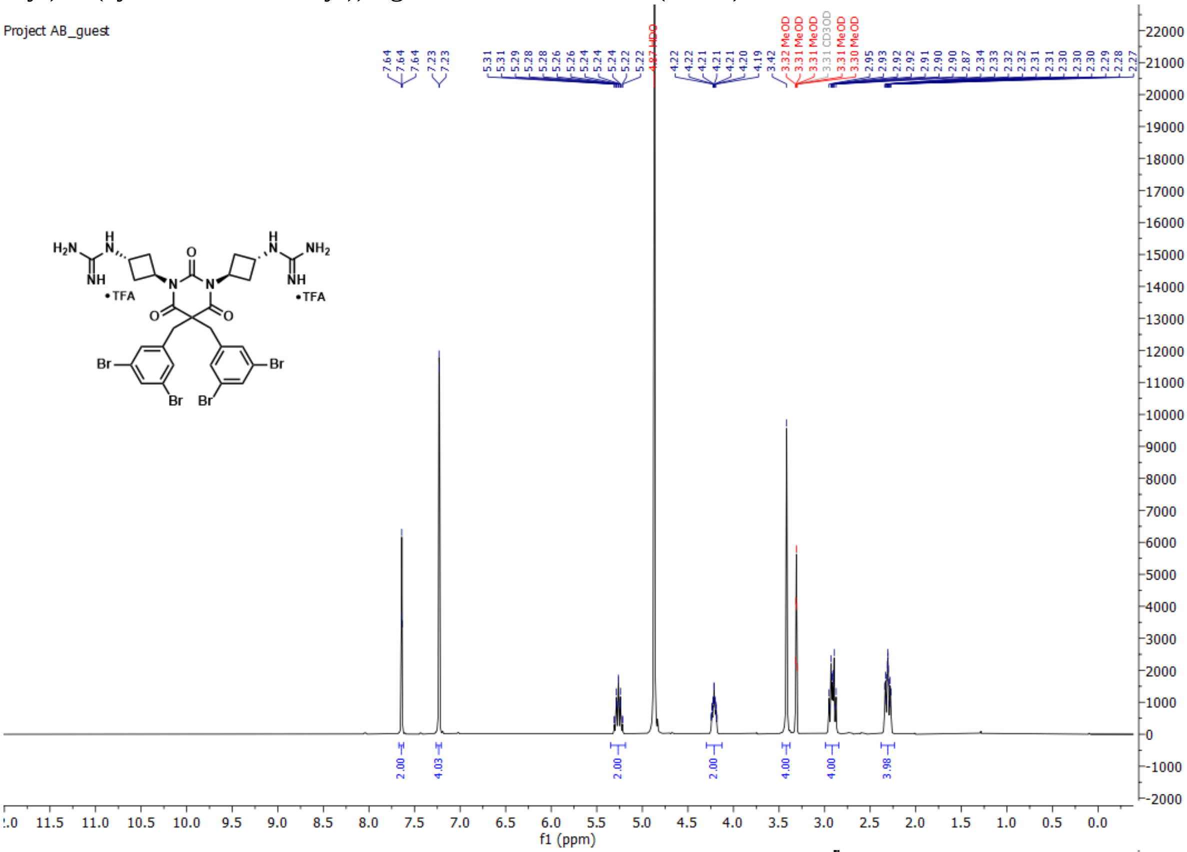

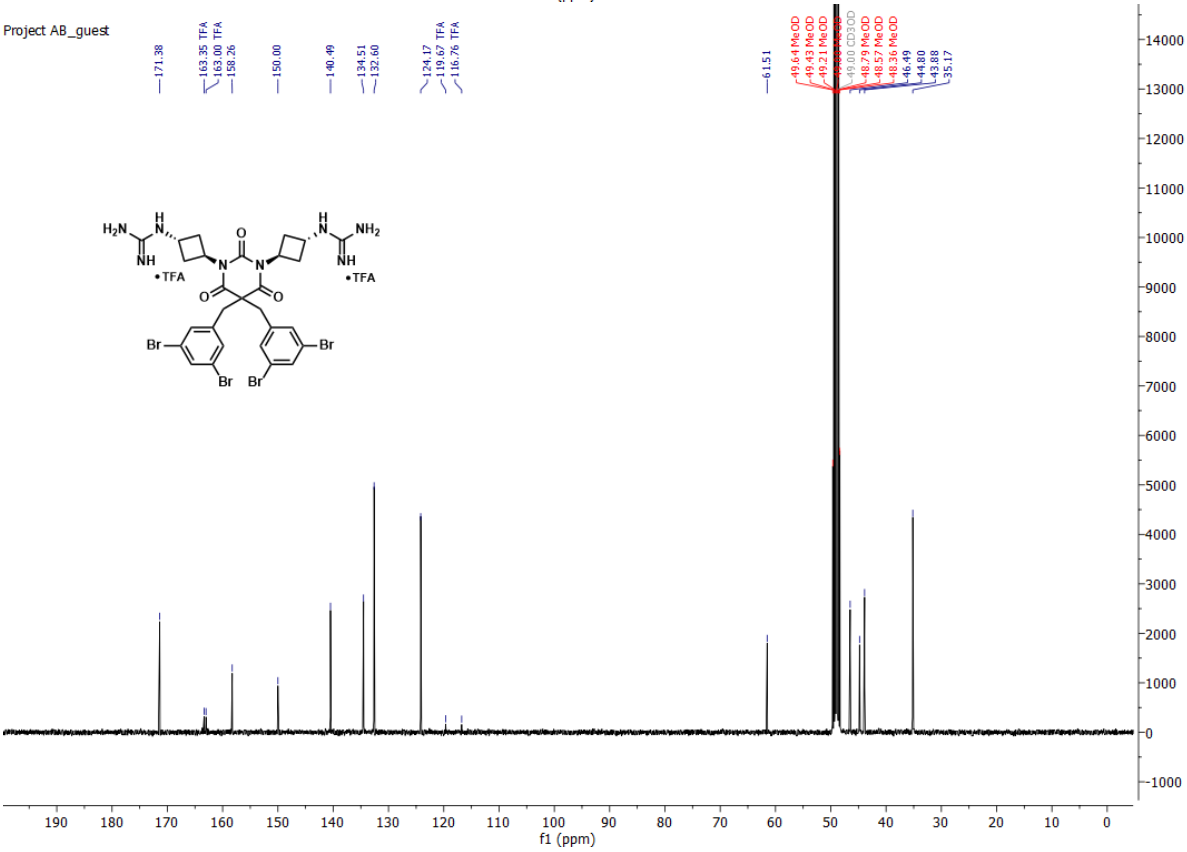

1,1'-((1*S*,1'*S*,4*s*,4'*s*)-(5,5-bis(3,5-dibromobenzyl)-2,4,6-trioxodihydropyrimidine-1,3(2*H*,4*H*)-diyl)bis(cyclohexane-4,1-diyl))diguanidine di-TFA salt (**18aG**)

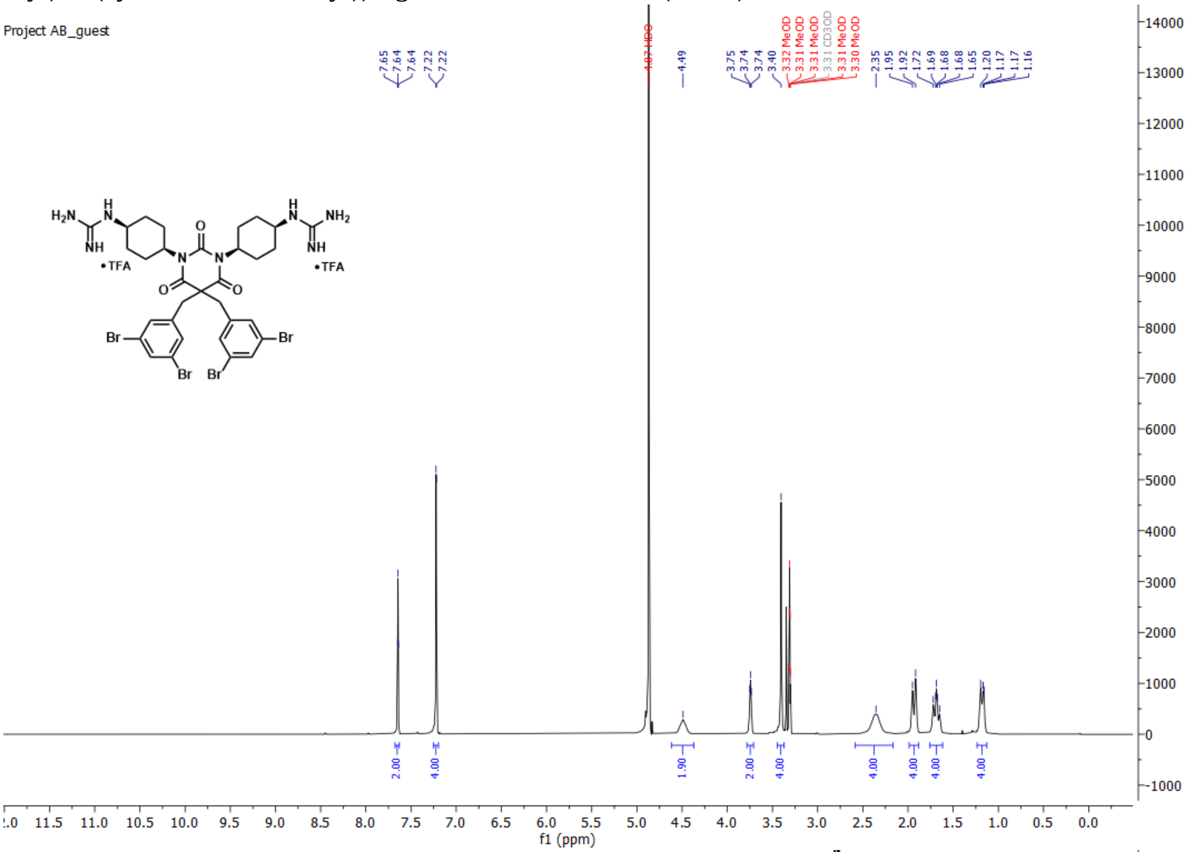

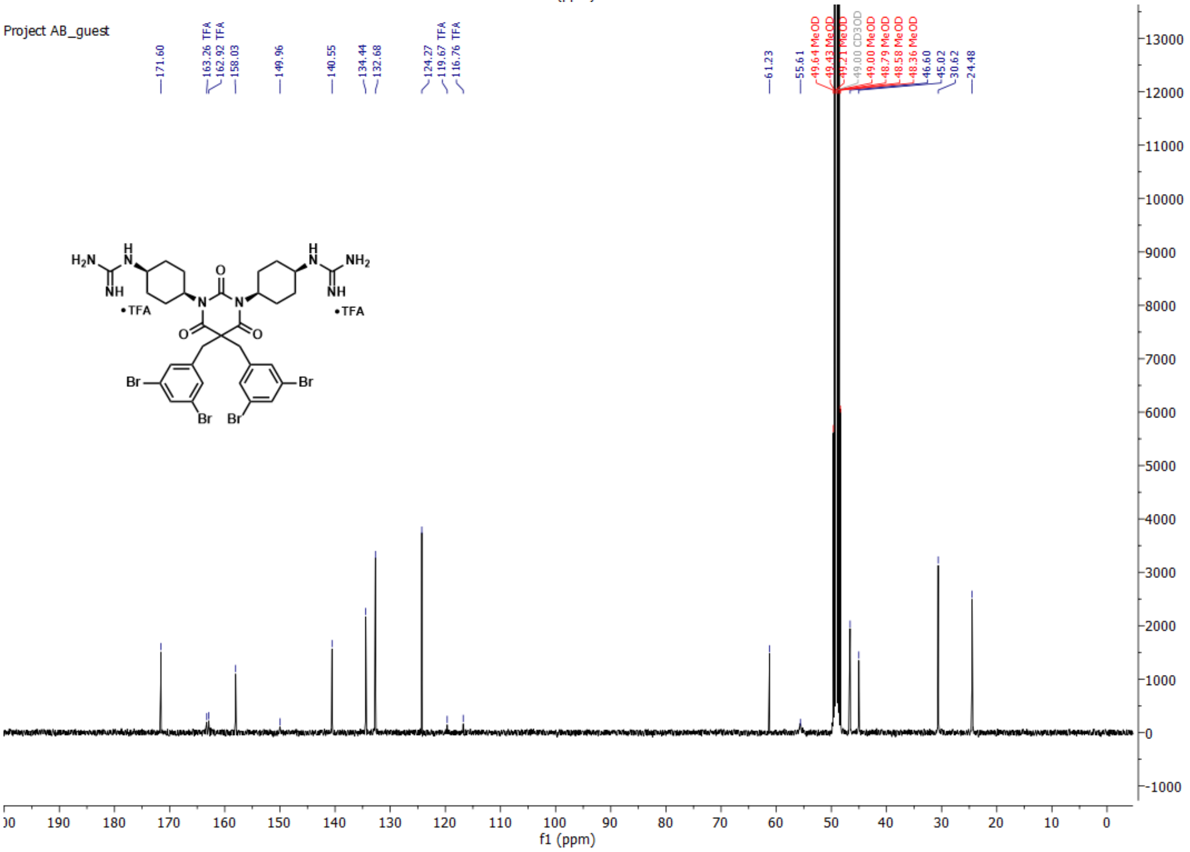

3.5 ^{1}H and ^{13}C NMR spectra of compounds in *series 5*

1,3-bis(3-aminopropyl)-5,5-bis((6-bromoquinolin-2-yl)methyl)pyrimidine-2,4,6(1*H*,3*H*,5*H*)-trione di-TFA salt (**13cA**)

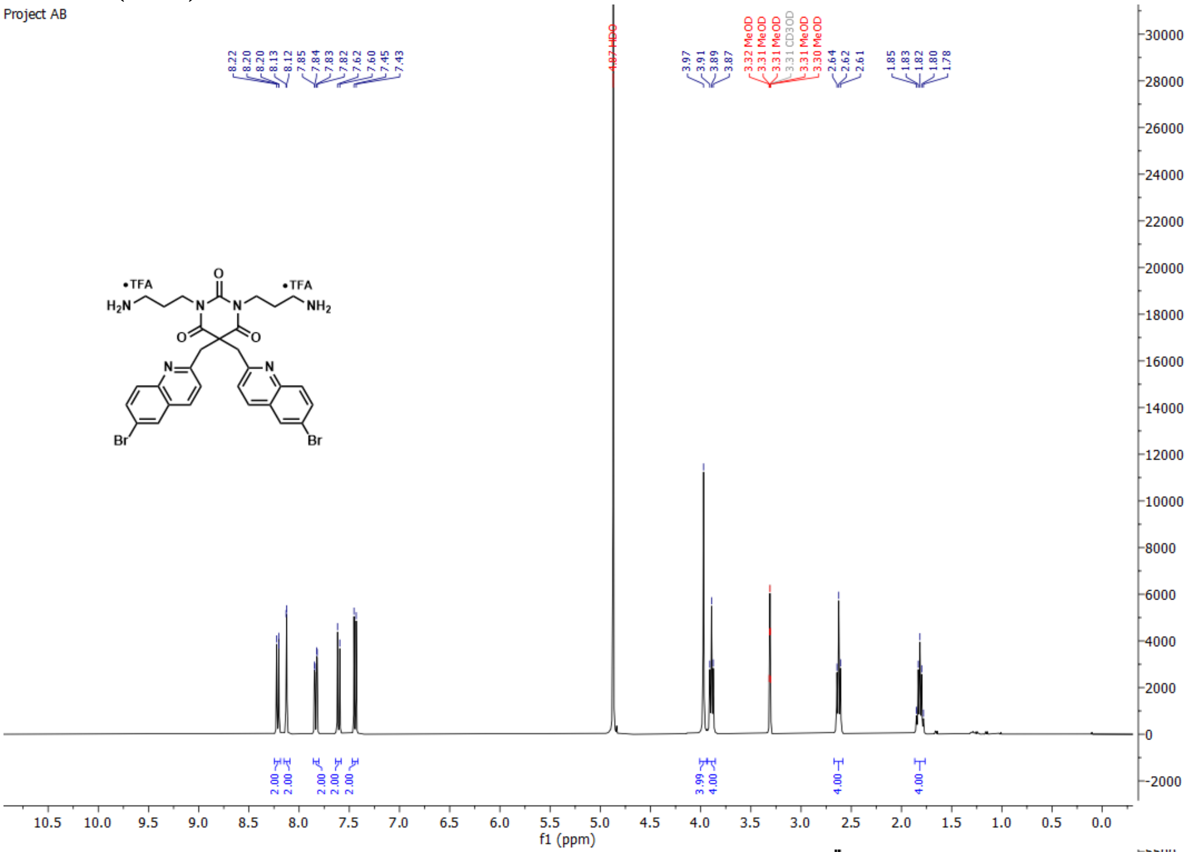

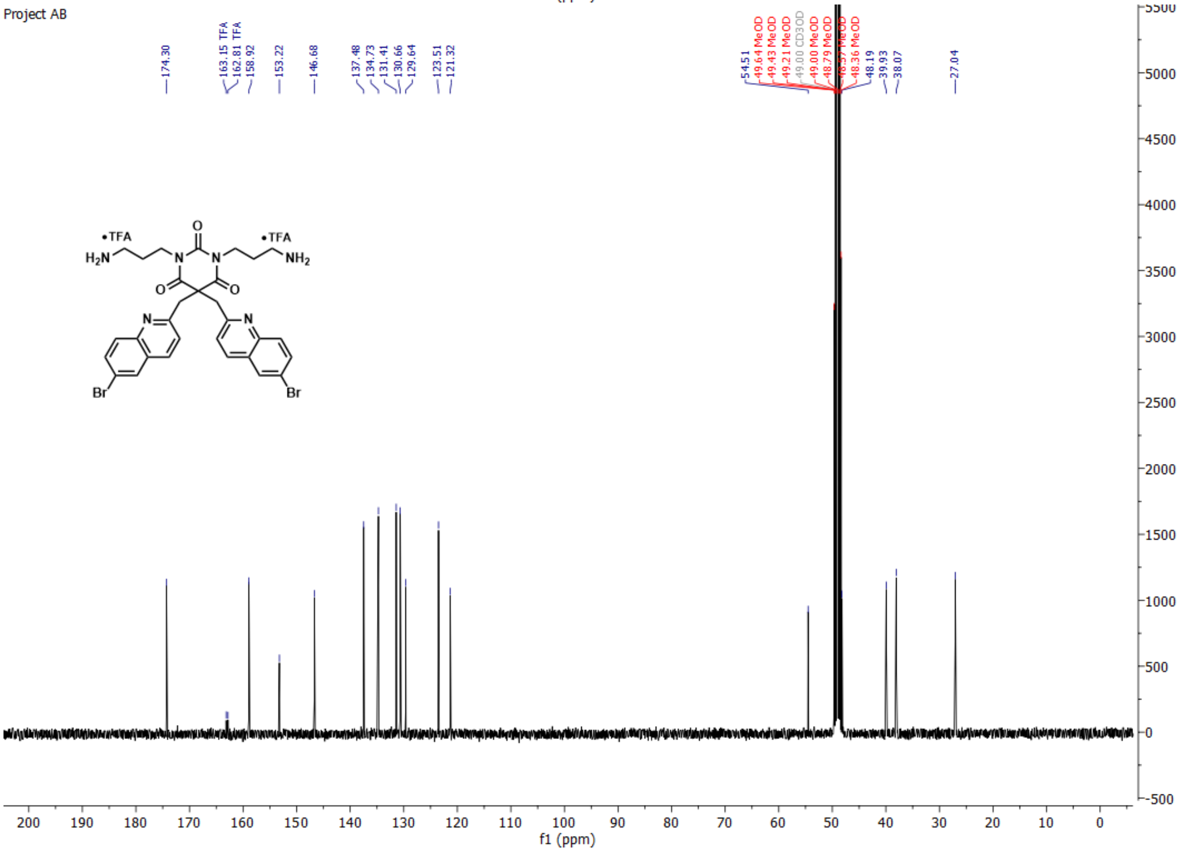

1,3-bis(3-aminopropyl)-5,5-bis(4-(trifluoromethyl)benzyl)pyrimidine-2,4,6(1*H*,3*H*,5*H*)-trione di-TFA salt (**13hA**)

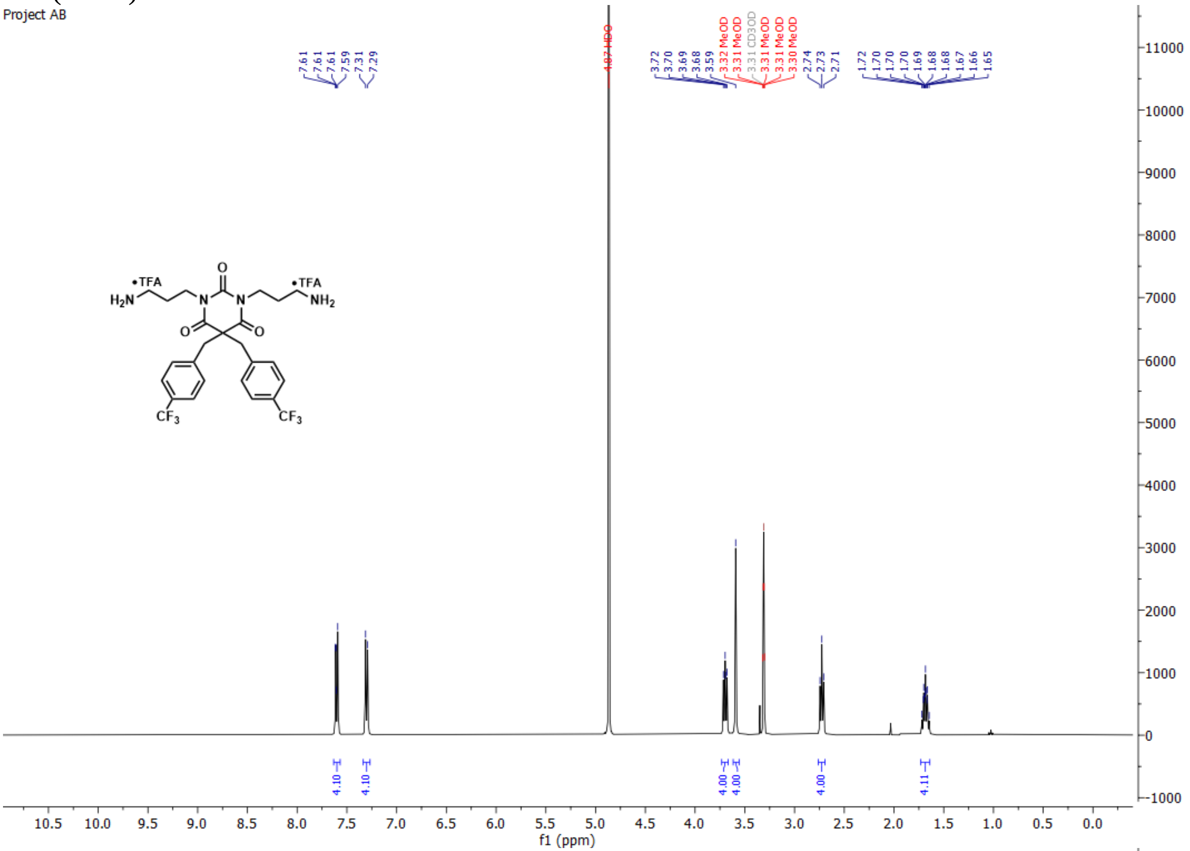

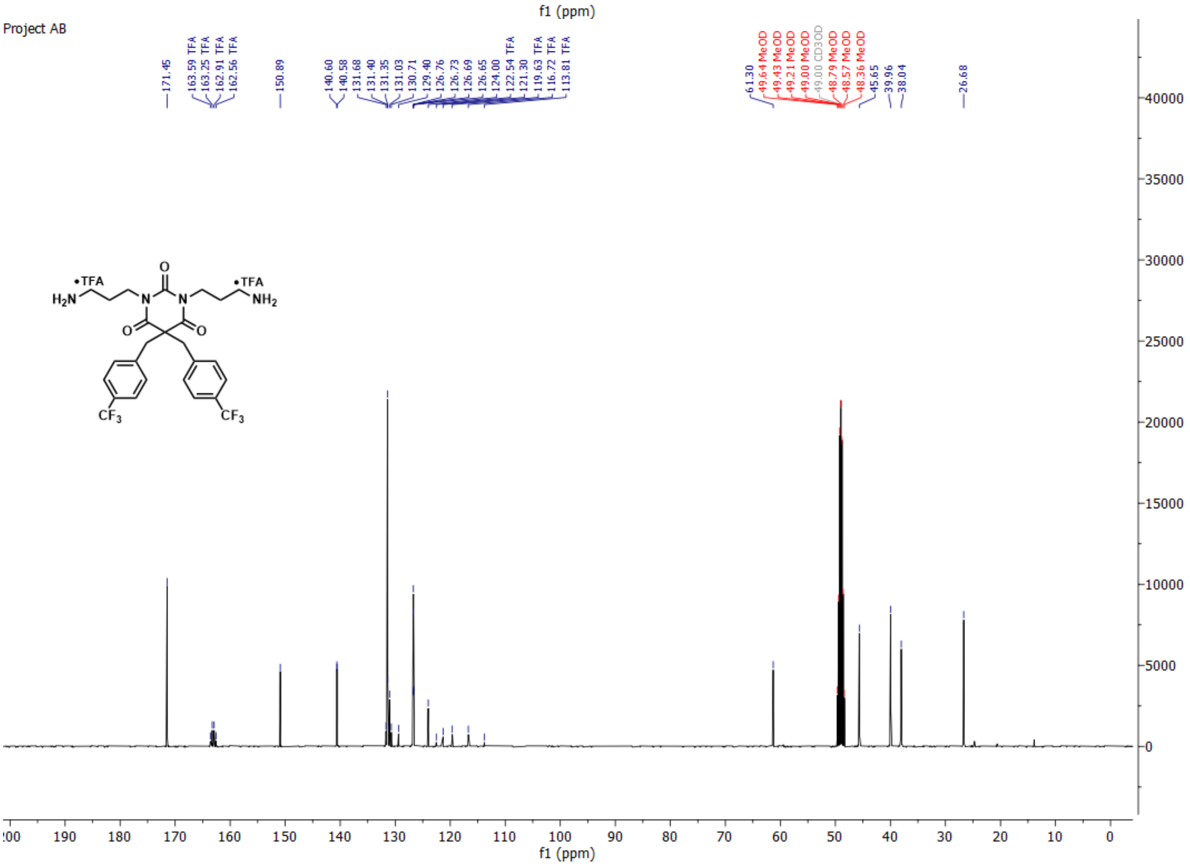

1,3-bis(3-aminopropyl)-5,5-bis(4-bromo-3-chlorobenzyl)pyrimidine-2,4,6(1*H*,3*H*,5*H*)-trione di-TFA salt (**13iA**)

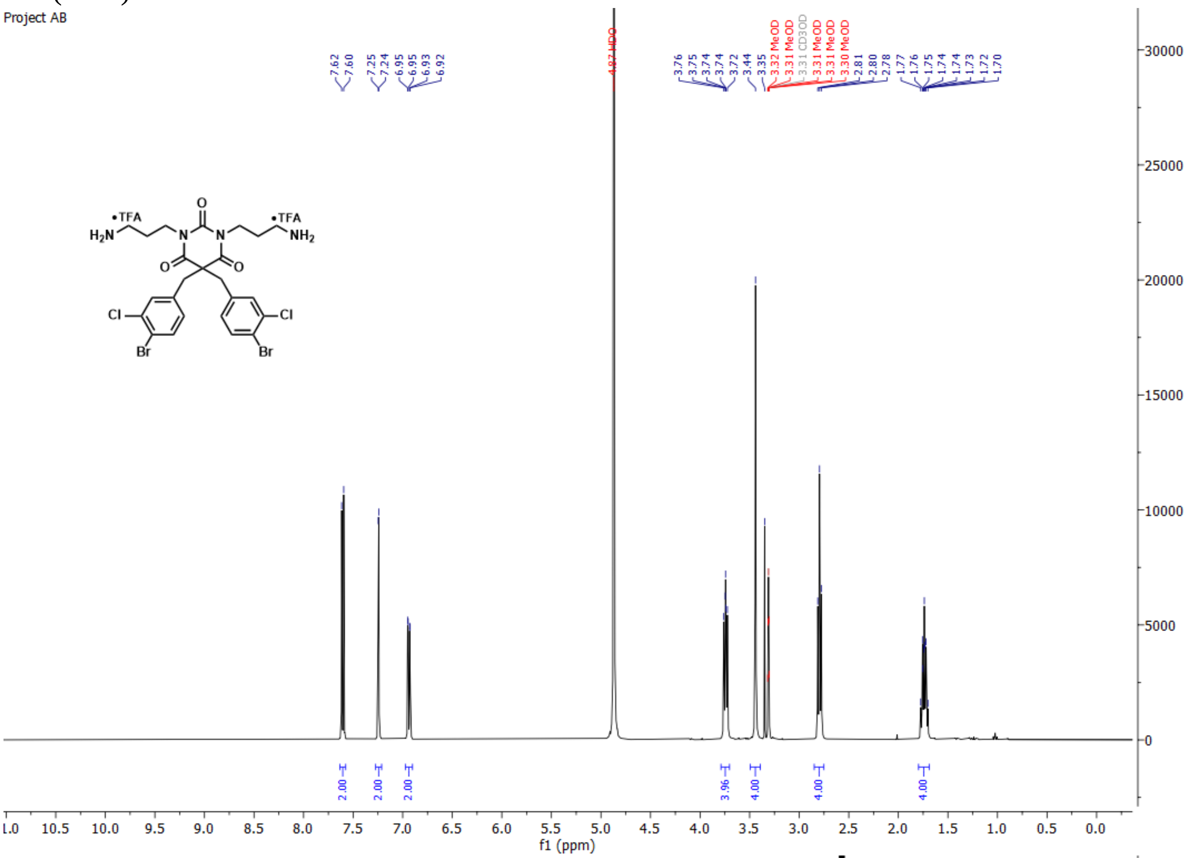

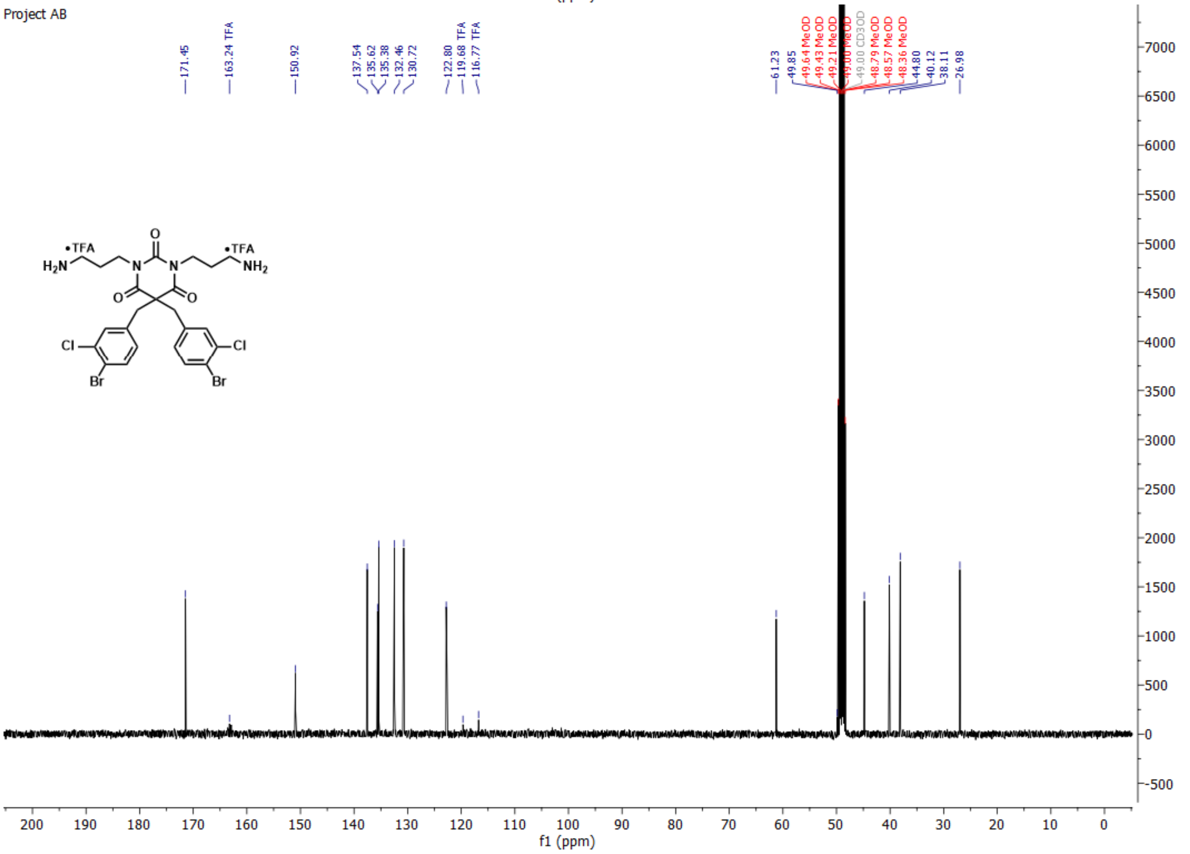

1,3-bis(3-aminopropyl)-5,5-bis((4-bromonaphthalen-1-yl)methyl)pyrimidine-2,4,6(1*H*,3*H*,5*H*)-trione di-TFA salt (**13eA**)

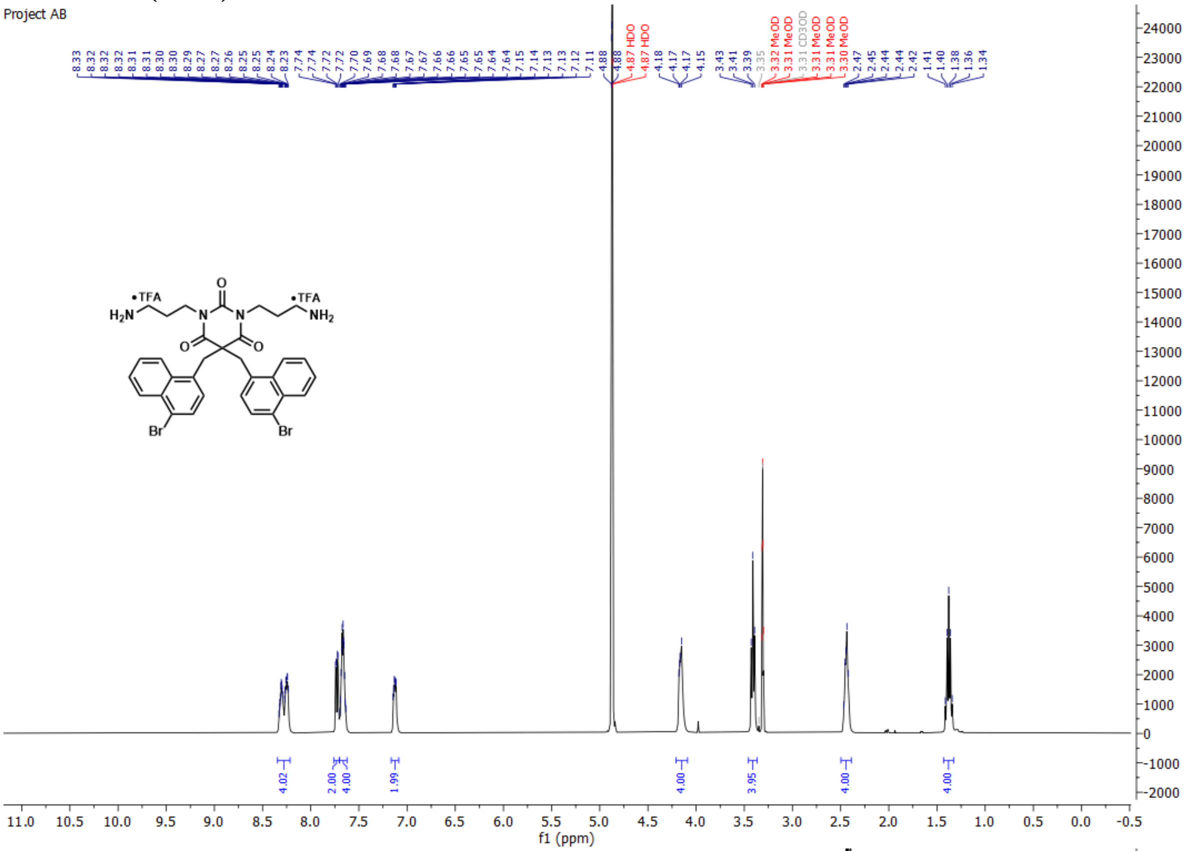

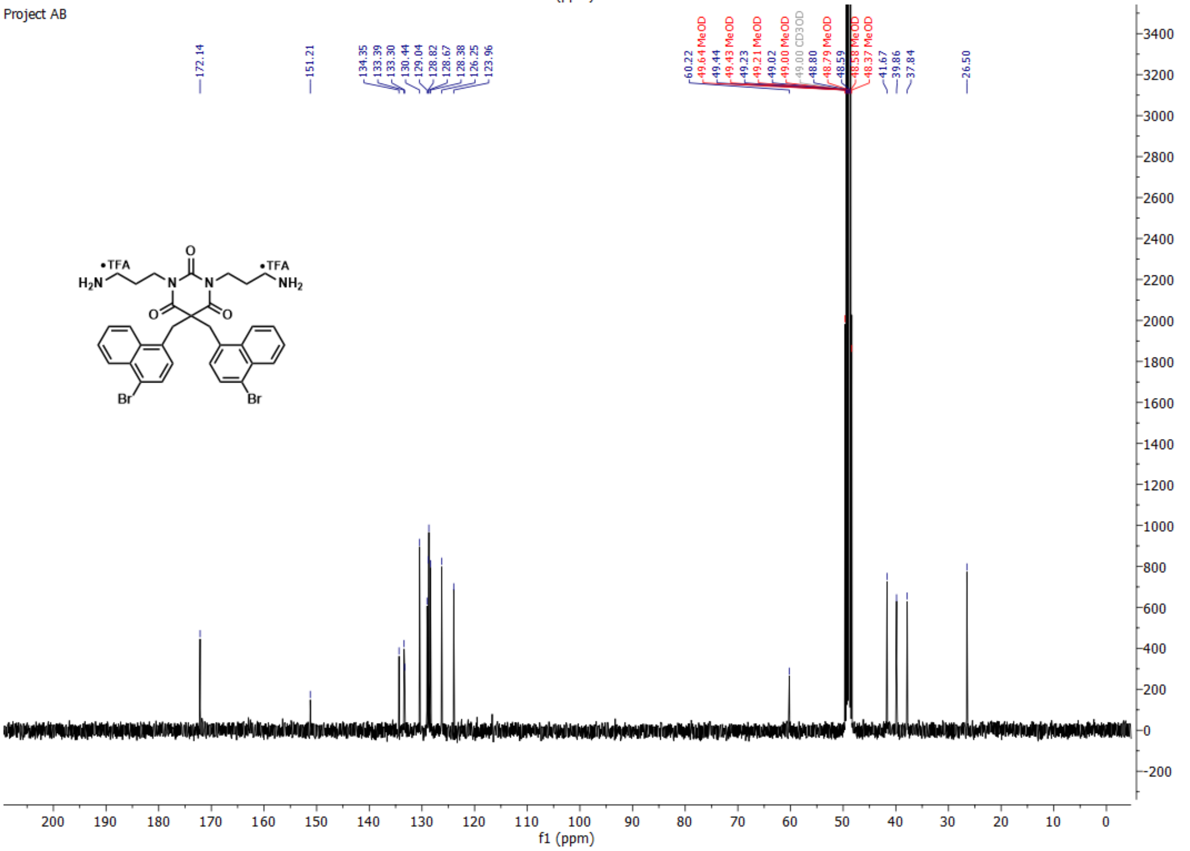

1,3-bis(3-aminopropyl)-5,5-bis(3,5-bis(trifluoromethyl)benzyl)pyrimidine-2,4,6(1*H*,3*H*,5*H*)-trione di-TFA salt (**13jA**)

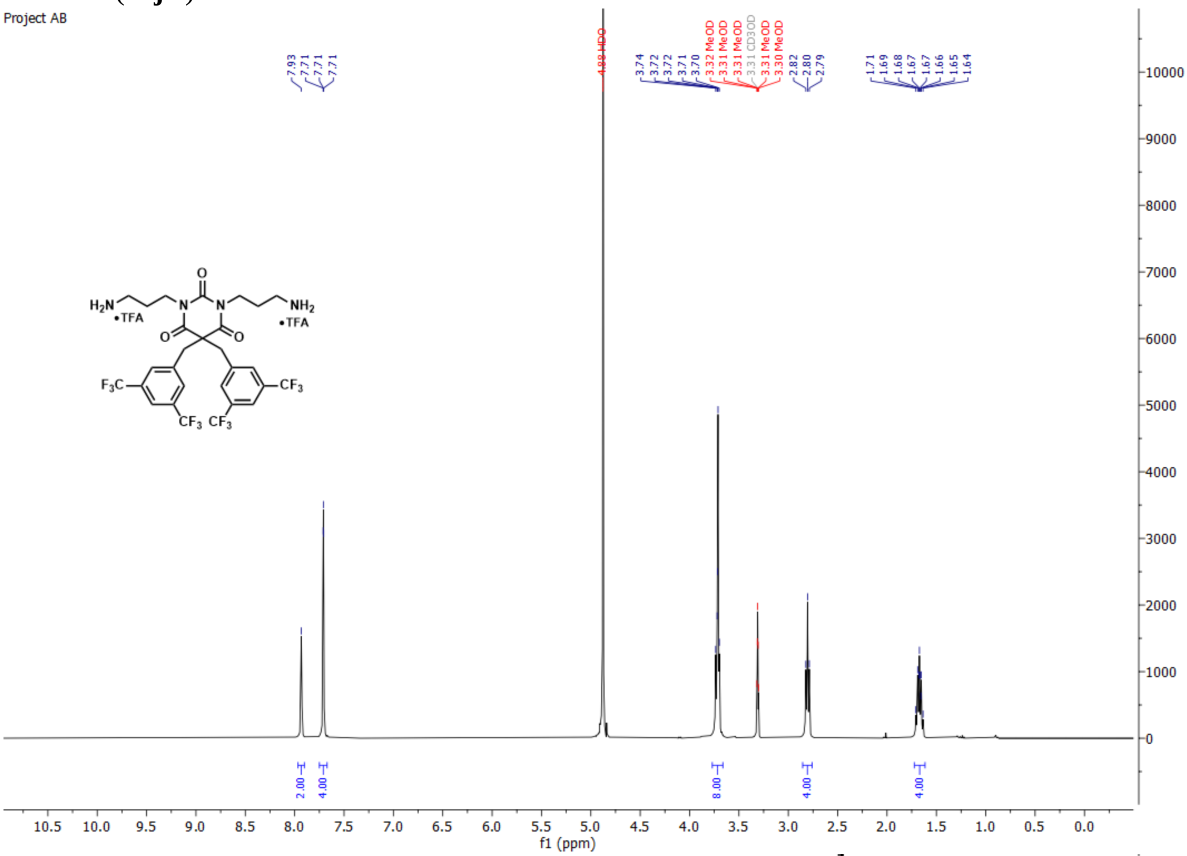

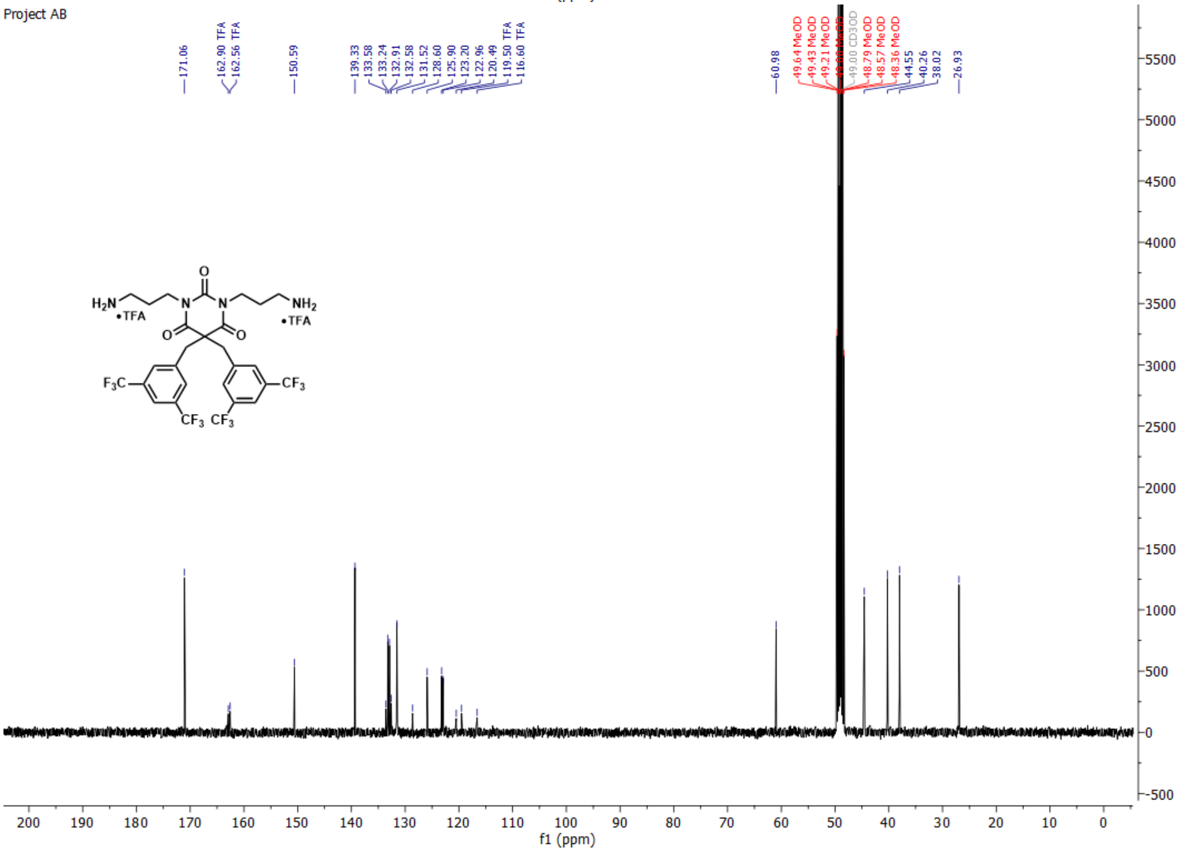

1,3-bis(3-aminopropyl)-5-(3,5-dibromobenzyl)-5-(4-(trifluoromethyl)benzyl)pyrimidine-2,4,6(1*H*,3*H*,5*H*)-trione di-TFA salt (**13lA**)

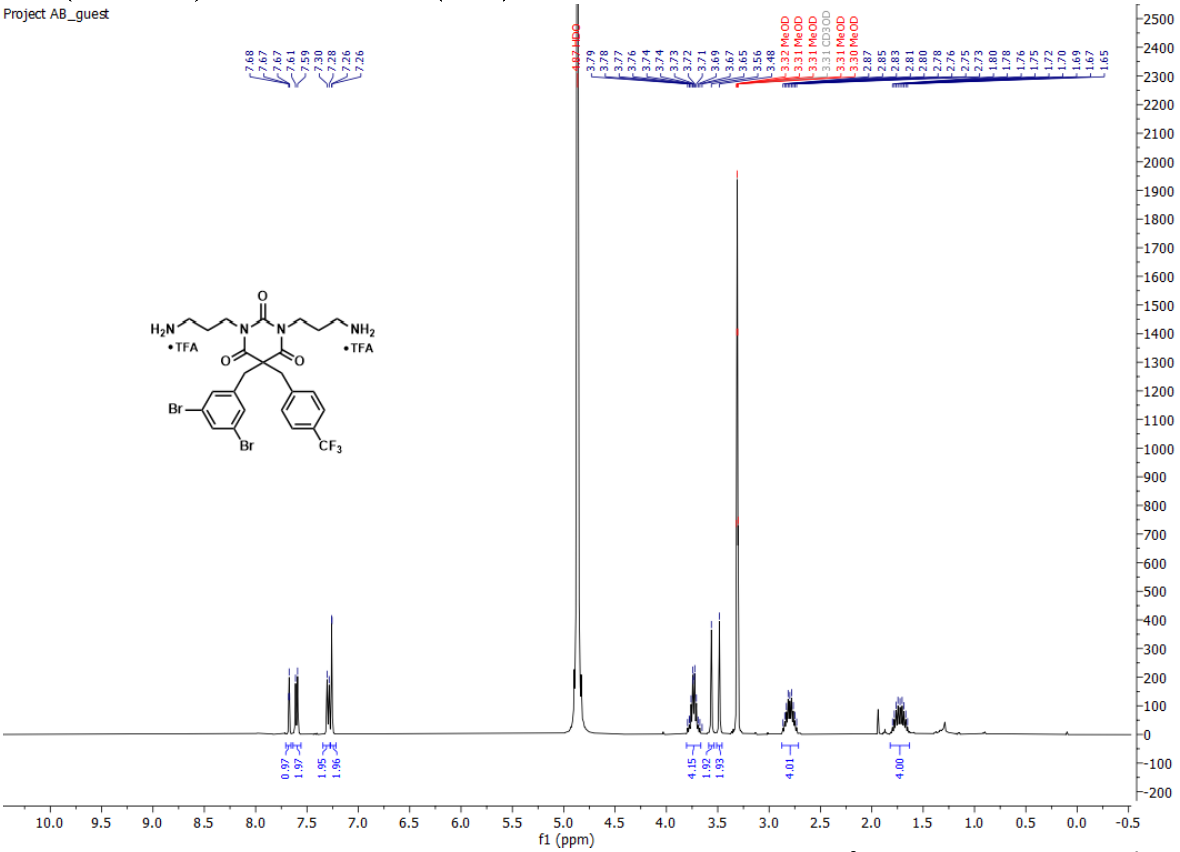

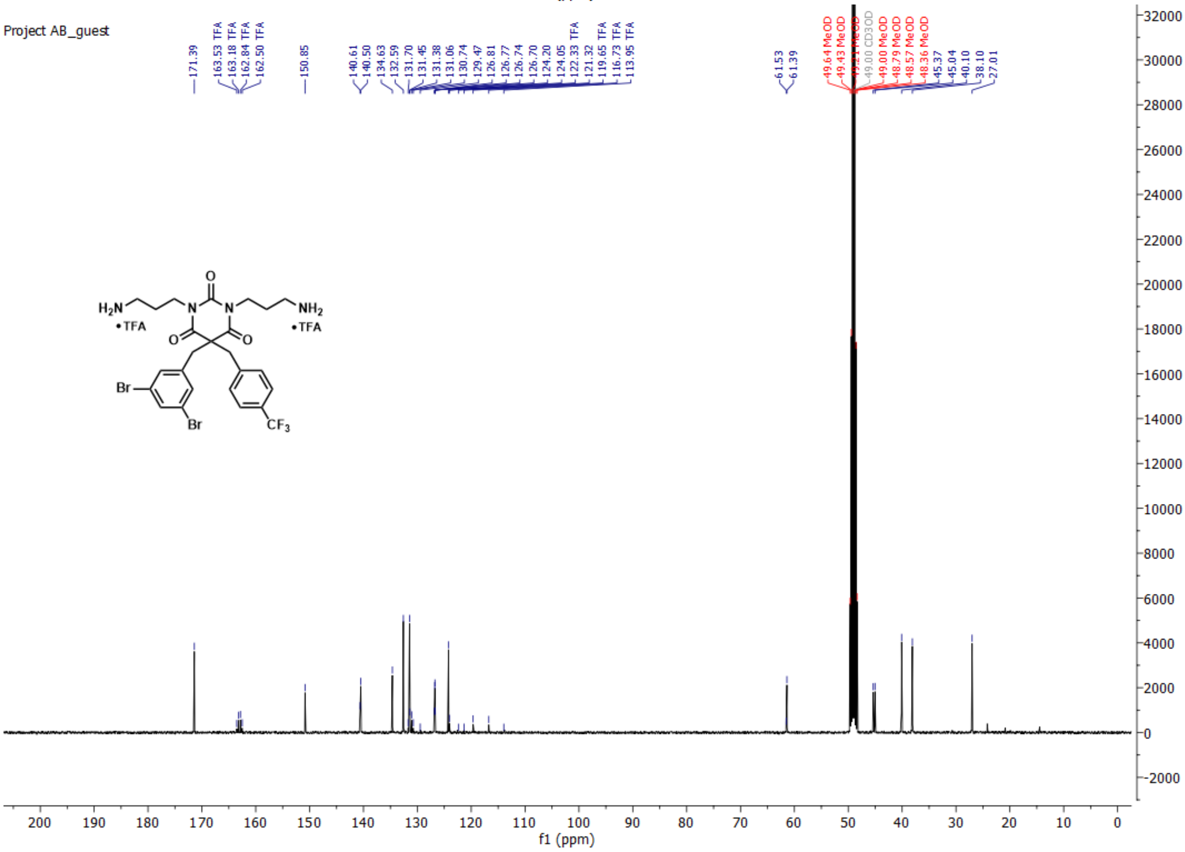

1,3-bis(3-aminopropyl)-5-(4-(*tert*-butyl)benzyl)-5-(3,5-dibromobenzyl)pyrimidine-2,4,6(1*H*,3*H*,5*H*)-trione di-TFA salt (**13pA**)

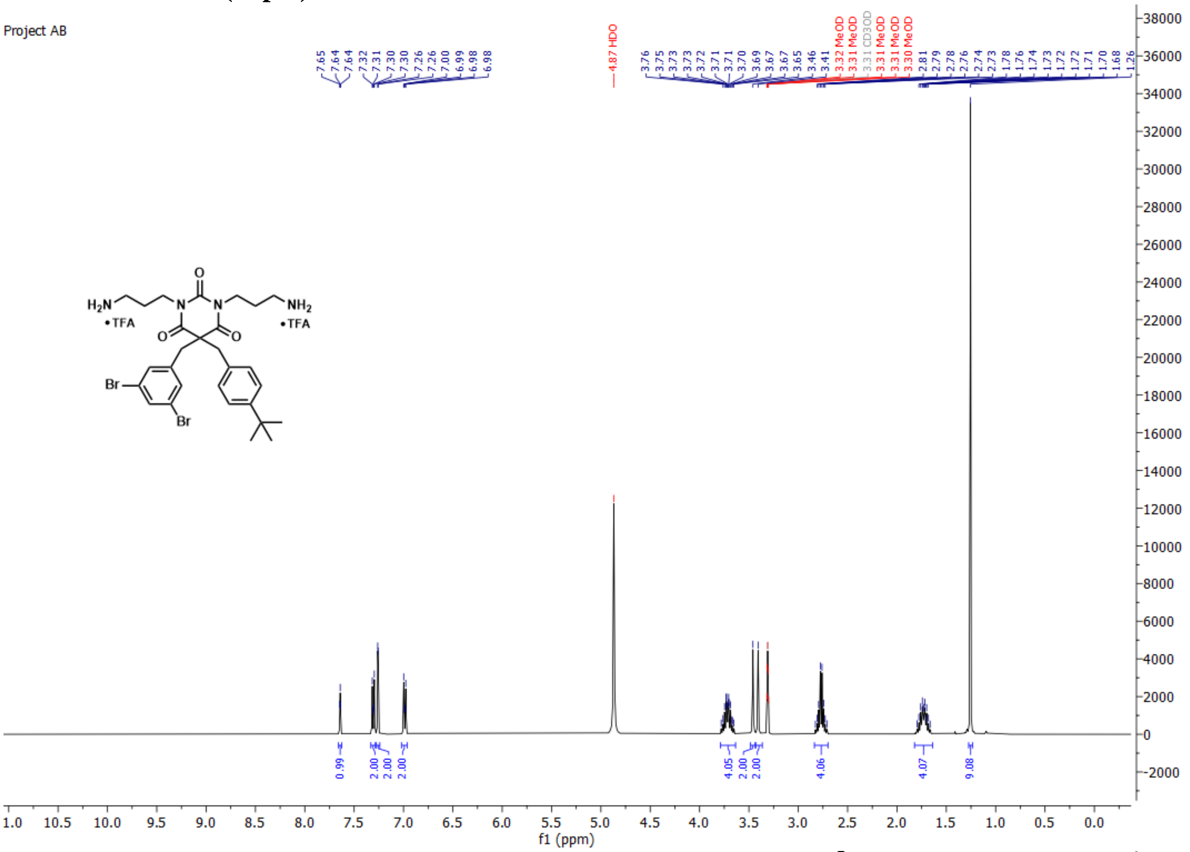

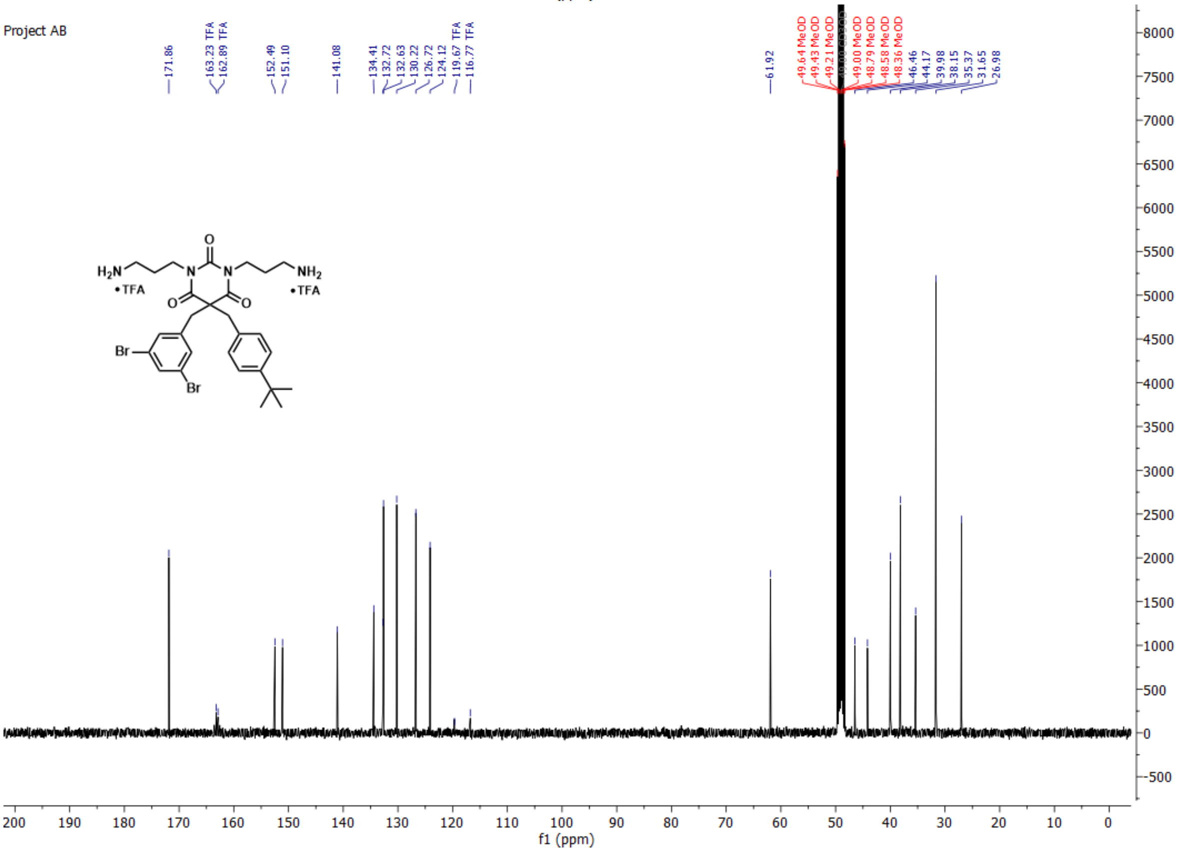

1,1'-((5,5-bis((6-bromoquinolin-2-yl)methyl)-2,4,6-trioxodihydropyrimidine-1,3(2*H*,4*H*)-diyl)bis(propane-3,1-diyl))diguanidine di-TFA salt (**13cG**)

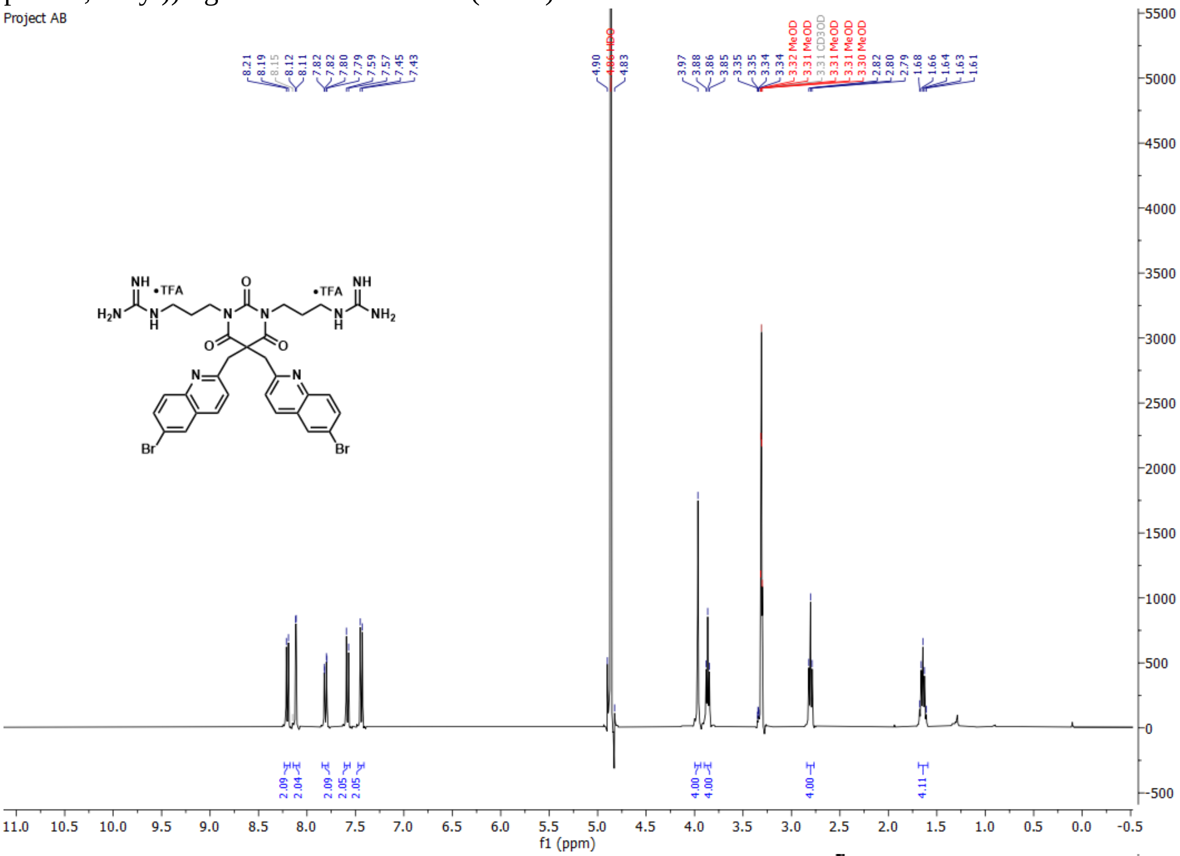

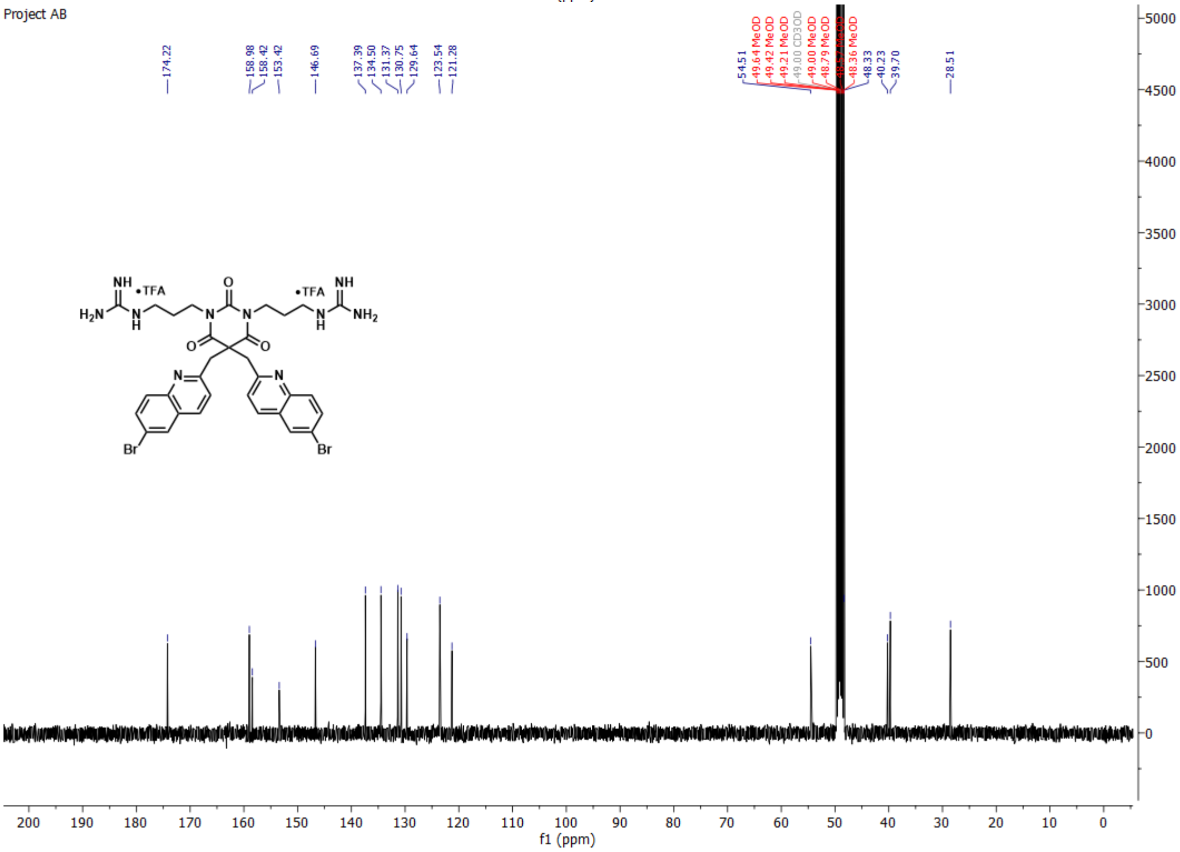

1,1'-((2,4,6-trioxo-5,5-bis(4-(trifluoromethyl)benzyl)dihydropyrimidine-1,3(2*H*,4*H*)-diyl)bis(propane-3,1-diyl))diguanidine di-TFA salt (**13hG**)

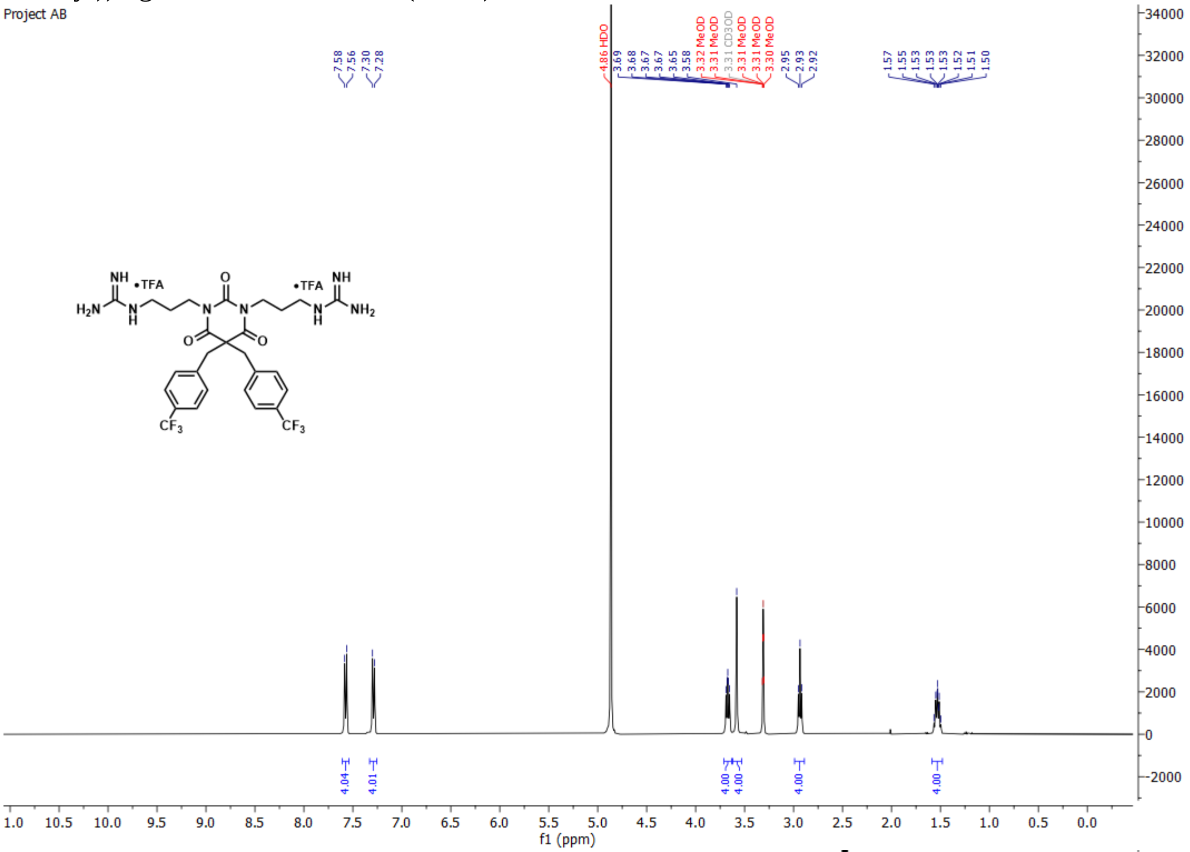

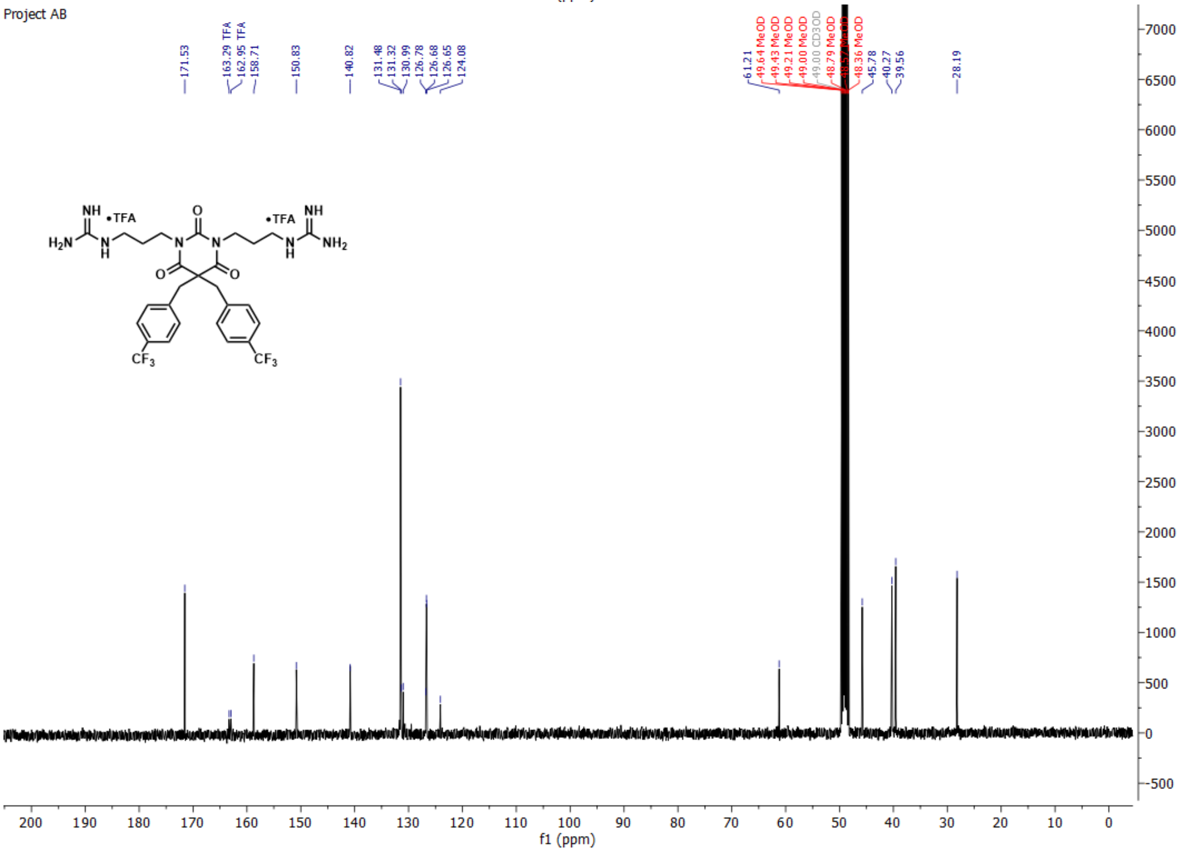

1,1'-((5,5-bis(4-bromo-3-chlorobenzyl)-2,4,6-trioxodihydropyrimidine-1,3(2*H*,4*H*)-diyl)bis(propane-3,1-diyl))diguanidine di-TFA salt (**13iG**)

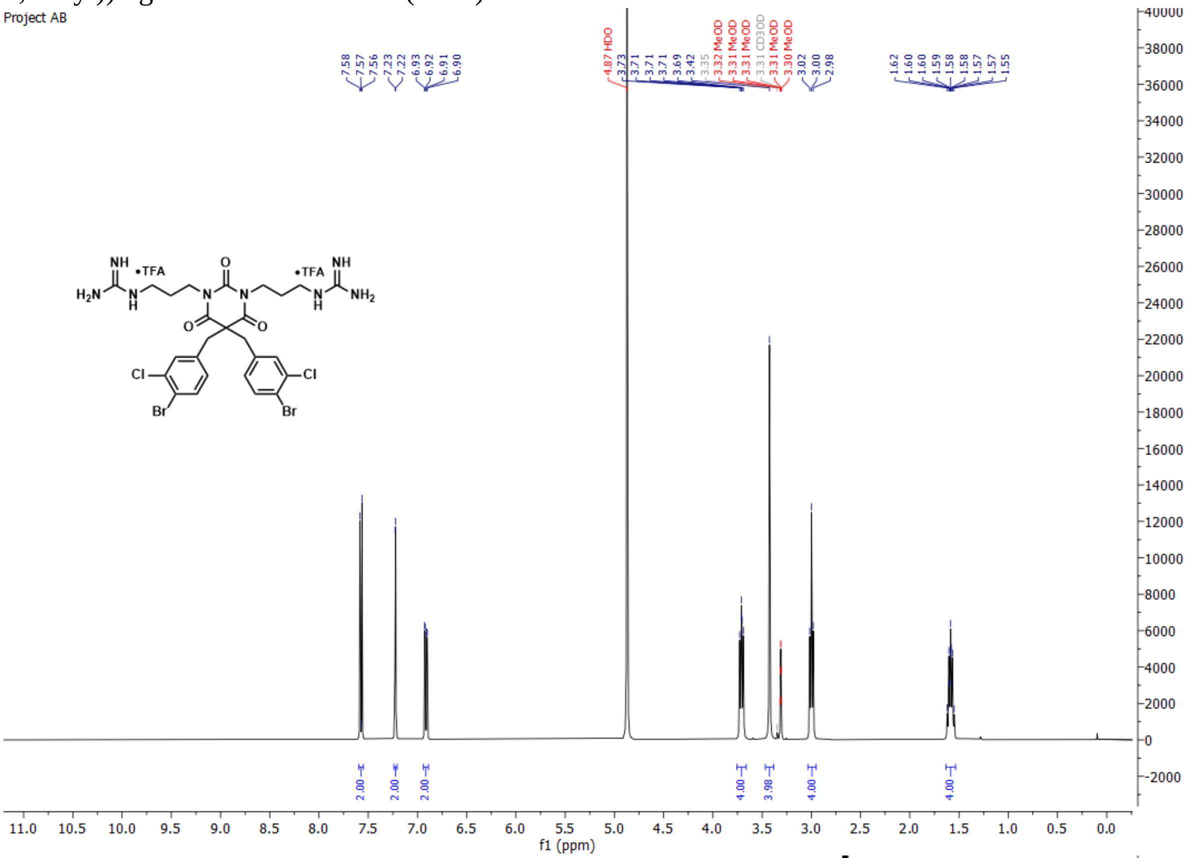

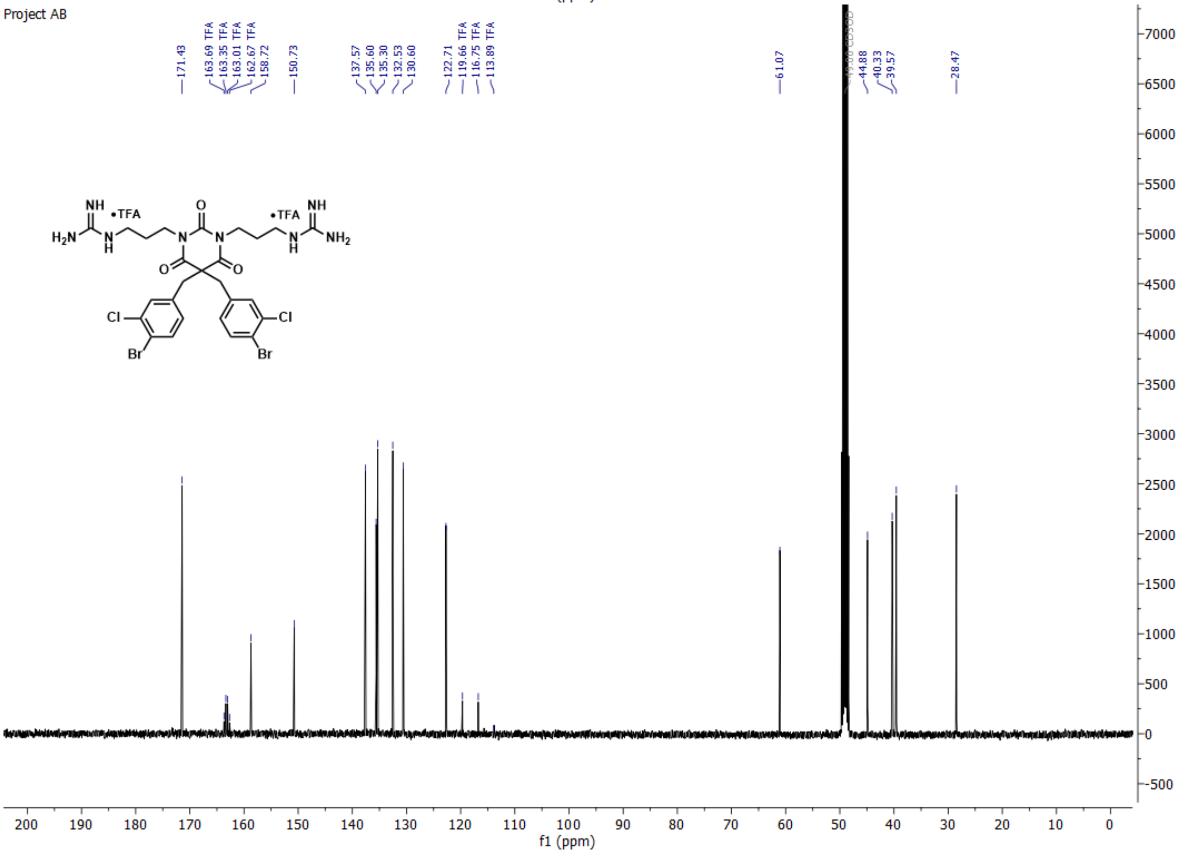

1,1'-((5,5-bis((4-bromonaphthalen-1-yl)methyl)-2,4,6-trioxodihydropyrimidine-1,3(2*H*,4*H*)-diyl)bis(propane-3,1-diyl))diguanidine di-TFA salt (**13eG**)

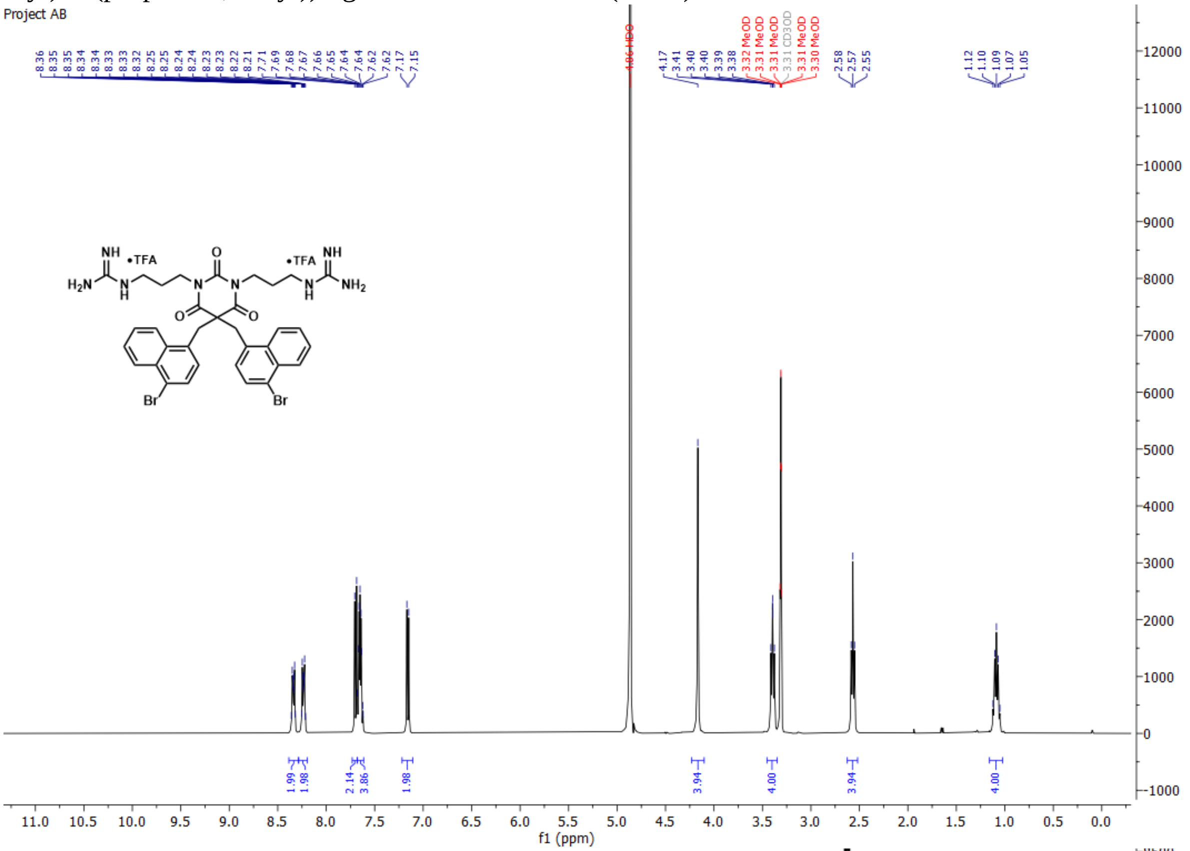

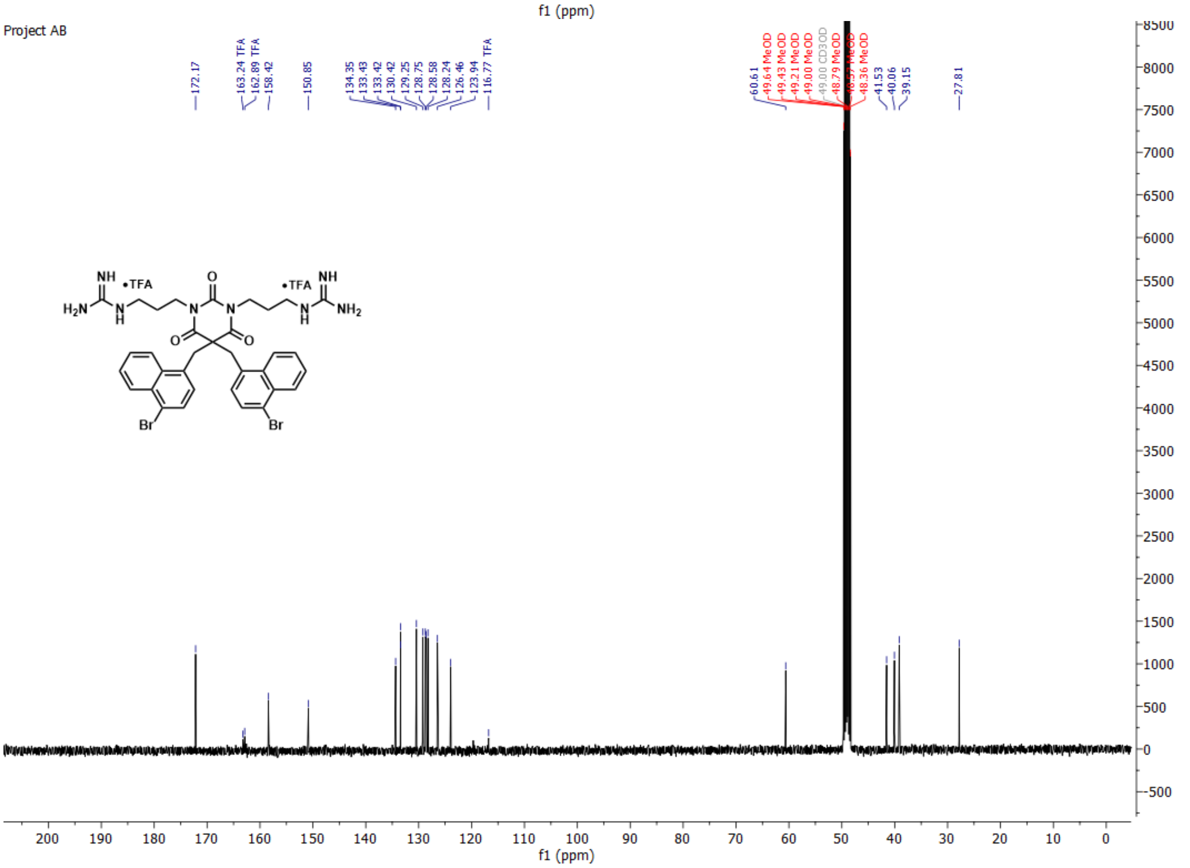

1,1'-((5,5-bis(3,5-bis(trifluoromethyl)benzyl)-2,4,6-trioxodihydropyrimidine-1,3(2*H*,4*H*)-diyl)bis(propane-3,1-diyl))diguanidine di-TFA salt (**13jG**)

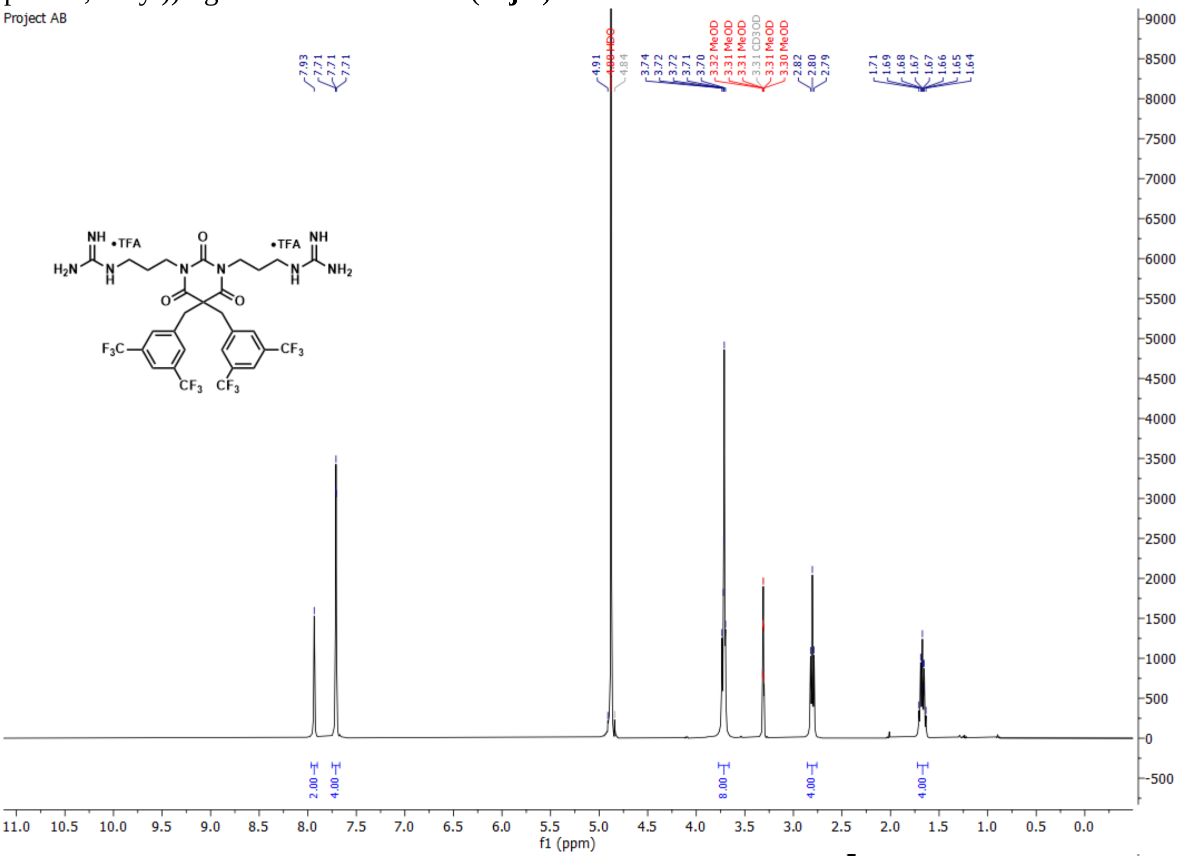

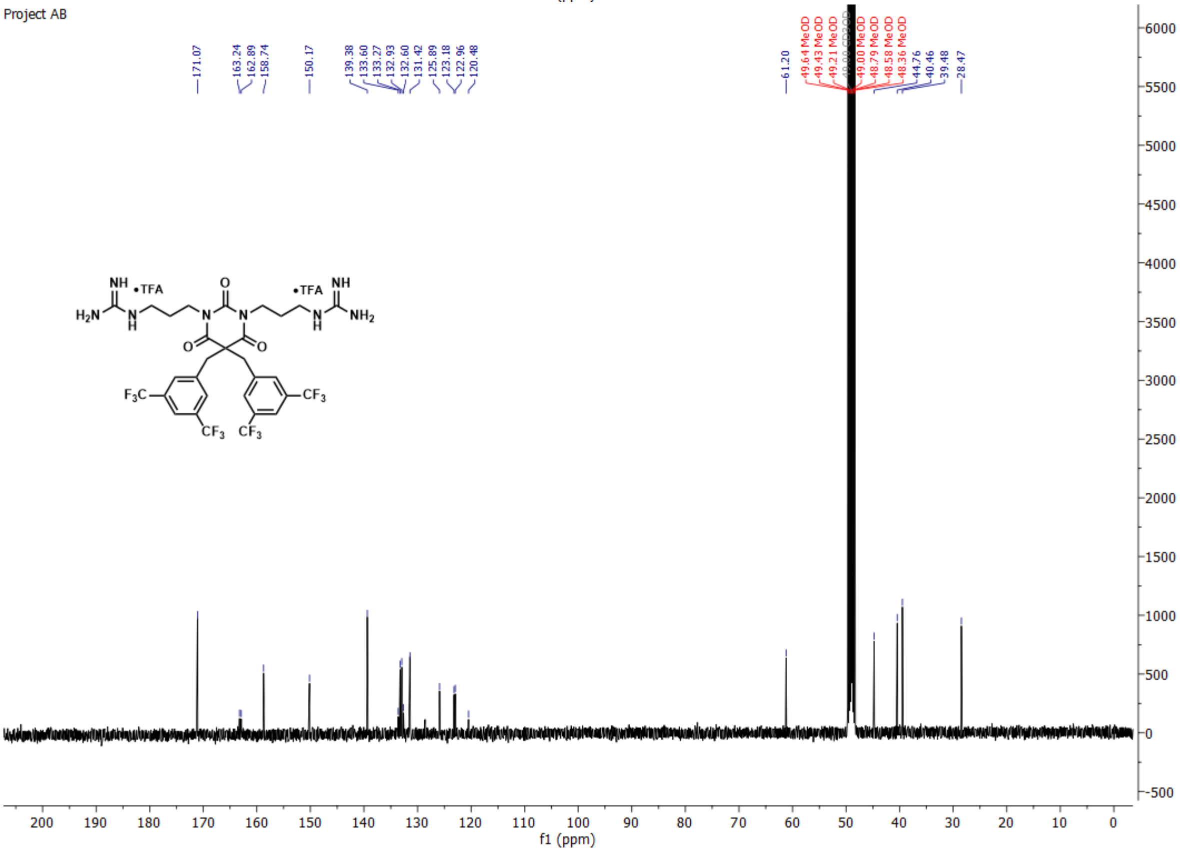

1,1'-((5-(3,5-dibromobenzyl)-2,4,6-trioxo-5-(4-(trifluoromethyl)benzyl)dihydropyrimidine-1,3(2*H*,4*H*)-diyl)bis(propane-3,1-diyl))diguanidine di-TFA salt (**13lG**)

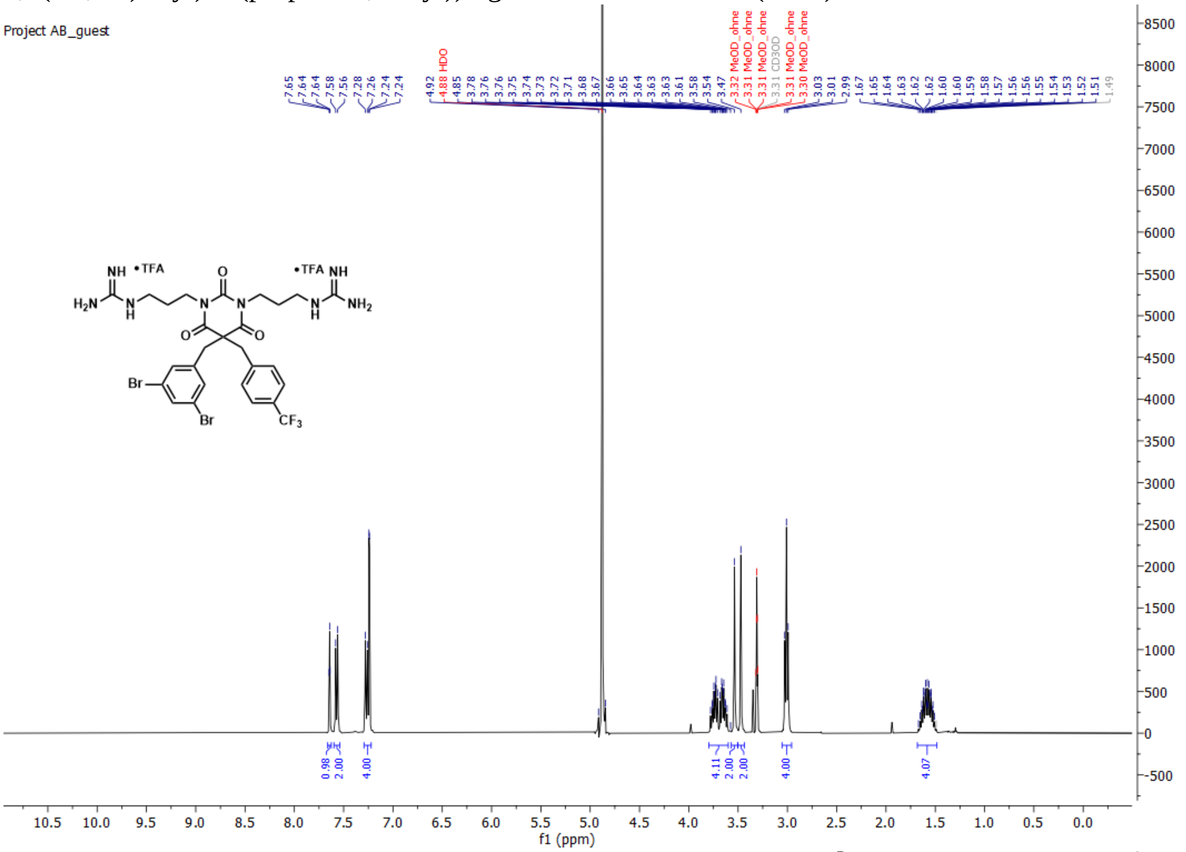

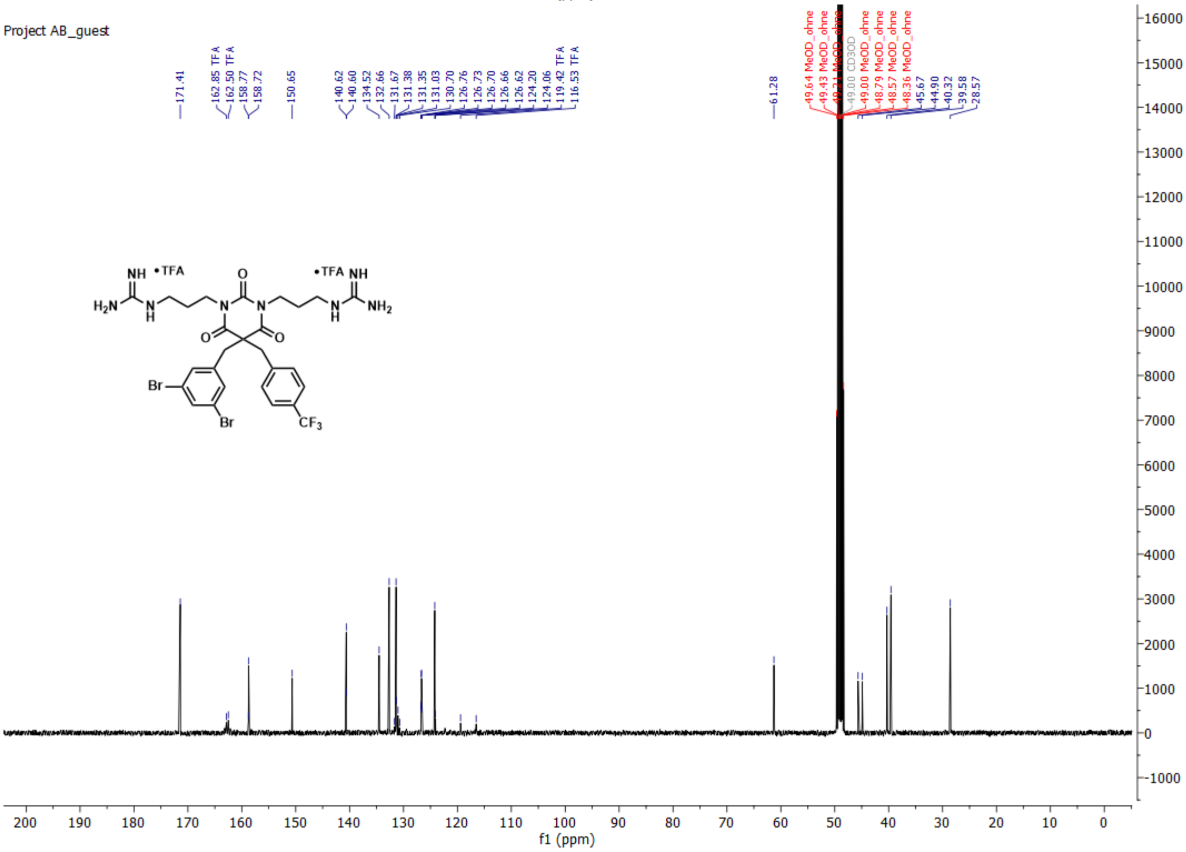

1,1'-((5-(4-(*tert*-butyl)benzyl)-5-(3,5-dibromobenzyl)-2,4,6-trioxodihydropyrimidine-1,3(2*H*,4*H*)-diyl)bis(propane-3,1-diyl))diguanidine di-TFA salt (**13pG**)

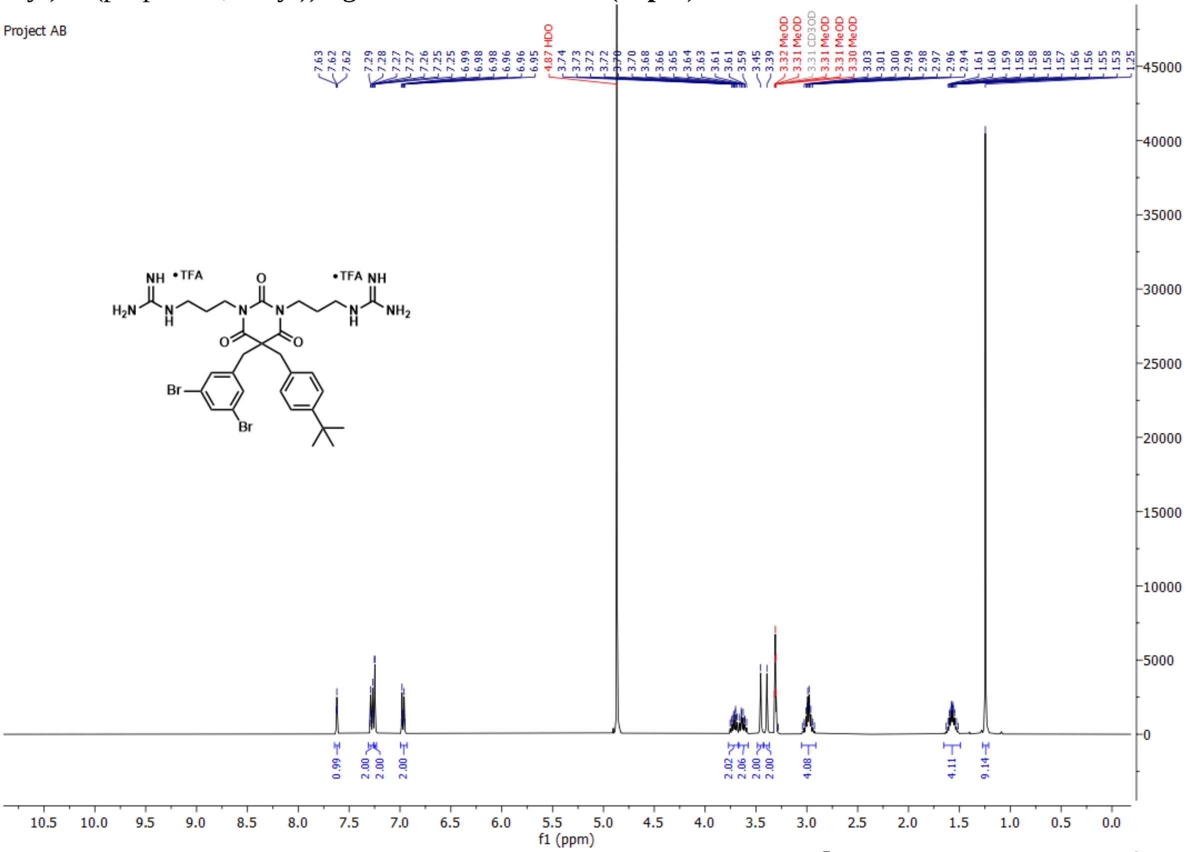

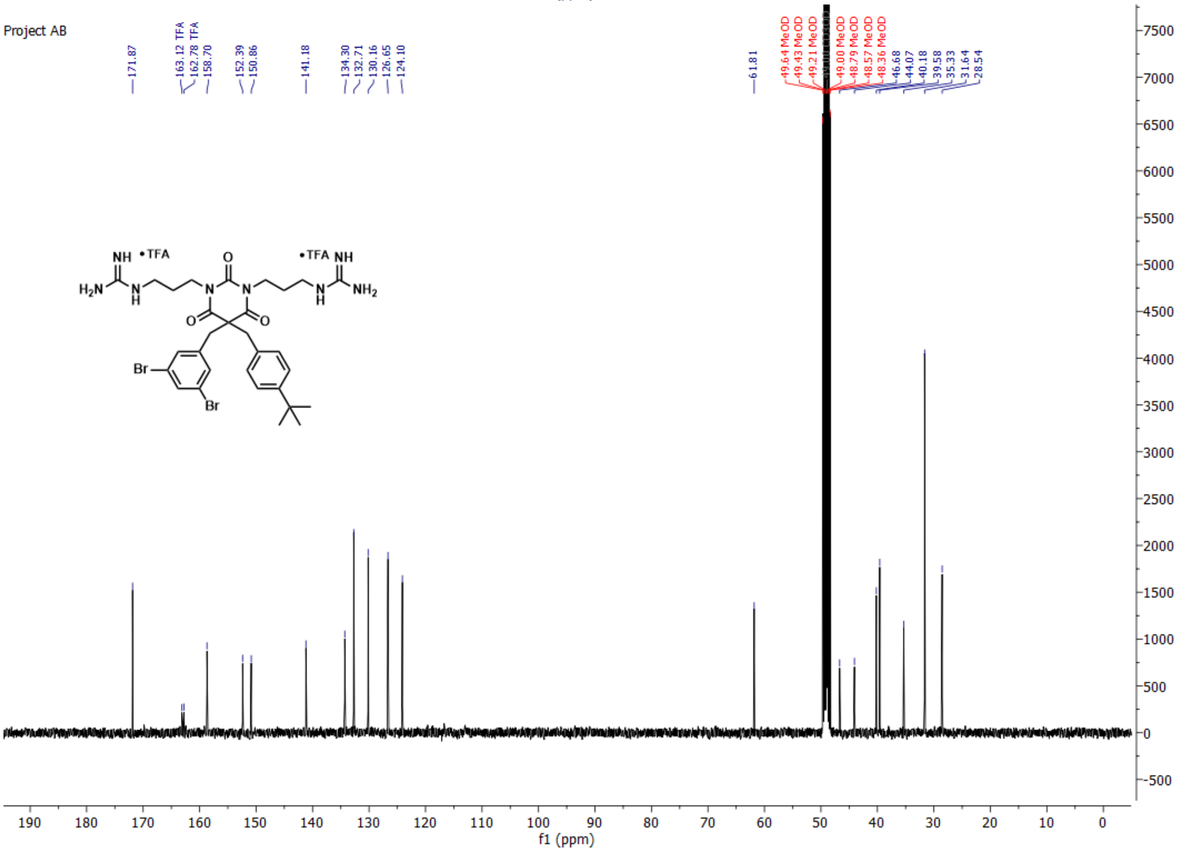

4 SFC analysis of final compounds

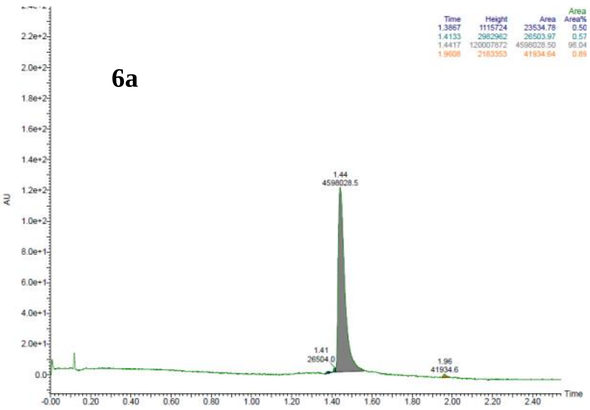

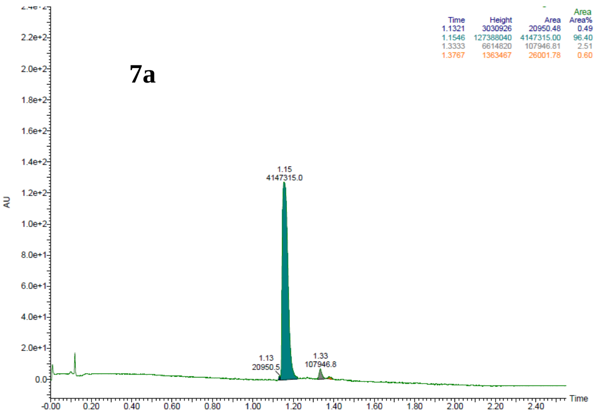

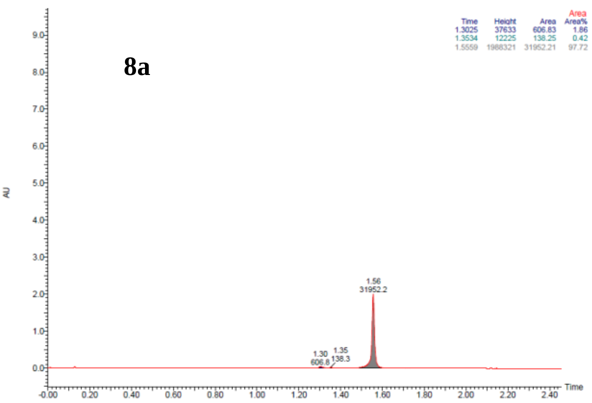

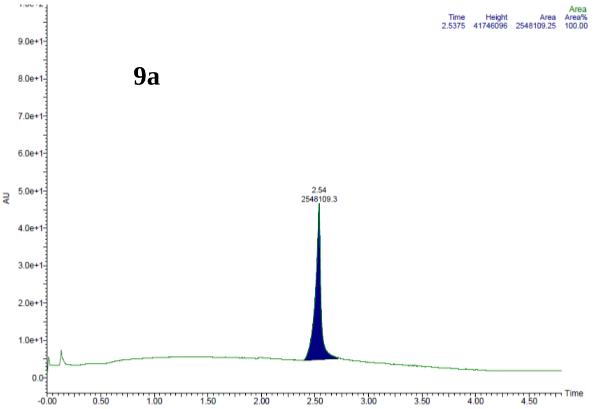

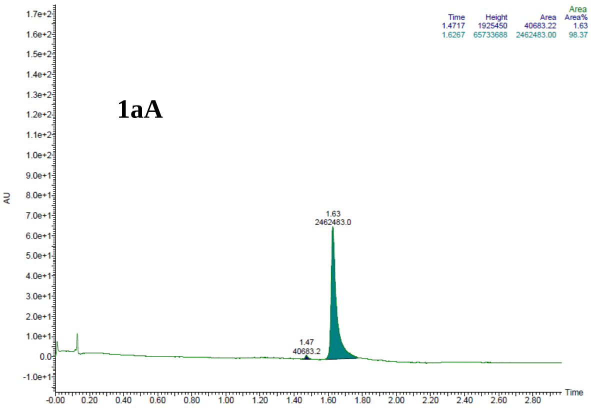

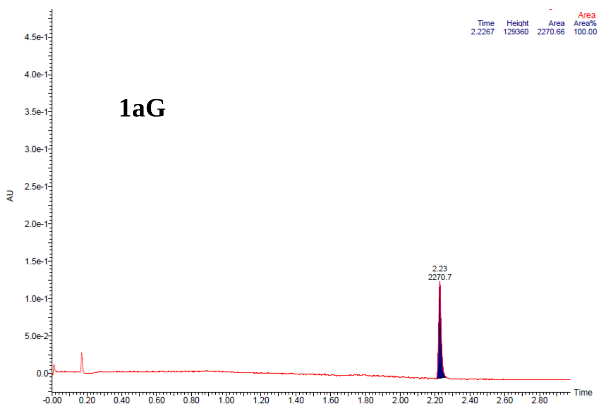

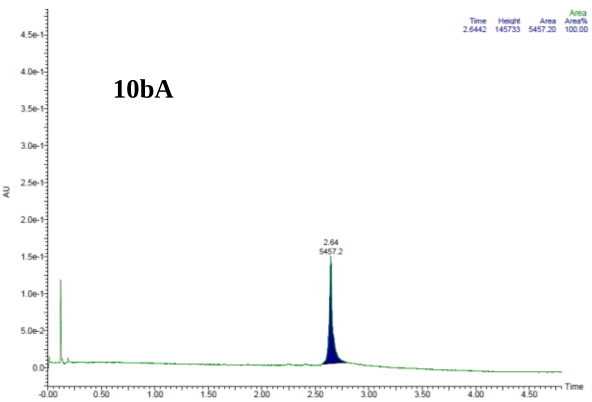

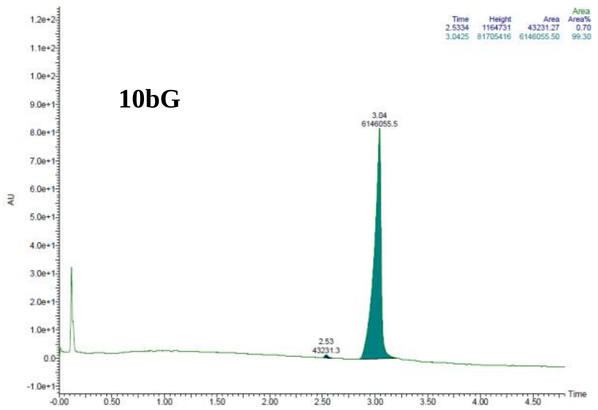

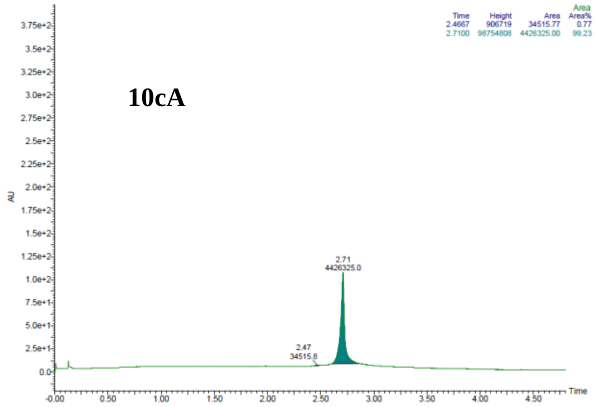

10cA

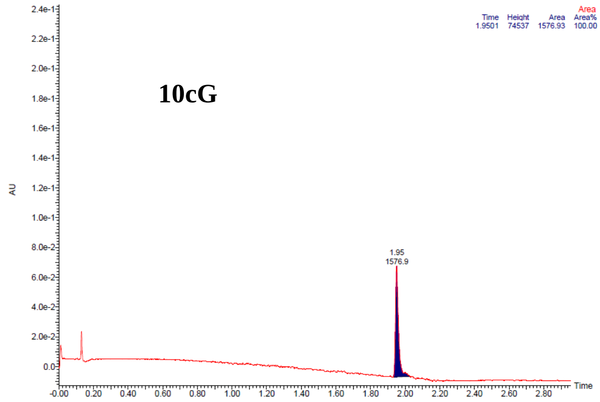

10cG

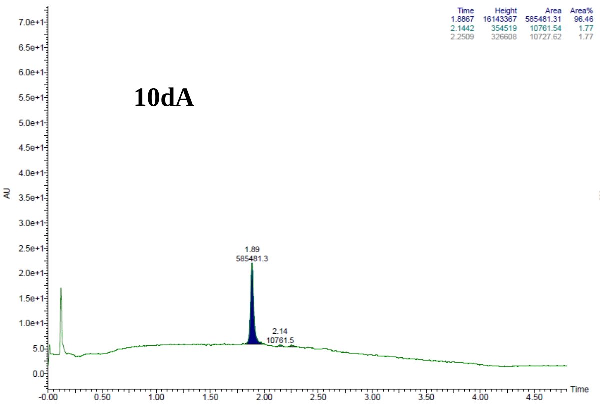

10dA

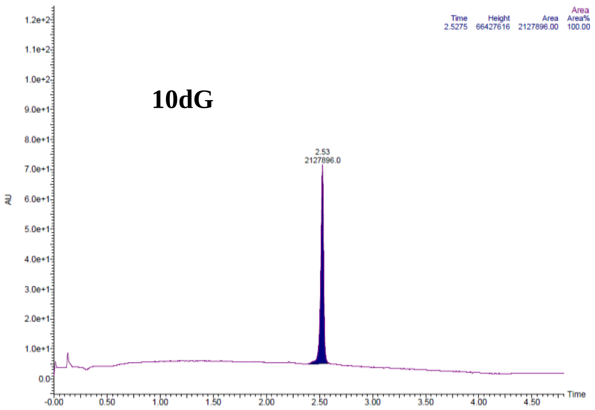

10dG

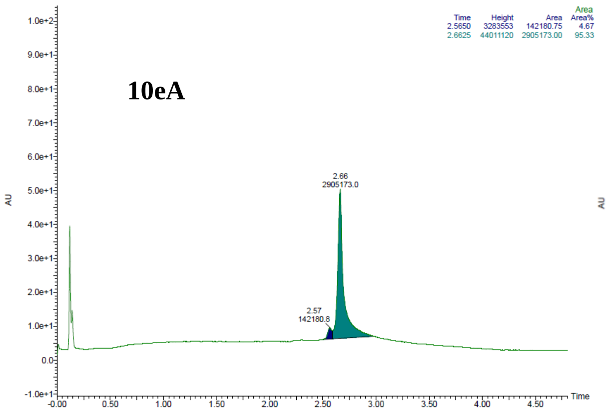

10eA

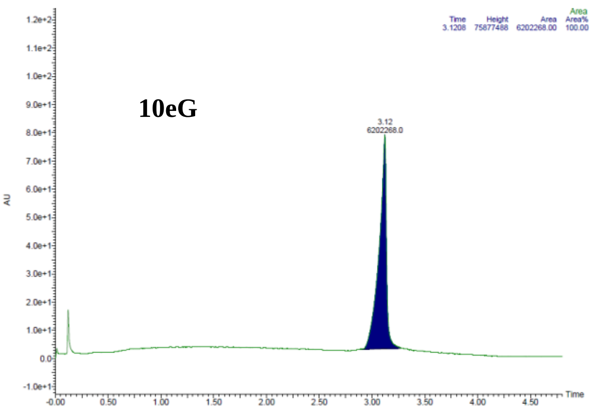

10eG

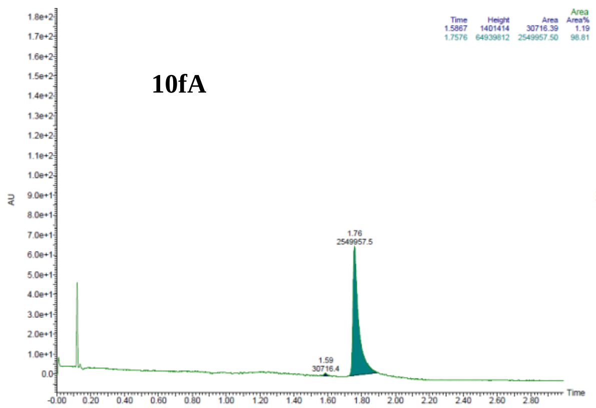

10fA

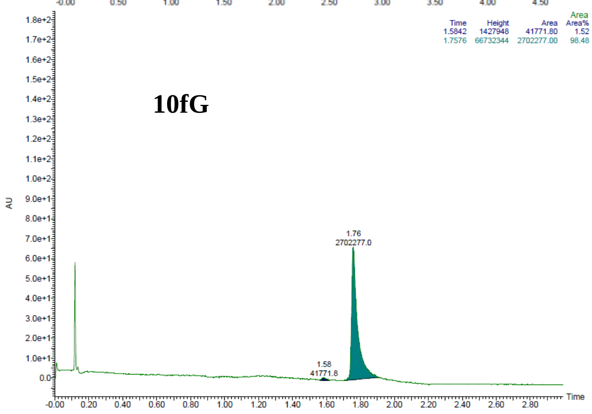

10fG

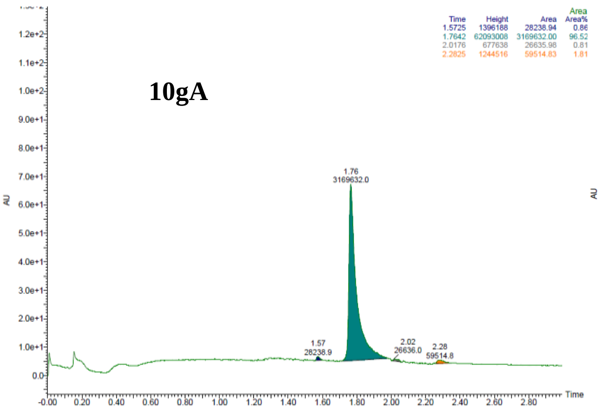
10gA
Time Height Area Area%
1.5725 1396188 28238.94 0.86
1.7642 62093008 3169632.00 96.52
2.0176 677638 26635.98 0.81
2.2825 1244516 59514.83 1.81
1.76 3169632.0
1.57 28238.9
2.02 26636.0
2.28 59514.8
AU
Time

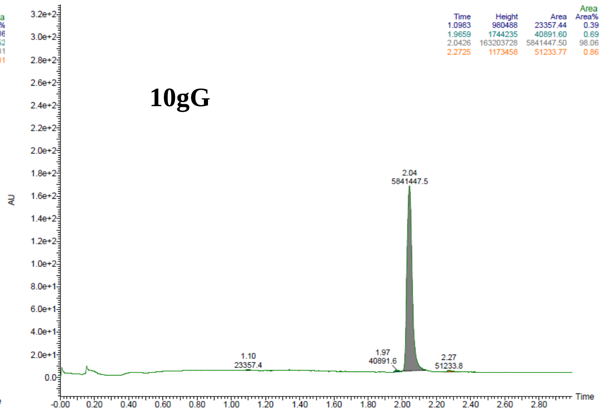
10gG
Time Height Area Area%
1.0983 960488 23357.44 0.39
1.9659 1744235 40891.60 0.69
2.0426 163203728 5841447.50 98.06
2.2725 1173458 51233.77 0.86
2.04 5841447.5
1.10 23357.4
1.97 40891.6
2.27 51233.8
AU
Time

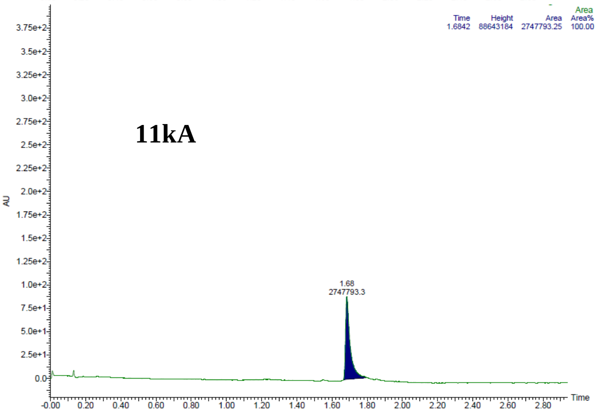
11kA
Time Height Area Area%
1.6842 88643184 2747793.25 100.00
1.68 2747793.3
AU
Time

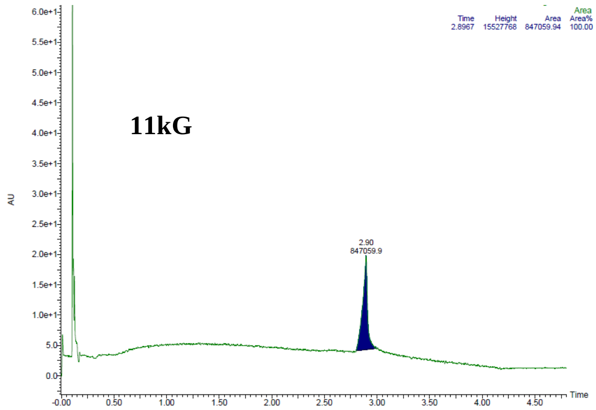
11kG
Time Height Area Area%
2.8967 15527768 847059.94 100.00
2.90 847059.9
AU
Time

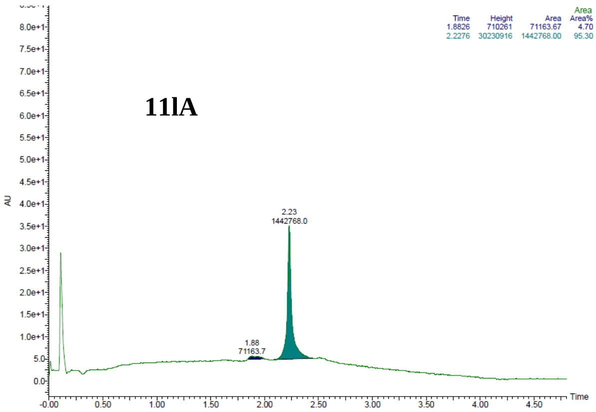
11lA
Time Height Area Area%
1.8826 710261 71163.67 4.70
2.2276 30230916 1442768.00 95.30
2.23 1442768.0
1.88 71163.7
AU
Time

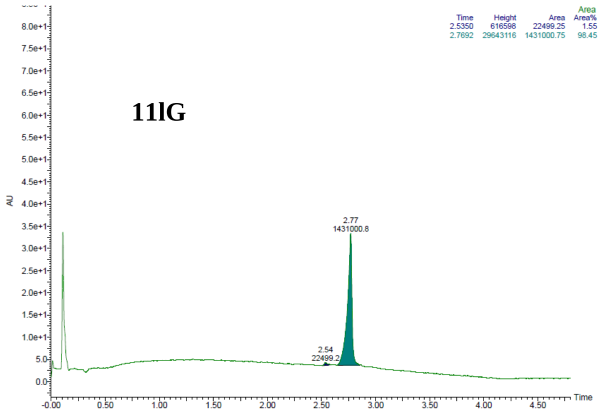
11lG
Time Height Area Area%
2.5350 616598 22499.25 1.55
2.7692 29643116 1431000.75 98.45
2.77 1431000.8
2.54 22499.2
AU
Time

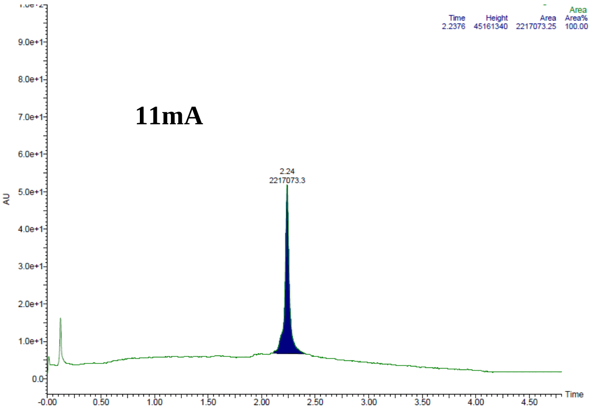
11mA
Time Height Area Area%
2.2376 45161340 2217073.25 100.00
2.24 2217073.3
AU
Time

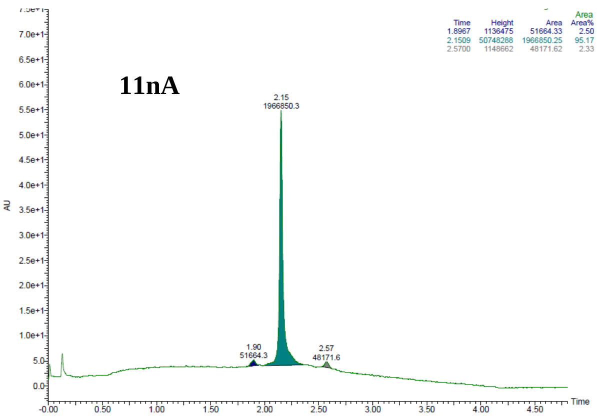
11nA
2.15
1966850.3
1.90
51664.3
2.57
48171.6
AU
Time

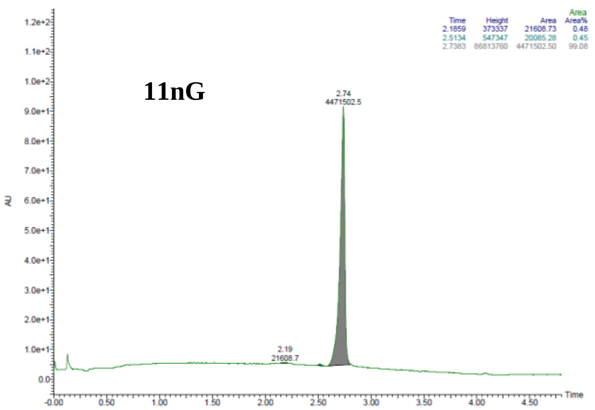
11nG
2.74
4471502.5
2.19
21608.7
AU
Time

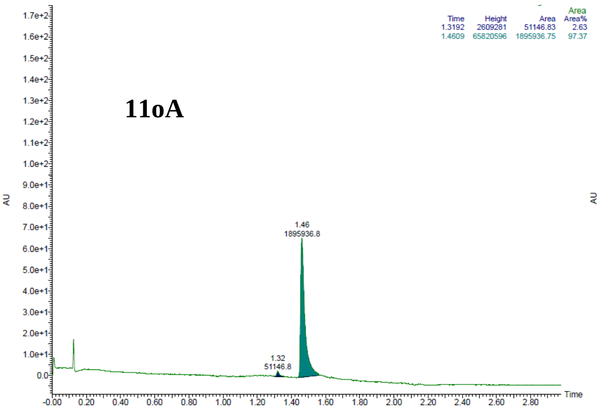
11oA
1.46
1895936.8
1.32
51146.8
AU
Time

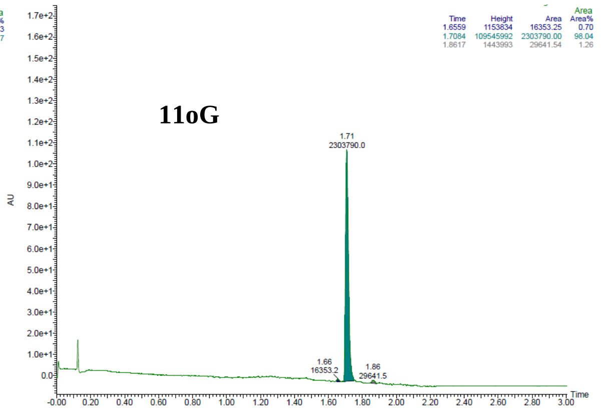
11oG
1.71
2303790.0
1.66
16353.2
1.86
29641.5
AU
Time

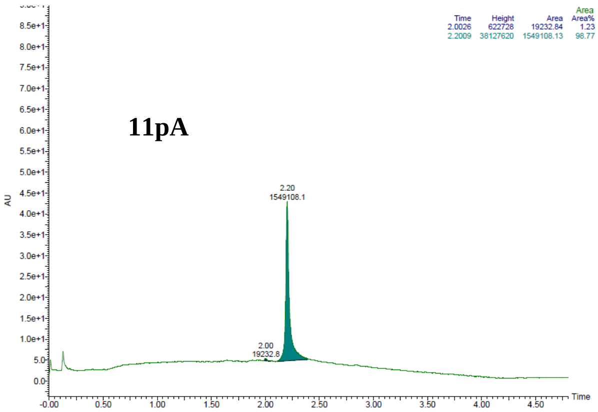
11pA
2.20
1549108.1
2.00
19232.8
AU
Time

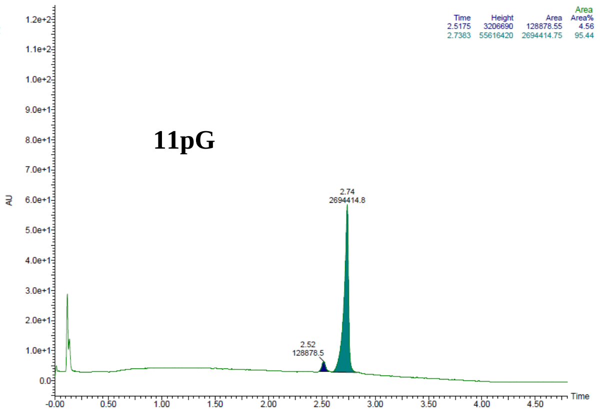
11pG
2.74
2694414.8
2.52
128878.5
AU
Time

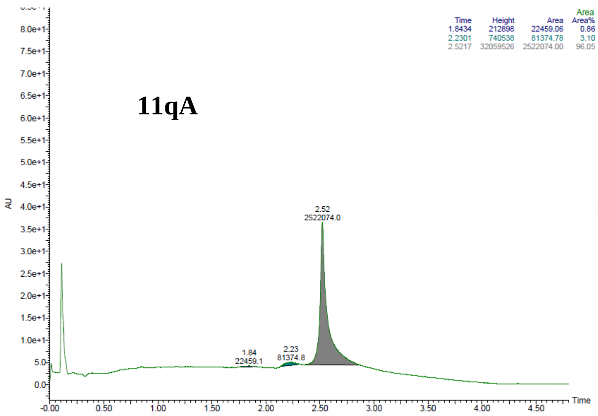
11qA
2.52
2522074.0
1.84
22459.1
2.23
81374.8
AU
Time

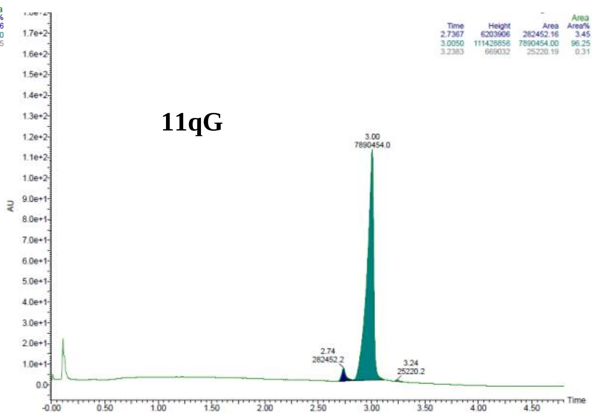
11qG
3.00
7890454.0
2.74
282452.2
3.24
25220.2
AU
Time

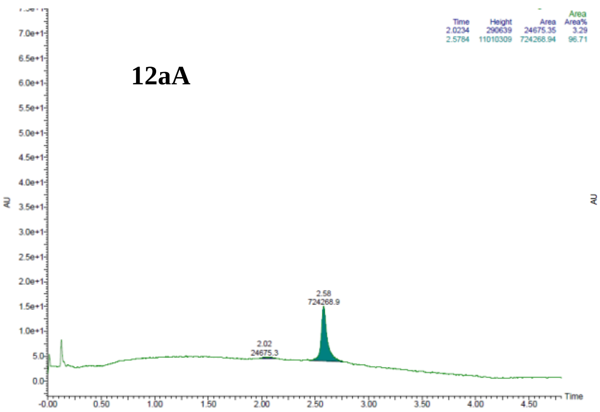
12aA
Time Height Area Area%
2.0234 290639 24675.35 3.29
2.5784 11010309 724268.94 96.71
2.58
724268.9
2.02
24675.3

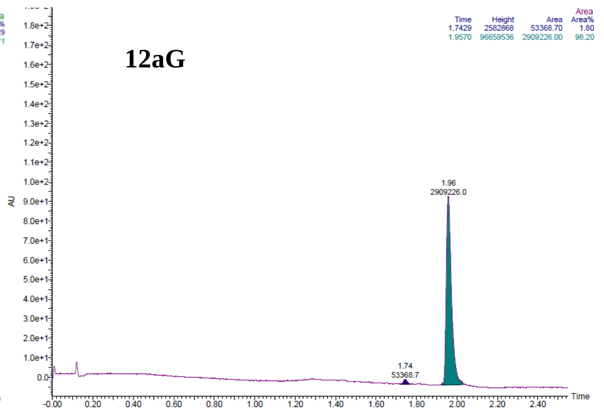
12aG
Time Height Area Area%
1.7429 2582868 53368.70 1.80
1.9570 96659536 2909226.00 98.20
1.96
2909226.0
1.74
53368.7

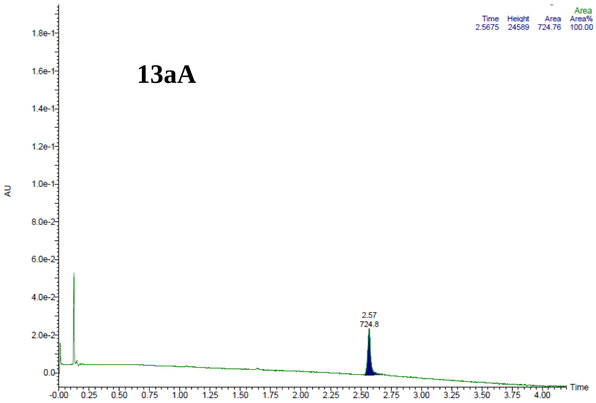
13aA
Time Height Area Area%
2.5675 24589 724.76 100.00
2.57
724.8

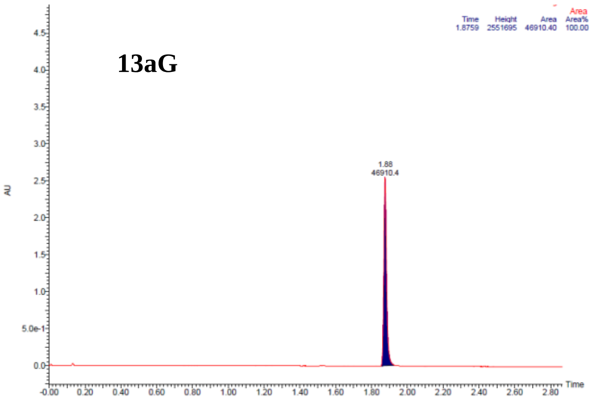
13aG
Time Height Area Area%
1.8759 2551695 46910.40 100.00
1.88
46910.4

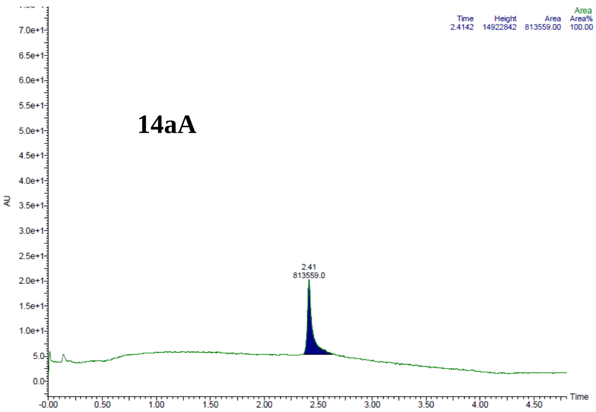
14aA
Time Height Area Area%
2.4142 14922842 813559.00 100.00
2.41
813559.0

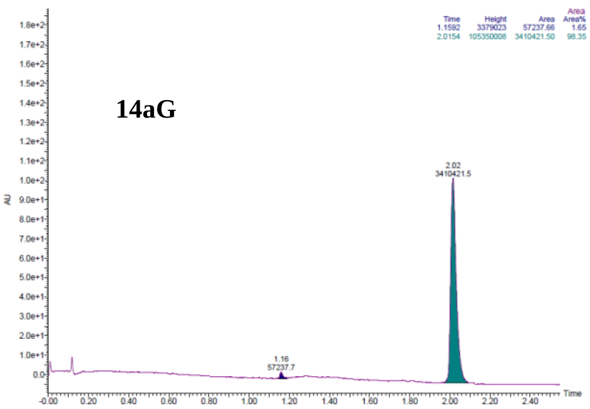
14aG
Time Height Area Area%
1.1592 3379023 57237.66 1.65
2.0154 105350008 3410421.50 98.35
2.02
3410421.5
1.16
57237.7

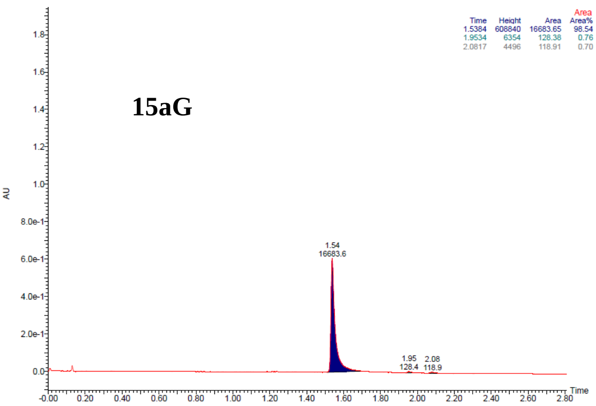
15aG
Time Height Area Area%
1.5384 608840 16683.65 98.54
1.9534 6354 128.38 0.76
2.0817 4496 118.91 0.70
1.54
16683.6
1.95
128.4
2.08
118.9

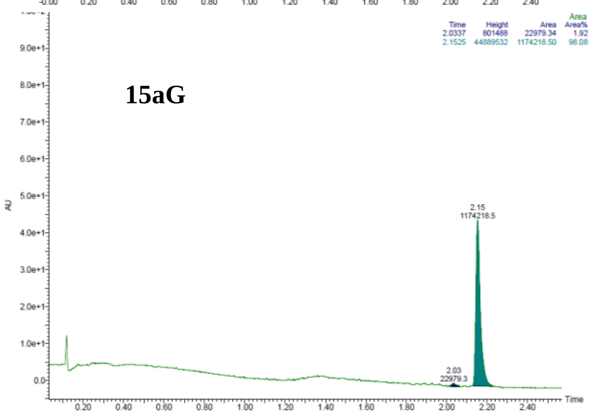
15aG
Time Height Area Area%
2.0337 801488 22979.34 1.92
2.1525 44889532 1174218.50 98.08
2.15
1174218.5
2.03
22979.3

16aA

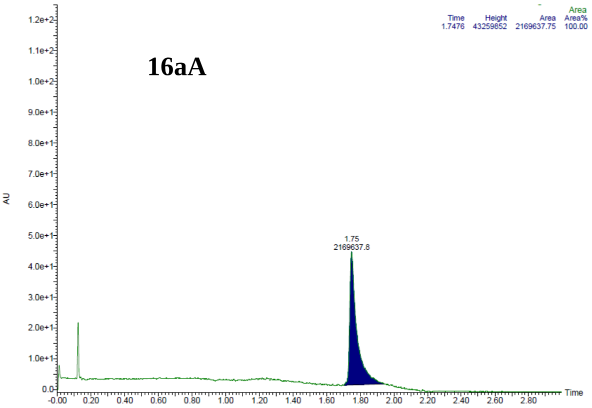

16aG

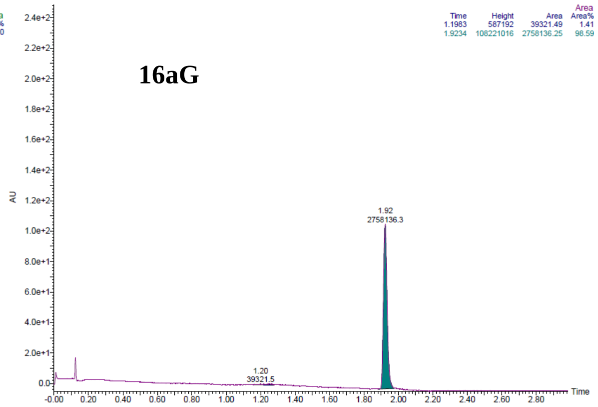

17aA

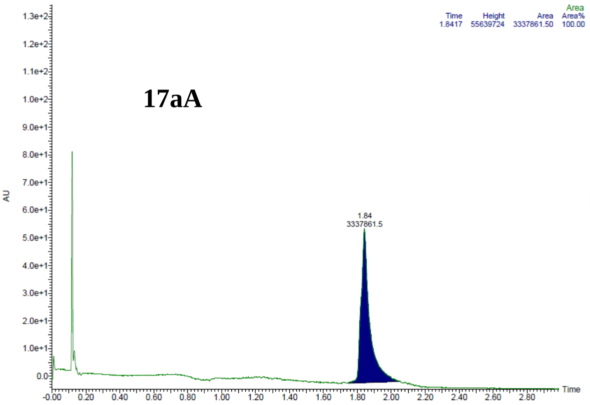

17aG

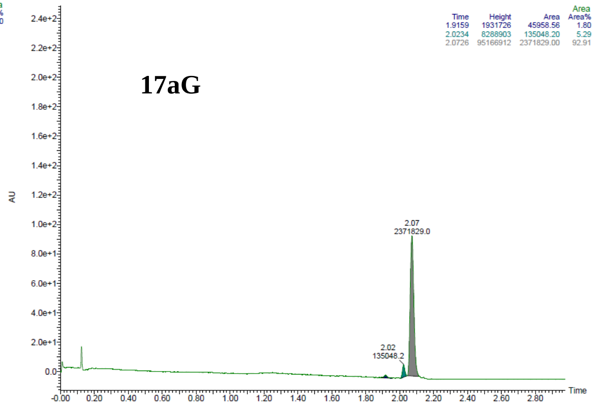

18aA

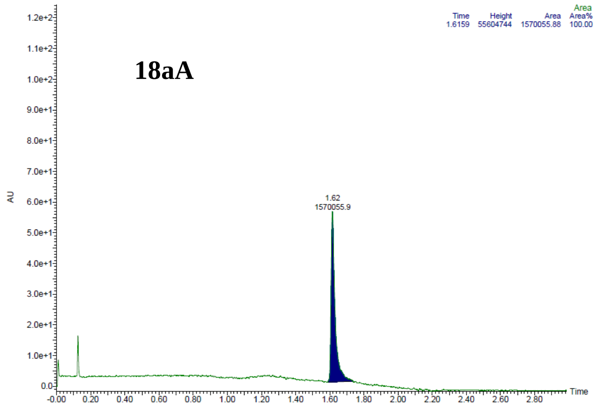

18aG

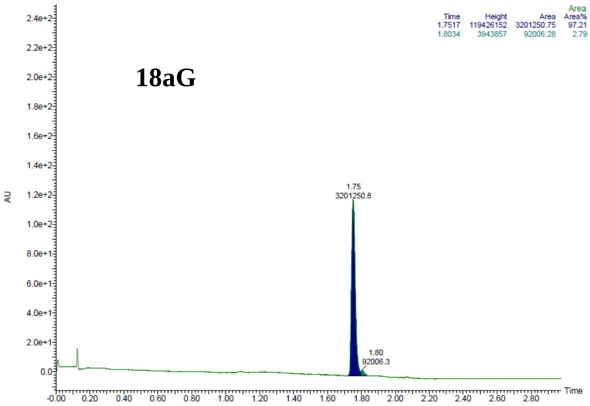

19aA

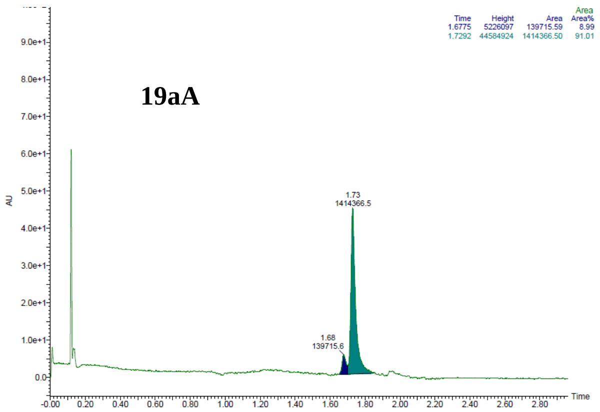

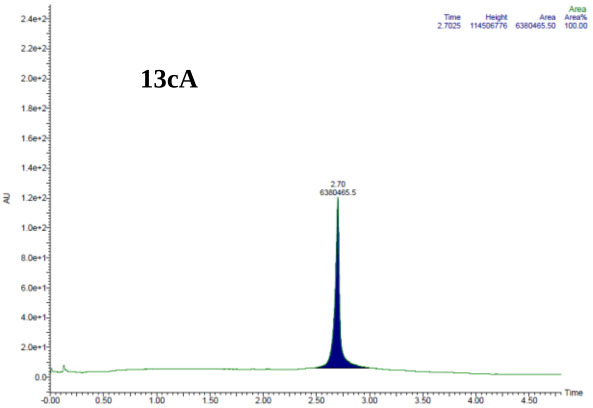
13cA
Time Height Area Area%
2.7025 114506776 6380465.50 100.00
2.70
6380465.5
AU
Time

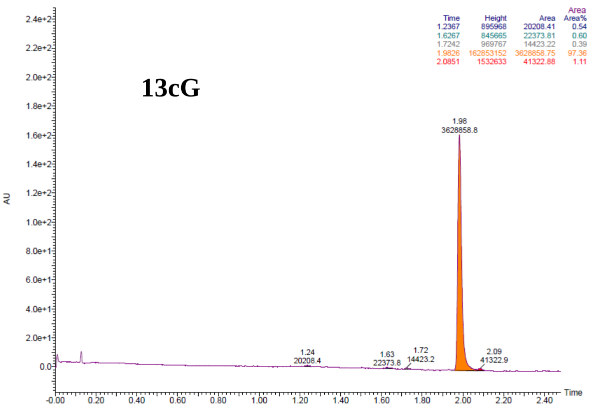
13cG
Time Height Area Area%
1.2367 895968 20208.41 0.54
1.6267 845665 22373.81 0.60
1.7242 969767 14423.22 0.39
1.9826 162853152 3628858.75 97.36
2.0851 1532633 41322.88 1.11
1.98
3628858.8
1.24
20208.4
1.63
22373.8
1.72
14423.2
2.09
41322.9
AU
Time

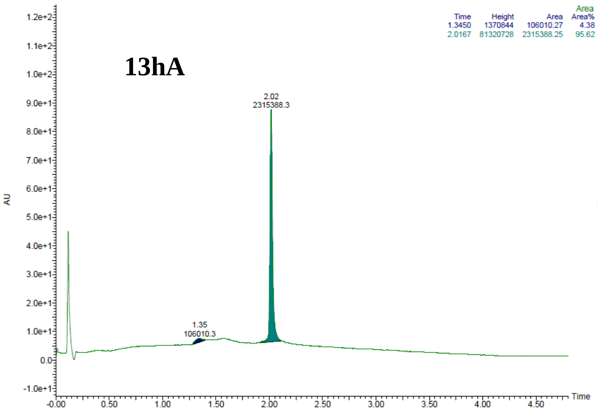
13hA
Time Height Area Area%
1.3450 1370844 106010.27 4.38
2.0167 81320728 2315388.25 95.62
2.02
2315388.3
1.35
106010.3
AU
Time

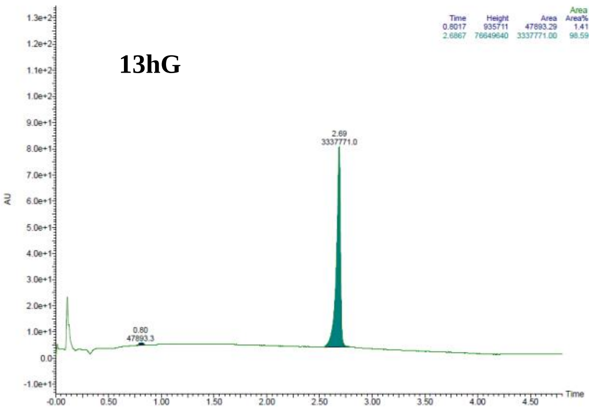
13hG
Time Height Area Area%
0.8017 935711 47893.29 1.41
2.6867 76649640 3337771.00 98.59
2.69
3337771.0
0.80
47893.3
AU
Time

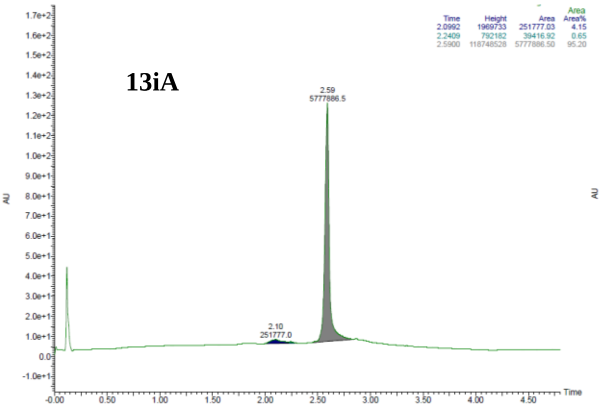
13iA
Time Height Area Area%
2.0992 1969733 251777.03 4.15
2.2409 792182 39416.92 0.65
2.5900 118748528 5777886.50 95.20
2.59
5777886.5
2.10
251777.0
AU
Time

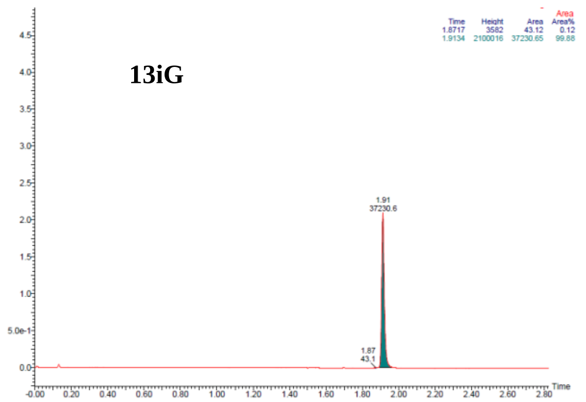
13iG
Time Height Area Area%
1.8717 3582 43.12 0.12
1.9134 2100016 37230.65 99.88
1.91
37230.6
1.87
43.1
AU
Time

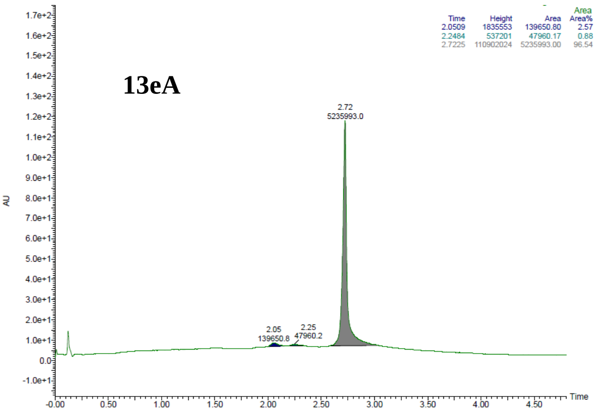
13eA
Time Height Area Area%
2.0509 1835553 139650.80 2.57
2.2484 537201 47960.17 0.88
2.7225 110902024 5235993.00 96.54
2.72
5235993.0
2.05
139650.8
2.25
47960.2
AU
Time

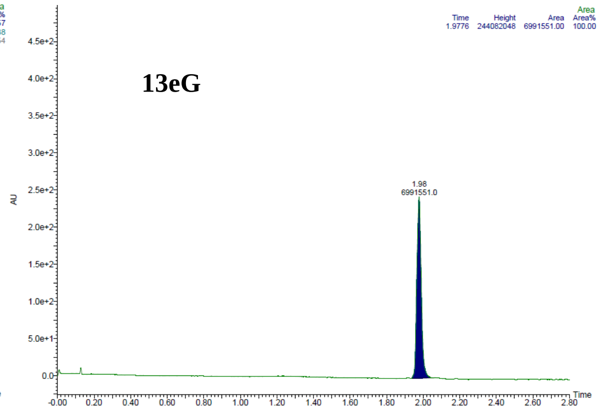
13eG
Time Height Area Area%
1.9776 244082048 6991551.00 100.00
1.98
6991551.0
AU
Time

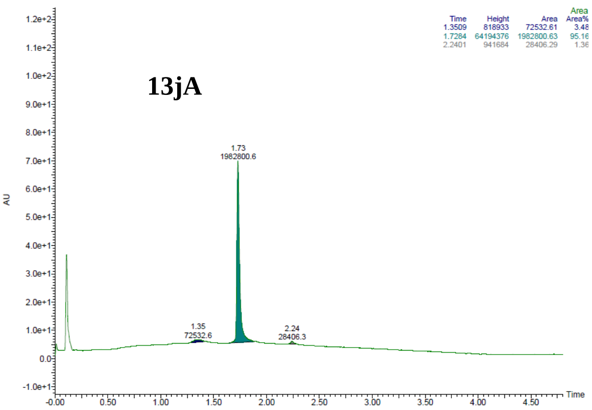
13jA
Time Height Area Area%
1.3509 818933 72532.61 3.48
1.7284 64194376 1982800.63 95.16
2.2401 941684 28406.29 1.36

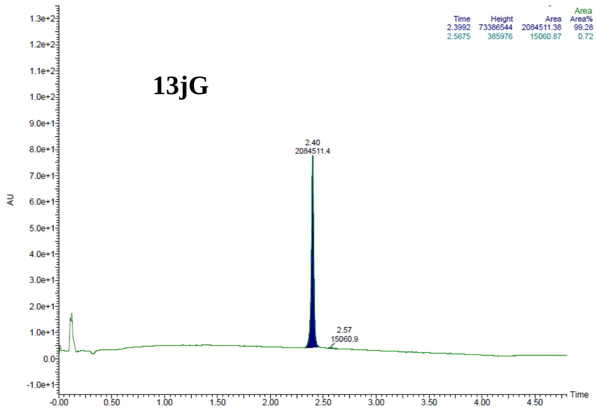
13jG
Time Height Area Area%
2.3992 73386544 2084511.38 99.28
2.5675 385976 15060.87 0.72

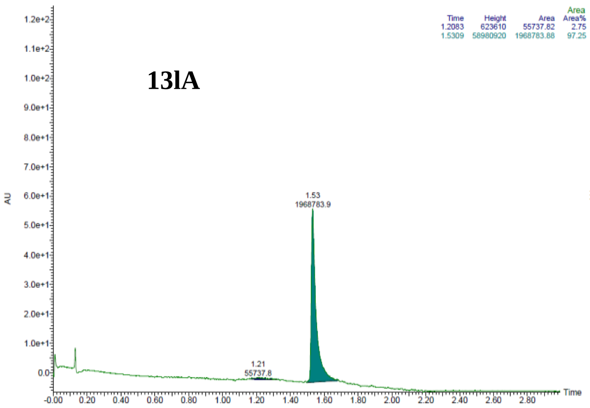
13lA
Time Height Area Area%
1.2083 623610 55737.82 2.75
1.5309 58980920 1968783.88 97.25

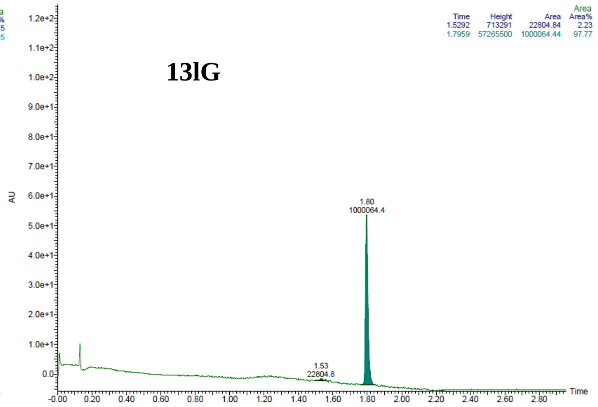
13lG
Time Height Area Area%
1.5292 713291 22804.84 2.23
1.7959 57265500 1000064.44 97.77

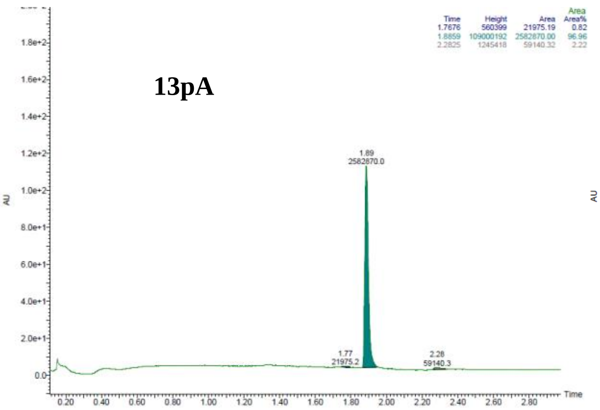
13pA
Time Height Area Area%
1.7676 560399 21975.19 0.82
1.8859 109000192 2582870.00 96.96
2.2825 1245418 59140.32 2.22

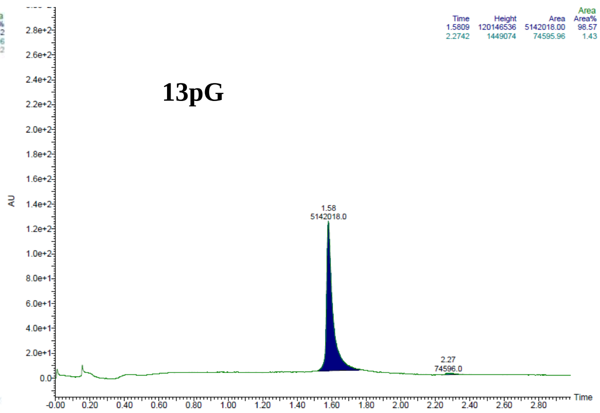
13pG
Time Height Area Area%
1.5809 120146536 5142018.00 98.57
2.2742 1449074 74595.96 1.43

5 Full selectivity index table

Table S1 Selectivity index (SI) of all compounds towards all bacterial strains tested. EC_{50} values are given in [µg/mL].

Code	Basic group	X	SI (MIC/EC_{50})[a] S. a	B. s	E. c	P. a	EC_{50}
6a	(N(Me)H)	*n*-butyl	9	18	9	5	73
7a	(NMe_2)	*n*-butyl	20	39	20	–	157
8a	(NMe_3)	*n*-butyl	>135	>67	–	–	>539
9a	(pyridinyl)	*n*-butyl	>280	>140	>70	–	>559
1aA	NH_2	*n*-butyl	20	40	20	10	79
1aG	guanidyl	*n*-butyl	31	31	31	8	62

Code	R[1]	X	SI (MIC/EC_{50})[a] S. a	B. s	E. c	P. a	EC_{50}	Code	SI (MIC/EC_{50})[a] S. a	B. s	E. c	P. a	EC_{50}
10bA	(2-methylquinoline)	*n*-butyl	–	–	–	–	>390	**10bG**	>54	>27	–	–	>432
10cA	(6-Br-2-methylquinoline)	*n*-butyl	>29	>117	–	–	>469	**10cG**	230	115	29	–	461
10dA	(*n*-hexyl)	*n*-butyl	>21	>42	–	–	>333	**10dG**	72	72	36	9	143
10eA	(4-Br-1-Me-Nal)	*n*-butyl	14	14	7	7	27	**10eG**	9	9	9	5	36
10fA	(2,4,5-tri-BrBn)	*n*-butyl	7	7	3	3	27	**10fG**	8	8	8	4	32
10gA	(2,4,6-tri-BrBn)	*n*-butyl	15	15	8	8	30	**10gG**	15	15	8	8	30

Code	Basic group	X	SI (MIC/EC_{50})[a] S. a	B. s	E. c	P. a	EC_{50}	Code	SI (MIC/EC_{50})[a] S. a	B. s	E. c	P. a	EC_{50}
11kA	(2-methylquinoline)	*n*-butyl	–	>56	–	–	>444	**11kG**	225	113	–	–	450
11lA	(4-CF_3Bn)	*n*-butyl	21	43	–	–	342	**11lG**	81	40	81	10	161
11mA	(cyclopentyl)	*n*-butyl	25	51	–	–	>407						
11nA	(*n*-hexyl)	*n*-butyl	36	36	9	9	144	**11nG**	29	15	15	7	58
11oA	(3,5-di-CF_3Bn)	*n*-butyl	12	46	12	12	93	**11oG**	18	18	18	9	36
11pA	(4-*tert*-butylBn)	*n*-butyl	12	12	12	6	47	**11pG**	20	20	20	10	39
11qA	(4-Br-1-Me-Nal)	*n*-butyl	21	21	10	10	82	**11qG**	15	15	15	7	58

Code	R[1]	X	SI (MIC/EC_{50})[a] S. a	B. s	E. c	P. a	EC_{50}	Code	SI (MIC/EC_{50})[a] S. a	B. s	E. c	P. a	EC_{50}
12aA	(3,5-di-BrBn)	(1,2-C_2H_4)	10	10	10	5	39	**12aG**	82	82	41	10	164
13aA	(3,5-di-BrBn)	(1,3-C_3H_6)	25	25	12	12	99	**13aG**	93	93	47	23	187
14aA	(3,5-di-BrBn)	(1,5-C_5H_{10})	6	6	3	3	24	**14aG**	5	5	5	4	29[b]
15aA	(3,5-di-BrBn)	(1,6-C_6H_{12})	8	8	8	2	30	**15aG**	14	14	14	2	57[b]
16aA	(3,5-di-BrBn)	(1,3-*cis*-cyclobutane)	6	13	13	6	50	**16aG**	37	37	19	9	75
17aA	(3,5-di-BrBn)	(1,3-*trans*-cyclobutane)	23	23	23	12	93	**17aG**	31	16	16	8	62
18aA	(3,5-di-BrBn)	(1,4-*cis*-cyclohexyl)	4	4	4	2	15	**18aG**	15	>30	8	8	30
19aA	(3,5-di-BrBn)	(1,4-*trans*-cyclohexyl)	8	8	8	4	16						

Code	R[1]	X	SI (MIC/EC_{50})[a] S. a	B. s	E. c	P. a	EC_{50}	Code	SI (MIC/EC_{50})[a] S. a	B. s	E. c	P. a	EC_{50}
13cA	(6-Br-2-methylquinoline)	*n*-propyl	–	>57	–	–	>455	**13cG**	>62	>124	–	–	>497
13hA	(4-CF_3Bn)	*n*-propyl	–	>25	–	–	>393	**13hG**	>54	>109	–	–	>435
13iA	(3-Cl, 4-BrBn)	*n*-propyl	40	81	40	20	323	**13iG**	174	174	44	–	348
13eA	(4-Br-1-Nal)	*n*-propyl	11	11	6	6	23	**13eG**	31	31	15	8	61
13jA	(3,5-di-CF_3Bn)	*n*-propyl	23	46	23	23	176	**13jG**	111	222	56	28	445
13lA[c]	R^2 = (4-CF_3Bn)	*n*-propyl	–	>55	>27	–	>438	**13lG**	>120	>120	>30	–	>480
13pA[c]	R^2 = (4-*tert*-butylBn)	*n*-propyl	11	11	6	6	23	**13pG**	169	169	85	11	169

Bacterial reference strains: S. a – *Staphylococcus aureus* ATCC 9144, B.s – *Bacillus subtilis* 168, E. c – *Escherichia coli* ATCC 25922, and P. a – *Pseudomonas aeruginosa* ATCC 27853; [a] No SI was calculated if MIC > 16 µg/mL; –: not calculated. [b] Precipitation in the RBC assay. [c] Mixed lipophilic side chain, 3,5-dibromobenzyl and R_2.

6 Biological methods

6.1 Minimum inhibitory concentration (MIC) assay

Stock solutions of the water-soluble compounds were prepared by dissolving them in ultrapure water (Milli-Q H_2O, Millipore, MA, USA). The less water-soluble compounds were first dissolved in 25 - 50 µL 100% DMSO before further dilution with ultrapure water. The DMSO concentration was always less than 1% in the working concentration of each compound. A modified broth microdilution susceptibility test[8], based on the CLSI M07-A9 protocol,[9] was used to determine minimal inhibitory concentrations (MIC). Briefly, the test compounds were two-fold diluted with ultrapure water in polystyrene 96-well flat-bottom microplates (NUNC, Roskilde, Denmark). The bacterial inoculum was diluted to 2.5 - 3 x 10^4 cells/mL in Mueller-Hinton broth (MHB, Difco Laboratories, USA) and added to the different diluted compounds in a ratio of 1:1. Positive control (ciprofloxacin, Sigma-Aldrich, USA), negative control (bacteria + water), and media control (media + water) were included in each experiment. The microplates were incubated for 48 h at 35 °C in an EnVision microplate reader (Perkin-Elmer, Turku, Finland). The lowest concentration of compounds that caused no bacterial growth, as determined by optical density (OD_{600}) measurements, was defined as the MIC value. All compounds were tested in 3 technical replicates.

6.2 Membrane integrity assays

6.2.1 Inner membrane

The inner membrane integrity assay was performed in a real-time manner using *Bacillus subtilis* 168 (ATCC 23857) and *Escherichia coli* K12 (ATCC MC1061) as test strains, both transformed with the reporter plasmid pCSS962 containing the gene encoding eukaryotic luciferase (*lucGR* gene).[10] Externally added D-luciferin was used as a substrate for the luciferase to detect light emission. *B. subtilis* and *E. coli* colonies were suspended in MH media supplemented with 5 µg/mL chloramphenicol (Merck KGaA, Darmstadt, Germany) and a mixture of 20 µg/mL chloramphenicol and 100 µg/mL ampicillin (Sigma-Aldrich, USA), respectively, and grown overnight at RT. Overnight cultures were further diluted and grown at RT for 2-3 hrs until they reached OD_{600} = 0.1. D-luciferin potassium salt (Synchem Inc., Elk Grove Village, IL, USA) was added to the bacterial cultures at a final concentration of 1 mM, and the background luminescence was measured before the actual assay. Black round-bottom 96-well microtiter plates (Nunc, Roskilde, Denmark) were prepared with two-fold dilution series of the compounds (10 µL per well) at final concentrations ranging from 50 to 1.56 µg/mL. Chlorhexidine acetate (Fresenius Kabi, Halden, Norway) and MQ-H_2O were used as positive and negative control, respectively. A Synergy H1 Hybrid Reader (BioTek, Winooski, VT, USA) was primed with bacterial suspension before the assay plate was loaded into the plate reader. Aliquots of 90 µL bacterial inoculum with D-luciferin were successively (well by well) injected into the test wells by an automated injector. The light (luminescence) emission, as a result of bacterial membrane disruption, was monitored every second for 3 minutes. Each study was performed at least three times independently, and the figures show a representative dataset.

6.2.2 Outer membrane

The outer membrane integrity assay was performed in a real-time manner using *E. coli*, the same strain as used in the inner membrane integrity assay. Externally added 1-*N*-phenylnapthylamine (NPN) was used as a substrate for the fluorescence to detect light emission. *E. coli* colonies were suspended in MH media and grown overnight at RT. Overnight cultures were further diluted and grown at RT for 2-3 hrs until they reached OD_{600} = 0.1. NPN (Sigma-Aldrich, USA) was added to the bacterial cultures at a final concentration of 20 µM in glucose hepes buffer (5mM), and the background fluorescence was measured before the actual assay. Black round-bottom 96-well microtiter plates were prepared with two-fold dilution series of the compounds (10 µL per well) at final concentrations ranging from 50 to 1.56 µg/mL. Chlorhexidine acetate and MQ-H_2O were used as positive and negative control. A Synergy H1 Hybrid Reader was primed with bacterial suspension before the assay plate was loaded into the plate reader. Aliquots of 90 µL bacterial inoculum with NPN were successively (well by well) injected into the test wells by an automated injector. The light (fluorescence) emission, as a result of bacterial outer membrane disruption, was monitored every second for 3 minutes. Each study was performed at least three times independently, and the figures show a representative dataset.

6.3 Viability assay

The real-time measurement of bacterial viability was performed by using *B. subtilis* 168 and *E. coli* K12, the same strains as used in the inner membrane integrity assay. However, in this assay B. subtilis 168 is carrying a constitutively expressed lux operon as a chromosomal integration in the sacA locus (PliaG) and *E. coli* K12 was transformed with the reporter plasmid pCGLS-1.[11, 12] *B. subtilis* and *E. coli* cultures were prepared the same way as the membrane integrity assay in MH media supplemented with 5 µg/mL chloramphenicol and a mixture of 20 µg/mL chloramphenicol and 100 µg/mL ampicillin, respectively. The continuous light production by these biosensors was monitored in the Synergy H1 Hybrid Reader, and the respective injector was primed with bacterial suspension. Black round-bottom 96-well microtiter plates were prepared with 10 µL of each compound at the final concentration ranging from 50 to1.56 µg/mL (two-fold dilutions), including Chlorhexidine as a positive control and MQ-H_2O as a negative control. An aliquot of 90 µL bacterial suspension was subsequently added by the automated injector. As a result of changes in bacterial viability, the decrease in light emission was monitored every second for 3 minutes. Each study was performed at least three times independently, and the figures show a representative dataset.

6.4 Red Blood Cell Haemolysis Assay

The protocol was adapted from Paulsen *et al.[1]* Haemolysis was determined using a heparinized fraction (10 IU/mL) of freshly drawn blood. The blood collected in ethylenediaminetetraacetic acid-containing test tubes (Vacutest, KIMA, Arzergrande, Italy) was used for the determination of the hematocrit (hct). The heparinized blood was washed 3× with pre-warmed phosphate-buffered saline (PBS) and adjusted to a final hct of 4%. Derivatives in DMSO (50 mM) were added to a 96-well polypropylene V-bottom plate (NUNC, Fisher Scientific, Oslo, Norway) and serially diluted. The test concentration range was 500–4 µM with DMSO contents ≤1%. A solution of 1% triton X-100 was used as a positive control for 100% haemolysis. As a negative control, a solution of 1% DMSO in PBS was includead. No signs of DMSO toxicity were detected. RBCs (1% v/v final concentration) were added to the well plate and incubated at 37 °C and 800 rpm for 1 h. After centrifugation (5 min, 3000*g*), 100 µL of each well was transferred to a 96-well flat-bottomed microtiter plate, and absorbance was measured at 545 nm with a microplate reader (VersaMaxTM, Molecular Devices, Sunnyvale, CA, USA). The percentage of haemolysis was calculated as the ratio of the absorbance in the derivative-treated and surfactant-treated samples, corrected for the PBS background. Three independent experiments were performed, and EC_{50} values are presented as averages.

7 Membrane integrity and viability assay

Table S2 Summary of the membrane integrity and viability assay against *B. subtilis* 168.

Code	MIC[1] (µg/ml, 24h)	MIA (activity and speed)[2]	VA (effects)[3]
	B. s		
7	4	+++	+
8	8	–	–
9	4	+	+
10cA	4	++	+
10cG	4	++	++
10dG	2	++++	++
11kG	4	+++	++
11lA	8	+++	+
11lG	4	++++	++
11nA	4	+++	+
11nG	4	++++	++
11oA	2	++++	++
11oG	2	++++	+++
11pA	4	++++	++
11pG	2	++++	+++
12aA	4	+++	++
12aG	2	++++	+++
13aA	4	+++	+++
13aG	2	++++	+++
16aG	2	++	+++
17aA	4	++	++
13cG	4	++	+
13hG	4	–	+
13iA	4	++	+
13iG	2	++++	++
13eG	2	+++	+++
13jA	4	+++	+
13jG	2	+++	+
13lG	4	++++	++
13pA	2	+++	++
13pG	1	++++	+++

B. s: *Bacillus subtilis* 168.

[1]MIC assay was also performed in biosensor assay, and the value was similar.

[2]For membrane integrity assay: High active, fast speed (++++) Medium active, Intermediate speed (+++), Medium active, Slow speed (++), Low active, Slow speed (+) and Not active (–).

[3]For viability assay: High effect (+++), Medium effect (++), Low effect (+) and No effect (–). The highest concentration (51.2 µg/mL) was used to compare and evaluate the membrane integrity and viability assay results.

Table S3 Summary of the membrane integrity and viability assay against *E. coli* K12.

Code	MIC[1] (µg/mL, 24h)	MIA (activity and speed)[2]	VA (effects)[3]
	E. c		
10dG	4	+++	++
11lG	4	++	++
11nG	4	+++	++
11oA	8	++	++
11oG	2	++	++
11pG	2	++	++
12aA	4	++++	++
13aA	8	++	+
13aG	4	+++	++
16aG	4	+	++
17aA	4	++	++
13eG	4	+	++
13jA	8	++	++
13jG	8	+++	++

E. c: *Escherichia coli* K12.

[1]MIC assay was also performed in biosensor assay, and the value was similar.

[2]For membrane integrity assay: High active, fast speed (++++) Medium active, Intermediate speed (+++), Medium active, Slow speed (++), Low active, Slow speed (+) and Not active (–).

[3]For viability assay: High effect (+++), Medium effect (++), Low effect (+) and No effect (–). The highest concentration (51.2 µg/mL) was used to compare and evaluate the membrane integrity and viability assay results.

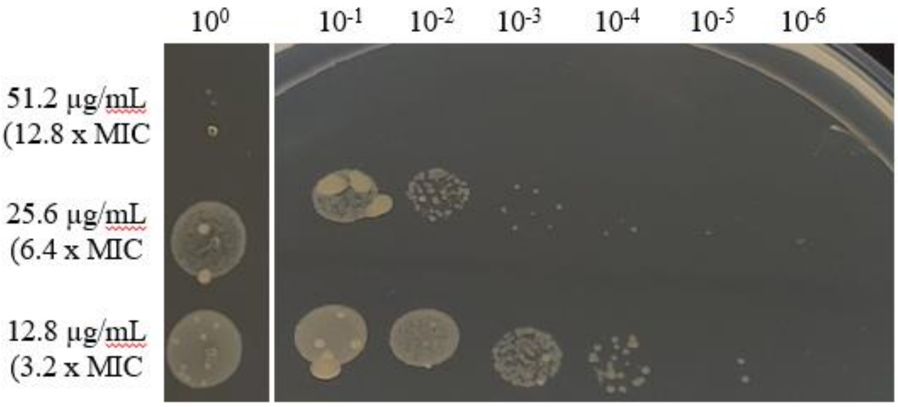

Figure S4. Bactericidal effect of barbiturate **11lG** against *E. coli* K12 after the outer membrane study with NPN. Horizontal: Dilution of the bacterial load.

8 Literature

[1] M.H. Paulsen, M. Engqvist, D. Ausbacher, T. Anderssen, M.K. Langer, T. Haug, G.R. Morello, L.E. Liikanen, H.-M. Blencke, J. Isaksson, E. Juskewitz, A. Bayer, M.B. Strøm, Amphipathic Barbiturates as Mimics of Antimicrobial Peptides and the Marine Natural Products Eusynstyelamides with Activity against Multi-resistant Clinical Isolates, J. Med. Chem., 64 (2021) 11395-11417.
[2] C. Huixiong, L. Jean-Philippe, G. Nohad, G. Christiane, An Efficient and Enantioselective Synthesis of Suitably Protected β-[1-(4-Malonyl)naphthyl]-L-alanine and β-[1-(4-Malonylmethyl)naphthyl]-L-alanine: Novel Fluorescent and Non-Hydrolysable Phosphotyrosine Mimetics, Eur. J. Org. Chem., 2006 (2006) 2329-2335.
[3] W.Z. Bi, C. Qu, X.L. Chen, S.K. Wei, L.B. Qu, S.Y. Liu, K. Sun, Y.F. Zhao, Copper(II) catalyzed heterobenzylic C(sp3)-H activation: Two efficient halogenation methodologies towards heterobenzyl halides, Tetrahedron, 74 (2018) 1908-1917.
[4] M. Donnier-Maréchal, P. Carato, P.-E. Larchanché, S. Ravez, R. Boulahjar, A. Barczyk, B. Oxombre, P. Vermersch, P. Melnyk, Synthesis and pharmacological evaluation of benzamide derivatives as potent and selective sigma-1 protein ligands, Eur. J. Med. Chem., 138 (2017) 964-978.
[5] M. Delor, J. Dai, T.D. Roberts, J.R. Rogers, S.M. Hamed, J.B. Neaton, P.L. Geissler, M.B. Francis, N.S. Ginsberg, Exploiting Chromophore–Protein Interactions through Linker Engineering To Tune Photoinduced Dynamics in a Biomimetic Light-Harvesting Platform, J. Am. Chem. Soc., 140 (2018) 6278-6287.
[6] P.H. Huy, J.C. Westphal, A.M.P. Koskinen, Concise, stereodivergent and highly stereoselective synthesis of cis- and trans-2-substituted 3-hydroxypiperidines – development of a phosphite-driven cyclodehydration, Beilstein J. Org. Chem., 10 (2014) 369-383.
[7] M. Botta, F. Corelli, G. Maga, F. Manetti, M. Renzulli, S. Spadari, Research on anti-HIV-1 agents. Part 2: Solid-phase synthesis, biological evaluation and molecular modeling studies of 2,5,6-trisubstituted-4(3H)-pyrimidinones targeting HIV-1 reverse transcriptase, Tetrahedron, 57 (2001) 8357-8367.
[8] E.M. Igumnova, E. Mishchenko, T. Haug, H.-M. Blencke, J.U.E. Sollid, E.G.A. Fredheim, S. Lauksund, K. Stensvåg, M.B. Strøm, Synthesis and antimicrobial activity of small cationic amphipathic aminobenzamide marine natural product mimics and evaluation of relevance against clinical isolates including ESBL–CARBA producing multi-resistant bacteria, Biorg. Med. Chem., 24 (2016) 5884-5894.
[9] F.R. Cockerill, Methods for Dilution Antimicrobial Susceptibility Tests for Bacteria That Grow Aerobically. Approved Standard. M07-A9 in: C.a.L.S. Institut (Ed.), Wayne, Pa : Clinical and Laboratory Standards Institut, 2012.
[10] M. Virta, K.E.O. Åkerman, P. Saviranta, C. Oker-Blom, M.T. Karp, Real-time measurement of cell permeabilization with low-molecular-weight membranolytic agents, J. Antimicrob. Chemother., 36 (1995) 303-315.
[11] J. Radeck, K. Kraft, J. Bartels, T. Cikovic, F. Dürr, J. Emenegger, S. Kelterborn, C. Sauer, G. Fritz, S. Gebhard, T. Mascher, The *Bacillus* BioBrick Box: generation and evaluation of essential genetic building blocks for standardized work with *Bacillus subtilis*, J. Biol. Eng., 7 (2013) 29.
[12] S. Frackman, M. Anhalt, K.H. Nealson, Cloning, organization, and expression of the bioluminescence genes of Xenorhabdus luminescens, J. Bacteriol., 172 (1990) 5767-5773.

Paper II

European Journal of Medicinal Chemistry 249 (2023) 115147

Contents lists available at ScienceDirect

European Journal of Medicinal Chemistry

journal homepage: www.elsevier.com/locate/ejmech

Research paper

Investigation of tetrasubstituted heterocycles reveals hydantoins as a promising scaffold for development of novel antimicrobials with membranolytic properties

Manuel K. Langer [a], Ataur Rahman [b], Hymonti Dey [b], Trude Anderssen [c], Hans-Matti Blencke [b], Tor Haug [b], Klara Stensvåg [b], Morten B. Strøm [c,*], Annette Bayer [a,*]

[a] Department of Chemistry, UiT – The Arctic University of Norway, NO-9037, Tromsø, Norway
[b] The Norwegian College of Fishery Science, Faculty of Biosciences, Fisheries and Economics, UiT – The Arctic University of Norway, NO-9037, Tromsø, Norway
[c] Department of Pharmacy, Faculty of Health Sciences, UiT – The Arctic University of Norway, NO-9037, Tromsø, Norway

A R T I C L E I N F O

Keywords:
Antimicrobial peptides (AMP)
Synthetic mimics of antimicrobial peptides (SMAMPs)
Peptidomimetics
Hydantoin
Membranolytic

A B S T R A C T

Mimics of antimicrobial peptides (AMPs) have been proposed as a promising class of antimicrobial agents. We report the analysis of five tetrasubstituted, cationic, amphipathic heterocycles as potential AMP mimics. The analysis showed that the heterocyclic scaffold had a strong influence on the haemolytic activity of the compounds, and the hydantoin scaffold was identified as a promising template for drug lead development. Subsequently, a total of 20 hydantoin derivatives were studied for their antimicrobial potency and haemolytic activity. We found 19 of these derivatives to have very low haemolytic toxicity and identified three lead structures, **2dA**, **6cG,** and **6dG** with very promising broad-spectrum antimicrobial activity. Lead structure **6dG** displayed minimum inhibitory concentration (MIC) values as low as 1 μg/mL against Gram-positive bacteria and 4–16 μg/mL against Gram-negative bacteria. Initial mode of action (MoA) studies performed on the amine derivative **6cG**, utilizing a luciferase-based biosensor assay, suggested a strong membrane disrupting effect on the outer and inner membrane of *Escherichia coli*. Our findings show that the physical properties and structural arrangement induced by the heterocyclic scaffolds are important factors in the design of AMP mimics.

1. Introduction

Antimicrobial resistance is now considered to have a similar impact on humans as global climate change [1]. Despite that, only around 30–40 new antimicrobial agents are currently in clinical trials and they are mainly derivatives of already marketed compound classes [2]. To combat the rising resistance, new and underdeveloped classes of compounds have to be utilized.

One promising group of antibiotic agents are the naturally occurring cationic antimicrobial peptides (AMPs), found in practically all higher forms of life [3]. Their amphipathic nature allows them to associate with the negatively charged bacterial outer membrane simultaneously as the lipophilic residues can insert and disrupt the membrane [3]. It is believed that due to the lack of a specific target, AMPs are less likely to induce antibiotic resistance development [4]. However, proteolytic instability [5], sometimes tedious synthetic procedures [6] and moderate activity [4] are among the drawbacks AMPs have been facing, thus retarding their development. To address these issues a range of synthetic AMP analogues have been reported including peptoids [7,8], oligoureas [9], γ-AApeptides [10,11] and other small synthetic mimics of antimicrobial peptides (SMAMPs) [6,12,13].

In recent years, we have focussed on the development of synthetic analogues of AMPs that fulfil and operate at the limit of the pharmacophore model for AMPs. That is, the presence of two cationic groups and two lipophilic groups of sufficient bulk to exert broad-spectrum activity [14]. Among these were β-amino amides [15,16], cyclic tetrapeptides [16], barbiturates [17] and others [18,19]. The barbituric acid framework **1** has proven to be a valuable scaffold for the preparation of highly active antimicrobials [17,20], and we were curious if our previous results would translate to other scaffold structures.

In this work we initially investigated five heterocyclic scaffolds **2–5** and **15** (Fig. 1), that would allow for the same substitution pattern of two lipophilic side chains and two cationic chains as demonstrated for barbituric acid **1** [17,20]. To achieve segregation of the cationic and

* Corresponding authors.
E-mail addresses: morten.strom@uit.no (M.B. Strøm), annette.bayer@uit.no (A. Bayer).

https://doi.org/10.1016/j.ejmech.2023.115147
Received 13 November 2022; Received in revised form 19 December 2022; Accepted 21 January 2023
Available online 24 January 2023

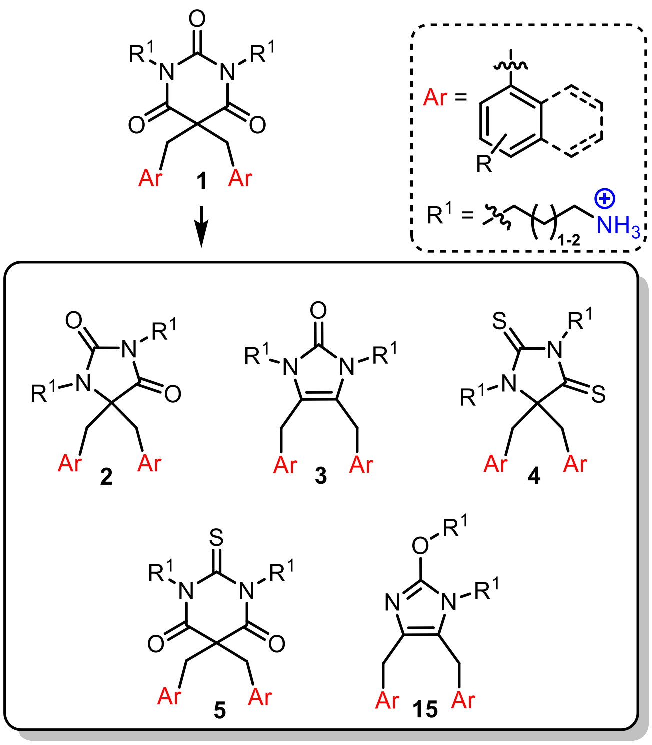

Fig. 1. Previously utilized barbituric acid **1** and core structures **2–5** and **15** used in this study. Ar = lipophilic side chain, R[1] = *n*-alkyl linker with a cationic head group. Red: lipophilic part, blue: cationic part.

lipophilic part we intended to attach the lipophilic side chains (Ar) at the bottom side of the heterocycles, bound to carbon atoms (Fig. 1). The *n*-alkyl linkers bearing the cationic head group (R[1]) were incorporated onto the top side, bound to the nitrogen atoms (Fig. 1).

We then constructed a small library based on the most promising scaffold, the hydantoin **2**, and evaluated the effect of different lipophilic and cationic side chains. For the most potent analogues, their membranolytic behaviour was studied.

2. Results and discussion

2.1. Design of the study

We planned three sets of compounds. In the first set all core structures (**2–5** and **15**) shown in Fig. 1 were synthesized with a combination of substituents (Fig. 2, left) that we had evaluated in previous studies of amphipathic, antimicrobial barbituric acid derivatives [17,20].

Lipophilic 3,5-dibromobenzyl (3,5-di-Br) side chains were found earlier to be beneficial for the antimicrobial potency [16,17]. Aliphatic *n*-propyl linkers exhibited a good balance between antimicrobial potency and haemolytic activity [20] and amine groups were most accessible. It should be noted that we did not aim for the 2-(hydroxy)-1*H*-imidazole **15A** in the initial plan, but **15A** was obtained as a side product during synthesis. The second set was comprised of tetrasubstituted hydantoins **2** (Fig. 2, right) with different lipophilic side chains, *n*-propyl linkers, and amines and guanidines as cationic head groups. The lipophilic side chains and cationic groups were chosen based on their performance in previous studies [16,17,20,21]. For the third set we used promising lipophilic side chains from the second set and incorporated *n*-butyl linkers to deliver hydantoins **6** (Fig. 2, right). The *n*-butyl linkers have previously demonstrated to result in more potent derivatives [17,20].

Imidazolidine-2,4-dione **2**, commonly known as hydantoin, is a privileged scaffold in medicinal chemistry, found in drugs against

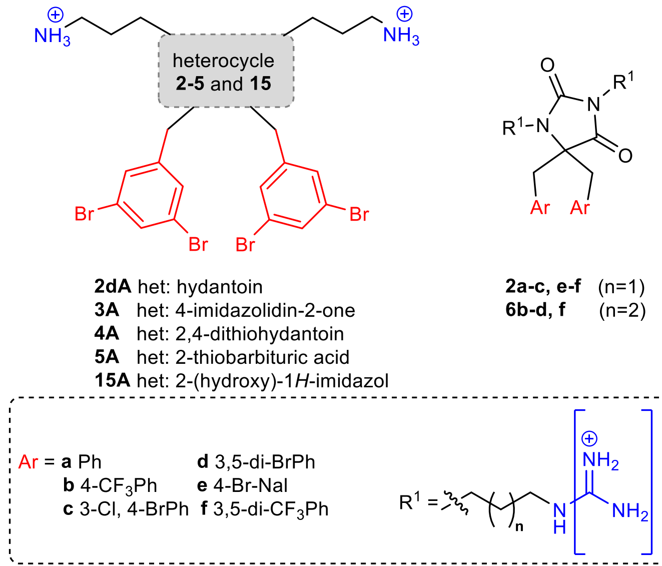

Fig. 2. Illustration of the three sets of compounds investigated. Brackets imply variations between cationic amine and guanidine groups.

various conditions [22–27]. However, it is only rarely seen in antimicrobial agents [6,28–30]. Of particular interest to this work, is a study by Cai and co-workers who demonstrated that suitably substituted hydantoins can effectively target bacterial membranes [6]. In the related 4-imidazolidin-2-one **3,** the lipophilic side chains were attached to two vicinal sp^2 hybridized carbons, providing more spatial separation and altered dihedral angle between the side chains. Additionally, removal of the amidic oxygen from hydantoin **2** led to a slight change in polarity. The changes in structure and physical properties may affect the compounds' ability to interact with the bacterial membrane. Lastly, we wanted to investigate the effect of sulphur on the biological activity. Thioamides are often utilized in peptide synthesis [31] and are known to hamper enzymatic degradation of peptides [32]. Sulphur is also found in a variety of different drugs [33,34], including some antimicrobial thio-peptides [35,36] and β-lactam antibiotics such as penicillins and cephalosporines [37]. In most of these structures the sulphur atom is part of a heterocyclic ring or a (di)sulfide, but not a thioamide or a related motif. Therefore, we were interested in joining those two areas by replacing some oxygens for sulphur atoms in the hydantoin and barbituric acid [17] core structures. The resulting structures were 2, 4-dithiohydantoin **4** and 2-thiobarbituric acid **5**.

2.2. Synthesis

2.2.1. Hydantoins 2 and 6

The hydantoin structure can be accessed from a range of different reactions [38–41], including the Read [42], Bucherer-Bergs [43] and Biltz [44] syntheses. To achieve higher substitution patterns and to facile the access of compound libraries, modern strategies have been developed such as multicomponent reactions [45,46].

Based on the required substitution pattern and the nature of substituents, we decided to utilize the Bucherer-Bergs reaction as the key step in our synthetic strategy towards hydantoins **2A** and **6A** (Scheme 1). To that end, we prepared symmetric ketones **6** from *p*-toluenesulfonylmethyl isocyanate (TosMIC) **7** [47]. TosMIC was α,α-dialkylated using phase-transfer catalysis (PTC) in DCM and an aqueous NaOH solution with the benzyl bromide of choice. The crude products were hydrolysed by treatment with concentrated HCl [47] to give symmetric ketones **8(a–f)** in 53–69% yield over two steps (o2s). The Bucherer-Bergs reaction is commonly performed in a mixture of EtOH/H_2O [43], with precipitation of the resulting hydantoins as the main driving force. Unfortunately, only the unsubstituted

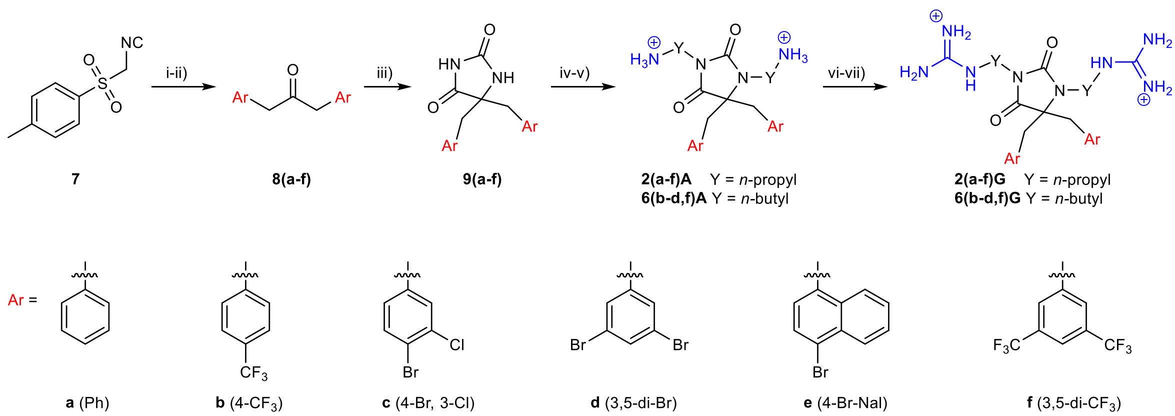

Scheme 1. Synthetic strategy towards target hydantoins **2** and **6**. Reaction conditions: i) $ArCH_2Br$, TBAB or TBAI, DCM, $NaOH_{(aq)}$ (20–35 wt%), r.t.; ii) $HCl_{(conc)}$, DCM/THF, r.t., 53–69% o2s; iii) KCN, NH_4CO_3, KOAc, DMSO or KCN, NH_4CO_3, EtOH/H_2O, 60–75 °C, 45–85%; iv) *N*-Boc-3-bromopropylamine or *N*-Boc-4-bromobutylamine, Cs_2CO_3, TBAI, acetone, 65 °C *then* v) TFA, DCM, r.t., 45–85% o2s; vi) *N,N*′-Di-Boc-1*H*-pyrazole-1-carboxamidine, DIPEA, THF, 45 °C *then* vii) TFA, DCM, r.t., 33–91% o2s.

diphenylpropan-2-one (Ar = Ph) could be prepared following this protocol. The other derivatives proved to be insoluble and the solvent needed to be changed to DMSO. Interestingly, an additional base, potassium acetate, was needed to obtain the hydantoins **9(a–f)** in moderate to high yields of 45–85%. For *N,N*′-dialkylation, the hydantoins **9(a–f)** were treated with *N*-Boc-3-bromopropylamine or *N*-Boc-4-bromobutylamine, caesium carbonate (Cs_2CO_3) and tetrabutylammonium iodide (TBAI) in acetone at elevated temperature.

Subsequent TFA/DCM induced Boc removal delivered the target hydantoins **2A** and **6A** in 45–85% over two steps. Conversion of the amine-modified hydantoins **2A** and **6A** to their guanidyl counterparts was achieved with *N,N*′-di-Boc-1*H*-pyrazole-1-carboxamidine and *N,N*-diisopropylethylamine (DIPEA) in THF. Ensuing Boc removal with TFA/DCM delivered guanidyl hydantoins **2G** and **6G** in 33–91% yield o2s.

2.2.2. 4-Imidazolidin-2-one *3A* and 2-(hydroxy)-1H-imidazole *15A*

We first set out to obtain the 4-imidazolidin-2-one derivative **3A** by a two-step process from the Boc protected hydantoin **2dA** (Ar = 3,5-di-BrPh) (see Supporting Information, Scheme S1 and Table S1). Even though the transformation was feasible, **3A** could not be purified satisfyingly. Therefore, we changed the synthetic strategy as shown in Scheme 2. Starting from 3,5-dibromobenzaldehyde **10**, we employed a Wittig reaction with $Ph_3PCH_2(OMe)Cl$ to generate the corresponding vinyl ether in 91% yield as a 1.5:1.0 mixture of the *E*- and *Z*-isomer as by ^{1}H NMR. Treatment of the vinyl ether with hydrochloric acid in THF and formic acid or TFA in DCM resulted in complex mixtures. Using *in-situ* generated HCl by combining oxalyl chloride, EtOH and H_2O [48] led to quick and full conversion to the desired aldehyde, but the results were not always reproducible. The most reliable results were finally achieved by using trimethylsilyl chloride (TMS-Cl) and sodium iodide in dry MeCN with high dilution [49]. The homologated aldehyde **11** was obtained in 60% yield. Aldehyde **11** was subsequently converted in a benzoin-type condensation to the α-hydroxy ketone **12** by treatment with Et_3N and catalytic amounts of 3-benzyl-5-(2-hydroxyethyl)-4-methylthiazolium chloride in dry PEG-400 [50]. We used PEG-400 instead of the more commonly employed EtOH [50], due to the low solubility of aldehyde **11**. Based on literature [51], we condensed the α-hydroxy ketone **12** with urea in the presence of glacial acetic acid in anhydrous PEG-400. We obtained 4-imidazolin-2-one **14** in 39% yield as the major product and found unexpectedly 4-oxazolin-2-one **13** in 18% yield. In previous reports, the side product was only observed when the benzoin reagent had electron donating substituents (4,4′-dimethoxybenzoin) or heterocyclic nitrogen (2,2′-pyridoin) [51]. The authors were reasoning that the electron donating *para*-methoxy substituents would render the hydroxyl group of the intermediate more nucleophilic as does the basic pyridinyl nitrogen by intramolecular hydrogen bonding. One possible explanation could be the bromine atom acting as a Lewis base, forming a hydrogen bond to the hydroxyl hydrogen. This interaction would be comparable to the basic pyridinyl hydrogen and would facilitate an intramolecular attack of the urea oxygen, leading to compound **13**.

We then alkylated 4-oxazolin-2-one **13** and 4-imidazolidin-2-one **14**, respectively, with *N*-boc-3-bromopropylamine using (*n*-hexadecyl)tri-*n*-butylphosphonium bromide as phase transfer catalyst and potassium carbonate as a base in a biphasic mixture of water and toluene under μ-wave irradiation. Subsequently, the di-alkylated products were

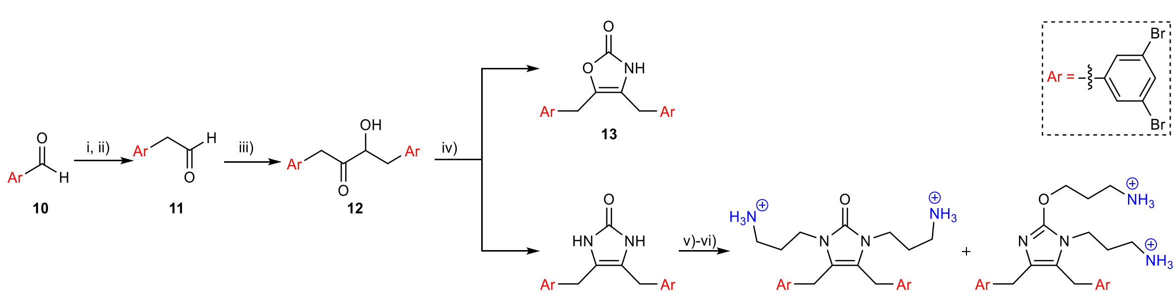

Scheme 2. Synthetic strategy towards tetrasubstituted 4-imidazolidin-2-one **3A** and its constitutional isomer **15A.** Ar = 3,5-dibromophenyl. Reaction conditions: i) $Ph_3PCH_2(OMe)Cl$, NaHMDS, THF (dry), −78 °C to r.t., 91%; *E/Z* = 1.5/1.0; ii) TMSCl, NaI, MeCN (dry), r.t., 60%; iii) 3-benzyl-5-(2-hydroxyethyl)-4-methylthiazolium chloride, Et_3N, PEG-400 (dry), 80 °C, 39%; iv) urea, AcOH, PEG-400 (dry), 130 °C, 18% for **13** and 39% for **14**; v) *N*-Boc-3-bromopropylamine, K_2CO_3, (*n*-hexadecyl)tri-*n*-butylphosphonium bromide, toluene:water, μ-wave, 130–150 °C *then* vi) TFA, DCM, r.t., 17–19% o2s.

deprotected with TFA/DCM. Synthesis of the derivative from 4-oxazolin-2-one **13** delivered a di-alkylated compound with an unresolved structure and was not further investigated.

Compound **14** delivered the desired *N,N′*-dialkylated 4-imidazolin-2-one **3A** in low yields (19% o2s). Surprisingly, *N,O*-dialkylated 2-(hydroxy)-1*H*-imidazole **15A** (17% o2s) was obtained from the same reaction mixture. The mono alkylated derivatives of structures **3A** and **15A** were obtained as well, partially explaining the low yields.

2.2.3. 2,4-Dithiohydantoin 4A

By employing *in situ* generated NH_4CN and CS_2 [52] we intended to obtain 2,4-thiohydantoin **4A** from ketone **8d** (Ar = 3,5-di-BrPh), but no conversion was observed. Instead hydantoin **9d** (3,5-di-Br) was treated with the Lawesson's reagent at elevated temperature [53] to deliver 2,4-thiohydantoin **16** (3,5-di-Br) in 82% yield (Scheme 3). *N,N′*-Dialkylation of **16** with *N*-Boc-3-bromopropylamine afforded 2,4-dithiohydantoin **4A** in 56% yield.

2.2.4. 2-Thiobarbituric acid 5A

In a first approach we tried to thiolate 5,5-bis(3,5-dibromobenzyl) barbituric acid with the Lawesson's reagent under the same conditions as used to obtained 2,4-dithiohydantoins (*vide supra*). Unfortunately, we obtained an inseparable mixture of the mono-, di- and tri-thiolated barbituric acid. Therefore, we decided to adapt our previously reported procedure [17] by replacing urea with thiourea. Treatment of di-benzylated diethyl malonate **17** and thiourea with NaH in a mixture of anhydrous THF and DMF gave the 5,5-dibenzylated-2-thiobarbituric acid **18** in low yields (Scheme 4). *N*-alkylation with *N*-Boc-3-bromopropylamine, Cs_2CO_3 and TBAI in acetone at elevated temperature, followed by TFA/DCM mediated Boc removal delivered the tetrasubstituted barbiturates **5A** and **1A** in very low yields (9%). Partial desulfurization had taken place, resulting in two mixtures of tetrasubstituted 2-thiobarbituric acid **5A** (X = S) and barbituric acid **1A** (X = O). Mixture 1 constituted a ratio of 2.4:1.0 (**5A:1A**) and mixture 2 constituted a ratio of 1.0:1.7 (**5A:1A**). The mixtures were inseparable but stable in solid state and were tested as such. Only when the mixtures were in solution, we could see slow desulfurization take place, potentially by low amounts of peroxide formation from atmospheric oxygen under light exposure [54,55].

2.3. SAR analysis

All compounds were screened for their antimicrobial activity against antibiotic susceptible Gram-positive and Gram-negative bacterial reference strains. Antimicrobial potency of each compound was expressed by their minimum inhibitory concentration (MIC) values. Haemolytic activity against human red blood cells (RBC), expressed by the EC_{50} value, was used as a measurement of cytotoxicity. The ideal compound should display high bacterial activity (low MIC values) and low or no toxicity towards human cells (high EC_{50} values) i.e. acting

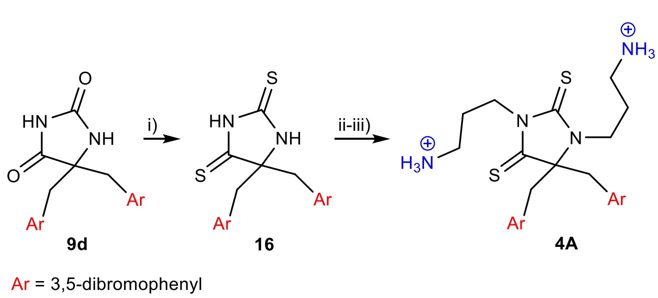

Scheme 3. Synthetic strategy towards 2,4-dithiohydantoin **4A**. Ar = 3,5-dibromophenyl. Reaction conditions: i) Lawesson's reagent, 1,4-dioxane, 115 °C, 82%; ii) *N*-Boc-3-bromopropylamine, Cs_2CO_3, TBAI, acetone, 55 °C then iii) TFA, DCM, r.t., 56%.

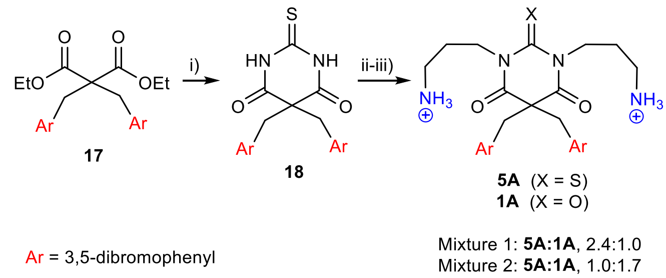

Scheme 4. Synthetic strategy towards 2-thiobarbituric acid **5A**. Mixtures of 2-thiobarbituric acid **5A** (X = S) and barbituric acid **1A** (X = O) were obtained. Ar = 3,5-dibromophenyl. Reaction conditions: i) Thiourea, NaH, anhydrous THF:DMF, 65 °C, 24%; ii) *tert*-butyl (3-bromopropyl)carbamate, Cs_2CO_3, TBAI, acetone, 70 °C, then iii) TFA, DCM, r.t., 9% o2s.

selectively against bacteria. As a reference compound we used the already reported barbiturate **1A** [20] (Table 1, entry 7). The commercially available antibiotic ciprofloxacin served as a positive control (entry 8). Capital **A** in the compound codes denotes cationic amine derivatives and capital **G** denotes cationic guanidine derivatives. For Series 2 and 3 the substituents on the phenyl groups are given in brackets for each compound to aid the discussion. The hydrophilicity of each core structure, bearing four substituents, was calculated using the ChemBioDraw Ultra software (PerkinElmer, v19.0.0.1.28).

2.3.1. Exploring new scaffolds

We started our investigation by comparing the different scaffolds **2dA**, **3A**, **4A**, **5A** and **15A** to identify the most promising candidate in terms of antimicrobial and haemolytic activity (Table 1). All scaffolds were decorated with the same lipophilic (Ar = 3,5-dibromophenyl) and cationic group (R^1 = 3-aminoprop-1-yl). The five membered hydantoin **2dA** (entry 1) was marginally less potent (MIC: 4–16 μg/mL) than the

Table 1
Antimicrobial activity (MIC in μg/mL) against bacterial reference strains and haemolytic activity against human RBC (EC_{50} in μg/mL) for compounds with different scaffold structures.

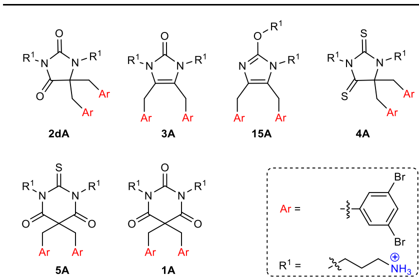

Entry	Comp. ID	CLogP[a]	Antimicrobial activity				EC_{50}
			S. a	B. s	E. c	P. a	
1	**2dA**	−1.69	8	4	16	8	344
2	**3A**	−0.47	2	1	4	8	52
3	**15A**	0.26	2	2	4	4	44
4	**4A**	−1.22	8	8	16	32	385
5	Mixture 1[b]	n.d.	8	4	8	16	305
6	Mixture 2[c]	n.d.	8	4	8	8	182
7 [20]	**1A**	−1.44	4	4	8	8	99
8	Ciprofloxacin		0.06	<0.03	<0.03	0.25	

Bacterial reference strains: S. a – *Staphylococcus aureus* ATCC 9144, B. s – *Bacillus subtilis* 168, E. c – *Escherichia coli* ATCC 25922, and P. a – *Pseudomonas aeruginosa* ATCC 27853.

[a] ClogP values were calculated for the respective tetrasubstituted core structures (calculated with ChemBioDraw Ultra). n.d.: not determined.

[b] Mixture of 2.4:1.0 (**5A:1A**).

[c] Mixture of 1.0:1.7 (**5A:1A**).

barbituric acid **1A** (entry 7), although it was estimated to be slightly more hydrophilic. Interestingly, hydantoin **2dA** was almost 3.5 times less haemolytic (EC_{50}: 344 μg/mL) than **1A** (EC_{50}: 99 μg/mL). The 4-imidazolidin-2-one core **3A** (entry 2) was one order of magnitude more lipophilic than the hydantoin core. **3A** demonstrated a 4-fold increase in antimicrobial potency (MIC: 1–4 μg/mL) against all strains except for the Gram-negative bacterium *Pseudomonas aeruginosa*, but also a 7-8-fold increase in haemolytic activity (EC_{50}: 52 μg/mL). The constitutional isomer 4-oxazolin-2-one **15A** (entry 3) gave a similar result (MIC: 2–4 μg/mL, EC_{50}: 44 μg/mL). Despite being very potent, the systemic application of these compounds is limited by their high haemolytic activity.

It did not become clear why these core structures were so distinctively more haemolytic than hydantoin **2dA**. The 2,4-dithiohydantion **4A** (entry 4) displayed a 4-fold decrease in activity against *P. aeruginosa* (MIC: 32 μg/mL) compared to its dioxo counterpart **2dA**. The dithio-derivative **4A** was only marginally less haemolytic (EC_{50}: 385 μg/mL) than **2dA** (EC_{50}: 344 μg/mL).

Mixture 1 (entry 5), being enriched with 2-thiobarbituric acid **5A** (ClogP = −0.52), exhibited reduced potency against the Gram-negative *P. aeruginosa* (MIC: 16 μg/mL) and the haemolytic activity (EC_{50}: 305 μg/mL) was decreased by a factor of three compared to **1A** (EC_{50} = 99 μg/mL). By reduction of the amount of **5A** in mixture 2 (entry 6), antimicrobial activity (MIC: 4–8 μg/mL) and more pronouncedly the haemolytic activity (EC_{50}: 182 μg/mL) approached the values found for **1A** (entry 7). In conclusion, the sulphur containing derivatives were less haemolytic and less potent against the Gram-negative *P. aeruginosa*. No major change in activity was observed against the other bacterial test strains. Combined with the synthetic challenges and the chemical instability, thionylated derivatives were not worthwhile to investigate further. Clearly the hydantoin scaffold was the most promising core structure for further development.

2.3.2. Hydantoins with n-propyl linkers (2)

A series of hydantoins **2** (Table 2) with *n*-propyl linkers connecting the cationic amino (**A**) or guanidino (**G**) groups to the core were constructed to screen additional lipophilic side chains (**a-c** and **e-f**) for their impact on the compounds' potency and haemolytic toxicity. We have chosen (pseudo)halogenated benzyl groups as lipophilic side chains based on their potential influence on the antimicrobial potency and haemolytic activity described in previous studies [16,17,20]. The trends observed in this study were similar to previous studies and will not be repeated in detail here. The compounds are ranged according to increasing lipophilicity.

Generally, the compounds in amine series **2(a-f)A** (Table 2, entry 1–6) exhibited improved antibacterial potency and increased haemolytic activity with higher CLogP values of the lipophilic side chains, except for hydantoin **2 fA** (3,5-di-CF_3). Derivatives **2aA** (Ph) and **2bA** (4-CF_3) were practically inactive against all strains (MIC: 16–>256 μg/mL). Amine hydantoin **2cA** (4-Br, 3-Cl) was only active against the Gram-positive strains, *Bacillus subtilis* and *Staphylococcus aureus* (MIC: 4–8 μg/mL), whereas the amine hydantoins **2(d-f)A** (entries 4–6) were

Table 2
Antimicrobial activity (MIC in μg/mL) against bacterial reference strains and haemolytic activity against human RBC (EC_{50} in μg/mL) for tetrasubstituted hydantoins **2** and **6**.

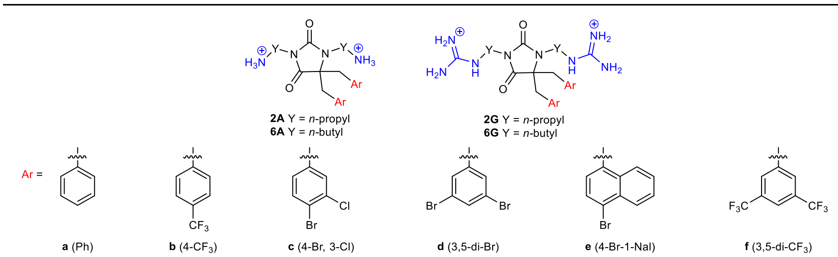

Entry	Comp. ID	Ar	Y	CLogP[a]	Antimicrobial activity				EC_{50}[b]
					S. a	B. s	E. c	P. a	
1	**2aA**	(Ph)	*n*-propyl	2.64	>256	256	>256	>256	>311
2	**2bA**	(4-CF_3)	*n*-propyl	3.52	64	16	256	>256	>379
3	**2cA**	(4-Br, 3-Cl)	*n*-propyl	4.08	8	4	32	32	368
4	**2dA**	(3,5-di-Br)	*n*-propyl	4.38	8	4	16	8	344
5	**2eA**	(4-Br-1-Nal)	*n*-propyl	4.68	4	4	8	8	69
6	**2fA**	(3,5-di-CF_3)	*n*-propyl	5.03	16	8	16	16	399
7	**2aG**	(Ph)	*n*-propyl	2.64	64	128	>256	>256	>353
8	**2bG**	(4-CF_3)	*n*-propyl	3.52	16	8	128	>256	>421
9	**2cG**	(4-Br, 3-Cl)	*n*-propyl	4.08	2	2	32	64	>467
10	**2dG**	(3,5-di-Br)	*n*-propyl	4.38	2	4	16	32	486
11	**2eG**	(4-Br-1-Nal)	*n*-propyl	4.68	2	2	8	32	206
12	**2fG**	(3,5-di-CF_3)	*n*-propyl	5.03	4	2	32	32	>489
13	**6bA**	(4-CF_3)	*n*-butyl	3.52	64	16	>128	>128	>393
14	**6cA**	(4-Br, 3-Cl)	*n*-butyl	4.08	8	4	64	64	>439
15	**6dA**	(3,5-di-Br)	*n*-butyl	4.38	8	2	32	32	364
16	**6fA**	(3,5-di-CF_3)	*n*-butyl	5.03	16	4	64	64	>461
17	**6bG**	(4-CF_3)	*n*-butyl	3.52	4	4	64	>128	>503
18	**6cG**	(4-Br, 3-Cl)	*n*-butyl	4.08	1	1	8	32	347
19	**6dG**	(3,5-di-Br)	*n*-butyl	4.38	1	1	4	16	206
20	**6fG**	(3,5-di-CF_3)	*n*-butyl	5.03	2	2	8	32	384
21	Ciprofloxacin				0.06	<0.03	<0.03	0.25	

Bacterial reference strains: S. a – *Staphylococcus aureus* ATCC 9144, B. s – *Bacillus subtilis* 168, E. c – *Escherichia coli* ATCC 25922, and P. a – *Pseudomonas aeruginosa* ATCC 27853.

[a] ClogP values were calculated for substituted benzyl groups (calculated with ChemBioDraw Ultra).

[b] Values given as *greater than* correspond to the highest concentration (500 μM) tested in the RBC assay.

potent against all strains tested (MIC: 4–16 μg/mL). The most potent amine derivative was **2eA** (4-Br-1-Nal), showing good broad-spectrum potency (MIC: 4–8 μg/mL). Interestingly, it was at least 5-times more haemolytic (EC_{50}: 69 μg/mL) than any of the other amine derivatives (**2A**). Hydantoin **2fA** (3,5-di-CF_3) was more lipophilic than **2eA** (4-Br-1-Nal) but less potent (MIC: 8–16 μg/mL) than the latter by a factor of two to four. The electron withdrawing trifluoromethyl groups may lead to a slight polarisation of the aromatic ring, thus reducing its ability to interact with the lipid membrane. The most promising amine derivative was **2dA** (3,5-di-Br), having broad-spectrum activity (MIC: 4–16 μg/mL) and negligible haemolytic activity (EC_{50}: 344 μg/mL). Surprisingly, it demonstrated slightly higher activity against *P. aeruginosa* than *Escherichia coli*

The guanidyl series **2(a-f)G** (Table 2, entry 7–12) exhibited the same general trend for antimicrobial potency and haemolytic activity as in the amine series, except for derivative **2fG** (3,5-di-CF_3). The guanidyl derivatives were generally more potent against the Gram-positive strains than their amine counterparts by a factor of two to four. Guanidyl hydantoins **2(b-f)G** (entries 8–12) exhibited good to very good potency (MIC: 2–16 μg/mL) against the Gram-positive strains. The potency against the Gram-negative *E. coli* was virtually unchanged compared to their amine correlates. However, the activity against the Gram-negative *P. aeruginosa* decreased two-fold for **2cG** (4-Br, 3-Cl) and **2fG** (3,5-di-CF_3), and four-fold for **2dG** (3,5-di-Br) and **2eG** (4-Br-1-Nal), correspondingly. All guanidyl derivatives were pronouncedly less haemolytic than their amine equivalents. The most promising guanidine derivative was **2eG** (4-Br-1-Nal), which demonstrated good potency against all bacterial strains (MIC: 2–8 μg/mL) except for *P. aeruginosa* and had low haemolytic toxicity (EC_{50}: 206 μg/mL). The combination of *n*-propyl linkers and guanidyl head groups having improved potency against Gram-positive strains and reduced potency against the Gram-negative *P. aeruginosa*, as well as reduced haemolytic activity, has also been observed for amphipathic barbiturates [20].

In summary, guanidyl derivatives **2(c-f)G** showed good potency against both Gram-positive test strains (MIC: 2–4 μg/mL), but none of the guanidyl derivatives **2G** were potent against *P. aeruginosa*. Amines **2dA** (3,5-di-Br) and **2eA** (4-Br-1-Nal) were the most potent derivatives of hydantoins **2**, with **2dA** (3,5-di-Br) being non haemolytic.

2.3.3. Hydantoins with n-butyl linkers (6)

In our previous study on tetrasubstituted barbiturates, a combination of guanidyl head groups and *n*-butyl linkers achieved the highest broad-spectrum activity. Due to the structural similarity, we reasoned that *n*-butyl linkers would boost the hydantoins' potency. We chose the most promising side chains **b** (4-CF_3), **c** (4-Br, 3-Cl), **d** (3,5-di-Br) and **f** (3,5-di-CF_3) from hydantoin derivatives **2**.

Amine hydantoins **6A** displayed the same potency against the Gram-positive strains as derivatives **2A** but had reduced activity against the Gram-negative strains by a factor of two to four (Table 2). None of the derivatives were haemolytic (EC_{50}: ≥364 μg/mL).

Upon guanylation, all compounds of **6G** became highly potent against the Gram-positive strains (MIC: 1–4 μg/mL). Guanidino hydantoin **6cG** (4-Br, 3-Cl) demonstrated good activity against all strains (MIC: 1–8 μg/mL), except for *P. aeruginosa*, with no noteworthy haemolytic activity (EC_{50}: 347 μg/mL). Hydantoin **6dG** (3,5-di-Br) had excellent activity against the Gram-positive strains (MIC: 1 μg/mL) and good to moderate activity against the Gram-negative strains (MIC: 4–16 μg/mL).

In summary, we did observe increased potency and haemolytic activity for the guanidyl compounds **6G** compared to their amine counterparts **6A** (*vide supra*). While being non-haemolytic, the potency of the amine derivatives was rather unsatisfying. The guanidyl compounds **6cG** (4-Br, 3-Cl) and **6dG** (3,5-di-Br), however, displayed promising antimicrobial potency and low to no haemolytic activity.

2.4. Selectivity index and counterion effect

The selectivity index (SI) is a simple descriptor given by the ratio of EC_{50}/MIC for the efficiency of antimicrobial agents. We have summarized the most promising compounds with their SI values in Table 3. Compounds were only considered active if the MIC value was ≤16 μg/mL. SI values for all other compounds can by found in the Supporting Information, Table S3.

Compounds **2cG** (4-Br, 3-Cl), **2fG** (3,5-di-CF_3), **6cA** (4-Br, 3-Cl) **2dG** (3,5-di-Br), **2eG** (4-Br-1-Nal), **6cG** (4-Br, 3-Cl) and **6fG** (3,5-di-CF_3) demonstrated excellent selectivity for the Gram-positive strains (entries 1–7). Hydantoins **2dG**, **2eG, 6cG** and **6fG** (entries 4–7) had additionally good selectivity (SI: >20) for *E. coli*. All seven derivatives showed low to no haemolytic toxicity. Derivatives **2dA** (3,5-di-Br), **2fA** (3,5-di-CF_3) and **6dG** (3,5-di-Br) had good SI values for all strains tested (entries 8–10). The hydantoins **2dA** (3,5-di-Br) and **2fA** (3,5-di-CF_3) had SI values >20 against the Gram-negative bacterium *P. aeruginosa*, while **6dG** (3,5-di-Br) had SI: 13 for *P. aeruginosa*. All these can be considered very promising compounds.

All compounds tested were obtained as di-trifluoroacetate (di-TFA) salts, which are non-physiological. Therefore, we converted **2cA**, **2cG**, **2dA** and **2dG** to physiological di-hydrochloride (di-HCl) salts, to assess if the biological behaviour would be altered (see Supporting Information, Table S2). We did not observe any major changes in the MIC or EC_{50} values for any of these four derivatives. Minor improvements in antimicrobial activity could be observed for the di-HCl salts of **2cA** (4-Br, 3-Cl) and **2cG** (4-Br, 3-Cl), but no clear trend was apparent. Also, the haemolytic activity was only influenced to a small extend and could often be correlated to the lower molecular weight of the di-HCl salts compared to the di-TFA salts.

2.5. Mode of action (MoA) studies

We have examined the effects of the compounds on the viability of bacterial cells and the membrane integrity of bacterial cells. Seven compounds were selected (based on structural alterations, MIC values, haemolytic activity, and SI) for MoA studies against *B. subtilis* 168 (see Supporting Information, Table S4), as they were primarily potent against Gram-positive bacteria. Six additional compounds with broad-spectrum activity were selected for MoA studies against both, *B. subtilis* 168 and *E. coli* K12 (see Supporting Information, Tables S4 and S5) [56]. These two well-known strains of *B. subtilis* and *E. coli*, in combination with the respective sensor plasmids that carry the reporter constructs, serve as models to study the modes of action in

Table 3
Selectivity index (SI) of the most promising narrow- and broad-spectrum antimicrobials. EC_{50} values are given in [μg/mL].

Entry	Comp. ID	SI (EC_{50}/MIC)[a]				EC_{50}[b]
		S. a	B. s	E. c	P. a	
1	**2cG**	>234	>234	–	–	>467
2	**2fG**	>122	>245	–	–	>489
3	**6cA**	>55	>110	–	–	>439
4	**2dG**	243	122	30	–	486
5	**2eG**	103	103	26	–	206
6	**6cG**	347	347	43	–	347
7	**6fG**	192	192	48	–	384
8	**2dA**	43	86	22	43	344
9	**2fA**	25	50	25	25	399
10	**6dG**	206	206	52	13	206

Bacterial reference strains: S. a – *Staphylococcus aureus* ATCC 9144, B. s – *Bacillus subtilis* 168, E. c – *Escherichia coli* ATCC 25922, and P. a – *Pseudomonas aeruginosa* ATCC 27853.

[a] –: No SI was calculated if MIC was >16 μg/mL.

[b] Values given as *greater than* correspond to the highest concentration (500 μM) tested in the RBC assay.

representatives of Gram-positive and Gram-negative bacteria, respectively.

To explore the MoA of promising compounds in *B. subtilis* 168 and *E. coli* K12, we conducted two luciferase-based biosensor tests – examining the effects on bacterial viability and membrane integrity. The biosensor-based viability test measures the viability of bacterial cells as light production by recombinantly expressed bacterial luciferase derived from the *Photorhabdus luminescens lux* operon [57,58]. External substrates do not affect light production by bacterial lux operons. Bacteria themselves provide a reduced flavin mononucleotide (FMNH2) and a long-chain aldehyde pool, which is the substrate for light production. Bacterial luciferase is a very efficient real-time sensor of bacterial viability because NADH, NADPH, and ATP are required to constantly fill the substrate pool.

The biosensor-based membrane integrity test is based on the *luc*GR gene (luciferase) of *Pyrophorus plagiophthalamus*, which is a luminous click beetle [59]. Unlike bacterial luciferase, the light reaction is closely dependent on externally added D-luciferin as a substrate. D-luciferin cannot cross the intact biological membrane properly at neutral pH. The uptake of D-luciferin is explored after the addition of antimicrobial substances to determine whether the membrane has been affected and becomes permeable for D-luciferin or not. If D-luciferin enters through damaged membranes, light production increases. Light production peaks quickly if the integrity of the membrane is compromised and then usually decreases during the consumption of the dying cells' ATP.

In general, most of the compounds tested influenced survival (viability) and showed strong membrane disrupting activity against *B. subtilis*, and some of them were active against both bacterial species. However, some compounds had more prominent effects on survival and faster membranolytic effects on *B. subtilis* than *E. coli*. When the concentration of the compounds exceeded the MIC value against the respective bacterium, both the viability and the integrity of the membrane were affected for most compounds. Furthermore, increasing concentrations affected both viability and membranolytic activity at an increasing rate, indicating a concentration-dependent killing effect. However, we were unable to determine the relationship between the structure/activity and the mode of action profiles. Compound **6cG** (4-Br, 3-Cl) was chosen as a broad-spectrum hydantoin to illustrate the results with regard to viability and membrane integrity (Figs. 3 and 4). During the 3 min test period, hydantoin **6cG** showed a substantial influence on the survival (viability) of *B. subtilis* (Fig. 3A, left). The derivative **6cG** showed a membrane-related action because the light emittance increased rapidly and dose-dependently (Fig. 3B, left), and the effect was prominent compared to chlorhexidine (CHX) (Fig. 3B, right). The CHX reference control is a bactericidal agent that affects the cell walls and membranes of both *B. subtilis* 168 [60] and *E. coli* K12 [61]. In the present study, the MIC value for CHX was determined to be 1.5 μg/mL against both *B. subtilis* 168 and *E. coli* K12. The disruptive membrane effect of hydantoin **6cG** on *B. subtilis* was shown to occur at a concentration of 25.6 and 51.2 μg/mL (blue and black line, Fig. 3B, left), which were 25.6 and 51.2 times higher than its MIC (1 μg/mL). Concentrations below 25.6 μg/mL showed a limited membrane disruption effect, with peak emissions not decreasing during the measurement period. The bacterial concentration in these experiments was approximately 100 times higher than that used in the MIC test, and this could explain why a higher concentration of **6cG** hydantoin was required to affect the viability and integrity of the membrane.

The effect of hydantoin **6cG** on the viability and membrane integrity of the Gram-negative *E. coli* showed somewhat incomparable effects as observed towards the Gram-positive *B. subtilis*. Being a broad-spectrum derivative, **6cG** could not influence the viability of *E. coli* as fast as the strong membranolytic agent CHX (Fig. 4A). Although a concentration-dependent declining trend of light emission was seen in the viability assay, only the highest concentration (51.2 μg/mL which is 6.4 x MIC) resulted in increased light emission in the inner membrane assay and it was not followed by a decline during the test period (indicating a less notable disruptive effect of the inner membrane) (Fig. 4B, left). The delay and reduction in the effect of **6cG** on membrane integrity could be caused by the outer membrane of *E. coli,* which may act as an additional barrier.

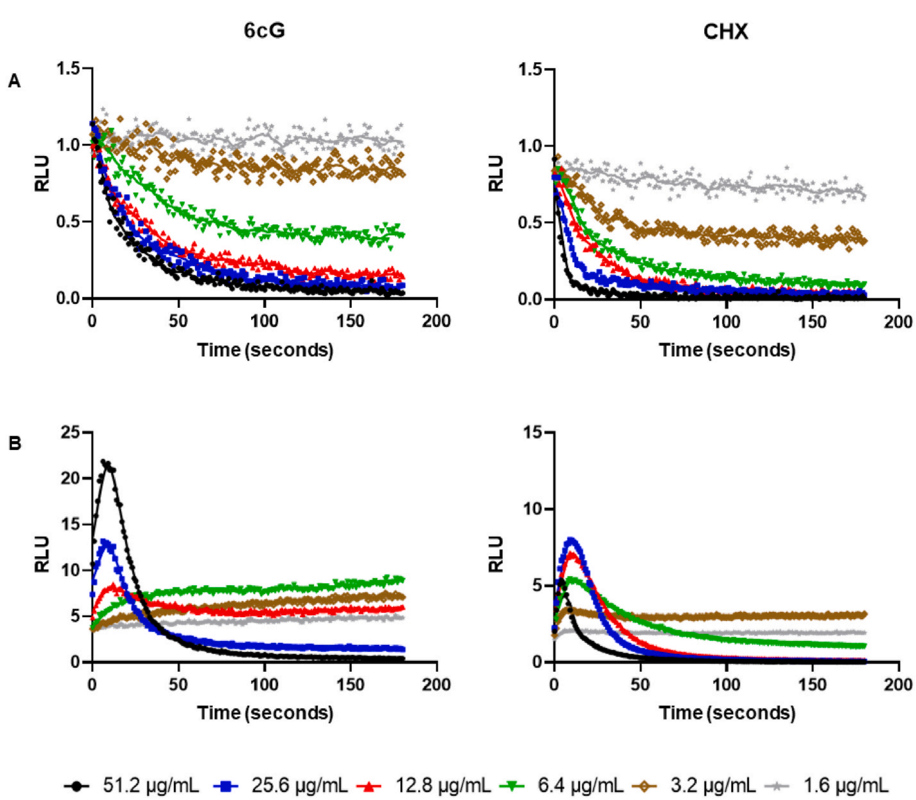

Fig. 3. The effects of **6cG** (broad spectrum) and chlorhexidine (CHX, positive control) on the kinetics of (**A**) viability and (**B**) membrane integrity in *B. subtilis* 168. Normalized light emission (normalized with a negative, untreated water control) is plotted as relative light units (RLU) over time (seconds). Light emission was measured each second for 180 s after adding the bacterial cell suspension (with 1 mM D-luciferin for the membrane integrity assay) to the analytes in separate wells. The figure shows a representative data set from at least three independent experiments.

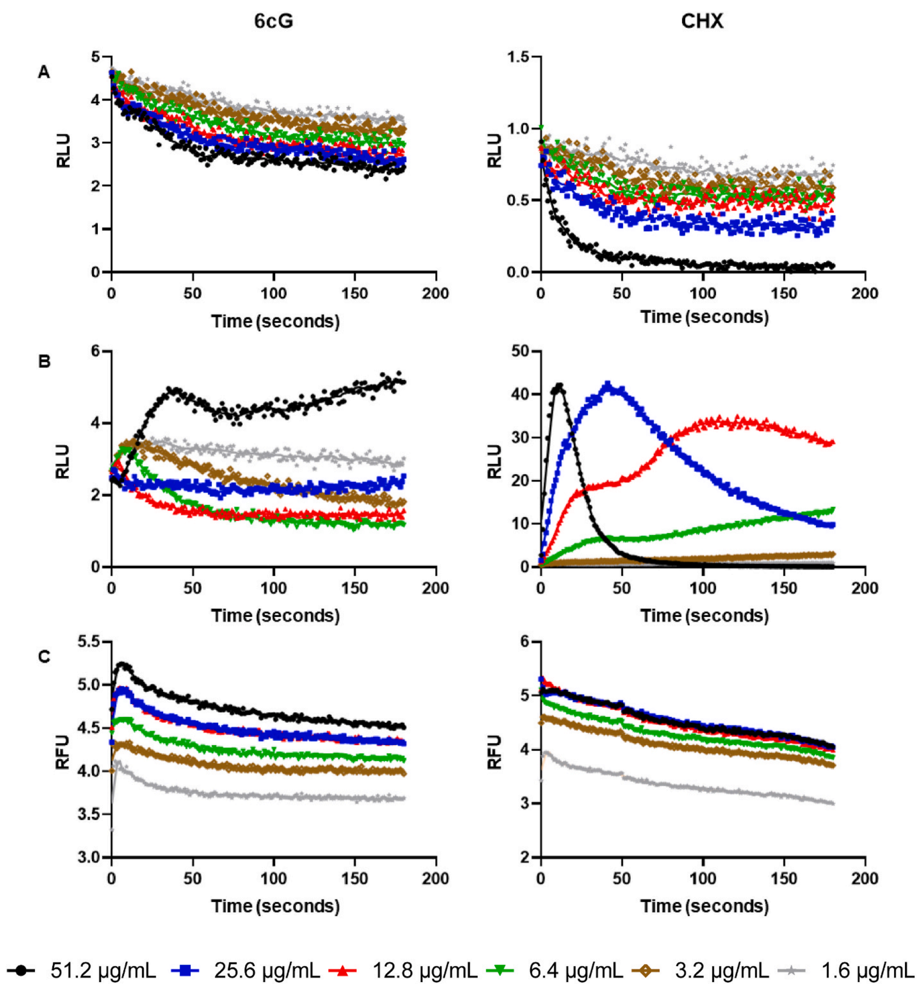

Fig. 4. The effects of **6cG** (broad spectrum) and chlorhexidine (CHX, positive control) on the kinetics of (A) viability, (B) inner membrane integrity, and (C) outer membrane integrity in *E. coli* K12. Normalized light emission (normalized with a negative, untreated water control) is plotted as relative light units (RLU) over time (seconds) for A and B. For C, normalized fluorescence (normalized with a negative, untreated water control) is plotted as relative fluorescence units (RFU) over time (seconds). Light emission/fluorescence was measured each second for 180 s after adding the bacterial cell suspension (with 1 mM D-luciferin for the inner membrane integrity assay and 20 μM 1-*N*-phenylnapthylamine for outer membrane integrity assay) to the analytes in separate wells. The figure shows a representative data set from at least three independent experiments.

We used the 1-*N*-phenylnapthylamine (NPN) fluorescent probe to determine whether **6cG** affected the outer membrane permeability of *E. coli*. The small NPN molecules (219 Da) have low fluorescence in water solutions, but if bound to phospholipids, they produce high fluorescence. Hydrophobic NPN cannot effectively pass through the outer membrane of intact *E. coli* cells, resulting in low fluorescence; however, if the outer membrane is damaged, NPN can reach the periplasmic space, bind to the phospholipids of the inner and outer membrane, and produce enhanced fluorescence [62]. In this test, high concentrations of hydantoin **6cG** produced high fluorescence levels (Fig. 4C, left), while no significant increase in luminescence was observed in the inner membrane integrity test, except in one concentration which is 51.2 μg/mL (Fig. 4B, left). This observation indicates that the presence of the outer membrane may be a rate-limiting step for this compound to act on the inner membrane. However, when the concentration of **6cG** increased, the fluorescence level was higher (Fig. 4C, left), indicating a rapid change in outer membrane permeability that was followed by membrane disruption as compared to CHX (Fig. 4C, right). At the same time, bacterial cell survival was reduced (Fig. 4A, left) and the integrity of the inner membrane was altered (Fig. 4B, left).

The viability of the bacterial cells was markedly reduced for a concentration of 51.2 μg/mL (6.4 x MIC) (see Fig. S1), and when samples from the NPN assay were spotted on an agar plate after the test period, a bactericidal effect of **6cG** was demonstrated. These results strongly suggest that when concentrations are high enough, hydantoin **6cG** disrupts the outer and inner membranes at the same speed. However, it cannot be excluded that higher concentrations of **6cG** cause a different MoA, leading the compound to cross the outer membrane without affecting the latter.

Our results indicate that the main MoA of most of the synthesized compounds is to interrupt the integrity of the bacterial membranes in a concentration-dependent manner – as demonstrated for the broad-spectrum hydantoin **6cG,** against both the Gram-positive *B. subtilis* and the Gram-negative *E. coli*. However, some cationic AMPs have a concentration-dependent dual mode of action [63]. For example, it is known that the N-terminal fragment 1–35 of Bac7 (a proline-arginine rich AMP) has an effect on the internal membrane at high concentrations and binds to the intracellular chaperone protein DnaK and 70S ribosomes, and affect these target molecules at low concentrations [64–66]. Hence, other targets may exist in addition to the bacterial cytoplasmic membranes. Further studies are needed to determine whether there are other additional modes of action for these compounds.

3. Conclusion

We investigated five scaffolds for their suitability to develop novel tetrasubstituted, amphipathic SMAMP antimicrobials, revealing the hydantoin structure as a promising template for antibacterial drug lead development. By screening different combinations of lipophilic side chains, *n*-alkyl linkers and cationic groups we identified the tetra-halogenated compounds **2dA** (3,5-di-Br), **6cG** (4-Br, 3-Cl) and **6dG** (3,5-di-Br) as very promising lead structures. The results obtained from the viability and membrane integrity assays, suggested a rapid membranolytic effect, as demonstrated for hydantoin **6cG** in *B. subtilis* and *E. coli*. Interestingly, both the inner and the outer membrane in *E. coli* seemed to be disrupted at a similar speed. We believe that our findings on the qualitative contribution of the scaffold structures can help the development of novel small molecule analogues of AMPs or SMAMPs.

4. Experimental section

For a detailed description of all chemical and biological experimental procedures, chemical analysis and further discussions see the Supporting Information. Additional raw data is available through the DataverseNO repository, link: https://doi.org/10.18710/A6AJN4.

Author contributions

M.K.L, A.B. and M.B.S. designed the compound library; M.K.L carried out all chemical experiments and analysis; A.R., H.D., H.-M.B., T.H. and K.S. determined the biological assays; A.R., H.D., T.A. performed the biological assays and M.K.L, A.R., H.D., H.-M.B., T.H., K.S., A.B. and M. B.S. analysed and interpreted the data. The manuscript was written through contributions of all authors. All authors have given approval to the final version of the manuscript.

Declaration of competing interest

The authors declare the following financial interests/personal relationships which may be considered as potential competing interests: Morten B Strøm and Annette Bayer have patent #Barbituric acid derivatives comprising cationic and lipophilic groups. WO2018178198A1. Issued to UiT.

Data availability

NMR data files are available at DataverseNO: https://doi.org/10.18710/A6AJN4.

Acknowledgements

MKL, AR and HD thank for a PhD fellowship provided by UiT as part of the AntifoMar (2560700) and LeadScAMR (2017/6770) grants. We thank Senior Engineer Jostein Johansen for help with the HRMS and Prof. Máté Erdélyi for sharing his knowledge.

Appendix A. Supplementary data

Supplementary data to this article can be found online at https://doi.org/10.1016/j.ejmech.2023.115147.

References

[1] O. Nolte, Antimicrobial resistance in the 21st century: a multifaceted challenge, Protein Pept. Lett. 21 (2014) 330–335.
[2] M. Miethke, M. Pieroni, T. Weber, M. Brönstrup, P. Hammann, L. Halby, P. B. Arimondo, P. Glaser, B. Aigle, H.B. Bode, R. Moreira, Y. Li, A. Luzhetskyy, M. H. Medema, J.-L. Pernodet, M. Stadler, J.R. Tormo, O. Genilloud, A.W. Truman, K. J. Weissman, E. Takano, S. Sabatini, E. Stegmann, H. Brötz-Oesterhelt, W. Wohlleben, M. Seemann, M. Empting, A.K.H. Hirsch, B. Loretz, C.-M. Lehr, A. Titz, J. Herrmann, T. Jaeger, S. Alt, T. Hesterkamp, M. Winterhalter, A. Schiefer, K. Pfarr, A. Hoerauf, H. Graz, M. Graz, M. Lindvall, S. Ramurthy, A. Karlén, M. van Dongen, H. Petkovic, A. Keller, F. Peyrane, S. Donadio, L. Fraisse, L.J.V. Piddock, I. H. Gilbert, H.E. Moser, R. Müller, Towards the sustainable discovery and development of new antibiotics, Nat. Rev. Chem. 5 (2021) 726–749.
[3] M. Pasupuleti, A. Schmidtchen, M. Malmsten, Antimicrobial peptides: key components of the innate immune system, Crit. Rev. Biotechnol. 32 (2012) 143–171.
[4] C.D. Fjell, J.A. Hiss, R.E. Hancock, G. Schneider, Designing antimicrobial peptides: form follows function, Nat. Rev. Drug Discov. 11 (2011) 37–51.
[5] G. Carmona, A. Rodriguez, D. Juarez, G. Corzo, E. Villegas, Improved protease stability of the antimicrobial peptide Pin2 substituted with D-amino acids, Protein J. 32 (2013) 456–466.
[6] M. Su, D. Xia, P. Teng, A. Nimmagadda, C. Zhang, T. Odom, A. Cao, Y. Hu, J. Cai, Membrane-active hydantoin derivatives as antibiotic agents, J. Med. Chem. 60 (2017) 8456–8465.
[7] R. Kapoor, P.R. Eimerman, J.W. Hardy, J.D. Cirillo, C.H. Contag, A.E. Barron, Efficacy of antimicrobial peptoids against Mycobacterium tuberculosis, Antimicrob. Agents Chemother. 55 (2011) 3058–3062.
[8] C. Ghosh, G.B. Manjunath, P. Akkapeddi, V. Yarlagadda, J. Hoque, D.S. Uppu, M. M. Konai, J. Haldar, Small molecular antibacterial peptoid mimics: the simpler the better, J. Med. Chem. 57 (2014) 1428–1436.
[9] A. Violette, S. Fournel, K. Lamour, O. Chaloin, B. Frisch, J.P. Briand, H. Monteil, G. Guichard, Mimicking helical antibacterial peptides with nonpeptidic folding oligomers, Chem. Biol. 13 (2006) 531–538.
[10] P. Teng, Y. Shi, P. Sang, J. Cai, γ-AApeptides as a new class of peptidomimetics, Chem. Eur J. 22 (2016) 5458–5466.
[11] Y. Shi, P. Teng, P. Sang, F. She, L. Wei, J. Cai, γ-AApeptides: design, structure, and applications, Acc. Chem. Res. 49 (2016) 428–441.
[12] P. Teng, A. Nimmagadda, M. Su, Y. Hong, N. Shen, C. Li, L.-Y. Tsai, J. Cao, Q. Li, J. Cai, Novel bis-cyclic guanidines as potent membrane-active antibacterial agents with therapeutic potential, Chem. Commun. 53 (2017) 11948–11951.
[13] M. Wang, R. Gao, M. Zheng, P. Sang, C. Li, E. Zhang, Q. Li, J. Cai, Development of bis-cyclic imidazolidine-4-one derivatives as potent antibacterial agents, J. Med. Chem. 63 (2020) 15591–15602.
[14] M.B. Strøm, B.E. Haug, M.L. Skar, W. Stensen, T. Stiberg, J.S. Svendsen, The pharmacophore of short cationic antibacterial peptides, J. Med. Chem. 46 (2003) 1567–1570.
[15] T. Hansen, T. Alst, M. Havelkova, M.B. Strøm, Antimicrobial activity of small β-peptidomimetics based on the pharmacophore model of short cationic antimicrobial peptides, J. Med. Chem. 53 (2010) 595–606.
[16] M.H. Paulsen, D. Ausbacher, A. Bayer, M. Engqvist, T. Hansen, T. Haug, T. Anderssen, J.H. Andersen, J.U.E. Sollid, M.B. Strøm, Antimicrobial activity of amphipathic α,α-disubstituted β-amino amide derivatives against ESBL – CARBA producing multi-resistant bacteria; effect of halogenation, lipophilicity and cationic character, Eur. J. Med. Chem. 183 (2019), 111671.
[17] M.H. Paulsen, M. Engqvist, D. Ausbacher, T. Anderssen, M.K. Langer, T. Haug, G. R. Morello, L.E. Liikanen, H.-M. Blencke, J. Isaksson, E. Juskewitz, A. Bayer, M. B. Strøm, Amphipathic barbiturates as mimics of antimicrobial peptides and the marine natural products eusynstyelamides with activity against multi-resistant clinical isolates, J. Med. Chem. 64 (2021) 11395–11417.
[18] E.M. Igumnova, E. Mishchenko, T. Haug, H.-M. Blencke, J.U.E. Sollid, E.G. A. Fredheim, S. Lauksund, K. Stensvåg, M.B. Strøm, Synthesis and antimicrobial activity of small cationic amphipathic aminobenzamide marine natural product mimics and evaluation of relevance against clinical isolates including ESBL–CARBA producing multi-resistant bacteria, Biorg. Med. Chem. 24 (2016) 5884–5894.
[19] T.A. Bakka, M.B. Strøm, J.H. Andersen, O.R. Gautun, Synthesis and antimicrobial evaluation of cationic low molecular weight amphipathic 1,2,3-triazoles, Bioorg. Med. Chem. Lett. 27 (2017) 1119–1123.
[20] M.K. Langer, A. Rahman, H. Dey, T. Anderssen, F. Zilioli, T. Haug, H.-M. Blencke, K. Stensvåg, M.B. Strøm, A. Bayer, A concise SAR-analysis of antimicrobial cationic amphipathic barbiturates for an improved activity-toxicity profile, Eur. J. Med. Chem. 241 (2022), 114632.
[21] M.H. Paulsen, E.A. Karlsen, D. Ausbacher, T. Anderssen, A. Bayer, P. Ochtrop, C. Hedberg, T. Haug, J.U. Ericson Sollid, M.B. Strøm, An amphipathic cyclic tetrapeptide scaffold containing halogenated $\beta^{2,2}$-amino acids with activity against multiresistant bacteria, J. Pept. Sci. 24 (2018) e3117.
[22] K. Kieć-Kononowicz, K. Stadnicka, A. Mitka, E. Pękala, B. Filipek, J. Sapa, M. Zygmunt, Synthesis, structure and antiarrhythmic properties evaluation of new basic derivatives of 5,5-diphenylhydantoin, Eur. J. Med. Chem. 38 (2003) 555–566.
[23] J. Handzlik, A.J. Bojarski, G. Satała, M. Kubacka, B. Sadek, A. Ashoor, A. Siwek, M. Więcek, K. Kucwaj, B. Filipek, K. Kieć-Kononowicz, SAR-studies on the importance of aromatic ring topologies in search for selective 5-HT7 receptor ligands among phenylpiperazine hydantoin derivatives, Eur. J. Med. Chem. 78 (2014) 324–339.
[24] T.R. Rodgers, M.P. LaMontagne, A. Markovac, A.B. Ash, Hydantoins as antitumor agents, J. Med. Chem. 20 (1977) 591–594.
[25] A.A. El-Barbary, A.I. Khodair, E.B. Pedersen, C. Nielsen, S-Glucosylated hydantoins as new antiviral agents, J. Med. Chem. 37 (1994) 73–77.
[26] S. Cortes, Z.-K. Liao, D. Watson, H. Kohn, Effect of structural modification of the hydantoin ring on anticonvulsant activity, J. Med. Chem. 28 (1985) 601–606.
[27] R. Sarges, R.C. Schnur, J.L. Belletire, M.J. Peterson, Spiro hydantoin aldose reductase inhibitors, J. Med. Chem. 31 (1988) 230–243.
[28] E. Szymańska, K. Kieć-Kononowicz, Antimycobacterial activity of 5-arylidene aromatic derivatives of hydantoin, Il Farmaco 57 (2002) 355–362.
[29] E. Szymańska, K. Kieć-Kononowicz, A. Białecka, A. Kasprowicz, Antimicrobial activity of 5-arylidene aromatic derivatives of hydantoin. Part 2, Il Farmaco 57 (2002) 39–44.
[30] J. Handzlik, E. Szymańska, J. Chevalier, E. Otrębska, K. Kieć-Kononowicz, J.-M. Pagès, S. Alibert, Amine–alkyl derivatives of hydantoin: new tool to combat resistant bacteria, Eur. J. Med. Chem. 46 (2011) 5807–5816.
[31] C.J. White, A.K. Yudin, Contemporary strategies for peptide macrocyclization, Nat. Chem. 3 (2011) 509–524.
[32] X. Chen, E.G. Mietlicki-Baase, T.M. Barrett, L.E. McGrath, K. Koch-Laskowski, J. J. Ferrie, M.R. Hayes, E.J. Petersson, Thioamide substitution selectively modulates proteolysis and receptor activity of therapeutic peptide hormones, J. Am. Chem. Soc. 139 (2017) 16688–16695.
[33] M. Feng, B. Tang, S.H. Liang, X. Jiang, Sulfur containing scaffolds in drugs: synthesis and application in medicinal chemistry, Curr. Top. Med. Chem. 16 (2016) 1200–1216.

[34] S. Pathania, R.K. Narang, R.K. Rawal, Role of sulphur-heterocycles in medicinal chemistry: an update, Eur. J. Med. Chem. 180 (2019) 486–508.
[35] M.C. Bagley, J.W. Dale, E.A. Merritt, X. Xiong, Thiopeptide antibiotics, Chem. Rev. 105 (2005) 685–714.
[36] X. Just-Baringo, F. Albericio, M. Álvarez, Thiopeptide antibiotics: retrospective and recent advances, Mar. Drugs 12 (2014) 317–351.
[37] H.C. Neu, β-Lactam Antibiotics: structural relationships affecting *in vitro* activity and pharmacologic properties, Rev. Infect. Dis. 8 (1986) 237–259.
[38] E. Ware, The chemistry of the hydantoins, Chem. Rev. 46 (1950) 403–470.
[39] M. Meusel, M. Gütschow, Recent developments in hydantoin chemistry, A review, Org. Prep. Proced. Int. 36 (2004) 391–443.
[40] C.A. López, G.G. Trigo, The chemistry of hydantoins, in: A.R. Katritzky (Ed.), Adv. Heterocycl. Chem., Academic Press, 1985, pp. 177–228.
[41] L. Konnert, F. Lamaty, J. Martinez, E. Colacino, Recent advances in the synthesis of hydantoins: the state of the art of a valuable scaffold, Chem. Rev. 117 (2017) 13757–13809.
[42] W.T. Read, Researches on hydantoins. Synthesis of the soporific, 4,4-phenylethyl-hydantoin (Nirvanol), J. Am. Chem. Soc. 44 (1922) 1746–1755.
[43] H.T.L. Bucherer V A, Syntheses of hydantoins. II. Formation of substituted hydantoins from aldehydes and ketones, J. Prakt. Chem. 141 (1934) 5–43.
[44] H. Biltz, Constitution of the products of the interaction of substituted carbamides on benzil and certain new methods for the preparation of 5,5-diphenylhydantoin, Ber. Dtsch. Chem. Ges. 41 (1908) 1379–1393.
[45] C. Hulme, L. Ma, J.J. Romano, G. Morton, S.-Y. Tang, M.-P. Cherrier, S. Choi, J. Salvino, R. Labaudiniere, Novel applications of carbon dioxide/MeOH for the synthesis of hydantoins and cyclic ureas via the Ugi reaction, Tetrahedron Lett. 41 (2000) 1889–1893.
[46] C. Hulme, H. Bienaymé, T. Nixey, B. Chenera, W. Jones, P. Tempest, A.L. Smith, Library generation via postcondensation modifications of isocyanide-based multicomponent reactions, in: Methods Enzymol., Academic Press, 2003, pp. 469–496.
[47] D.V. Leusen, A.M.V. Leusen, Synthetic uses of tosylmethyl isocyanide (TosMIC), in: Organic Reactions, 2004, pp. 417–666.
[48] R. Sakata, T. Soeta, Y. Ukaji, One-Carbon homologation of pyrrole carboxaldehyde via wittig reaction and mild hydrolysis of vinyl ether - toward the synthesis of a stericcaly locked phytochrome chromophore, Heterocycles 91 (2015) 593–603.
[49] Z. Kosarych, T. Cohen, Rapid, high-yield cleavage of enol and dienol methyl ethers under mild conditions using chlorotrimethylsilane/sodium iodide, Tetrahedron Lett. 21 (1980) 3959–3962.
[50] H. Stetter, R.Y. Rämsch, Über die präparative Nutzung der 1,3-thiazoliumsalzkatalysierten Acyloin- und Benzoin-Bildung; IV1, Herstellung von Acyloinen mit funktionellen Gruppen, 1981, pp. 477–478. Synthesis, 1981.
[51] Y.B. Kim, C.S. Kim, C.K. Lee, Condensation reactions of aryl acyloins with ureas in ethylene glycol, J. Heterocycl. Chem. 31 (1994) 1653–1656.
[52] H.C. Carrington, Thiohydantoins. Part I. Preparation of 5 : 5-disubstituted 2 : 4-dithiohydantoins from the corresponding ketones, J. Chem. Soc. (1947) 681–683, 131.
[53] M. Marinov, S. Minchev, N. Stoyanov, G. Ivanova, M. Spassova, V. Enchev, Synthesis, spectroscopic characterization and *ab initio* investigation of thioanalogues of spirohydantoins, Croat. Chem. Acta 78 (2005) 9–16.
[54] G. Wenska, S. Paszyc, Photolysis of thiopurines in the presence of oxygen, Z. Naturforsch. B Chem. Sci. 36 (1981) 1628–1631.
[55] M. Terada, R. Watanabe, II.3.6 barbiturates, in: Drugs and Poisons in Humans, Springer Berlin, Heidelberg, 2005, pp. 301–313.
[56] M. Virta, K.E.O. Åkerman, P. Saviranta, C. Oker-Blom, M.T. Karp, Real-time measurement of cell permeabilization with low-molecular-weight membranolytic agents, J. Antimicrob. Chemother. 36 (1995) 303–315.
[57] J. Chatterjee, E.A. Meighen, Biotechnological applications of bacterial bioluminescence (lux) genes, Photochem. Photobiol. 62 (1995) 641–650.
[58] J. Lehtinen, M. Virta, E.-M. Lilius, Fluoro-luminometric real-time measurement of bacterial viability and killing, J. Microbiol. Methods 55 (2003) 173–186.
[59] M. Virta, K.E. Akerman, P. Saviranta, C. Oker-Blom, M.T. Karp, Real-time measurement of cell permeabilization with low-molecular-weight membranolytic agents, J. Antimicrob. Chemother. 36 (1995) 303–315.
[60] E. Juskewitz, E. Mishchenko, V.K. Dubey, M. Jenssen, M. Jakubec, P. Rainsford, J. Isaksson, J.H. Andersen, J.U. Ericson, Lulworthinone: *In vitro* mode of action investigation of an antibacterial dimeric naphthopyrone isolated from a marine fungus, Mar. Drugs 20 (2022) 277.
[61] T. Kuyyakanond, L.B. Quesnel, The mechanism of action of chlorhexidine, FEMS Microbiol. Lett. 100 (1992) 211–215.
[62] B. Loh, C. Grant, R.E. Hancock, Use of the fluorescent probe 1-*N*-phenylnaphthylamine to study the interactions of aminoglycoside antibiotics with the outer membrane of *Pseudomonas aeruginosa*, Antimicrob. Agents Chemother. 26 (1984) 546–551.
[63] M. Graf, M. Mardirossian, F. Nguyen, A.C. Seefeldt, G. Guichard, M. Scocchi, C. A. Innis, D.N. Wilson, Proline-rich antimicrobial peptides targeting protein synthesis, Nat. Prod. Rep. 34 (2017) 702–711.
[64] E. Podda, M. Benincasa, S. Pacor, F. Micali, M. Mattiuzzo, R. Gennaro, M. Scocchi, Dual mode of action of Bac7, a proline-rich antibacterial peptide, Biochim. Biophys. Acta 1760 (2006) 1732–1740.
[65] M.L. Scocchi C, P. Decarli, G. Mignogna, P. Christen, R. Gennaro, The proline-rich antibacterial peptide Bac7 binds to and inhibits *in vitro* the molecular chaperone DnaK, Int. J. Pept. Res. Therapeut. 15 (2009) 147–155.
[66] M. Mardirossian, R. Grzela, C. Giglione, T. Meinnel, R. Gennaro, P. Mergaert, M. Scocchi, The host antimicrobial peptide Bac71-35 binds to bacterial ribosomal proteins and inhibits protein synthesis, Chem. Biol. 21 (2014) 1639–1647.

Supporting Information

for

Investigation of Tetrasubstituted Heterocycles Reveals Hydantoins as a Promising Scaffold for Development of Novel Antimicrobials with Membranolytic Properties

Manuel K. Langer[a], Ataur Rahman[b], Hymonti Dey[b], Trude Anderssen[c], Hans-Matti Blencke[b], Tor Haug[b], Klara Stensvåg[b], Morten B. Strøm[a]*, Annette Bayer[b]*

[a] *Department of Chemistry, UiT – The Arctic University of Norway, NO-9037 Tromsø, NORWAY.*
[b] *The Norwegian College of Fishery Science, Faculty of Biosciences, Fisheries and Economics, UiT – The Arctic University of Norway, NO-9037 Tromsø, NORWAY.*
[c] *Department of Pharmacy, Faculty of Health Sciences, UiT – The Arctic University of Norway, NO-9037 Tromsø, NORWAY.*
** Shared senior authorship and corresponding authors.*

Table of Contents

1. 4-imidazolidin-2-ones *via N*-acyliminium ion rearrangement

Based on the pioneering work of Speckamp and co-workers[1] *N*-acyliminium intermediates have been used in a variety of cationic cyclisations.[2] Far less explored are the *N*-acyliminium ion triggered rearrangements, predominantly Cope-type, which are mostly reported as the underlying mechanism for certain cyclisations.[3] But when Kohn et al. studied the preparation of annulated imidazolidinones from 4-hydroxy-5,5-dimethylimidazolidin-2-one, they also observed a 1,2-methylshift to the corresponding 4-imidazolin-2-one.[4]. As the 4-hydroxy-imidazolidinones can be accessed by reducing the corresponding hydantoins, we envisioned a similar sequence, starting from the di-Boc protected hydantoin Boc-**9a** and the previously prepared hydantoins Boc-**2aA** and Boc-**2da** (**Scheme S1**).

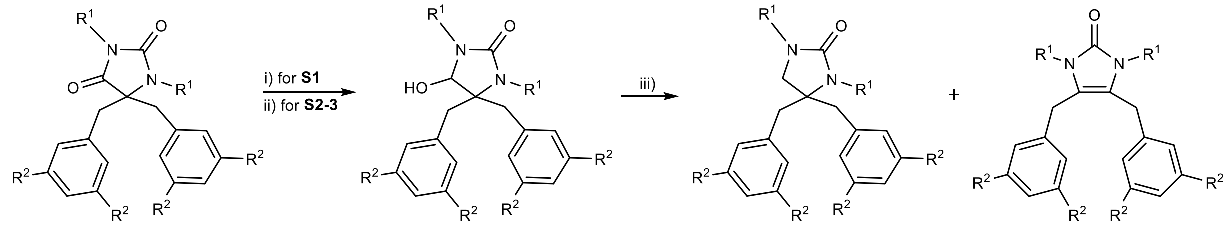

Boc-**9a** R^1 = Boc, R^2 = H
Boc-**2aA** R^1 = $(CH_2)_3NHBoc$, R^2 = H
Boc-**2dA** R^1 = $(CH_2)_3NHBoc$, R^2 = Br

S1 R^1 = Boc or H, R^2 = H
S2 R^1 = $(CH_2)_3NHBoc$, R^2 = H
S3 R^1 = $(CH_2)_3NHBoc$, R^2 = Br

S4 R^1 = R^2 = H

S5 R^1 = $(CH_2)_3NH_2$, R^2 = H
3A R^1 = $(CH_2)_3NH_2$, R^2 = Br

Scheme S1. Synthetic strategy towards **3A** *via* a cationic rearrangement from an *in situ* generated *N*-acyliminium ion. Reaction conditions: i) $NaBH_4$, EtOH, r.t., 16 h, no yield determined; ii) DIBAL, DCM (dry), -78 to 0 °C, 3 h, 56-70%; iii) see **Table S1**.

Using Boc-**9a** was appealing, because a later introduction of the alkyl linkers would be advantageous for building libraries. $NaBH_4$ mediated reduction of the amidic carbonyl of Boc-**9a** delivered intermediate **S1**. Upon sequential treatment of the latter one with catalytic amounts of *para*-toluenesulfonic acid (*p*-TsOH) at 120 °C followed by TFA in DCM (Table S1, Entry 1) deoxygenated imidazolidine **S4** was obtained. Consequently, we decided to employ **2aA** and **2dA** instead. Both tetrasubstituted hydantoins could be reduced by DIBAL in DCM to yield 4-hydroxy-imidazolidinones **S2** and **S3** in 56% and 70%, respectively. Refluxing intermediate **S2** with a catalytic amount of *p*-TsOH in anhydrous toluene[4] (Table S1, Entry 2) led to quantitative conversion. During this process we observed partial degradation of the Boc groups and decided to treat the crude with TFA in DCM and obtained fully deprotected 4-imidazolidin-2-one **S5** in a yield of 74%. Both TFA alone and with additional trifluoro acetic acid anhydride (TFAA) (Entry 3 and 4) effectively promoted the rearrangement. Using formic acid (Entry 4) led to a mixture of the desired product alongside unreacted starting material with zero to two Boc-groups being intact. When treating halo-aryl containing derivative **S3** with TFA (Entry 5), we observed only partial rearrangement to **3A**. Presumably, partial Boc removal takes place prior to the *N*-acyliminium ion formation, leading to a positively net charged compound and thus raising the barrier for the dehydration and subsequent introduction of another positive charge. Even though we could demonstrate the practical value of this strategy towards 4-imidazolidin-2-ones, the final products **S5** and **3A** were difficult to purify, supposedly due to partial fragmentation of the intermediate *N*-acyliminium ion. We decided therefore to abolish this strategy.

Table S1. Reaction conditions for the cationic rearrangement and subsequent Boc-deprotection

Entry	Reactant	Acid (eq)	Solvent[a]	Temperature [°C]	Time [h]	Product (Yield [%])
1	**S1**	1. p-TsOH (0.20) 2. TFA (20.0 eq)	1. Toluene 2. DCM	1. 120 2. 25	1. 24 2. 18	**S4** (34)
2[b]	**S2**	1. p-TsOH (0.20) 2. TFA (20.0)	1. Toluene 2. DCM	1. 120 2. 25	1. 5.5 2. 18	**S5** (74)
3	**S2**	TFA (20.0 eq)	DCM	25	18	**S5** (82)
4	**S2**	TFAA (1.30)	TFA:DCM (2:1)	50	18	**S5** (83)
5	**S2**	Formic acid (1.05)	DCM	50	4	n.d.[c]
6	**S3**	TFA (15.0)	DCM	25	22	**S17A** (43%)

[a] Anhydrous solvents were used. [b] Upon completion of the rearrangement toluene was removed and replaced by DCM. [c] A mixture of reactant, Boc-deprotected reactant and the rearranged product was obtained.

2. Counterion effect

Physicochemical properties like adsorption, solubility and membrane permeability of basic and acidic drugs can be greatly influenced by their counterions.[5] We converted the di-trifluoroacetate (di-TFA) salts of hydantoins **2c** (3-Cl, 4-Br) and **2d** (3,5-di-Br) into their di-hydrochloride (di-HCl) salts to improve their water solubility[6] and to evaluate the impact of counterions on their biological activity (**Table S2**).

Table S2. MIC and EC_{50} values in [µg/mL] of selected di-trifluoroacetate (TFA) and di-hydrochloride (HCl) salts. Improved values are shown in green.

Comp. ID	Side chain	MIC (TFA)				EC_{50} (TFA)	MIC (HCl)				EC_{50} (HCl)	Solubility[a]
		S. a	B. s	E. c	P. a		S. a	B. s	E. c	P. a		
2cA	(3-Cl, 4-Br)	8	4	32	32	368	8	2	16	32	>400	+/+
2dA	(3,5-di-Br)	8	4	16	8	344	8	2	16	4	289	+/+
2cG	(3-Cl, 4-Br)	2	2	32	8	>467	<1	2	16	64	342	–/–
2dG	(3,5-di-Br)	2	1	16	16	486	2	2	16	32	303	–/–

S. a – *Staphylococcus aureus* ATCC 9144, B.s – *Bacillus subtilis* 168, E. c – *Escherichia coli* ATCC 25922, and P. a – *Pseudomonas aeruginosa* ATCC 27853. [a] If solubility in pure water is equal or greater than 1 mg/mL it is denoted with (+), if lower (–).

Water solubility was assessed qualitatively, by setting the threshold at 1 mg/mL. Di-TFA and di-HCl salts of the amine derivatives **2A** were water soluble, but neither of the salt forms of **2G** were water soluble according to the established criteria. The amine derivatives **2A** demonstrated a minor increase in antimicrobial potency against individual strains by a factor of two. The guanidyl derivatives **2G** did not follow a clear trend, except for Gram-negative *P. aeruginosa*. The di-HCl salts of both guanidyl hydantoins were less potent against *P. aerugrinosa*, especially **2cG** showed an 8-fold decrease in potency for undetermined reasons. The haemolytic activity of the amine derivatives **2A** was comparable for both salt forms, but the di-HCl salts of the guanidyl analogues seemed to be more haemolytic than the di-TFA salts. The effect was less pronounced when EC_{50} values given in µM were compared, but it was still observable. In summary, the di-HCl salts of the amine derivatives **2A** showed slightly improved biological properties, whereas for the guanidyl derivatives **2G** no clear conclusion could be drawn.

3. Experimental Details

3.1 General methods

Unless otherwise noted, purchased chemicals were used as received without further purification. Solvents were dried according to standard procedures over molecular sieves of appropriate size.

Normal phase flash chromatography was carried out on silica gel 60 (230−400 mesh) or on an interchim® PuriFlash XS420 flash system with the sample preloaded on a Samplet® cartridge belonging to a Biotage SP-1 system. Purification by reversed phase (RP) C18 column chromatography (H_2O with 0.1 % TFA/MeCN with 0.1 % TFA) was performed on an interchim® PuriFlash XS420 flash system with the sample preloaded on a Samplet® cartridge.

Thin layer chromatography was carried out using Merck TLC Silica gel 60 F254 and visualized by short-wavelength ultraviolet light or by treatment with an appropriate stain.

NMR spectra were obtained on a 400 MHz Bruker Advance III HD spectrometer equipped with a 5 mm SmartProbe BB/1H (BB = 19F, 31P-15N) at 20 °C. The chemical shifts are reported in ppm relative to the solvent residual peak ($CDCl_3$: δH 7.26 and δC 77.16; Methanol-d4: δH 3.31 and δC 49.00; deuterium oxide: δH 4.79; DMSO-d6 δH 2.51 and δC 39.52). ^{13}C NMR spectra were obtained with ^{1}H decoupling. Data are represented as follows: chemical shift, multiplicity (s = singlet, d = doublet, t = triplet, q = quartet, qn = quintet, dt = doublet of triplet, m = multiplet), coupling constant (*J* in Hz) and integration. The raw data was analyzed with MestReNova (Version 14.0.0-23239).

High-resolution mass spectra (HRMS) were recorded from methanol solutions on an LTQ Orbitrap XL (Thermo Scientific) either in negative or in positive electrospray ionization (ESI) mode. The data was analyzed with Thermo Scientific Xcalibur software.

All final products were lyophilized for 48 h to yield their di-TFA salts.

The purity of all tested compounds was determined to be ≥95%. The analyses were carried out on a Waters ACQUITY UPC^2 system equipped with a TorusTM DEA 130Å, 1.7 µm, 2.1 mm x 50 mm column. Compounds were detected on a Waters ACQUITY PDA detector spanning wavelengths from 205 to 650 nm, coupled to a Waters ACQUITY QDA detector for low resolution mass (LRMS) detection. The derivatives were eluted with a mobile phase consisting of supercritical CO_2 and MeOH containing 0.1 % NH_3 and a linear gradient of 2 – 40 % MeOH over 2 or 4 min followed by isocratic 0.5 min of 40% MeOH. The flow rate was 1.5 mL/min.

3.2 Synthesis of building blocks

1-bromo-4-(bromomethyl)naphthalene **S6**[7], *tert*-butyl (3-bromopropyl)carbamate **S7**[8], and *tert*-butyl (4-bromobutyl)carbamate **S8**[9] were prepared as described in literature.

Note: All compounds were obtained as di-TFA salts. TFA is typically observed at 162.1 (q, J = 35.7 Hz) and 117.7 (q, J = 290.3 Hz) in ^{13}C-NMR and is not reported for each compound individually.

3.3 General procedures

<u>*General Procedure A: Synthesis of symmetrical ketones **8***</u>

Substituted benzyl bromide, TosMiC and TBAB or TBAI were mixed with DCM and a $NaOH_{(aq)}$ solution was added. The mixture was stirred vigorously until TLC indicated full conversion. The layers were separated, and the organic layer was washed with water twice. The organic layer was dried over Na_2SO_4, filtered and the solvent was removed under reduced pressure. The disubstituted TosMiC derivative was obtained as a viscous oil.
The crude oil was taken up in a suitable solvent and $HCl_{(conc.)}$ was added. The solution was stirred at room temperature until TLC indicated full conversion. Water was added and the pH was adjusted to 8–9 with a 2 N $NaOH_{(aq)}$ solution. The aqueous layer was extracted with DCM (3x) and the combined organics were washed with a 10% $NaHCO_{3(aq)}$ solution (2x), dried over Na_2SO_4, filtered and the solvent was removed under reduced pressure. The crude product was purified by column chromatography on silica gel with EtOAc/heptane as eluent. Some of the ketones were not obtained pure but used for the next synthetic step.

*General Procedure B: Synthesis of Hydantoins **9** by the Bucherer-Bergs reaction*

The symmetrical ketone **8** was taken up in DMSO and NH_4CO_3, KOAc and KCN were added. The solution was stirred at 60 °C until all starting material had been consumed. Water was added and the pH was adjusted to 1-2 by dropwise addition of 1 N $HCl_{(aq)}$, upon which a white solid precipitated. The mixture was stirred for 30 min at ambient temperature and then filtered. The residue was washed with water and chloroform extensively. The solids were collected and lyophilized for 24 h to yield the desired hydantoins.

General Procedure C: N,N'-dialkylation and subsequent Boc-removal

Hydantoin **9**, *tert*-butyl (3-bromopropyl)carbamate **S7** or *tert*-butyl (4-bromobutyl)carbamate **S8**, Cs_2CO_3 and TBAI were mixed with acetone and stirred at 65–75 °C until no more starting material and mono-alkylated compound could be observed (HRMS). The reaction mixture was allowed to cool to ambient temperature before water and EtOAc were added. The layers were separated and the aqueous layer was extracted twice more with EtOAc. The combined organics were dried over $MgSO_4$, filtered and the solvent was removed under reduced pressure. The crude products were purified by automated column chromatography on silica gel with EtOAc in heptane as eluent to deliver the Boc protected *N,N'*-dialkylated intermediates Boc-**2A** and Boc-**6A**.
The Boc protected *N,N'*-dialkylated intermediates were dissolved in DCM and TFA was added. The resulting mixture was stirred at ambient temperature until HRMS indicated the cleavage of all Boc groups. The solvent was removed and the crude products were purified by automated RP column chromatography with a gradient of MeCN in H_2O (both containing 0.1% TFA). Fractions containing the target compound were collected, most of the solvent was removed under reduced pressure and the residual solution lyophilized for 48 h. The desired hydantoins **2A** and **6A** were obtained as di-TFA salts.

General procedure D: Guanidine formation

The d-TFA salts of **2A** or **6A** were mixed with THF and DIPEA and stirred at ambient temperature for 10 min. *N*,*N'*-Di-Boc-1*H*-pyrazole-1-carboxamidine was added and the solution was stirred at elevated temperatures until TLC indicated full conversion. The mixture was allowed to cool to ambient temperature and sat. $NH_4Cl_{(aq)}$ solution and EtOAc were added. The layers were separated and the aqueous layer was extracted twice more with EtOAc. The combined organics were dried over Na_2SO_4, filtered and the solvent was removed. The crude products were purified by automated flash column chromatography on silica gel and EtOAc in heptane as eluent to yield the Boc-protected guanidine containing hydantoins Boc-**2G** or Boc-**6G**.
The Boc-protected guanidines were stirred with TFA in DCM at ambient temperature until HRMS indicated full conversion. The solvent was removed and the crude products were purified by automated RP column chromatography with a gradient of MeCN in H_2O (both containing 0.1% TFA). Fractions containing the product were collected, most of the solvent was removed and the residual solution was lyophilized for 48 h. The desired guanylated hydantoins **2G** and **6G** were obtained as di-TFA salts.

General Procedure E: Preparation of hydrochloric (HCl) salts

The previously obtained TFA salts were taken up in MeOH and HCl in MeOH (1.25 M, 10.0 eq) was added. The solvent was removed and the residue was lyophilized for 24 h. The procedure was repeated twice more to yield the respective HCl salts in ≥95% purity. The absence of fluorine was confirmed by ^{19}F NMR (not included).

3.4 Experimental procedures for the synthesis of hydantoins

3.4.1 Synthesis of symmetric ketones 8

The following compounds were synthesized according to General Procedure A:

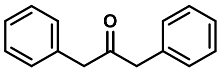

1,3-diphenylpropan-2-one **8a**.
Bromomethyl benzene (1.75 g, 10.24 mmol, 2.0 eq), TosMIC (1.00 g, 5.12 mmol, 1.0 eq), TBAB (661 mg, 2.05 mmol, 0.4 eq), NaOH (35 wt%, 35 mL) and DCM (70 mL) were stirred for 14 h. The addition product was obtained as a brown oil.
The addition product, HCl (37%, 2.0 mL), DCM (30 mL) and THF (7 mL) were stirred at ambient temperature for 17 h. Purification by column chromatography on silica gel with 5 % EtOAc in heptane as eluent delivered **8a** (857 mg, 1.78 mmol, 53% o2s) as a colorless liquid. **^{1}H NMR** (400 MHz, Chloroform-*d*) δ 7.45 – 7.33 (m, 6H), 7.29 – 7.22 (m, 4H), 3.80 (s, 4H). **^{13}C NMR** (101 MHz, Chloroform-*d*) δ 205.4, 134.0 (2C), 129.4 (4C), 128.6 (4C), 126.9 (2C), 48.9 (2C). **HRMS** (ESI): calcd for $C_{15}H_{14}ONa^+$ $[M+Na]^+$ 233.0937, found: 233.0938.

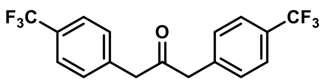

1,3-bis(4-(trifluoromethyl)phenyl)propan-2-one **8b**.
4-(trifluoromethyl)benzyl bromide (4.90 g, 20.50 mmol, 2.0 eq), TosMIC (2.00 g, 10.24 mmol, 1.0 eq), TBAB (1.65 g, 5.12 mmol, 0.5 eq), NaOH (20 wt%, 50 mL) and DCM (100 mL) were stirred for 24 h. The addition product was obtained as a brown oil.
The addition product, HCl (37%, 8 mL), DCM (33 mL) and THF (7 mL) were stirred at ambient temperature for 17 h. Purification by column chromatography on silica gel with 15% EtOAc in heptane as eluent delivered impure **8b** (2.43 g, 7.02 mmol, 69% o2s) as an off-white solid. **^{1}H NMR** (400 MHz, Methanol-*d4*) δ 7.59 (d, *J* = 8.1 Hz, 4H), 7.36 (d, *J* = 8.0 Hz, 4H), 3.98 (s, 4H). **^{13}C NMR** (101 MHz, Methanol-*d4*) δ 206.1, 140.2 (2C), 131.5 (4C), 130.2 (q, J = 32 Hz, 2C), 126.28 (q, *J* = 3.9, 4C), 125.8 (q, *J* = 271.0 Hz, 2C), 49.5 (2C). **HRMS** (ESI): calcd for $C_{17}H_{11}F_6O^-$ [M-H]$^-$ 345.0720, found: 345.0717.

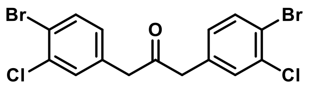

1,3-bis(4-bromo-3-chlorophenyl)propan-2-one **8c**.
1-bromo-4-(bromomethyl)-2-chlorobenzene (1.75 g, 6.15 mmol, 2.0 eq), TosMIC (600 mg, 3.07 mmol, 1.0 eq), TBAB (396 mg, 1.23 mmol, 0.4 eq), NaOH (20 wt%, 12 mL) and DCM (25 mL) were stirred for 24 h. The addition product was obtained as a brown oil.
The addition product, HCl (37%, 1.5 mL), DCM (20 mL) and THF (5 mL) were stirred at ambient temperature for 6.5 h. Purification by column chromatography on silica gel with 12% EtOAc in heptane as eluent delivered impure **8c** (0.96 g, 3.97 mmol, 59% o2s) as an off-white solid. **^{1}H NMR** (400 MHz, Chloroform-*d*) δ 7.56 (d, *J* = 8.2 Hz, 2H), 7.24 (d, *J* = 2.1 Hz, 2H), 6.90 (dd, *J* = 8.2, 2.1 Hz, 2H), 3.69 (s, 4H). **^{13}C NMR** (101 MHz, Chloroform-*d*) δ 203.0, 134.9, 134.3, 134.1, 131.9, 129.2, 122.2, 48.3 (2C). **HRMS** (ESI): calcd for $C_{15}H_9Br_2Cl_2O^-$ [M-H]$^-$ 432.8403, found: 432.8404.

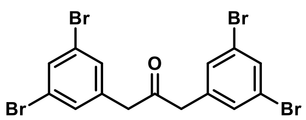

1,3-bis(3,5-dibromophenyl)propan-2-one **8d**.[10]
1,3-dibromo-5-(bromomethyl)benzene (4.04 g, 12.30 mmol, 2.0 eq), TosMIC (1.20 g, 6.15 mmol, 1.0 eq), TBAB (793 mg, 2.55 mmol, 0.4 eq), NaOH (20 wt%, 60 mL) and DCM (125 mL) were stirred for 14 h. The addition product was obtained as a brown oil.
The addition product, HCl (37%, 5 mL), DCM (40 mL) and THF (7 mL) were stirred at ambient temperature for 5 h. The title compound was precipitated from DCM by addition of EtOH. The solids were collected and washed with H_2O and EtOH to yield pure **8d** (1.94 g, 3.68 mmol, 60 % o2s) as a white solid. **^{1}H NMR** (400 MHz, DMSO-*d6*) δ 7.71 (t, *J* = 1.8 Hz, 2H), 7.44 (d, *J* = 1.8 Hz, 4H), 3.94 (s, 4H). **^{13}C NMR** (101 MHz, DMSO-*d6*) δ 203.7, 139.8 (2C), 132.0 (4C), 131.5 (4C), 122.6 (2C), 47.2 (2C). **HRMS** (ESI): calcd for $C_{15}H_9Br_4O^-$ [M-H]$^-$ 520.7392, found: 520.7393.

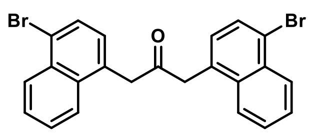

1,3-bis(4-bromonaphthalen-1-yl)propan-2-one **8e.**
1-bromo-4-(bromomethyl)naphthalene **S6** (1.84 g, 6.15 mmol, 2.0 eq), TosMIC (600 mg, 3.07 mmol, 1.0 eq), TBAB (396 mg, 1.23 mmol, 0.4 eq), NaOH (20 wt%, 30 mL) and DCM (65 mL) were stirred for 14 h. The addition product was obtained as a brown oil.
The addition product, HCl (37%, 6.0 mL), DCM (30 mL) and THF (7 mL) were stirred at ambient temperature for 17 h. Upon addition of water and EtOH a white solid precipitated. The solids were collected and washed with water to deliver **8e** (820 mg, 3.07 mmol, 57% o2s) as a white solid. **^{1}H NMR** (400 MHz, Chloroform-*d*) δ 8.31 – 8.24 (m, 2H), 7.70 (d, *J* = 7.6 Hz, 2H), 7.63 (dt, *J* = 8.5, 0.8 Hz, 2H), 7.58 (ddd, *J* = 8.2, 6.9, 1.2 Hz, 2H), 7.43 (ddd, *J* = 8.3, 6.8, 1.3 Hz, 2H), 7.10 (d, *J* = 7.6 Hz, 2H), 4.10 (s, 4H). **^{13}C NMR** (101 MHz, Chloroform-*d*) δ 205.4, 133.4, 132.3, 130.8, 129.7, 128.9, 128.2, 127.5, 127.4, 124.4, 123.0, 47.2. **HRMS** (ESI): calcd for $C_{23}H_{16}Br_2ONa^+$ [M+Na]$^+$ 488.9460, found: 488.9458.

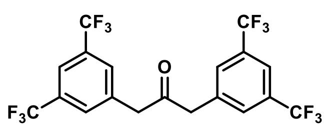

1,3-bis(3,5-bis(trifluoromethyl)phenyl)propan-2-one **8f**.
3,5-bis(trifluoromethyl)benzyl bromide (2.25 g, 7.32 mmol, 2.2 eq), TosMIC (650 mg, 3.33 mmol, 1.0 eq), TBAI (246 mg, 0.67 mmol, 0.2 eq), NaOH (30 wt%, 12 mL) and DCM (12 mL) were stirred for 24 h. The addition product was obtained as a brown oil.
The addition product, HCl (37%, 4.2 mL), DCM (20 mL) and THF (4 mL) were stirred at ambient temperature for 17 h. Purification by column chromatography on silica gel with 10% EtOAc in heptane as eluent delivered **8f** (857 mg, 1.78 mmol, 53% o2s) as an off-white solid. **^{1}H NMR** (400 MHz, Methanol-*d4*) δ 7.84 (s, 2H), 7.82 (s, 4H), 4.18 (s, 4H). **^{13}C NMR** (101 MHz, Methanol-*d4*) δ 203.2, 137.4, 131.2 (q, *J* = 32.9 Hz, 2C), 130.3 – 130.1

(m, 2C), 123.5 (q, J = 272.0 Hz, 2C), 120.3 – 120.1 (m, 1C). *Methylene-carbons were not observed, due to overlap with the deuterated solvent.* **HRMS** (ESI): calcd for $C_{19}H_9F_{12}O^-$ [M-H]$^-$ 481.0467, found: 481.0461.

3.4.2 Synthesis of hydantoins 9

The following compounds were prepared according to general procedure B:

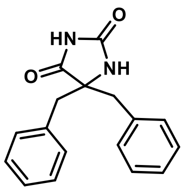

5,5-dibenzylimidazolidine-2,4-dione **9a**.
8a (36 mg, 0.17 mmol, 1.0 eq), KCN (22 mg, 0.34 mmol, 2.0 eq), NH_4CO_3 (82 mg, 0.86 mmol, 5.0 eq), water (0.5 mL) and EtOH (0.5 mL) were stirred at 75 °C for 24 h. Pure **9a** (35 mg, 125 µmol, 73%) was obtained as a white solid. **^{1}H NMR** (400 MHz, DMSO-*d6*) δ 9.97 (s, 1H), 8.00 (s, 1H), 7.33 – 7.12 (m, 10H), 3.10 (d, J = 13.4 Hz, 2H), 2.86 (d, J = 13.4 Hz, 2H). **^{13}C NMR** (101 MHz, Methanol-*d4*) δ 179.1, 158.6, 136.1 (2C), 131.4 (4C), 129.2 (4C), 128.2 (2C), 70.3, 43.9 (2C). **HRMS** (ESI): calcd for $C_{17}H_{16}N_2O_2^-$ [M-H]$^-$ 279.1139, found: 279.1137.

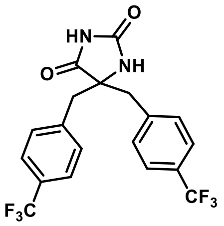

5,5-bis(4-(trifluoromethyl)benzyl)imidazolidine-2,4-dione **9b**.
8b (1.76 g, 5.07 mmol, 1.0 eq), KCN (826 mg, 12.69 mmol, 2.5 eq), NH_4CO_3 (1.95 g, 20.30 mmol, 4.0 eq), KOAc (996 mg, 10.15 mmol, 2.0 eq) and DMSO (15 mL) were stirred at 60 °C for 21 h. Pure **9b** (1.76 g, 4.23 mmol, 83%) was obtained as a slightly brown solid. **^{1}H NMR** (400 MHz, DMSO-*d6*) δ 10.01 (s, 1H), 8.16 (s, 1H), 7.67 (d, J = 8.0 Hz, 4H), 7.40 (d, J = 7.9 Hz, 4H), 3.23 (d, J = 13.3 Hz, 2H), 3.00 (d, J = 13.3 Hz, 2H). **^{13}C NMR** (101 MHz, DMSO-*d6*) δ 174.7, 155.6, 139.9 (2C), 131.0 (4C), 127.6 (q, J = 31.6 Hz, 4C), 124.9 (q, J = 3.8 Hz, 4C), 124.3 (q, J = 274 Hz, 2C), 66.0, 41.8 (2C). **HRMS** (ESI): calcd for $C_{19}H_{13}F_6N_2O_2^-$ [M-H]$^-$ 415.0887, found: 415.0882.

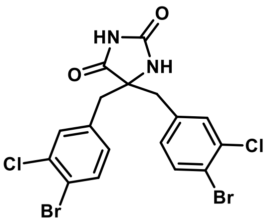

5,5-bis(4-bromo-3-chlorobenzyl)imidazolidine-2,4-dione **9c**.
8c (737 mg, 1.69 mmol, 1.0 eq), KCN (275 mg, 4.22 mmol, 2.5 eq), NH_4CO_3 (648 mg, 6.75 mmol, 4.0 eq), KOAc (331 mg, 3.37 mmol, 2.0 eq) and DMSO (7 mL) were stirred at 60 °C for 16 h. Pure **9c** (387 mg, 0.76 mmol, 45%) was obtained as an off-white solid. **^{1}H NMR** (400 MHz, DMSO-*d6*) δ 10.30 (s, 1H), 8.14 (s, 1H), 7.70 (d, J = 8.2 Hz, 2H), 7.39 (d, J = 2.0 Hz, 2H), 7.06 (dd, J = 8.2, 2.0 Hz, 2H), 3.09 (d, J = 13.4 Hz, 2H), 2.85 (d, J = 13.5 Hz, 2H). **^{13}C NMR** (101 MHz, DMSO-*d6*) δ 175.7, 156.4, 136.7, 133.4, 132.5, 132.0, 130.7, 120.0, 66.6, 40.8 (2C). **HRMS** (ESI): calcd for $C_{17}H_{11}Br_2Cl_2N_2O_2^-$ [M-H]$^-$ 502.8570, found: 502.8570.

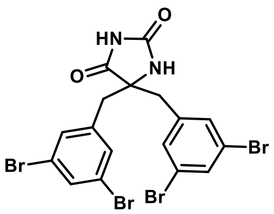

5,5-bis(3,5-dibromobenzyl)imidazolidine-2,4-dione **9d**.
8d (1.21 g, 2.30 mmol, 1.0 eq), KCN (374 mg, 5.75 mmol, 2.5 eq), NH_4CO_3 (884 mg, 9.20 mmol, 4.0 eq), KOAc (451 mg, 4.60 mmol, 2.0 eq) and DMSO (9 mL) were stirred at 60 °C for 16 h. Pure **9d** (1.17 g, 1.96 mmol, 85%) was obtained as a grey solid. **^{1}H NMR** (400 MHz, DMSO-*d6*) δ 10.42 (s, 1H), 8.22 (s, 1H), 7.73 (t, J = 1.8 Hz, 2H), 7.37 (d, J = 1.9 Hz, 4H), 3.09 (d, J = 13.4 Hz, 2H), 2.84 (d, J = 13.4 Hz, 2H). **^{13}C NMR** (101 MHz, DMSO-*d6*) δ 175.7, 154.7, 139.6 (2C), 132.8 (4C), 132.0 (4C), 122.0 (2C), 67.0, 40.77 (2C). **HRMS** (ESI): calcd for $C_{17}H_{11}Br_4N_2O_2^-$ [M-H]$^-$ 590.7560, found: 590.7562.

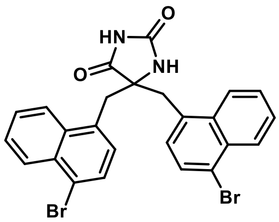

5,5-bis((4-bromonaphthalen-1-yl)methyl)imidazolidine-2,4-dione **9e**.
8e (842 mg, 1.80 mmol, 1.0 eq), KCN (410 mg, 6.29 mmol, 3.5 eq), NH_4CO_3 (1.21 g, 12.59 mmol, 7.0 eq), KOAc (410 mg, 4.18 mmol, 2.0 eq) and DMSO (7 mL) were stirred at 75 °C for 90 h. Pure **9e** (627 mg, 1.16 mmol, 65%) was obtained as a red solid. **^{1}H NMR** (400 MHz, DMSO-*d6*) δ 9.91 (s, 1H), 8.41 (dt, J = 8.0, 2.8 Hz, 2H), 8.21 – 8.11 (m, 2H), 8.06 (d, J = 1.7 Hz, 1H), 7.83 (d, J = 7.8 Hz, 2H), 7.73 – 7.63 (m, 4H), 7.42 (d, J = 7.8 Hz, 2H), 3.86 (d, J = 14.2 Hz, 2H), 3.54 (d, J = 14.2 Hz, 2H). **^{13}C NMR** (101 MHz, DMSO-*d6*) δ 176.8, 155.6, 133.6, 132.4, 131.1, 129.5, 129.3, 127.4, 126.7, 126.6, 126.0, 121.4, 68.0, 37.7. **HRMS** (ESI): calcd for $C_{25}H_{17}Br_2N_2O_2^-$ [M-H]$^-$ 534.9662, found: 534.9660.

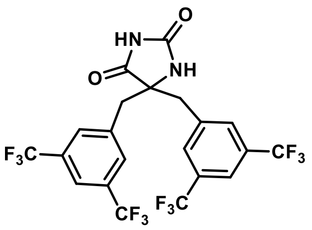

5,5-bis(3,5-bis(trifluoromethyl)benzyl)imidazolidine-2,4-dione **9f**.
8f (806 mg, 1.67 mmol, 1.0 eq), KCN (272 mg, 4.18 mmol, 2.5 eq), NH_4CO_3 (642 mg, 6.69 mmol, 4.0 eq), KOAc (410 mg, 4.18 mmol, 2.50eq) and DMSO (15 mL) were stirred at 60 °C for 20 h. Pure **9f** (470 mg, 0.85 mmol, 51%) was obtained as a white solid. **^{1}H NMR** (400 MHz, DMSO-*d6*) δ 10.38 (s, 1H), 8.34 (s, 1H), 8.02 (s, 2H), 7.84 (s, 4H), 3.40 (d, *J* = 13.3 Hz, 2H), 3.12 (d, *J* = 13.4 Hz, 2H). **^{13}C NMR** (101 MHz, DMSO-*d6*) δ 175.6, 155.5, 138.2 (2C), 131.0 – 130.8 (m, 4C), 129.9 (q, *J* = 32.7 Hz, 4C), 123.3 (q, *J* = 272.8 Hz, 4C). 121.1 – 120.8 (m, 2C), 68.1, 40.9 (2C). **HRMS** (ESI): calcd for $C_{21}H_{11}F_{12}N_2O_2^-$ [M-H]$^-$ 551.0634, found: 551.0628

3.4.3 Synthesis of *N,N'*-dialkylated hydantoins 2A

The following compound were prepared according to General Procedure C:

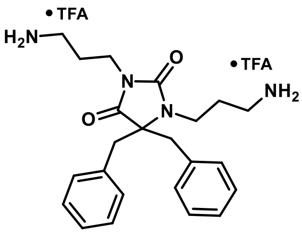

1,3-bis(3-aminopropyl)-5,5-dibenzylimidazolidine-2,4-dione **2aA**.
9a (168 mg, 0.60 mmol, 1.0 eq), *tert*-butyl (3-bromopropyl)carbamate **S7** (429 mg, 1.8 mmol, 3.0 eq), Cs_2CO_3 (586 mg, 1.8 mmol, 3.0 eq), TBAI (44 mg, 120 µmol, 0.2 eq) and acetone (8.0 mL) were stirred at 65 °C for 72 h. Purification by column chromatography on silica gel with a gradient of 0-70% EtOAc in heptane delivered the intermediate Boc-**2aA** (302 mg, 508 µmol, 85%) as a white solid.
TFA (460 µL, 6.00 mmol, 10.0 eq) and DCM (3.0 mL) were added and the solution was stirred at ambient temperature for 3.5 h. The crude was purified by RP chromatography with a gradient of 0-70% MeCN/H_2O + 0.1% TFA to yield the di-TFA salt of **2aA** (272 mg, 437 µmol, 73% o2s) as a white solid. **^{1}H NMR** (400 MHz, Methanol-*d4*) δ 7.33 – 7.22 (m, 6H), 7.21 – 7.15 (m, 4H), 3.65 – 3.58 (m, 2H), 3.35 (d, *J* = 14.5 Hz, 2H), 3.26 (d, *J* = 14.5 Hz, 2H), 3.25 (t, *J* = 6.7 Hz, 2H), 2.86 (t, *J* = 7.3 Hz, 2H), 2.27 (t, *J* = 7.3 Hz, 2H), 2.02 (qn, *J* = 7.4 Hz, 2H), 1.47 (qn, *J* = 7.4 Hz, 2H). **^{13}C NMR** (101 MHz, Methanol-*d4*) δ 175.9, 158.6, 135.9 (2C), 131.0 (4C), 129.7 (4C), 128.7 (2C), 73.6, 41.7 (2C), 39.5, 38.4, 37.7, 35.9, 28.2, 26.8. **HRMS** (ESI): calcd for $C_{23}H_{31}N_4O_2^+$ [M+H]$^+$ 395.2442, found 395.2445. **SFC**: 93.2%.

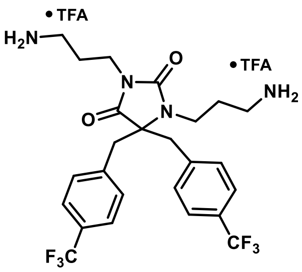

1,3-bis(3-aminopropyl)-5,5-bis(4-(trifluoromethyl)benzyl)imidazolidine-2,4-dione **2bA**.
9b (250 mg, 0.60 mmol, 1.0 eq), *tert*-butyl (3-bromopropyl)carbamate **S7** (429 mg, 1.80 mmol, 3.0 eq), Cs_2CO_3 (586 mg, 1.8 mmol, 3.0 eq), TBAI (44 mg, 120 µmol, 0.2 eq) and acetone (8 mL) were stirred at 65 °C for 72 h. Purification by column chromatography on silica gel with a gradient of 0-70% EtOAc in heptane delivered the intermediate Boc-**2bA** (434 mg, 594 µmol, 99%) as a white solid.
TFA (551 µL, 7.20 mmol, 12.0 eq) and DCM (2.5 mL) were added and the solution was stirred at ambient temperature for 16 h. The crude was purified by RP chromatography with a gradient of 0-70% MeCN/H_2O + 0.1% TFA to yield the di-TFA salt of **2bA** (388 mg, 512 µmol, 85% o2s) as a white solid. **^{1}H NMR** (400 MHz, Methanol-*d4*) δ 7.60 (d, *J* = 8.1 Hz, 4H), 7.40 (d, *J* = 8.0 Hz, 4H), 3.69 – 3.62 (m, 2H), 3.41 (s, 4H), 3.27 (t, *J* = 6.9 Hz, 2H), 2.99 (t, *J* = 7.3 Hz, 2H), 2.44 (t, *J* = 7.0 Hz, 2H), 2.08 (qn, *J* = 7.4 Hz, 2H), 1.50 (qn, *J* = 6.9 Hz, 2H). **^{13}C NMR** (101 MHz, Methanol-*d4*) δ 175.2, 158.2, 140.3 (2C), 131.9 (4C), 130.9 (q, *J* = 32.5 Hz, 2C), 126.4 (q, *J* = 3.8 Hz, 4C). 125.5 (q, *J* = 271.3 Hz, 4C), 72.9, 41.2 (2C), 39.5, 38.4, 37.7, 35.9, 28.3, 26.8. **HRMS** (ESI): calcd for $C_{25}H_{29}F_6N_4O_2^+$ [M+H]$^+$ 531.2189, found 531.2186. **SFC**: >99.0%.

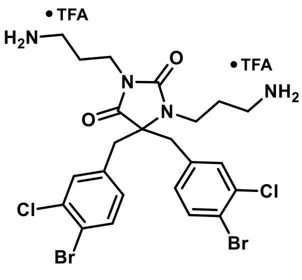

1,3-bis(3-aminopropyl)-5,5-bis(4-bromo-3-chlorobenzyl)imidazolidine-2,4-dione **2cA**.
9c (127 mg, 0.25 mmol, 1.0 eq), *tert*-butyl (3-bromopropyl)carbamate **S7** (179 mg, 0.75 mmol, 3.0 eq), Cs_2CO_3 (244 mg, 0.75 mmol, 3.0 eq), TBAI (18 mg, 50 µmol, 0.2 eq) and acetone (1.5 mL) were stirred at 65 °C for 70 h. Purification by column chromatography on silica gel with a gradient of 0-55% EtOAc in heptane delivered the slightly impure intermediate Boc-**2cA** (201 mg, 245 µmol, 98%) as a white foam.
TFA (230 µL, 3.00 mmol, 12.0 eq) and DCM (1.5 mL) were added and the solution was stirred at ambient temperature for 16 h. The crude was purified by RP chromatography with a gradient of 0-70% MeCN/H_2O + 0.1% TFA to yield the di-TFA salt of **2cA** (170 mg, 203 µmol, 81% o2s) as a white solid. **^{1}H NMR** (400 MHz, Methanol-*d4*) δ 7.62 (d, *J* = 8.3 Hz, 2H), 7.34 (d, *J* = 2.1 Hz, 2H), 7.05 (dd, *J* = 8.3, 2.1 Hz, 2H), 3.64 – 3.55 (m, 2H), 3.36 – 3.31 (m, 2H), 3.29 – 3.25 (m, 4H), 3.00 (t, *J* = 7.3 Hz, 2H), 2.58 (t, *J* = 6.9 Hz, 2H), 2.06 (qn, *J* = 7.4 Hz, 2H), 1.58 (qn, *J* = 7.0 Hz, 2H). **^{13}C NMR** (101 MHz, Methanol-*d4*) δ 175.1, 158.1, 137.1

(2C), 135.3 (2C), 135.0 (2C), 132.9 (2C), 131.2 (2C), 122.4 (2C), 72.6, 40.4 (2C), 39.4, 38.4, 37.8, 36.0, 28.4, 27.1. **HRMS** (ESI): calcd for $C_{23}H_{27}Br_2Cl_2N_4O_2^+$ [M+H]$^+$ 618.9872, found 618.9878. **SFC**: 96.7%.

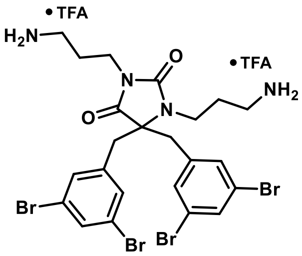

1,3-bis(3-aminopropyl)-5,5-bis(3,5-dibromobenzyl)imidazolidine-2,4-dione **2dA**.
9d (149 mg, 0.25 mmol, 1.0 eq), *tert*-butyl (3-bromopropyl)carbamate **S7** (179 mg, 0.75 mmol, 3.0 eq), Cs_2CO_3 (244 mg, 0.75 mmol, 3.0 eq), TBAI (18 mg, 50 µmol, 0.2 eq) and acetone (1.5 mL) were stirred at 65 °C for 70 h. Purification by column chromatography on silica gel with a gradient of 15-70% EtOAc in heptane delivered the impure intermediate Boc-**2dA** (169 mg, 159 µmol, 74%) as a white foam.
TFA (191 µL, 2.50 mmol, 10.0 eq) and DCM (2.0 mL) were added and the solution was stirred at ambient temperature for 4 h. The crude was purified by RP chromatography with a gradient of 0-70% MeCN/H_2O + 0.1% TFA to yield the di-TFA salt of **2dA** (153 mg, 163 µmol, 65% o2s) as a white solid. **^{1}H NMR** (400 MHz, Methanol-*d4*) δ 7.67 (t, *J* = 1.7 Hz, 2H), 7.36 (d, *J* = 1.7 Hz, 4H), 3.59 (dd, *J* = 8.5, 6.6 Hz, 2H), 3.41 – 3.33 (m, 2H), 3.27 (s, 4H), 3.00 (t, *J* = 7.2 Hz, 2H), 2.67 (t, *J* = 7.0 Hz, 2H), 2.06 (qn, *J* = 7.3 Hz, 2H), 1.63 (qn, *J* = 7.0 Hz, 2H). **^{13}C NMR** (101 MHz, Methanol-*d4*) δ 174.9, 158.1, 140.0 (2C), 134.3 (2C), 133.0 (4C), 123.9 (4C), 72.5, 40.3 (2C), 39.3, 38.4, 37.9, 36.2, 28.5, 27.3. **HRMS** (ESI): calcd for $C_{23}H_{27}Br_4N_4O_2^+$ [M+H]$^+$ 706.8862, found 706.8856. **SFC**: >99.0%.

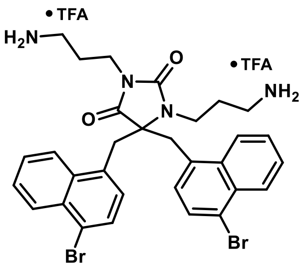

1,3-bis(3-aminopropyl)-5,5-bis((4-bromonaphthalen-1-yl)methyl)imidazolidine-2,4-dione **2eA**.
9e (135 mg, 0.25 mmol, 1.0 eq), *tert*-butyl (3-bromopropyl)carbamate **S7** (179 mg, 0.75 mmol, 3.0 eq), Cs_2CO_3 (244 mg, 0.75 mmol, 3.0 eq), TBAI (18 mg, 50 µmol, 0.2 eq) and acetone (1.5 mL) were stirred at 65 °C for 70 h. Purification by column chromatography on silica gel with a gradient of 10-25% EtOAc in heptane delivered the slightly impure intermediate Boc-**2eA** (208 mg, 244 µmol, 98%) as a yellow solid.
TFA (191 µL, 2.50 mmol, 10.0 eq) and DCM (1.5 mL) were added and the solution was stirred at ambient temperature for 3.5 h. The crude was purified by RP chromatography with a gradient of 0-70% MeCN/H_2O + 0.1% TFA to yield the di-TFA salt of **2eA** (132 mg, 150 µmol, 60% o2s) as a yellow solid. **^{1}H NMR** (400 MHz, Methanol-*d4*) δ 8.33 – 8.22 (m, 4H), 7.77 (d, *J* = 7.8 Hz, 2H), 7.71 – 7.62 (m, 4H), 7.18 (d, *J* = 7.8 Hz, 2H), 4.05 (d, *J* = 15.3 Hz, 2H), 3.86 (d, *J* = 15.3 Hz, 2H), 3.79 – 3.69 (m, 2H), 3.10 (t, *J* = 6.8 Hz, 2H), 2.83 (t, *J* = 7.4 Hz, 2H), 2.14 (t, *J* = 6.8 Hz, 2H), 1.70 (qn, *J* = 7.5 Hz, 2H), 1.01 (qn, *J* = 6.8 Hz, 2H). **^{13}C NMR** (101 MHz, Methanol-*d4*) δ 175.3, 158.2, 134.9 (2C), 133.4 (2C), 132.7 (2C), 130.4 (2C), 129.1 (2C), 128.8 (2C), 128.7 (2C), 128.3 (2C), 126.1 (2C), 123.7 (2C), 71.7, 39.7, 38.3, 37.4, 37.1 (2C), 35.7, 28.2, 26.7. **HRMS** (ESI): calcd for $C_{31}H_{33}Br_2N_4O_2^+$ [M+H]$^+$ 651.0965, found 651.0965. **SFC**: >99.0%.

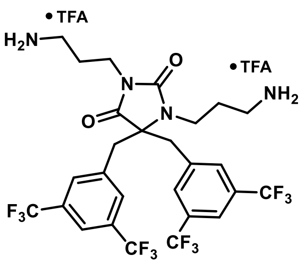

1,3-bis(3-aminopropyl)-5,5-bis(3,5-bis(trifluoromethyl)benzyl)imidazolidine-2,4-dione **2fA**.
9f (200 mg, 0.36 mmol, 1.0 eq), *tert*-butyl (3-bromopropyl)carbamate **S7** (259 mg, 1.09 mmol, 3.0 eq), Cs_2CO_3 (354 mg, 1.09 mmol, 3.0 eq), TBAI (27 mg, 72 µmol, 0.2 eq) and acetone (5.0 mL) were stirred at 65 °C for 72 h. Purification by column chromatography on silica gel with a gradient of 10-25% EtOAc in heptane delivered the slightly impure intermediate Boc-**2fA** (225 mg, 260 µmol, 72%) as a white solid.
TFA (277 µL, 3.63 mmol, 10.0 eq) and DCM (2.0 mL) were added and the solution was stirred at ambient temperature for 17 h. The crude was purified by RP chromatography with a gradient of 10-65% MeCN/H_2O + 0.1% TFA to yield the di-TFA salt of **2fA** (144 mg, 161 µmol, 45% o2s) as a white solid. **^{1}H NMR** (400 MHz, Methanol-*d4*) δ 7.92 (s, 2H), 7.80 (d, *J* = 1.7 Hz, 4H), 3.72 (dd, *J* = 8.5, 6.5 Hz, 2H), 3.56 (d, *J* = 14.2 Hz, 2H), 3.45 (d, *J* = 14.3 Hz, 2H), 3.26 (dd, *J* = 7.9, 6.5 Hz, 2H), 3.06 (t, *J* = 7.3 Hz, 2H), 2.63 (t, *J* = 7.0 Hz, 2H), 2.14 (q, *J* = 7.3 Hz, 2H), 1.48 (qn, *J* = 7.1 Hz, 2H). **^{13}C NMR** (101 MHz, Methanol-*d4*) δ 174.5, 157.6, 138.8 (2C), 132.8 (q, *J* = 33.3 Hz, 4C), 132.1 – 131.8 (m, 4C), 124.7 (q, *J* = 272.1 Hz, 4C) 122.8 – 122.4 (m, 2C) 71.7, 40.3 (2C), 39.3, 38.4, 37.8, 36.2, 28.9, 27.0. **HRMS** (ESI): calcd for $C_{27}H_{27}F_{12}N_4O_2^+$ [M+H]$^+$ 667.1937, found 667.1940. **SFC**: 96.8%.

3.4.4 Synthesis of *N,N′*-dialkylated hydantoins 2G

The following compounds were prepared according to General Procedure D:

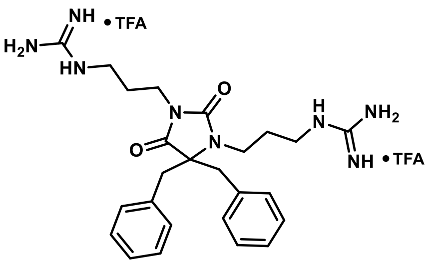

1,1'-((4,4-dibenzyl-2,5-dioxoimidazolidine-1,3-diyl)bis(propane-3,1-diyl))diguanidine **2aG.**

2aA (120 mg, 193 µmol, 1.0 eq), *N,N′*-Di-Boc-1*H*-pyrazole-1-carboxamidine (150 mg, 482 µmol, 2.50 eq), DIPEA (134 µL, 771 µmol, 4.00 eq) and THF (1 mL) were stirred at 45 °C for 2.0 h. The crude was purified with a gradient of 10-45% EtOAc in heptane to yield Boc-**2aG** (126 mg, 143 µmol, 74%) as a white foam.

TFA (221 µL, 2.89 mmol, 15.0 eq) and DCM (2 mL) were added and the solution was stirred at ambient temperature for 24 h. The crude was purified by RP chromatography with a gradient of 10-55% MeCN/H_2O + 0.1% TFA to yield the di-TFA salt of **2aG** (86 mg, 122 µmol, 63% o2s) as a white powder. **^{1}H NMR** (400 MHz, Methanol-*d4*) δ 7.31 – 7.21 (m, 6H), 7.16 (dd, *J* = 7.6, 1.9 Hz, 4H), 3.57 – 3.49 (m, 2H), 3.34 (d, *J* = 14.6 Hz, 2H), 3.25 (d, *J* = 14.5 Hz, 2H), 3.17 (dt, *J* = 11.1, 6.8 Hz, 4H), 2.58 (t, *J* = 6.9 Hz, 2H), 1.94 – 1.84 (m, 2H), 1.31 (qn, *J* = 6.8 Hz, 2H). **^{13}C NMR** (101 MHz, Methanol-*d4*) δ 176.1, 158.7, 158.6, 158.4, 135.9 (2C), 130.9 (4C), 129.6 (4C), 128.6 (2C), 73.4, 41.8 (2C), 40.2, 40.0, 39.4, 36.2, 29.4, 28.3. **HRMS** (ESI): calcd for $C_{25}H_{35}N_8O_2^+$ $[M+H]^+$ 479.2877, found 479.2868. **SFC**: >99.0%.

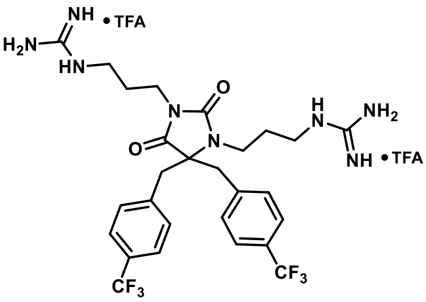

1,1'-((2,5-dioxo-4,4-bis(4-(trifluoromethyl)benzyl)imidazolidine-1,3-diyl)bis(propane-3,1-diyl))diguanidine **2bG.**

2bA (103 mg, 136 µmol, 1.0 eq), *N,N′*-Di-Boc-1*H*-pyrazole-1-carboxamidine (105 mg, 340 µmol, 2.50 eq), DIPEA (95 µL, 543 µmol, 4.00 eq) and THF (1 mL) were stirred at 45 °C for 2.0 h. The crude was purified with a gradient of 10-52% EtOAc in heptane to yield Boc-2**bG** (120 mg, 118 µmol, 87%) as a white foam.

TFA (156 µL, 2.04 mmol, 15.0 eq) and DCM (1 mL) were added and the solution was stirred at ambient temperature for 24 h. The crude was purified by RP chromatography with a gradient of 10-60% MeCN/H_2O + 0.1% TFA to yield the di-TFA salt of **2bG** (89 mg, 106 µmol, 78% o2s) as a white powder. **^{1}H NMR** (400 MHz, Methanol-*d4*) 7.60 (d, *J* = 8.0 Hz, 4H), 7.38 (d, *J* = 8.0 Hz, 4H), 3.64 – 3.54 (m, 2H), 3.44 (d, *J* = 14.4 Hz, 2H), 3.39 (d, *J* = 14.4 Hz, 2H), 3.21 (dt, *J* = 9.2, 7.0 Hz, 4H), 2.70 (t, *J* = 6.9 Hz, 2H), 1.99 – 1.90 (m, 2H), 1.38 – 1.26 (m, 4H). **^{13}C NMR** (101 MHz, Methanol-*d4*) δ 175.2 (2C), 158.3, 140.4 (2C), 131.8 (4C), 126.4 (q, *J* = 3.8 Hz, 4C), 72.8, 41.3 (2C), 40.2, 40.0, 39.4, 36.4, 29.6, 28.3. *CF_3 carbon and the neighboring carbon were not observed due to too low intensity*. **HRMS** (ESI): calcd for $C_{27}H_{33}F_6N_8O_2^+$ $[M+H]^+$ 615.2625, found 615.2626. **SFC**: >99.0%.

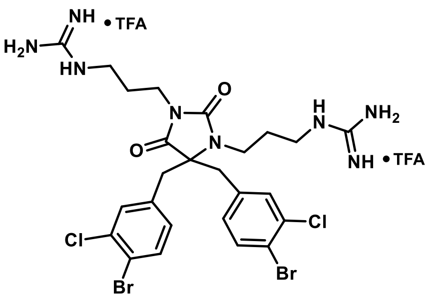

1,1'-((4,4-bis(4-bromo-3-chlorobenzyl)-2,5-dioxoimidazolidine-1,3-diyl)bis(propane-3,1-diyl))diguanidine **2cG.**

2cA (57 mg, 68 µmol, 1.0 eq), *N,N′*-Di-Boc-1*H*-pyrazole-1-carboxamidine (53 mg, 170 µmol, 2.50 eq), DIPEA (47 µL, 272 µmol, 4.00 eq) and THF (1 mL) were stirred at 45 °C for 2.0 h. The crude was purified with a gradient of 10-52% EtOAc in heptane to yield impure Boc-**2cG** (120 mg, 109 µmol, 159%) as a white foam.

TFA (78 µL, 102 mmol, 15.0 eq) and DCM (1 mL) were added and the solution was stirred at ambient temperature for 24 h. The crude was purified by RP chromatography with a gradient of 10-60% MeCN/H_2O + 0.1% TFA to yield the di-TFA salt of **2cG** (44 mg, 47 µmol, 69% o2s) as a white powder. **^{1}H NMR** (400 MHz, Methanol-*d4*) δ 7.60 (d, *J* = 8.3 Hz, 2H), 7.33 (d, *J* = 2.1 Hz, 2H), 7.03 (dd, *J* = 8.3, 2.1 Hz, 2H), 3.59 – 3.50 (m, 2H), 3.29 – 3.20 (m, 8H), 2.78 (t, *J* = 7.0 Hz, 2H), 1.95 (qn, *J* = 7.1 Hz, 2H), 1.39 (qn, *J* = 7.1 Hz, 2H). **^{13}C NMR** (101 MHz, Methanol-*d4*) δ 175.2, 158.7, 158.6, 158.0, 137.2 (2C), 135.4 (2C), 135.0 (2C), 132.9 (2C), 131.1 (2C), 122.4 (2C), 72.6, 40.4 (2C), 40.2, 40.0, 39.4, 37.8, 36.4, 29.7, 28.6. **HRMS** (ESI): calcd for $C_{25}H_{31}Br_2Cl_2N_8O_2^+$ $[M+H]^+$ 703.0308, found 703.0312. **SFC**: >99.0%.

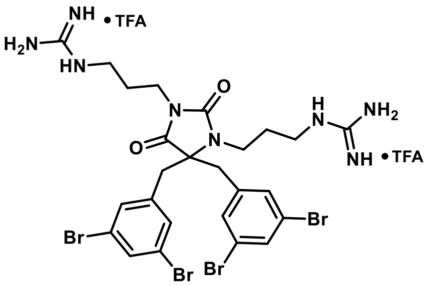

1,1'-((4,4-bis(3,5-dibromobenzyl)-2,5-dioxoimidazolidine-1,3-diyl)bis(propane-3,1-diyl))diguanidine **2dG**.

2dA (53 mg, 57 µmol, 1.0 eq), *N*,*N′*-Di-Boc-1*H*-pyrazole-1-carboxamidine (44 mg, 141 µmol, 2.50 eq), DIPEA (39 µL, 226 µmol, 4.00 eq) and THF (1 mL) were stirred at 45 °C for 2.0 h. The crude was purified with a gradient of 10-52% EtOAc in heptane to yield Boc-**2dG** (60 mg, 50 µmol, 89%) as a white foam.

TFA (65 µL, 848 µmol, 15.0 eq) and DCM (1 mL) were added and the solution was stirred at ambient temperature for 24 h. The crude was purified by RP chromatography with a gradient of 10-60% MeCN/H_2O + 0.1% TFA to yield the di-TFA salt of **2dG** (50 mg, 49 µmol, 87% o2s) as a white powder. **^{1}H NMR** (400 MHz, Methanol-*d4*) δ 7.66 (t, *J* = 1.7 Hz, 2H), 7.34 (d, *J* = 1.8 Hz, 4H), 3.57 – 3.46 (m, 2H), 3.30 – 3.22 (m, 8H), 2.87 (t, *J* = 7.0 Hz, 2H), 2.01 – 1.90 (m, 2H), 1.46 (qn, *J* = 7.1 Hz, 2H). **^{13}C NMR** (101 MHz, Methanol-*d4*) δ 175.1, 158.7, 158.6, 157.9, 140.1 (2C), 134.2 (2C), 133.0 (4C), 123.9 (4C), 72.7, 40.4 (2C), 40.2, 40.0, 39.5, 36.5, 29.7, 28.8. **HRMS** (ESI): calcd for $C_{25}H_{31}Br_4N_8O_2^+$ [M+H]$^+$ 790.9309, found 790.9310. **SFC**: >99.0%.

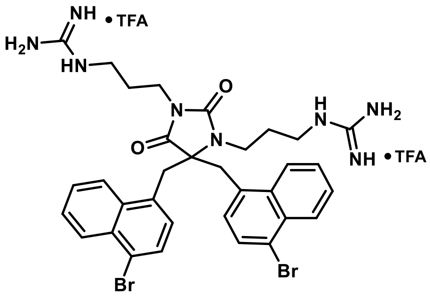

1,1'-((4,4-bis((4-bromonaphthalen-1-yl)methyl)-2,5-dioxoimidazolidine-1,3-diyl)bis(propane-3,1-diyl))diguanidine **2eG.**

2eA (27 mg, 31 µmol, 1.0 eq), *N*,*N′*-Di-Boc-1*H*-pyrazole-1-carboxamidine (24 mg, 77 µmol, 2.50 eq), DIPEA (21 µL, 123 µmol, 4.00 eq) and THF (1 mL) were stirred at 45 °C for 2.0 h. The crude was purified with a gradient of 10-45% EtOAc in heptane to yield Boc-**2eG** (27 mg, 24 µmol, 77%) as a clear liquid.

TFA (35 µL, 460 µmol, 15.0 eq) and DCM (1 mL) were added and the solution was stirred at ambient temperature for 24 h. The crude was purified by RP chromatography with a gradient of 10-55% MeCN/H_2O + 0.1% TFA to yield the di-TFA salt of **2eG** (20 mg, 21 µmol, 68% o2s) as a white powder. **^{1}H NMR** (400 MHz, Methanol-*d4*) δ 8.28 (ddt, *J* = 7.7, 4.6, 2.2 Hz, 4H), 7.74 (d, *J* = 7.8 Hz, 2H), 7.70 – 7.60 (m, 4H), 7.16 (d, *J* = 7.8 Hz, 2H), 4.06 (d, *J* = 15.4 Hz, 2H), 3.85 (d, *J* = 15.3 Hz, 2H), 3.71 – 3.59 (m, 2H), 3.04 (dt, *J* = 10.4, 6.9 Hz, 4H), 2.32 (t, *J* = 7.0 Hz, 2H), 1.47 (qn, *J* = 7.0 Hz, 2H), 0.72 (qn, *J* = 7.0 Hz, 2H). **^{13}C NMR** (101 MHz, Methanol-*d4*) δ 175.7, 158.5, 158.3, 158.0, 135.0 (2C), 133.5 (2C), 132.7 (2C), 130.4 (2C), 129.0 (2C), 128.7 (2C), 128.6 (2C), 128.2 (2C), 126.1 (2C), 123.7 (2C), 71.7, 40.1, 40.1, 39.0, 37.0 (2C), 36.2, 29.2, 28.1. **HRMS** (ESI): calcd for $C_{33}H_{37}Br_2N_8O_2^+$ [M+H]$^+$ 735.1401, found 735.1393. **SFC**: >99.0%.

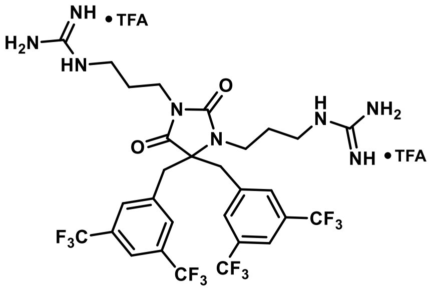

1,1'-((4,4-bis(3,5-bis(trifluoromethyl)benzyl)-2,5-dioxoimidazolidine-1,3-diyl)bis(propane-3,1-diyl))diguanidine **2fG**.

2fA (83 mg, 93 µmol, 1.0 eq), *N*,*N′*-Di-Boc-1*H*-pyrazole-1-carboxamidine (72 mg, 232 µmol, 2.50 eq), DIPEA (65 µL, 371 µmol, 4.00 eq) and THF (1 mL) were stirred at 45 °C for 2.0 h. The crude was purified with a gradient of 10-50% EtOAc in heptane to yield Boc-**2fG** (48 mg, 42 µmol, 45%) as a clear liquid.

TFA (107 µL, 1.39 mmol, 15.0 eq) and DCM (1 mL) were added and the solution was stirred at ambient temperature for 24 h. The crude was purified by RP chromatography with a gradient of 15-55% MeCN/H_2O + 0.1% TFA to yield the di-TFA salt of **2fG** (30 mg, 31 µmol, 33% o2s) as a white powder. **^{1}H NMR** (400 MHz, Methanol-*d4*) δ 7.94 – 7.89 (m, 2H), 7.83 – 7.76 (m, 4H), 3.67 – 3.60 (m, 2H), 3.57 (d, *J* = 14.3 Hz, 2H), 3.50 (d, *J* = 14.3 Hz, 2H), 3.30 (t, *J* = 6.8 Hz, 2H), 3.20 – 3.12 (m, 2H), 2.80 (t, *J* = 6.9 Hz, 2H), 2.07 – 1.96 (m, 2H), 1.34 – 1.19 (m, 2H). **^{13}C NMR** (101 MHz, Methanol-*d4*) δ 174.7, 158.8, 158.6, 157.5, 138.9 (2C), 132.8 (q, *J* = 33.3 Hz, 4C), 132.0 – 131.7 (m, 4C), 124.7 (q, *J* = 272.0 Hz, 4C). 122.6 – 122.4 (m, 2C), 72.3, 40.4 (2C), 40.2, 40.0, 39.2, 36.4, 29.8, 28.5. **HRMS** (ESI): calcd for $C_{29}H_{31}F_{12}N_8O_2^+$ [M+H]$^+$ 751.2373, found 751.2375. **SFC**: >99.0%.

3.4.5 Synthesis of *N,N'*-dialkylated hydantoins 6A

The following compounds were prepared according to General Procedure C:

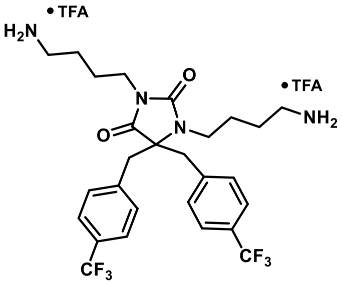

1,3-bis(4-aminobutyl)-5,5-bis(4-(trifluoromethyl)benzyl)imidazolidine-2,4-dione **6bA.**

9b (69 mg, 166 µmol, 1.0 eq), *tert*-butyl (4-bromobutyl)carbamate **S8** (104 mg, 414 µmol, 2.5 eq), Cs_2CO_3 (189 mg, 580 µmol, 3.5 eq), TBAI (6.1 mg, 17 µmol, 0.1 eq) and acetone (2.0 mL) were stirred at 75 °C for 72 h. Purification by column chromatography on silica gel with a gradient of 15-50% EtOAc in heptane delivered the impure intermediate Boc-**6bA** (110 mg, 145 µmol, 88%) as a colorless solid.

TFA (127 µL, 1.66 mmol, 10.0 eq) and DCM (1.5 mL) were added and the solution was stirred at ambient temperature for 24 h. The crude was purified by RP chromatography with a gradient of 15-55% MeCN/H_2O + 0.1% TFA to yield the di-TFA salt of **6bA** (64 mg, 81 µmol, 49% o2s) as a white solid. **^{1}H NMR** (400 MHz, Methanol-*d4*) δ 7.60 (d, *J* = 8.0 Hz, 4H), 7.38 (d, *J* = 8.0 Hz, 4H), 3.58 – 3.49 (m, 2H), 3.39 (s, 4H), 3.12 (t, *J* = 7.3 Hz, 2H), 2.97 (t, *J* = 7.2 Hz, 2H), 2.74 (t, *J* = 7.7 Hz, 2H), 1.82 – 1.64 (m, 4H), 1.31 – 1.18 (m, 2H), 1.05 (h, *J* = 7.4, 6.8 Hz, 2H). **^{13}C NMR** (101 MHz, Methanol-*d4*) δ 175.1, 157.8, 140.5 – 140.4 (m, 2H), 131.9 (4C), 130.7 (q, *J* = 32.3 Hz, 2C), 126.3 (q, *J* = 3.9 Hz, 4C), 125.6 (q, *J* = 271.2 Hz, 2C), 72.5, 42.0, 41.3 (2C), 40.2, 39.7, 38.2, 27.2, 26.3, 25.6, 25.4. **HRMS** (ESI): calcd for $C_{27}H_{33}F_6N_4O_2^+$ [M+H]$^+$ 559.2502, found 559.2503. **SFC**: 96.6%.

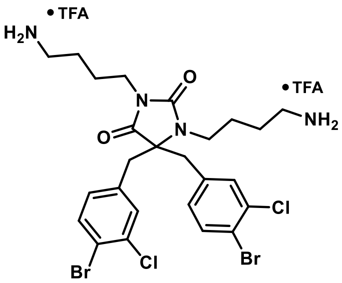

1,3-bis(4-aminobutyl)-5,5-bis(4-bromo-3-chlorobenzyl)imidazolidine-2,4-dione **6cA**.

9c (73 mg, 144 µmol, 1.0 eq), *tert*-butyl (4-bromobutyl)carbamate **S8** (91 mg, 360 µmol, 2.5 eq), Cs_2CO_3 (164 mg, 504 µmol, 3.5 eq), TBAI (5.3 mg, 14 µmol, 0.1 eq) and acetone (2.0 mL) were stirred at 75 °C for 72 h. Purification by column chromatography on silica gel with a gradient of 15-50% EtOAc in heptane delivered the impure intermediate Boc-**6cA** (92 mg, 108 µmol, 75%) as a colorless solid.

TFA (111 µL, 1.44 mmol, 10.0 eq) and DCM (1.5 mL) were added and the solution was stirred at ambient temperature for 24 h. The crude was purified by RP chromatography with a gradient of 15-55% MeCN/H_2O + 0.1% TFA to yield the di-TFA salt of **6cA** (71 mg, 81 µmol, 56% o2s) as a white solid. **^{1}H NMR** (400 MHz, Methanol-*d4*) δ 7.60 (d, *J* = 8.3 Hz, 2H), 7.34 (d, *J* = 2.1 Hz, 2H), 7.03 (dd, *J* = 8.3, 2.1 Hz, 2H), 3.48 (t, *J* = 7.5 Hz, 2H), 3.25 (s, 4H), 3.19 (t, *J* = 7.2 Hz, 2H), 2.98 (t, *J* = 7.2 Hz, 2H), 2.81 (t, *J* = 7.6 Hz, 2H), 1.81 – 1.65 (m, 4H), 1.35 – 1.23 (m, 2H), 1.20 – 1.08 (m, 2H). **^{13}C NMR** (101 MHz, Methanol-*d4*) δ 175.1, 157.8, 137.2 (2C), 135.2 (2C), 135.0 (2C), 133.1 (2C), 131.2 (2C), 122.2 (2C), 72.4, 41.9, 40.4 (2C), 40.2, 40.1, 38.3, 27.3, 26.2, 26.0, 25.5. **HRMS** (ESI): calcd for $C_{25}H_{31}Br_2Cl_2N_4O_2^+$ [M+H]$^+$ 647.0185, found 647.0192. **SFC**: 97.3%.

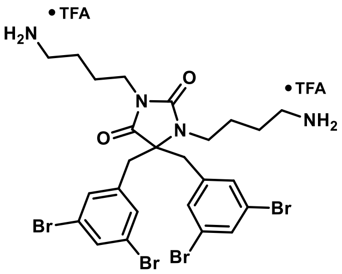

1,3-bis(4-aminobutyl)-5,5-bis(3,5-dibromobenzyl)imidazolidine-2,4-dion **6dA**.

9d (73 mg, 123 µmol, 1.0 eq), *tert*-butyl (4-bromobutyl)carbamate **S8** (77 mg, 306 µmol, 2.5 eq), Cs_2CO_3 (140 mg, 429 µmol, 3.5 eq), TBAI (4.5 mg, 12 µmol, 0.1 eq) and acetone (2.5 mL) were stirred at 75 °C for 72 h. Purification by column chromatography on silica gel with a gradient of 15-50% EtOAc in heptane delivered the impure intermediate Boc-**6dA** (91 mg, 97 µmol, 79%) as a colorless solid.

TFA (94 µL, 1.23 mmol, 10.0 eq) and DCM (1.5 mL) were added and the solution was stirred at ambient temperature for 24 h. The crude was purified by RP chromatography with a gradient of 15-55% MeCN/H_2O + 0.1% TFA to yield the di-TFA salt of **6dA** (73 mg, 76 µmol, 62% o2s) as a white solid. **^{1}H NMR** (400 MHz, Methanol-*d4*) δ 7.66 (t, *J* = 1.7 Hz, 2H), 7.34 (d, *J* = 1.7 Hz, 4H), 3.49 – 3.41 (m, 2H), 3.29 – 3.24 (m, 4H), 3.22 (d, *J* = 7.4 Hz, 2H), 3.02 – 2.95 (m, 2H), 2.87 (t, *J* = 7.6 Hz, 2H), 1.72 (qn, *J* = 3.6 Hz, 4H), 1.40 (qn, *J* = 7.4 Hz, 2H), 1.34 – 1.23 (m, 2H). **^{13}C NMR** (101 MHz, Methanol-*d4*) δ 175.1, 157.6, 140.2 (2C), 134.2 (2C), 133.1 (4C), 123.9 (4C), 72.6, 42.0, 40.5 (2C), 40.3, 40.0, 38.5, 27.2, 26.2, 26.2, 25.6. **HRMS** (ESI): calcd for $C_{25}H_{31}Br_4N_4O_2^+$ [M+H]$^+$ 734.9175, found 734.9179. **SFC**: 96.1%.

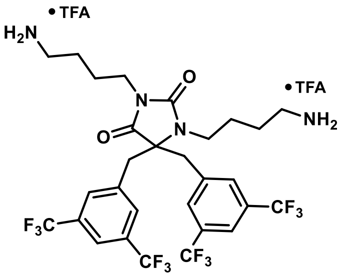

1,3-bis(4-aminobutyl)-5,5-bis(3,5-bis(trifluoromethyl)benzyl)imidazolidine-2,4-dione **6fA**.

9f (72 mg, 130 µmol, 1.0 eq), *tert*-butyl (4-bromobutyl)carbamate **S8** (82 mg, 326 µmol, 2.5 eq), Cs_2CO_3 (149 mg, 456 µmol, 3.5 eq), TBAI (4.8 mg, 13 µmol, 0.1 eq) and acetone (2.0 mL) were stirred at 75 °C for 72 h. Purification by column chromatography on silica gel with a gradient of 15-50% EtOAc in heptane delivered the impure intermediate Boc-**6fA** (103 mg, 115 µmol, 88%) as a colorless solid.

TFA (100 µL, 1.30 mmol, 10.0 eq) and DCM (1.5 mL) were added and the solution was stirred at ambient temperature for 24 h. The crude was purified by RP chromatography with a gradient of 8-48% MeCN/H_2O + 0.1% TFA to yield the di-TFA salt of **6fA** (96 mg, 104 µmol, 80% o2s) as a white solid. **^{1}H NMR** (400 MHz, Methanol-*d4*) δ 7.92 (d, *J* = 2.0 Hz, 2H), 7.81 – 7.77 (m, 4H), 3.59 – 3.53 (m, 2H), 3.54 (d, *J* = 14.3 Hz, 2H), 3.49 (d, *J* = 14.3 Hz, 2H), 3.10 (dd, *J* = 8.4, 6.7 Hz, 2H), 2.96 (t, *J* = 6.8 Hz, 2H), 2.79 – 2.69 (m, 2H), 1.76 (qn, *J* = 3.3 Hz, 4H), 1.37 – 1.25 (m, 2H), 1.08 (tt, *J* = 9.4, 6.5 Hz, 2H). **^{13}C NMR** (101 MHz, Methanol-*d4*) δ 174.7, 157.2, 139.0 (2C), 132.7 (q, *J* = 33.2 Hz, 4C), 132.0 – 1.31.7 (m, 4C), 124.7 (q, *J* = 272.0 Hz, 4C), 122.6 – 122.4 (m, 2C), 72.2, 42.0, 40.5 (2C), 40.2, 39.7, 38.3, 27.4, 26.2, 25.7, 25.3. **HRMS** (ESI): calcd for $C_{29}H_{31}F_{12}N_4O_2^+$ $[M+H]^+$ 695.2250, found 695.2254. **SFC**: 95.5%.

3.4.6 Synthesis of *N,N'*-dialkylated hydantoins 6G

The following compounds were prepared according to General Procedure D:

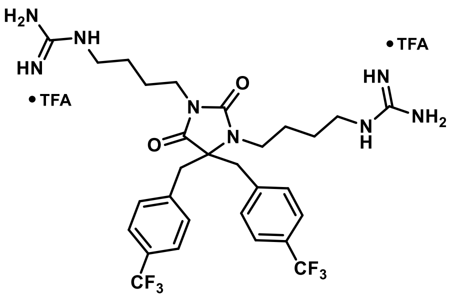

1,1'-((2,5-dioxo-4,4-bis(4-(trifluoromethyl)benzyl)imidazolidine-1,3-diyl)bis(butane-4,1-diyl))diguanidine **6bG**.

6bA (29 mg, 37 µmol, 1.0 eq), *N,N'*-Di-Boc-1*H*-pyrazole-1-carboxamidine (29 mg, 92 µmol, 2.50 eq), DIPEA (26 µL, 148 µmol, 4.0 eq) and THF (0.75 mL) were stirred at 45 °C for 2.5 h. The crude was purified with a gradient of 20-55% EtOAc in heptane to yield pure Boc-**6bG** (38 mg, 36 µmol, 99%) as a clear solid.

TFA (85 µL, 1.11 mmol, 30.0 eq) and DCM (0.75 mL) were added and the solution was stirred at ambient temperature for 44 h. The crude was purified by RP chromatography with a gradient of 20-60% MeCN/H_2O + 0.1% TFA to yield the di-TFA salt of **6bG** (25 mg, 29 µmol, 78% o2s) as a white powder. **^{1}H NMR** (400 MHz, Methanol-*d4*) δ 7.59 (d, *J* = 8.1 Hz, 4H), 7.38 (d, *J* = 8.0 Hz, 4H), 3.54 (dd, *J* = 9.1, 6.7 Hz, 2H), 3.39 (s, 4H), 3.22 (t, *J* = 7.1 Hz, 2H), 3.14 (t, *J* = 6.5 Hz, 2H), 3.00 (t, *J* = 6.9 Hz, 2H), 1.82 – 1.69 (m, 2H), 1.69 – 1.58 (m, 2H), 1.15 – 1.02 (m, 4H). **^{13}C NMR** (101 MHz, Methanol-*d4*) δ 175.3, 158.7, 158.6, 158.0, 140.5 (2C), 131.9 (4C), 130.8 (q, *J* = 32.3 Hz, 2C), 126.3 (q, *J* = 3.9 Hz, 4C), 125.6 (q, *J* = 271.4 Hz, 2C), 72.5, 42.2, 42.0, 41.5, 41.4 (2C), 38.4, 27.5 (2C), 26.5, 25.8. **HRMS** (ESI): calcd for $C_{29}H_{37}F_6N_8O_2^+$ $[M+H]^+$ 643.2938, found 643.2936. **SFC**: >99%.

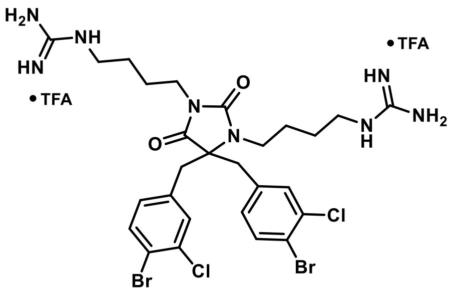

1,1'-((4,4-bis(4-bromo-3-chlorobenzyl)-2,5-dioxoimidazolidine-1,3-diyl)bis(butane-4,1-diyl))diguanidine **6cG.**

6cA (28 mg, 32 µmol, 1.0 eq), *N,N'*-Di-Boc-1*H*-pyrazole-1-carboxamidine (25 mg, 80 µmol, 2.50 eq), DIPEA (22 µL, 128 µmol, 4.0 eq) and THF (0.75 mL) were stirred at 45 °C for 2.5 h. The crude was purified with a gradient of 20-55% EtOAc in heptane to yield pure Boc-**6cG** (35 mg, 31 µmol, 97%) as a clear solid.

TFA (74 µL, 0.96 mmol, 30.0 eq) and DCM (0.75 mL) were added and the solution was stirred at ambient temperature for 44 h. The crude was purified by RP chromatography with a gradient of 20-60% MeCN/H_2O + 0.1% TFA to yield the di-TFA salt of **6cG** (28 mg, 29 µmol, 91% o2s) as a white powder.

^{1}H NMR (400 MHz, Methanol-*d4*) δ 7.59 (d, *J* = 8.2 Hz, 2H), 7.33 (d, *J* = 2.1 Hz, 2H), 7.03 (dd, *J* = 8.3, 2.1 Hz, 2H), 3.53 – 3.44 (m, 2H), 3.27 – 3.16 (m, 8H), 3.06 (t, *J* = 7.1 Hz, 2H), 1.81 – 1.69 (m, 2H), 1.69 – 1.58 (m, 2H), 1.25 – 1.06 (m, 4H). **^{13}C NMR** (101 MHz, Methanol-*d4*) δ 175.2, 158.7, 158.6, 158.0, 137.3 (2C), 135.3 (2C), 134.9 (2C), 133.0 (2C), 131.2 (2C), 122.3 (2C), 72.4, 42.2, 42.1, 41.8, 40.5 (2C), 38.5, 27.6, 27.5, 26.5, 26.1. **HRMS** (ESI): calcd for $C_{27}H_{35}Br_2Cl_2N_8O_2^+$ $[M+H]^+$ 731.0621, found 731.0630. **SFC**: >99%.

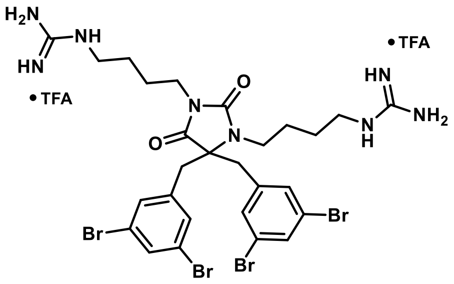

1,1'-((4,4-bis(3,5-dibromobenzyl)-2,5-dioxoimidazolidine-1,3-diyl)bis(butane-4,1-diyl))diguanidine **6dG**.

6dA (31 mg, 32 µmol, 1.0 eq), *N,N′*-Di-Boc-1*H*-pyrazole-1-carboxamidine (25 mg, 80 µmol, 2.50 eq), DIPEA (22 µL, 129 µmol, 4.0 eq) and THF (0.75 mL) were stirred at 45 °C for 2.5 h. The crude was purified with a gradient of 20-55% EtOAc in heptane to yield pure Boc-**6dG** (36 mg, 29 µmol, 92%) as a clear solid.

TFA (74 µL, 963 µmol, 30.0 eq) and DCM (0.75 mL) were added and the solution was stirred at ambient temperature for 44 h. The crude was purified by RP chromatography with a gradient of 10-45% MeCN/H_2O + 0.1% TFA to yield the di-TFA salt of **6dG** (25 mg, 24 µmol, 74% o2s) as a white powder. **^{1}H NMR** (400 MHz, Methanol-*d4*) δ 7.65 (t, *J* = 1.7 Hz, 2H), 7.34 (d, *J* = 1.7 Hz, 4H), 3.45 (t, *J* = 7.7 Hz, 2H), 3.28 – 3.19 (m, 8H), 3.11 (t, *J* = 6.8 Hz, 2H), 1.79 – 1.57 (m, 2H), 1.34 – 1.17 (m, 4H). **^{13}C NMR** (101 MHz, Methanol-*d4*) δ 175.1, 158.7, 158.6, 157.8, 140.2 (2C), 134.1 (2C), 133.1 (4C), 123.9 (4C), 72.6, 42.2 (2C), 41.9, 40.5 (2C), 38.7, 27.5 (2C), 26.7, 26.4. **HRMS** (ESI): calcd for $C_{27}H_{35}Br_4N_8O_2^+$ $[M+H]^+$ 818.9611, found 818.9613. **SFC**: >99%.

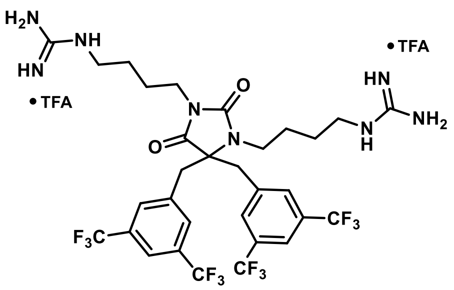

1,1'-((4,4-bis(3,5-bis(trifluoromethyl)benzyl)-2,5-dioxoimidazolidine-1,3-diyl)bis(butane-4,1-diyl))diguanidine **6fG**.

6fA (33 mg, 36 µmol, 1.0 eq), *N,N′*-Di-Boc-1*H*-pyrazole-1-carboxamidine (28 mg, 89 µmol, 2.50 eq), DIPEA (25 µL, 143 µmol, 4.0 eq) and THF (0.75 mL) were stirred at 45 °C for 2.5 h. The crude was purified with a gradient of 20-55% EtOAc in heptane to yield pure Boc-**6fG** (40 mg, 34 µmol, 95%) as a clear solid.

TFA (82 µL, 1.07 mmol, 30.0 eq) and DCM (0.75 mL) were added and the solution was stirred at ambient temperature for 44 h. The crude was purified by RP chromatography with a gradient of 20-60% MeCN/H_2O + 0.1% TFA to yield the di-TFA salt of **6fG** (31 mg, 31 µmol, 86% o2s) as a white powder. **^{1}H NMR** (400 MHz, Methanol-*d4*) δ 7.91 (s, 2H), 7.81 – 7.77 (m, 4H), 3.60 – 3.52 (m, 2H), 3.55 (d, *J* = 14.3 Hz, 2H), 3.49 (d, *J* = 14.3 Hz, 2H), 3.23 (t, *J* = 7.0 Hz, 2H), 3.10 (t, *J* = 6.8 Hz, 2H), 3.00 (t, *J* = 6.8 Hz, 2H), 1.78 (q, *J* = 8.4, 7.7 Hz, 2H), 1.74 – 1.63 (m, 2H), 1.17 – 1.04 (m, 4H). **^{13}C NMR** (101 MHz, Methanol-*d4*) δ 174.8, 158.7, 158.6, 157.5, 139.0 (2C), 132.7 (q, *J* = 33.3 Hz, 4C), 132.0 – 131.7 (m, 4C), 124.7 (q, *J* = 272.1 Hz, 4C), 122.6 – 122.3 (m, 2C), 72.2, 42.2, 42.0, 41.5, 40.5 (2C), 38.5, 27.7, 27.5, 26.5, 25.9. **HRMS** (ESI): calcd for $C_{31}H_{35}F_{12}N_8O_2^+$ $[M+H]^+$ 779.2686, found 779.2689. **SFC**: >99%.

3.5 Synthesis of different core structures 3-5 and 15

3.5.1 2,4-Dithiohydantoins

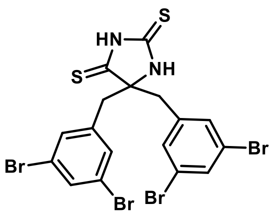

5,5-bis(3,5-dibromobenzyl)imidazolidine-2,4-dithione **16**.

Hydantoin **9d** (175 mg, 294 µmol, 1.0 eq) was mixed with anhydrous 1,4-dioxane (2.5 mL) in an oven dried vial under inert atmosphere. Lawesson's reagent (475 mg, 1.17 mmol, 4.0 eq) was added and the solution was stirred at 115 °C for 40 h. The mixture became yellow and clear at elevated temperature. The mixture was allowed to cool to ambient temperature and the solvent was removed under reduced pressure. Purification by column chromatography on silica gel with a gradient of 10-15 % EtOAc in heptane and subsequent lyophilization delivered **16** (152 mg, 242 µmol, 82%) as a yellow solid.

^{1}H NMR (400 MHz, DMSO-*d6*) δ 12.91 (s, 1H), 10.97 (d, *J* = 1.7 Hz, 1H), 7.72 (t, *J* = 1.8 Hz, 2H), 7.37 (d, *J* = 1.8 Hz, 4H), 3.17 (d, *J* = 13.5 Hz, 2H), 3.10 (d, *J* = 13.5 Hz, 2H). **^{13}C NMR** (101 MHz, DMSO-*d6*) δ 206.5, 180.4, 138.5 (2C), 132.3 (4C), 132.2 (2C), 121.9 (4C), 80.6, 43.5. **HRMS** (ESI): calcd for $C_{17}H_{11}Br_4N_2S_2^-$ $[M-H]^-$ 622.7103, found: 622.7109.

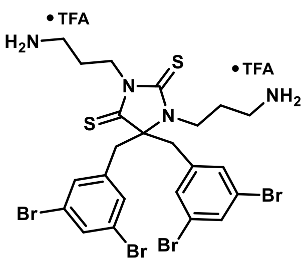

1,3-bis(3-aminopropyl)-5,5-bis(3,5-dibromobenzyl)imidazolidine-2,4-dithione **4A**.

2,4-dithiohydantoin **16** (75 mg, 119 µmol, 1.0 eq), *tert*-butyl (3-bromopropyl)carbamate **S7** (92 mg, 388 µmol, 3.25 eq), Cs_2CO_3 (97 mg, 0.299 µmol, 2.5 eq), TBAI (8.8 mg, 24 µmol, 0.2 eq) and acetone (2.0 mL) were stirred at 55 °C for 72 h. The mixture was allowed to cool to ambient temperature before water and EtOAc were added. The layers were separated, and the aqueous layer was extracted with EtOAc twice. The combined organics were dried over $MgSO_4$, filtered and the solvent was removed under reduced pressure. Purification by automated flash column chromatography on silica gel with a gradient of 10-45% EtOAc in heptane delivered the impure intermediate Boc-**4A** (169 mg, 159 µmol, 74%) as a yellow foam.

Boc-**4A**, TFA (138 µL, 1.79 mmol, 15.0 eq) and DCM (1.0 mL) were combined, and the mixture stirred for 24 h at ambient temperature. The solvent was removed and the crude purified by RP chromatography with a gradient of 20-60% MeCN/H_2O + 0.1% TFA to yield the di-TFA salt of **4A** (65 mg, 67 µmol, 56% o2s) as a white solid.

Note: *Peaks in the NMR that are not accounted for are likely to be the S-alkylated isomers.*

^{1}H NMR (400 MHz, Methanol-*d4*) δ 7.56 (t, *J* = 1.8 Hz, 2H), 7.31 (d, *J* = 1.8 Hz, 4H), 3.61 – 3.55 (m, 2H), 3.37 (t, *J* = 7.2 Hz, 2H), 3,36 (d, *J* = 13.0 Hz, 2H), 3.26 (d, *J* = 12.9 Hz, 2H), 3.17 (t, *J* = 7.2 Hz, 2H), 2.74 (t, *J* = 7.3 Hz, 2H), 2.25 (qn, *J* = 7.2 Hz, 2H), 1.56 – 1.43 (m, 2H). **^{13}C NMR** *not obtained*. **HRMS** (ESI): calcd for $C_{23}H_{27}Br_4N_4S_2^+$ $[M+H]^+$ 738.8405, found: 738.8405. **SFC**: *not obtained*.

3.5.2 Thiobarbituric acid

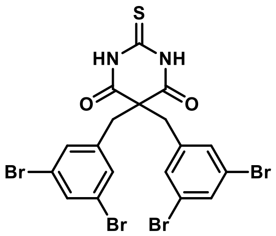

5,5-bis(3,5-dibromobenzyl)-2-thioxodihydropyrimidine-4,6(1H,5H)-dione **18**.

Diethyl 2,2-bis(3,5-dibromobenzyl)malonate[11] (1.10 g, 1.67 mmol, 1.0 eq) was dissolved in 15 mL of anhydrous THF:DMF (2:1) under inert atmosphere and cooled to 0 °C. Thiourea (1.27 g, 16.7 mmol, 10.0 eq) and NaH (201 mg, 5.02 mmol, 3.0 eq, 60% in mineral oil) were added and the mixture was stirred at that temperature for 30 min. The suspension was then heated to 65 °C for 5 days, cooled to ambient temperature and EtOAc was added. The organic layer was washed with 5% $LiCl_{(aq)}$ solution thrice, dried over $MgSO_4$, filtered and the solvent was removed under reduced pressure. The crude solids were purified by column chromatography on silica gel with 5% EtOAc in heptane to yield **18** (261 mg, 408 µmol, 24%) as a yellow foam.

^{1}H NMR (400 MHz, Chloroform-*d*) δ 9.20 (s, 2H), 7.58 (t, *J* = 1.8 Hz, 2H), 7.23 (d, *J* = 1.8 Hz, 4H), 3.33 (s, 4H).**^{13}C NMR** (101 MHz, Chloroform-*d*) δ174.0, 168.4, 137.6 (2C), 134.2 (2C), 131.6 (4C), 123.6 (4C), 59.9, 43.3 (2C). **HRMS** (ESI): calcd for $C_{18}H_{11}Br_4N_2O_2S^-$ $[M-H]^-$ 634.7280, found: 634.7275.

The following compound was synthesized according to General procedure C:

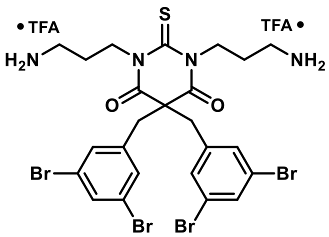

1,3-bis(3-aminopropyl)-5,5-bis(3,5-dibromobenzyl)-2-thioxodihydropyrimidine-4,6(1H,5H)-dione **5A**.

2-Thiobarbituric acid **18** (106 mg, 166 µmol, 1.0 eq), *tert*-butyl (3-bromopropyl)carbamate **S7** (118 mg, 497 µmol, 3.0 eq), Cs_2CO_3 (119 mg, 364 µmol, 2.2 eq), TBAI (12 mg, 33 µmol, 0.2 eq) and acetone (1.5 mL) were stirred at 70 °C for 87 h. Purification by automated column chromatography on silica with a gradient of 5-45% EtOAc in heptane delivered the impure intermediate Boc-**5A** (83 mg, 87 µmol, 53%) as a yellow solid.

TFA (102 µL, 1.33 mmol, 8.0 eq) and DCM (1.0 mL) were added and the solution was stirred at ambient temperature for 17 h. The crude was purified by RP chromatography with a gradient of 20-60% MeCN/H_2O + 0.1% TFA to yield two batches of a mixture of desulfurized (**1A**) and thionylated product (**5A**) as their di-TFA salts. Yield adjusted to pure **5A** (15 mg, 15 µmol, 9% o2s) Analytical data is only referring to the thionylated product. *Note: De-sulfurization has taken place.*

Mixture 1: white solid, 2-thiobarbituric acid **5A** : barbituric acid **1A** 2.4:1.0[a],
Mixture 2: slightly yellow solid, 2-thiobarbituric acid **5A** : barbituric acid **1A** 1.0:1.7[a]

Analytical data for the 2-thiobarbituric acid derivative **5A**:

^{1}H NMR (400 MHz, Methanol-*d4*) δ 7.65 (t, *J* = 1.7 Hz, 2H), 7.25 (d, *J* = 1.7 Hz, 4H), 4.26 – 4.18 (m, 4H), 3.48 (s, 4H), 2.94 (t, *J* = 7.3 Hz, 4H), 1.93 – 1.81 (m, 4H). **^{13}C NMR** (101 MHz, Methanol-*d4*) δ 179.1, 169.8, 140.3 (2C), 134.7 (2C), 132.6 (4C), 124.2 (4C), 61.9, 46.5 (2C), 45.1 (2C), 38.3 (2C), 26.6 (2C). **HRMS** (ESI): calcd for $C_{24}H_{27}Br_4N_4O_2S^+$ $[M+H]^+$ 750.8583, found: 750.8592. **SFC**: *not obtained*.

Analytical data for desulfurized derivative was identical to the data obtained previously.[12]

[a] Ratio was determined by NMR

3.5.3 4-imidazolidin-2-one and its constitutional isomers

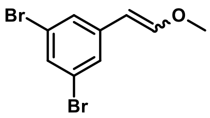

(E)/(Z)-1,3-dibromo-5-(2-methoxyvinyl)benzene **S9**.
(Methoxymethyl)triphenylphosphonium chloride (7.27 g, 21.2 mmol, 1.6 eq) was taken up in dry THF (40 mL) under inert atmosphere and cooled to -78 °C. NaHMDS (21.2 mL, 21.2 mmol, 1.6 eq; 1.0 M in THF) was added slowly and the resulting mixture was stirred at 0 °C for 30 min. The mixture was re-cooled to -78 °C and 3,5-dibromobenzaldehyde **10** (3.50 g, 13.2 mmol, 1.0 eq) was added slowly. Stirring was continued at -78 °C for 30 min and then at ambient temperature for another 2 h. Water and EtOAc were added and the layers were separated. The aqueous layer was extracted with EtOAc twice and the combined organics were dried over $MgSO_4$, filtered and the solvent was removed under reduced pressure. Heptane was added to the crude solids, and the suspension was sonicated for 5 min. The organic layer was decanted, and the procedure was repeated 3 times. The organic layers were combined, and the solvent was removed under reduced pressure. The crude product was purified by column chromatography on silica gel with 0-5% EtOAc in heptane to yield **S9** (3.54 g, 12.1, 91%) as a slightly yellow liquid. A 1.5 : 1.0 mixture of the *(E):(Z)* isomers was obtained. **HRMS** (ESI): calcd for $C_9H_9Br_2O^+$ $[M+H]^+$ 290.9015 found: *not found*.
Cis-**ABML444:** **^{1}H NMR** (400 MHz, Chloroform-*d*) δ 7.64 (d, *J* = 1.7 Hz, 2H), 7.41 (t, *J* = 1.8 Hz, 1H), 6.20 (d, *J* = 7.0 Hz, 1H), 5.08 (d, *J* = 7.0 Hz, 1H), 3.82 (s, 3H). **^{13}C NMR** (101 MHz, Chloroform-*d*) δ 150.3, 139.6, 130.9, 129.6 (2C), 122.7 (2C), 103.3, 57.0.
Trans-**ABML444:** **^{1}H NMR** (400 MHz, Chloroform-*d*) δ 7.40 (t, *J* = 1.7 Hz, 1H), 7.28 (d, *J* = 1.8 Hz, 2H), 7.04 (d, *J* = 12.9 Hz, 1H), 5.65 (d, *J* = 12.9 Hz, 1H), 3.69 (s, 3H). **^{13}C NMR** (101 MHz, Chloroform-*d*) δ 151.0, 140.4, 130.9, 126.7 (2C), 123.2 (2C), 102.9, 57.0.

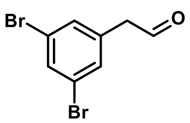

2-(3,5-dibromophenyl)acetaldehyde **11**.
The mixture of *(E)/(Z)*-**S9** (2.87 g, 9.83 mmol, 1.0 eq) was taken up in anhydrous MeCN (197 mL, c = 0.05 M) and NaI (3.09, 20.6 mmol, 2.1 eq) was added. To the vigorously stirring mixture TMSCl (2.63 mL, 20.6 mmol, 2.1 eq) was added and the suspension was stirred at ambient temperature for 110 min. A 0.5 M $Na_2SO_{3(aq)}$ solution was added and the layers were separated. The aqueous layer was extracted with Et_2O thrice and the combined organics were dried over $MgSO_4$, filtered and the solvent was removed under reduced pressure. The crude solids were taken up in CCl_4, filtered and the solvent was removed under reduced pressure. The crude orange solids were quickly filtered over a short silica plug to yield aldehyde **11** (1.63 g, 5.68 mmol, 60%) as a white solid. *Note: The product decomposes on silica upon extended exposure.*
^{1}H NMR (400 MHz, Chloroform-*d*) δ 9.75 (t, *J* = 1.9 Hz, 1H), 7.62 (t, *J* = 1.8 Hz, 1H), 7.32 (d, *J* = 1.8 Hz, 2H), 3.67 (d, *J* = 1.9 Hz, 2H). **^{13}C NMR** (101 MHz, Chloroform-*d*) δ 197.5, 135.7, 133.4, 131.6 (2C), 123.5 (2C), 49.5. **HRMS** (ESI): calcd for $C_8H_7Br_2O^+$ $[M+H]^+$ 276.8858, found: *not found*.

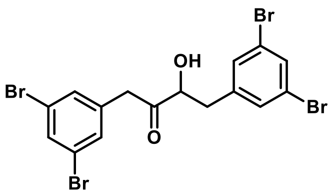

1,4-bis(3,5-dibromophenyl)-3-hydroxybutan-2-one **12**.
Aldehyde **11** (1.63 g, 5.86 mmol, 1.0 eq) and 3-benzyl-5-(2-hydroxyethyl)-4-methylthiazolium chloride (119 mg, 440 µmol, 0.07 eq) were mixed with anhydrous PEG-400 (18 mL) under inert atmosphere. Triethylamine (409 µL, 2.93 mmol, 0.50 eq) was added and the resulting mixture was stirred at 80 °C for 5 h. The oil bath was removed ice-water was added and stirring was continued for 1.0 h. Water and BRINE were added and the aqueous layer was extracted with Et_2O thrice. The combined organics were washed with water twice, dried over $MgSO_4$, filtered and the solvent was removed under reduced pressure. The crude product was purified by column chromatography on silica gel with 10% EtOAc in heptane to yield **12** (635 mg, 1.14 mmol, 39%) as a yellow solid.
^{1}H NMR (400 MHz, Chloroform-*d*) δ 7.60 (t, *J* = 1.8 Hz, 1H), 7.57 (t, *J* = 1.8 Hz, 1H), 7.31 (d, *J* = 1.8 Hz, 2H), 7.24 (d, *J* = 1.8 Hz, 2H), 4.49 – 4.40 (m, 1H), 3.78 (d, *J* = 16.5 Hz, 1H), 3.72 (d, *J* = 16.4 Hz, 1H), 3.16 (s, 1H), 3.10 (dd, *J* = 14.2, 4.2 Hz, 1H), 2.79 (dd, *J* = 14.2, 7.7 Hz, 1H). **^{13}C NMR** (101 MHz, Chloroform-*d*) δ 207.0, 140.1, 136.2, 133.2, 132.9, 131.4 (2C), 131.2 (2C), 123.2 (2C), 123.1 (2C), 76.6, 44.3, 39.2. *Note*: *Residual EtOAc and heptane were observed.* **LRMS** (ESI): calcd for $C_{16}H_{11}Br_4O_2^-$ $[M–H]^-$ 550.7, found 550.7.

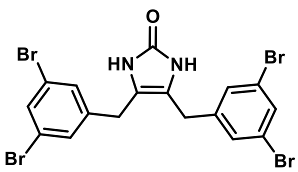

4,5-bis(3,5-dibromobenzyl)-1,3-dihydro-2H-imidazol-2-one **14**.
Acyloin **12** (543 mg, 0.98 mmol, 1.0 eq) was mixed with dry urea (205 mg, 3.42 mmol, 3.5 eq) in a heat dried flask. Glacial acetic acid (2 mL) and anhydrous PEG-400 (2 mL) were added and the mixture was heated to 130 °C for 110 min. After cooling to ambient temperature water was added and a white solid formed. The suspension was stirred for 45 min at ambient temperature, before the solids were filtered off. The residue was washed with water twice. The crude solids were purified by automated flash

column chromatography on silica gel with a gradient of 60-80% EtOAc/heptane + 2.5% MeOH. The title compound **14** (221 mg, 381 µmol, 39%) was obtained as a white solid.
^{1}H NMR (400 MHz, DMSO-*d6*) δ 9.78 (s, 2H), 7.65 (t, *J* = 1.8 Hz, 2H), 7.39 (d, *J* = 1.8 Hz, 4H), 3.69 (s, 4H). *Note: Residual MeOH was observed at δ 4.10 (q, J = 5.3 Hz), 3.17 (d, J = 5.2 Hz).* **^{13}C NMR** (101 MHz, DMSO-*d6*) δ 154.2, 144.3 (2C), 131.2 (2C), 130.3 (4C), 122.4 (4C), 115.5 (2C), 28.4. *Residual MeOH was observed at 48.6.* **HRMS** (ESI): calcd for $C_{17}H_{13}Br_4N_2O^+$ [M+H]$^+$ 576.7756, found: 576.7756.

The following constitutional isomer was obtained from the reaction mixture of compound **14**:

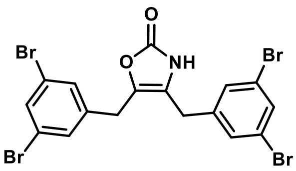

4,5-bis(3,5-dibromobenzyl)oxazol-2(3H)-imine **13.**
Same chemicals and procedure as for **14**. The title compound **13** (100 mg, 172 µmol, 18%) was obtained as a white solid.
^{1}H NMR (400 MHz, DMSO-*d6*) δ 10.61 (s, 1H), 7.72 (t, *J* = 1.7 Hz, 1H), 7.71 (t, *J* = 1.8 H, 1H), 7.49 (d, *J* = 1.8 Hz, 2H), 7.41 (d, *J* = 1.7 Hz, 2H), 3.89 (s, 2H), 3.77 (s, 2H). **^{13}C NMR** (101 MHz, DMSO-*d6*) δ 155.0, 142.5 (2C), 133.5, 131.7, 131.7, 130.5 (2C), 130.4 (2C), 122.6 (2C), 122.5 (2C), 120.2, 28.5, 27.5. *Note: Residual $CDCl_3$ was observed at 79.3, 79.0, 78.6.* **LRMS** (ESI): calcd for $C_{17}H_{10}Br_4NO_2^-$ [M-H]$^-$ 575.9, found 575.7.

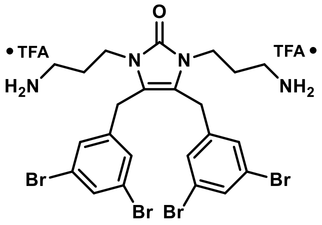

1,3-bis(3-aminopropyl)-4,5-bis(3,5-dibromobenzyl)-1,3-dihydro-2H-imidazol-2-one **3A**.
4-imidazolidin-2-one **14** (100 mg, 172 µmol, 1.0 eq), *tert*-butyl (3-bromopropyl)carbamate **S7** (329 mg, 1.38 mmol, 8.0 eq), K_2CO_3 (135 mg, 0.98 mmol, 5.7 eq) and (*n*-hexadecyl)tri-*n*-butylphosphonium bromide (88 mg, 172 µmol, 1.0 eq) were mixed with toluene (0.5 mL) and water (0.5 mL). The resulting mixture was heated under microwave irradiation to 130 °C for 90 min and then to 150 °C for 60 min. After cooling to ambient temperature, water was added and the aqueous layer was extracted with toluene thrice. The combined organics were dried over $MgSO_4$, filtered and the solvent was removed. The crude yellow solid was purified by automated column chromatography on silica gel with a gradient of 15-45% EtOAc/heptane + 2.5% MeOH. Boc-**3A** (35 mg, 39 µmol, 23%) was obtained as a slightly yellow solid.
Boc-**3A** (35 mg, 39 µmol, 1.0 eq) was taken up in DCM (500 µL) and TFA (75 µL, 0.98 mmol, 25 eq) was added. The solution was stirred at ambient temperature for 20 h before removal of the solvent. The crude amine was purified by RP chromatography with a gradient of 20-55% MeCN/H_2O + 0.1% TFA. The title compound **3A** (30 mg, 33 µmol, 19% o2s) was obtained as a white di-TFA salt.
^{1}H NMR (400 MHz, Methanol-*d4*) δ 7.60 (t, *J* = 1.8 Hz, 2H), 7.27 (d, *J* = 1.8 Hz, 4H), 3.99 (s, 4H), 3.72 (t, *J* = 6.8 Hz, 4H), 2.89 (t, *J* = 7.1 Hz, 4H), 1.77 (qn, *J* = 6.9 Hz, 4H). **^{13}C NMR** (101 MHz, Metahnol-*d4*) δ 155.5, 143.7 (2C), 133.7 (2C), 131.1 (4C), 124.4 (4C), 119.7 (2C), 39.2 (2C), 37.7 (2C), 28.6, 28.4 (2C). **HRMS** (ESI): calcd for $C_{23}H_{27}Br_4N_4O_1^+$ [M+H]$^+$ 690.8913 found 690.8924. **SFC:** >99%.

The constitutional isomer **15A** was obtained from the reaction mixture of **3A**:

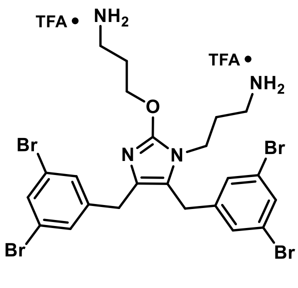

3-(2-(3-aminopropoxy)-4,5-bis(3,5-dibromobenzyl)-1H-imidazol-1-yl)propan-1-amine **15A**.
Chemicals and procedure as stated above for **3A**. Boc-**15A** was obtained impure as a yellow foam (no yield determined).
After TFA treatment and purification by RP chromatography with a gradient of 20-60% MeCN/H_2O + 0.1% TFA, the di-TFA salt of **15A** (27 mg, 29 µmol 17% o2s) was obtained as a white solid.
^{1}H NMR (400 MHz, Methanol-*d4*) δ 7.58 (t, *J* = 1.8 Hz, 1H), 7.54 (t, *J* = 1.8 Hz, 1H), 7.31 (d, *J* = 1.7 Hz, 2H), 7.17 (d, *J* = 1.8 Hz, 2H), 4.62 – 4.54 (m, 2H), 4.07 (s, 2H), 3.90 (s, 2H), 3.87 – 3.80 (m, 2H), 3.18 (t, *J* = 7.4 Hz, 2H), 2.91 (t, *J* = 7.9 Hz, 2H), 2.24 (qn, *J* = 6.5 Hz, 2H), 1.90 (qn, *J* = 7.8 Hz, 2H). **^{13}C NMR** (101 MHz, Methanol-*d4*) δ 151.4, 144.1, 143.1, 133.9, 133.4, 131.5 (2C), 131.1 (2C), 128.0 124.4 (2C), 124.1 (2C), 123.3, 70.6, 41.2, 37.9, 37.6, 31.3, 28.4 (2C), 28.0. **HRMS** (ESI): calcd for $C_{23}H_{27}Br_4N_4O_1^+$ [M+H]$^+$ 690.8907, found 690.8907. **SFC:** 96.5%.

3.5.4 4-imidazolidin-2-one *via N*-acyliminium ion rearrangement

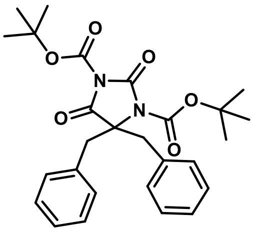

Di-tert-butyl 4,4-dibenzyl-2,5-dioxoimidazolidine-1,3-dicarboxylate Boc-**9a.**
5,5-disubstituted hydantoin **9a** (100 mg, 357 µmol, 1.0 eq) was taken up in THF (2.0 mL) and cooled to 0 °C. 4-DMAP (3.3 mg, 27 µmol, 0.1 eq) and Boc_2O (234 mg, 1.07 mmol, 3.0 eq) were added the cooling bath was removed and the resulting solution was stirred at 45 °C for 20 h. The solution was allowed to cool to ambient temperature and DCM was added. The organic layer was washed with 0.1 M $HCl_{(aq)}$ thrice, dried over $MgSO_4$, filtered and the solvent was removed. The crude was purified by automated column chromatography on silica gel with a gradient of 10-38% EtOAc in heptane to yield Boc-**9a** (156 mg, 325 µmol, 91%) as a white solid.
^{1}H NMR (400 MHz, Chloroform-*d*) δ 7.29 – 7.20 (m, 6H), 7.15 – 7.09 (m, 4H), 3.69 (d, *J* = 13.7 Hz, 2H), 3.38 (d, *J* = 13.6 Hz, 2H), 1.63 (s, 9H), 1.43 (s, 9H). **^{13}C NMR** (101 MHz, Chloroform-*d*) δ 170.1, 149.4, 146.9, 144.5, 133.9 (2C), 129.6 (4C), 128.8 (4C), 127.8 (2C), 85.9, 84.5, 71.8, 40.8 (2C), 28.1 (3C), 27.6 (3C). **HRMS** (ESI): calcd for $C_{27}H_{32}N_2O_6Na^+$ $[M+Na]^+$ 503.2153, found: 503.2155.

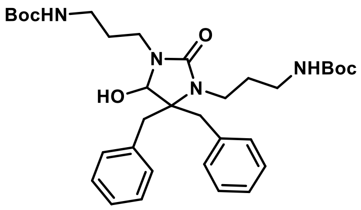

Di-tert-butyl ((4,4-dibenzyl-5-hydroxy-2-oxoimidazolidine-1,3-diyl)bis(propane-3,1-diyl))dicarbamate **S2**
Boc-**2aA** (226 mg, 380 µmol, 1.0 eq) was dissolved in anhydrous DCM (2.5 mL) under inert atmosphere and cooled to -78 °C. DIBAL-H (1 M in DCM, 570 µL, 570 µmol, 1.5 eq) was added and the resulting mixture was stirred at -78 °C for 3h. 10% Rochelle's $salt_{(aq)}$ solution was added and the suspension was stirred at ambient temperature for 30 min. The aqueous layer was extracted with Et_2O thrice and the combined organics were washed twice with 10% Rochelle's $salt_{(aq)}$ solution, dried over $MgSO_4$, filtered and the solvent was removed under reduced pressure. The crude was purified by automated column chromatography on silica gel with a gradient of 15-60% EtOAc in heptane to yield **S2** (126 mg, 211 µmol, 56%) as a colorless solid.
^{1}H NMR (400 MHz, Chloroform-*d*) δ 7.53 – 7.45 (m, 2H), 7.37 – 7.23 (m, 3H), 7.22 – 7.12 (m, 3H), 6.95 – 6.81 (m, 2H), 5.60 (t, J = 6.9 Hz, 1H), 5.04 (d, J = 6.7 Hz, 1H), 4.73 (d, J = 6.8 Hz, 1H), 4.59 (s, 1H), 3.81 – 3.66 (m, 1H), 3.50 (d, J = 13.5 Hz, 1H), 3.43 – 3.31 (m, 1H), 3.26 – 3.14 (m, 1H), 3.10 – 2.98 (m, 1H), 2.84 (d, J = 14.1 Hz, 1H), 2.80 (d, J = 13.5 Hz, 1H), 2.80 – 2.58 (m, 4H), 2.48 (d, J = 14.1 Hz, 1H), 1.86 – 1.64 (m, 2H), 1.44 (s, 9H), 1.41 (s, 9H), 1.24 – 1.19 (m, 2H). *Residual DCM (5.29, s), EtOAc (4.14 (q, J = 7.2 Hz), 2.06 (s), 1.27 (t, J = 7.1 Hz)) and heptane (0.93 – 0.86 (m, 1H)) were observed*. **^{13}C NMR** (101 MHz, Chloroform-*d*) δ 159.8, 156.7, 156.4, 136.9 (2C), 135.8 (2C), 131.1 (2C), 129.8 (2C), 128.6 (2C), 128.5 (2C), 127.0 (2C), 126.9 (2C), 84.2, 79.3, 79.2, 67.4, 40.6, 39.9, 37.7, 37.5, 37.3, 31.7, 29.5, 28.6 (3C), 28.6 (3C). *Residual EtOAc (171.3, 60.5, 21.2, 14.2), heptane (32.0, 22.8, 14.3) and "grease" (29.1) were observed.* **HRMS** (ESI): calcd for $C_{33}H_{49}N_4O_6^+$ $[M+H]^+$ 597.3647, found: 597.3647.

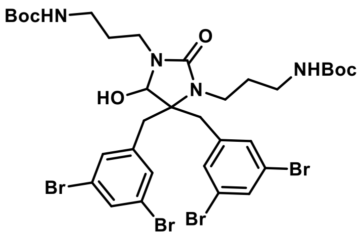

Di-tert-butyl ((4,4-bis(3,5-dibromobenzyl)-5-hydroxy-2-oxoimidazolidine-1,3-diyl)bis(propane-3,1-diyl))dicarbamate **S3.**
Boc-**2dA** (131 mg, 144 µmol, 1.0 eq) was dissolved in anhydrous DCM under inert atmosphere and cooled to -78 °C. DIBAL-H (432 µL, 432 µmol, 3.0 eq) was added and the resulting mixture was allowed to warm to 0 °C and stirred for 3h. 10% Rochelle's $salt_{(aq)}$ solution was added and after stirring at ambient temperature for 60 min, the aqueous layer was extracted with DCM thrice. The combined organics were washed twice with 10% Rochelle's $salt_{(aq)}$ solution, dried over $MgSO_4$, filtered and the solvent was removed under reduced pressure. The crude was purified by automated column chromatography on silica gel with a gradient of 50-85% EtOAc in heptane to yield **S3** (92 mg, 101 µmol, 70%) as a white solid.
^{1}H NMR (400 MHz, Chloroform-*d*) δ 7.62 (d, J = 1.8 Hz, 2H), 7.59 (t, J = 1.7 Hz, 1H), 7.50 (t, J = 1.7 Hz, 1H), 7.01 (d, J = 1.7 Hz, 2H), 5.58 (s, 1H), 5.50 (s, 1H), 4.93 (t, *J* = 6.7 Hz, 1H), 4.75 (d, J = 6.3 Hz, 1H), 3.80 – 3.64 (m, 2H), 3.46 (d, J = 13.3 Hz, 1H), 3.42 – 3.31 (m, 1H), 3.19 – 3.09 (m, 2H), 3.09 – 2.80 (m, 5H), 2.77 (d, J = 14.0 Hz, 1H), 2.70 (d, J = 13.4 Hz, 1H), 2.40 (d, J = 14.0 Hz, 1H), 1.86 – 1.73 (m, 2H), 1.73 – 1.61 (m, 2H), 1.45 (s, 9H), 1.44 (s, 9H), 1.24 – 1.18 (m, 2H). *Residual heptane was observed at 1.33 – 1.22 (m) and 0.90 – 0.85 (m).* **^{13}C NMR** (101 MHz, Chloroform-*d*) δ 159.5, 157.3, 156.4, 140.6, 139.5, 133.0 (3C), 132.7, 131.5 (2C), 123.1 (2C), 122.9 (2C), 83.7, 80.5, 79.4, 67.0, 40.5, 39.2, 37.8 (2C), 37.6, 37.4 31.8, 30.5, 28.6 (6C). *Residual heptane was observed at 32.0, 29.2, 22.8, 14.3*. **HRMS** (ESI): calcd for $C_{33}H_{44}Br_4N_4O_6Na^+$ $[M+Na]^+$ 930.9887, found: 930.9886.

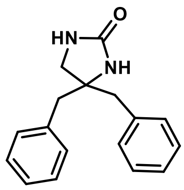

4,4-dibenzylimidazolidin-2-one **S4**.

Boc-**9a** (156 mg, 325 µmol, 1.0 eq) was dissolved in EtOH, $NaBH_4$ (61 mg, 1.62 mmol, 5.0 eq) was added and the mixture was stirred at ambient temperature for 16 h. 0.1 M HCl was added to destroy residual $NaBH_4$, followed by the addition of water. The aqueous layer was extracted with Et_2O thrice. The combined organics were dried over $MgSO_4$, filtered and the solvent was removed under reduced pressure. The crude was purified by automated column chromatography on silica gel with a gradient of 15-55% EtOAc in heptane to yield impure-**S1** (16 mg, 33 µmol, 10%) as a white solid. **S1** was obtained as a mixture of compounds having between zero to two Boc groups and was used without further purification.

S1 (16 mg, 33 µmol, 1.0 eq) was dissolved in anhydrous toluene (0.75 mL) in an oven dried flask under inert atmosphere and p-TsOH (1.6 mg, 8.3 µmol, 0.25 eq) was added. The resulting mixture was heated to 120 °C for 24 h. The mixture was allowed to cool to ambient temperature and the solvent was removed. To the resulting crude DCM (0.75 mL) and TFA (64 µL, 828 µmol, 25 eq) were added and the resulting solution was stirred at ambient temperature for 20 h. The solvent was removed and the crude product was purified by automated column chromatography on silica gel with a gradient of 15-55% EtOAc in heptane to yield impure **S4** (3 mg, 11 µmol, 24%) as a white solid.

^{1}H NMR (400 MHz, Methanol-*d4*) δ 7.37 – 7.20 (m, 10H), 4.19 (s, 2H), 2.97 (d, *J* = 13.8 Hz, 2H), 2.89 (d, *J* = 13.8 Hz, 2H). **^{13}C NMR** (101 MHz, Methanol-*d4*) δ 161.8, 137.0 (2C), 131.7 (4C), 129.5 (4C), 128.1 (2C), 72.1, 62.6, 45.9 (2C). **LRMS** (ESI): calcd for $C_{17}H_{18}N_2O^+$ $[M+H]^+$ 267.1, found 267.1.

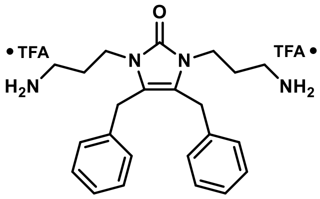

1,3-bis(3-aminopropyl)-4,5-dibenzyl-1,3-dihydro-2H-imidazol-2-one **S5**.

S2 (18 mg, 30 µmol, 1.0 eq) was dissolved in DCM (750 µL) and TFA (46 µL, 603 µmol, 20.0 eq) was added. The resulting clear solution was stirred at ambient temperature for 18 h. The solvent was removed under reduced pressure and the crude was purified by RP column chromatography with a gradient of 10-45% $MeCN/H_2O$ + 0.1% TFA to yield the impure di-TFA salt of **S5** (15 mg, 25 µmol, 82%) as a slightly yellow solid.

^{1}H NMR (400 MHz, Methanol-*d4*) δ 8.09 (s, 6H), 7.34 – 7.26 (m, 4H), 7.26 – 7.19 (m, 4H), 7.10 (d, J = 7.3 Hz, 4H), 3.86 (s, 4H), 3.64 (s, 4H), 2.71 (s, 4H), 1.48 (s, 4H).**^{13}C NMR** (101 MHz, Methanol-*d4*) δ 154.9, 137.0 (2C), 129.3 (4C), 127.9 (4C), 127.5 (2C), 119.3 (2C), 37.6 (2C), 36.2 (2C), 29.2 (2C), 26.5 (2C).**HRMS** (ESI): calcd for $C_{23}H_{31}N_4O^+$ $[M+H]^+$ 379.2492, found: 379.2499.

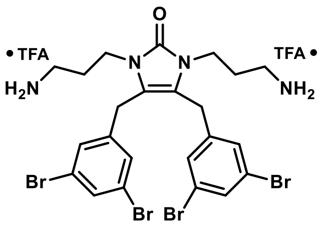

1,3-bis(3-aminopropyl)-4,5-bis(3,5-dibromobenzyl)-1,3-dihydro-2H-imidazol-2-one **3A**.

S3 (92 mg, 101 µmol, 1.0 eq) was dissolved in DCM (1 mL) and TFA (116 µL, 1.51 mL, 15.0 eq) was added. The mixture was stirred at ambient temperature for 22 h. A second portion of TFA (116 µL, 1.51 mL, 15.0 eq) was added and the mixture was heated to 45 °C for 20 h. The solution was allowed to cool to ambient temperature after a total of 42 h and the solvent was removed. The crude was purified by RP column chromatography with a gradient of 10-55% $MeCN/H_2O$ + 0.1% TFA to yield the impure di-TFA salt of **3A** (40 mg, 43 µmol, 43%) as a slightly yellow solid. The spectroscopic data was identical to the ones reported (*vide supra*).

4. NMR spectra

4.1 Symmetrical ketones **8**

1,3-diphenylpropan-2-one **8a**.

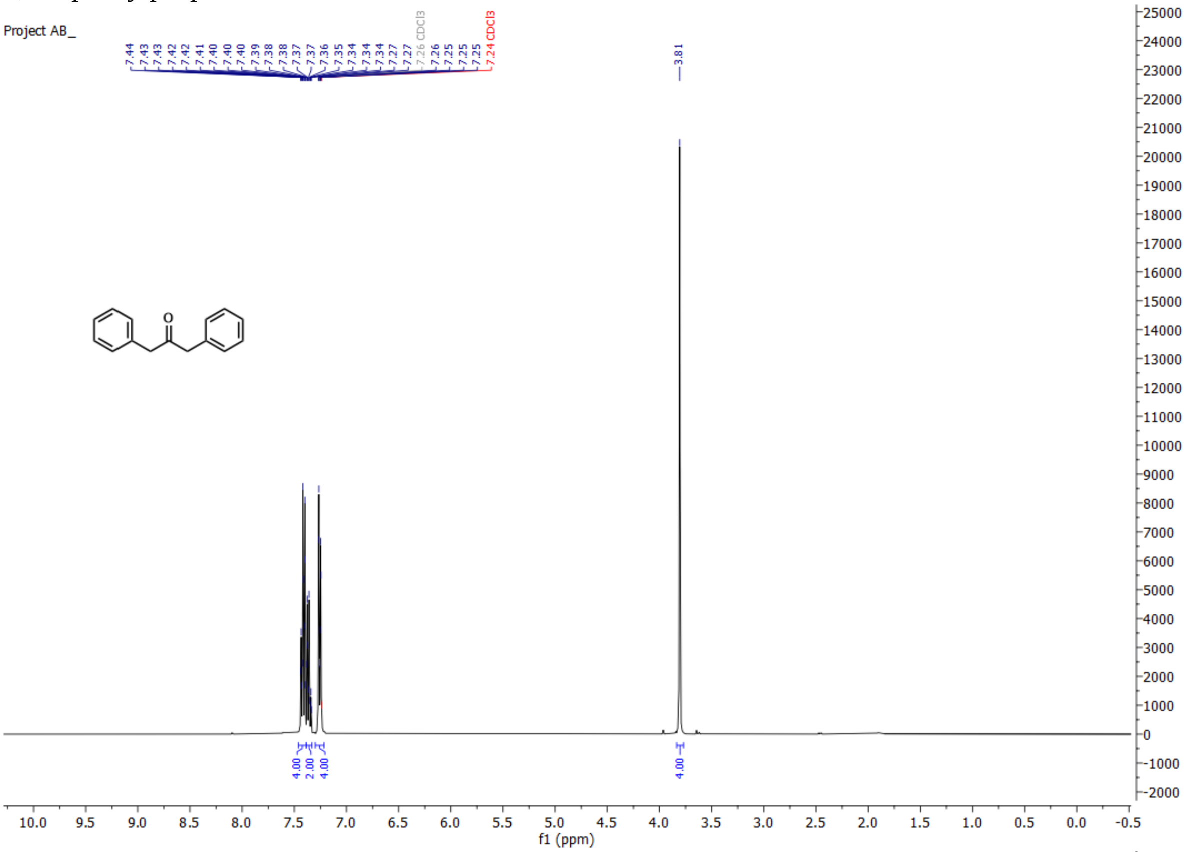

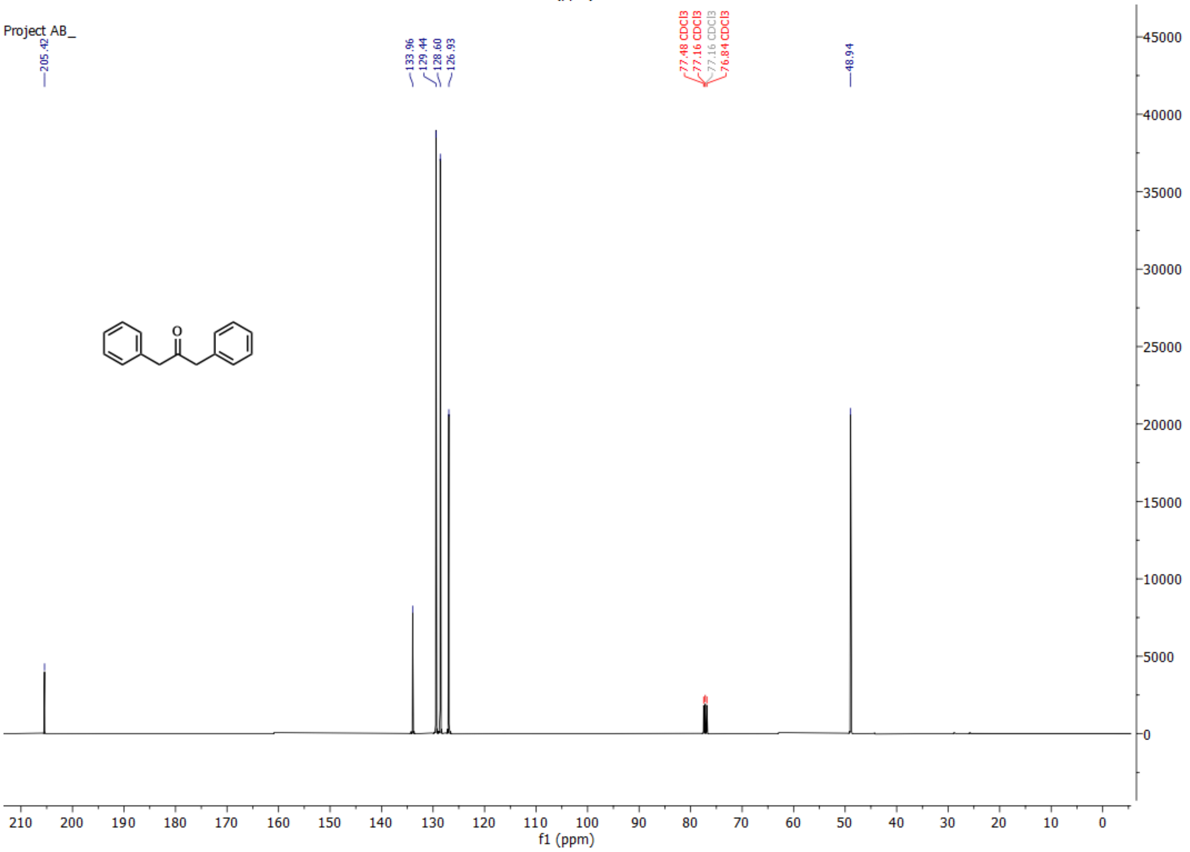

1,3-bis(4-(trifluoromethyl)phenyl)propan-2-one **8b**.

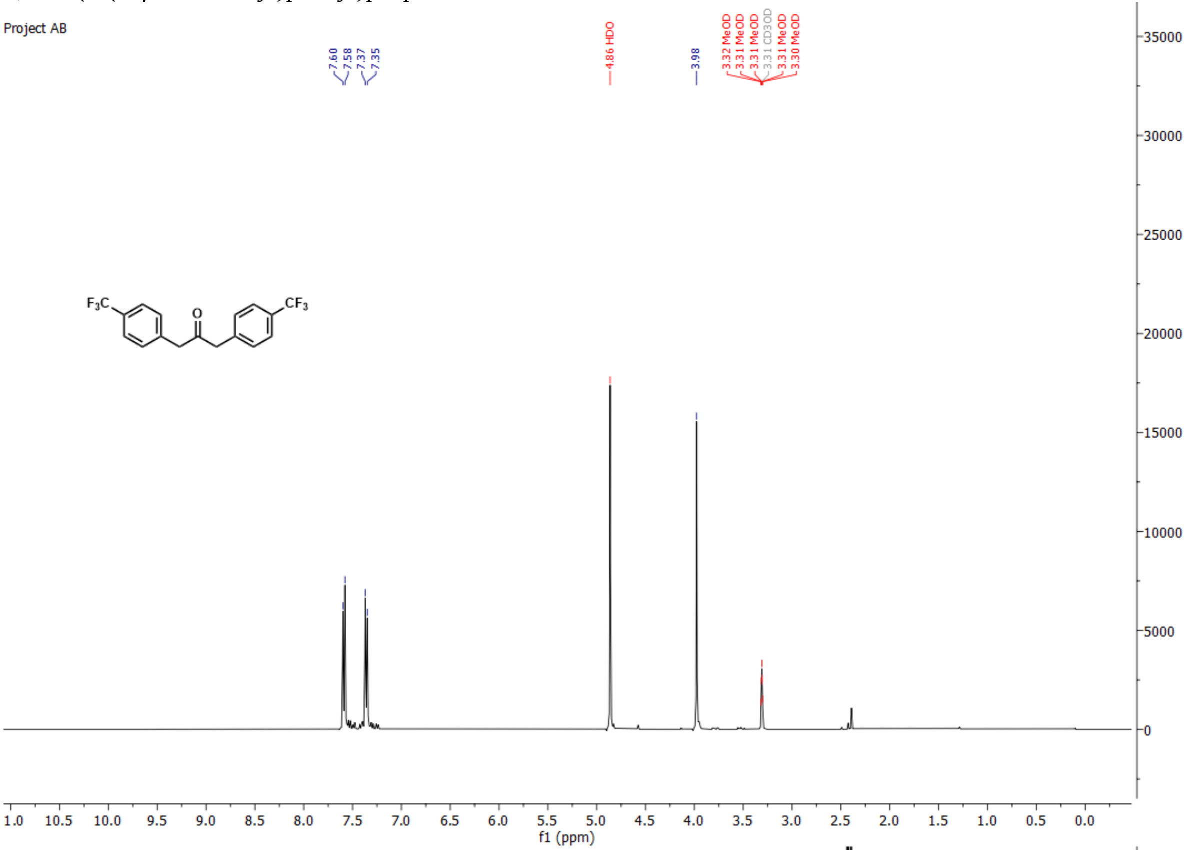

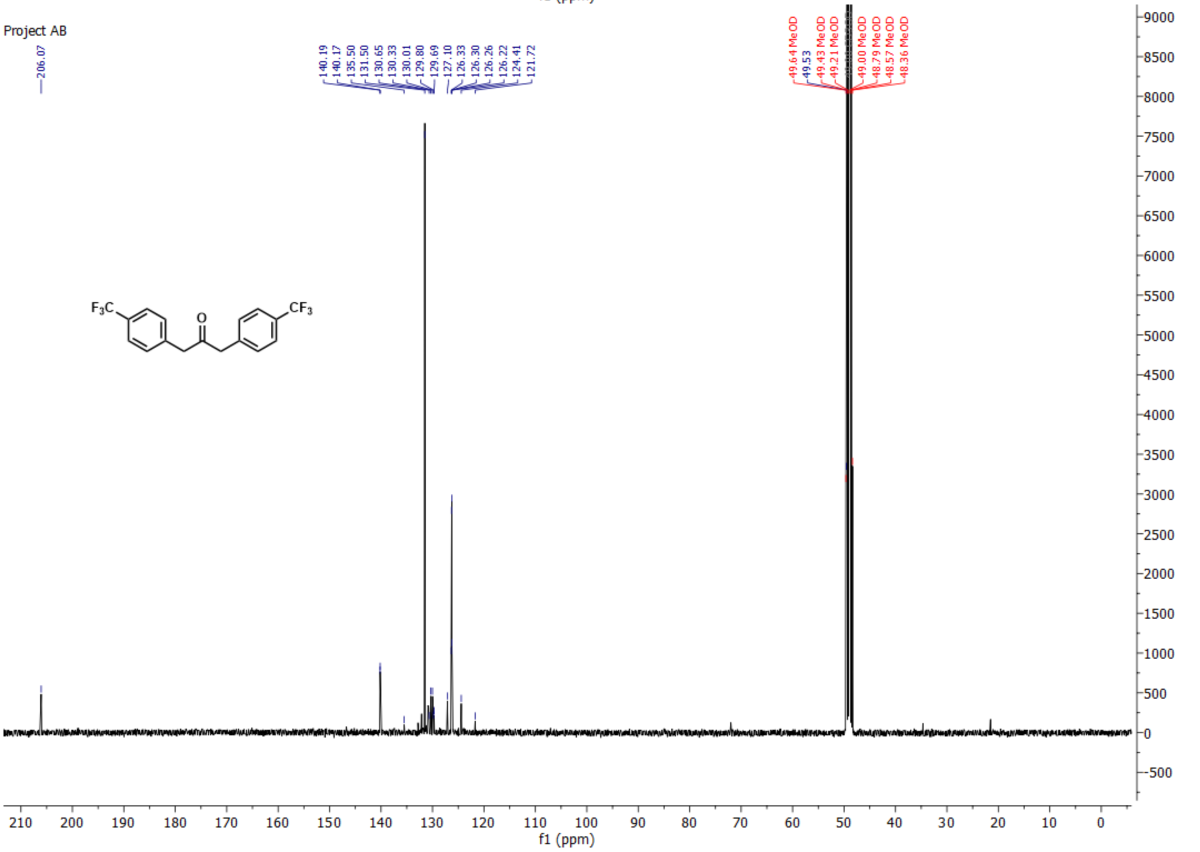

1,3-bis(4-bromo-3-chlorophenyl)propan-2-one **8c**.

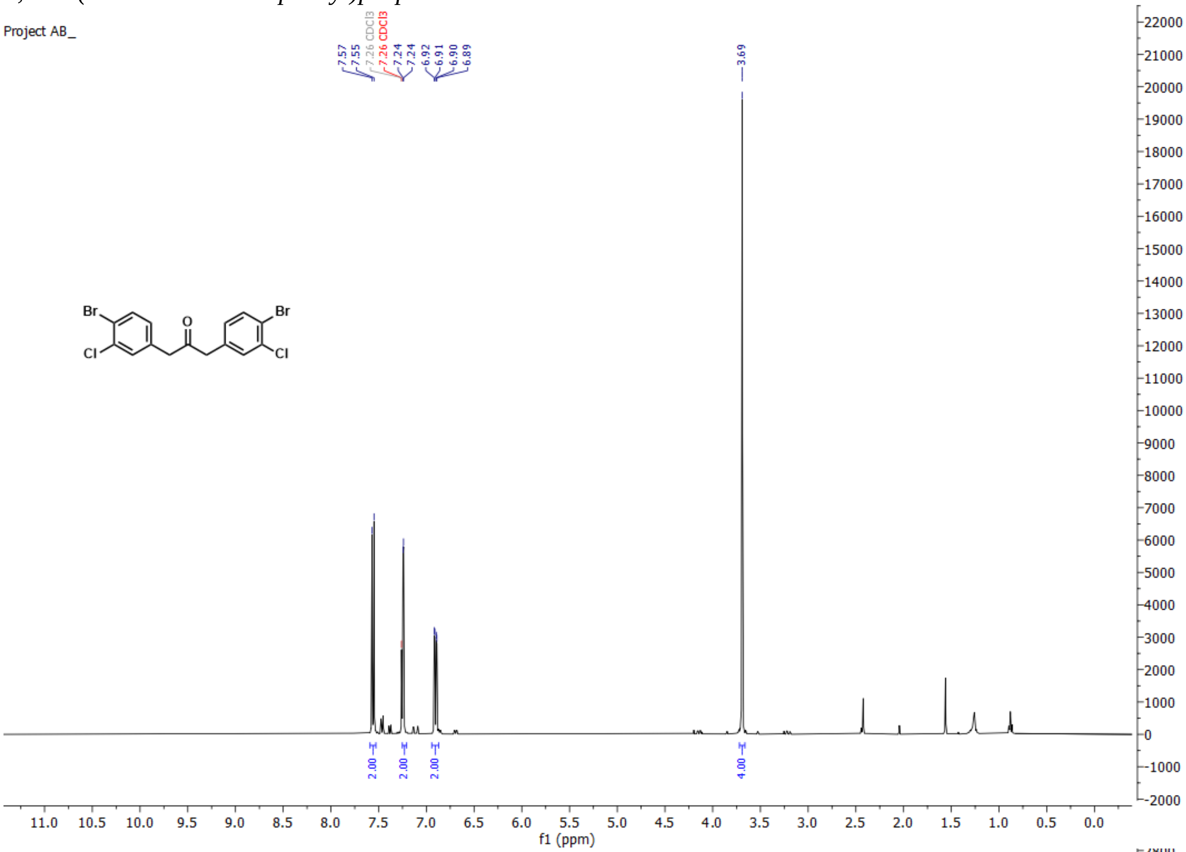

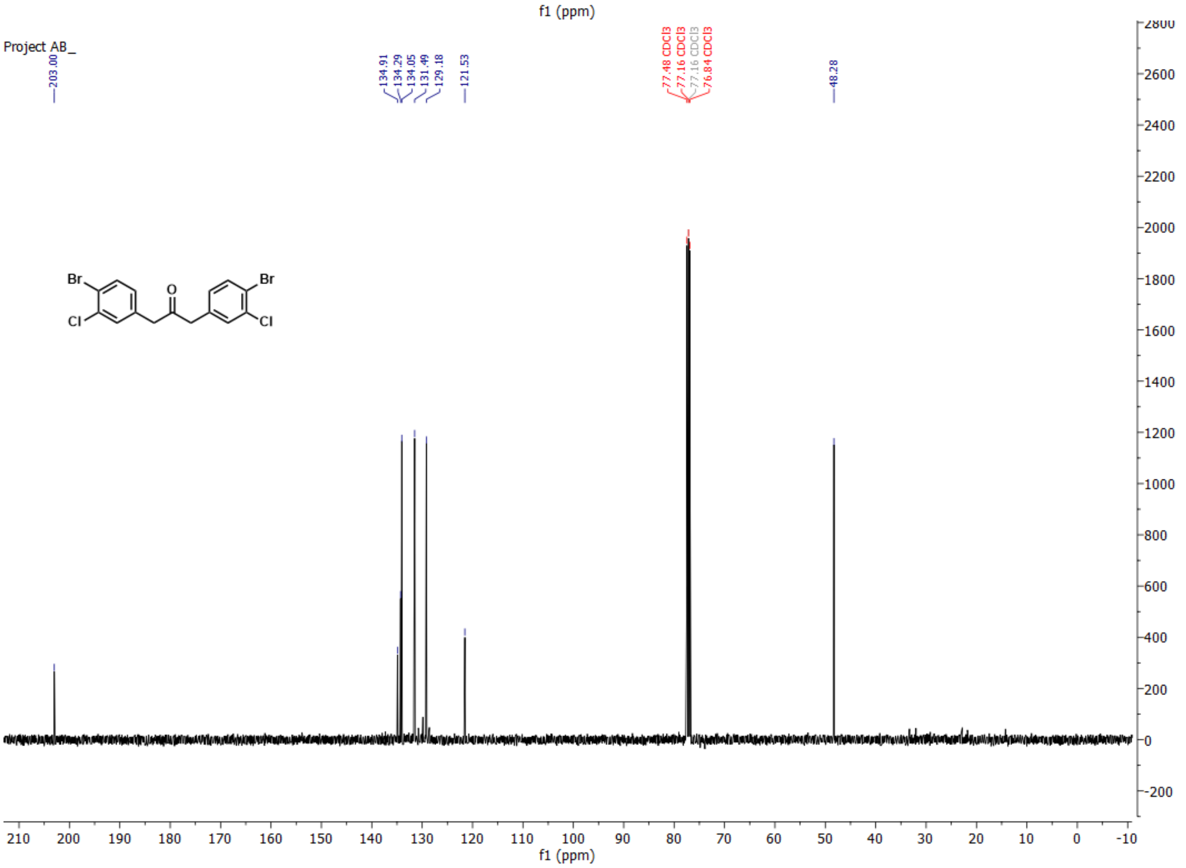

1,3-bis(3,5-dibromophenyl)propan-2-one **8d**.

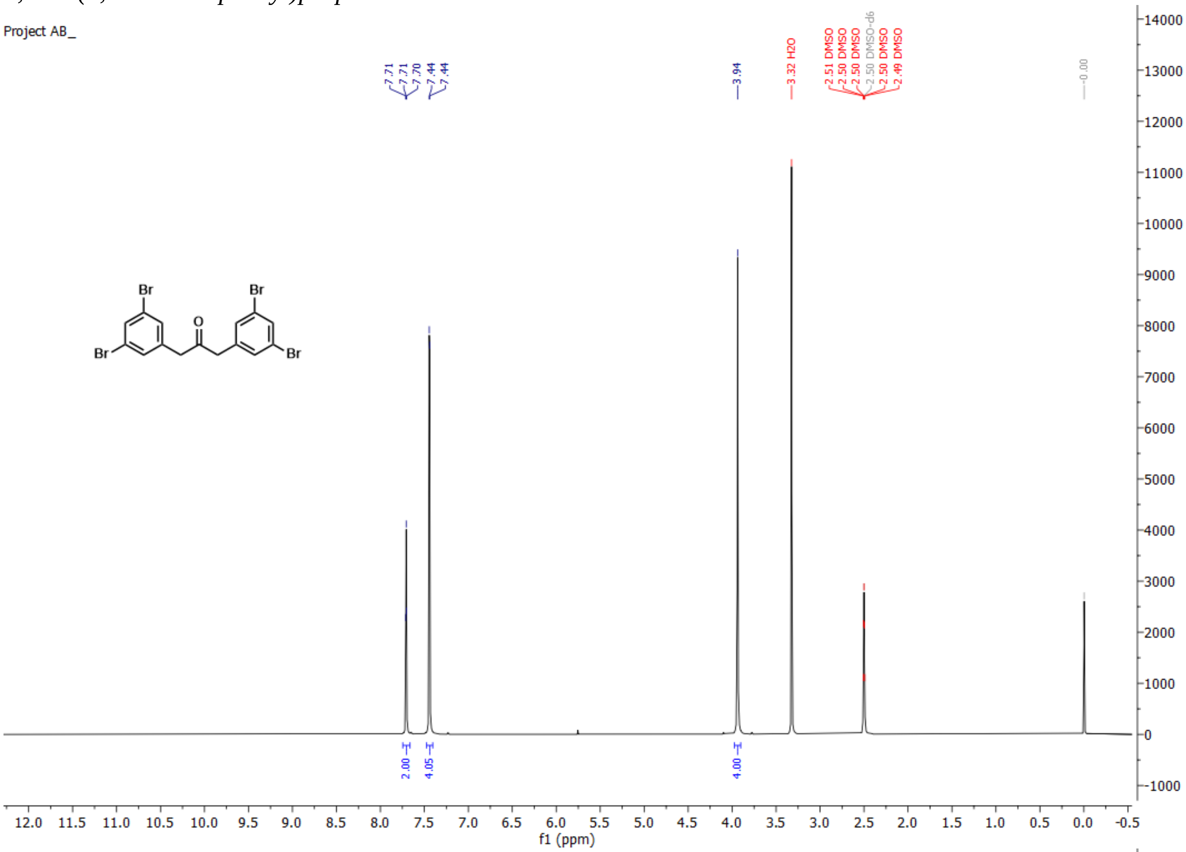

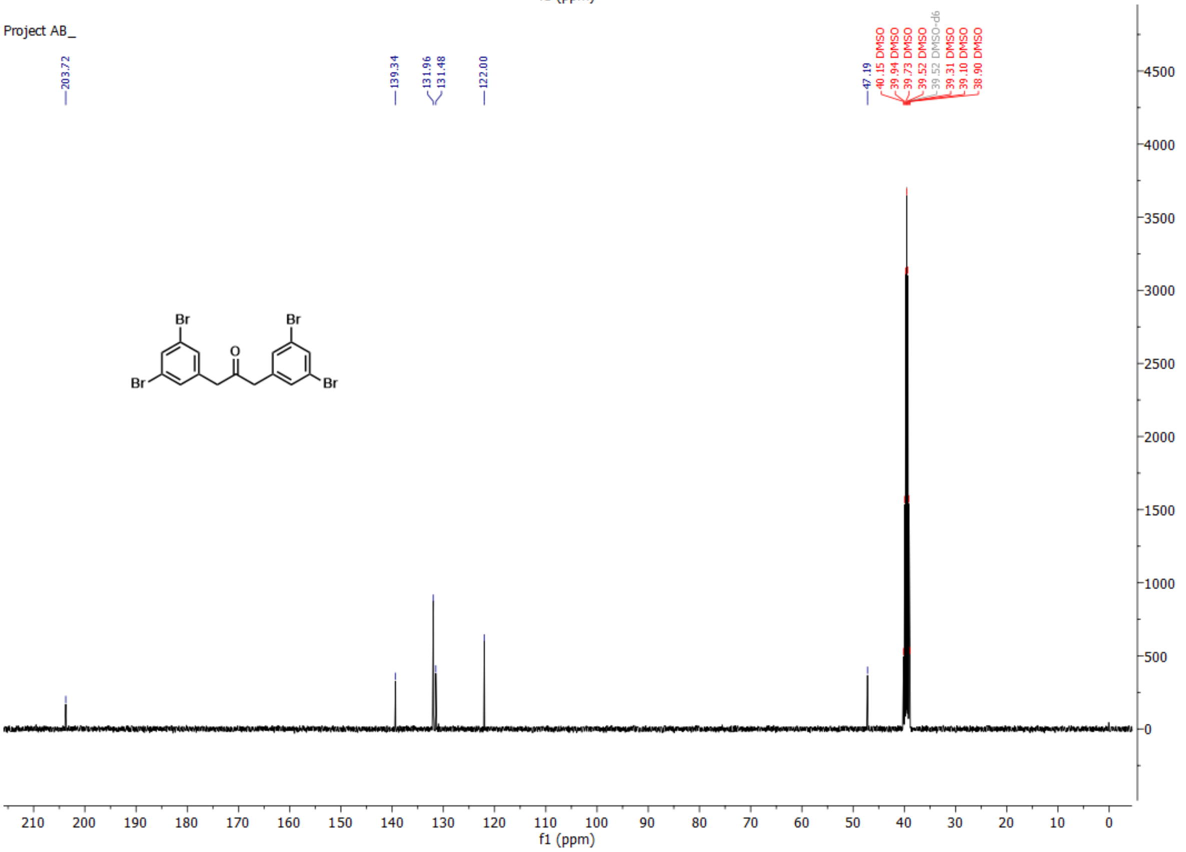

1,3-bis(4-bromonaphthalen-1-yl)propan-2-one **8e**.

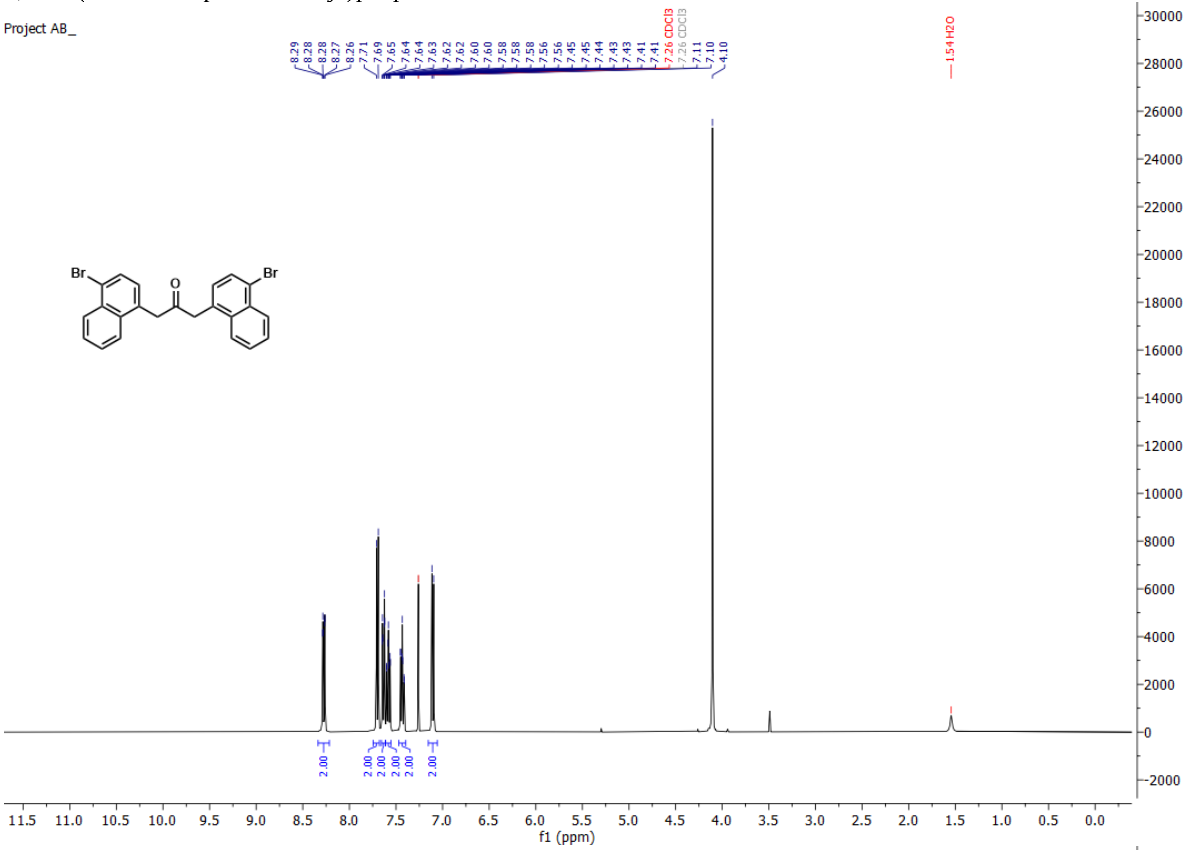

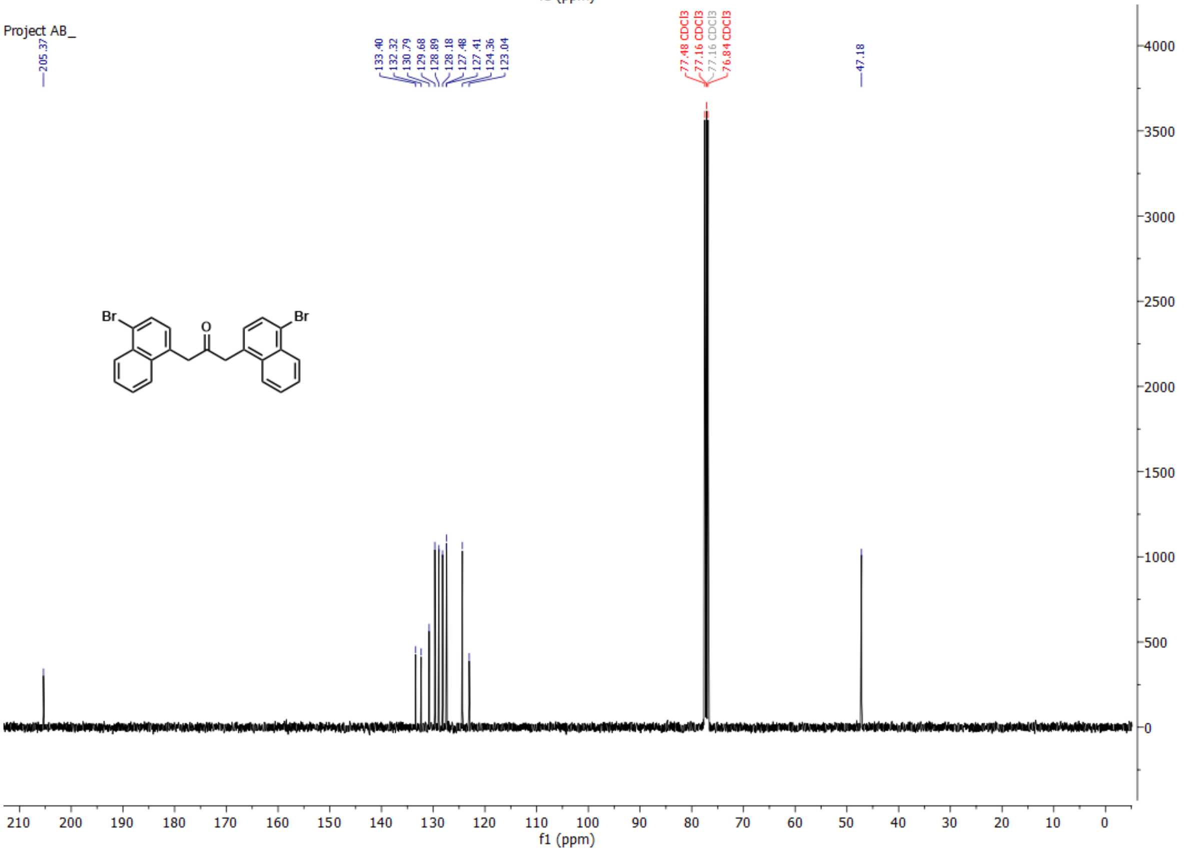

1,3-bis(3,5-bis(trifluoromethyl)phenyl)propan-2-one **8f**.

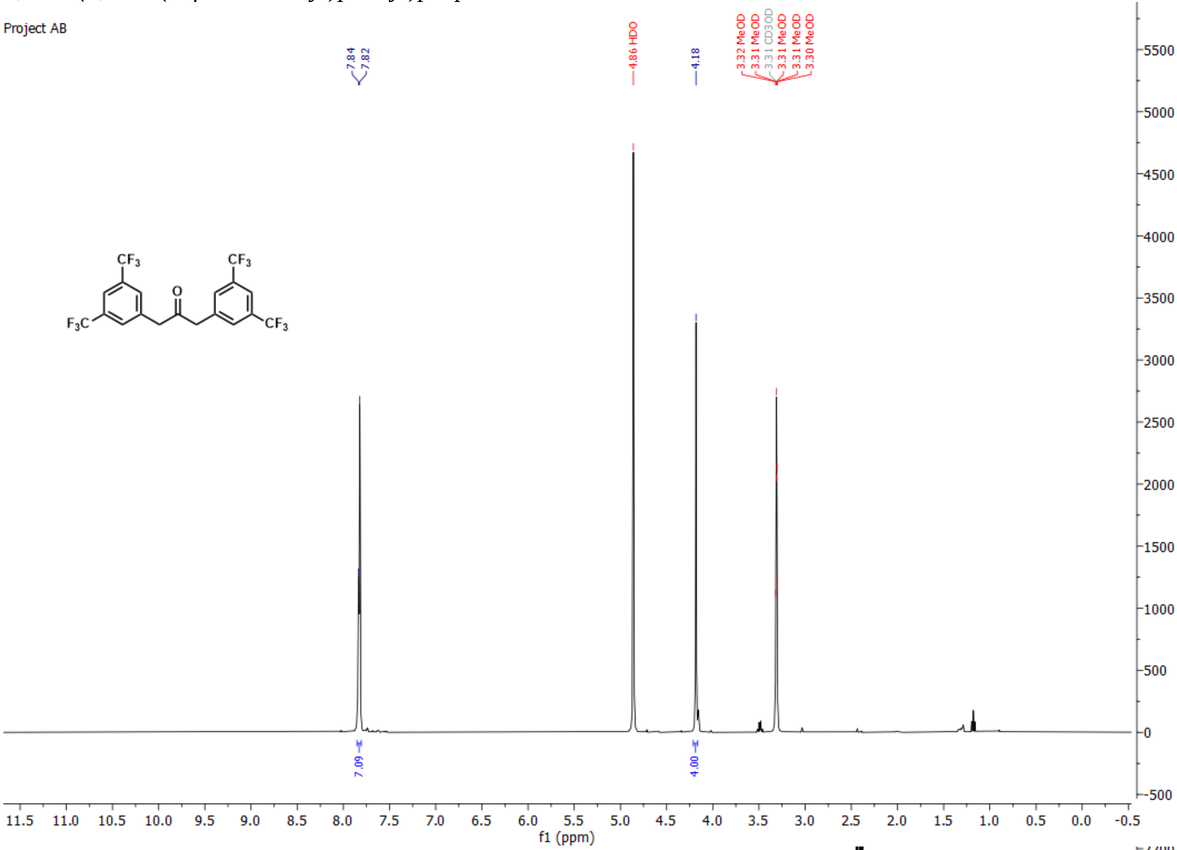

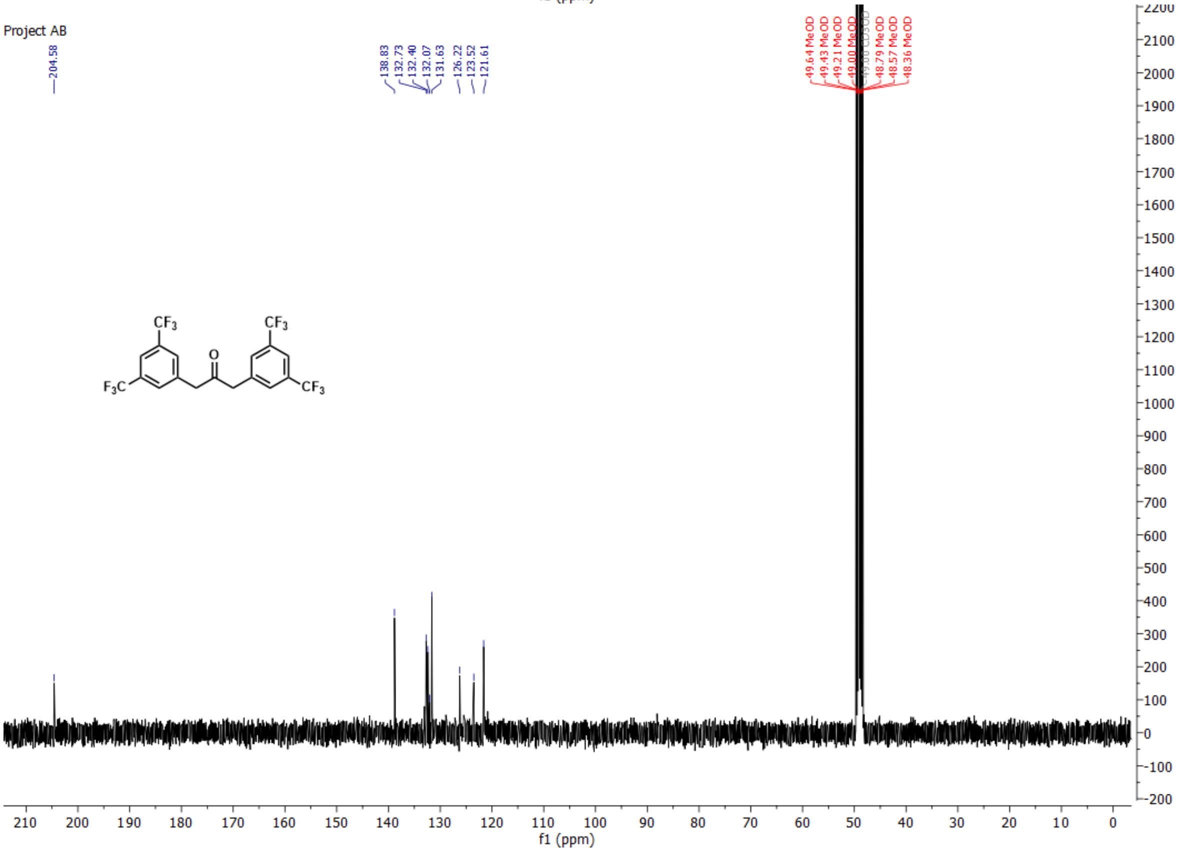

4.2 Hydantoins **9**

5,5-dibenzylimidazolidine-2,4-dione **9a**.

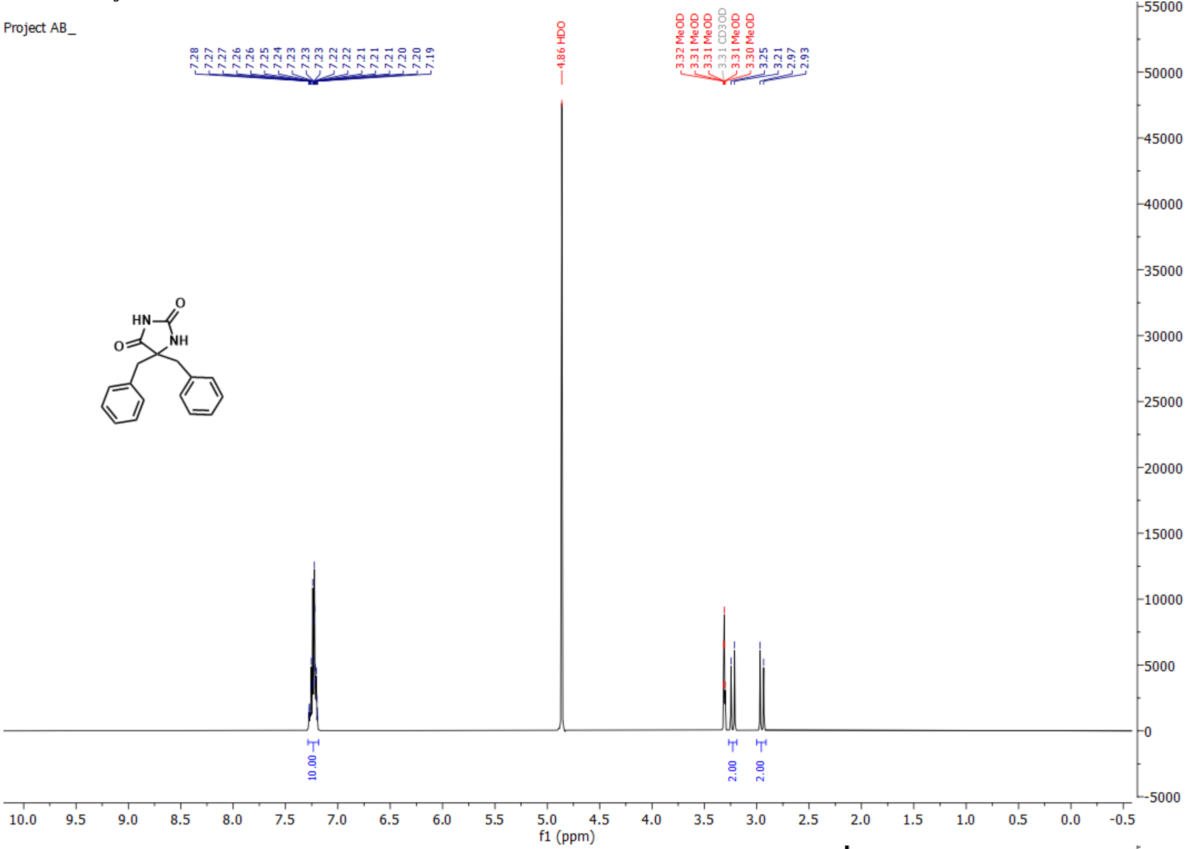

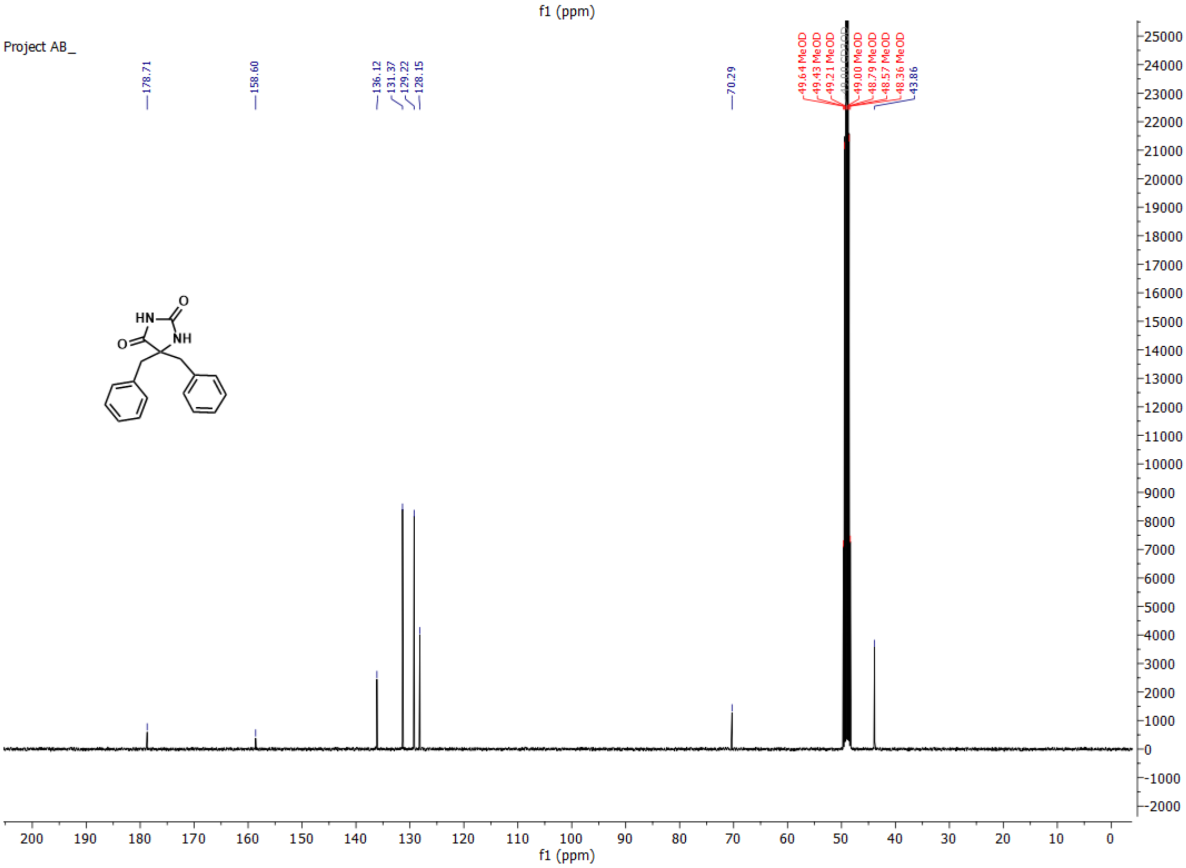

5,5-bis(4-(trifluoromethyl)benzyl)imidazolidine-2,4-dione **9b**.

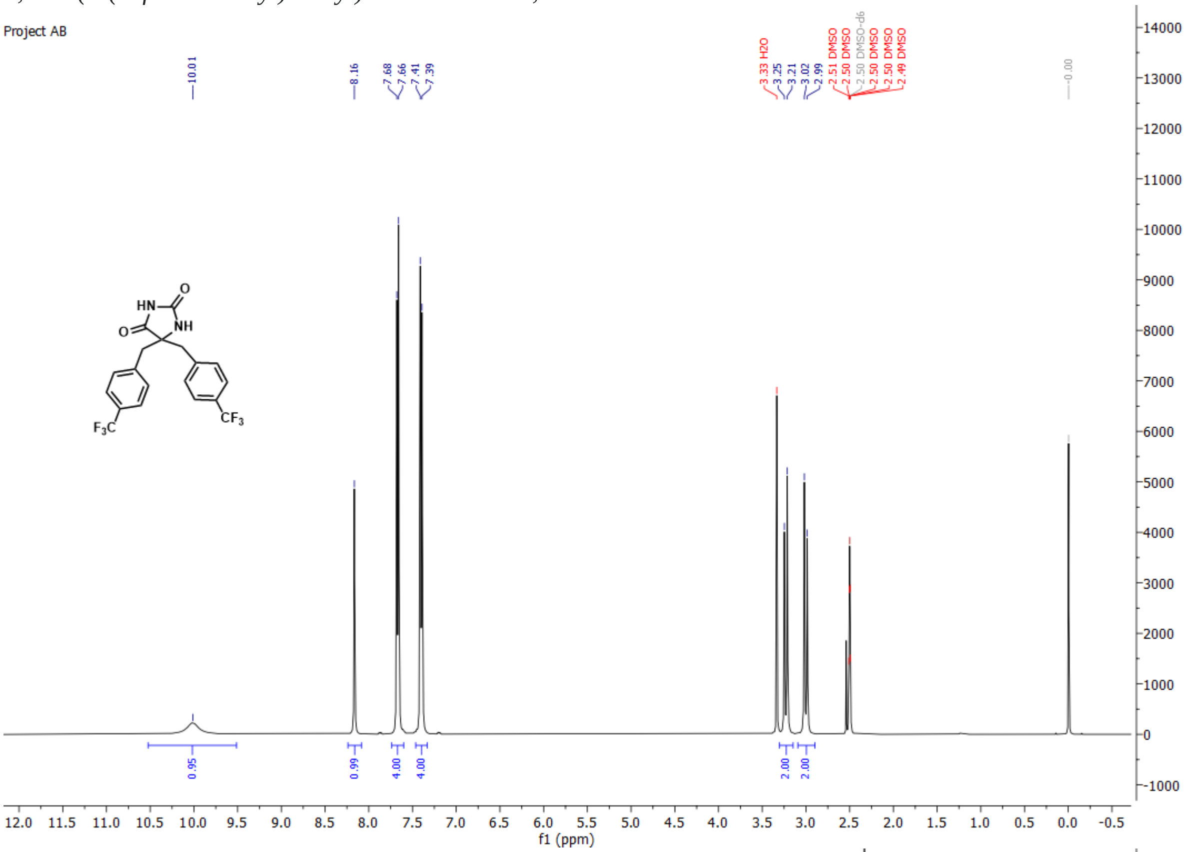

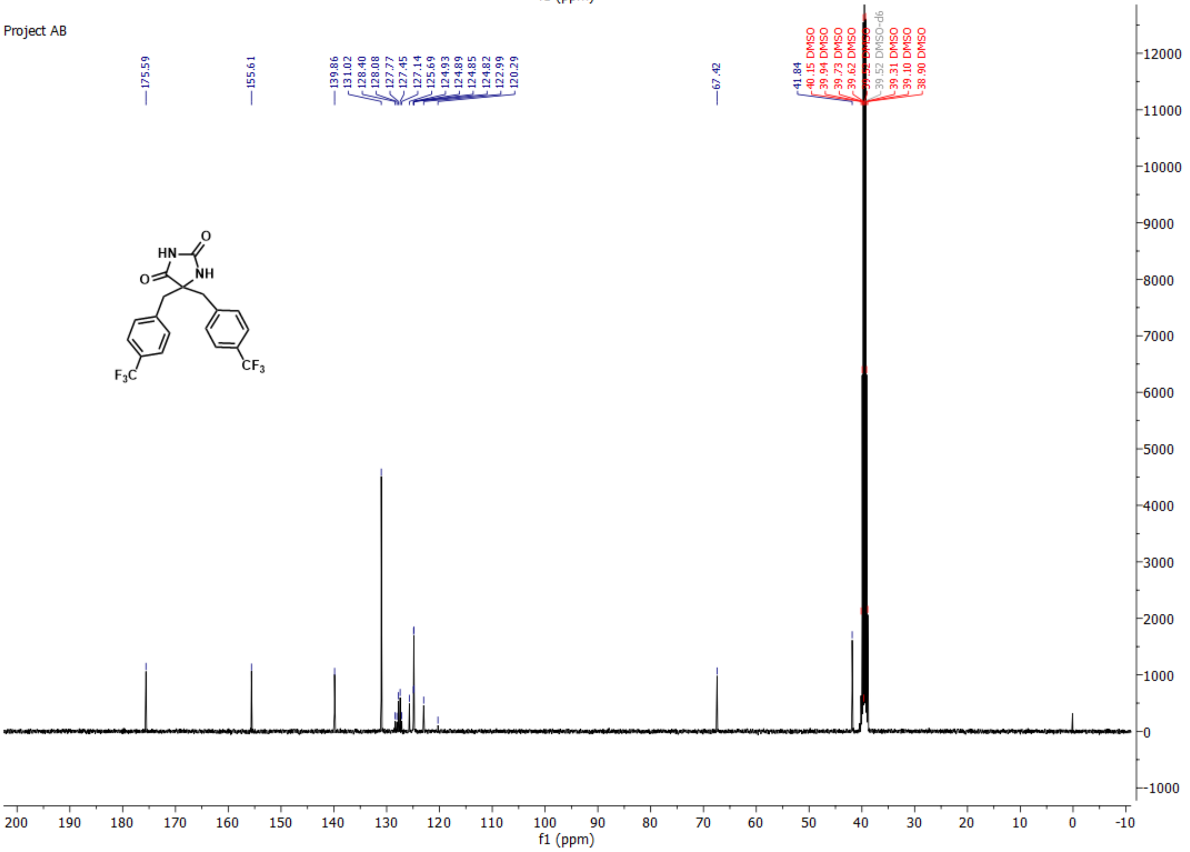

5,5-bis(4-bromo-3-chlorobenzyl)imidazolidine-2,4-dione **9c**.

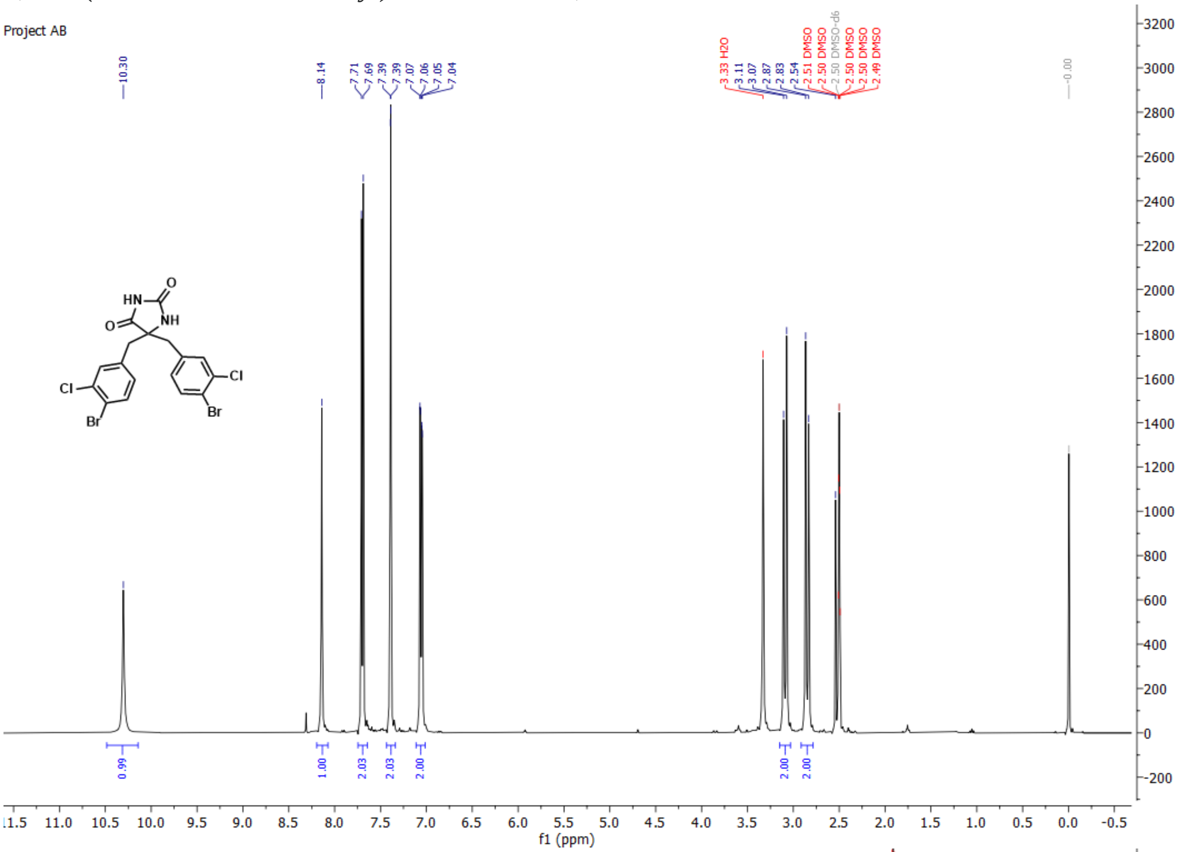

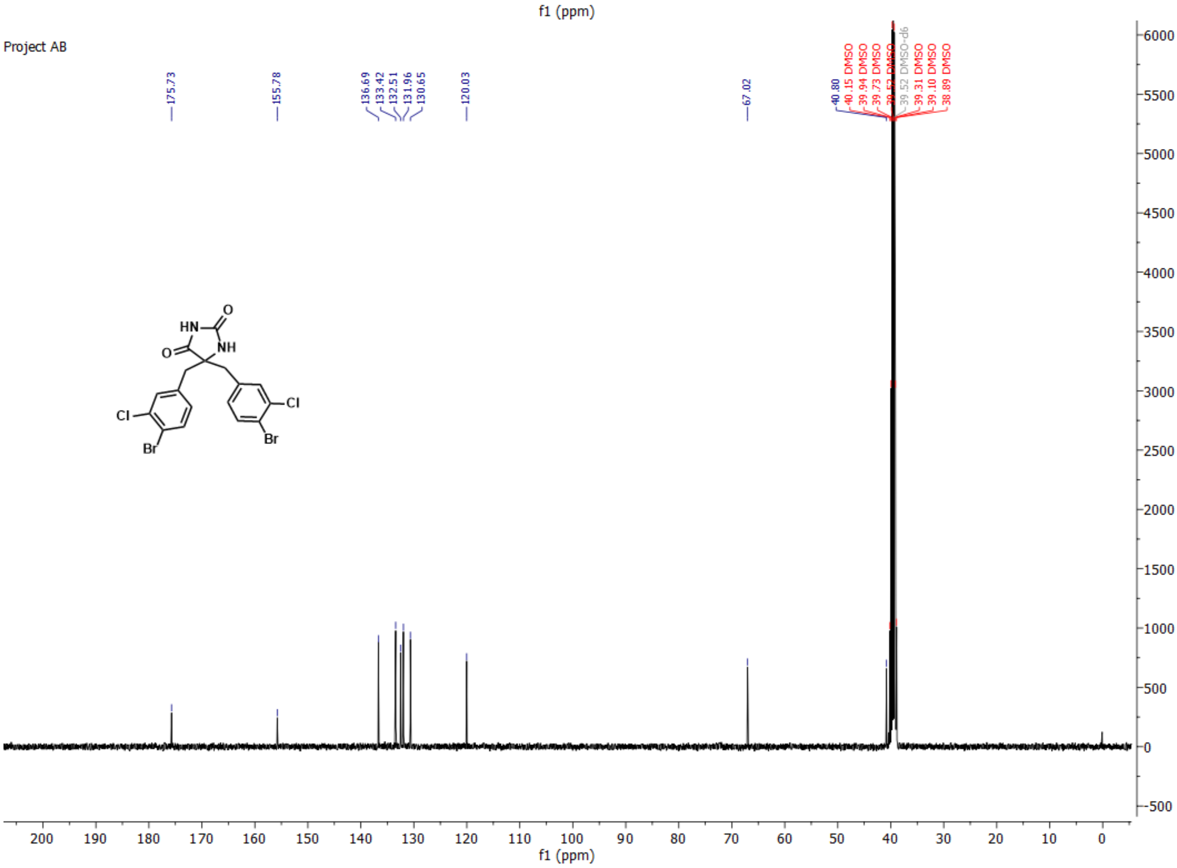

5,5-bis(3,5-dibromobenzyl)imidazolidine-2,4-dione **9d**.

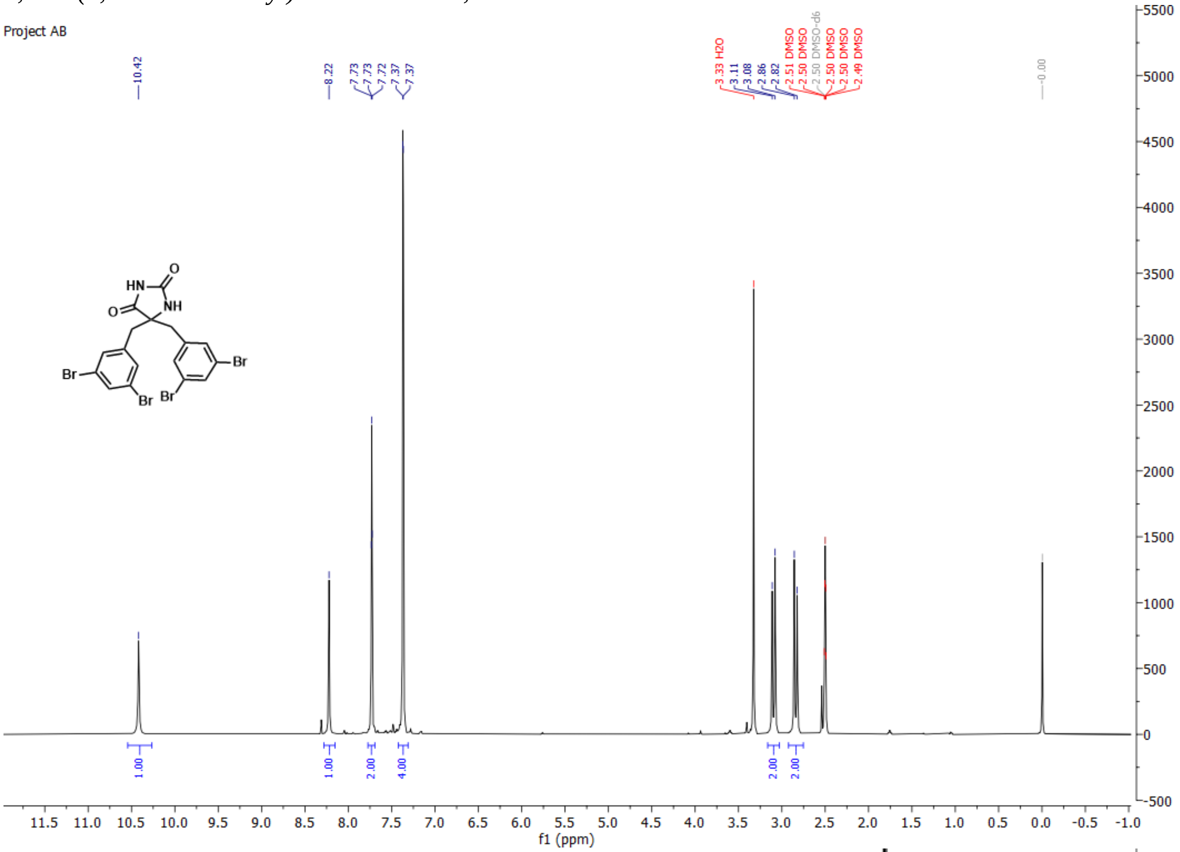

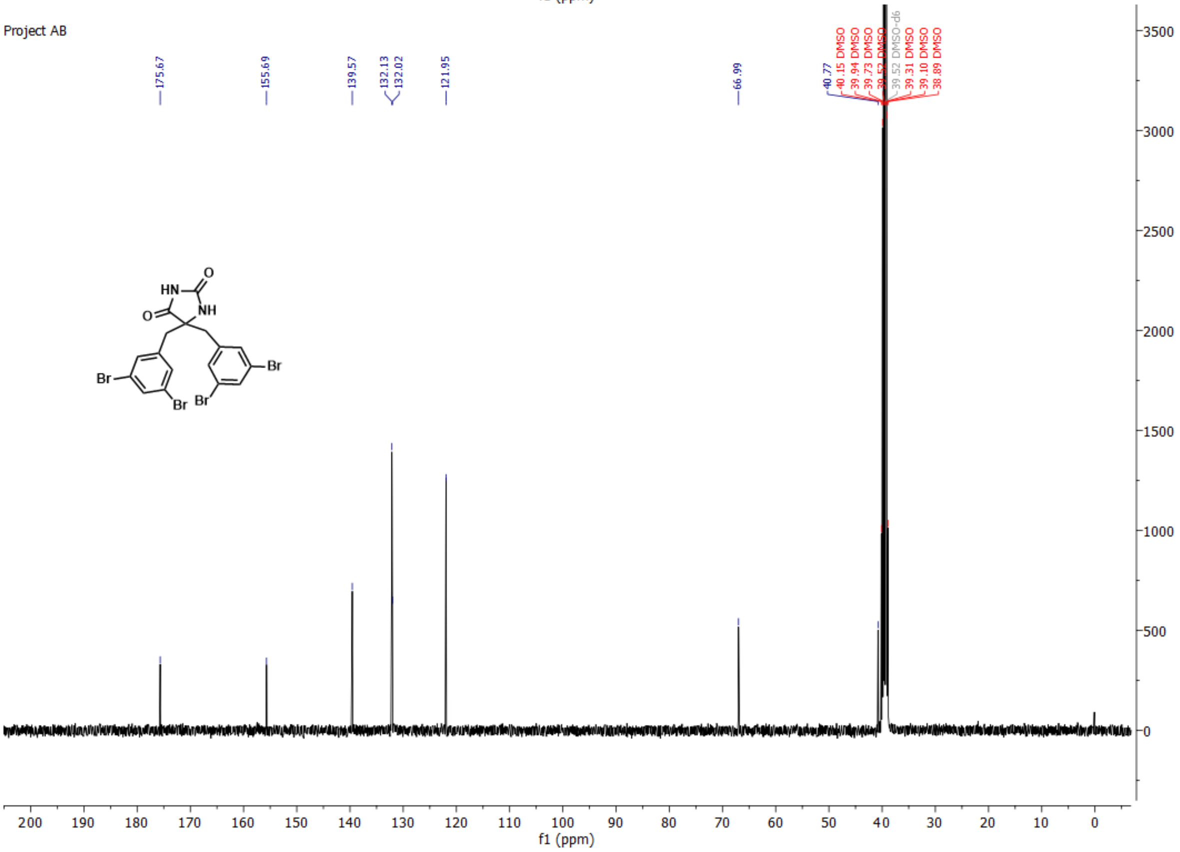

5,5-bis((4-bromonaphthalen-1-yl)methyl)imidazolidine-2,4-dione **9e**.

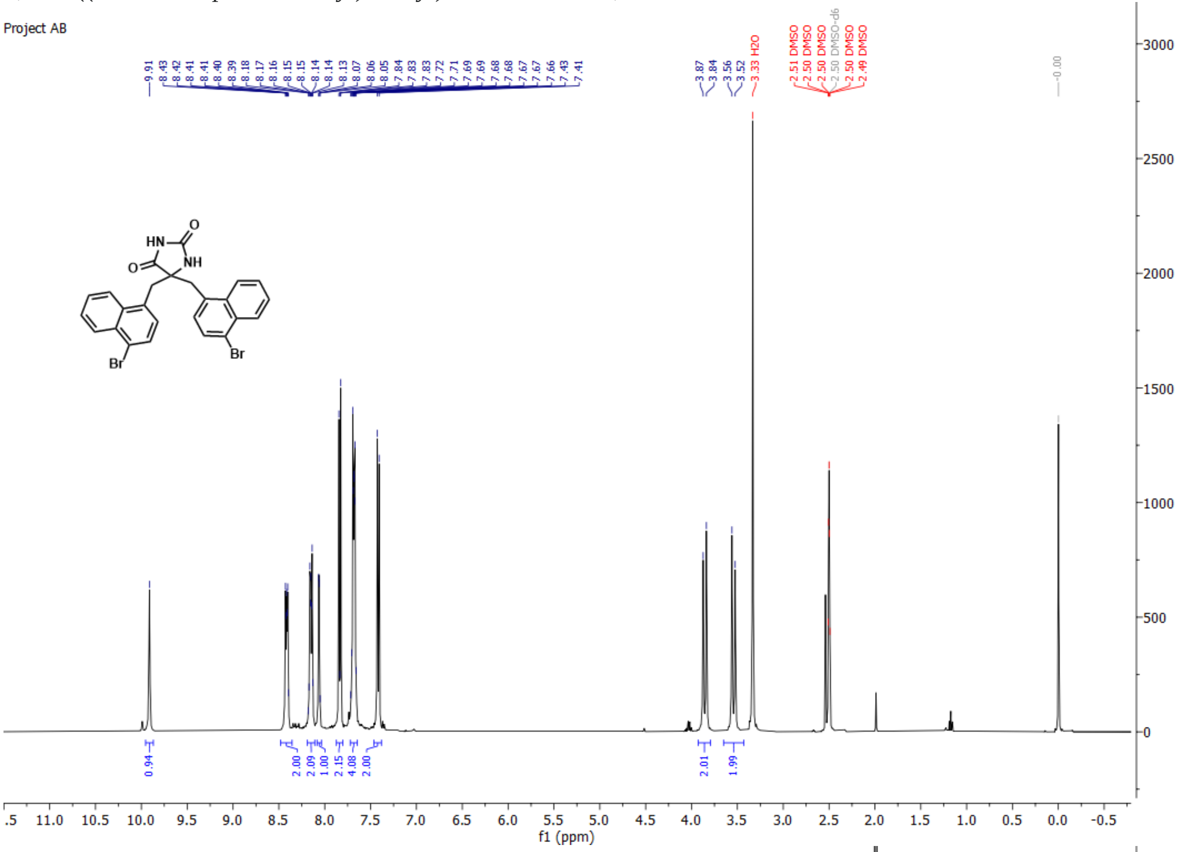

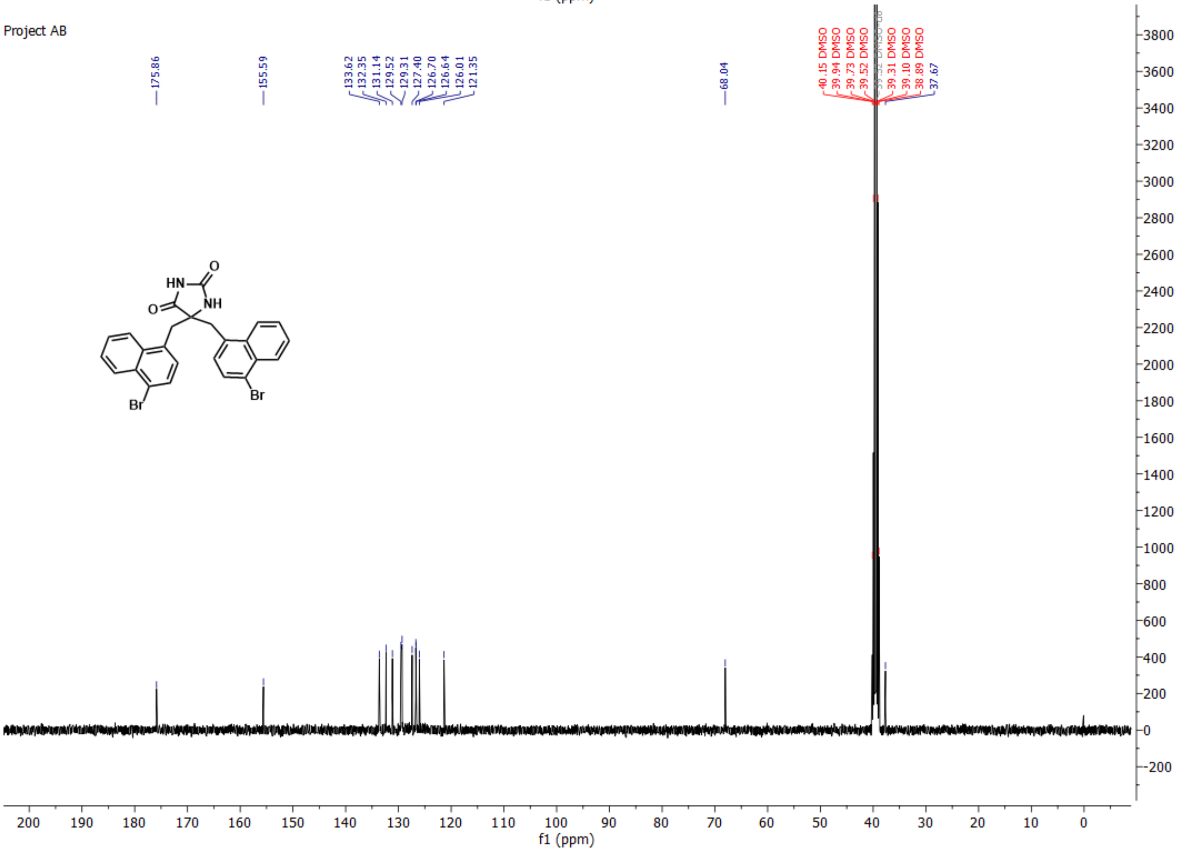

5,5-bis(3,5-bis(trifluoromethyl)benzyl)imidazolidine-2,4-dione **9f**.

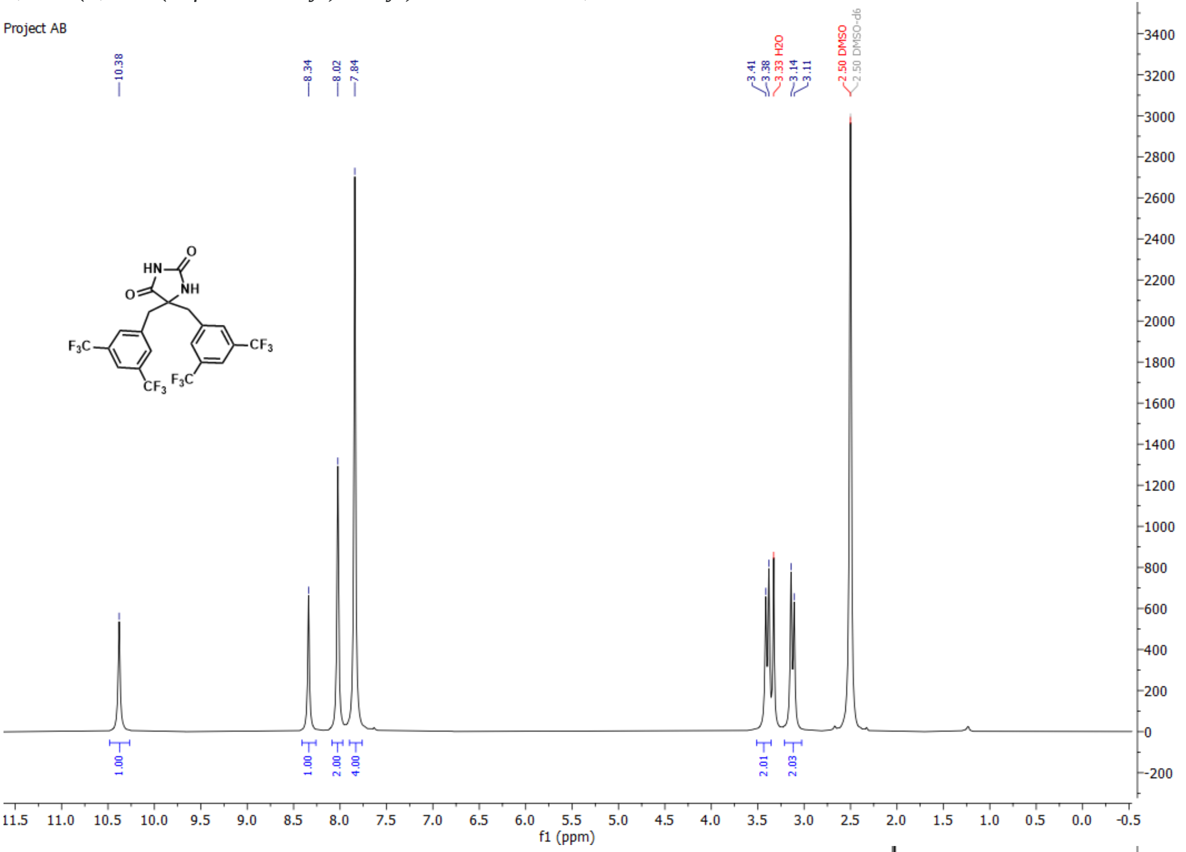

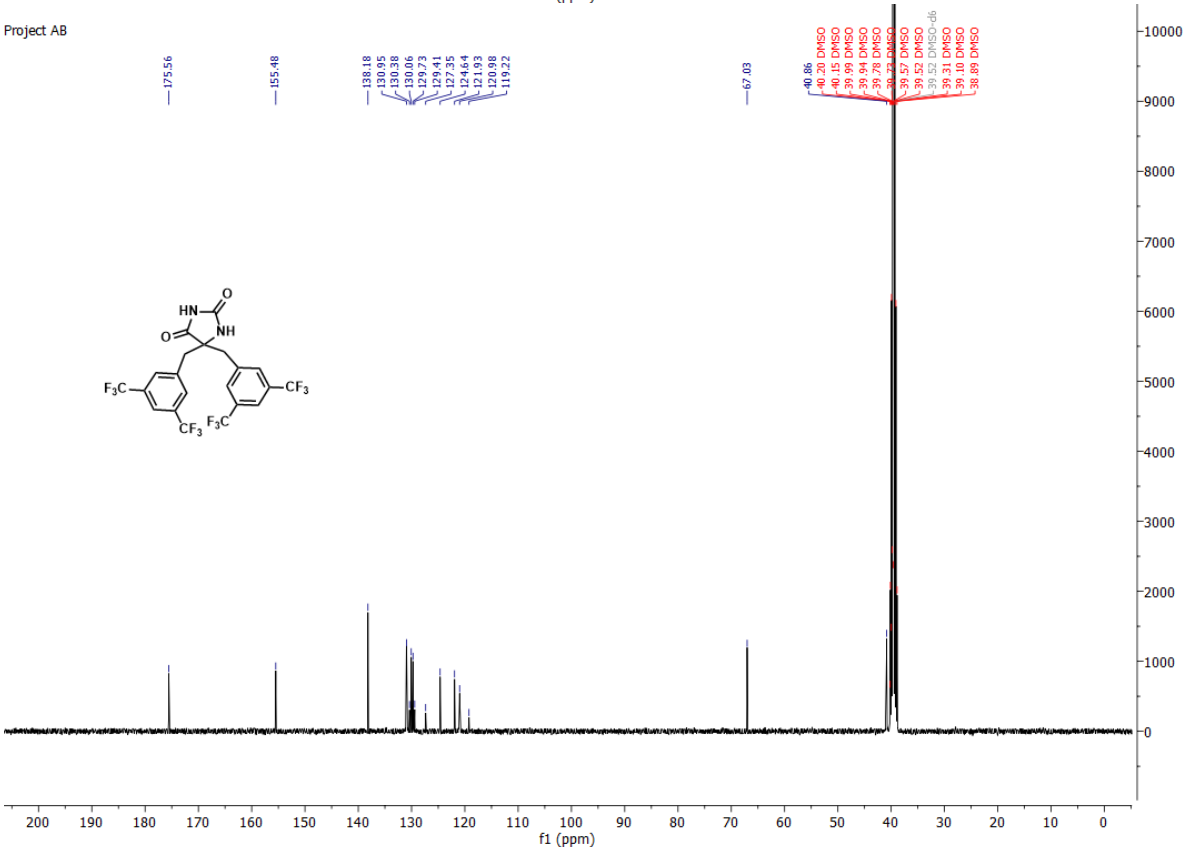

4.3 *N,N'*-dialkylated hydantoins 2A

1,3-bis(3-aminopropyl)-5,5-dibenzylimidazolidine-2,4-dione **2aA**.

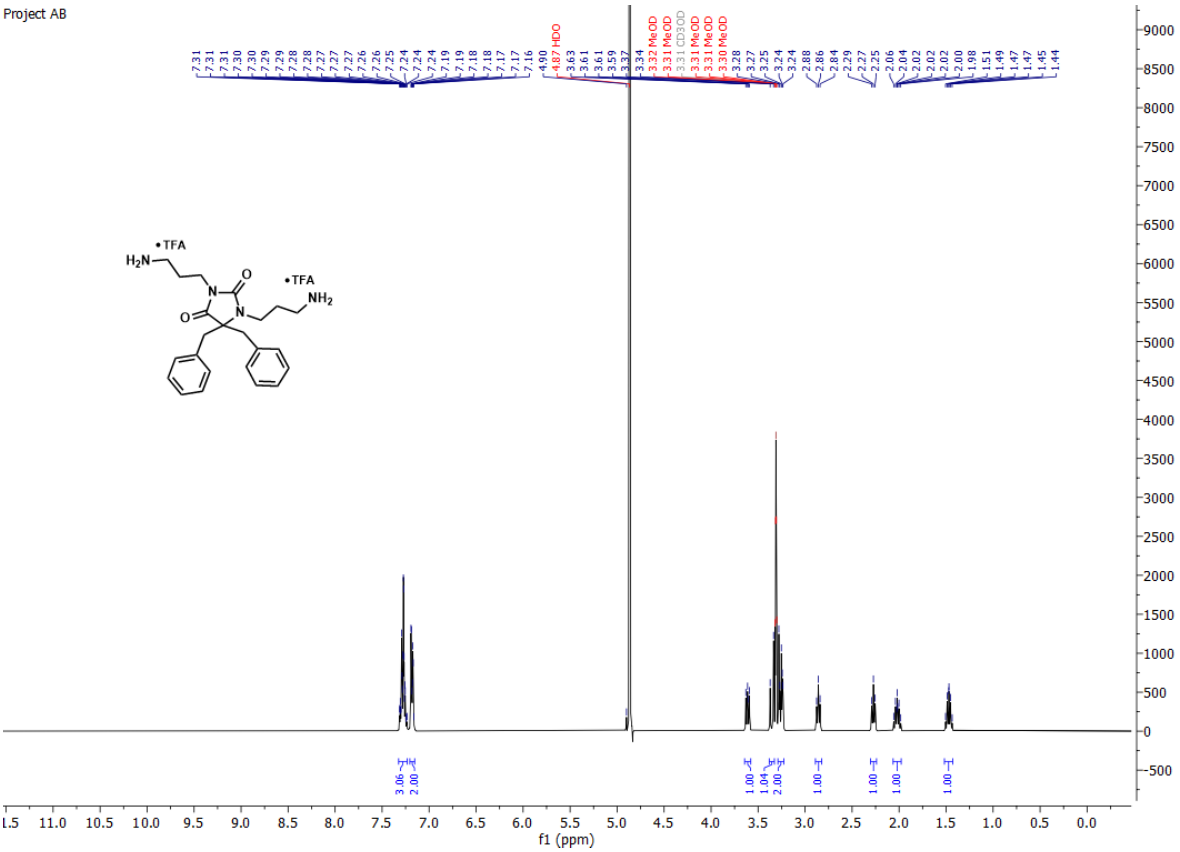

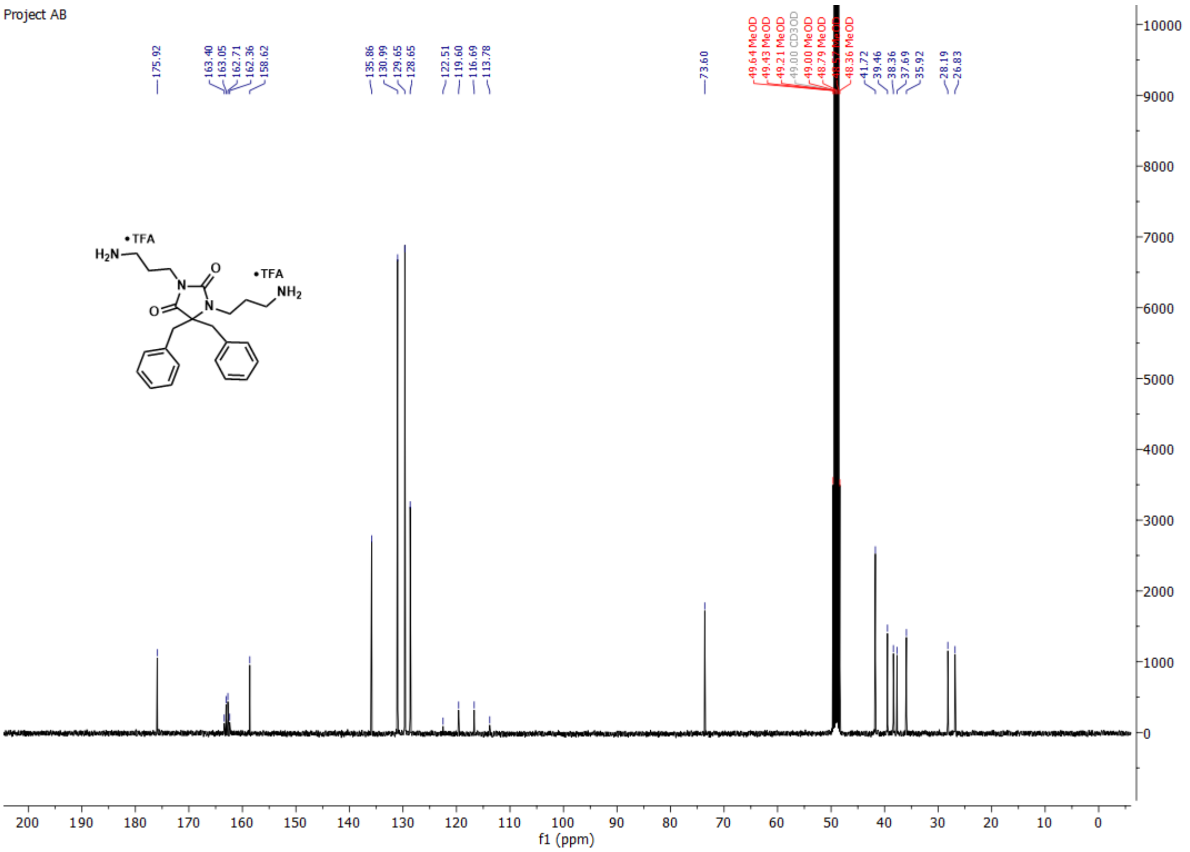

1,3-bis(3-aminopropyl)-5,5-bis(4-(trifluoromethyl)benzyl)imidazolidine-2,4-dione **2bA**.

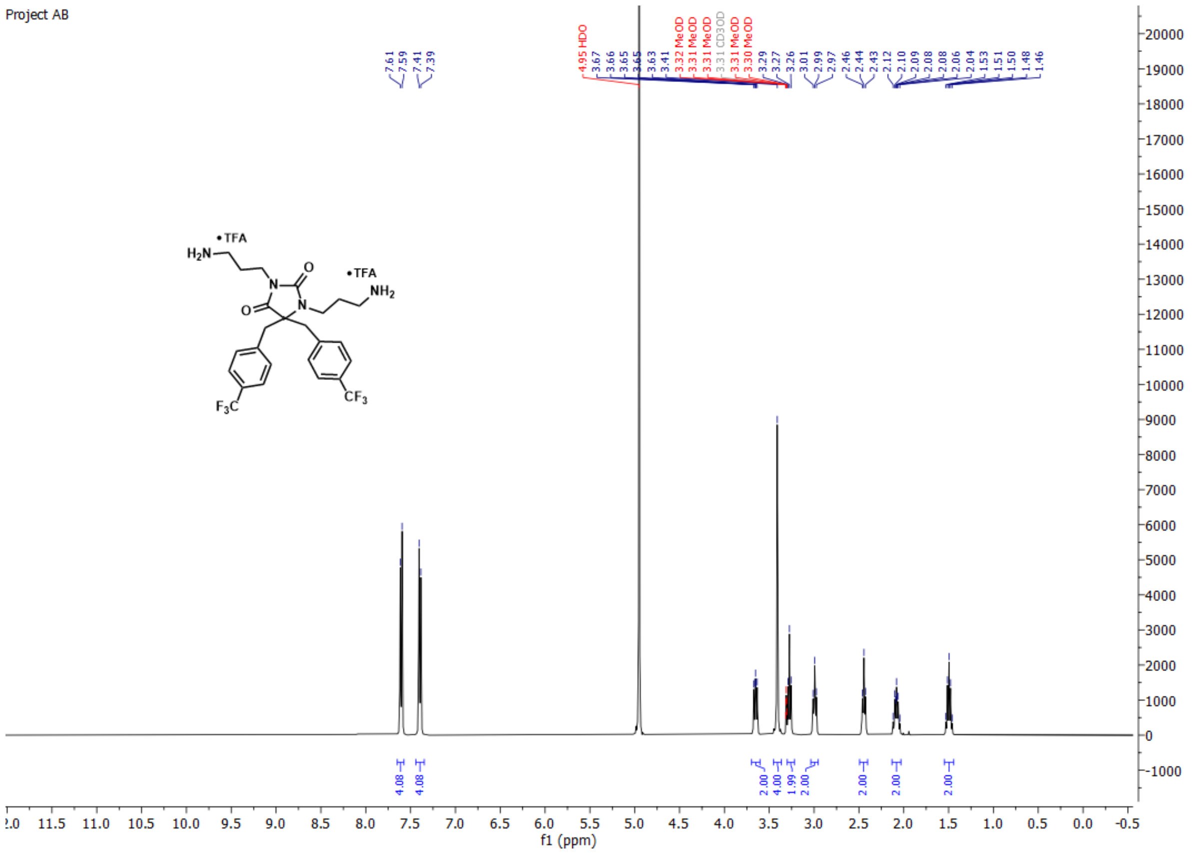

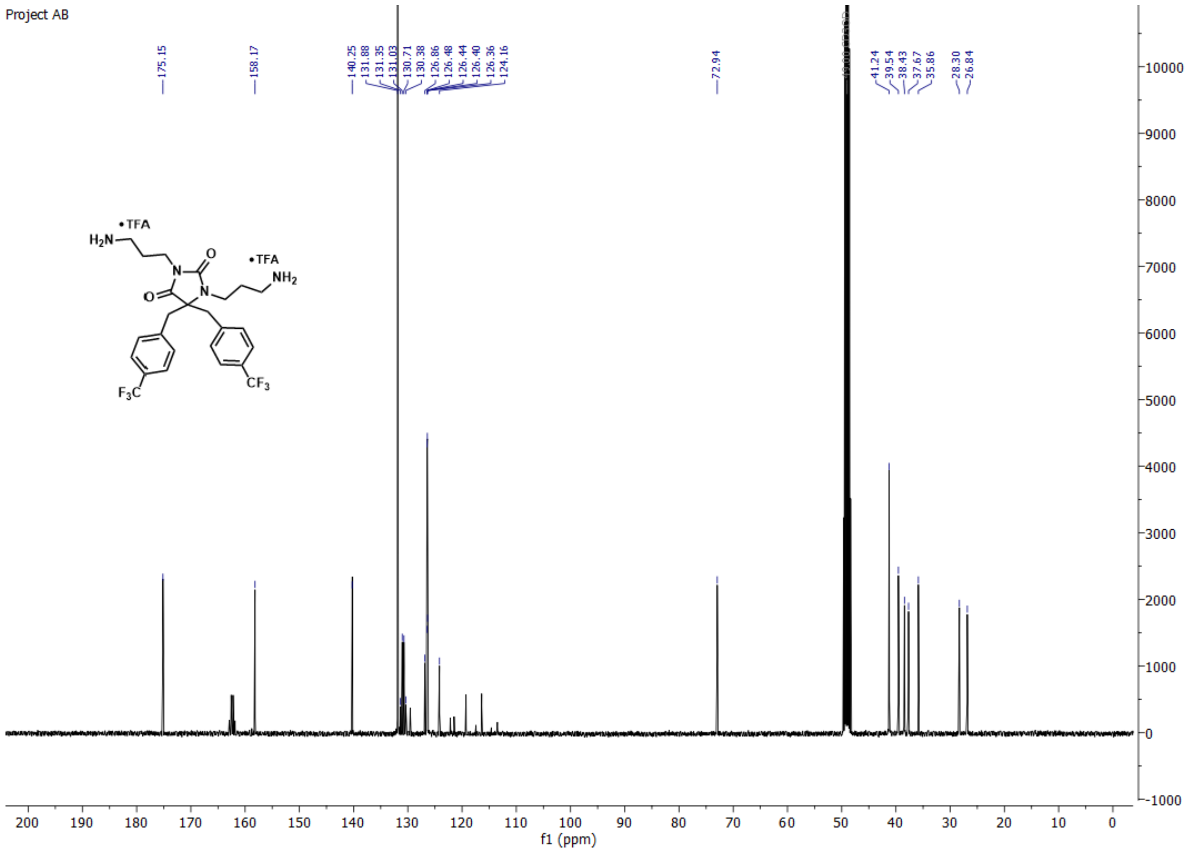

1,3-bis(3-aminopropyl)-5,5-bis(4-bromo-3-chlorobenzyl)imidazolidine-2,4-dione **2cA**.

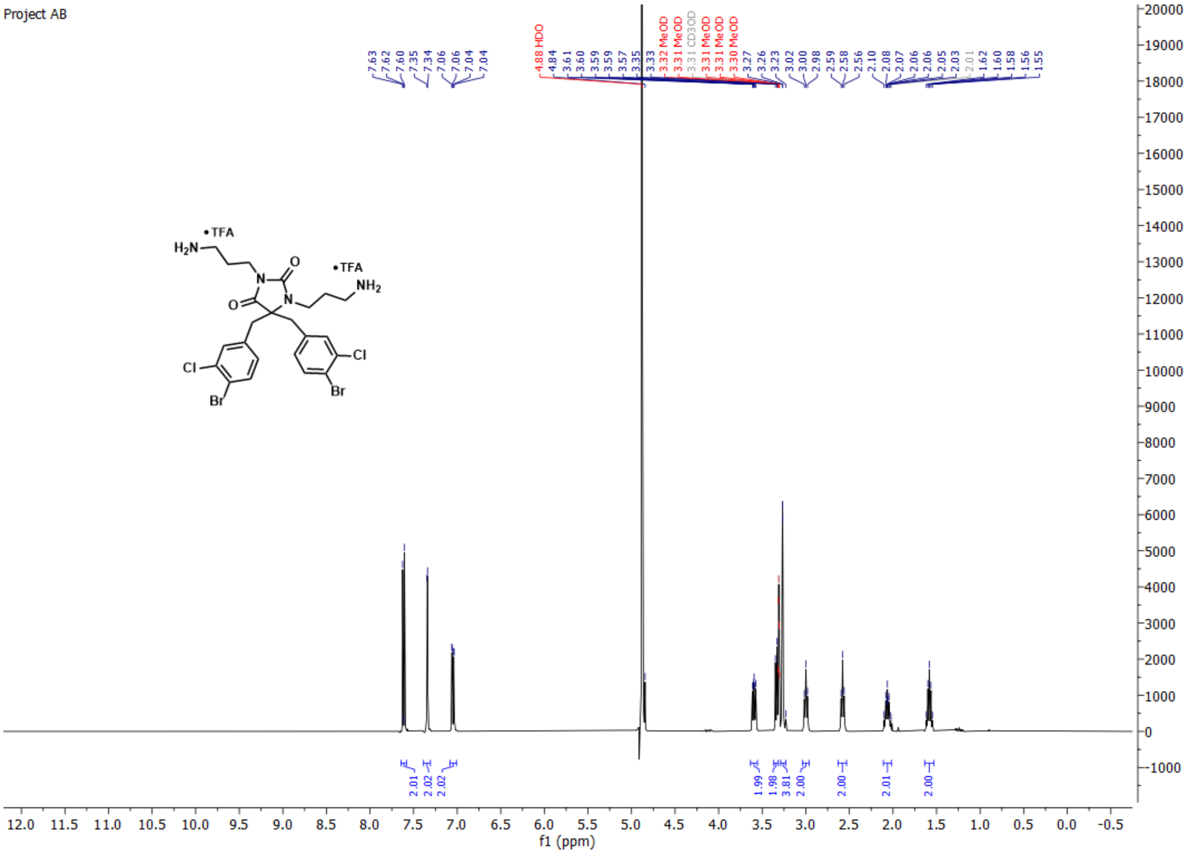

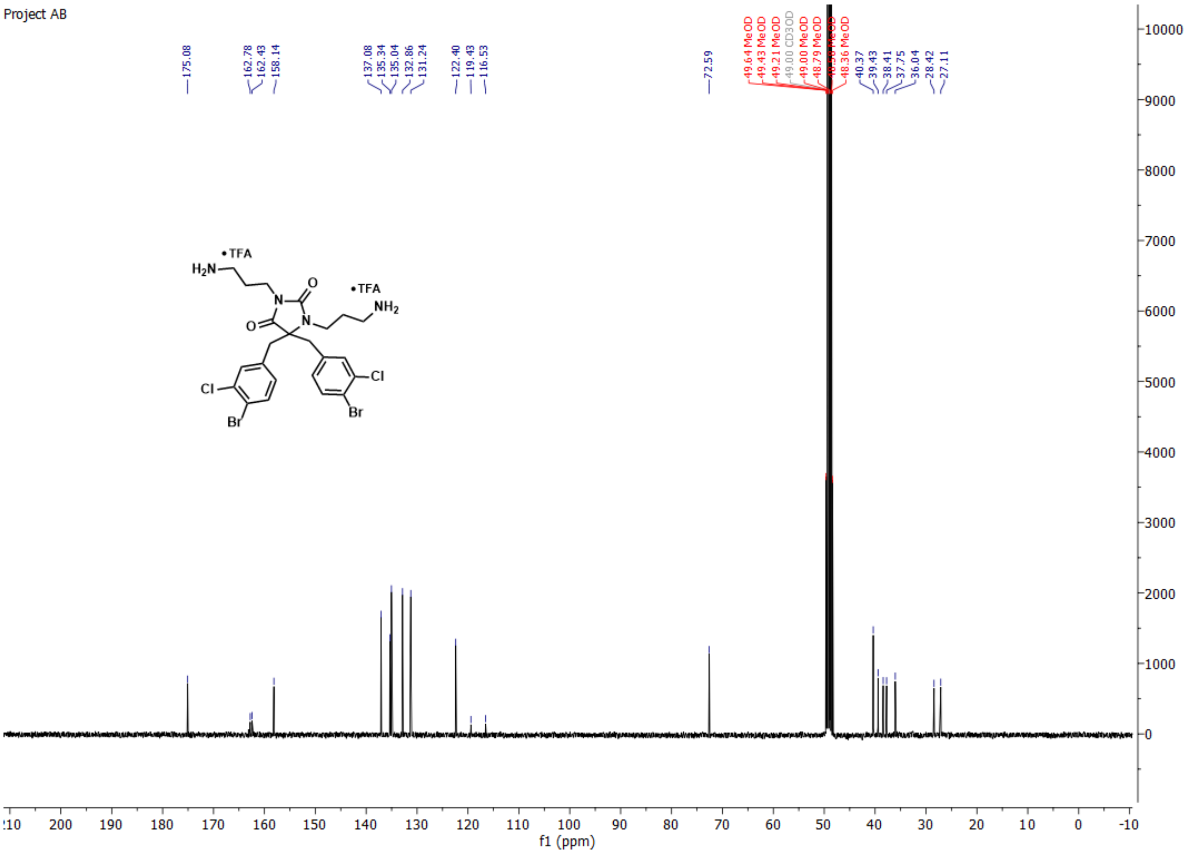

1,3-bis(3-aminopropyl)-5,5-bis(3,5-dibromobenzyl)imidazolidine-2,4-dione **2dA**.

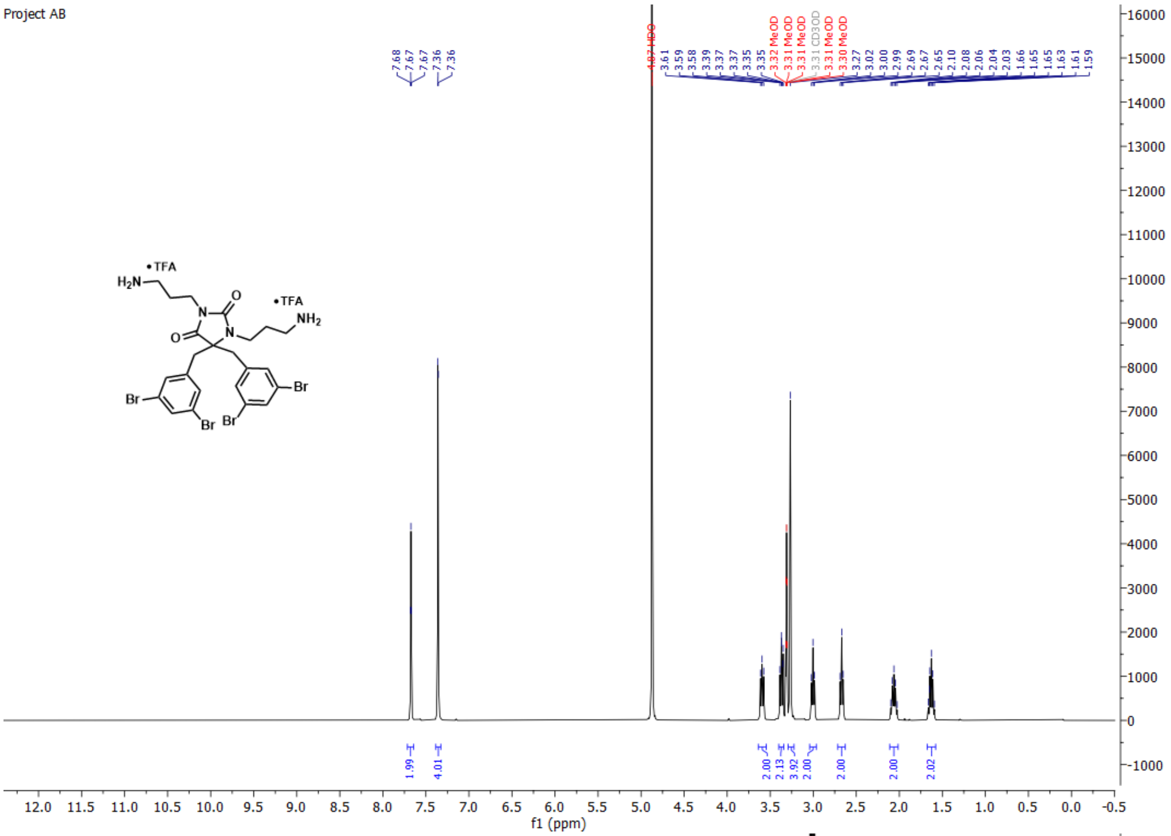

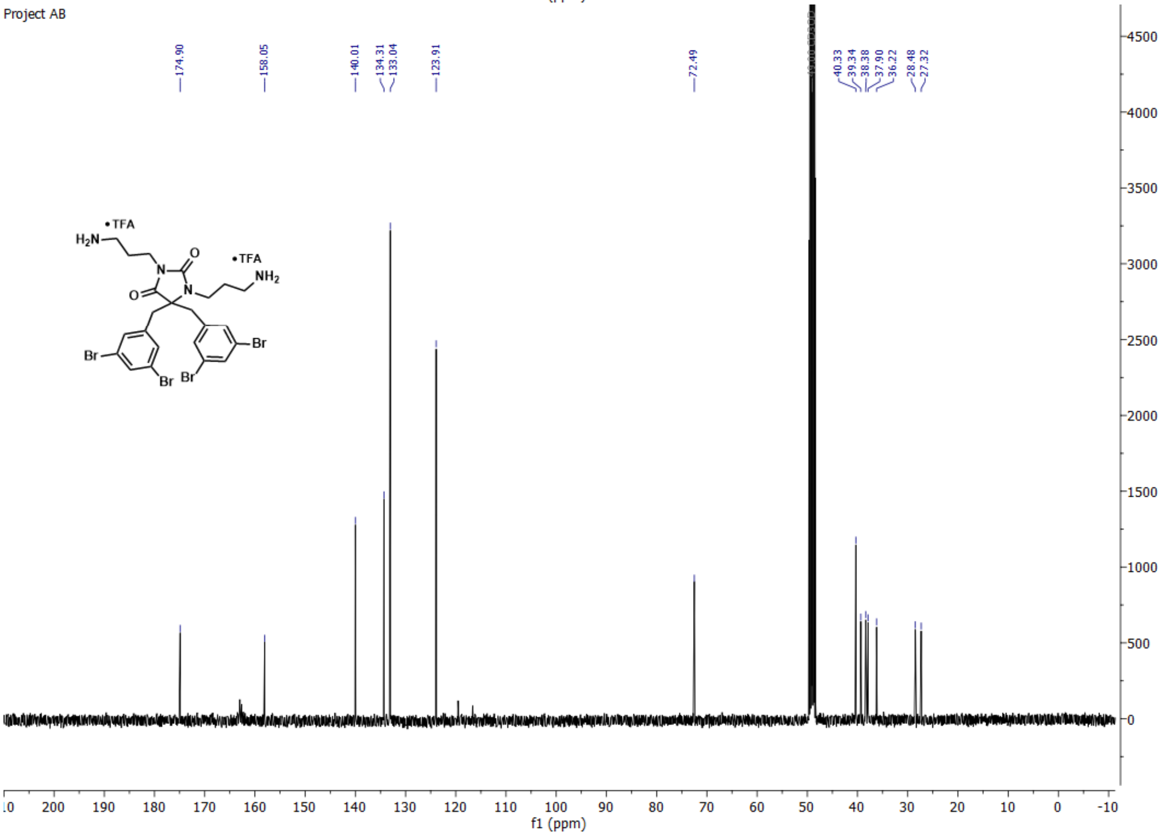

1,3-bis(3-aminopropyl)-5,5-bis((4-bromonaphthalen-1-yl)methyl)imidazolidine-2,4-dione **2eA**.

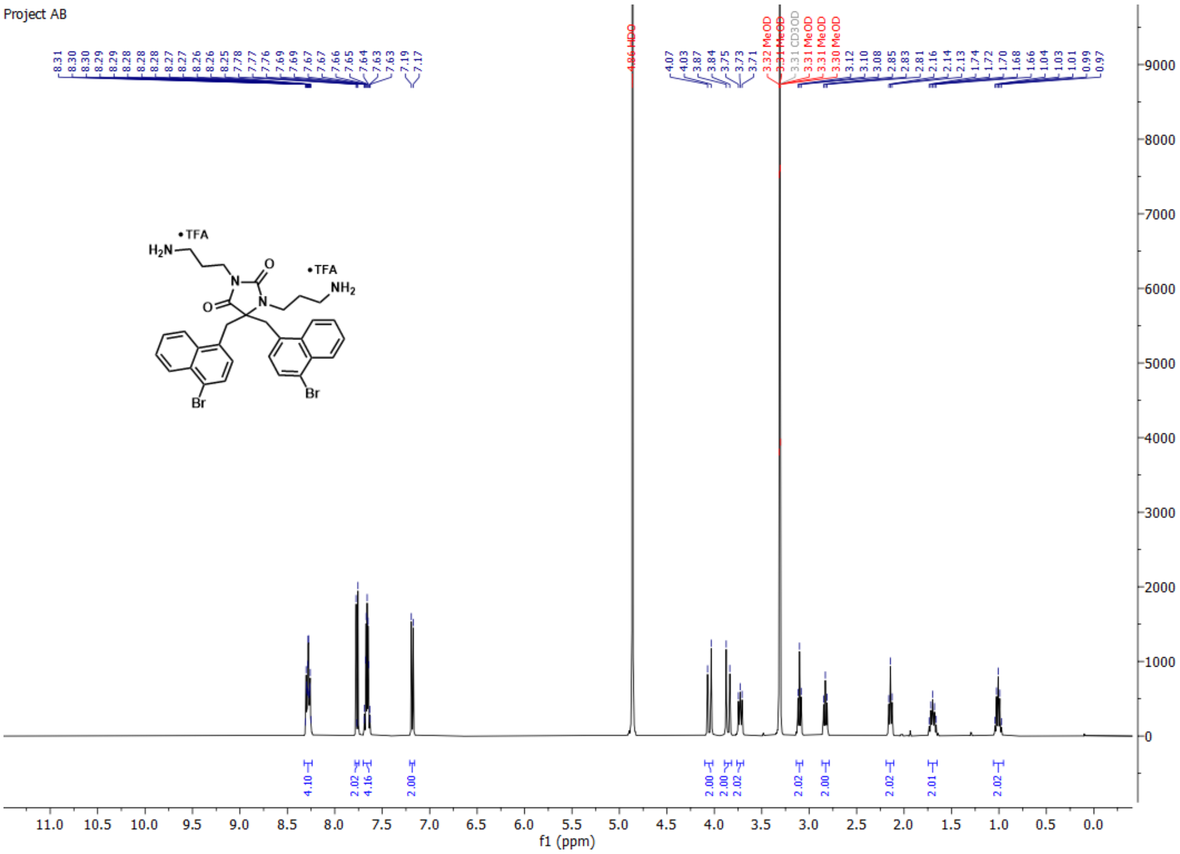

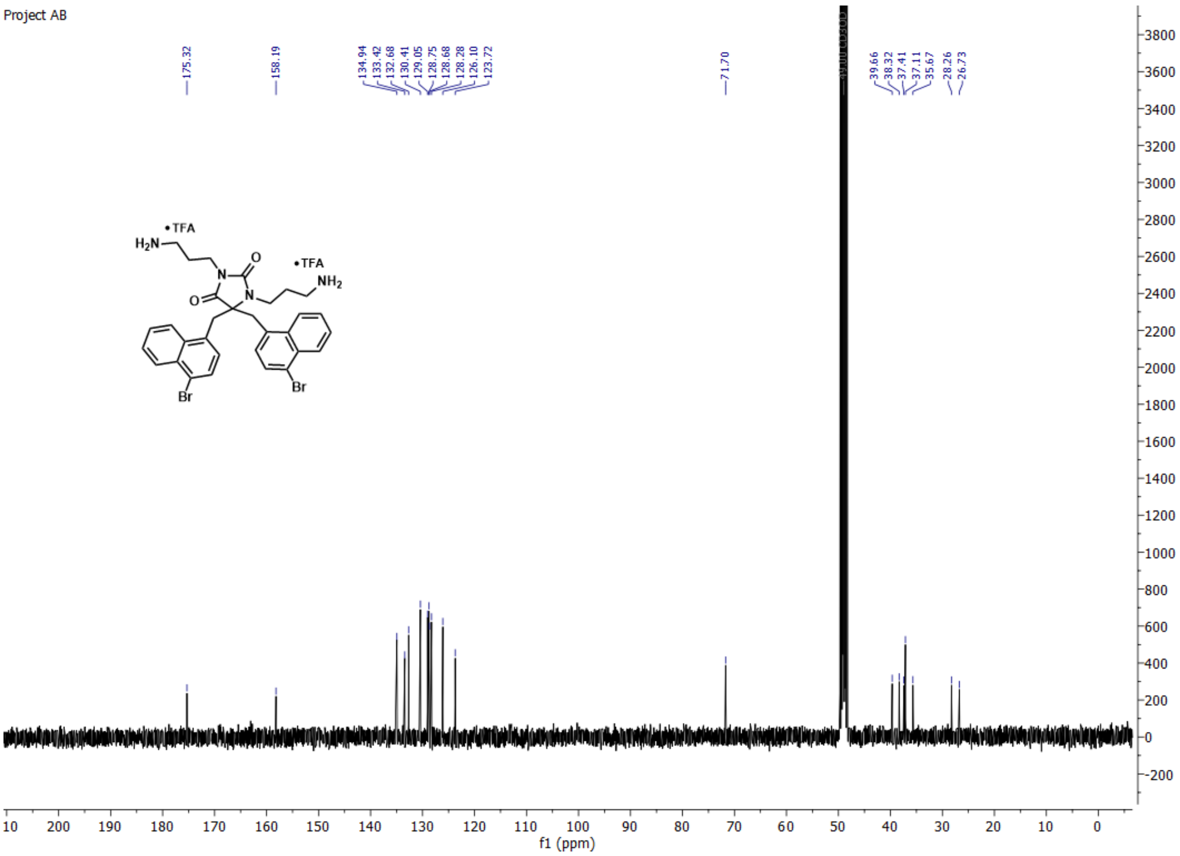

1,3-bis(3-aminopropyl)-5,5-bis(3,5-bis(trifluoromethyl)benzyl)imidazolidine-2,4-dione **2fA**.

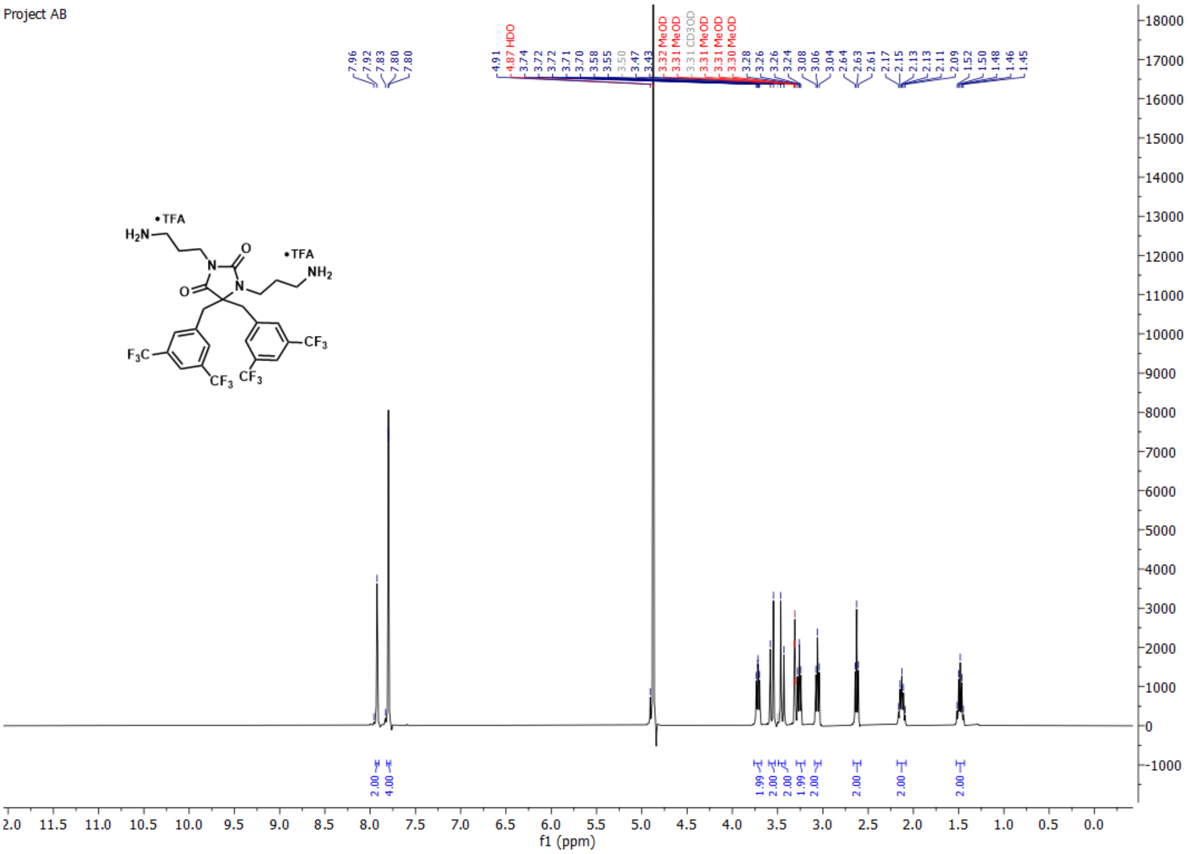

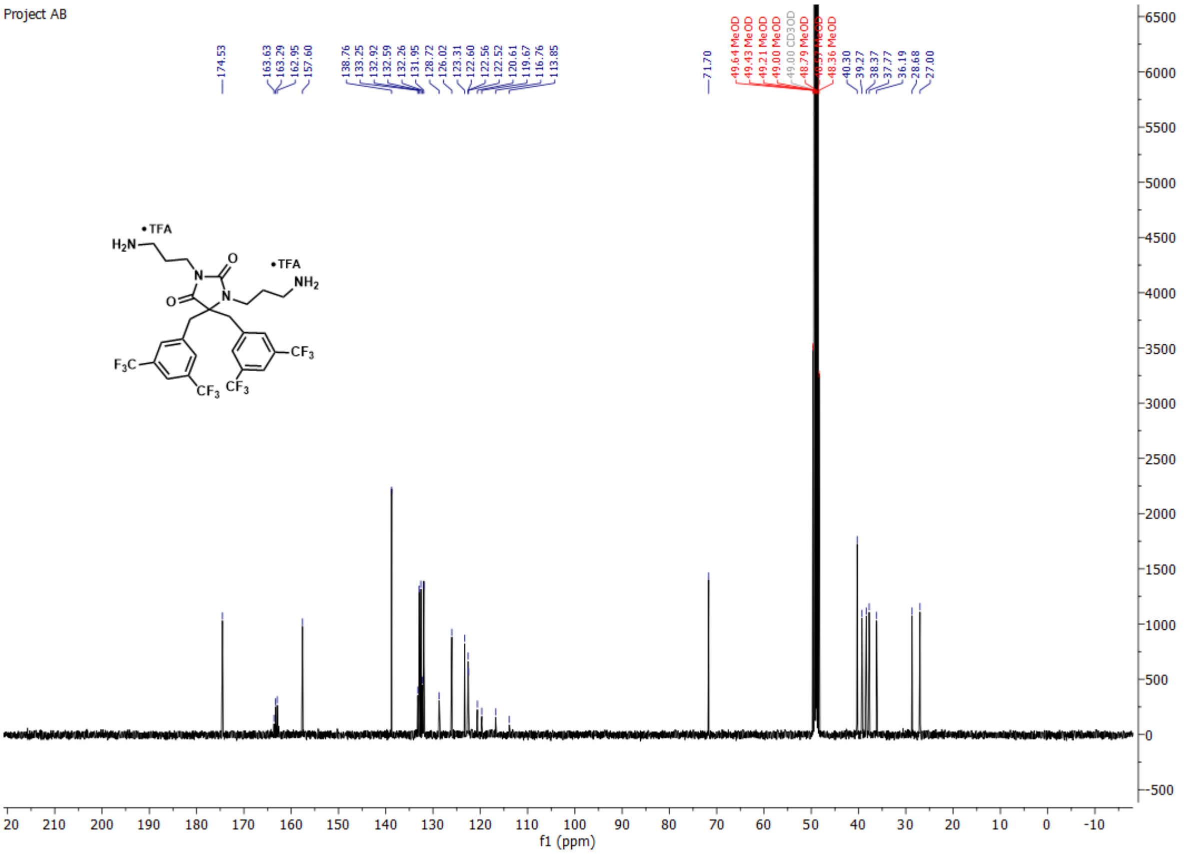

4.4 *N,N'*-dialkylated hydantoins **2G**

1,1'-((4,4-dibenzyl-2,5-dioxoimidazolidine-1,3-diyl)bis(propane-3,1-diyl))diguanidine **2aG**.

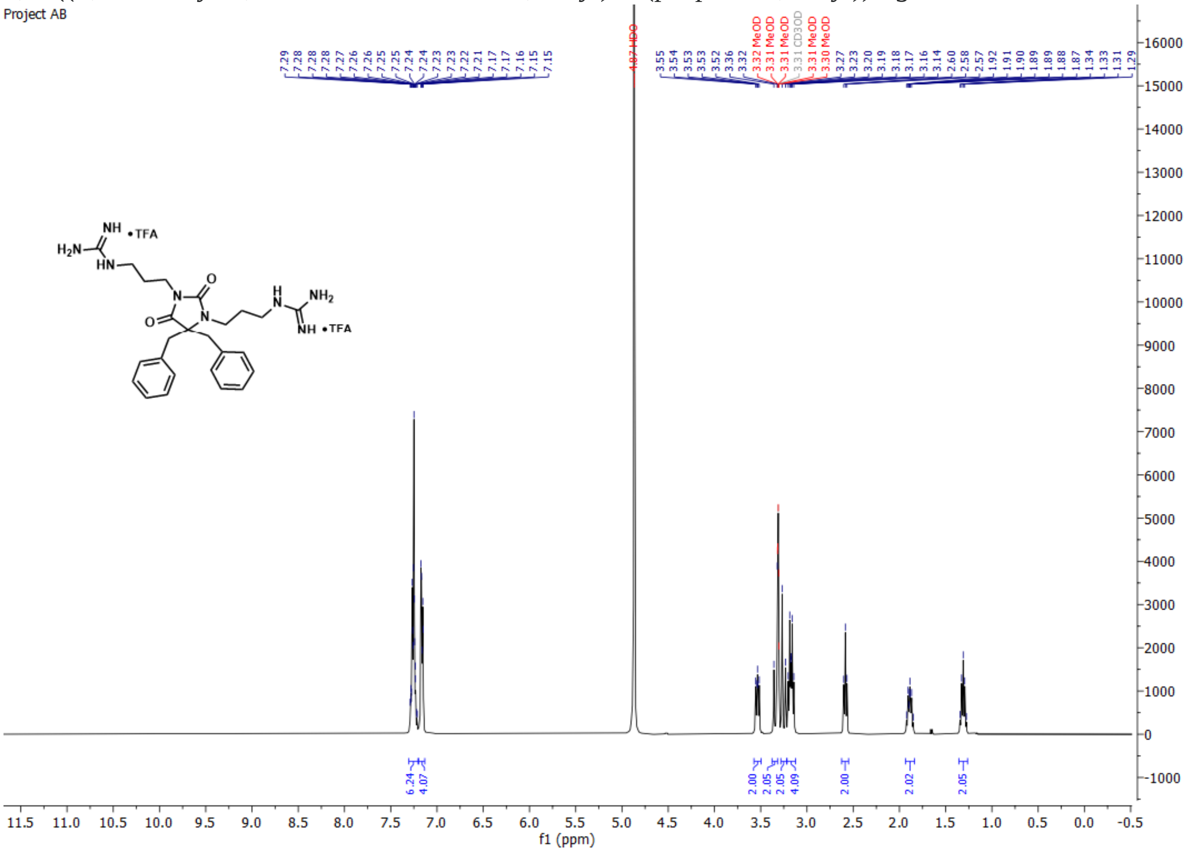

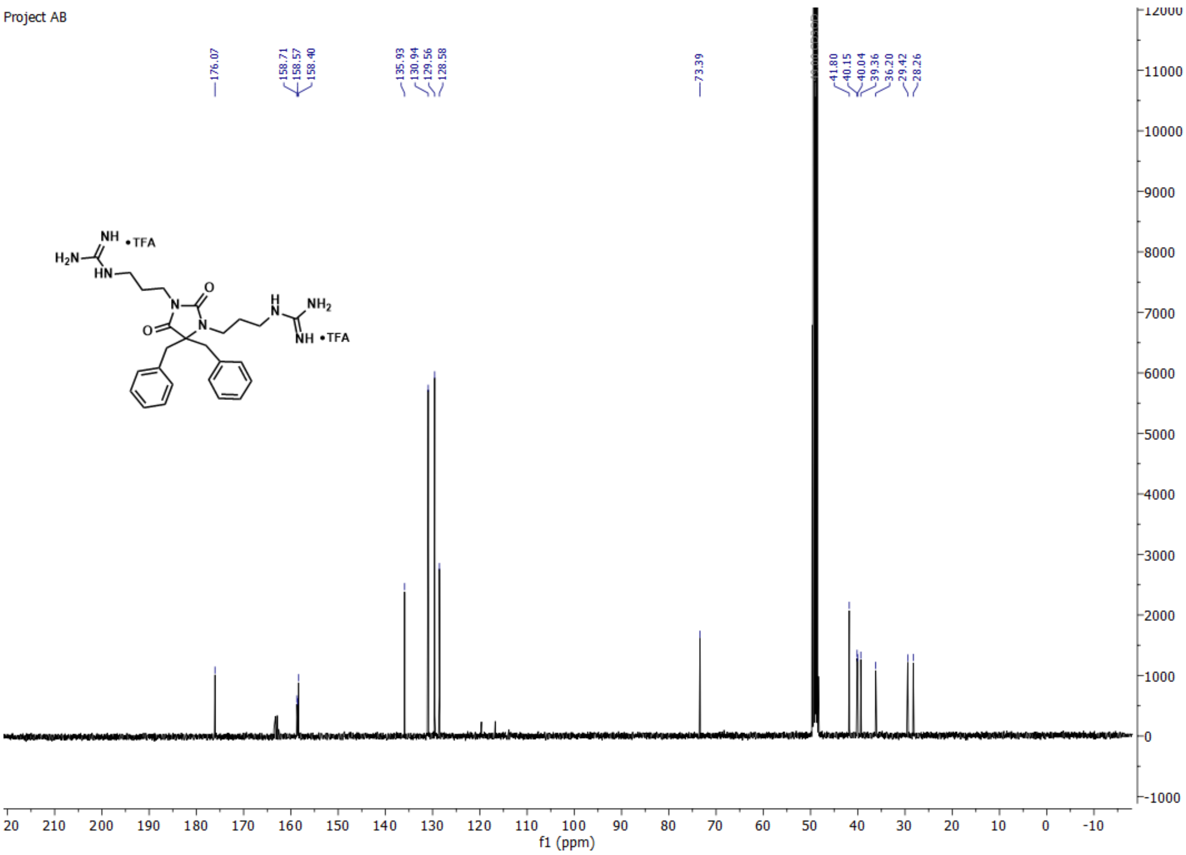

1,1'-((2,5-dioxo-4,4-bis(4-(trifluoromethyl)benzyl)imidazolidine-1,3-diyl)bis(propane-3,1-diyl))diguanidine **2bG**.

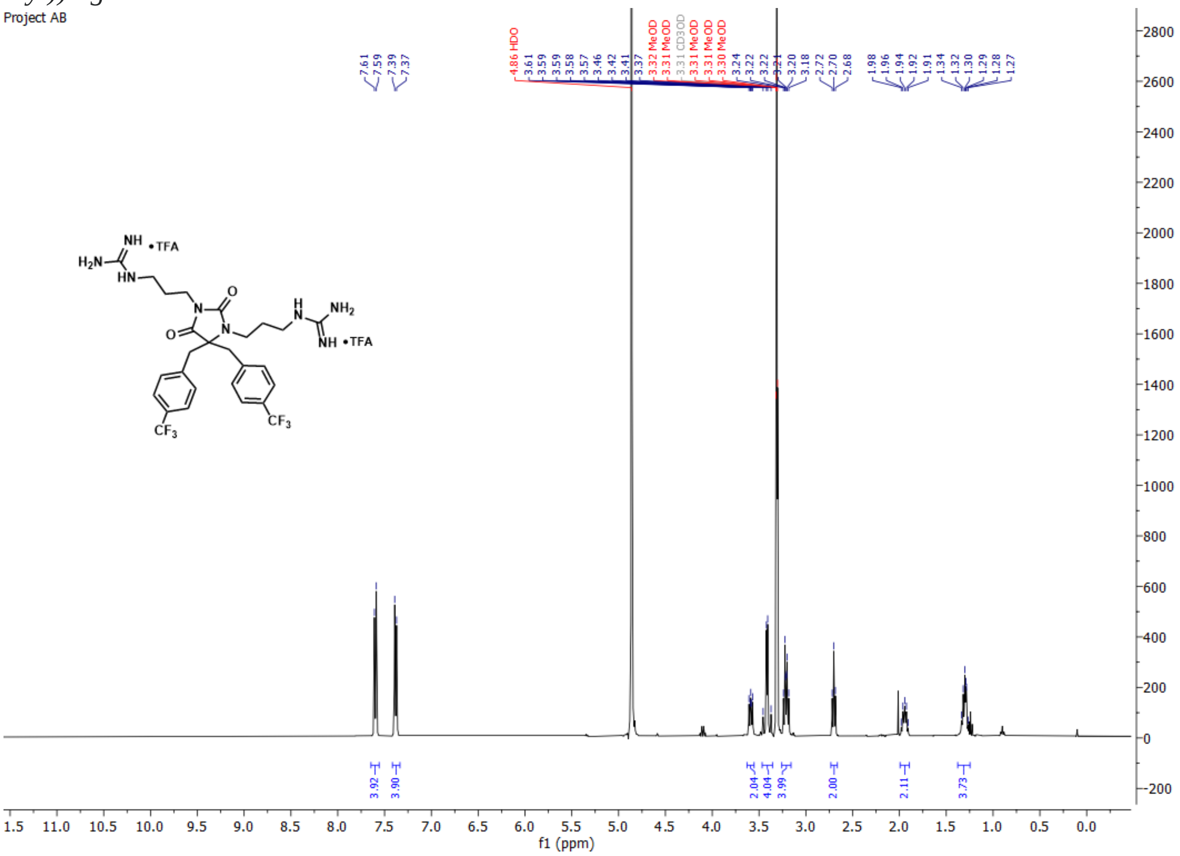

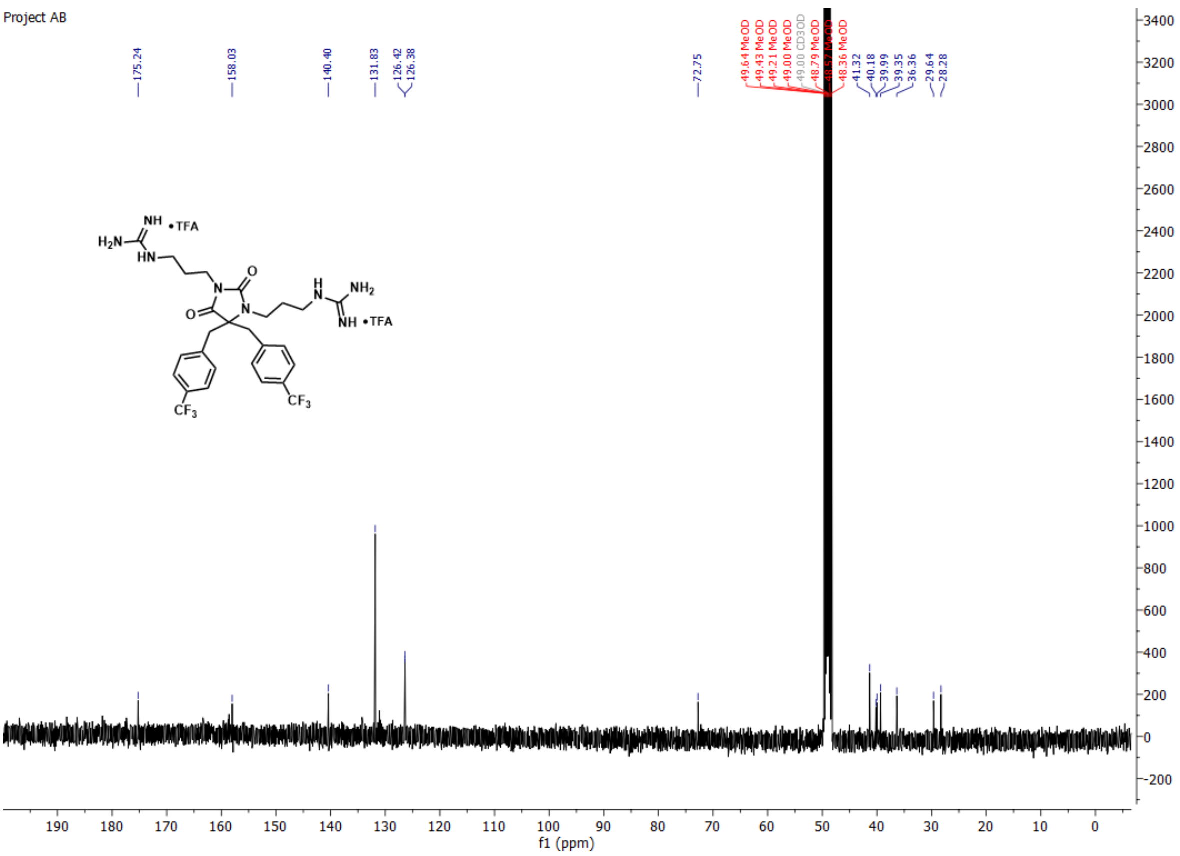

1,1'-((4,4-bis(4-bromo-3-chlorobenzyl)-2,5-dioxoimidazolidine-1,3-diyl)bis(propane-3,1-diyl))diguanidine **2cG**.

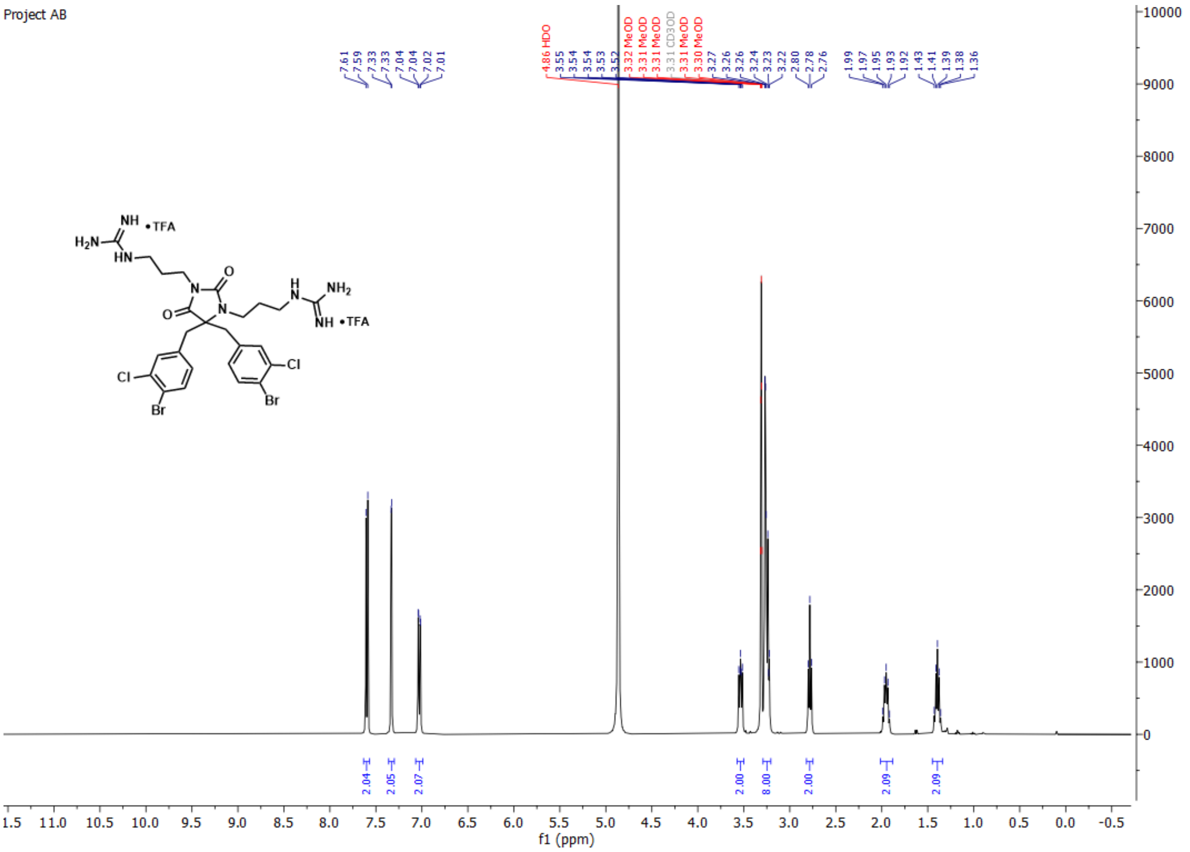

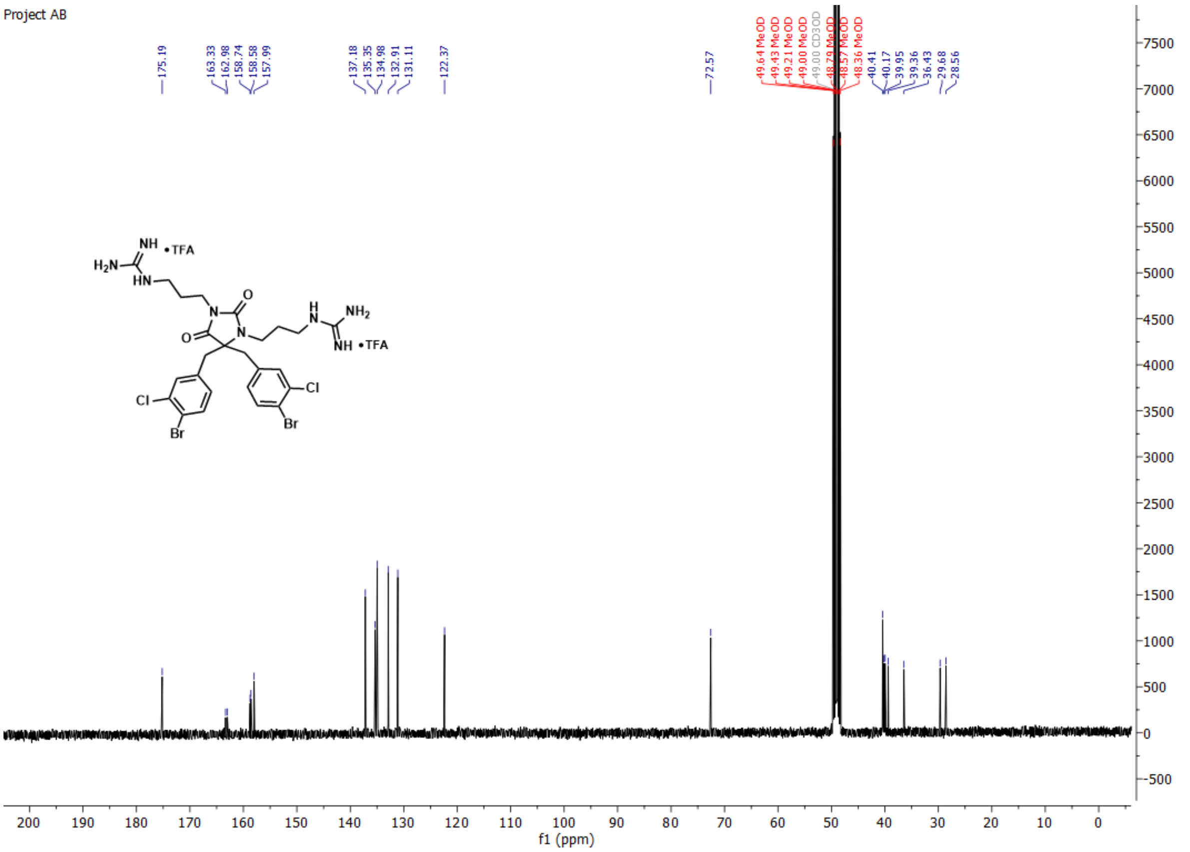

1,1'-((4,4-bis(3,5-dibromobenzyl)-2,5-dioxoimidazolidine-1,3-diyl)bis(propane-3,1-diyl))diguanidine **2dG**.

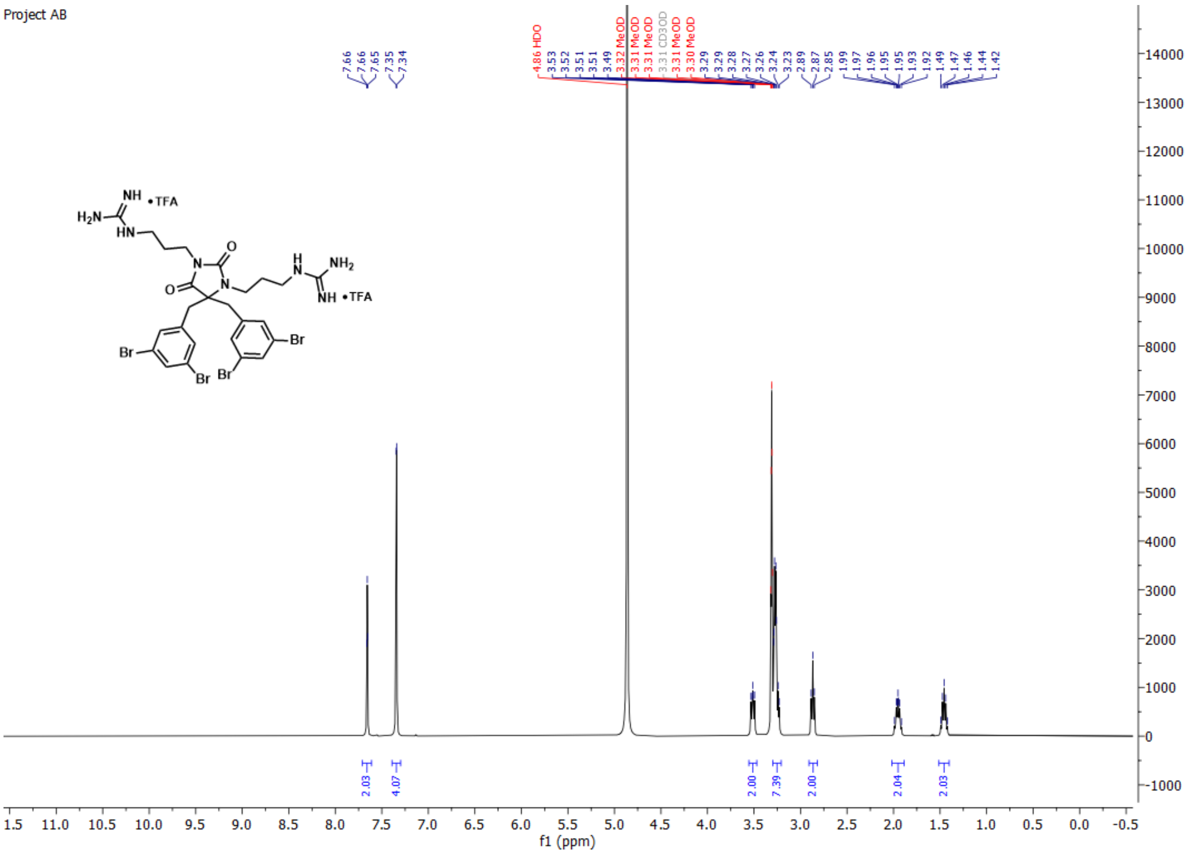

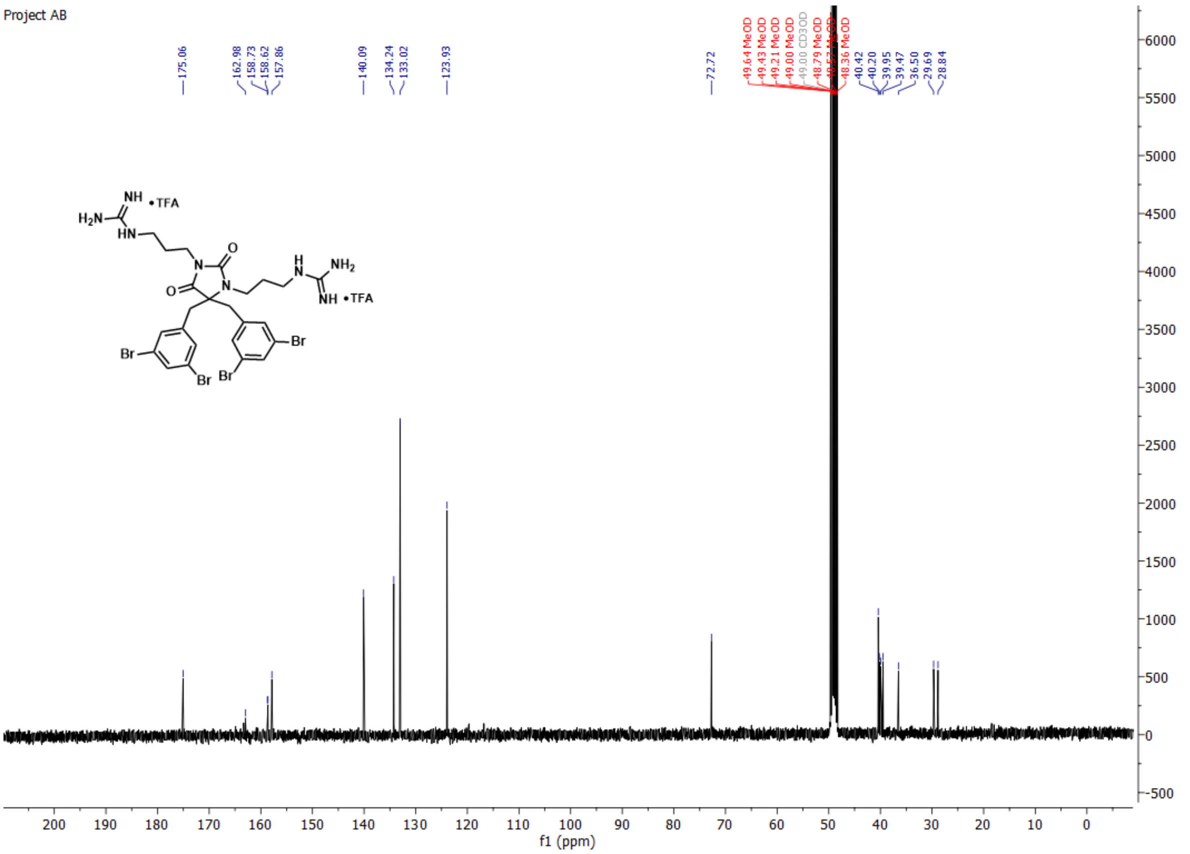

1,1'-((4,4-bis((4-bromonaphthalen-1-yl)methyl)-2,5-dioxoimidazolidine-1,3-diyl)bis(propane-3,1-diyl))diguanidine **2eG**.

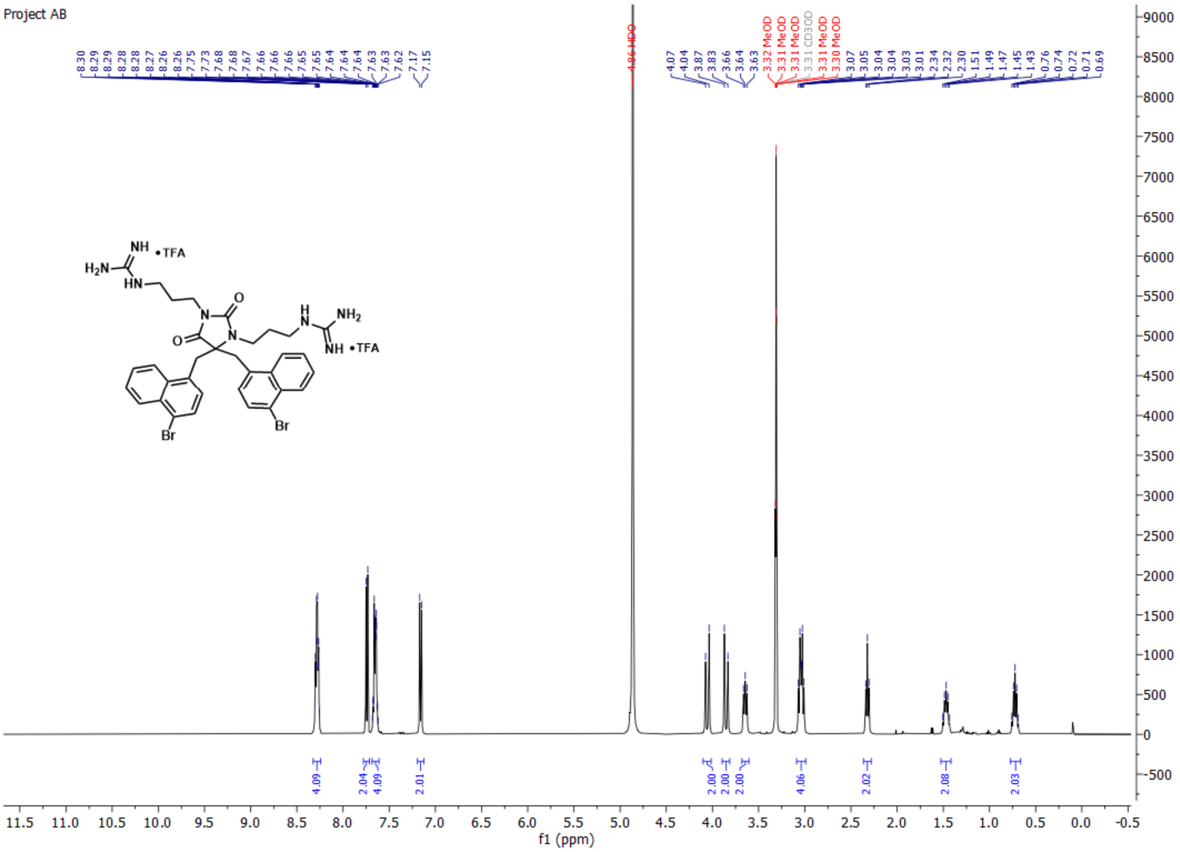

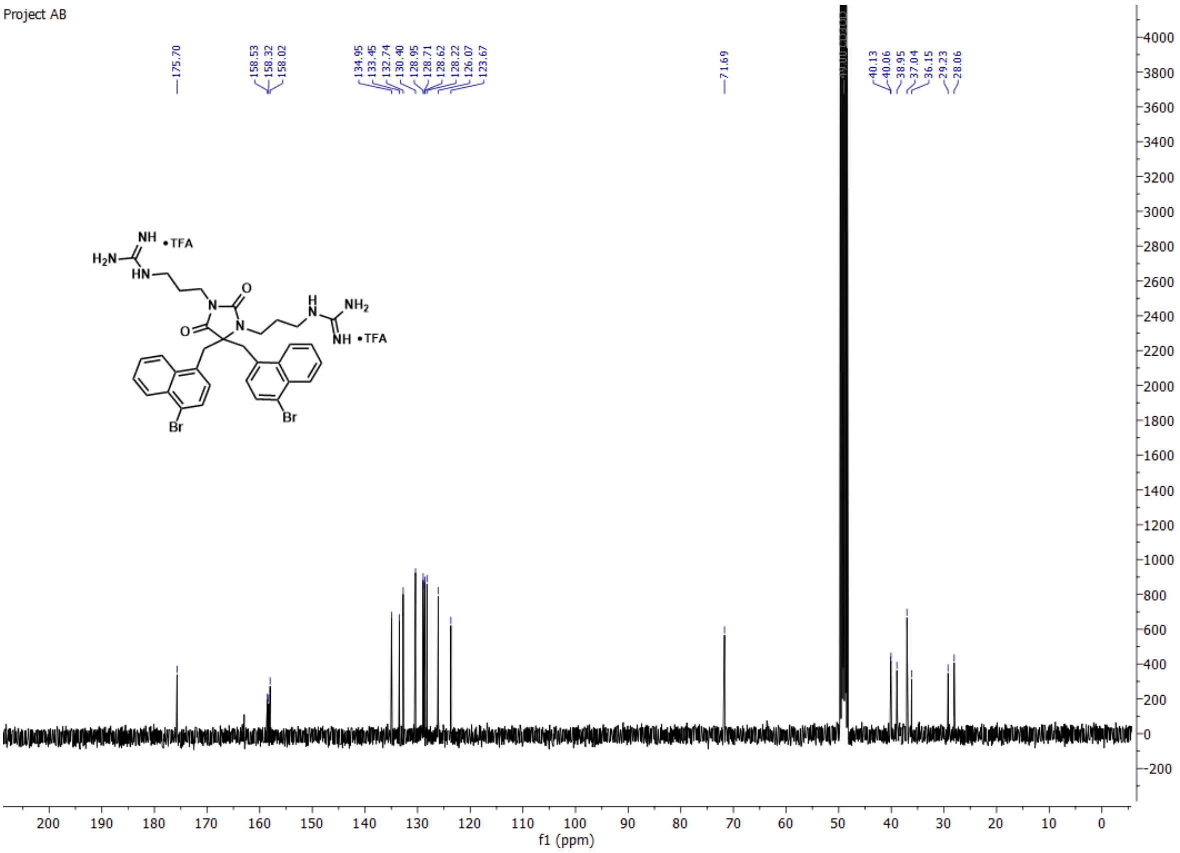

1,1'-((4,4-bis(3,5-bis(trifluoromethyl)benzyl)-2,5-dioxoimidazolidine-1,3-diyl)bis(propane-3,1-diyl))diguanidine **2fG**.

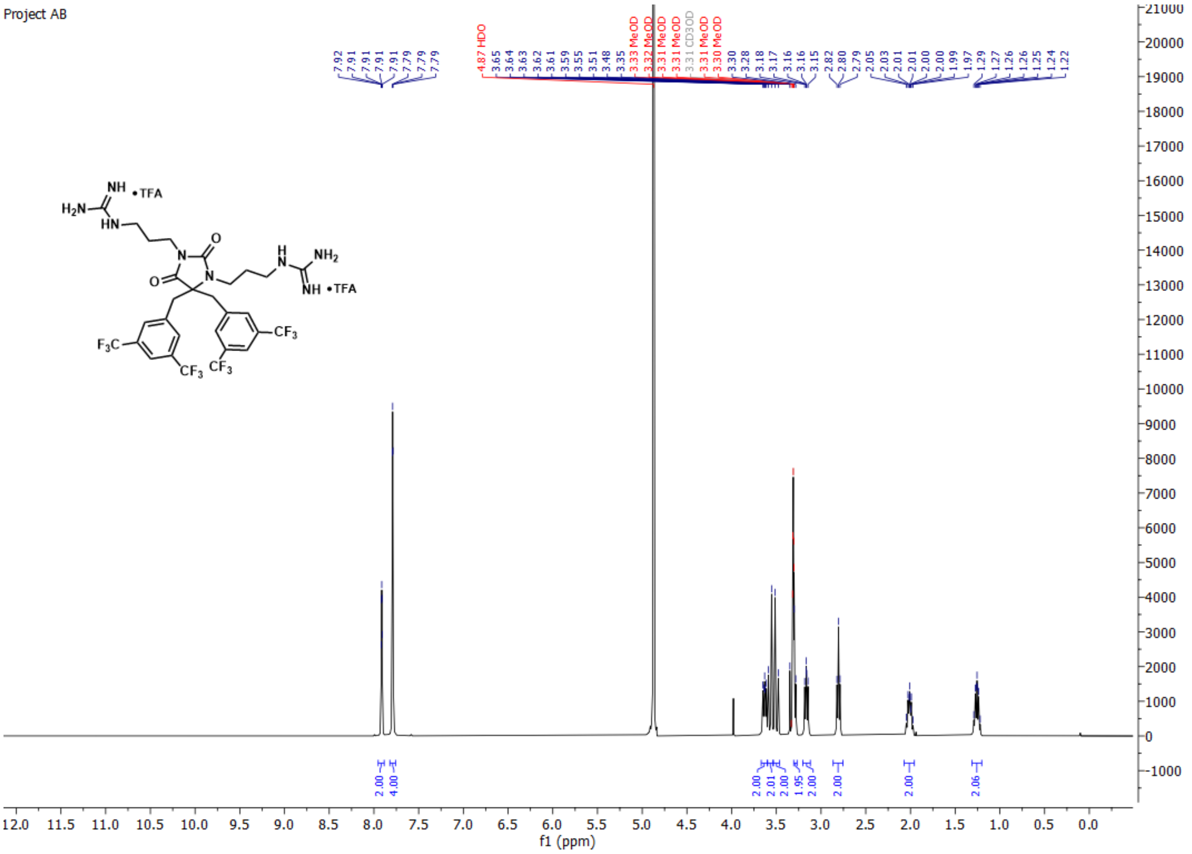

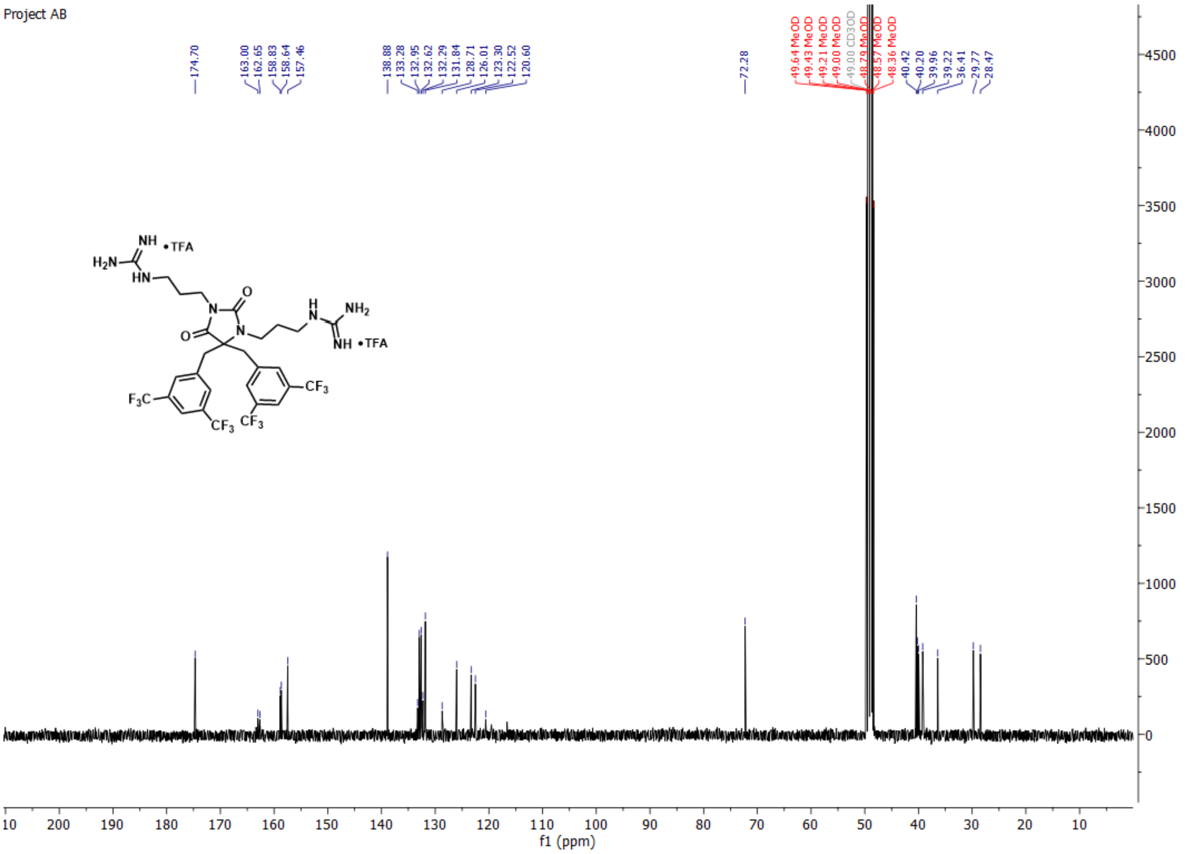

4.5 *N,N'*-dialkylated hydantoins **6A**

1,3-bis(4-aminobutyl)-5,5-bis(4-(trifluoromethyl)benzyl)imidazolidine-2,4-dione **6bA**.

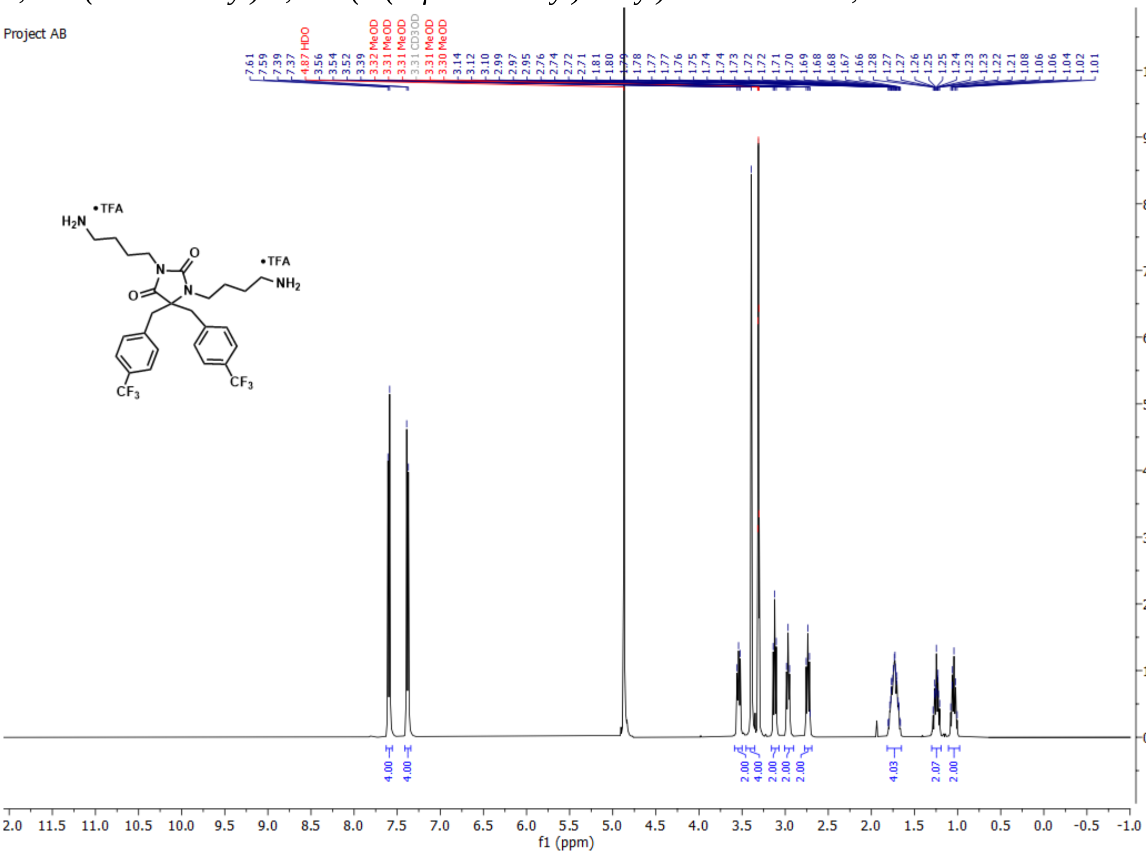

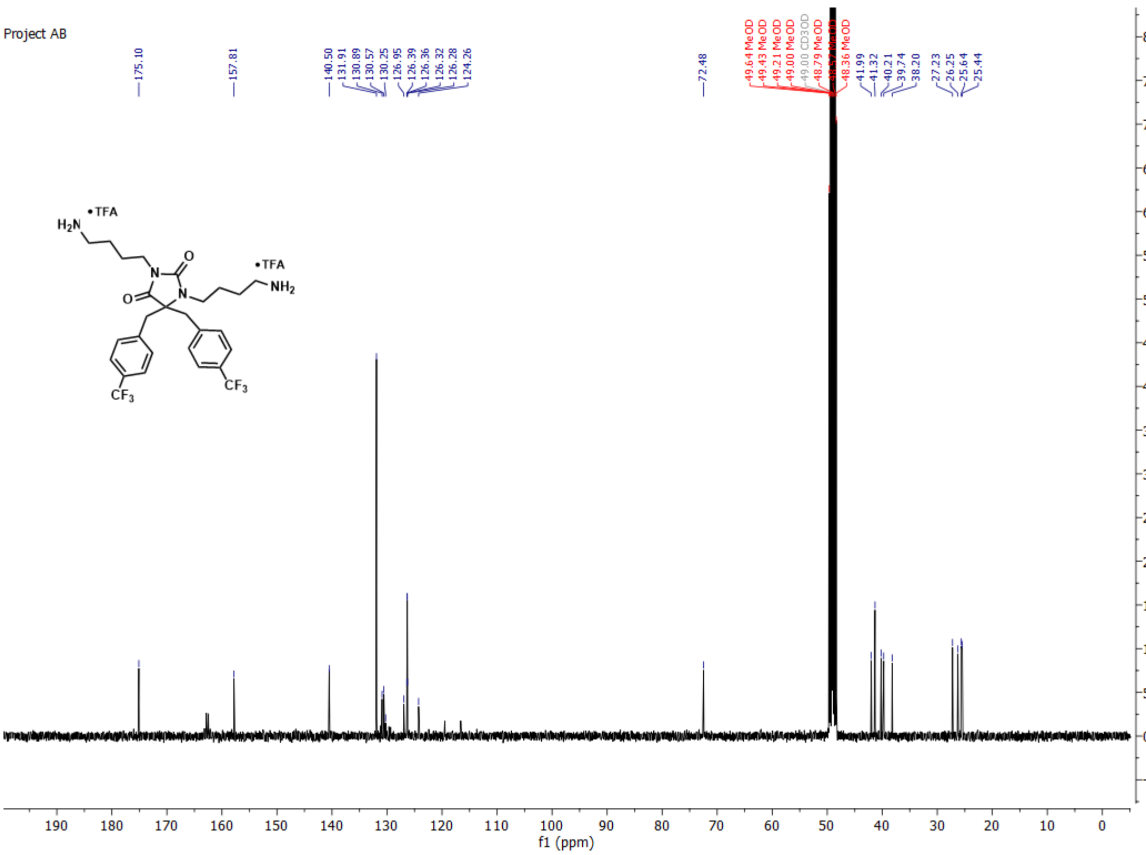

1,3-bis(4-aminobutyl)-5,5-bis(4-bromo-3-chlorobenzyl)imidazolidine-2,4-dione **6cA**.

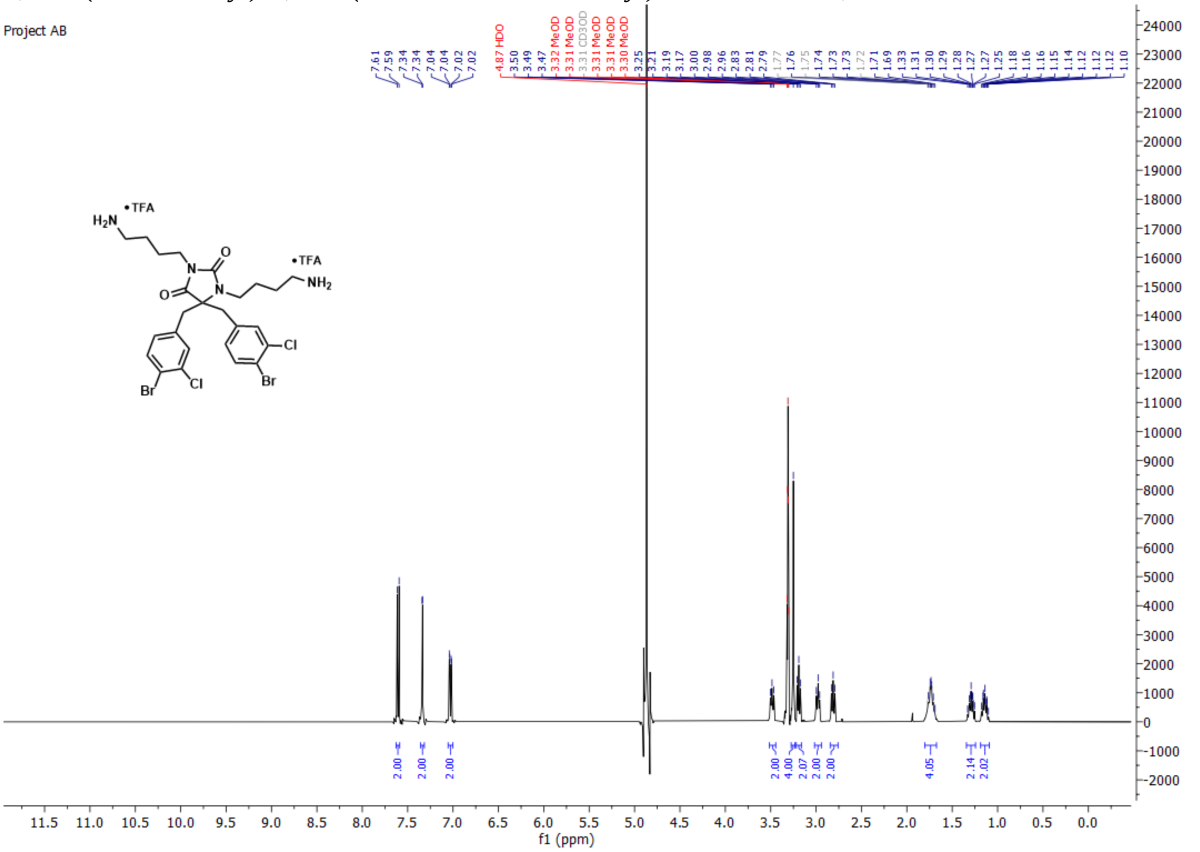

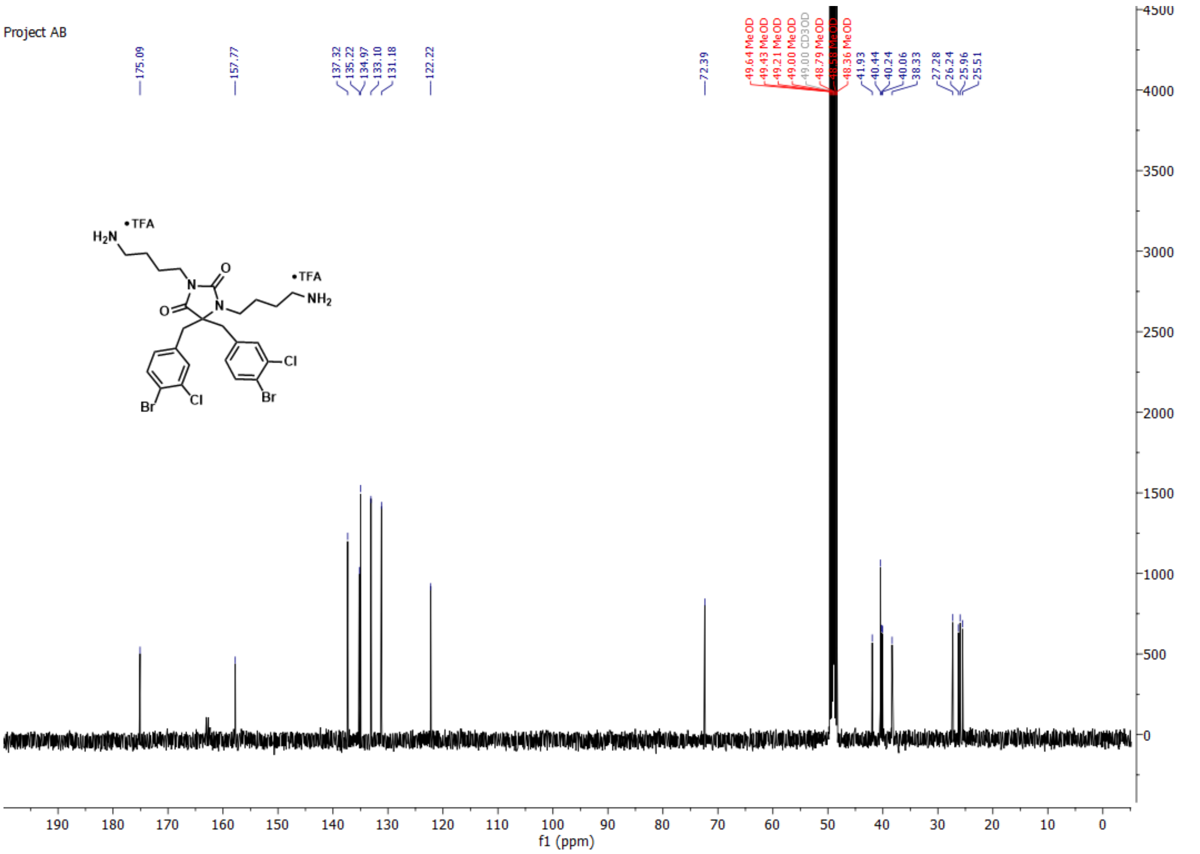

1,3-bis(4-aminobutyl)-5,5-bis(3,5-dibromobenzyl)imidazolidine-2,4-dion **6dA**.

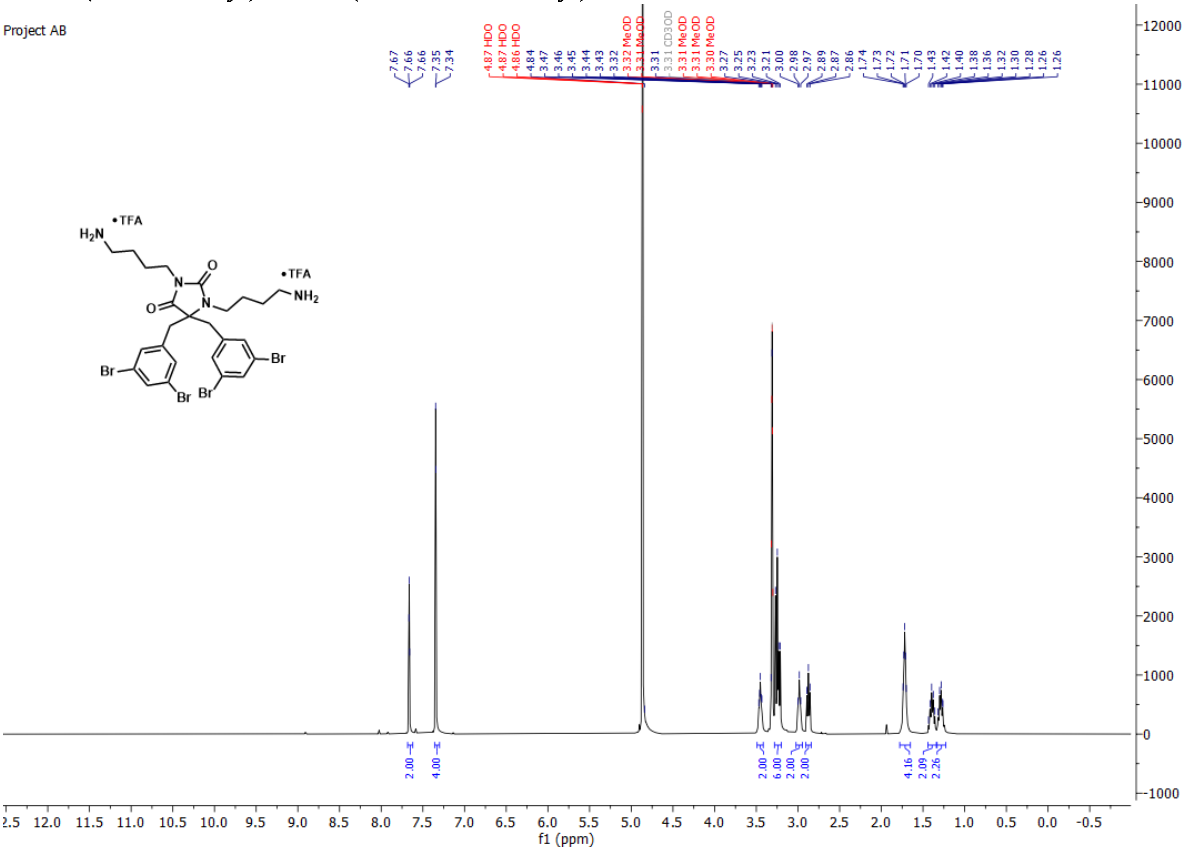

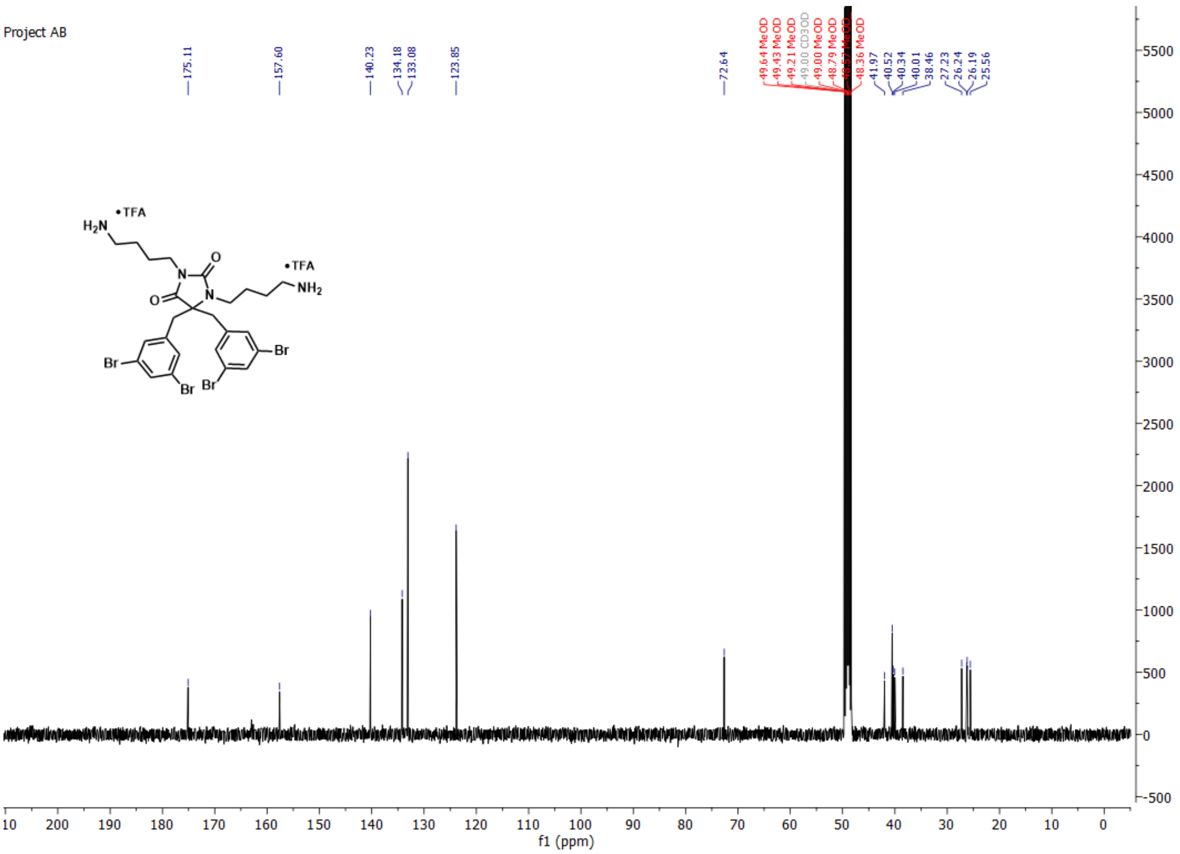

1,3-bis(4-aminobutyl)-5,5-bis(3,5-bis(trifluoromethyl)benzyl)imidazolidine-2,4-dione **6fA**.

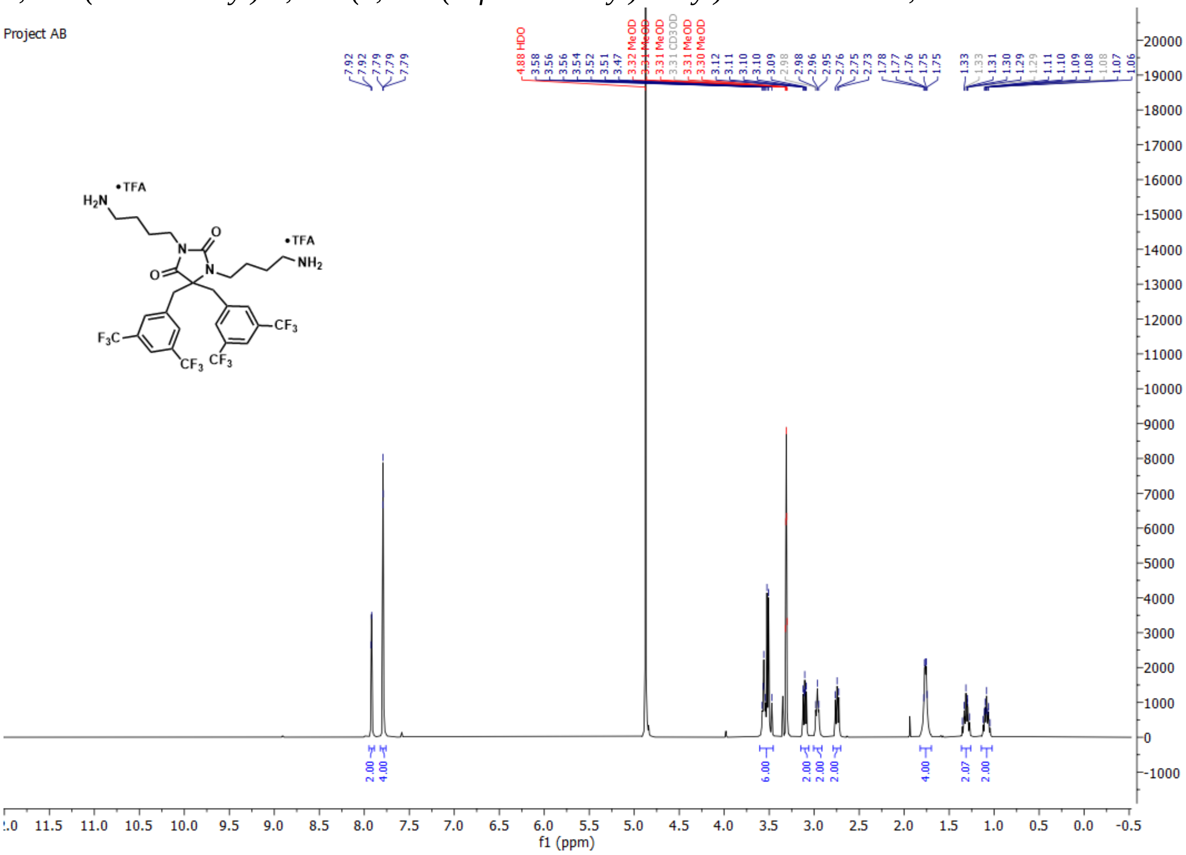

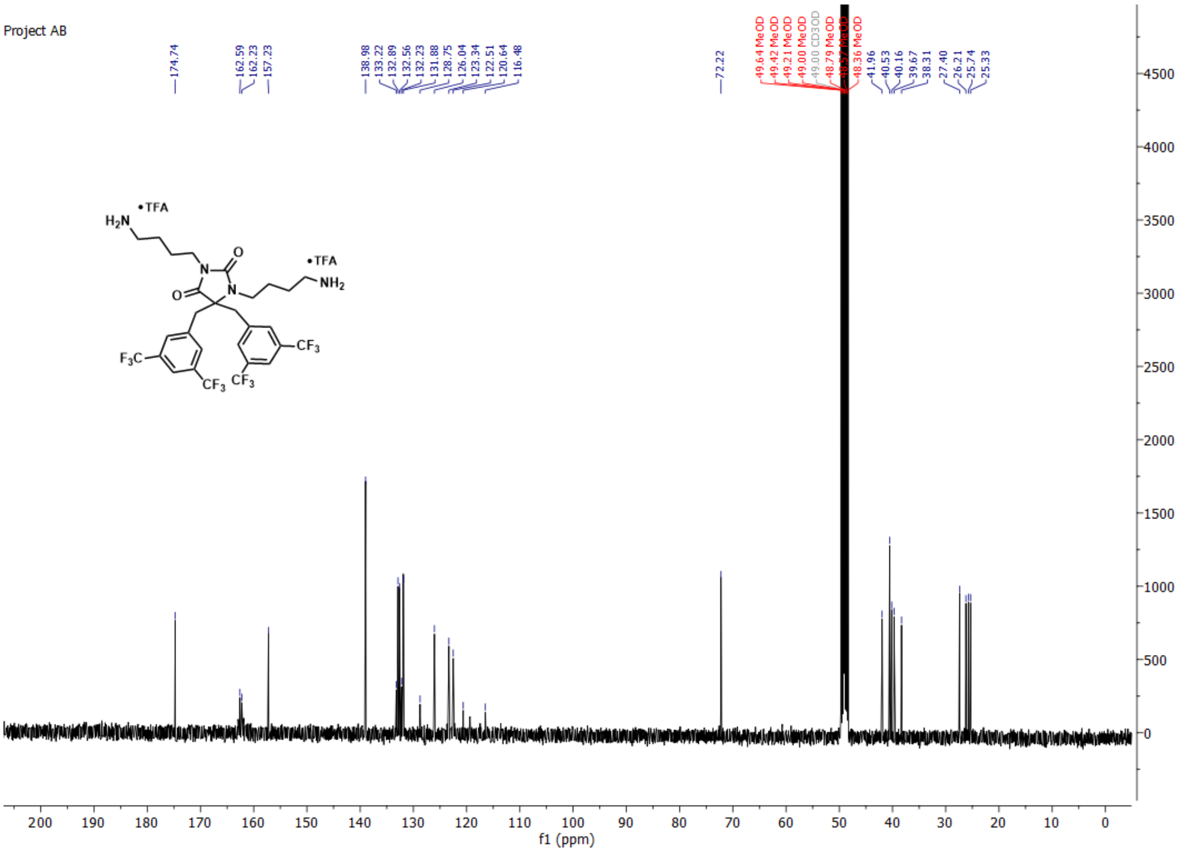

4.6 *N,N'*-dialkylated hydantoins **6G**

1,1'-((2,5-dioxo-4,4-bis(4-(trifluoromethyl)benzyl)imidazolidine-1,3-diyl)bis(butane-4,1-diyl))diguanidine **6bG**.

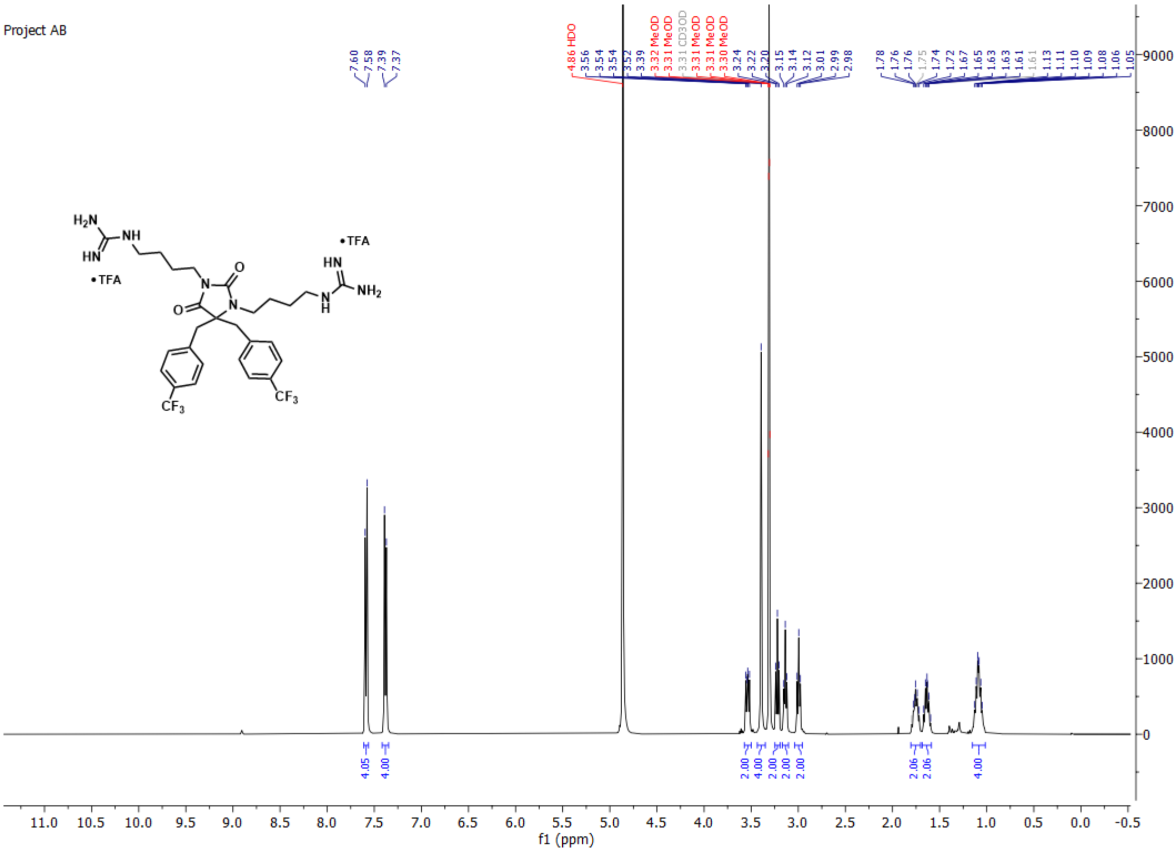

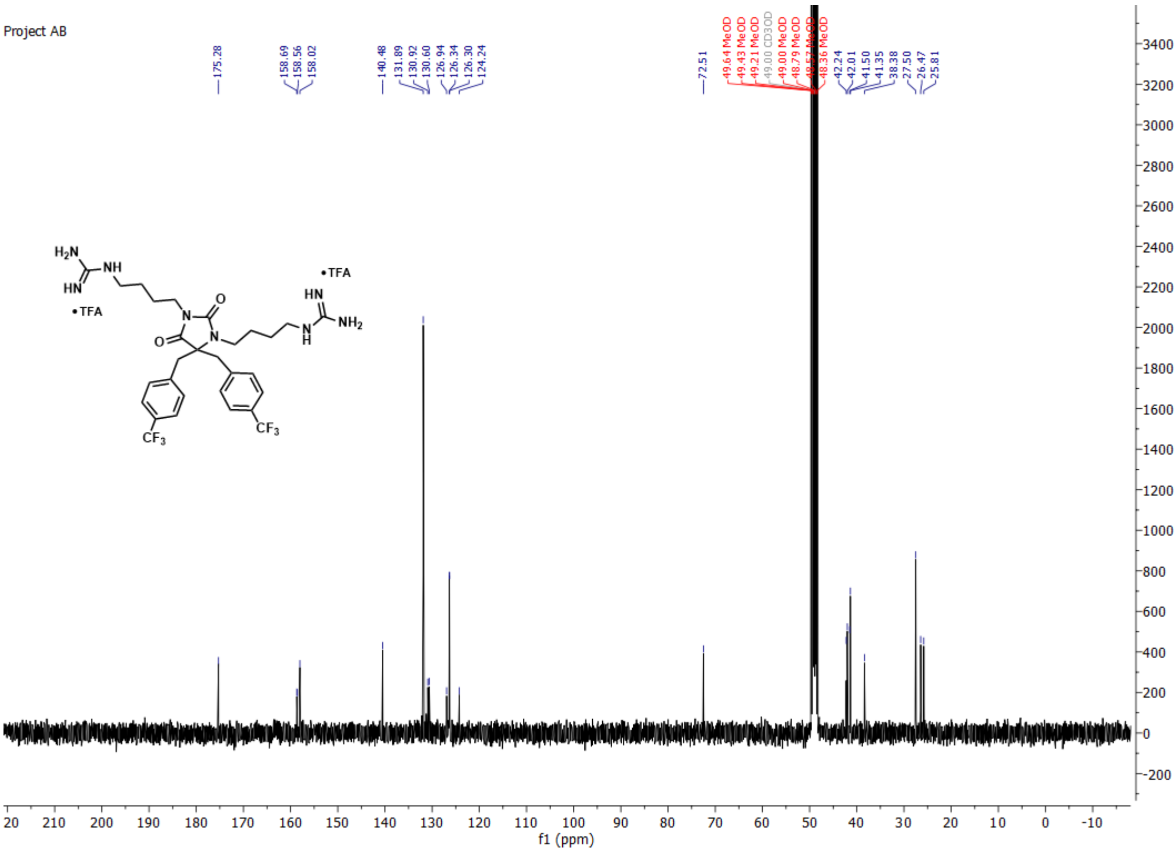

1,1'-((4,4-bis(4-bromo-3-chlorobenzyl)-2,5-dioxoimidazolidine-1,3-diyl)bis(butane-4,1-diyl))diguanidine **6cG**.

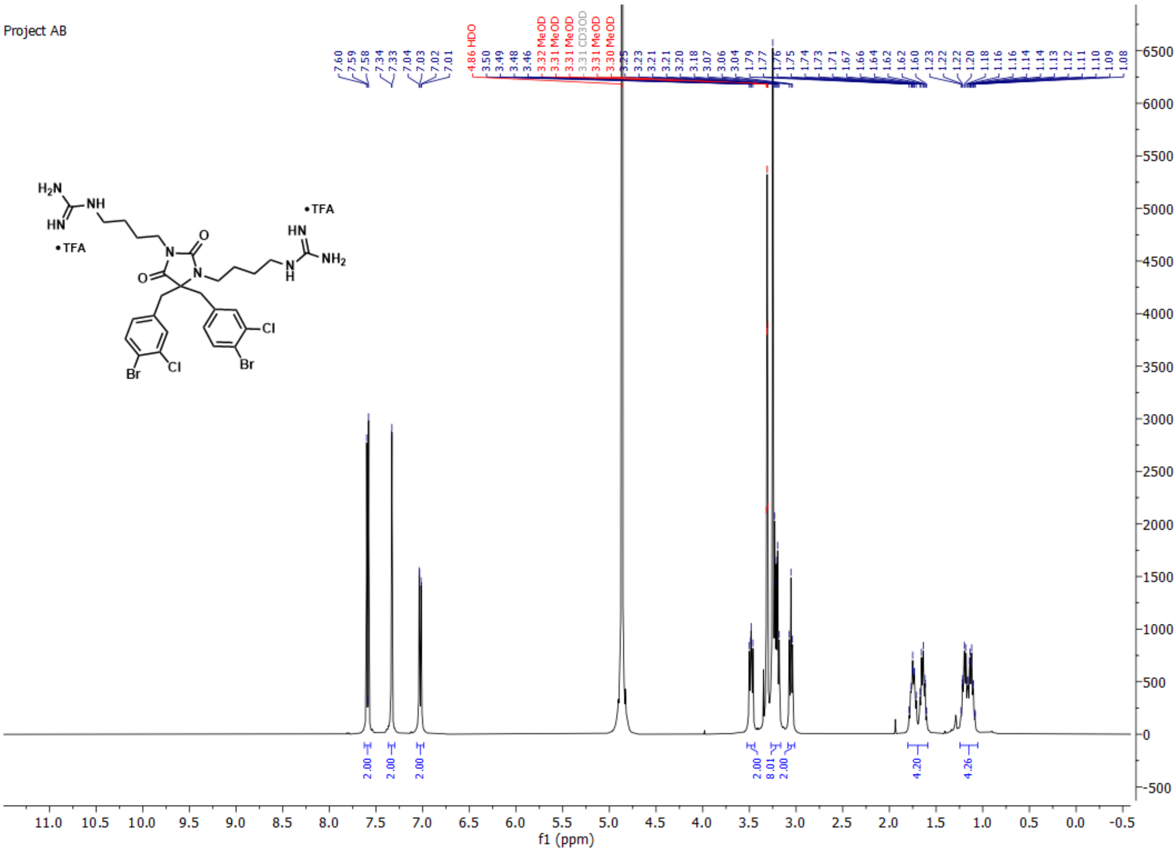

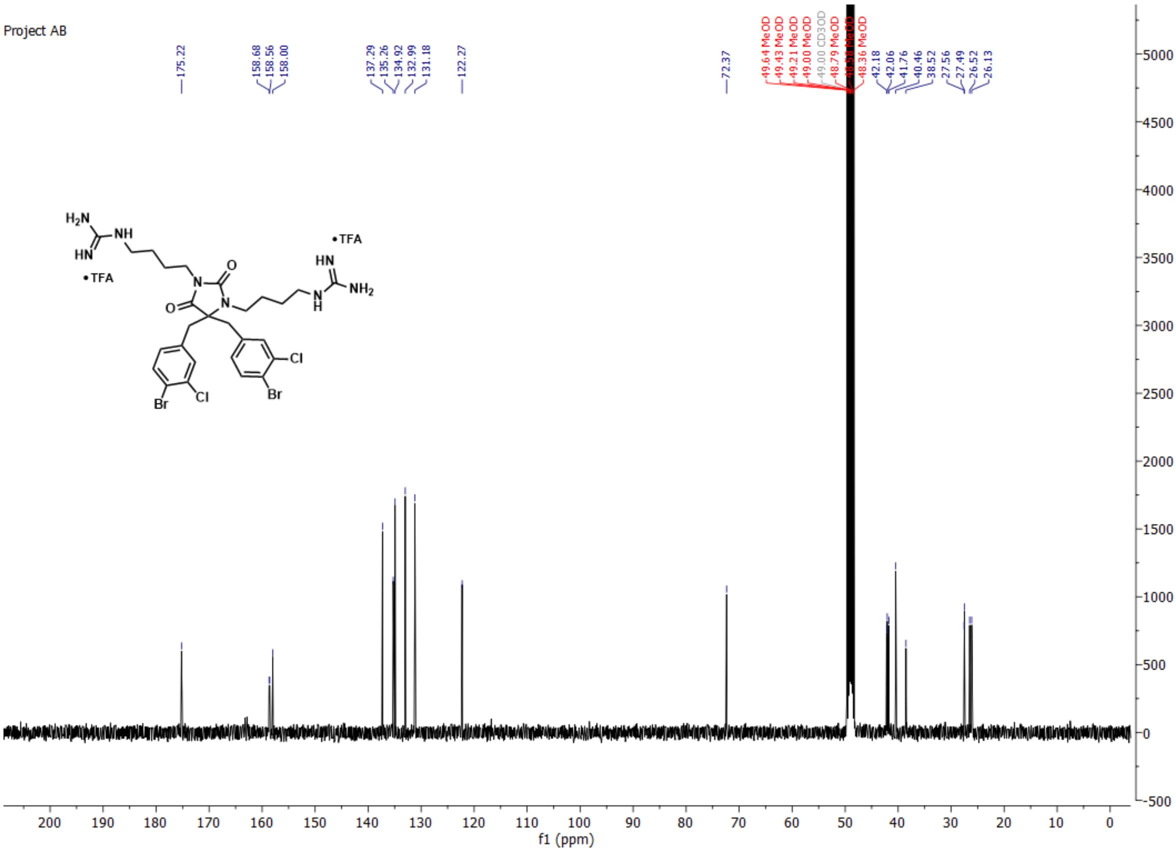

1,1'-((4,4-bis(3,5-dibromobenzyl)-2,5-dioxoimidazolidine-1,3-diyl)bis(butane-4,1-diyl))diguanidine **6dG**.

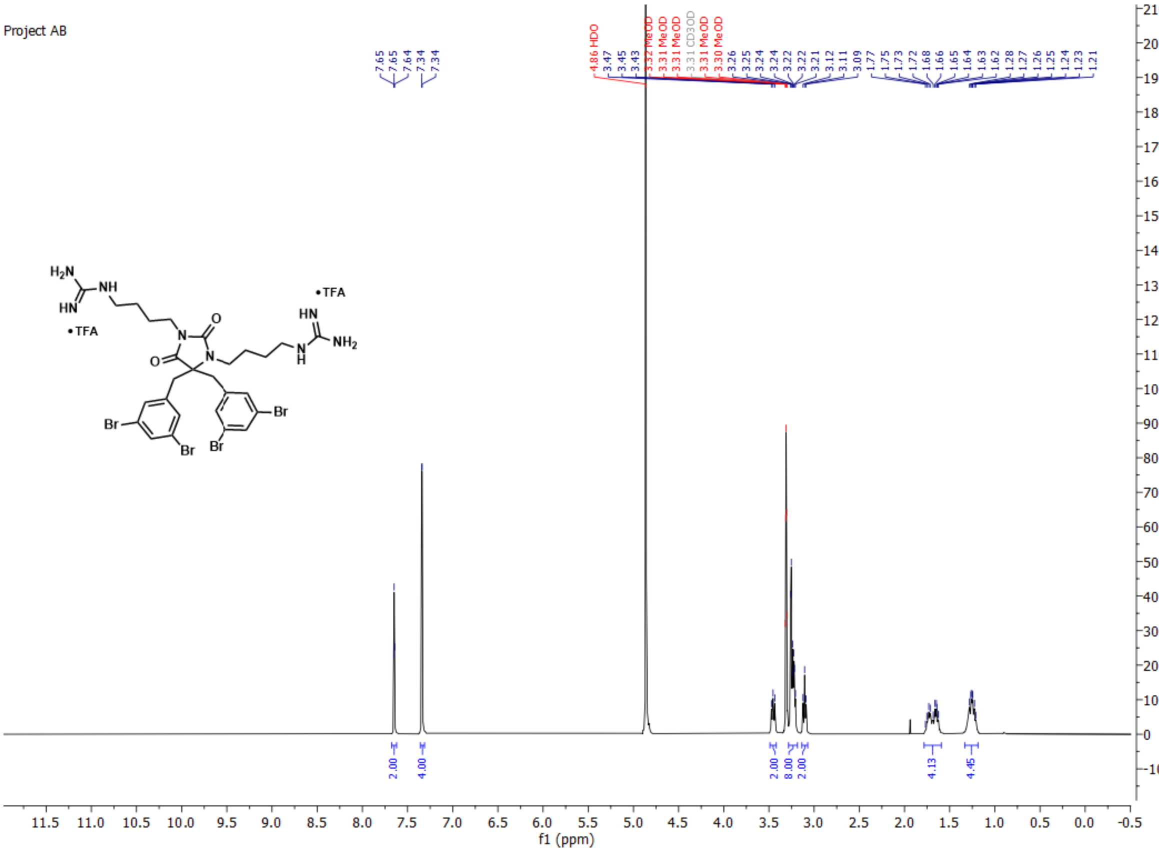

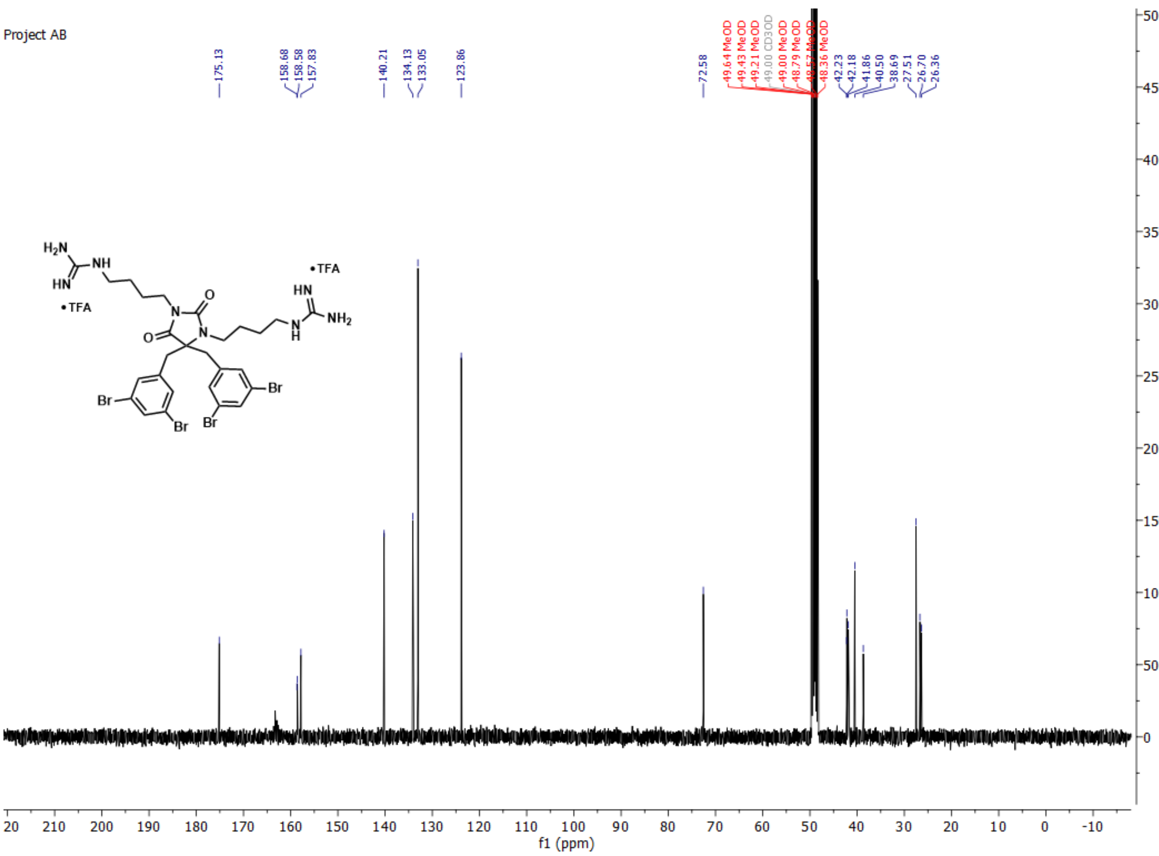

1,1'-((4,4-bis(3,5-bis(trifluoromethyl)benzyl)-2,5-dioxoimidazolidine-1,3-diyl)bis(butane-4,1-diyl))diguanidine **6fG**.

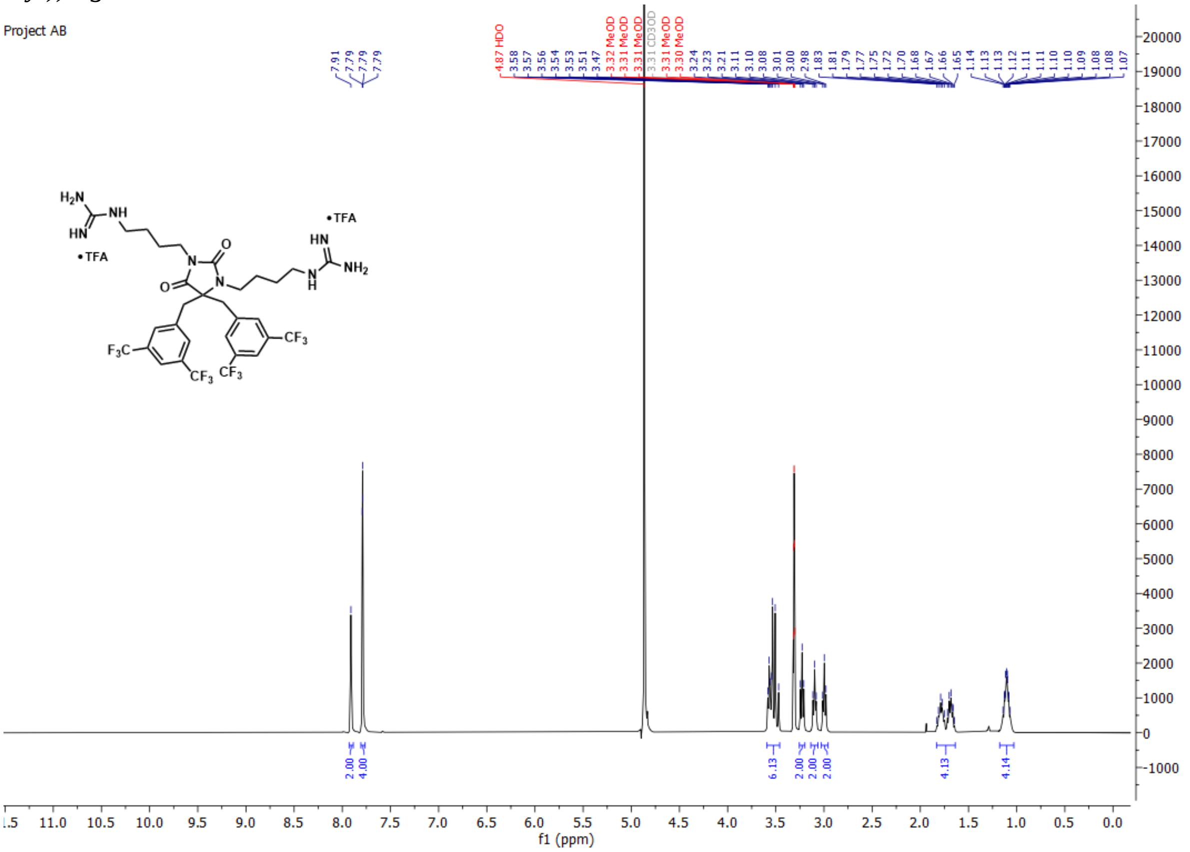

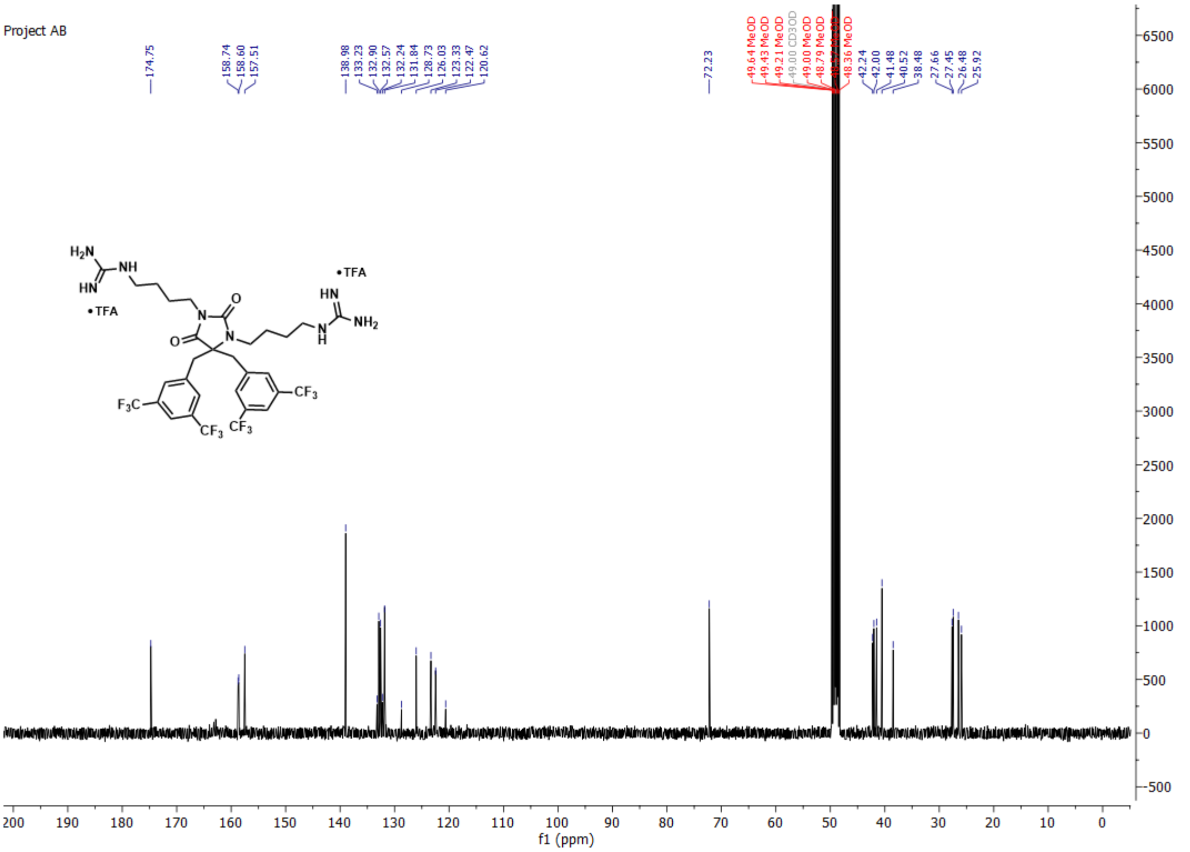

4.7 2,4-Dithiohydantoin core

5,5-bis(3,5-dibromobenzyl)imidazolidine-2,4-dithione **16**.

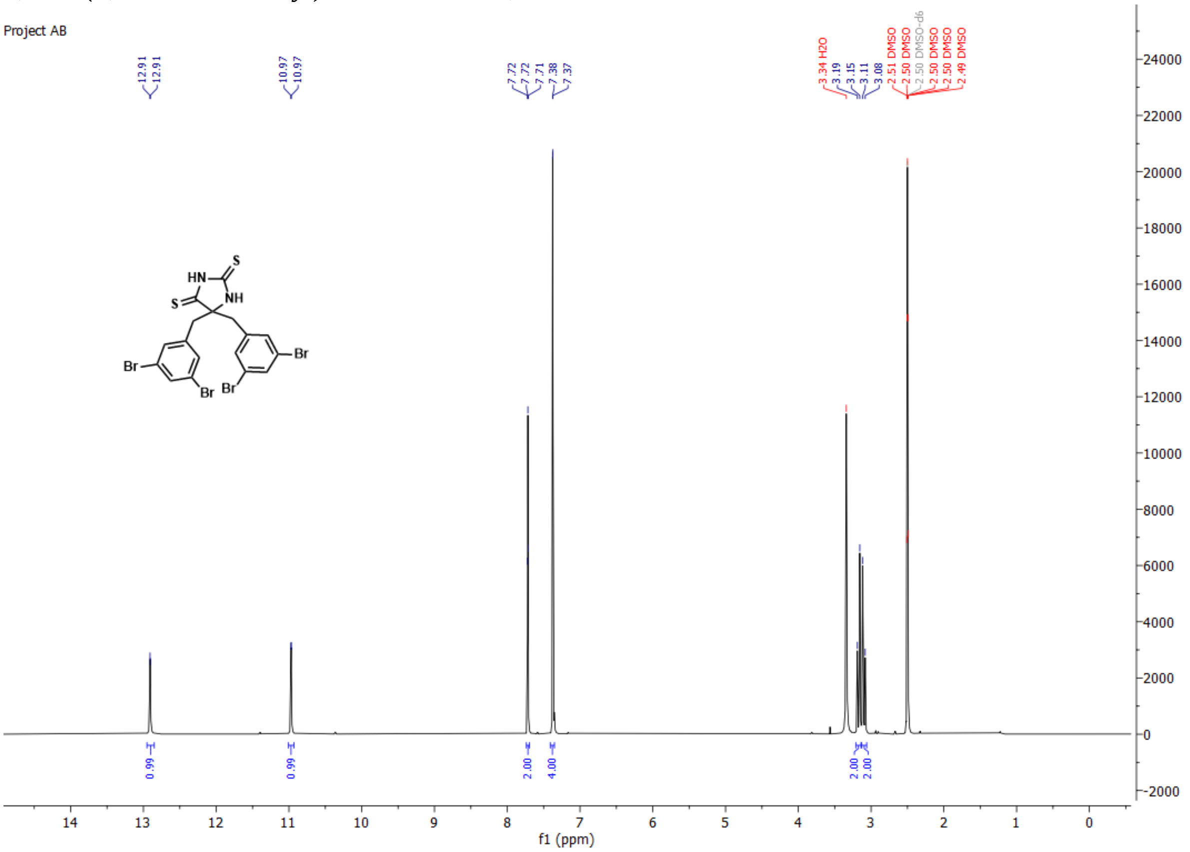

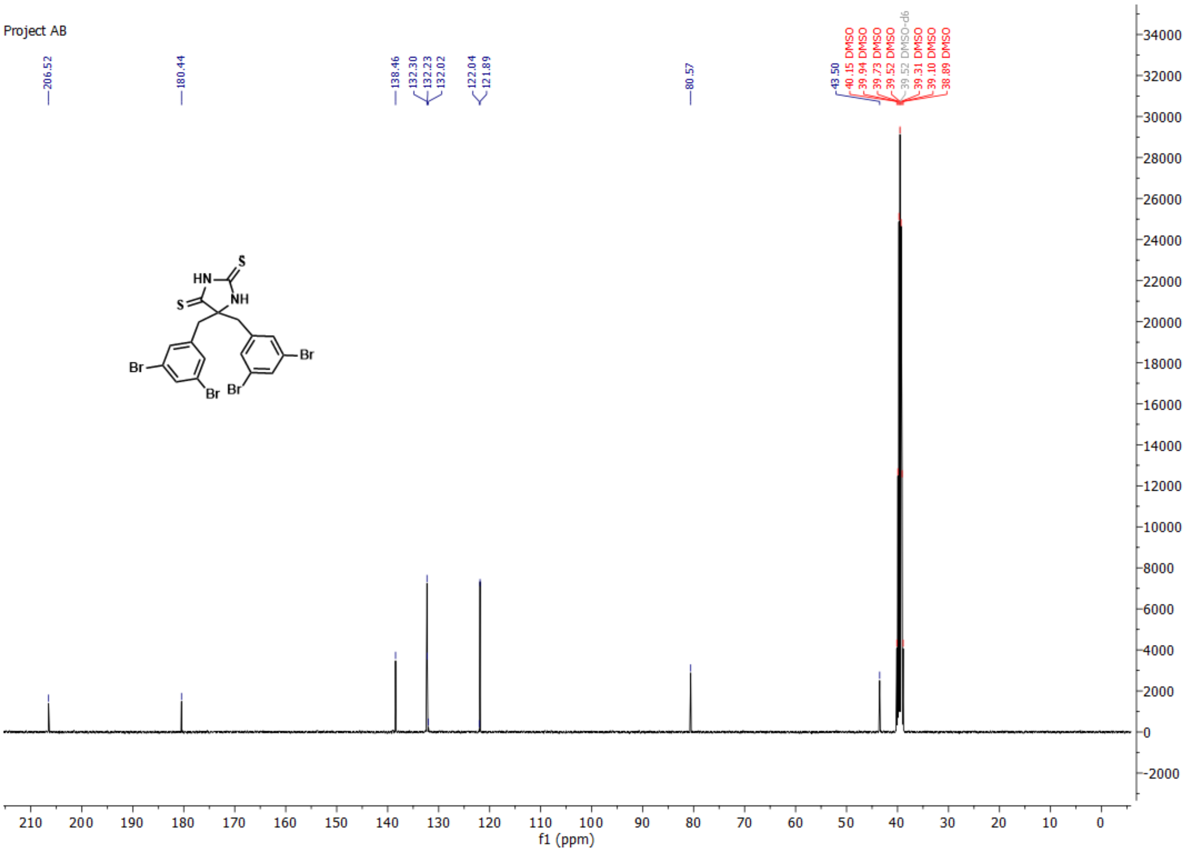

1,3-bis(3-aminopropyl)-5,5-bis(3,5-dibromobenzyl)imidazolidine-2,4-dithione **4A**.

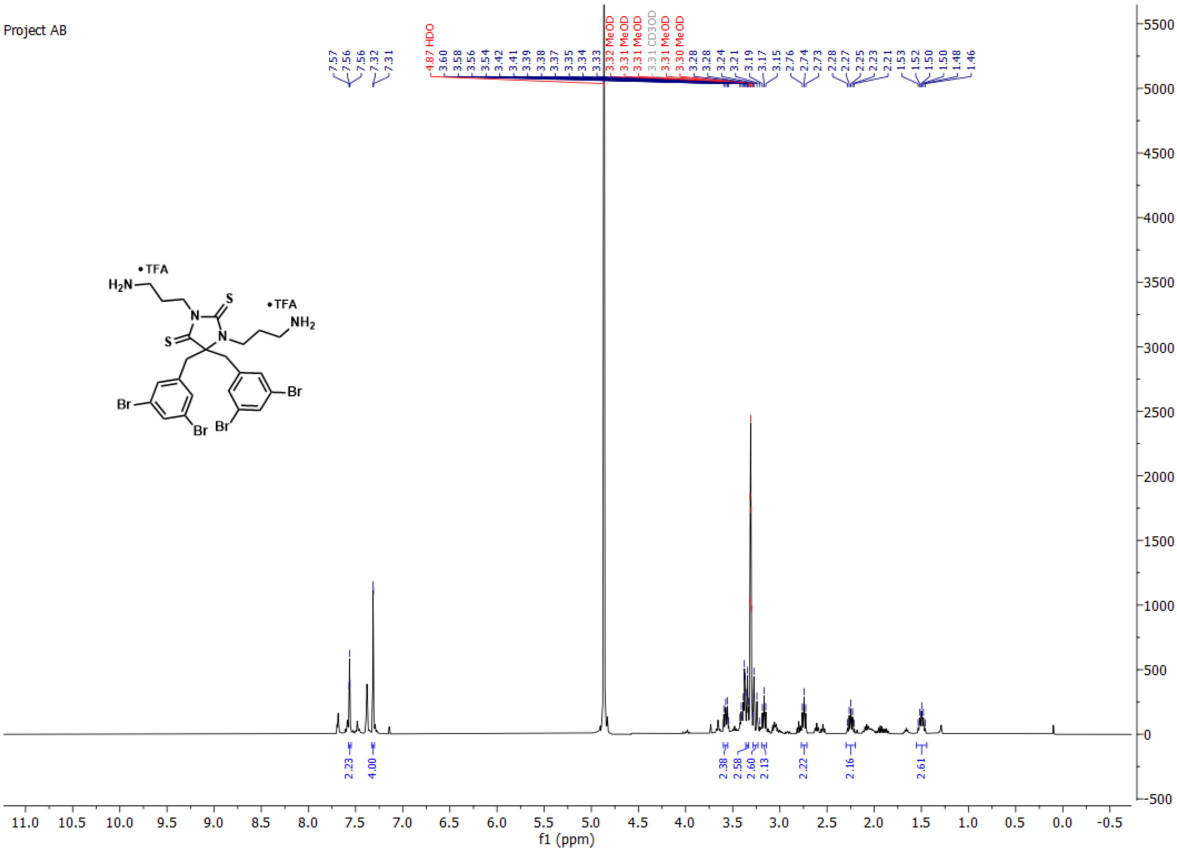

No ^{13}C-NMR was obtained.

4.8 2-Thiobarbituric acid core

5,5-bis(3,5-dibromobenzyl)-2-thioxodihydropyrimidine-4,6(1H,5H)-dione **18**.

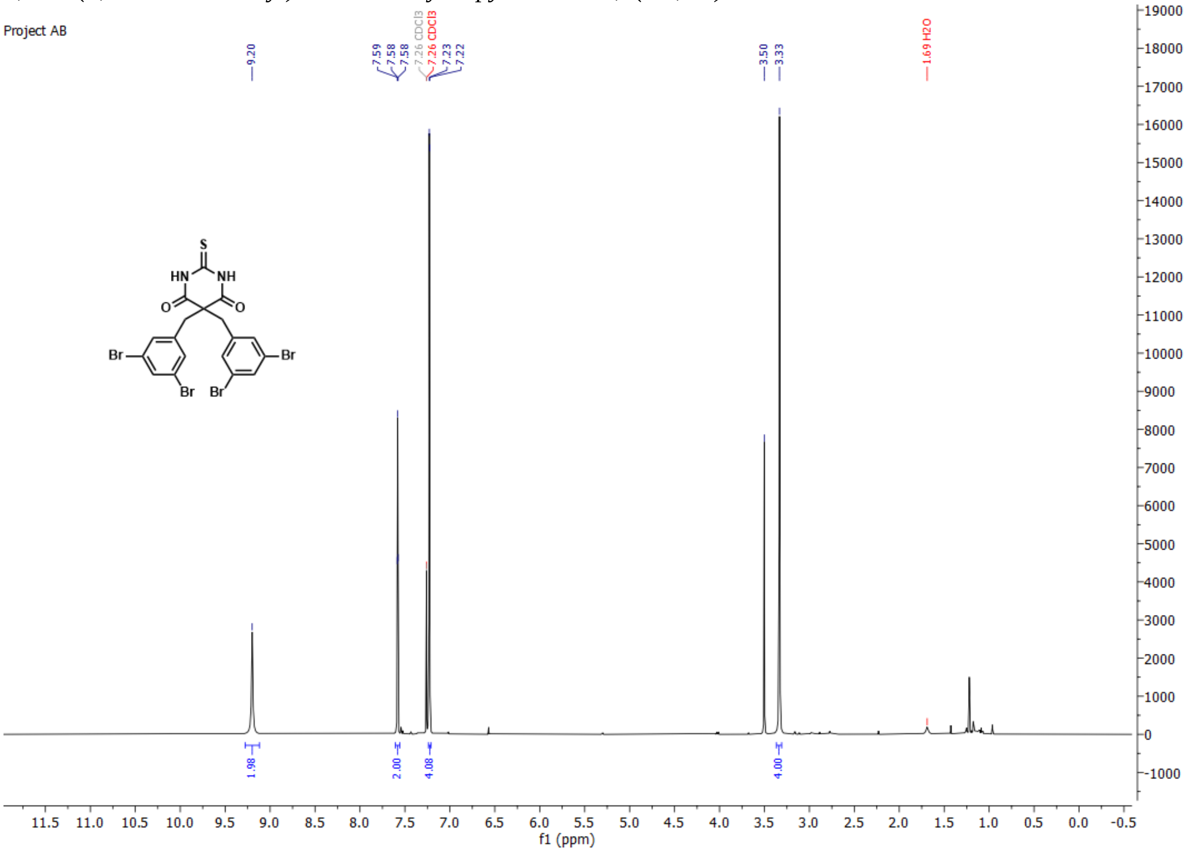

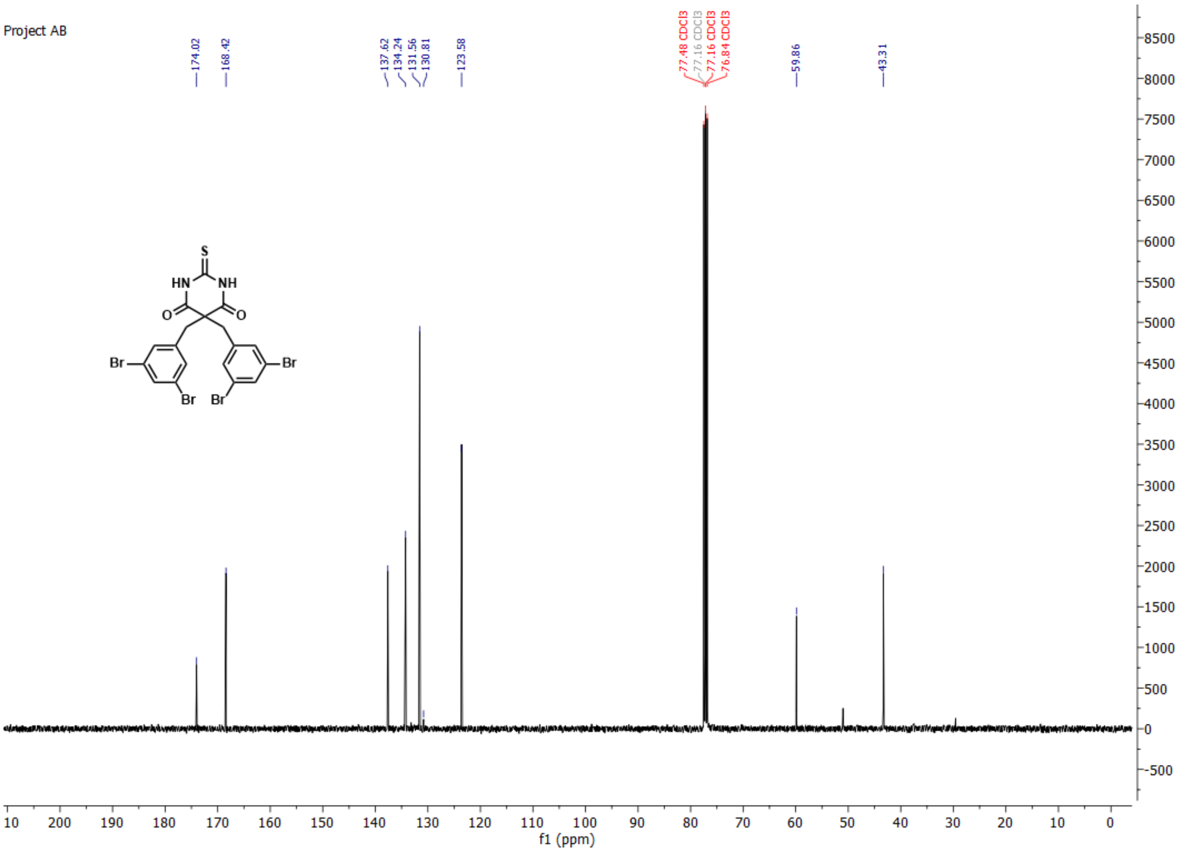

1,3-bis(3-aminopropyl)-5,5-bis(3,5-dibromobenzyl)-2-thioxodihydropyrimidine-4,6(1H,5H)-dione **5A**.

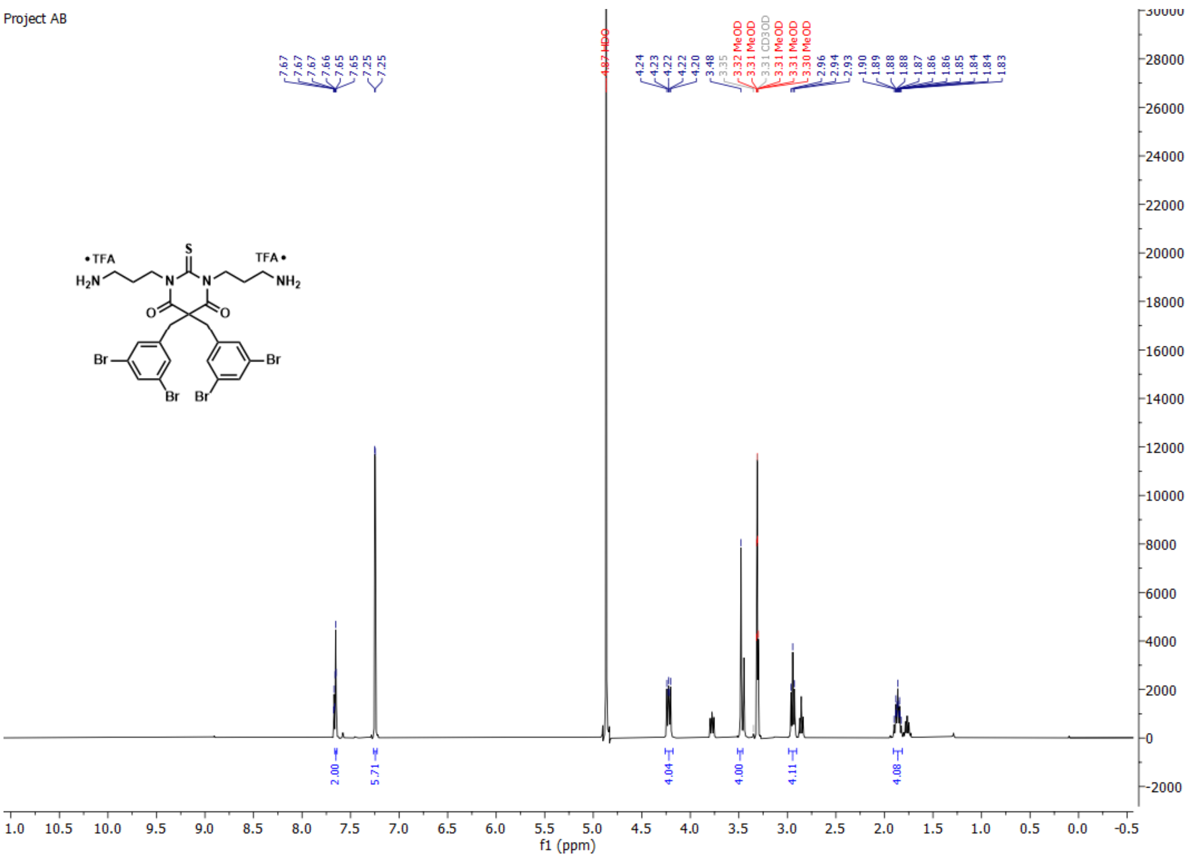

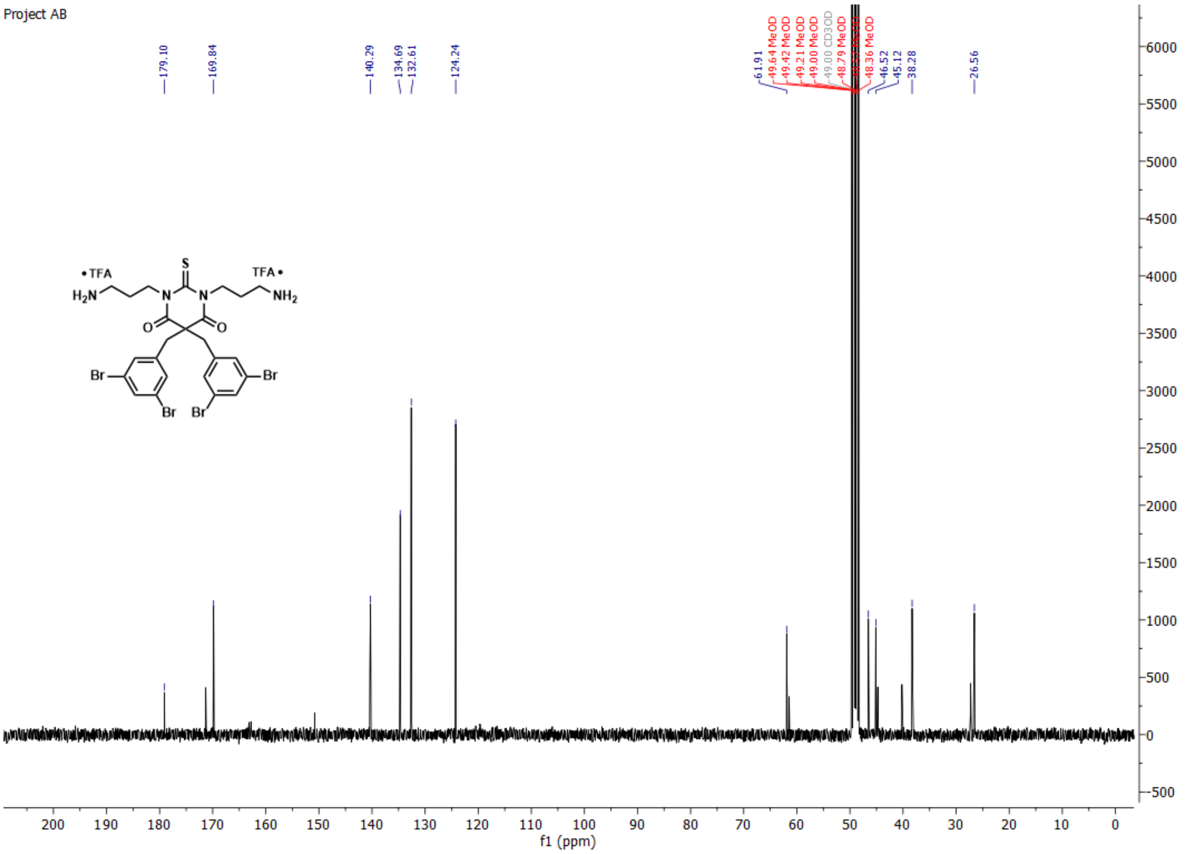

4.9 4-imidazolidin-2-one and its constitutional isomers

(E)/(Z)-1,3-dibromo-5-(2-methoxyvinyl)benzene **S9**.

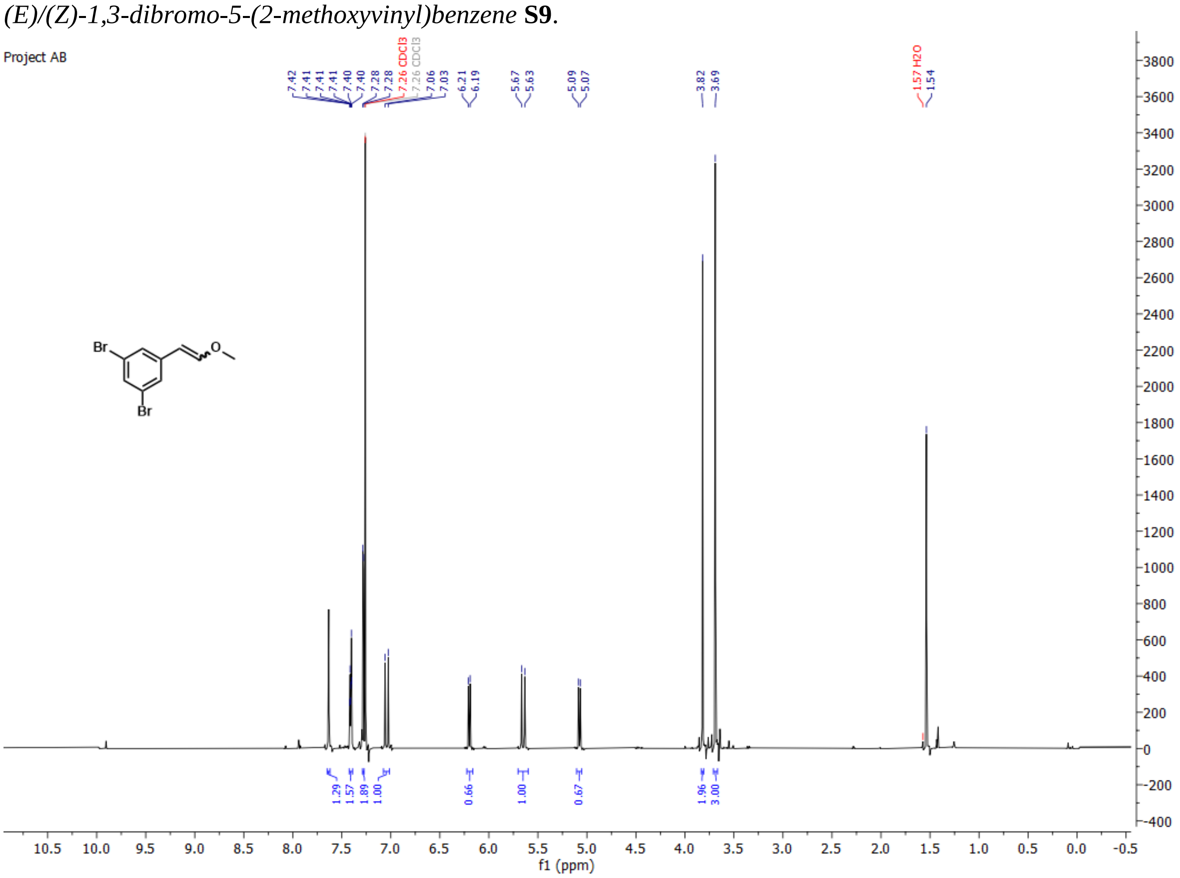

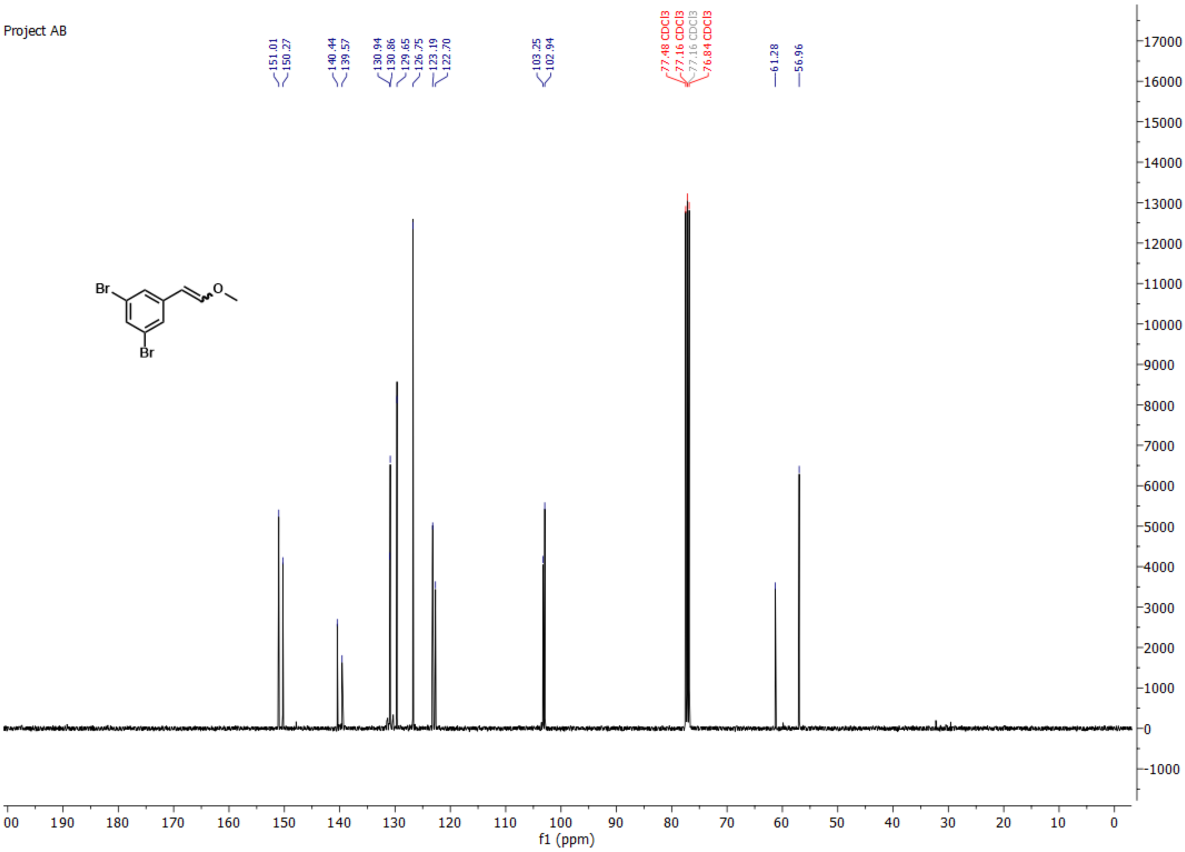

2-(3,5-dibromophenyl)acetaldehyde **11**.

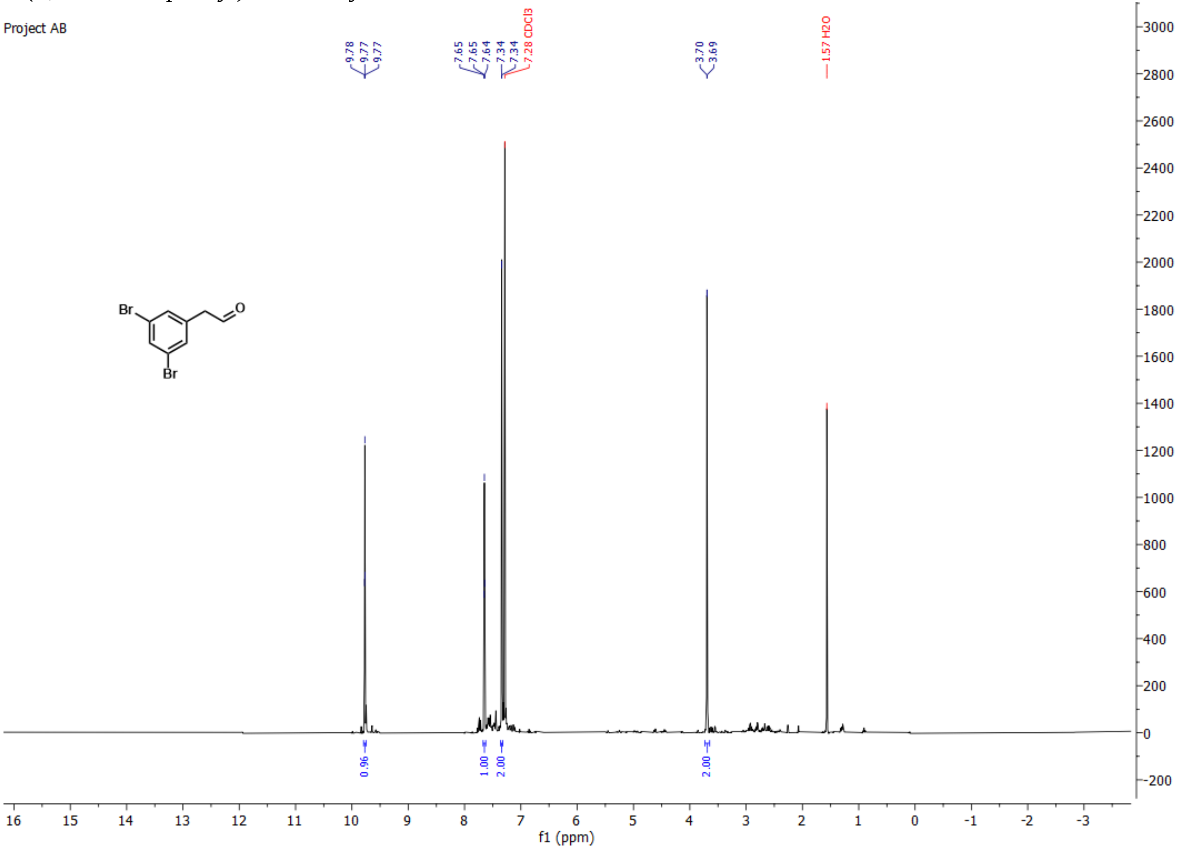

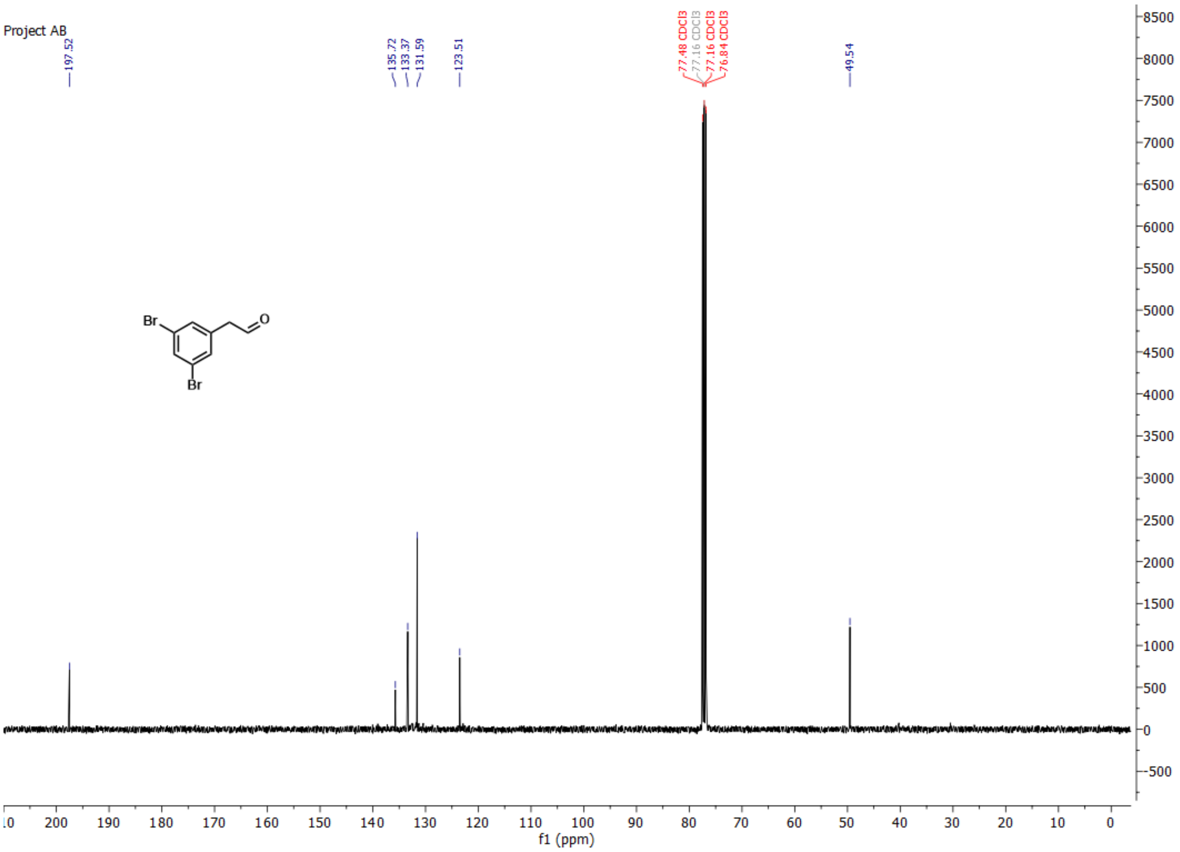

1,4-bis(3,5-dibromophenyl)-3-hydroxybutan-2-one **12**.

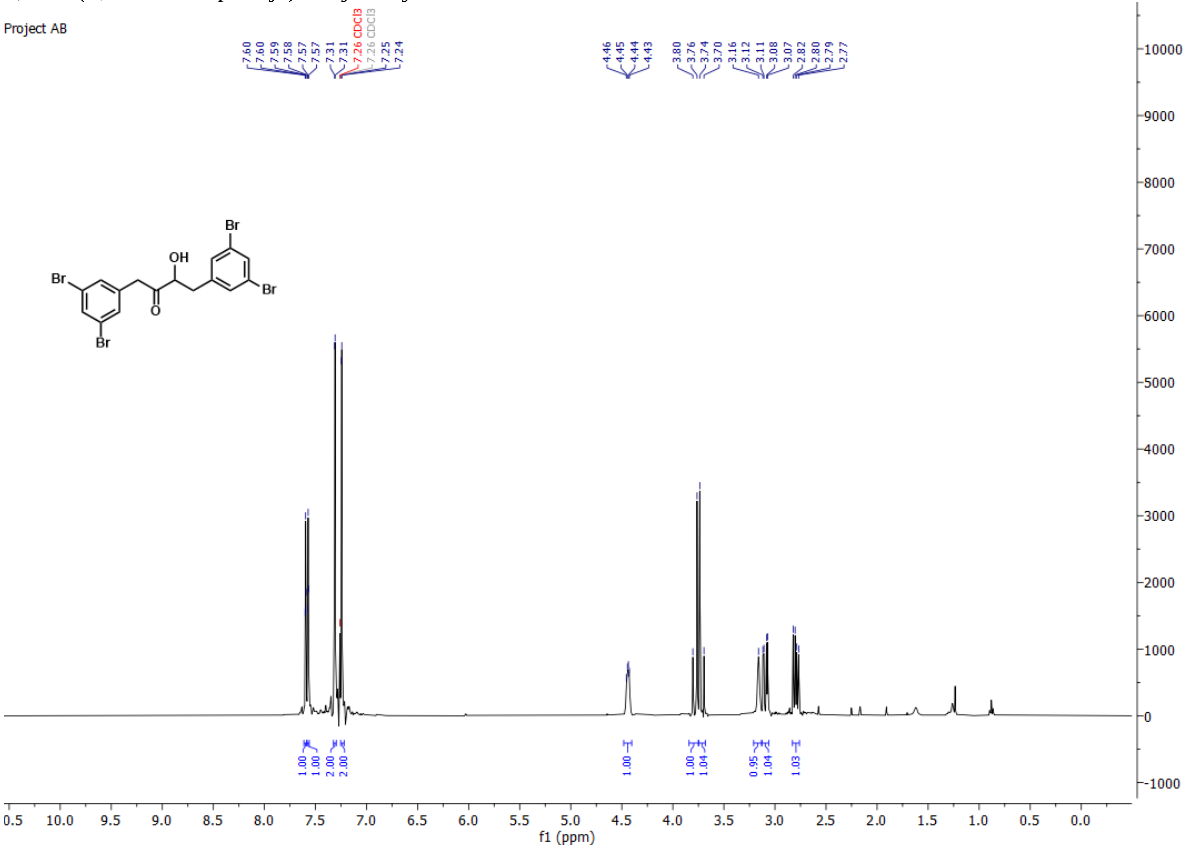

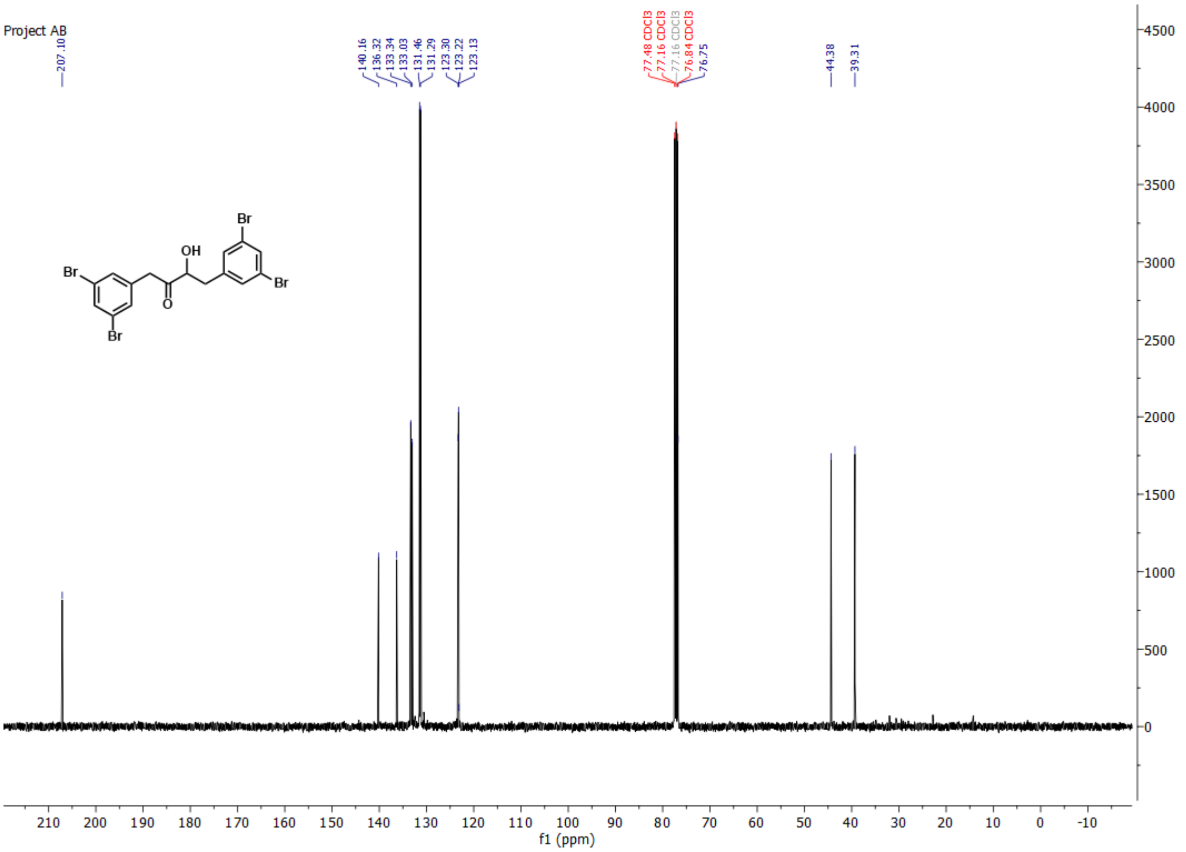

4,5-bis(3,5-dibromobenzyl)-1,3-dihydro-2H-imidazol-2-one **14**.

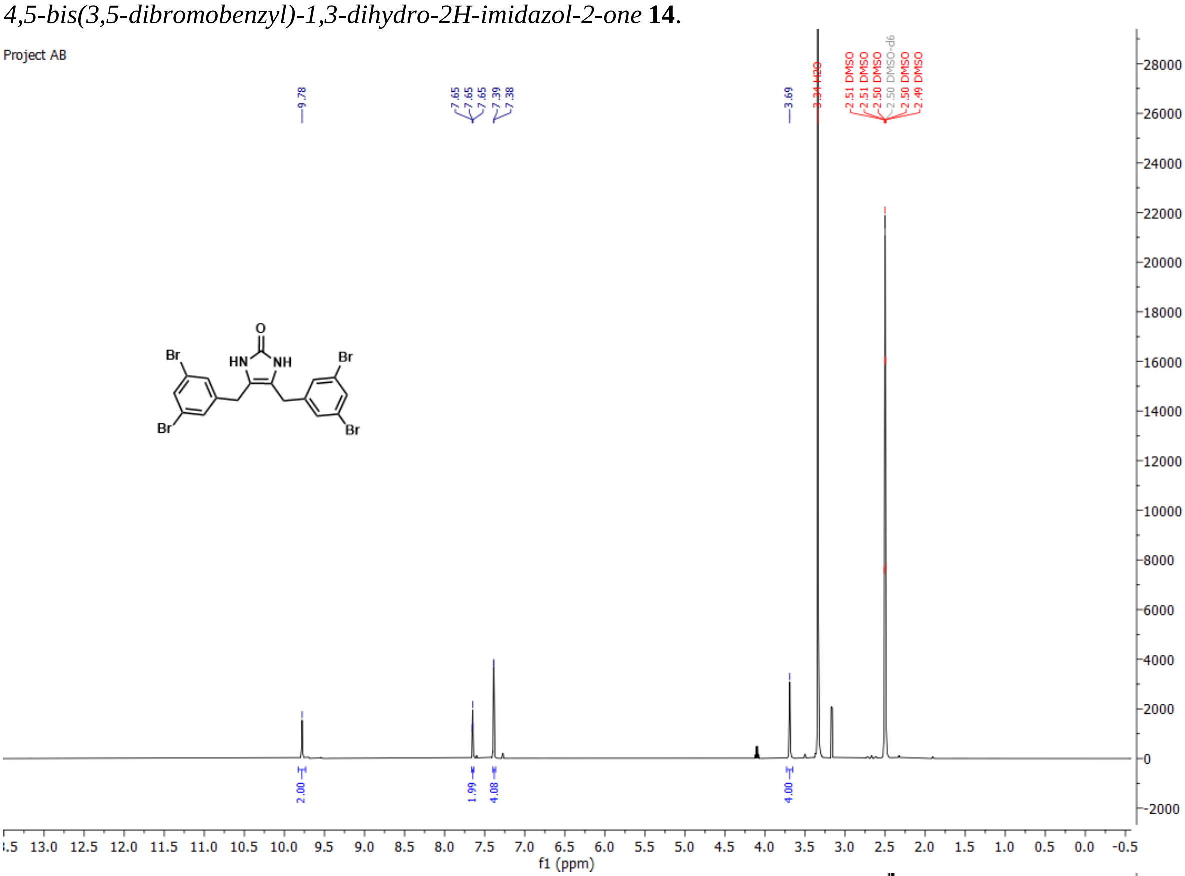

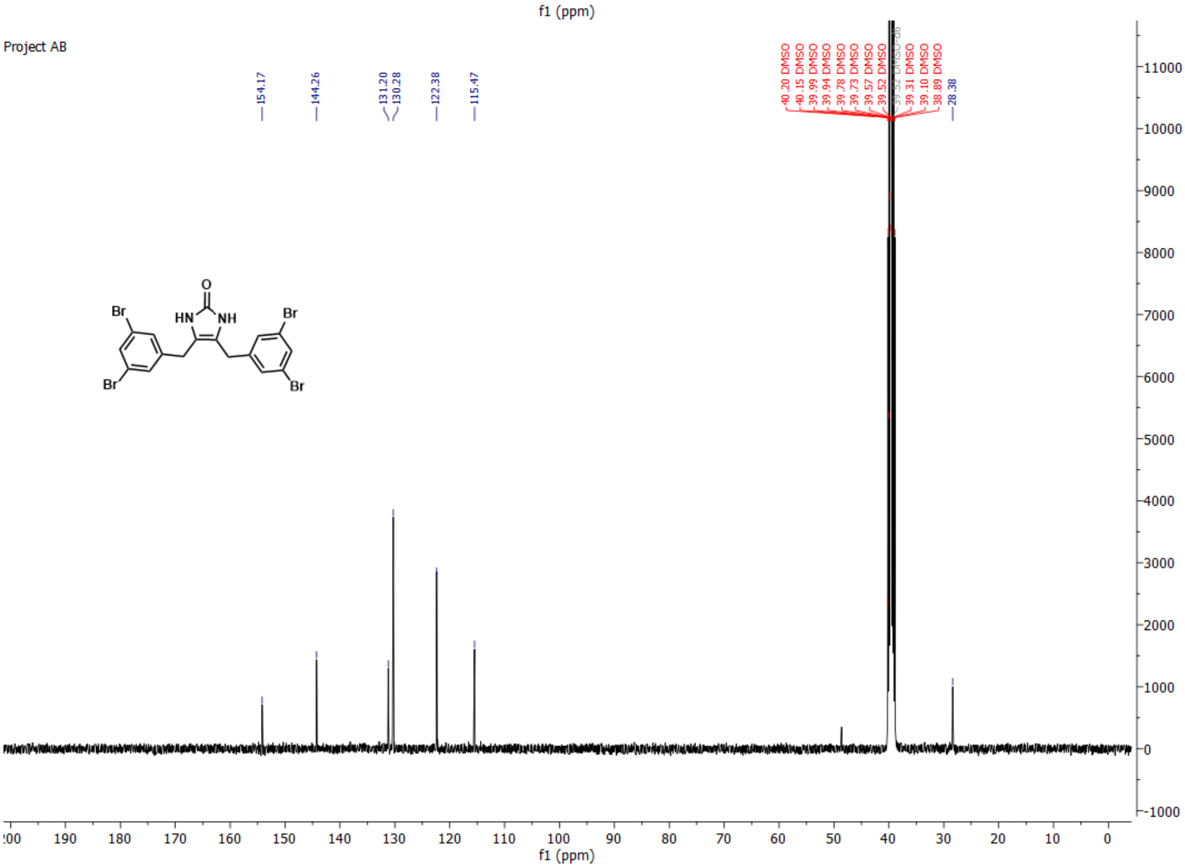

4,5-bis(3,5-dibromobenzyl)oxazol-2(3H)-imine **13**.

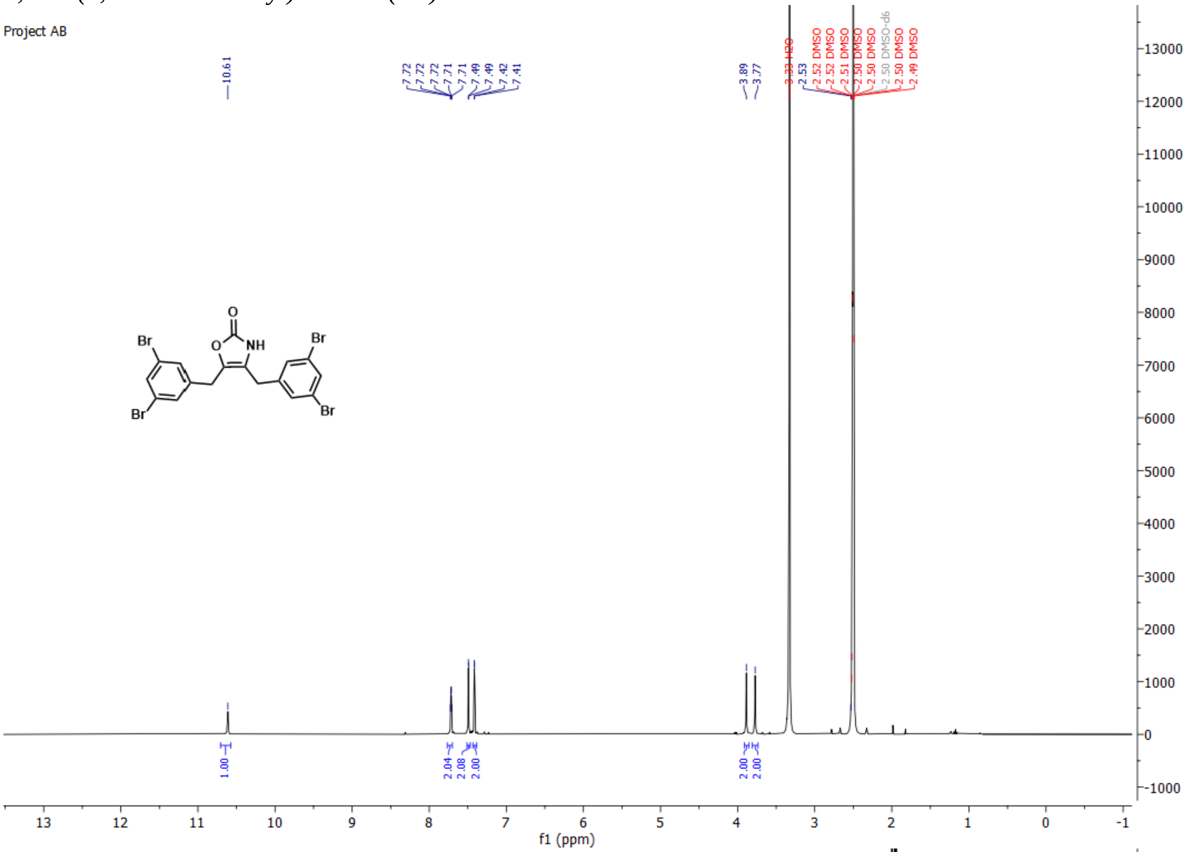

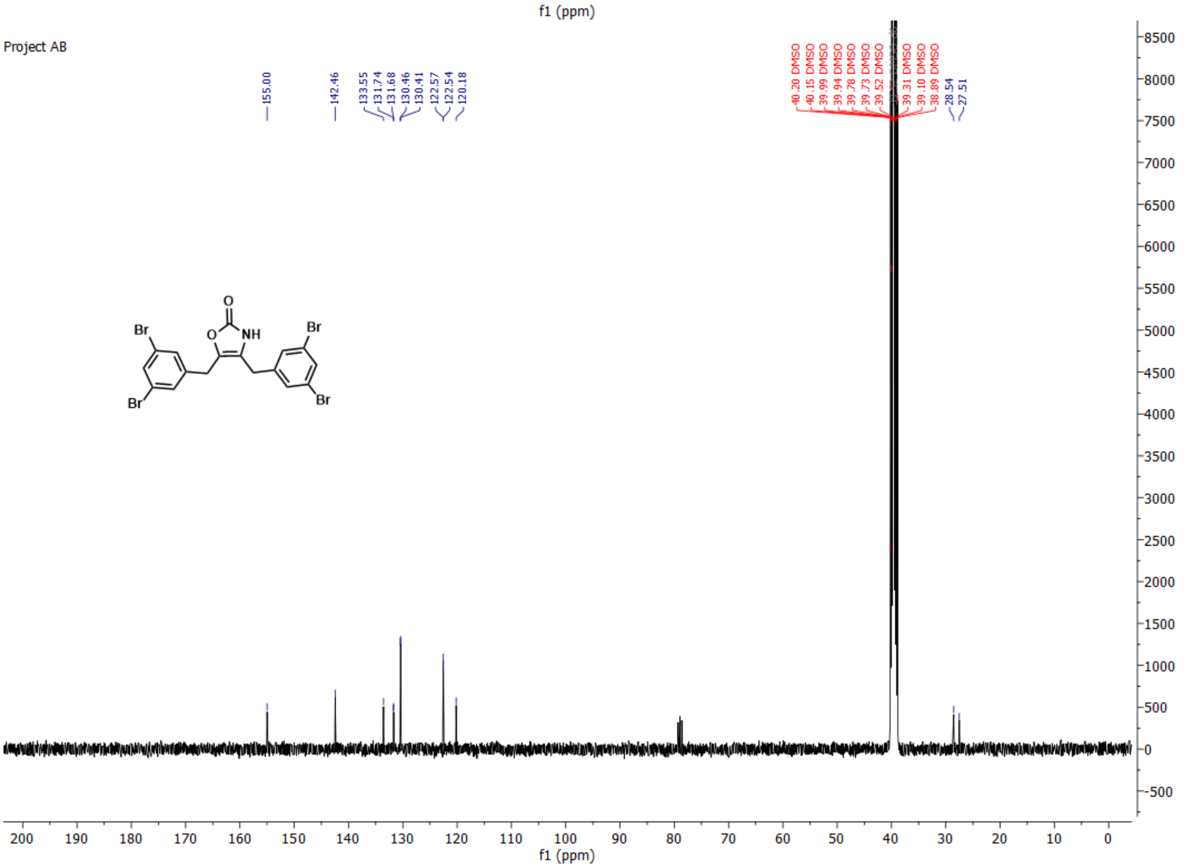

1,3-bis(3-aminopropyl)-4,5-bis(3,5-dibromobenzyl)-1,3-dihydro-2H-imidazol-2-one **3A**.

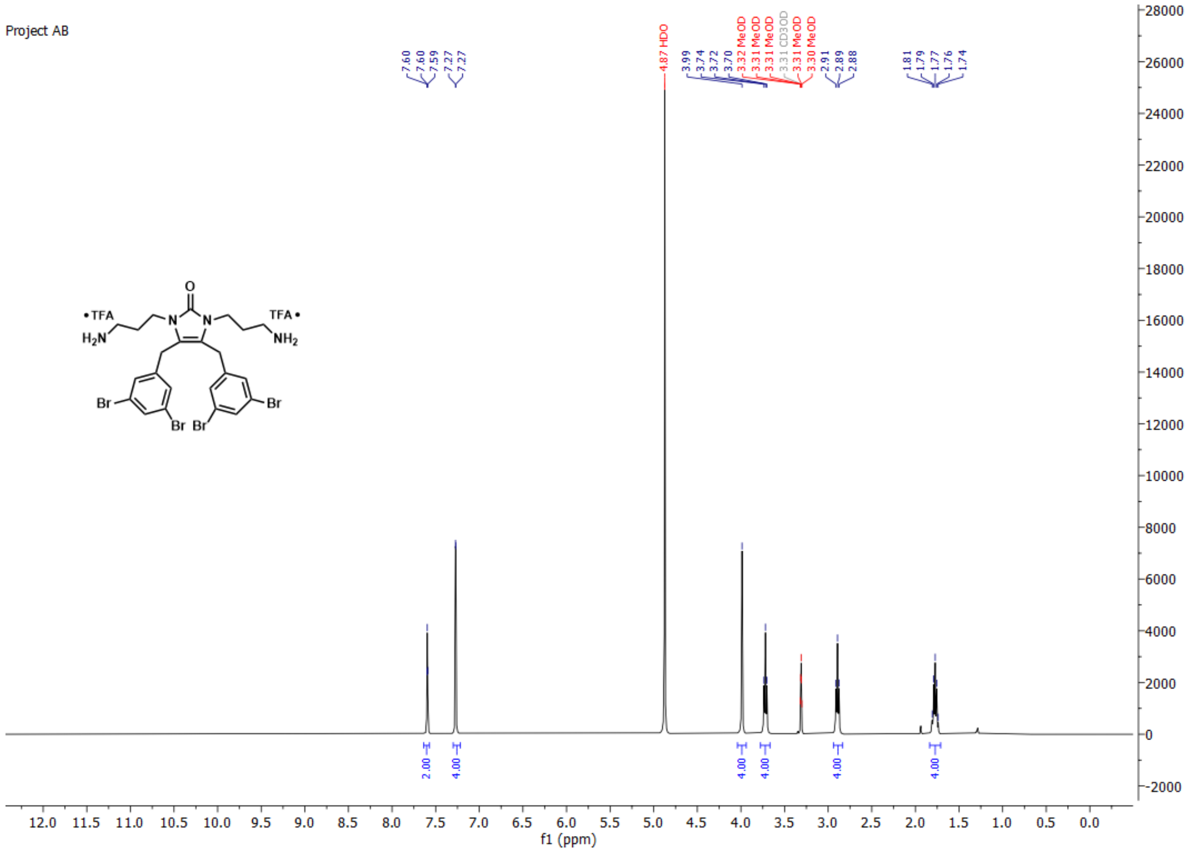

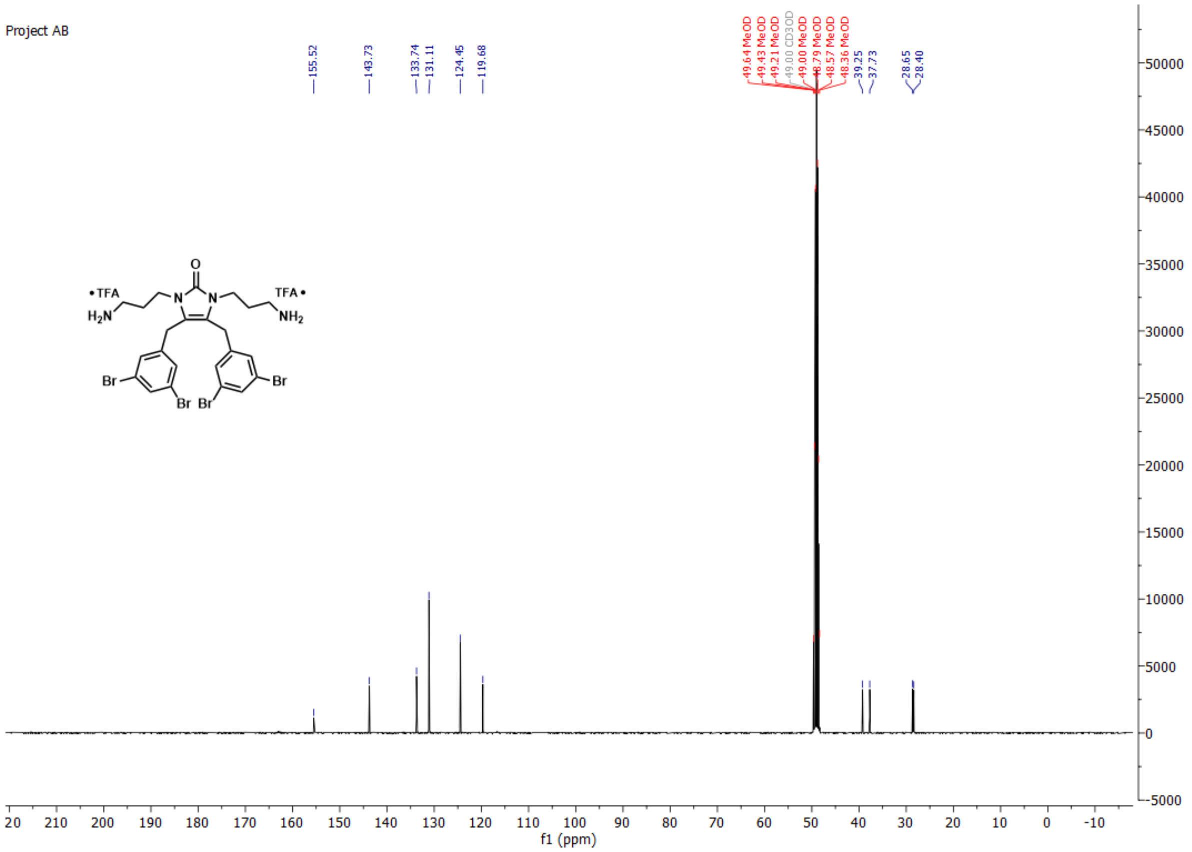

3-(2-(3-aminopropoxy)-4,5-bis(3,5-dibromobenzyl)-1H-imidazol-1-yl)propan-1-amine **15A**.

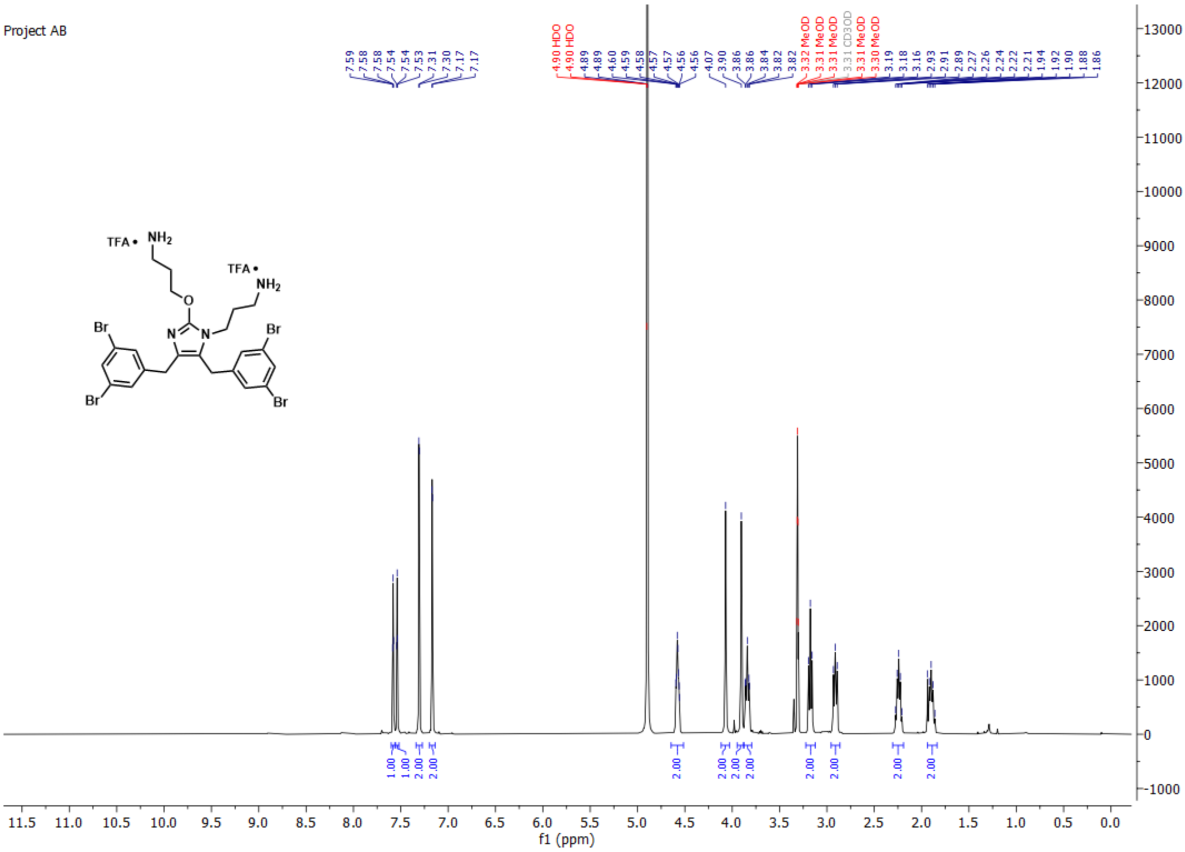

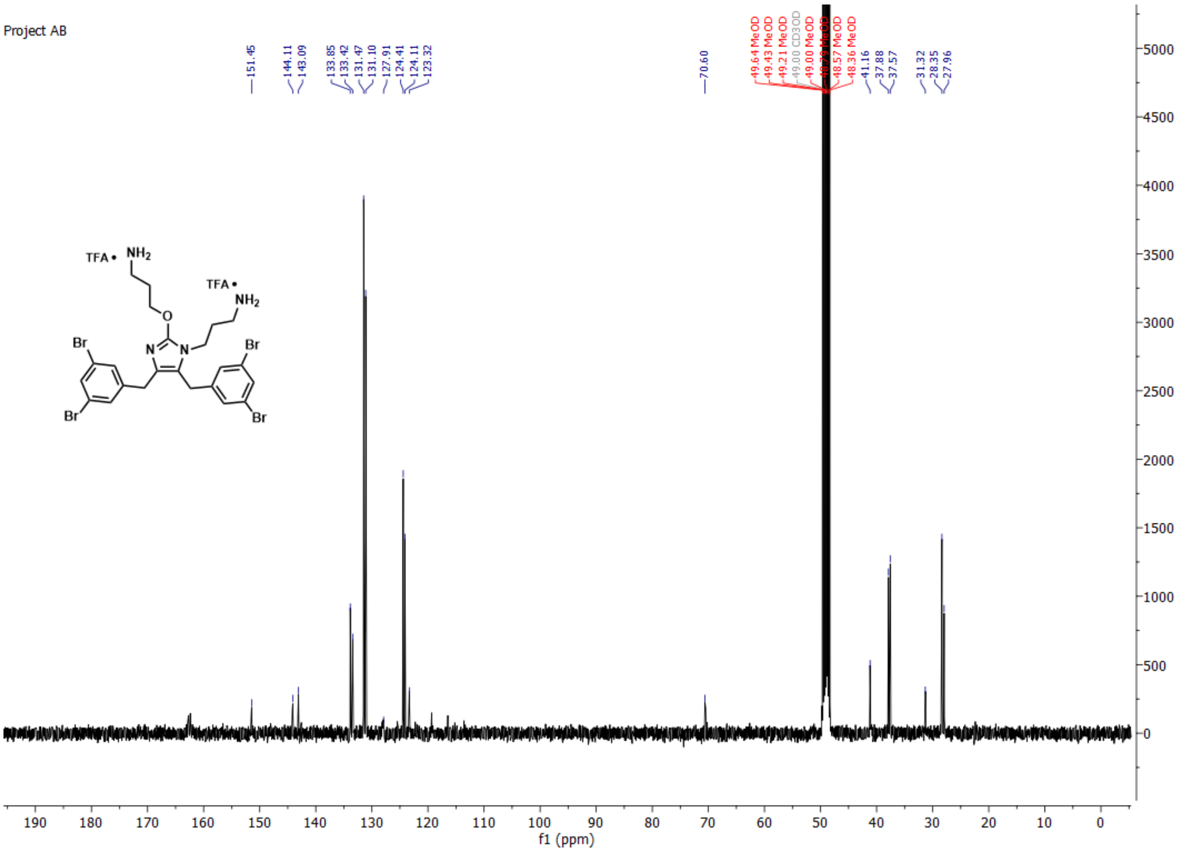

4.10 4-imidazolidin-2-one *via N*-acyliminium ion rearrangement

Di-tert-butyl 4,4-dibenzyl-2,5-dioxoimidazolidine-1,3-dicarboxylate Boc-**9a**.

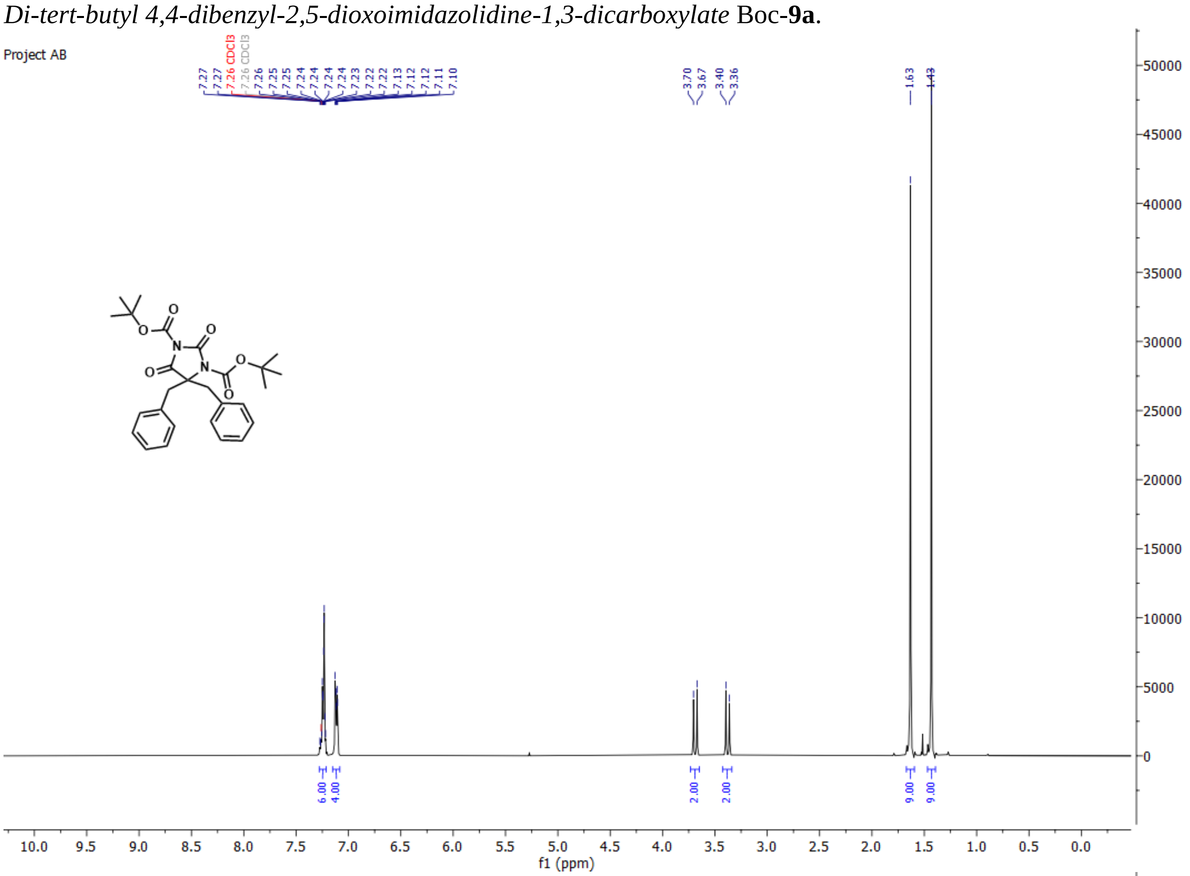

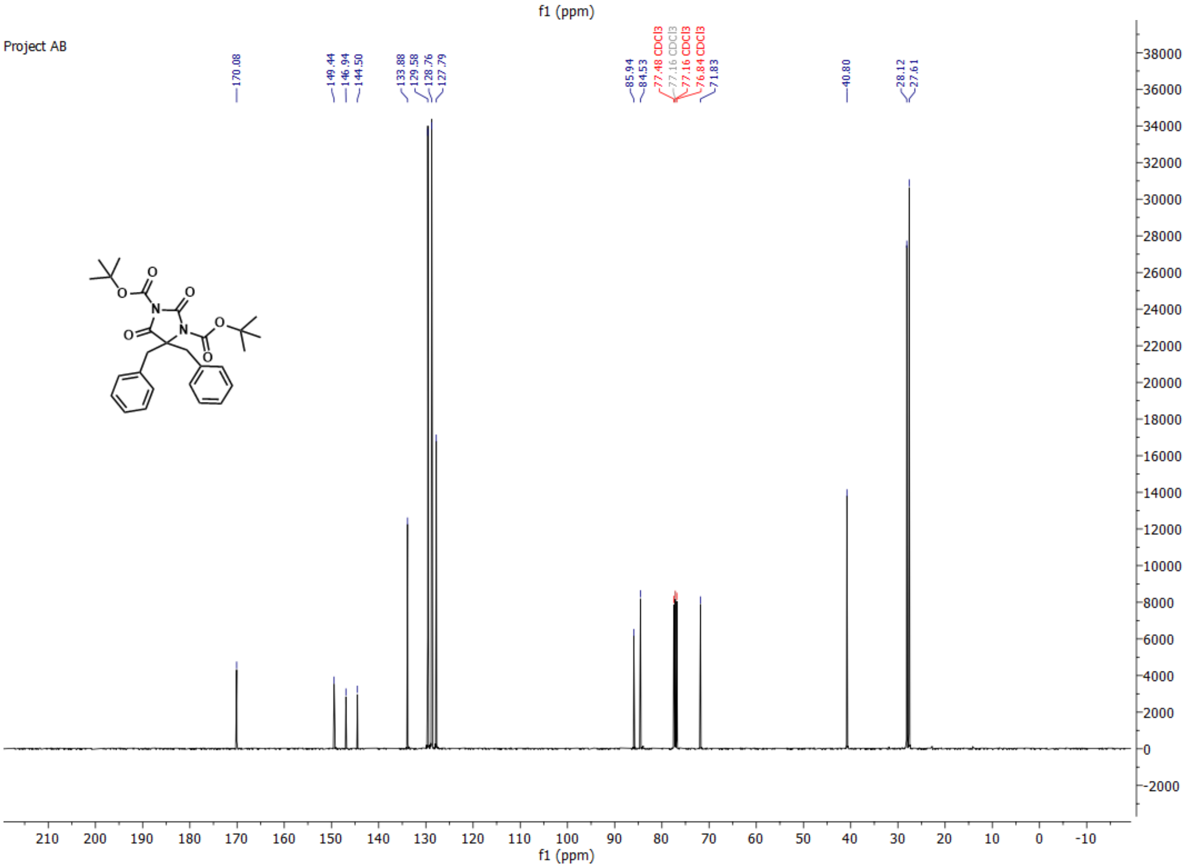

Di-tert-butyl ((4,4-dibenzyl-5-hydroxy-2-oxoimidazolidine-1,3-diyl)bis(propane-3,1-diyl))dicarbamate **S2**.

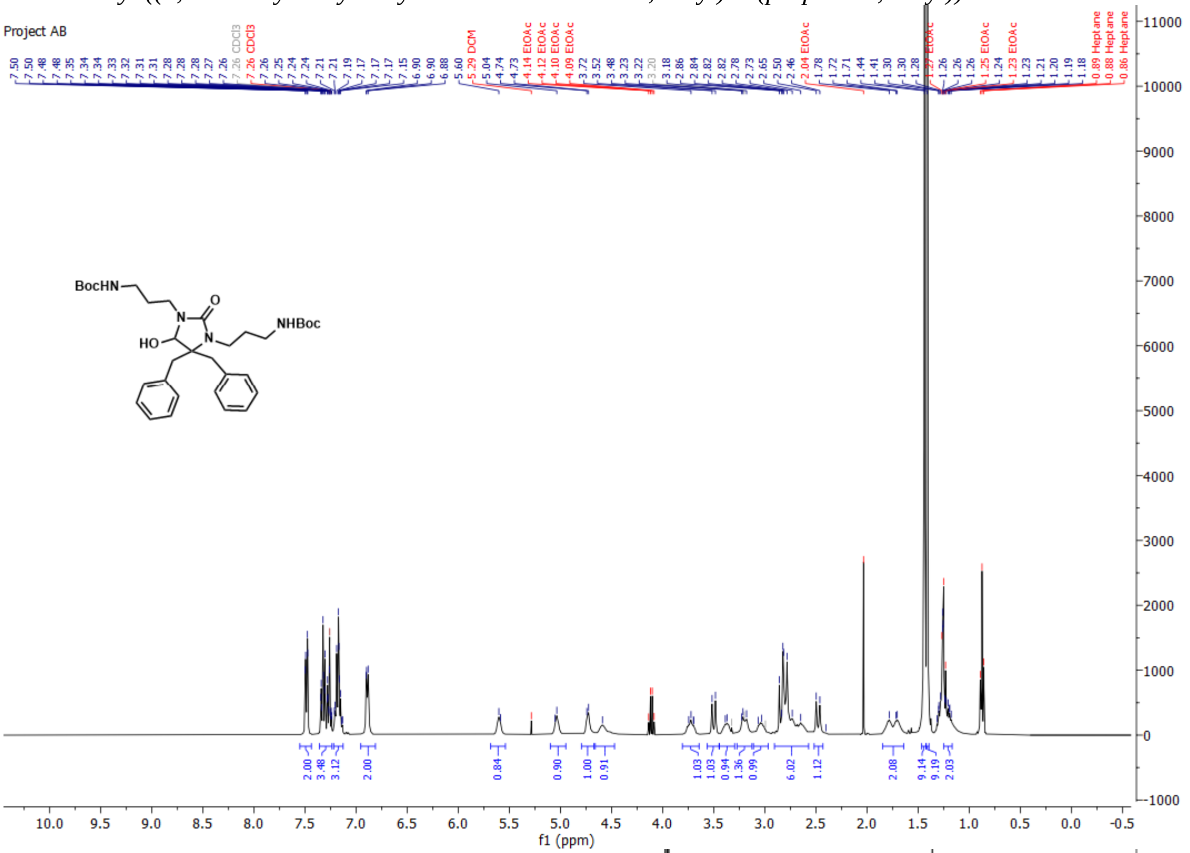

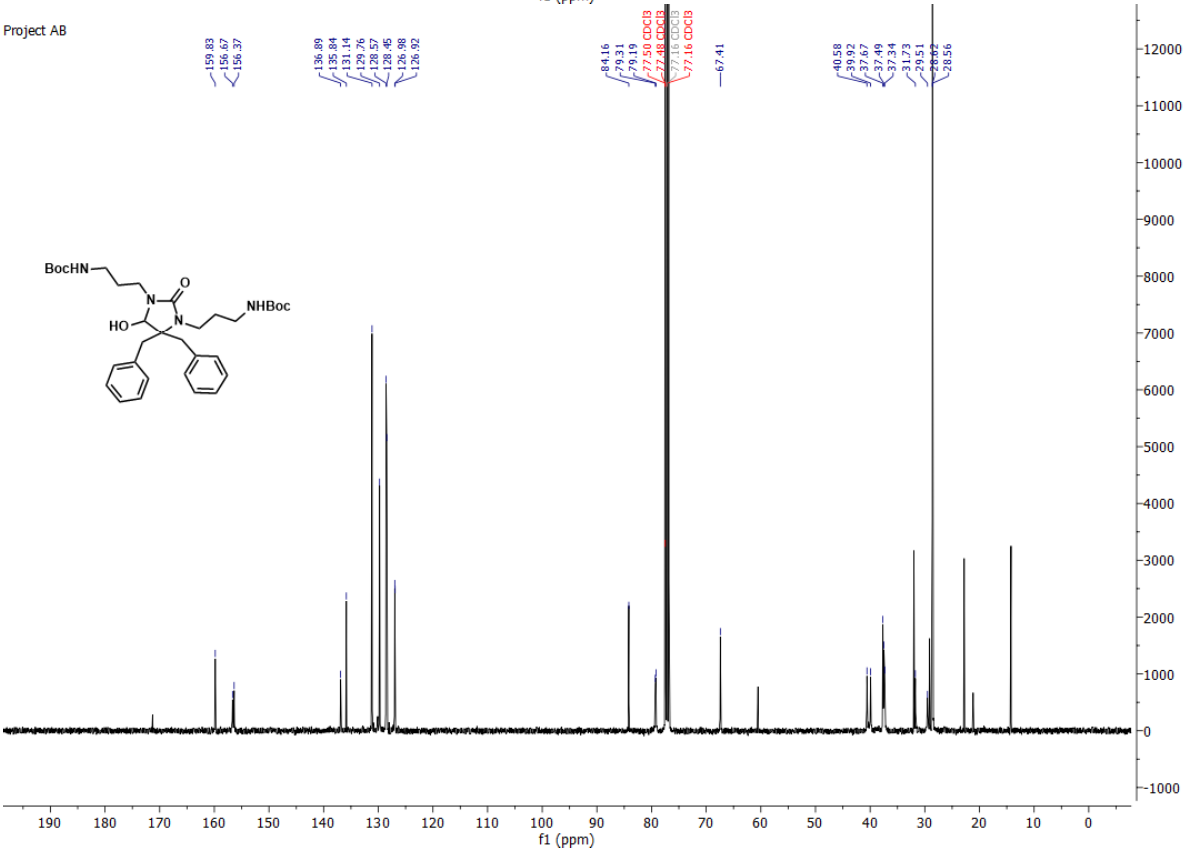

Di-tert-butyl ((4,4-bis(3,5-dibromobenzyl)-5-hydroxy-2-oxoimidazolidine-1,3-diyl)bis(propane-3,1-diyl))dicarbamate **S3**.

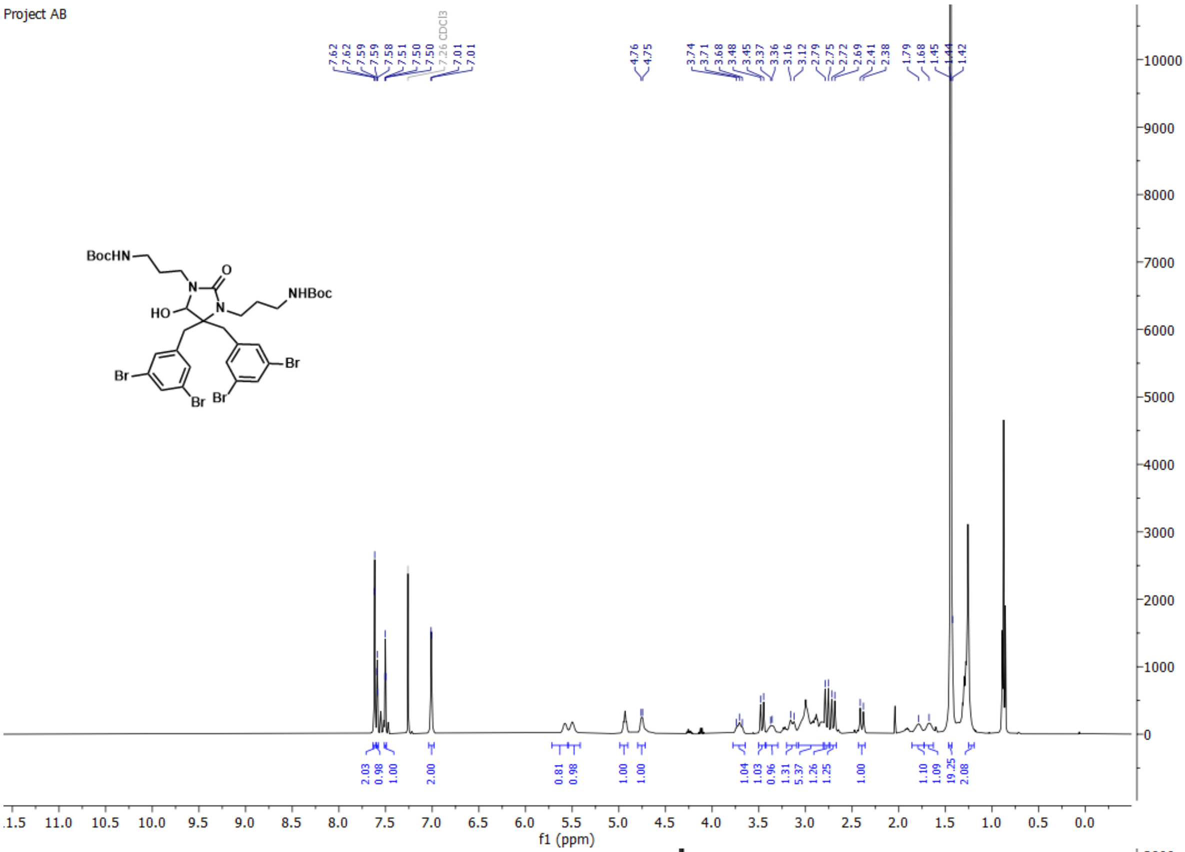

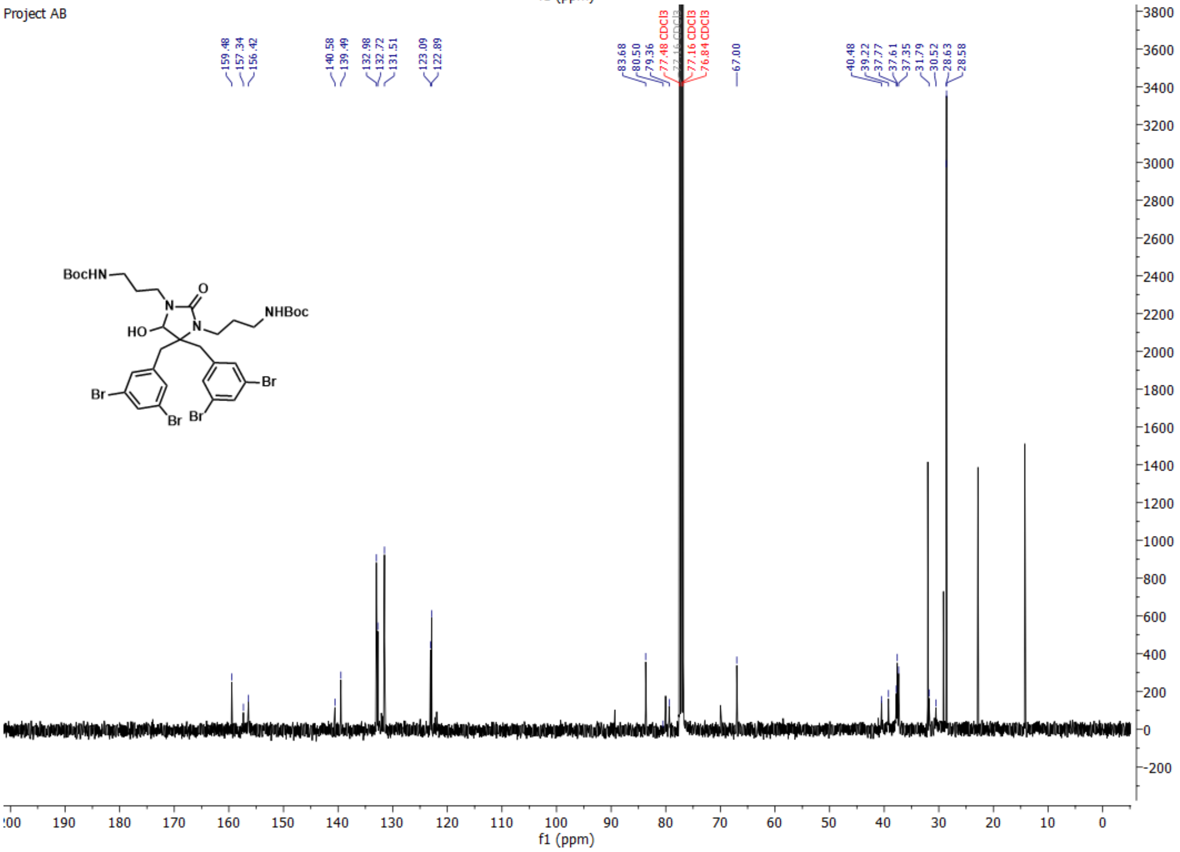

4,4-dibenzylimidazolidin-2-one **S4**.

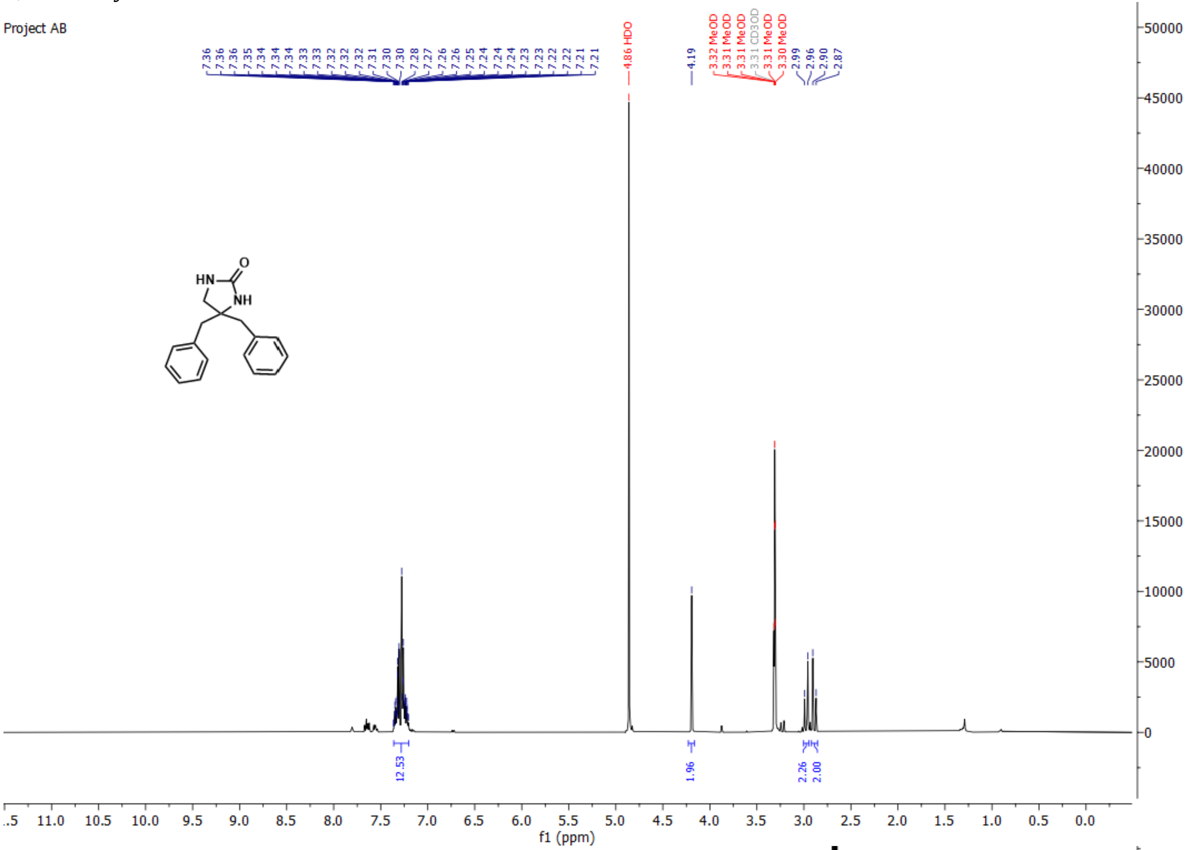

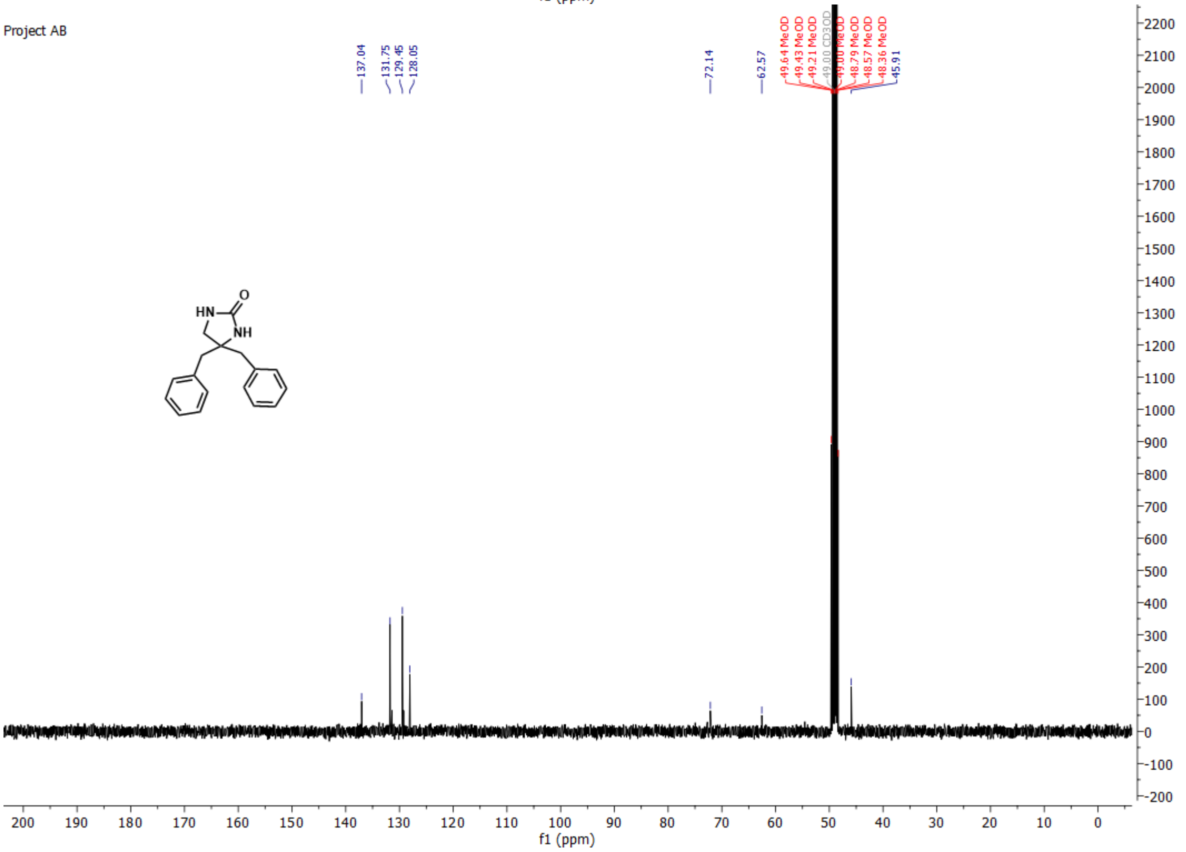

1,3-bis(3-aminopropyl)-4,5-dibenzyl-1,3-dihydro-2H-imidazol-2-one **S5**.

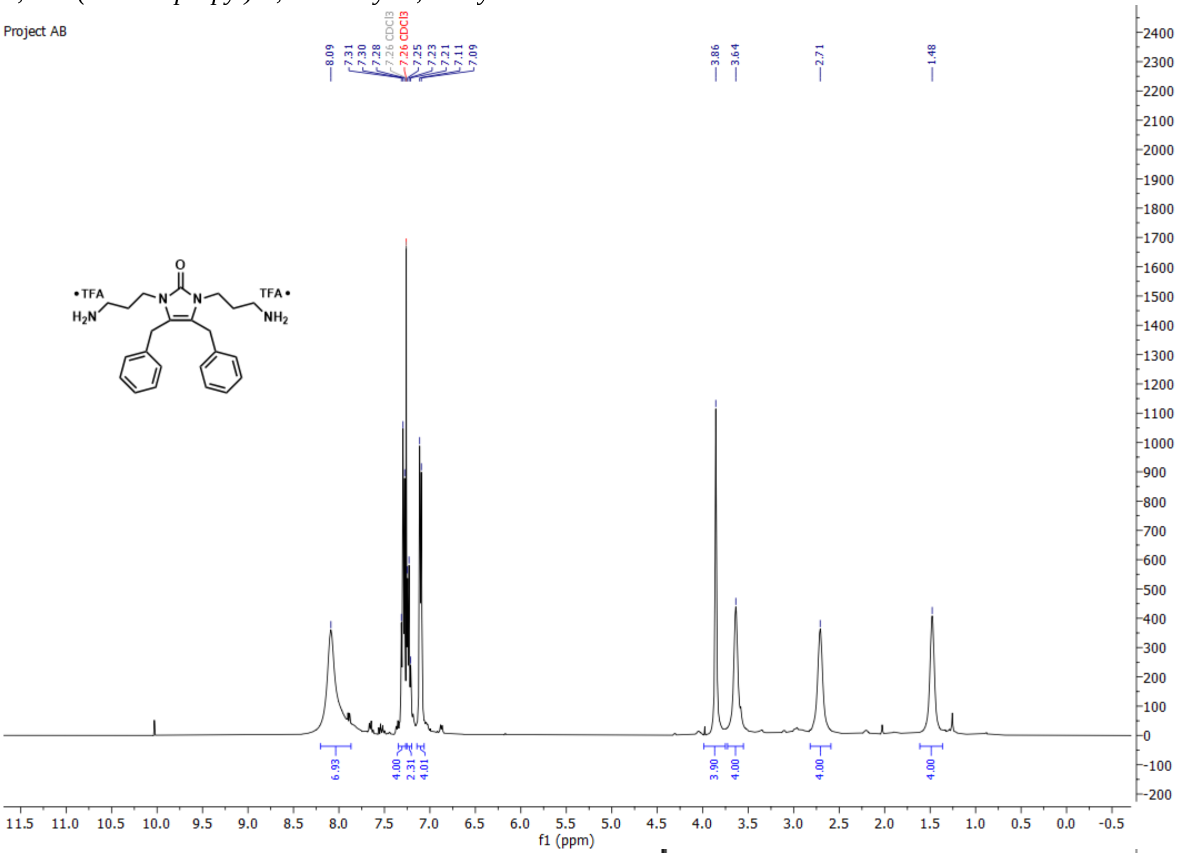

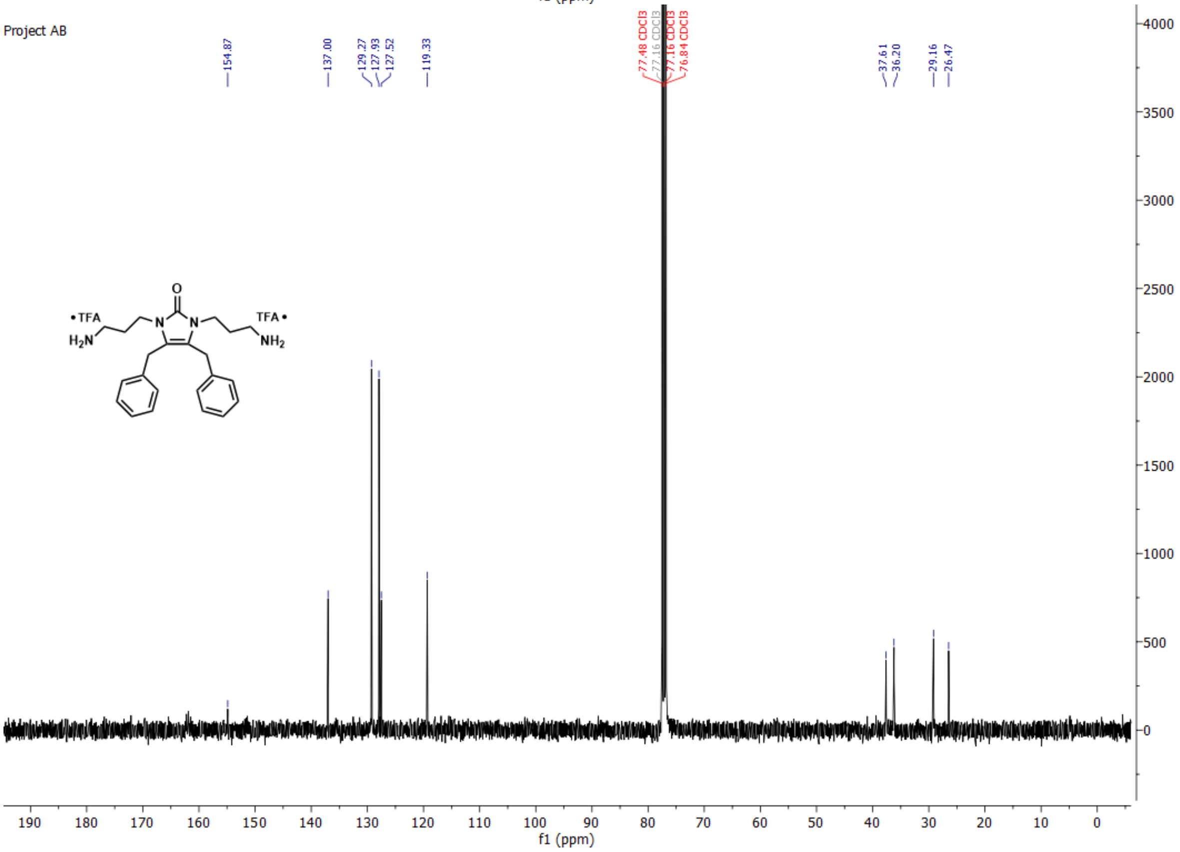

5. SFC traces

5.1 Scaffolds **3A**, **4A**, **5A** and **15A**

For compounds **4A** and **5A** no SFC traces were obtained.

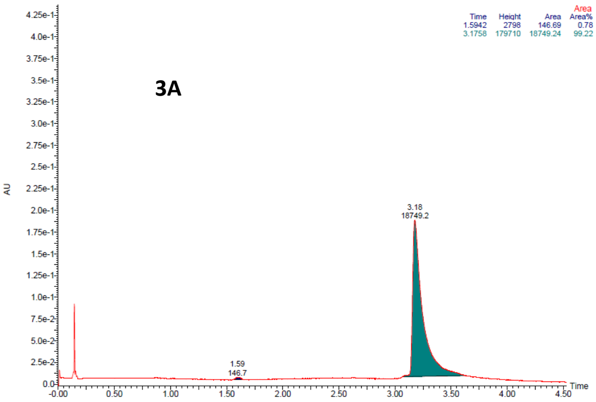

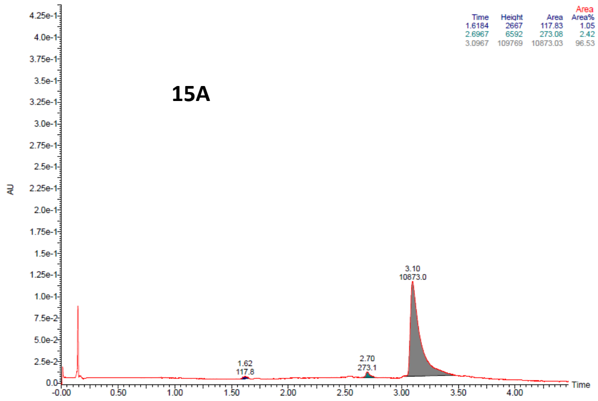

5.2 Hydantoins **2A** and **2G**

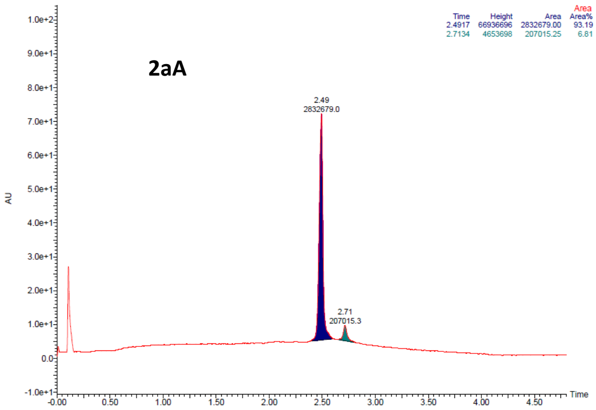

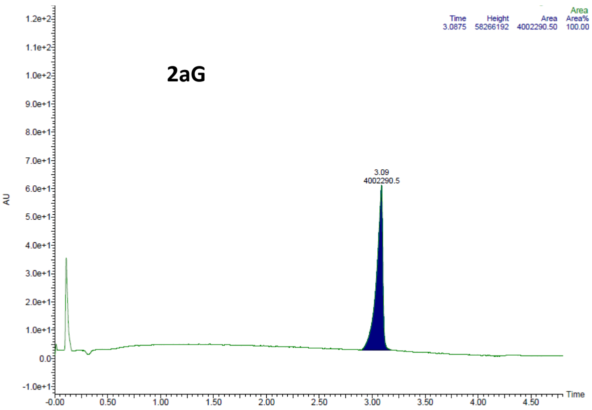

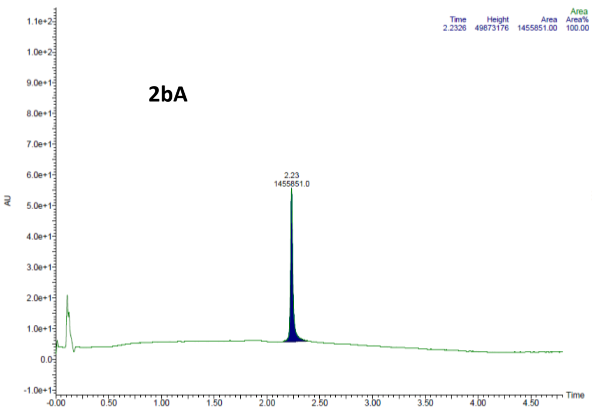

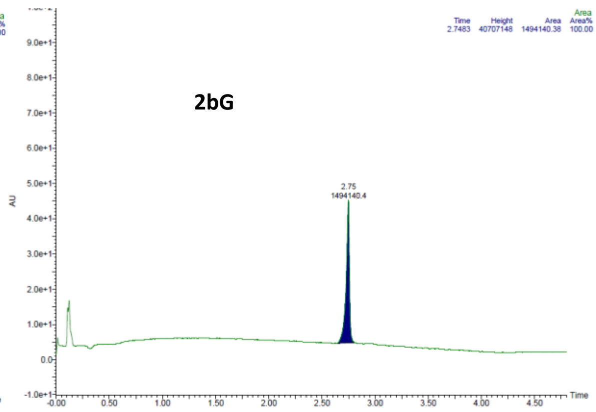

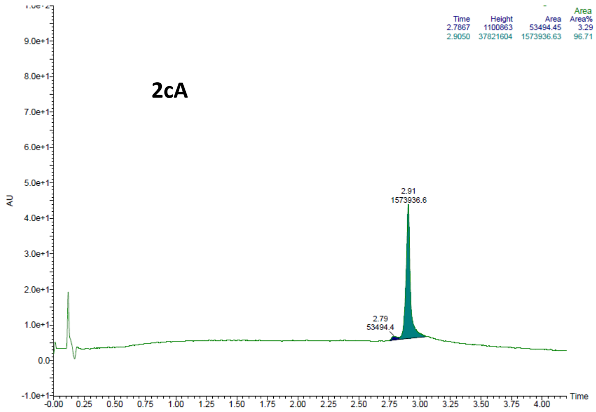
2cA
Time Height Area Area%
2.7867 1100863 53494.45 3.29
2.9050 37821604 1573936.63 96.71
2.91
1573936.6
2.79
53494.4
AU
Time
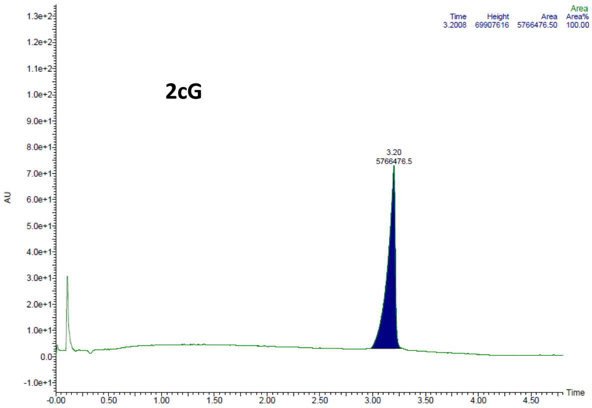
2cG
Time Height Area Area%
3.2008 69907616 5766476.50 100.00
3.20
5766476.5
AU
Time
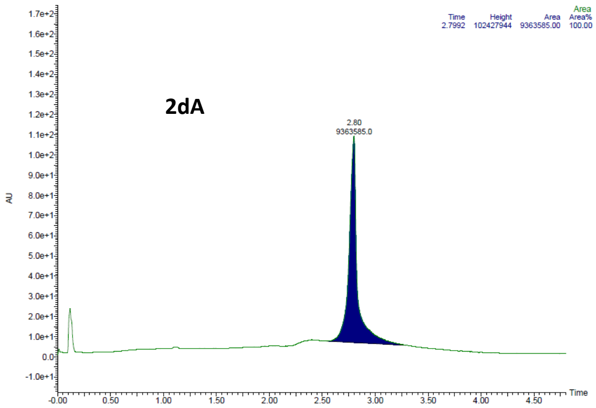
2dA
Time Height Area Area%
2.7992 102427944 9363585.00 100.00
2.80
9363585.0
AU
Time
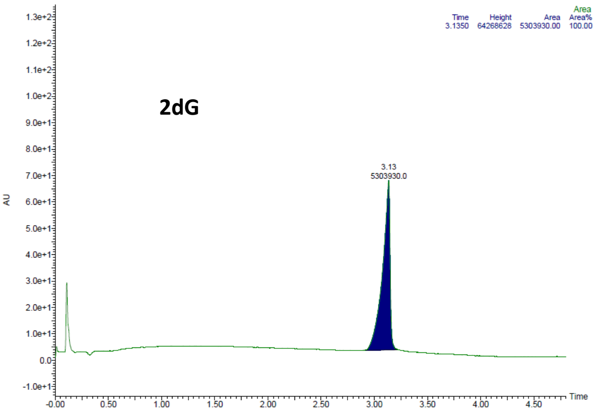
2dG
Time Height Area Area%
3.1350 64268628 5303930.00 100.00
3.13
5303930.0
AU
Time
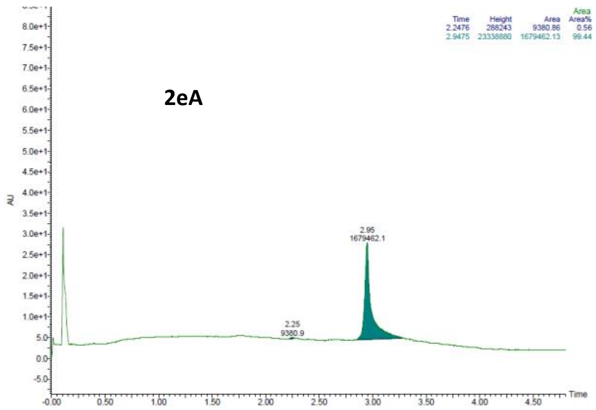
2eA
Time Height Area Area%
2.2476 288243 9380.86 0.56
2.9475 23338880 1679462.13 99.44
2.95
1679462.1
2.25
9380.9
AU
Time
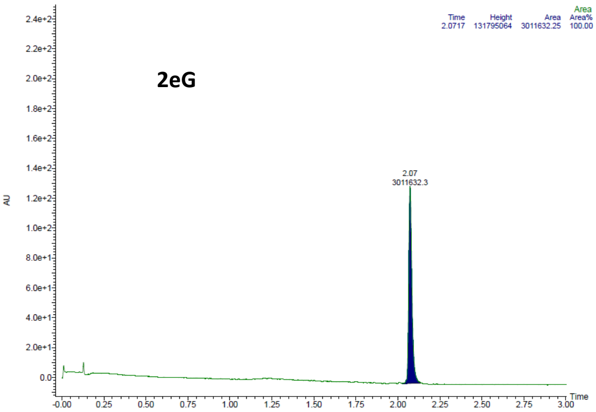
2eG
Time Height Area Area%
2.0717 131795064 3011632.25 100.00
2.07
3011632.3
AU
Time
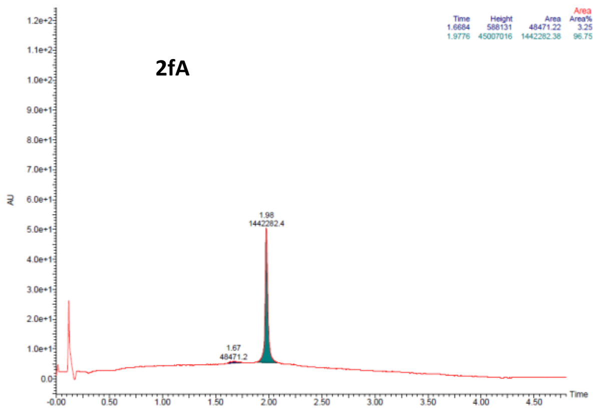
2fA
Time Height Area Area%
1.6684 588131 48471.22 3.25
1.9776 45007016 1442282.38 96.75
1.98
1442282.4
1.67
48471.2
AU
Time
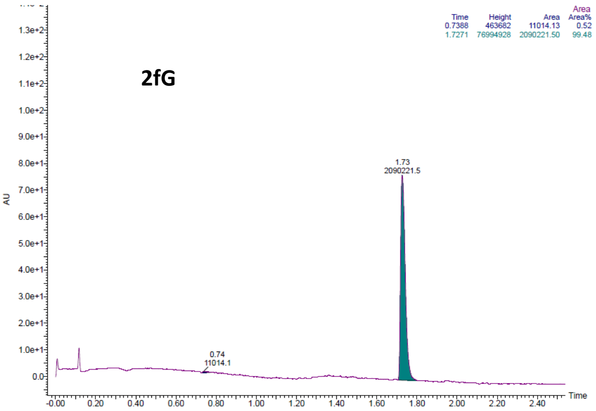
2fG
Time Height Area Area%
0.7388 463682 11014.13 0.52
1.7271 76994928 2090221.50 99.48
1.73
2090221.5
0.74
11014.1
AU
Time

5.3 Hydantoins **6A** and **6G**

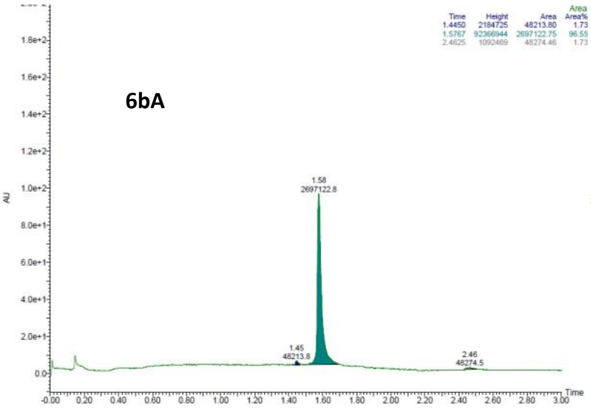

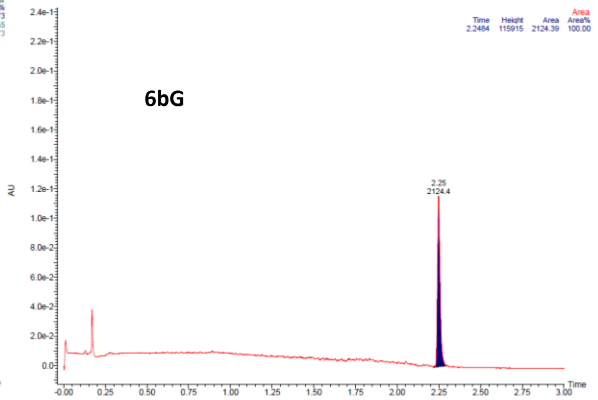

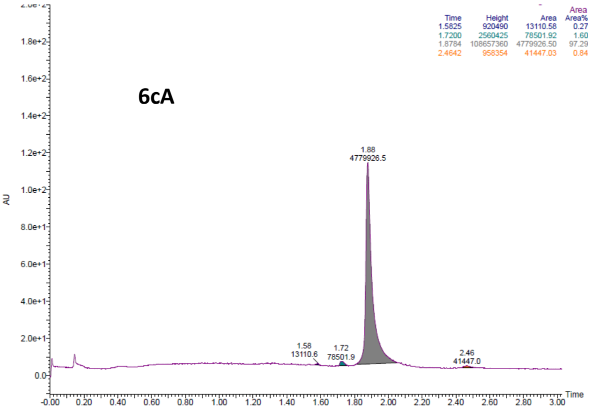

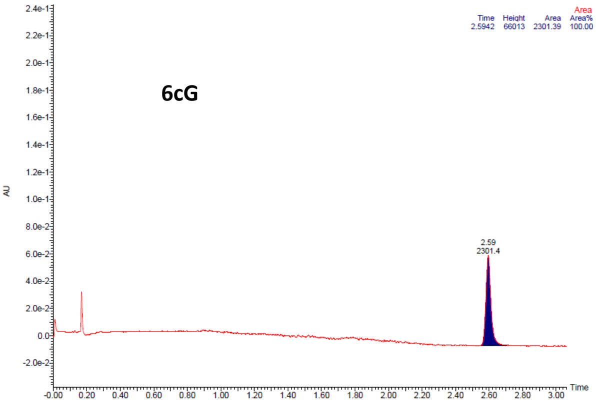

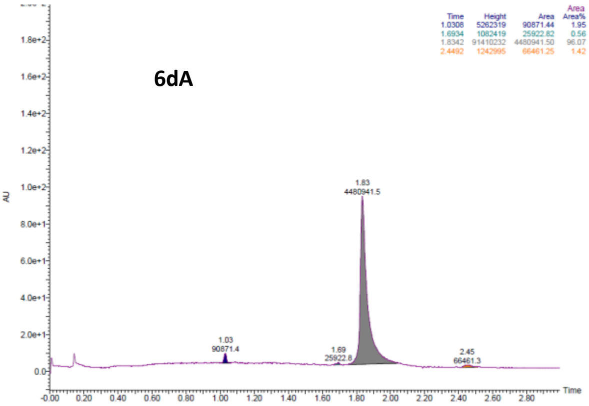

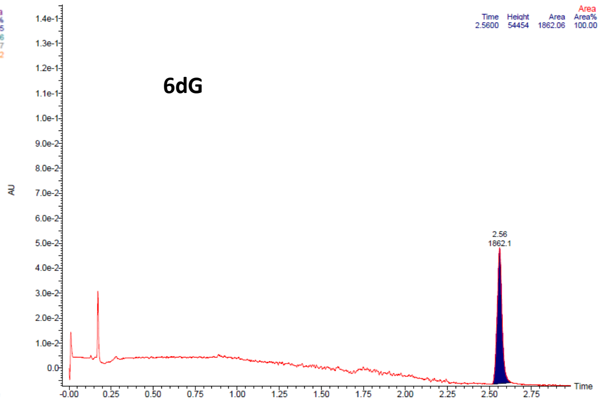

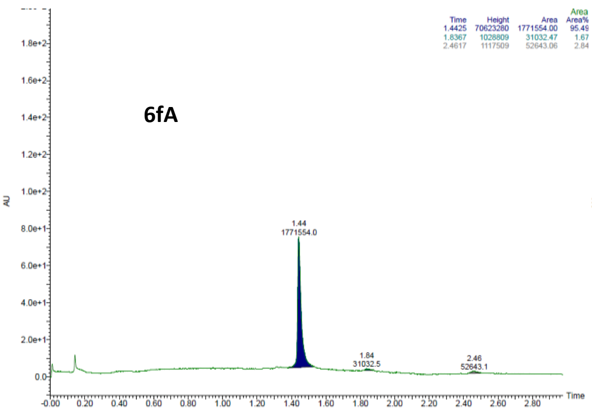

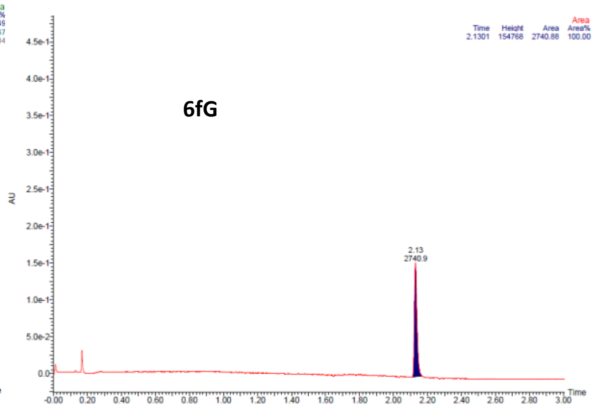

6. Full selectivity index table

Table S3. Selectivity index (SI) of all compounds towards all bacterial strains tested. EC_{50} values are given in [µg/mL].

			SI (MIC/EC_{50})				
Code	Core	ClogP[b]	S. a	B. s	E. c	P. a	EC_{50}[c]
2dA	Hydantoin	-1.69	43	86	22	43	344
4A	2,4-dithiohydantoin	-1.22	48	48	24	–	385
3A	4-imidazolidin-2-one	-0.47	24	48	24	6	48
15A	2-(hydroxy)-1*H*-imidazol	0.26	22	22	11	11	44
Mix 1	2-thiobarbituric acid	-0.10	38	76	39	19	305
Mix 2	2-thiobarbituric acid	-0.10	23	46	23	23	182
1A	Barbituric acid	-1.44	25	25	12	12	99

				SI (MIC/EC_{50})						SI (MIC/EC_{50})				
Code	Ar	Y	ClogP[b]	S. a	B. s	E. c	P. a	EC_{50}[c]	Code	S. a	B. s	E. c	P. a	EC_{50}[c]
2aA	(Ph)	*n*-propyl	2.64	–	–	–	–	>311	**2aG**	–	–	–	–	>353
2bA	(4-CF_3Ph)	*n*-propyl	3.52	–	>24	–	–	>379	**2bG**	>26	>65	–	–	>421
2cA	(3-Cl, 4-BrPh)	*n*-propyl	4.08	46	92	–	–	368	**2cG**	>234	>234	–	–	>467
2dA	(3,5-di-BrPh)	*n*-propyl	4.38	43	86	22	43	344	**2dG**	243	122	30	–	486
2eA	(4-Br-1-Nal)	*n*-propyl	4.68	17	17	6	6	69	**2eG**	103	103	26	–	206
2fA	(3,5-di-CF_3Ph)	*n*-propyl	5.03	25	50	25	25	399	**2fG**	>122	>245	–	–	>489

				SI (MIC/EC_{50})						SI (MIC/EC_{50})				
Code	Ar	Y	ClogP[b]	S. a	B. s	E. c	P. a	EC_{50}[c]	Code	S. a	B. s	E. c	P. a	EC_{50}[c]
6bA	(4-CF_3Ph)	*n*-butyl	3.52	–	>25	–	–	>393	**6bG**	>126	>126	–	–	>503
6cA	(3-Cl, 4-BrPh)	*n*-butyl	4.08	>55	>110	–	–	>439	**6cG**	347	347	43	–	347
6dA	(3,5-di-BrPh)	*n*-butyl	4.38	46	182	–	–	364	**6dG**	206	206	52	13	206
6fA	(3,5-di-CF_3Ph)	*n*-butyl	5.03	>29	>115	–	–	>461	**6fG**	192	192	48	–	384

Bacterial reference strains: S. a – *Staphylococcus aureus* ATCC 9144, B.s – *Bacillus subtilis* 168, E. c – *Escherichia coli* ATCC 25922, and P. a – *Pseudomonas aeruginosa* ATCC 27853. [a] –: No SI was calculated if MIC was >16 µg/mL.

7. Biological Methods

7.1 Minimum inhibitory concentration (MIC) assay

Based on the CLSI M07-A9 protocol,[13] a modified broth microdilution sensitivity test[14] was used to determine the minimum inhibitory concentration (MIC). Initially, a stock solution of water-soluble compounds was prepared by dissolving it in ultrapure water (Milli-Q H2O, Millipore, MA, United States). Before being further diluted with ultrapure water, the less water-soluble compounds were first dissolved in 25 - 50 µL 100% DMSO. The concentration of DMSO is always less than 1% in each compound's working concentration. The test components were then two-fold diluted with ultrapure water in polystyrene microplates with 96 wells of flat bottom (NUNC, Roskilde, Denmark). The bacterial inoculum was diluted into Mueller-Hinton broth (MHB, Difco Laboratories, USA) at 2.5- 3 x 10^4 cells / ml and added to the different diluted compounds in a 1:1 ratio. In each experiment, positive control (ciprofloxacin, Sigma-Aldrich, USA), negative control (bacteria + water), and medium control (media + water) were included. The microplates were incubated in EnVision microplate readers at 35 °C for 48 hours (Perkin-Elmer, Turku, Finland). The lowest concentration of compounds that did not cause bacterial growth was defined as MIC by optical density measurements (OD600). All components have been tested in 3 technical repetitions.

7.2 Membrane integrity assay

7.2.1 Inner membrane

Bacillus subtilis 168 (ATCC 23857) and *Escherichia coli* K12 (ATCC MC1061) were used as test strains to perform the inner membrane integrity assay in real time. Both strains were transformed with the reporter plasmid pCSS962 containing the gene encoding eukaryotic luciferase (*lucGR* gene).[15] D-luciferin, which was added externally, was used as a substrate for luciferase to detect light emissions. MH media supplemented with 5 µg/mL chloramphenicol (Merck KGaA, Darmstadt, Germany) and a mixture of 20 µg/mL chloramphenicol and 100 µg/mL ampicillin (Sigma-Aldrich, USA), respectively, were used to suspend *B. subtilis* and *E. coli* colonies and grown overnight at RT. The overnight culture was further diluted and grown at RT for 2-3 hours until OD600 = 0.1. A final concentration of 1 mM of D-luciferin potassium salt (Synchem Inc., Elk Grove Village, IL, USA) was added to the bacterial cultures and the background light is measured before the actual tests. Black microtiter plates (96 wells, round-bottom; Nunc, Roskilde, Denmark) were prepared with a twofold series of dilutions of compounds (10 µL per well) at final concentrations of 51.2 to 1.6 µg/mL. MQ-H_2O and chlorhexidine acetate (Fresenius Kabi, Halden, Norway) were used as negative and positive control, respectively. The bacterial suspension was primed before loading the assay plate into the Synergy H1 Hybrid Plate Reader (BioTek, Winooski, VT, USA). The 90 µL bacterial inoculum with D-luciferin was injected sequentially (well by well) by automated injection into test wells. Light emission (luminescence) due to bacterial membrane disturbance was monitored every second for 3 minutes. Each study was conducted at least three times independently and the figures show a representative set.

7.2.2 Outer membrane

The integrity testing of the outer membrane was carried out in real time using E. coli, the integrity same strain used in the testing of the integrity of the inner membrane. 1-N-phenylnapthylamine (NPN), which was added externally, was used as a substrate for fluorescent detection. The MH medium was used to suspend E. *coli* colonies and grown overnight at RT. The overnight cultures were further diluted and grown in RT for 2-3 hours until OD600 = 0.1. NPN (Sigma-Aldrich, USA) was added to bacterial cultures at a final concentration of 20 µM in glucose hepes buffer (5mM). Background fluorescence was measured before the actual assay. Black 96-well microtiter plates (round bottom) are prepared with a two-fold series of compounds (10 µL per well) diluted at final concentrations between 51.2 and 1.6 µg/mL. MQ-H_2O and chlorhexidine acetate were used as negative and positive control. The bacterial suspension was primed before the assay plate was loaded into the Synergy H1 hybrid plate reader. Bacterial inoculum (aliquots of 90 µL) with NPN was sequentially (well by well) injected into the test wells by an automated injector. As a result of bacterial outer membrane disruption, light (fluorescence) emission was monitored every second for 3 minutes. Each study has been carried out independently at least three times and the figures show a representative set.

7.3 Viability assay

B. subtilis 168 and *E. coli* K12, the same strains used in the inner membrane integrity assay, were used to perform the bacterial viability assay in real time. However, *E. coli* K12 was transformed with the reporter plasmid pCGLS-

1 and *B. subtilis* 168 has a constitutively expressed lux operon as a chromosomal integration at the sacA locus (PliaG).[16] MH medium supplemented with 5 µg/mL chloramphenicol and a mixture of 20 µg/mL chloramphenicol and 100 µg/mL ampicillin, respectively, were used to culture *B. subtilis* and *E. coli*, the same way as the membrane integrity assay. The respective injector was primed with bacterial suspension and continuous light production by these biosensors was monitored in the Synergy H1 hybrid reader. 10 µL of each compound at the final concentration ranging from 51.2 to1.6 µg/mL (two-fold dilutions) was prepared in black round-bottom 96-well microtiter plates. Chlorhexidine was used as a positive control and MQ-H_2O as a negative control. The automated injector added bacterial suspension (aliquot of 90 µL) consequently. Due to changes in bacterial viability, the reduction of light emission was monitored every second for 3 minutes. Each study was carried out at least three times individually and the figures show a representative set.

7.4 Red Blood Cell Haemolysis Assay

The protocol was adapted from Paulsen et al.[11] Haemolysis was determined using a heparinized fraction (10 IU/mL) of freshly drawn blood. The blood collected in ethylenediaminetetraacetic acid-containing test tubes (Vacutest, KIMA, Arzergrande, Italy) was used for the determination of the hematocrit (hct). The heparinized blood was washed 3× with pre-warmed phosphate-buffered saline (PBS) and adjusted to a final hct of 4%. Derivatives in DMSO (50 mM) were added to a 96-well polypropylene V-bottom plate (NUNC, Fisher Scientific, Oslo, Norway) and serially diluted. The test concentration range was 500–4 µM with DMSO contents ≤1%. A solution of 1% triton X-100 was used as a positive control for 100% haemolysis. As a negative control, a solution of 1% DMSO in PBS was included. No signs of DMSO toxicity were detected. RBCs (1% v/v final concentration) were added to the well plate and incubated at 37 °C and 800 rpm for 1 h. After centrifugation (5 min, 3000g), 100 µL of each well was transferred to a 96-well flat-bottomed microtiter plate, and absorbance was measured at 545 nm with a microplate reader (VersaMaxTM, Molecular Devices, Sunnyvale, CA, USA). The percentage of haemolysis was calculated as the ratio of the absorbance in the derivative-treated and surfactant-treated samples, corrected for the PBS background. Three independent experiments were performed, and EC_{50} values are presented as averages.

8. Membrane integrity and viability assay

Table S4. Summary of the membrane integrity and viability assay against *B. subtilis* 168.

Code	MIC[1] (µg/mL, 24h)	MIA (activity and speed)[2]	VA (effects)[3]
	B. s		
2bG	8	–	–
2cA	4	++	+
2cG	2	+++	++
2dA	4	++	+
2dG	4	++++	++
2eG	2	++++	+++
2fG	2	+++	++
6bG	4	++	++
6cA	4	++	+
6cG	1	++++	+++
6dA	2	++	+
6dG	1	++++	+++
6fG	2	+++	+++
CHX	1.5	++++	+++

B. s: *Bacillus subtilis* 168

[1]MIC assay was also performed in biosensor assay, and the value was similar.

[2]For membrane integrity assay: High active, fast speed (++++) Medium active, Intermediate speed (+++), Medium active, Slow speed (++), Low active, Slow speed (+) and Not active (–).

[3]For viability assay: High effect (+++), Medium effect (++), Low effect (+) and No effect (–). The highest concentration (51.2 µg/mL) was used to compare and evaluate the membrane integrity and viability assay results.

Table S5. Summary of the membrane integrity and viability assay against *E. coli* K12.

Code	MIC[1] (µg/mL, 24h)	MIA (activity and speed)[2]	VA (effects)[3]
	E. c		
2dA	16	+	+
2dG	16	+	+
2eG	8	+	+
6cG	8	+	+
6dG	4	+	+
6fG	8	+	+
CHX	1.5	++++	+++

E. c: *Escherichia coli* K12

[1]MIC assay was also performed in biosensor assay, and the value was similar.

[2]For membrane integrity assay: High active, fast speed (++++) Medium active, Intermediate speed (+++), Medium active, Slow speed (++), Low active, Slow speed (+) and Not active (–).

[3]For viability assay: High effect (+++), Medium effect (++), Low effect (+) and No effect (–). The highest concentration (51.2 µg/mL) was used to compare and evaluate the membrane integrity and viability assay results.

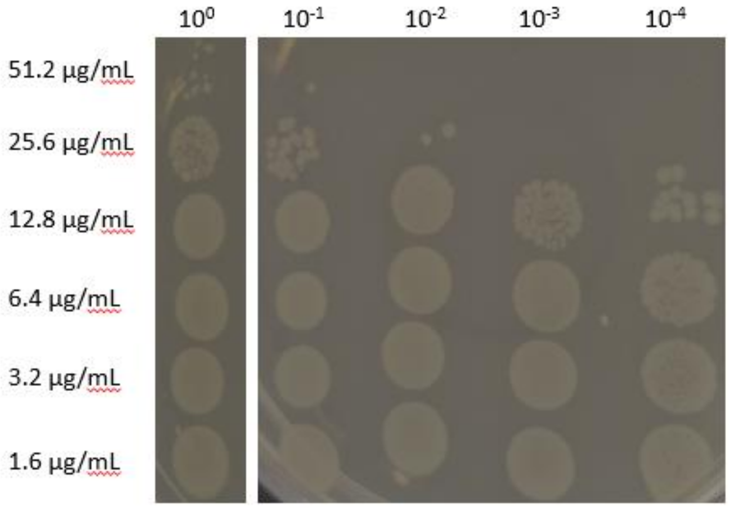

Figure S1. Bactericidal effect of hydantoin **6cG** against *E. coli* K12 after the outer membrane study with NPN. Horizontal: Dilution of the bacterial load.

9. Literature

[1] J. Dijkink, H. E. Schoemaker, W. N. Speckamp, *Tetrahedron Lett.* **1975**, *16*, 4043-4046.

[2] H. Hiemstra, W. N. Speckamp, in *Alkaloids Chem. Biol., Vol. 32* (Ed.: A. Brossi), Academic Press, **1988**, pp. 271-339.

[3] aD. J. Hart, T. K. Yang, *J. Org. Chem.* **1985**, *50*, 235-242; bH. Ent, H. De Koning, W. N. Speckamp, *J. Org. Chem.* **1986**, *51*, 1687-1691.

[4] H. Kohn, Z. K. Liao, *J. Org. Chem.* **1982**, *47*, 2787-2789.

[5] aD. Gupta, D. Bhatia, V. Dave, V. Sutariya, S. Varghese Gupta, *Molecules (Basel, Switzerland)* **2018**, *23*, 1719; bA. T. M. Serajuddin, *Adv. Drug Del. Rev.* **2007**, *59*, 603-616.

[6] P. L. Gould, *Int. J. Pharm.* **1986**, *33*, 201-217.

[7] C. Huixiong, L. Jean-Philippe, G. Nohad, G. Christiane, *Eur. J. Org. Chem.* **2006**, *2006*, 2329-2335.

[8] M. Donnier-Maréchal, P. Carato, P.-E. Larchanché, S. Ravez, R. Boulahjar, A. Barczyk, B. Oxombre, P. Vermersch, P. Melnyk, *Eur. J. Med. Chem.* **2017**, *138*, 964-978.

[9] J. Simonin, S. K. V. Vernekar, A. J. Thompson, J. D. Hothersall, C. N. Connolly, S. C. R. Lummis, M. Lochner, *Bioorg Med Chem Lett* **2012**, *22*, 1151-1155.

[10] L. Tao, F. Luoyi, G. Hao, X. Zeming, Z. Yanpeng, J. Nianqiang, J. Long, L. Gaofeng, L. Yang, W. Jiaobing, *Angew. Chem. Int. Ed.* **2017**, *56*, 9473-9477.

[11] M. H. Paulsen, M. Engqvist, D. Ausbacher, T. Anderssen, M. K. Langer, T. Haug, G. R. Morello, L. E. Liikanen, H.-M. Blencke, J. Isaksson, E. Juskewitz, A. Bayer, M. B. Strøm, *J. Med. Chem.* **2021**.

[12] M. K. Langer, Rahman, A.; Dey. H.; Anderssen, T.; Zilioli, F.; Haug, T.; Blencke, H.-M.; Stensvåg, K.; Strøm, M. B.; Bayer, A., *(submitted Manuscript)* **2022**.

[13] F. R. Cockerill, 9th ed. (Ed.: C. a. L. S. Institut), Wayne, Pa : Clinical and Laboratory Standards Institut, **2012**.

[14] E. M. Igumnova, E. Mishchenko, T. Haug, H.-M. Blencke, J. U. E. Sollid, E. G. A. Fredheim, S. Lauksund, K. Stensvåg, M. B. Strøm, *Biorg. Med. Chem.* **2016**, *24*, 5884-5894.

[15] M. Virta, K. E. O. Åkerman, P. Saviranta, C. Oker-Blom, M. T. Karp, *J. Antimicrob. Chemother.* **1995**, *36*, 303-315.

[16] aJ. Radeck, K. Kraft, J. Bartels, T. Cikovic, F. Dürr, J. Emenegger, S. Kelterborn, C. Sauer, G. Fritz, S. Gebhard, T. Mascher, *J. Biol. Eng.* **2013**, *7*, 29; bS. Frackman, M. Anhalt, K. H. Nealson, *J. Bacteriol.* **1990**, *172*, 5767-5773.

Paper III

Paper IV